Design of C5-Substituted 2′-Deoxyuridines, Small Fluorescent Molecule and Study of Photophysical/Biophysical Properties

A Dissertation Submitted to the
Indian Institute of Technology Guwahati
As Partial Fulfillment for the Award of Degree of

Doctor of Philosophy
in Chemistry
by

Hiranya Gogoi
Roll No. 126122016

Under The Supervision of

Prof. Subhendu Sekhar Bag

Department of Chemistry
Indian Institute of Technology Guwahati
Guwahati 781039
May 2019

Dedicated to

My
Parents
And
Those who have helped me

Nothing in life is to be feared, it is only to be understood.

-Marie Curie

INDIAN INSTITUTE OF TECHNOLOGY, GUWAHATI
Department of Chemistry

DECLARATION

I do hereby declare that the research work embodied in this thesis entitled "***Design of C5-Substituted 2'-Deoxyuridines, Small Fluorescent Molecule and Study of Photophysical/Biophysical Properties***" has been carried out by me under the supervision of **Prof. Subhendu Sekhar Bag** in the Department of Chemistry, Indian Institute of Technology Guwahati, India.

In keeping with the general practice of reporting scientific observations, due acknowledgments have been made wherever the work described is based on the findings of other investigators.

IIT Guwahati
May, 2019

Hiranya Gogoi

Dr. Subhendu Sekhar Bag, FRSC
Professor
Department of Chemistry
Indian Institute of Technology
Guwahati-781039
Assam, INDIA

Ph: +91-361-258-2324(O)
Ph: +91-361-258-4324 (R)
Fax: +91-361-258-2349
E-mail: ssbag75@iitg.ernet.in
ssbag75@yahoo.co.in

CERTIFICATE

This is to certify that the research work presented in this thesis entitled "***Design of C5-Substituted 2'-Deoxyuridines, Small Fluorescent Molecule and Study of Photophysical/Biophysical Properties***" is an authentic record of the results obtained from the research work carried out by **Mr. Hiranya Gogoi** under my supervision in the Department of Chemistry, Indian Institute of Technology Guwahati, India. This work is original and has not been submitted elsewhere for a degree or award.

IIT Guwahati
May, 2019

Prof. Subhendu Sekhar Bag
(Thesis Supervisor)

ACKNOWLEDGMENT

It is with high regards and profound respect that I express a deep sense of sincere gratitude to my supervisor **Prof. Subhendu Sekhar Bag** for his stimulating guidance, precious constructive suggestions and decisive insights during the entire course of my research work.

I would like to thank my Doctoral Committee members, **Prof. Anil Kumar Saikia** (chairman), **Dr. Chandan Mukherjee** (member) and **Prof. Animes Kumar Golder** (member) for their intellectual input, encouragement, valuable suggestions and comments during the entire course of my research work.

I wish to thank my lab mates Rajen da, Sangita ba, Subhashis da, Suman da, Manoj da, Afsana ba, Suranjan and Mohan for their cooperation, support and pleasant company throughout my research work. Without their help, it would have been impossible to complete my research work.

Sincere thanks go to my other lab mates Dipankar da, Momina ba, Tridip da and Anindya for their cooperation and sharing some happy moments inside and outside the laboratory.

I would like to acknowledge my juniors Anupama, Sayantan, Krisanu, Shilpa, Samir, Sourav, Queen, Aniket, Suravi and Sinchini for their help, support and pleasant company in the laboratory. Thanks to all of my friends, juniors, seniors and trainees whom I met during my research life in IIT Guwahati for their help.

My honest regards to all the faculty members of our department for their encouragement and help. I want to express my thanks to Dr. Babulal Das, Mr. Chandan Borgohain and Dr. Kh. Kesho Singh for their help in collecting various experimental data and our technical and official staffs for their help and support.

I owe the success to my parents (Mr. Jagat Gogoi and Mrs. Kunjalata Gogoi) who have been a constant source of inspiration to carry out my career. I wish to thank them for giving me the freedom to pursue a career path of my choice and their constant support and encouragement in realizing my dreams. I want to express my thanks to my brother and sisters and all the family members for their support.

I would like to express my deep gratitude to the Lakshminath Bezbaroa Central Library for providing physical and digital access to research materials, space and environment for study and financial assistance. Thanks to all library staff for their help.

And last but not least, I would like to acknowledge the Department of Chemistry, IIT Guwahati for giving me the opportunity and fellowship to carry out my research work. I am also thankful to the CIF IIT Guwahati for providing instrument facilities.

Hiranya Gogoi

Hiranya Gogoi

Present Address:

C/O: Prof. Subhendu Sekhar Bag
Department of Chemistry
Indian Institute of Technology Guwahati
Guwahati – 781039, Assam, India
Phone: +91 361 2582324
Email: g.hiranya@iitg.ac.in
hiranyagogoi32@gmail.com

Permanent Address:

Vill – Erapather
P. O. – Bhadoi Panchali
Dist. – Dibrugarh
Pin – 786191
Assam, India
Mobile**:** +91 9678347743

Area of Interest

Design and synthesis of modified fluorescent nucleosides for chemical and biochemical application.

Education:

2019	**Ph. D.** [Thesis submitted] **Title:** "Design of C5-Substituted 2′-Deoxyuridines, Small Fluorescent Molecule and Study of Photophysical/Biophysical Properties."
2012	**Master of Science** (*in Organic Chemistry*) Gauhati University, Assam
2009	**Bachelor of Science** *(Chemistry Hons.)* Duliajan College Dibrugarh University

Honors/Awards:

- Graduate Aptitude Test (**GATE**) in Chemistry, 2012, awarded by MHRD, Government of India.

List of Publications

1. ●Design of "Click" Fluorescent Labeled 2'-deoxyuridines via C5-[4-(2-Propynyl(methyl)amino)]phenyl Acetylene as a Universal Linker: Synthesis, Photophysical Properties, and Interaction with BSA● Bag*, Subhendu Sekhar; **Gogoi, Hiranya** ● *J Org Chem* **2018,** *83* (15), 7606-7621.

2. ●Design of a fused triazolyl 2-quinolinone unnatural nucleoside via tandem CuAAC-Ullmann coupling reaction and study of photophysical property● Bag*, Subhendu Sekhar; Das, Suman Kalyan.; **Gogoi, Hiranya**● *Tetrahedron* **2018,** *74* (18), 2218-2229.

Communicated

1. ●Sensing BSA Protein with Fluorescent Unnatural Tetrazolylpyrene Nucleoside● Bag*, Subhendu Sekhar**;** **Gogoi, Hiranya;** Pradhan, Manoj Kumar**;** Talukdar, Sangita**.**
2. ●Design, Synthesis and Studies on the Photophysical/Biophysical Properties/Interaction of Fluorescent Triazolyl Fluorene-Labeled 2'-deoxyuridine Nucleoside● Bag*, Subhendu Sekhar; **Gogoi, Hiranya.**
3. ●Studies on the Interaction of Pyrenylamido Triazolyl Aromatic Amino Acid Scaffold with Short Abasic DNAs● Bag*, Subhendu Sekhar**;** **Gogoi, Hiranya;** Jana**,** Subhashis**.**

List of Conferences/Symposiums

1. XIIth J-NOST Conference for Research Scholars, November 24-27, **2016**, CSIR-CDRI, Lucknow, India.
2. Recent Trends in Chemical Science (RTCS), October 12-13, **2017**, Department of Chemistry, NIT Meghalaya, India.

ABSTRACT

The dissertation entitled "**DESIGN OF C5-SUBSTITUTED 2′-DEOXYURIDINES, SMALL FLUORESCENT MOLECULE AND STUDY OF PHOTOPHYSICAL/BIOPHYSICAL PROPERTIES**" is an embodiment of research aimed towards the synthesis and studies on photophysical/biophysical properties of (a) nucleosides containing triazolyl donor/acceptor aromatics at C5 position of 2'-deoxyuridine, (b) study of interaction of fluorescently labeled nucleoside/fluorescent unnatural nucleoside with model protein biomolecule (BSA), (c) nucleosides containing fluorene aromatics at C5 position of 2'-deoxyuridine and (d) studies on the interaction of an AIE fluorescent probe, pyrenylamido triazolyl aromatic amino acid **PyAm-^{Ar}TAA,** with short abasic DNAs. Towards this journey, few fluorescent C5-substituted 2′-deoxyuridine nucleosides have been synthesized and their photophysical properties evaluated. The biophysical properties of two triazolyl nucleoside, one tetrazolyl nucleoside and one triazolyl aromatic amino acid have been investigated.

Thus, this thesis contains a total of 5 Chapters including one Review Chapter (**Chapter 1**). Each chapter contains its individual experimental and reference sections. **Chapter 1** is a review of the applications of various types of fluorescent and non-fluorescent C5-substituted 2′-deoxyuridines. **Chapter 2** deals with the synthesis of a post-synthetically modifiable universal linker, 4-(Propynyl(methyl)amino)phenylacetylene, containing 2′-deoxyuridine nucleoside and then to generate fluorescent C5- donor/acceptor aromatics substituted 2'-deoxyuridine nucleosides. The study of photophysical properties of such nucleosides has also been included in this chapter. **Chapter 3** deals with the studies on the interaction of a ratiometric fluorescent probe, pyrene-labeled dual fluorescent 2'-deoxyuridine, and a tetrazolylpyrene unnatural fluorescent nucleoside with BSA. **Chapter 4** focuses on the synthesis of fluorescent C5-triazolylfluorene-labeled 2'-deoxyuridines and studies on their photophysical/biophysical properties. **Chapter 5** deals with the studies on the interaction of an AIE fluorescent probe, pyrenylamido triazolyl aromatic amino acid **PyAm-^{Ar}TAA,** with short abasic DNAs.

CHAPTER 1: APPLICATIONS OF C5-SUBSTITUTED 2'-DEOXYURIDINES: A REVIEW

This chapter highlights the applications of various types of fluorescent and non-fluorescent C5-substituted 2′-deoxyuridines. The C5-substituted 2'-deoxyuridines are known for their potential antiviral properties for a long time. 5-iodo-2'-deoxyuridine (IDU) is the first synthetic nucleoside showing effective antiviral properties and was synthesized in 1959. Later, more

effective antiviral agents such as BVDU and IVDU have been synthesized. Eventually, safer and more effective practices have led to the synthesis of numerous uridine analogous exhibiting antiviral as well as anticancer properties ((**Figure A1**).

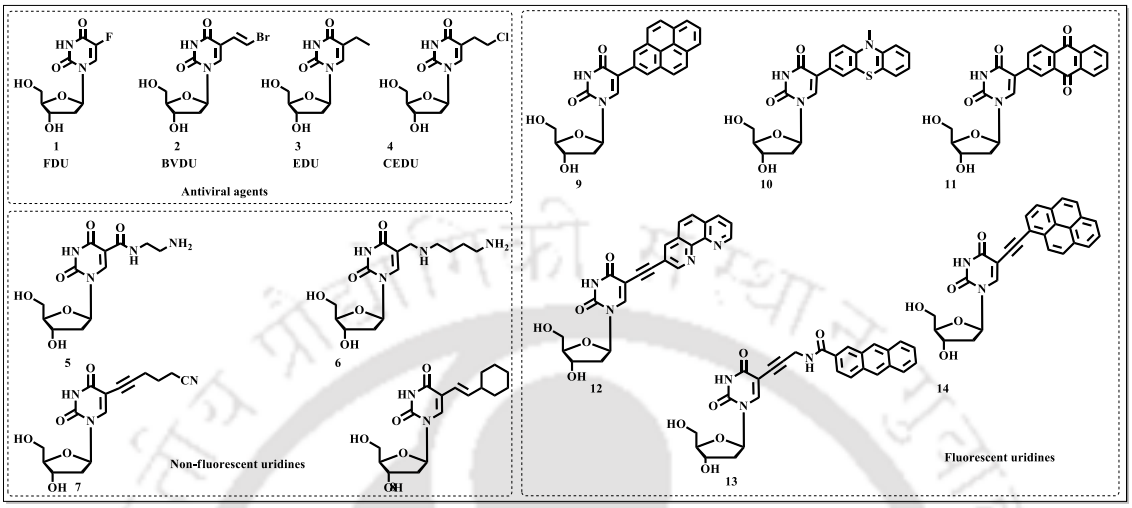

Figure A1. Different types of C5-substituted 2'-deoxyuridines.

In 1973, Kropinski *et al.* have discovered a modified base 5-(4-aminobutylaminomethyl-2′-deoxyuridine in the DNA of bacteriophage ϕW-14 with a higher melting temperature compared to its natural analog DNA without a modified base. The results of the assay have established the idea among researchers that DNA can be stabilized to more extent than the natural ones. Thus, the earlier modifications of DNA mainly focused on the effects of substituents on the stability of DNA duplexes. Development of methodologies and knowledge led to the synthesis of alkenyl and alkynyl 5-substituted uridines which provide incorporation of diverse functionality into DNA leading to modulated covalent, electrostatic interaction properties within DNA. In many cases, when incorporated into DNA, short alkenyl and alkynyl chains have shown higher duplex stability than alkyl chains with the same carbon numbers.

On the other hand, understanding the structure, properties, and functions of biological macromolecules, cells and microorganisms often utilize fluorescence-based techniques for a long time. Thus, a number of fluorescence-based techniques have been developed which contributed significantly to the field of molecular genetics. In this regard, the molecules which have good photophysical properties can be very helpful for understanding the various chemical, biochemical and biological phenomena. Thus, the nucleosides can be modified to impart rich photophysical properties. Such modifications can be done at the base or at the sugar of a nucleoside. We limited our discussion with the various types of base modified fluorescent

uridines at the C5 position, their synthesis and applications in this chapter. **Figure A1** represents various types of C5-substituted 2'-deoxyuridines.

Thus, this chapter contains a critical survey of applications of few C5-substituted 2'-deoxyuridines.

CHAPTER 2: DESIGN, SYNTHESIS AND PHOTOPHYSICAL PROPERTIES OF FLUORESCENT C5-SUBSTITUTED 2′-DEOXYURIDINES

This chapter elaborates the design concept and the synthesis of a post-synthetically modifiable universal linker, 4-(Propynyl(methyl)amino)phenylacetylene, containing 2′-deoxyuridine nucleoside and then to generate fluorescent C5- donor/acceptor aromatics substituted 2'-deoxyuridine nucleosides. The photophysical properties of the synthesized nucleosides have also been explored and discussed in this chapter.

Understanding the biological events associated with inter-biomolecular interactions, such as dielectric properties in DNA, proteins, cell membranes and structures, functions, dynamics of biomolecules is a very indispensable research area in current years. In this respect, highly solvatochromic fluorescent probes and fluorescently labeled biomolecular building blocks such as solvofluorochromic nucleosides/ amino acids have been successfully utilized for the sensing and detection of such biomolecular events. The fluorescently labeled nucleosides also find many applications such as DNA sequencing, chemical and biochemical sensing processes, single nucleotide polymorphism (SNPs) typing and many more biotechnological applications. Fluorescently labeled nucleosides/nucleotides that display a strong enhanced signal upon hybridization with a target DNA can be used for the detection of single nucleotide polymorphism (SNPs typing).

As a part of our continuous research efforts in the design of solvofluorochromic molecules/biomolecular building blocks, we thought that it would be worthwhile to design dual emissive modified nucleosides. Based on our experience, literature reports and wider applicability, we considered the design of C5-labeled 2'-uridines as model nucleoside probes useable for DNA analysis in the future. Till the date, there is no report wherein C5-position of 2′-deoxyuridine is linked with an electron donor unit as a post-synthetically modifiable functional group which effectively can generate a modulated fluorescence property of a fluorophore if attached at the terminus or the terminal alkyne can be reacted with a fluorophoric azide functionality. Inspired by our previous result on “installation/modulation of fluorescence response” of various small fluorescent molecules and an interesting dual emission behavior

from pyrene when attached to *N*,*N*-dimethylanilino triazole donor unit and motivated by the importance of dual emitting probe for DNA analysis, we thought that it would be worthwhile to generate a set of fluorescent 2'-deoxyuridine nucleosides which could show interesting intramolecular charge transfer property or dual emission. We further thought that attaching an electron donor phenylacetylene unit as a post-synthetically modifiable functional group at the C5-position of 2'-deoxyuridine would be beneficial to generate a set of fluorescent 2'-deoxyuridines with modulated fluorescence property of a fluorophore via azide-alkyne cycloaddition reaction. Furthermore, the same nucleoside, if incorporated into DNA, can offer the opportunity of generating fluorescent oligonucleotide probes via post-synthetic click reaction with modulated fluorescence property.

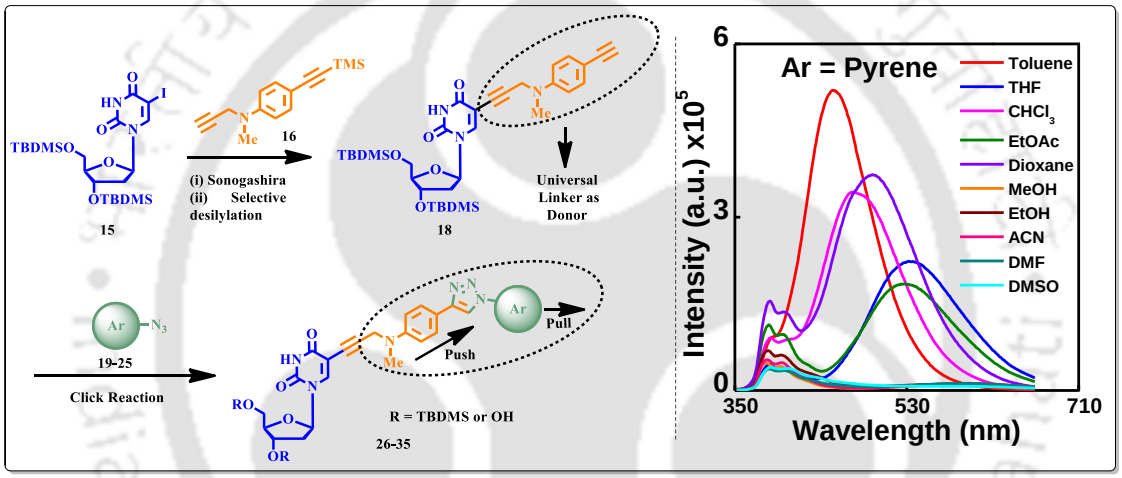

Scheme A1. Graphical representation of the design concept for the synthesis of universal linker containing modified 2′-deoxyuridine and its fluorescent analogs and the dual fluorescent spectra of a representative pyrenyl fluorescent nucleoside.

Therefore in this chapter, we have reported the rational design and synthesis of triazolyl push-pull fluorophore-labeled uridines via the intermediacy of C5-{4-(2-propynyl(methyl)amino)}phenyl acetylene as a universal linker. Our design involves the synthesis of a universal linker, 4-(Propynyl(methyl)amino)phenylacetylene and its incorporation into C5-position of 2′-deoxyuridine. The universal linker containing 2′-deoxyuridine can then undergo Huisgen 1, 3-dipolar cycloaddition reaction with donor-acceptor chromophore containing fluorogenic azides to afford the target fluorescent uridines. The donor aromatic substituted triazole moiety is thought to allow an intramolecular charge transfer (ICT) process from triazole-linked moiety to the fluorophoric units leading to solvatochromic fluorescence at a longer wavelength. Moreover, the fluorophores, such as

pyrene, coupled electronically with donor aryltriazoles, could show dual fluorescence property or interesting modulated solvatochromic emission response. Thus, our design would ultimately lead to predetermined photophysical properties of the fluorophores and hence of the nucleoside.

The synthesized nucleosides have shown interesting solvatochromic characteristic and/or intramolecular charge transfer (ICT) feature. Few of them also exhibit dual emitting characteristics evidencing our designing concept. The HOMO-LUMO distribution shows that the emissive states of these nucleosides can be characterized with more significant electron redistribution between the C5-{4-(2-propynyl(methyl)amino)}phenyl triazolyl donor moiety and the aromatic chromophores linked to it leading to modulated emission property. The solvent polarity sensitivity of these nucleosides has also been tested. The synthesized triazolyl benzonitrile-, naphthyl- and pyrenyl- nucleosides have been found to exhibit interesting intramolecular charge transfer (ICT) and dual (LE/ICT) emission property. The dual fluorescent nucleosides having ratiometric fluorescence property could be utilized for DNA analysis if incorporated in a DNA for the generation of fluorescent oligonucleotide probes. All experimental results are presented in this chapter.

CHAPTER 3: STUDIES ON THE INTERACTION OF TRIAZOLYLPYRENE-LABELED FLUORESCENT 2'-DEOXYURIDINE AND UNNATURAL TETRAZOLYLPYRENE NUCLEOSIDES WITH BSA

This chapter describes the studies on the interaction of a triazolylpyrene-labeled fluorescent 2'-deoxyuridine and an unnatural fluorescent tetrazolylpyrene nucleoside with bovine serum albumin (BSA) protein utilizing UV-visible and fluorescence spectroscopy. Protein-ligand interactions are of paramount importance for all processes taking place in living organisms. These interactions regulate the states and functions of proteins which are important for regulation of biological functions. Therefore, the study of such interactions is crucial for the development of newer drug candidates. A small molecule with unique photophysical properties responding to the microenvironment exceptionally and bearing information related to biological protein-ligand binding sites and events is significant for drug discovery and many other research topics. Therefore, molecular design and proteomics are two topmost research topics in the field of drug discovery. However, a large number of experimental trials required to gain insight into the properties and functions of a particular protein and develop smart molecules accordingly. Therefore, highly abundant proteins like serum albumins often used as models in order to investigate protein-small molecule interactions which ultimately assist in

designing biologically active compounds. Therefore, aqueous complexation studies of synthetic molecules with serum albumins such as bovine serum albumin (BSA) gain significant research interest during the last decade.

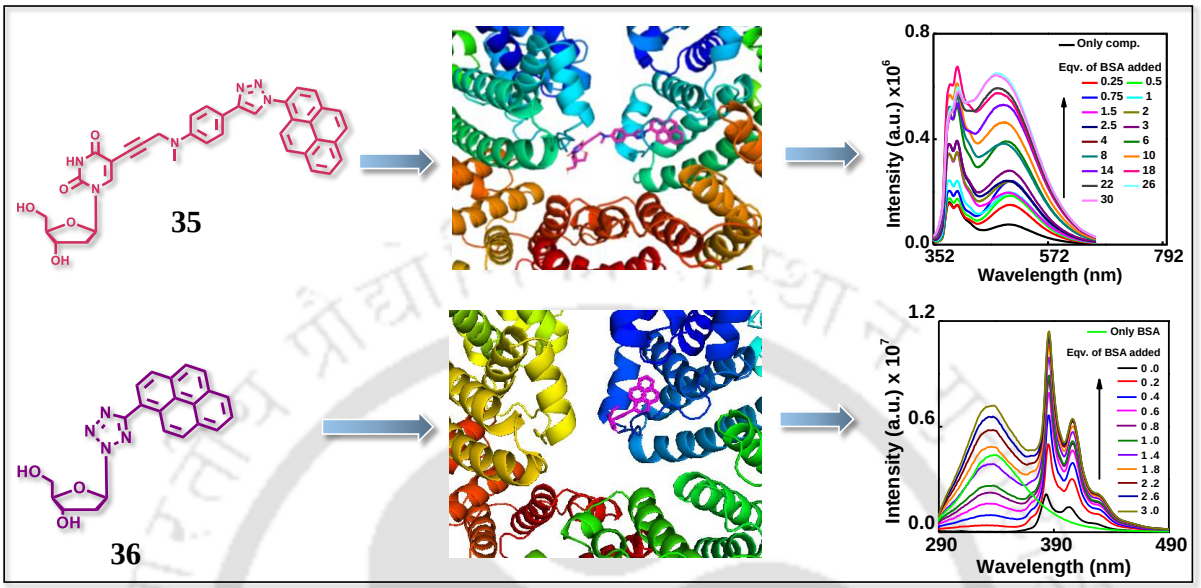

Figure A2. Schematic presentation of the interactions of BSA with pyrene-labeled nucleosides.

With the above background and the observed photophysical properties of our previously reported pyrene-labeled fluorescent probes, **35** and **36** (**Figure A2**), we envisaged that these nucleosides might offer some interesting binding interactions with a biomolecule such as a model protein BSA. Thus, from the UV-visible and fluorescence study, we have successfully shown that our click chemistry derived triazolyl and tetrazolyl fluorophoric nucleosides **35** and **36**, respectively, serve as versatile fluorescent light-up probes for BSA protein detection in the aqueous media. The enhancement in the fluorescence intensity of both of these nucleoside probes upon addition of BSA indicates strong interaction with high binding constant. All experimental results are presented in this chapter.

CHAPTER 4: SYNTHESIS AND STUDIES ON THE PHOTOPHYSICAL/BIOPHYSICAL PROPERTIES OF TRIAZOLYLFLUORENE-LABELED 2′-DEOXYURIDINES

This chapter elaborates the synthesis of triazolylfluorene-labeled 2′-deoxyuridines and studies on their photophysical properties and interaction of one of them with calf thymus DNA (ctDNA). Fluorene is a rigid and planar molecule containing two benzene rings fused by a five-

membered ring. The structural importance of fluorene is its planar structure and delocalized π-electron cloud. The fluorene moiety can be utilize as spacers via aromatic coupling at the 2 and 7 positions for the design and synthesis of fluorescent probes. Also, the C-H functionalization at the C9 position of the fluorene is highly facile. For such structural features, fluorene has been utilized as building blocks for the synthesis of various organic molecules including dyes, polymers etc. Many of these molecules have been exploited for their applications in cell imaging and detection of explosives. However, a very few examples of fluorene containing nucleosides are available in the literature. Electronic conjugation between a triazole and a fluorene scaffold could lead to the generation of a modulated photophysical property within the parent molecule, which might be useful for the investigation of biological events. Therefore, the synthesis of triazolylfluorene decorated nucleosides with novel photophysical properties is an interesting topic of research.

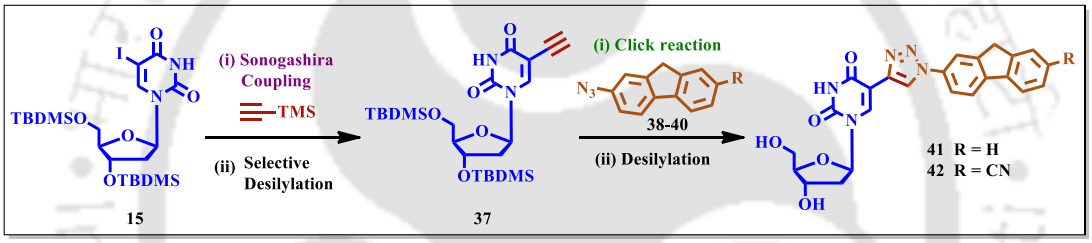

Scheme A2. Graphical representation of the synthesis of triazolylfluorene-labeled 2′-deoxyuridines.

With the above background, we have synthesized few fluorescent nucleosides wherein the C5 position of 2'-deoxyuridine is electronically conjugated with fluorene analogues via Sonogashira cross-coupling and copper-catalyzed click chemistry. We envisaged that these nucleosides might offer some interesting photophysical properties and binding interaction with DNAs and/or proteins. From the study on photophysical properties of the synthesized nucleosides, we have observed that the two of the synthesized nucleosides show interesting dual emission properties in various organic solvents which are very important for monitoring the DNA microenvironment. We also have studied the interaction of cyanofluorenyl 2'-deoxyuridine **42** (**Scheme A2**) with ctDNA and observed that this nucleoside is capable of sensing ctDNA via generation of an enhanced fluorescence signal. All experimental results are presented in this chapter.

CHAPTER 5: STUDIES ON THE AGGREGATION INDUCED FLUORESCENCE EMISSION PROPERTY OF PYRENYLAMIDO TRIAZOLYL AROMATIC AMINO ACID AND ITS INTERACTION WITH SHORT ABASIC DNAs

This chapter described the studies on the aggregation induced fluorescence emission (AIE) property of a fluorescent pyrenylamido triazolyl aromatic amino acid scaffold **PyAm-^{Ar}TAA** and the interaction with short abasic DNAs.

The development of fluorescent molecules with the ability to recognize DNA sequence alteration via the generation of highly specific fluorescence signal are of recent attraction in biology and in bioorganic and medicinal chemistry. In this respect, the probe with AIE property would be advantageous as these fluorophores in any concentration can be utilized as light-up fluorescent probes. In particular, sensing of DNA lesions is crucial for reliable disease diagnosis and the design of new chemotherapeutics. The most commonly encountered DNA lesions are abasic DNA, mismatched DNA, base modified DNA, single-strand breaks, double-strand breaks, and intrastrand cross-linked DNA. Out of all DNA lesions, however, an abasic site [Ap or Φ] DNA is most frequent and can lead to deleterious mutations. Therefore, the design of fluorescent probes for the detection and stabilization of abasic DNA is paramount importance for the cellular survival and development of new chemotherapeutic agents.

Over the years, many platforms have been developed for the detection and stabilization of DNA abasic site (Ap site). Thus, fluorescent oligonucleotide probes containing non-nucleosidic base surrogates have been utilized for Ap site recognition and stabilization. Similarly, fluorimetric sensing, as well as stabilization of an abasic DNA, has also been achieved with the use of nucleosidic base surrogates. However, these methods require preparation of fluorescent modified DNA probes which in turn need complicated probe design and high cost analysis. Therefore, the best alternative strategy is to employ a ligand/ molecule which can fit within the gap created by the Ap site. Therefore, the label-free detection of Ap site is very much desirable to offer simple and low-cost strategy. The fluorescent molecules having a comparable volume of an A: T pair and good intercalating property are, in general, the suitable candidates to cover the gap space created by an Ap site and thus, are capable of sensing and stabilizing Ap DNA via inter-/intrastrand π-π stacking interaction.

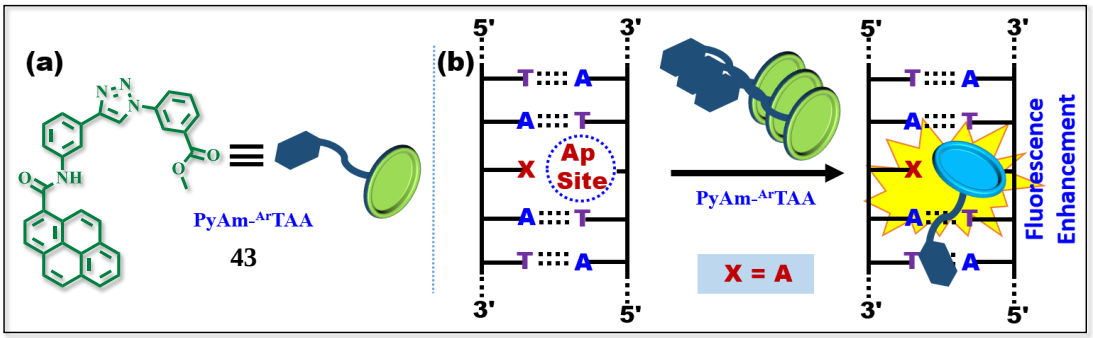

Scheme A3. The chemical structure of the AIE probe and the schematics of the concept of binding of the probe **PyAm-^{Ar}TAA** to an abasic site opposite to A base (X = A).

With the above background and concept, we studied the interaction of an AIE probe **PyAm-^{Ar}TAA (43**, **Scheme A3)** with short 13-mer DNA duplexes containing an abasic site opposite to all four natural bases utilizing a "Just Mix & Read" label-free strategy which does not need any annelation and relies on simple read out the fluorescence signal from the probe. We have successfully demonstrated that the bare fluorescent pyrenylamido aromatic triazolo amino acid scaffold, **PyAm-^{Ar}TAA**, serves as a good AIE light-up probe for label-free detection of DNA abasic site specifically opposite to base adenine (A) without affecting the DNA duplex stability. All the experimental results are presented in this chapter.

Abbreviations

A	Adenine
Abs	Absorbance
Ac	Acyl
ACMA	9-amino-6-chloro-2-methoxyacridine
ACN	Acetonitrile
ACQ	Aggregation caused quenching
ADP	adenosine diphosphate
ADT	AutoDockTools
Ag	Silver
AIDS	Acquired immune deficiency syndrome
AIE	Aggregation induced emission
AIEE	Aggregation induced emission enhancement
AMP	Adenosine monophosphate
AP	Apurinic/apyrimidinic
APCI	Atmospheric-pressure chemical ionization
ATP	Adenosine triphosphate
B3LYP	Becke, three-parameter, Lee-Yang-Parr
BDF	Base discriminating fluorescent
BER	Base excision repair
BODIPY	4,4-difluoro-4-bora-3a,4a-diaza-s-indacene
BSA	Bovine serum albumin
BVDU	(E) -5-(2-bromo)-2'-deoxyuridine
C	Cytosine
CD	Circular Dichroism
$CDCl_3$	Deuterated chloroform
CEDU	5-(2-chloroethyl)-2'-deoxyuridine
$CHCl_3$	Chloroform
CI	Configuration interaction
CNT	Concentrative nucleoside transporter
Comp.	Compound
Conc.	Concentration
CPL	Circularly polarized luminescence
CPN	Conjugated polymer nanoparticle
Cr	Chromium
CT	Charge transfer
ctDNA	Calf thymus DNA
Cu	Copper
CuAAC	Copper catalyzed azide-alkyne cycloaddition
CuI	Copper iodide
$CuSO_4$	Copper sulfate
5-dU	5-substituted-2′-deoxyuridine
D-A	Donor-acceptor
DCM	Dichloromethane
DFT	Density functional theory
Diox	Dioxane
DMF	Dimethyl formamide
DMSO	Dimethyl dimethyl sulfoxide
DMSO-d_6	Deuterated DMSO

DNA	Deoxyribonucleic acid
DNT	2,4-dinitrotoluene
DOL	Degree of labeling
DSA	Distyrylanthracene
dsDNA	Double-stranded DNA
ED_{50}	Median effective dose
EdU	5-ethyl-2'-deoxyuridine
ENT	Equilibrative nucleoside transporter
Eqv.	Equivalent
ESF	Environmentally sensitive fluorescent
ESI	Electrospray ionization
ESIPT	Excited state intramolecular proton transfer
Et_3N	Trimethylamine
EtOAC	Ethyl acetate
EtOH	Ethanol
eV	Electron volt
FDU	5-fluoro -2'-deoxyuridine
Fe	Iron
Fl	Fluorescence
FNA	Functional nucleic acid
FISH	Fluorescent in situ hybridization
Freq.	Frequency
FRET	Fluorescence resonance energy transfer
FT-IR	Fourier-transform infrared spectroscopy
G	Guanine
GFP	Green fluorescent protein
GO	Graphene Oxide
h	Hour
^1H NMR	Proton NMR
HBV	Hepatitis B virus
HCMV	Human cytomegalovirus
Hex	Hexane
HIV-1	Human immunodeficiency virus 1
H_2O_2	Hydrogen peroxide
HOMO	Highest occupied molecular orbital
HPS	Hexaphenylsilole
HRMS	High resolution mass spectroscopy
HSA	Human serum albumin
HSV-1	Herpes simplex virus 1
IC_{50}	Half maximal inhibitory concentration
ICD	Induced circular dichroism
ICT	Intramolecular charge transfer
IDU	5-iodo-2'-deoxyuridine
IdUTP	5-iodo-2'-deoxyuridine triphosphate
IR	Infrared Spectroscopy
IVDU	(E)-5-(2-iodovinyl)-2'-deoxyuridine
K	Kelvin
k	Rate constant
KBr	Potassium bromide
K_2CO_3	Potassium carbonate

KOH	Potassium hydroxide
LE	Locally-excited
LED	Light-emitting diode
LELCs	Light-emitting liquid crystals
LGA	Lamarckian genetic algorithm
LUMO	Lowest unoccupied molecular orbital
Max	Maxima
MB	Molecular beacon
MeOH	Methanol
min	Minute
mM	Mili molar
m.p.	Melting point
MPPS	1-methyl-1,2,3,4,5-pentaphenylsilole
µM	Micro molar
NaCl	Sodium chloride
Na_2HPO_4	Sodium hydrogen phosphate
$NaH_2PO_4.H_2O$	Sodium dihydrogen phosphate monohydrate
Na_2SO_4	Sodium sulfate
NDP	Nucleoside diphosphate
NER	Nucleotide excision repair
NIR	Near-infrared
nm	Nanometer
NMP	Nucleoside monophosphate
NMR	Nuclear Magnetic Resonance
NT	Nucleoside transporter
NTP	Nucleoside triphosphate
O_2	Oxygen
ODF	Oligodeoxyfluoroside
ODN	Oligodeoxyribonucleotide
OLED	Organic light-emitting diodes
PAH	Polycyclic aromatic hydrocarbons
Pb	Lead
PCR	Polymerase chain reaction
Pd	Palladium
PEG	Polyethylene glycol
PET	Photoinduced electron transfer
Ph	Phenyl
ppm	Parts per million
PRODAN	6-propionyl-2-dimethylaminonaphthalene
Prop.	Properties
PyAm-^{Ar}TAA	Pyrenylamido aromatic triazolo amino acid
RDX	1,3,5-trinitroperhydro-1,3,5-triazine
RIM	Restriction of intramolecular motion
RIR	Restriction of intramolecular rotation
RIV	Restriction of intramolecular vibration
RNA	Ribonucleic acid
r.t.	Room temperature
SNP	Single nucleotide polymorphism
ssDNA	Single-stranded DNA
T	Thymine

TBAF	Tetra-n-butylammonium fluoride
TBDMS	Tertiary-butyldimethylsilyl
t-BuOH	Tertiary butanol
TDDFT	Time-dependent density functional theory
TFE	Trifluoroethanol
TFO	Triplex forming oligonucleotide
THF	Tetrahydrofuran
TICT	Twisted intramolecular charge transfer
TLC	Thin layer chromatography
TMS	Trimethylsilyl
TNP	2,4,6-trinitrophenol
TNT	2,4,6-trinitrotoluene
TPE	Tetraphenylethylene
TCSPC	Time-correlated single photon counting
$^{Tz}B_{Do}$	Tetrazolyl donor nucleosidic base
UV	Ultra violet
VV	Vaccinia virus
VZV	Varicella zoster virus
UDP	Uridine diphosphate
W-C	Watson-Crick
Wt	Water
Zn	Zinc

Notations

pH	Potential of hydrogen
Φ	Abasic site
Φ_f	Quantum yield
ε	Molar extinction co-efficient
τ	Decay time
Å	Angstrom (10^{-8} cm)
$\tilde{\nu}$	Wavenumber
λ	Wavelength
T_m	Primer Melting Temperature
λ_{max}^{abs}	Absorption maxima
λ_{max}^{fl}	Fluorescence maxima
Δf	Solvent polarity parameter
δ	Chemical Shift in NMR
s	singlet
d	doublet
t	triplet
q	quartet
m	mutliplet
bs	broad singlet
dd	double doublet
dt	doublet of triplet
ddd	doublet of doublet of doublet
J	coupling constant in Hz

Contents

Page No.

CHAPTER 1: APPLICATIONS OF C5-SUBSTITUTED 2'-DEOXYURIDINES: A REVIEW

1.1.	Introduction	1-5
1.2.	Need for Modified Nucleosides	5-6
1.3.	Types of Modification	6-10
1.4.	5-Substituted (C5) Modified Pyrimidine Nucleosides	10-11
1.5.	Non-Fluorescent 5-Substituted Modified 2'-Deoxyuridines and Their Applications	11-18
	1.5.1. 5-Aminoalkyl-2'-Deoxyuridines and Their Applications	11-13
	1.5.2. 5-Alkenyl 2'-Deoxyuridines and Their Applications	13-15
	1.5.3. 5-Alkynyl 2'-Deoxyuridines and Their Applications	15-18
1.6.	5-Substituted 2'-Deoxyuridines in Clinical Research	18-23
1.7.	Fluorescently Labeled 5-Substituted 2'-Deoxyuridines and Their Applications	23-30
	1.7.1. Applications of 5-Substituted 2'-Deoxyuridines Directly Linked to Fluorophores	24-26
	1.7.2. Applications of 5-Substituted 2'-Deoxyuridines Linked to Fluorophores via an Alkenyl Linker	26-28
	1.7.3. Applications of 5-Substituted 2'-Deoxyuridines Linked to Fluorophores via an Alkynyl Linker	28-30
1.8.	Probing Biomolecular Microenvironment with Fluorescent Nucleosides	31-33
1.9.	Summary and Future Prospect	33-35
1.10.	References	35-48

CHAPTER 2: DESIGN, SYNTHESIS AND PHOTOPHYSICAL PROPERTIES OF FLUORESCENT C5-SUBSTITUTED 2′-DEOXYURIDINES

2.1.	Introduction	49-51
2.2.	Sonogashira Cross-Coupling Reaction	51-53
2.3.	Click Chemistry	53-54
2.4.	Click Chemistry as a Tool in Nucleic Acid Research for Generating Fluorescent Nucleosides	55-59
	2.4.1. Pre-Synthetic Modification of DNA	56
	2.4.2. Post-Synthetic Modification of DNA	57-59
2.5.	Background	59-60
2.6.	Aim and Objective	60-61
2.7.	Result and Discussion	62-78
	2.7.1. Synthesis of Fluorescently Labeled 2′-Deoxyuridines	62-64
	2.7.2. Study of Photophysical Properties	64-75
	2.7.3. Theoretical Calculations	75-78
2.8.	Conclusion	78-79
2.9.	Experimental Section	79-90
	2.9.1. General Experimental	79
	2.9.2. Synthesis and Characterizations	80-89
	2.9.3. Photophysical Studies of the Synthesized Nucleosides	89
	2.9.4. Theoretical Calculation	90
	2.9.5. B3LYP/6-31G* Optimized Structure and Cartesian Coordinates of the Synthesized Compounds	90-96
2.10.	^{1}H and ^{13}C NMR Spectra of Few Selected Nucleosides	97-102
2.11.	References	103-112

CHAPTER 3: STUDIES ON THE INTERACTION OF TRIAZOLYL PYRENE-LABELED FLUORESCENT 2'-DEOXYURIDINE AND UNNATURAL TETRAZOLYLPYRENE NUCLEOSIDES WITH BSA

3.1.	Introduction		113-116
	3.1.1.	Protein-Ligand Interaction	113-115
	3.1.2.	Bovine Serum Albumin (BSA): Highly Recognized Protein Model	115-116
3.2.	Some Recent Small Molecule Probes of BSA		116-120
3.3.	Protein-Nucleic Acid Interactions		120-121
3.4	Nucleoside as Drug: Nucleoside-Protein Interaction		121-122
3.5.	Background		122
3.6.	Objective		122-123
3.7.	Result and Discussion		123-131
	3.7.1.	UV-visible and Fluorescence Photophysical Properties of Pyrene-Labeled Nucleosides	123-124
	3.7.2.	Theoretical Calculations	124-125
	3.7.3.	Study of UV-visible and Fluorescence Photophysical Properties of Triazolylpyrene-Labeled Nucleoside **2.45G** in presence of BSA	125-128
	3.7.4.	Study of UV-visible and Fluorescence Photophysical Properties of Tetrazolylpyrene-Labeled Nucleoside **1.262** in presence of BSA	128-130
	3.7.5.	Determination of Protein-Probe Binding Constant	130-131
	3.7.6.	Circular Dichroism (CD) Study	131
	3.7.7.	Molecular Docking Study	131-138
		3.7. 7.1. Molecular Docking Study of Triazolylpyrene-Labeled Nucleoside	132-135
		3.7. 7.2. Molecular Docking Study of Tetrazolylpyrene-Labeled Nucleoside	135-138
3.8.	Conclusion		138
3.9.	Experimental Section		138-142
	3.9.1.	Materials	138-139

3.9.2. Preparation of BSA Solution 139
3.9.3. Preparation of Nucleoside Solution 139
3.9.4. Photophysical Study 139-140
3.9.5. Molecular Docking 140
3.9.6. TDDFT Calculations 141
3.9.7. B3LYP/6-31G* Optimized Structure and Cartesian Coordinates of the Tetrazolylpyrene Nucleoside **1.262** 141-142
3.10. References 142-150

CHAPTER 4: SYNTHESIS AND STUDIES ON THE PHOTOPHYSICAL/BIOPHYSICAL PROPERTIES OF TRIAZOLYL FLUORENE-LABELED 2′-DEOXYURIDINES

4.1. Introduction 151
4.2. Fluorene Derivatives and Their Applications 151-161
4.2.1. Fluorene Analogues as Metal Ion Sensor 152-154
4.2.2. Fluorene Analogues Utilized for Cell Imaging 154-158
4.2.3. Fluorene Analogues Utilized for Detection of Explosives 158-161
4.3. Nucleosides containing Fluorene Derivatives 161-164
4.4. Background 165
4.5. Objective 165-166
4.6. Result and Discussion 166-172
4.6.1. Synthesis of Fluorene-Labeled Nucleosides 166-167
4.6.2. Study of Photophysical Properties 168-172
4.6.3. Theoretical Calculations 173-174
4.6.4. Study of Interaction of Nucleoside **4.64C** with ctDNA 174-177
4.6.4.1. Study of UV-visible and Fluorescence Photophysical Properties of Cyanofluorenyl Triazolyl Nucleoside (**4.64C**) in Presence of ctDNA 174-175
4.6.4.2. Determination of Binding Constant 175-176
4.6.4.3. Molecular Docking 176-177
4.7. Conclusion 177

4.8. Experimental Section 177-190
4.8.1. General Experimental 177-178
4.8.2. Synthesis and Characterizations 178-183
4.8.3. Photophysical Studies of the Nucleosides 184
4.8.4. Studies on the Interaction of Nucleoside **4.64C** with ctDNA 184-185
4.8.5. Molecular Docking 185
4.8.6. Theoretical Calculations 186
4.8.7. B3LYP/6-31G* Optimized Structure and Cartesian Coordinates of the Synthesized Compounds 186-190
4.9. ^{1}H and ^{13}C NMR Spectra of Few Selected Nucleosides 191-196
4.10. References 197-201

CHAPTER 5: STUDIES ON THE AGGREGATION INDUCED FLUORESCENCE EMISSION PROPERTY OF PYRENYLAMIDO TRIAZOLYL AROMATIC AMINO ACID AND ITS INTERACTION WITH SHORT ABASIC DNAs

5.1. Introduction: Aggregation-Induced Emission 202-210
5.1.1. Study to Prove Aggregation-Induced Emission 204-205
5.1.2. Various Types of Probes Showing Aggregation-Induced Emission 205-207
5.1.3. Applications of Probes Showing Aggregation-Induced Emission 208-210
5.2. Applications of Probes Showing Aggregation-Induced Emission in DNA Research 211-215
5.3. Applications of Fluorescent Probes in Abasic DNA Detection 215-227
5.3.1. Abasic DNA: Its Structure, Generation and Reactivity 215-218
5.3.2. Stabilization of Abasic Site by Non-Nucleosidic Base Surrogates 218-221
5.3.3. Targeting Abasic Site with Nucleosidic Base Surrogates 221-223
5.3.4. Label-Free Detection of Abasic Site 223-227
5.4. Background 227
5.5. Objective 228-229

5.6. Result and Discussion 229-238
5.6.1. Study on Photophysical Properties of **PyAm-^{Ar}TAA** 229-233
5.6.2. Interaction of **PyAm-^{Ar}TAA** with Short Abasic DNAs 233-237
5.6.2.1. Spectral Studies of **PyAm-^{Ar}TAA** with Short Abasic DNAs 233-235
5.6.2.2. Titration Study of PyAm-ArTAA with ODN 1●5 235-236
5.6.2.3. Determination of **A●Φ**–Probe Binding Constant 236-237
5.6.2.4. Circular Dichroism (CD) Study 237
5.6.2.5. Molecular Docking Study of ODN 1●5 with **PyAm-^{Ar}TAA** 237-238
5.7. Conclusion 238-239
5.8. Experimental Section 239-242
5.8.1. Materials 239
5.8.2. Preparation of Abasic DNA Solutions 239-240
5.8.3. Photophysical Study 240
5.8.4. Molecular Docking 240-241
5.8.5. B3LYP/6-31G* Optimized Structure and Cartesian Coordinates of **PyAm-^{Ar}TAA** 241-242
5.9. References 242-265

Summary and Outlook 266-269

Chapter 1

APPLICATIONS OF C5-SUBSTITUTED 2'-DEOXYURIDINES: A REVIEW

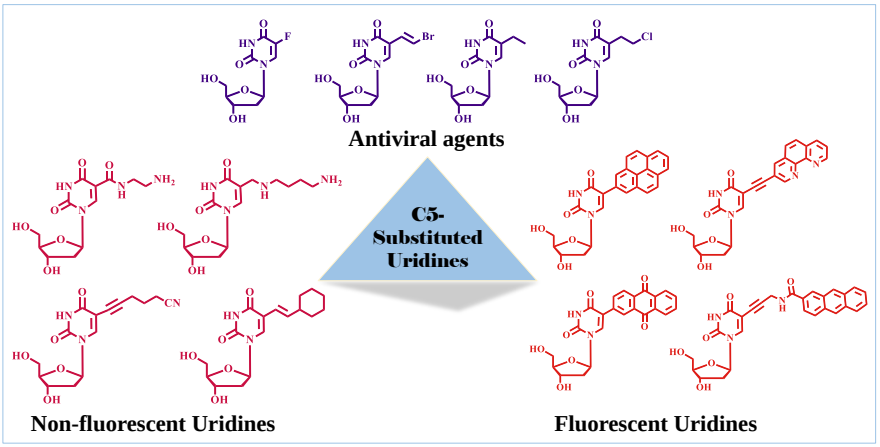

1.1. Introduction

1.1.1. Nucleosides, Nucleotides and Nucleic Acids

Nucleic acids are one of the most essential building blocks of living cells. Chemists and biochemists recognize nucleic acids as the center of importance in biological systems. Structurally, nucleic acids exist in long polymeric structures consist of nucleotides. Even though their compositions are simple nucleotide monomers, these biopolymers take an active part in various complex cellular functions. For example, deoxyribonucleic acid (DNA) stores, access and replicates genetic information as a linear nucleotide code. On the other hand, ribonucleic acid (RNA) transports genetic information from DNA to the ribosome which ultimately leads to protein synthesis. The role of nucleic acids as a genetic carrier was not realized until about 70 years ago. During last half century, numerous experiments and investigations were performed significantly on the structure of DNA, [1-7] structure-function relationships between DNA and RNA [8, 9] and fundamental processes like DNA replication, RNA transcription and protein synthesis.[10-15] The observations and results of these investigations lead to modern molecular biology and form the basis of nucleic acids as a genetic carrier. The transportation of genetic information from DNA into RNA and then to a protein known as the central dogma of molecular biology originally put forward by Francis Crick (**Figure 1.1**).[16, 17]

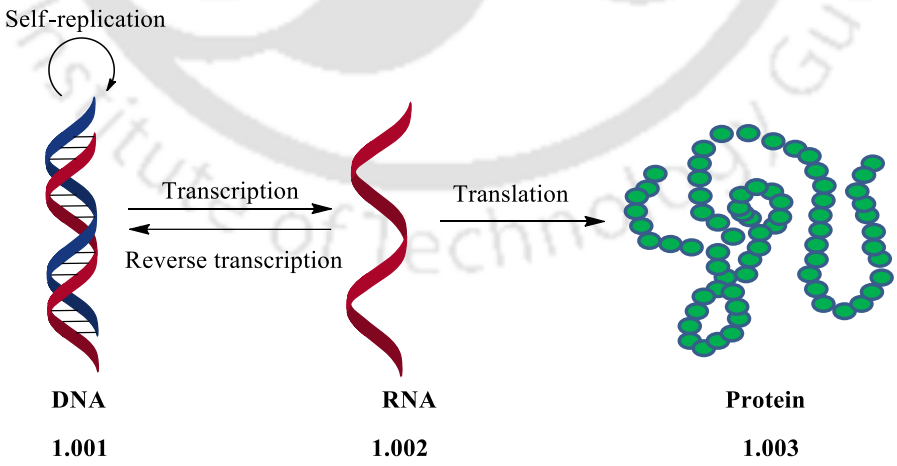

Figure 1.1. The central dogma of molecular biology

According to the theory of central dogma, an individual DNA molecule serves as templates for complementary DNA strands during the replication process, while as complementary RNA molecules during the transcription process. Sequentially, the RNA molecules serve as fingerprints for the arrangements of amino acids by ribosomes during the process of translation. The principle of this paradigm have withstood the test of time and experimentation and continues to represent as guiding principle for molecular biologists involving in all areas of basic biological, biomedical and genetic research. However, certain additions are necessary which are based on observations and discovery of some unusual transcriptions. These include the occurrence of RNA synthesis and RNA-directed DNA synthesis (reverse transcription), as found in some viruses and plant species.[18] Later on, various experiments and their findings indicate the involvement of RNA in more complex biological activities than DNA.[19, 20]

1.1.2. Structure of Nucleic Acids

Deoxyribonucleic acid (DNA) and ribonucleic acid (RNA) are the two types of nucleic acids present in living cells as mentioned before. Both are polymers of repeating subunits called nucleotides. The arrangement of nucleotide subunits in the primary structure of a nucleic acid responsible for the flow of genetic information within a cell. Each nucleotide monomer consists of (i) a pentose (5 carbon) sugar, (ii) a base, which is essentially a cyclic nitrogen-containing compound, and (iii) a phosphate group. There are two types of sugar present in nucleic acids, deoxyribose which is present only in DNA and ribose which is present in RNA. Therefore, the two nucleic acids are named according to the sugars present in them. The only structural difference between these two sugars is the absence of oxygen at 2'-position of deoxyribose sugar (**1.004**, **1.005**, **Figure 1.2**). The bases present in nucleic acids resemble either a purine ring system or a pyrimidine ring system and termed accordingly as purines and pyrimidines (**Figure 1.2**). These bases are also called as nucleobases as they primarily found in nucleic acids. In DNA, four different bases are found naturally: adenine (A), guanine (G), cytosine (C) and thymine (T). The first two are derivatives of purine whereas the other two are derivatives of pyrimidine. In RNA, we find the same first three nucleobases as in DNA but instead of thymine, another pyrimidine derivative uracil (U) is present as a fourth nucleobase. In addition to these major bases, there is also a large range of minor bases which occur less frequently than others. A wide variety of modified nucleobases are found in RNAs, whereas the DNA of eukaryotes consists of simply modified nucleobases involving the methylation of

the C5-position of cytosine or the exocyclic amino group of adenine. These modifications support a mechanism of regulation and expression of individual genes at the DNA level in eukaryotes. [21] The third component of a nucleotide monomer is a phosphate group which is derived from phosphoric acid (**1.006**, **Figure 1.2**).

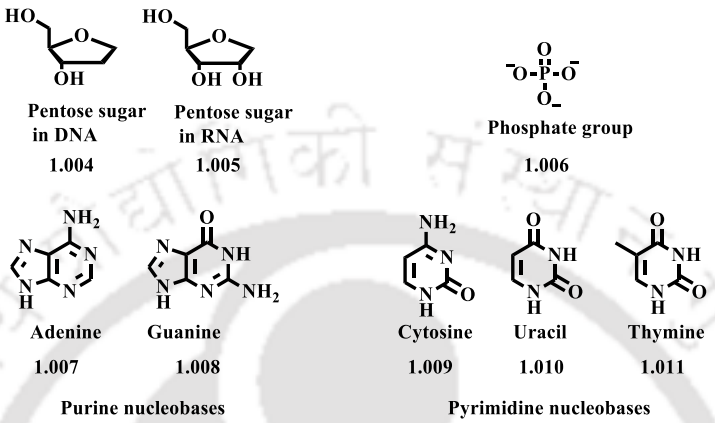

Figure 1.2. Components of a nucleotide.

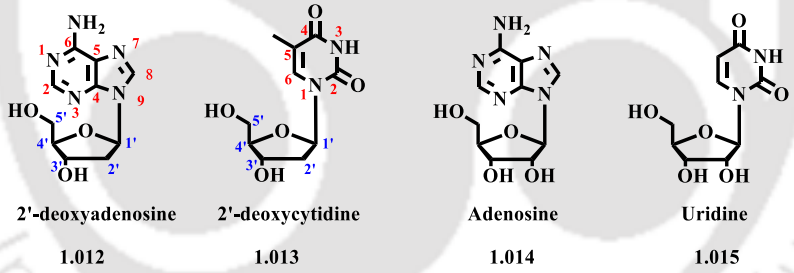

Figure 1.3. Natural nucleosides and their ring numbering system.

The structure composed by any one of the nucleobases with either one of the two sugar moieties via a glycosidic bond is known as nucleoside (**Figure 1.3**). When the sugar moiety is ribose then we have ribonucleoside, on the other hand, if it is deoxyribose then we have a deoxyribonucleoside. Accordingly, nucleosides with individual bases and ribose sugar are termed as adenosine, guanidine, cytidine, thymidine, uridine respectively. On the hand, nucleosides with individual bases and deoxyribose sugar are termed as deoxyadenosine, deoxyguanidine, deoxycytidine, deoxythymidine, and deoxyuridine respectively. Structurally, a nucleotide is a nucleoside phosphate. These nucleotide monomers are connected together to

form a polymeric structure by 3', 5'-phosphodiester bonds leading to the primary structure nucleic acids (**Figure 1.4**).

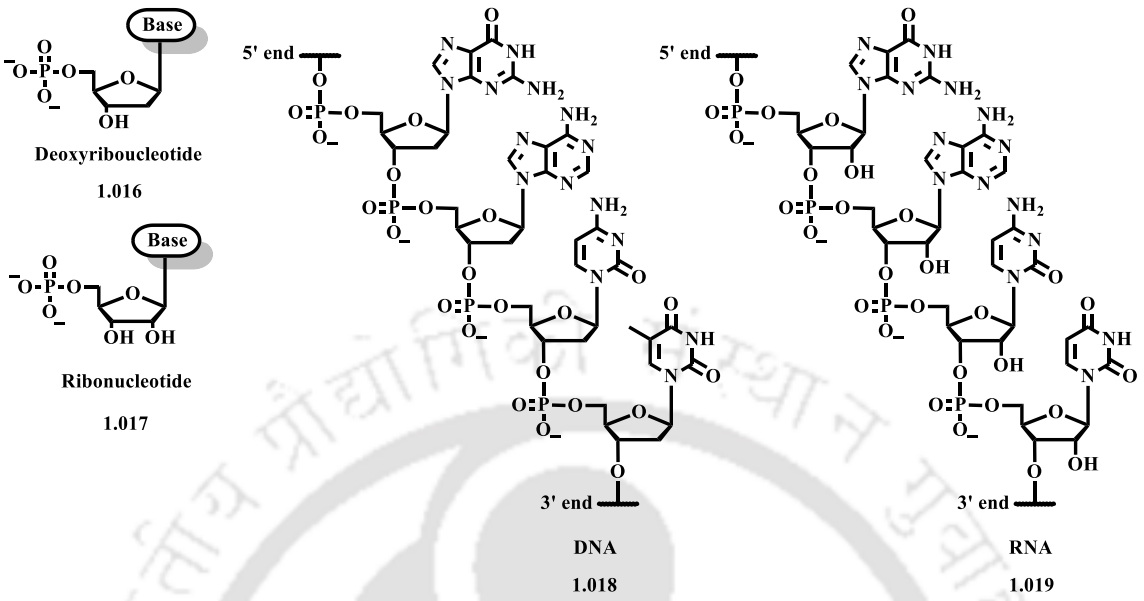

Figure 1.4. The molecular structure of Nucleotides, DNA and RNA.

In addition, one or two additional phosphates can be inserted into the first phosphate group of a nucleoside molecule via a pyrophosphate linkage. The nucleosides with one phosphate group are called nucleoside monophosphates (NMPs), those with two and three phosphate groups are called nucleoside diphosphates (NDPs) and nucleoside triphosphates (NTPs) respectively. One of the most important nucleobases involved in these compounds is adenine which forms adenosine mono, di and triphosphate molecules (AMP, ADP, and ATP) (**Figure 1.5**). These molecules are well-known for their vital roles in many biological processes.

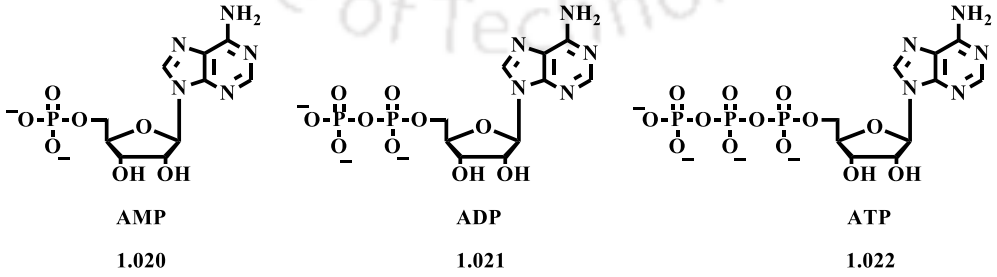

Figure 1.5. Adenosine phosphates.

One of the most important structural features of DNA is the specific pairing of nucleobases. In a natural DNA, adenine always pairs with thymine and cytosine always pairs with guanine and vice versa. This base pairing is specific in DNA and during polymerase-mediated replication, it forms the basis of the genetic alphabet, ultimately leading to the basis of the genetic code.[22, 23] However, the genetic alphabets and hence the information stored in them by no means should be restricted to only two base pairs. It became a logical thought among the scientific community that an expanded genetic alphabet could provide us a platform for the encoding of additional information which might be beneficial not only for various in vitro and in vivo applications but also for a variety of biotechnology applications. Toward the expansion of genetic alphabet, an unnatural third base pair can be formed between two identical unnatural nucleotides (self-pairs) or two different unnatural nucleotides (hetero pairs). The incorporation of such unnatural base pairs into DNA would expand the potential of DNA in terms of information and functions such as site-directed labeling of oligonucleotides and in vitro selections with oligonucleotides functionalized with diverse chemical structures.[24-26] Thus, the design and synthesis of unnatural base pairs is an interesting research area leading towards the expansion of genetic alphabet which would find widespread applications in biotechnology including the production of unnatural proteins and organisms.[27-29]

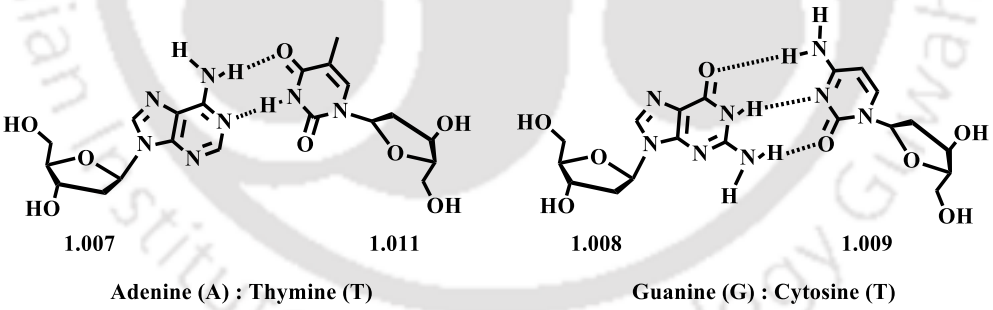

Figure 1.6: Presentation of hydrogen bonding between the DNA bases.

1.2. Need for Modified Nucleosides

The study of nucleic acids is a broad area extended over numerous fields of science. The diverse structural features and chemical functional groups present in nucleic acids allow them to interact with many different molecules. These molecules can act as some sorts of gene regulatory proteins which can alter the natural flow of genetic information through DNA or

RNA.[30, 31] In addition, molecules from extracellular sources can stabilize DNA or RNA to a greater extent and may also artificially alter or inhibit their functions. These biologically active molecules are either naturally occurring or chemically synthesized. Incorporation of such molecules into nucleic acids have a substantial contribution in the field of nucleic acid research and towards the development of chemotherapeutic regimens.[32]

Fluorescence is one of the most intrusive, rapid, highly responsive and simple analytical techniques.[33] Understanding the structure, properties, and functions of biological macromolecules, cells and microorganisms often depend on fluorescence-based techniques for a long time.[34-40] The molecules which have good photophysical properties can be very helpful for understanding the various chemical, biochemical and biological phenomena. Naturally occurring nucleotide bases in nucleic acids show extremely poor fluorescence property.[41-43] These bases show very short fluorescent decay times and hence provide poor structural information. The development of fluorescent biomolecular building blocks having good photophysical properties can provide a better understanding of molecular environments, events and therefore is a highly demanding research area. Fluorescently labeled nucleosides often find their applications in the following research topics:-

(i) Detection of single nucleotide polymorphisms (SNPs).
(ii) Determination of nucleic acid structure and function.
(iii) Study of the nucleic acid microenvironment.
(iv) Detection and monitoring of biological ligand binding events.

1.3. Types of Modification

Modified nucleosides can be classified mainly into two categories: (i) Base-modified and (ii) Sugar-modified nucleosides.

(i) Base-modified nucleosides: - In the synthetic oligonucleotide research area, the synthesis of nucleobase modified nucleosides is probably the most common and most explored topic among researchers. Natural pyrimidine nucleobases can be modified via substitutions generally in C2, C4 N3, C5 and C6 positions (**1.023-1.027**, **Figure 1.7**).[44-51]Among these, C5-substituted products are the most explored for their applications in medicinal and biochemistry.[44] Similarly in natural purine nucleobases, substitutions can be done effectively at C2, C6 and C8 positions (**1.028-1.031**, **Figure 1.7**).[52-56] An example of naturally occurring biologically active purine analog is 7-deazapurine (pyrrolo[2,3-d]pyrimidine).[57] Due to its

applications in many currently available drugs, the synthesis of its substituted nucleoside analogs is a recent topic of interest. Several modified 7-deazapurine nucleoside analogs have been utilized in various investigations.[58-63] Some examples of such types of nucleoside analogs are shown in **Figure 1.7** (**1.032-1.035**).

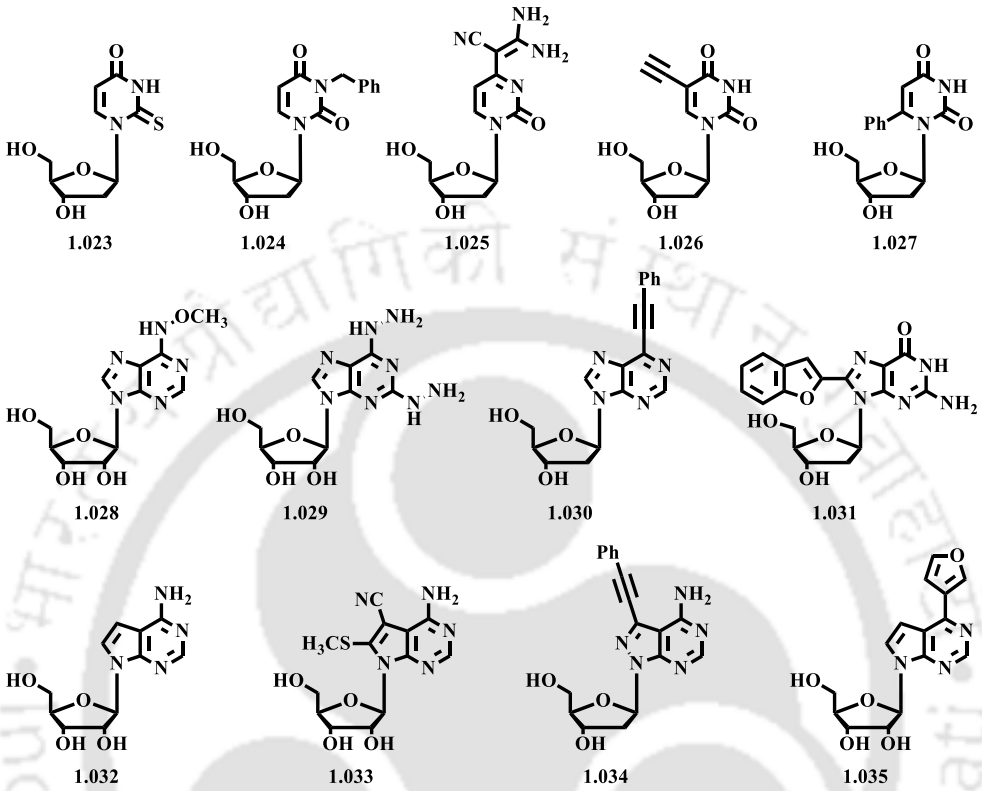

Figure 1.7. Selected examples of base-modified nucleosides.

Some simple examples of base-modified nucleosides are isosteres of the natural DNA bases.[64] Generally, in these modified bases, the exocyclic carbonyl groups are replaced with C-F groups and N-H groups are replaced with C-H groups (**Figure 1.8**). These modified nucleosides have been utilized in several investigations.[65-68] The compounds **1.038** to **1.043** represent a broad family of nucleosides known as C-nucleosides, where the sugar moiety is linked to a base through a C-C single bond. Several naturally occurring C-nucleosides and their synthetic analogs contributed significantly in the field of medicinal chemistry.[69] A direct advantage of C-nucleosides is their higher stability against enzymatic and acid-catalyzed hydrolysis when compared to corresponding N-nucleosides.

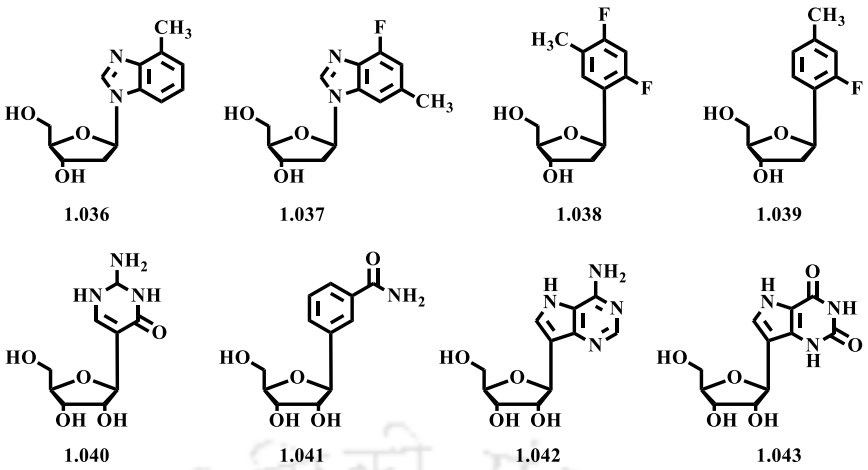

Figure 1.8. Selected examples of base isosteres and C-nucleosides.

As mentioned in the above section, natural nucleobases show weak photophysical properties. However, nucleosides can be modified to impart useful photophysical properties. Fluorescent nucleoside analogs often developed by modification on the natural nucleobases or by utilizing fluorophores with remarkable photophysical properties as base surrogates. Such fluorescent nucleoside base analogs can be classified as chromophoric base, Pteridine, expanded nucleobase, extended nucleobase, and isomorphic base analogs. Chromophoric base analogs are obtained by replacing natural bases with polycyclic aromatic hydrocarbons (PAH) (**1.044-1.047**, **Figure 1.9**).[70-72] These nucleoside analogs display high emission quantum efficiencies but lack Watson-Crick (W-C) hydrogen bonding ability. Pteridines are highly emissive planar heterobicyclic aromatic compounds. These compounds are naturally occurring and have chemical structures similar to purines (**1.048-1.051**, **Figure 1.9**). The initiation and development of pteridine labeled nucleosides were mostly done by Hawkins and co-workers.[73, 74] Expanded nucleobase analogs are developed by either fusion or insertion of aromatic rings into purine and pyrimidine bases (**1.052-1.055**, **Figure 1.9**). In many cases, such modifications lead to the generation of highly emissive nucleobases with H-bonding complementarity similar to that of natural nucleobases. Extended nucleobase analogs are often developed by attaching fluorophores with known photophysical properties to the nucleobases either through rigid or flexible linkers (**1.056-1.059**, **Figure 1.9**).[75, 76] The parent fluorophores normally retained their photophysical properties when attached to the nucleobases via electronically nonconjugated linkers. On the other hand, attachment via electronically conjugated linkers typically generate new fluorophores with unique photophysical properties. Isomorphic nucleobase analogs (**1.060-1.063**, **Figure 1.9**) are heterocycles which have a close resemblance to the

corresponding natural nucleobases in terms of structure and W-C base pairing property.[75, 77, 78] When compared to other nucleobase analogs, a practical advantage of these analogs is their close resemblance to the natural nucleobases and minimal or non-perturbing nature. Because of the non-perturbing nature, isomorphic base labeled probes found numerous applications in the field of nucleic acid research.[75, 77-79]

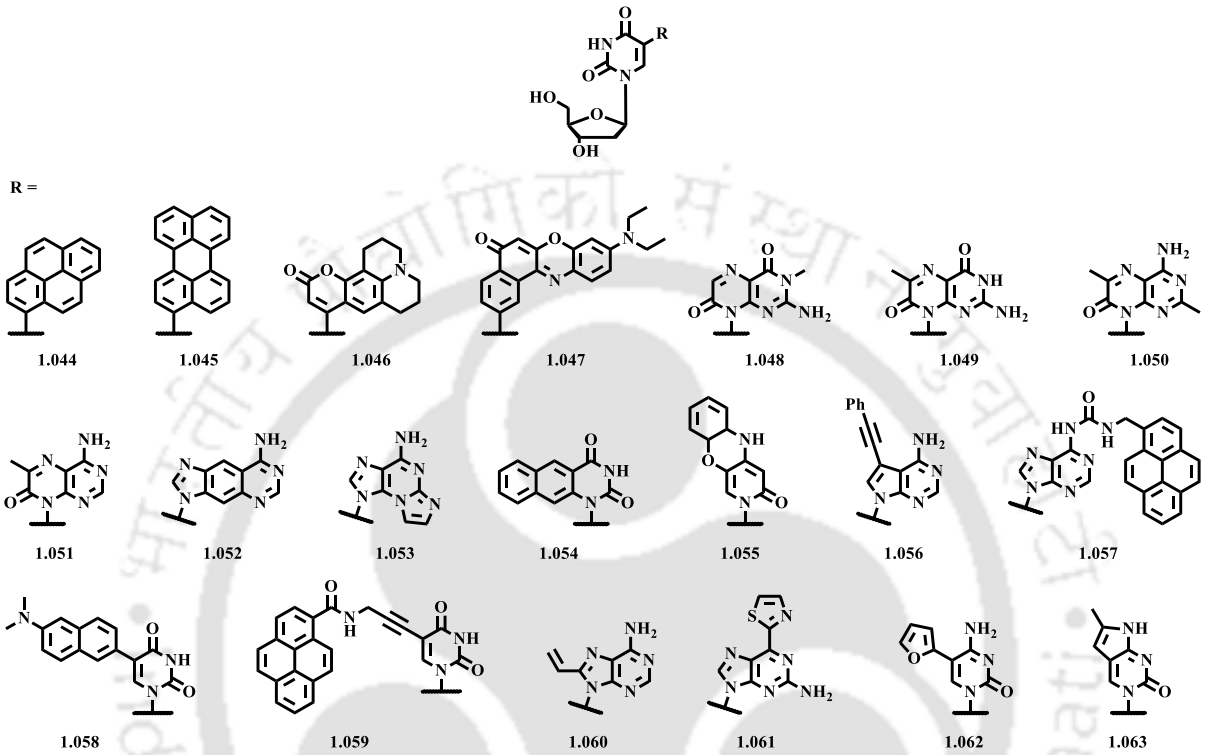

Figure 1.9. Selected examples of fluorescent base analogs.

(ii) Sugar-modified nucleosides: - Research for the effective, selective and nontoxic antiviral agents initiated a variety of strategies for the development of modified nucleoside analogs. In many cases, these strategies involved the modification of the sugar moiety of natural nucleosides. For example, acyclic nucleosides like acyclovir and ganciclovir are clinically used for the treatment of herpes viruses. Dideoxynucleosides and their analogs such as didanosine (ddI), zalcitabine (ddC), stavudine (d4T) and avacavir are used for the treatment of AIDS (**Figure 1.10**).

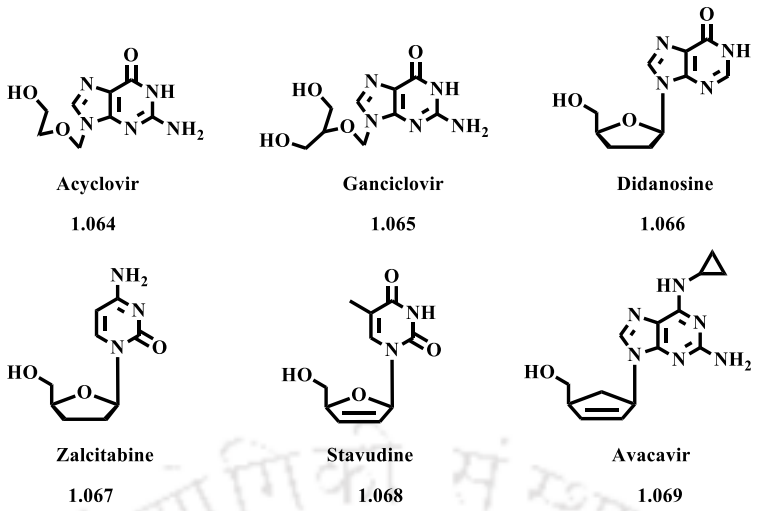

Figure 1.10. Selected examples of clinically approved sugar modified nucleoside drugs.

Our research area is focused on the base modified pyrimidine nucleosides at C5-position, therefore we will not discuss the sugar modified nucleosides broadly. Some different types of biologically active sugar modified nucleosides are shown in **Figure 1.11**. Below sections will restrict the discussion about the C5 modification of 2′-deoxyuridine only. Therefore the examples will include the modified 2′-deoxyuridines wherein C5-position is modified.

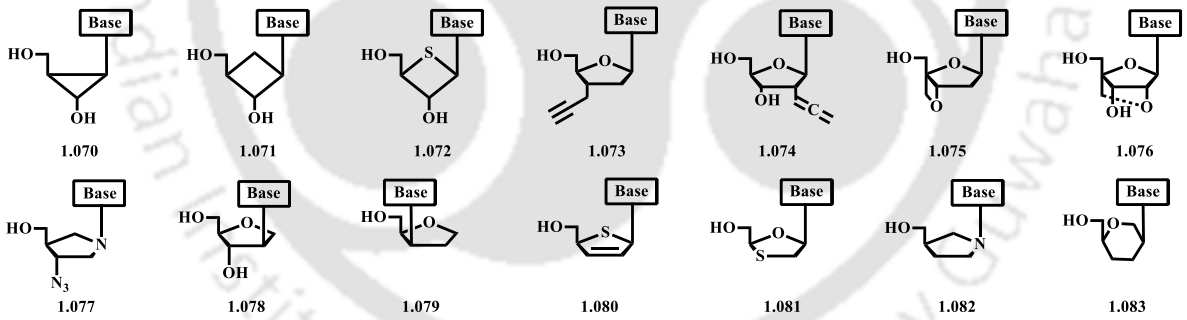

Figure 1.11. Selected examples of sugar modified nucleosides.

1.4. 5-Substituted (C5) Modified Pyrimidine Nucleosides

5-substituted pyrimidine nucleosides consist of a special group of compounds highly recognized for their applications in pharmaceutical molecular genetics. Incorporation of diverse functionalities in the C5-position of pyrimidine nucleosides/nucleotides has been a continuous interest in order to improve their physicochemical properties such as metabolic

stability, oral bioavailability, and pharmacokinetics.[80, 81] These molecules have shown potential antiviral activities against diverse classes of viruses and will be discussed later in this chapter.

The evolution of molecular techniques for the analysis of nucleic acids has a great impact on the development of molecular genetics. The molecular techniques used in this endeavor mostly related to the utilization of modified oligonucleotide probes. As a site for modification and attachment of molecular signaling components, the C5-position of pyrimidine nucleosides is possibly the ideal site as this site remains in the major groove of the B-DNA. As there is no significant steric hindrance at the major groove, even very large groups can be incorporated without destabilizing the DNA structure. Thus a wide selection of biologically active molecules is possible for incorporation at the C5-position of pyrimidine nucleosides/nucleotides for interpretation of molecular genetics. Moreover, C5-substituted pyrimidine derivatives are well-known for their high compatibility with the endogenous kinases and DNA polymerases needed for their incorporation into DNA.[82-84]

1.5. Non-Fluorescent 5-Substituted Modified 2'-Deoxyuridines and Their Applications

1.5.1. 5-Aminoalkyl-2'-Deoxyuridines and Their Applications

In 1973, Kropinski *et al.*[85] discovered a hypermodified base 5-(4-aminobutylaminomethyl)-2′-deoxyuridine (**1.084**, **Figure 1.12**) in the DNA of bacteriophage ϕW-14 with higher melting temperature than the same natural DNA without a modified base. The results of that assay establish the idea among researchers that DNA can be stabilized to more extent than the natural ones. Following the discovery of Kropinski and his colleagues, Takeda *et al.*[86] synthesized a series of ODNs containing 5-(4-aminobutylaminomethyl)uracil instead of thymidine and monitored their duplex stability in terms of melting temperature. In the investigation, they observed that the stability of duplexes definitely enhanced for some specific base pairs. After this, a variety of the C5-modified nucleosides with aminoalkyl side chains have been investigated during the period and are listed in **Figure 1.12**. The amino substituted saturated alkanes (**1.085-1.087**) were reported as non-stabilizing.[87-89] However, the amino substituted side chains containing amide functionality (**1.088-1.097**) were reported to enhance stabilization.[90-95] The amide groups present in these nucleosides can stack and effectively form hydrogen bonds with nearby bases which are possible reasons behind the

enhanced stabilization. The guanidinium substituted C5 side chain (**1.098**) has been reported to stimulate the cellular uptake of oligonucleotides.[96] Kuwahara *et al.*[97] synthesized pyrimidine nucleoside triphosphates containing amino acids with similar aminoalkyl side chains and are listed in **Figure 1.13**.[98] Incorporation of these molecules into DNA could provide diverse modified DNA libraries with significant protein-like properties.

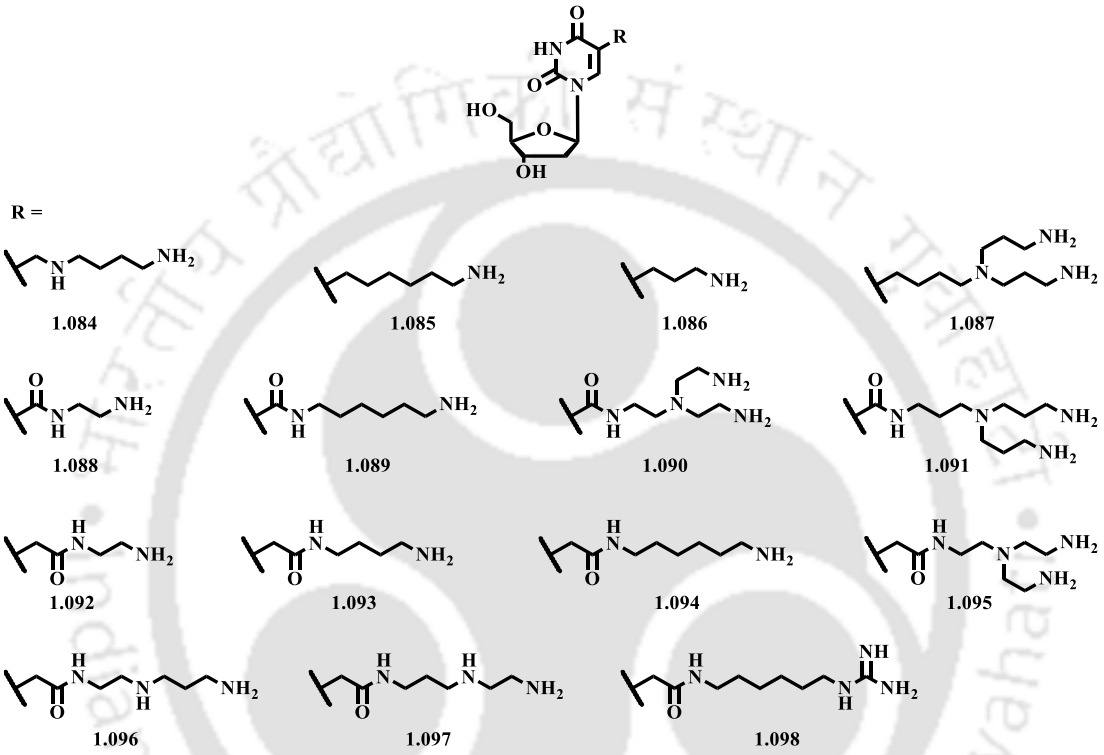

Figure 1.12. Selected examples of 5-aminoalkyl-2′-deoxyuridines.

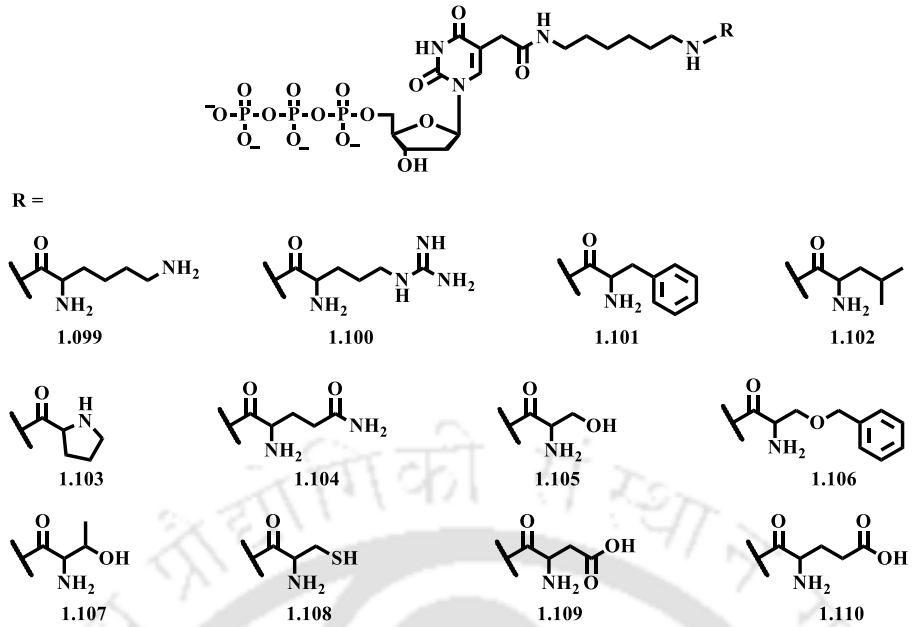

Figure 1.13. Selected examples of 2′-deoxyuridine triphosphates containing amino acids.

1.5.2. 5-Alkenyl 2'-Deoxyuridines and Their Applications

The functional groups of natural nucleic acids are not suited for general acid-base catalysis due to their pH range.[99] To address this limitation, Sakthivel *et al*. [100] synthesized a novel series of 5-(3-amino-1-propenyl)-2'-deoxyuridines and their triphosphate derivatives (**1.111-1.117**, **Figure 1.14**). These compounds could be good examples to provide the potential for covalent binding, electrostatic interactions, and metal-ion catalysis and are listed the **Figure 1.14**.

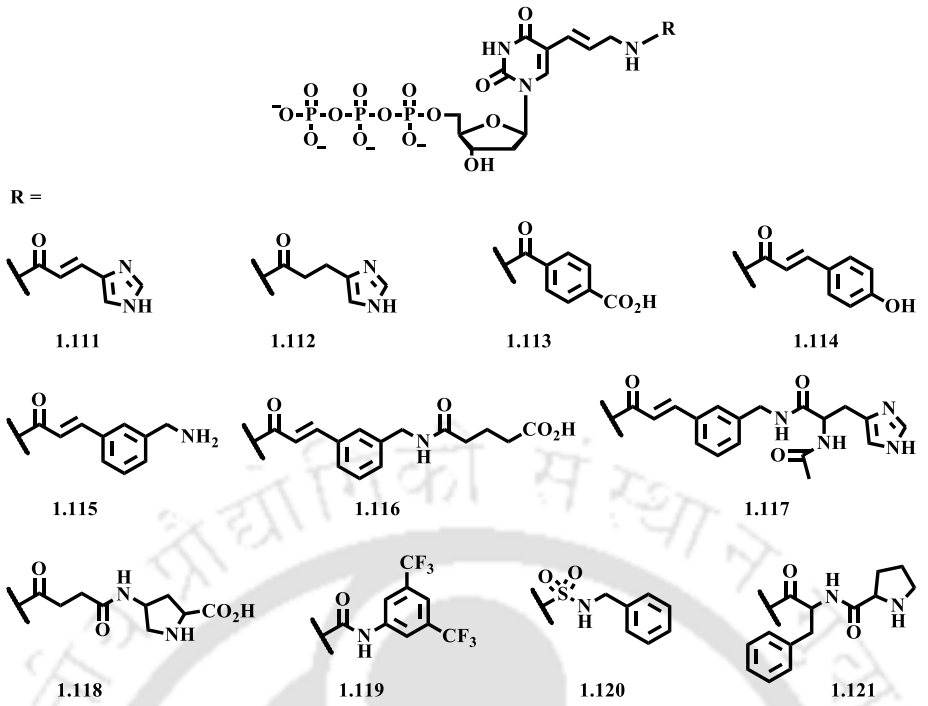

Figure 1.14. Selected examples of 5-(3-amino-1-propenyl)-2'-deoxyuridine triphosphates.

The analogs **1.115** and **1.116** were the first reported examples of cationic and anionic nucleotide analogs incorporated into DNA by PCR, which can alter the electrostatic properties of DNA. Hollenstein *et al.*[101] reported similar 2′-deoxyuridine triphosphates containing proline, urea and sulfonamide groups (**1.118-1.121**, **Figure 1.14**) for incorporation into DNA. More recent C5-substituted analogs of 2'-deoxyuridine containing alkenyl side chains are listed in **Figure 1.15**.[102-108]

DNA can be functionalized with primary amine and imidazole functions with potential catalytic properties utilizing these alkenyl linkers, which could be beneficial for in vitro selection of potential nucleic acid based catalysts. The compounds **1.130** and **1.131 (Figure 1.15)** have been utilized for the synthesis of triple-helix forming oligonucleotides (TFO)s.[104] Z-alkenyl linker (**1.131**) reported as destabilizing to the formation of TFOs to a great extent, while TFOs having E-alkenyl linker (**1.130**) reported as unpurturbing in nature, exhibiting stability similar to the unmodified structures.

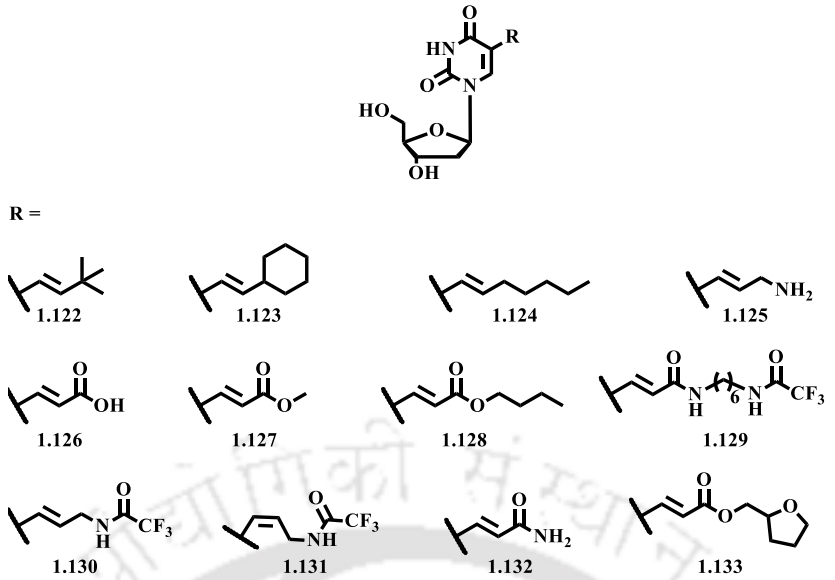

Figure 1.15. Selected examples of 5-alkenyl-2′-deoxyuridine analogs.

1.5.3. 5-Alkynyl 2'-Deoxyuridines and Their Applications

One of the most explored C5 modifications in pyrimidine nucleosides is the attachment of an alkynyl linker. Acetylenes and their highly conjugated homologs are well-known for their ability to generate strong electronic transmission between consecutive subunits. The linear sp hybridized carbon chain can provide rigid structures which should facilitate the exact location of the substituents attached with alkynyl functionalized oligonucleotide probes and thus can provide a better understanding of substituent-nucleotide interaction. A comprehensive study on this was done by Froehler and co-workers in the early 1990s, where they have reported the antisense properties of oligonucleotides labeled with 5-(1-propynyl) uracil and 5-(1-propynyl) cytosine.[109-111] Both of the modified bases showed increased affinity of a particular sequence for hybridization with complementary RNA, when incorporated in multiple positions of the sequence. Subsequent studies have reported the ability of the C5 propynyl group to stabilize DNA not only through base stacking interactions but also through cooperative interactions among them, when present in consecutive positions in a sequence.[112, 113] In 2004, Richert and co-workers reported extensive studies of C5 substituents containing acetylenic linker which are shown in **Figure 1.16**. They incorporated these substituents in the oligonucleotide 5'-CTTTTCU*TTCTT-3', where U* was one of the modified deoxyuridines.[114]

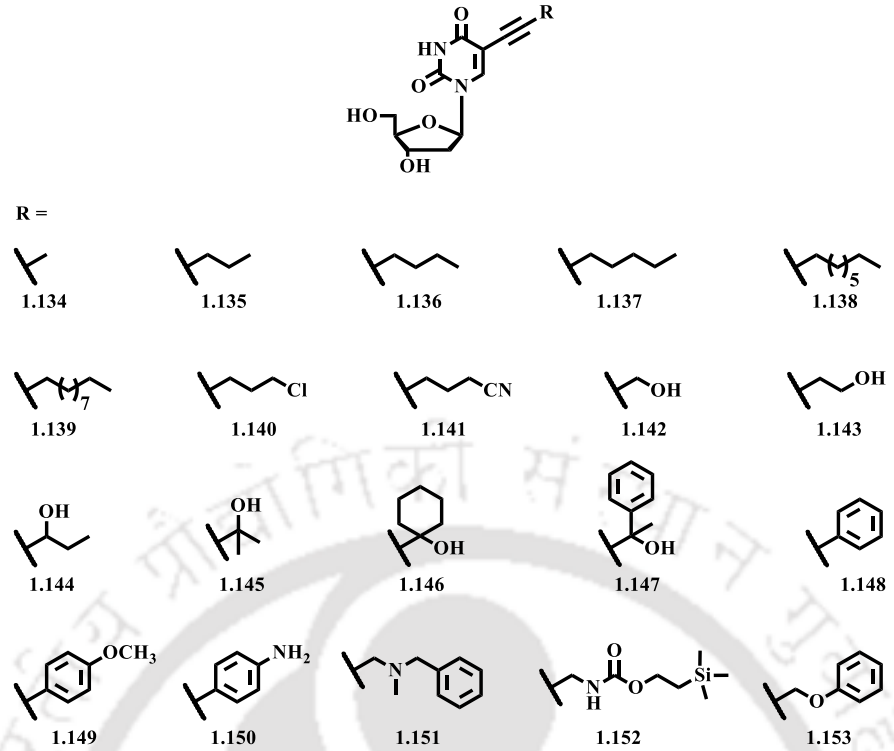

Figure 1.16. Selected examples of 5-alkynyl-2'-deoxyuridine analogs reported by Richert and co-workers.

The C5 propynyl analog (**1.134**) was found to show higher stabilizing effect than thymidine, while longer alkynyl substituents up to five carbons (**1.135-1.137**) showed a more stabilizing effect than propynyl. The hydroxyl ethyl group (**1.143**) was reported as most duplex-stabilizing within the series showing a T_m value of 42.9 °C in 100mM NaCl concentration, which is higher than both the propynyl (39.4 °C) and thymidine (39 °C). Most of the other substituents were reported as destabilizing to the duplex formation.

In 2009, Howorka *et al.*[115] described the synthesis of C5-substituted 2'-deoxyuridines and their 5'-triphosphate derivatives bearing alkynyl linkers with carboxyl, alkyl and amino group at the terminal. The synthesized compounds are shown in the scheme **Figure 1.17**. The authors explored the effect of these substituents on the enzymatic incorporation into DNA using Deep $Vent_R$ exo^- and Taq DNA polymerase. According to the authors, most of the substituents can be incorporated into oligonucleotides efficiently by both of the polymerases. However, better results were reported with Deep Vent than with the Taq polymerase. Interestingly, both of the polymerases showed difficulties incorporating the amino-propargyl derivative (**1.154**) and almost no incorporation was observed.

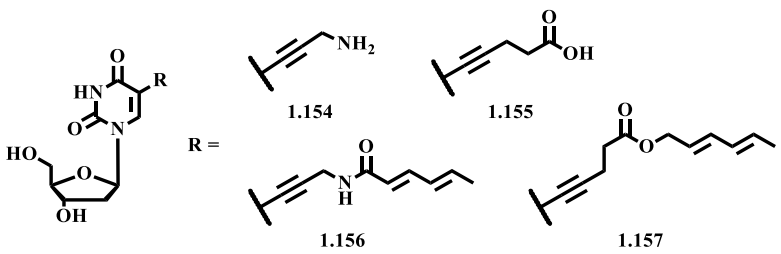

Figure 1.17. Selected examples of 5-alkenyl-2′-deoxyuridine analogs.

The chemistry of covalently linked nucleosides have been explored for their applications as interstrand cross-linkers in DNA duplexes, [116-122] inhibitors of ribonucleotide reductase [123] and HIV reverse transcriptase, [124] models for the repair mechanism of DNA photolesions,[125] supramolecular self-assembly[126] and protein binding.[127] Some selected examples of covalently linked 2'-deoxyuridines connected via alkynyl and diynyl linkers are shown in **Figure 1.18**.[128-131] Sniady *et al.* synthesized covalently linked 2′-deoxyuridine dinucleosides via ethynyl and short diynyl spacers (**1.158-1.160, Figure 1.18)**.[130] These compounds can be converted to their furopyrimidine derivatives. Crisp *et al.* utilized a semi-flexible diynyl spacer containing long alkyl chain to synthesize such types of compounds (**1.163-1.164, Figure 1.18)**.[128] These compounds have been studied for the formation of intramolecular hydrogen bonding between the two nucleobases and intensity of hydrogen bond formation was measured in terms of ^{1}H NMR chemical shifts.

Seela *et al.*[129, 131] employed azide-alkyne cycloaddition (click reaction) to link nucleosides using a moderately long diynyl spacer (**1.161**, **Figure 1.18**). It was reported that all of these 1,2,3-triazole functionalized nucleosides (**1.162**, **1.166** and **1.167**) exhibited enhanced duplex stabilization which is superior to that of the propynyl group for several oligonucleotide sequences. It is interesting to observe that such bulky groups do not perturb DNA stability. The presence of the polar character of the side chains and highly polar 1,2,3-triazole moiety in these molecules possibly enabled them to get solvated by H_2O molecules due to which no perturbation was observed. The compounds **1.166** and **1.167** can be further modified into a circular structure using a bis azide, 1,4-bis(azidomethyl)benzene (**1.165**). This type of bis-click circularization is a very useful strategy utilizing oligonucleotides for the construction of circular RNA, peptides and other macrocycles.

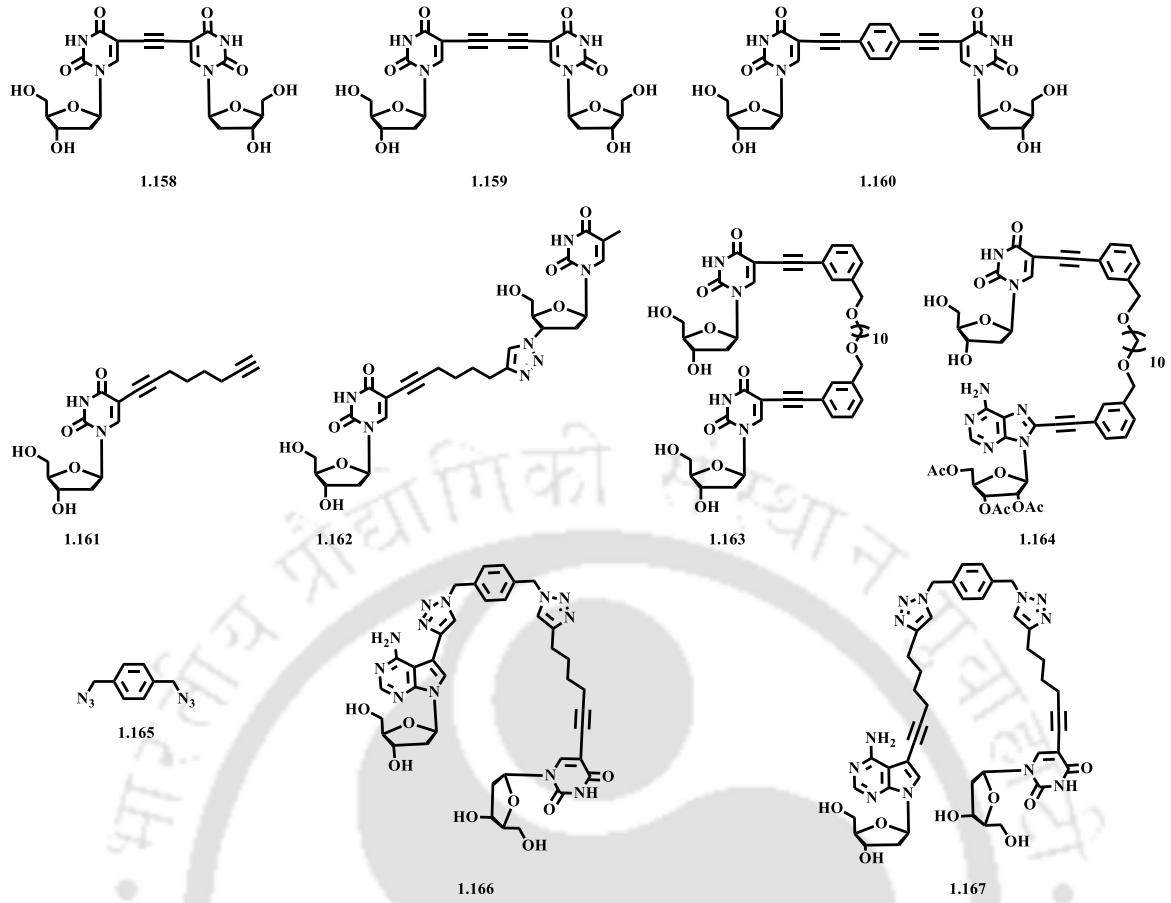

Figure 1.18. Selected examples of covalently linked dinucleosides and their linkers.

1.6. 5-Substituted 2'-Deoxyuridines in Clinical Research

5-iodo-2'-deoxyuridine (IDU) (**1.168**, **Figure 1.18**) was the first synthetic nucleoside analog with effective antiviral properties and was synthesized in 1959. It is used in the treatment of herpetic keratitis and ocular herpes virus infections.[132, 133] The suggested mechanism of action of IDU is the involvement of its active triphosphate derivative (IDUTP), which inhibits the growth of viral DNA when incorporated. However, the use of IDU for the treatment of herpes infections is limited due to its toxicity. Research for non-toxic and more effective antiviral agents leads to the development of several modified uridines: 5-ethyl-2'-deoxyuridine (EDU), (E) -5-(2-bromo)-2'-deoxyuridine (BVDU), (E)-5-(2-iodovinyl)-2'-deoxyuridine (IVDU), 5-(2-chloroethyl)-2'-deoxyuridine (CEDU) etc. The EDU is commercially known as acedurid and used for the treatment of herpetic keratitis and reported as less-mutagenic in comparison to IDU. Among these analogs, BVDU and IVDU were found to show the highest antiviral activity against HSV-1 and VZV infections.[133, 134]

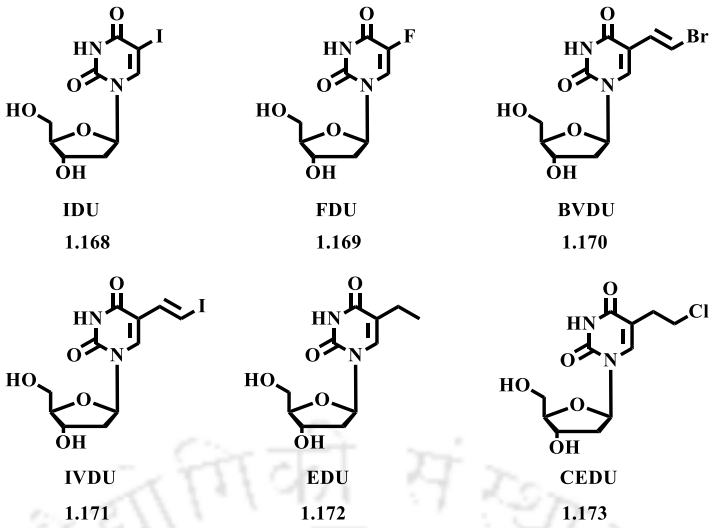

Figure 1.19. Selected examples of 5-substituted-2′-deoxyuridines licensed for clinical antiviral use.

The possible mechanism of action for BVDU includes the involvement of its active triphosphate derivative. According to the literature, the BVDU converted to BVDU triphosphate by virus-encoded kinases, which then possibly interfere with viral DNA polymerases or incorporated into viral DNA.[133, 134] It was reported that the chloroethyl derivative CEDU in lower doses is more effective than BVDU but its potential application is limited due to its mutagenic properties. Some fluorinated pyrimidines and their nucleosides exhibit potent antitumor activity and among them, 5-fluorouracil and 5-fluorodeoxyuridine (FDU) (**1.169**, **Figure 1.18**) are the most important examples. Both 5-fluoro -2'-deoxyuridine and 5-fluorouracil are used for the treatment of breast cancer and a variety of tumors.[135, 136] However, FDU is not specifically tumor selective and dose-limiting intestinal toxicity is observed in certain cases.[137]

5-isopropyl-2'-deoxyuridine (**1.174**, **Figure 1.20**) was also reported to exhibit antiviral activity against HSV-1, but comparatively weaker than BVDU.[138] Acetals are well-known prodrug candidates.[139] Fan *et al.*[140] reported a nucleoside acetal, 5-(dimethoxymethyl)-2'-deoxyuridine (**1.175**, **Figure 1.20**) with potent anti-orthopoxvirus activity. The antiviral activity of the compound suggested being related to oxygen atoms on the substituent, which permits binding to more hydrophilic protein targets through hydrogen bonding interactions. Safadi *et al.*[141] reported similar 5-substituted 2'-deoxyuridine derivatives and explored for their antiviral activity against HIV-1 (**1.176-1.178, Figure 1.20**). According to the authors, 5-

hydroxymethyl-2'-deoxyuridine (**1.154**) exhibited moderate activity while 5-carbamoyl-2'-deoxyuridine (**1.177**) and 5-carbamoylmethyl-2'-deoxyuridine (**1.178**) exhibited potential activity against HIV-1.

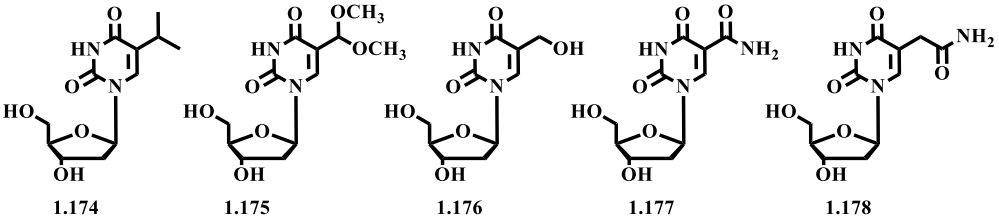

Figure 1.20. Selected examples of 5-substituted-2′-deoxyuridines with antiviral properties.

Alkynyl modifications of uridines constitute a large group of molecules which have been explored for diverse biochemical studies. In 2007, Meneni *et al.*[142] synthesized a series of 5-alkynyl uridines (**1.179-1.186**, **Figure 1.21**) via Sonogashira coupling and explored their anticancer property. These nucleosides were studied for their antitumor properties in vitro using two human breast cultures MCF-7 and MDA-MB-231. Among the series, 5-ethynyl -2'-deoxyuridine (**1.179**) reported as most potent exceeding the potency of cisplatin and 5-fluorouracil. P-tolyethynyl-2'-deoxyuridine (**1.183**) was also found to show high potency with MCF-7 but the results were negative with MDA-MB-231. Lower antitumor activity was reported for **1.184**, **1.185** which have longer or bulkier aliphatic substituents in the aromatic ring. Cristofoli *et al.* studied iodoethynyl (**1.187**, **Figure 1.21**) and trimethylsilylethynyl (**1.188**) 2′-deoxyuridines to acquire antiviral structure-activity relationships. These compounds also showed enhanced antiviral activity against HSV-1, HSV-2, and VSV.[143]

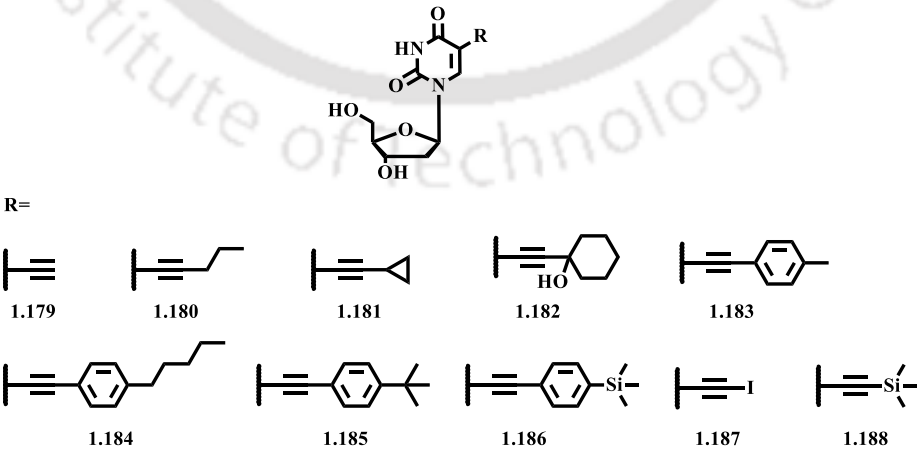

Figure 1.21. 5-alkynyl-2′-deoxyuridines reported by Meneni *et al.* and Cristofoli *et al.*

Korshun and co-workers synthesized several 5-arylethynyl-2′-deoxyuridines (**1.189- 1.194**, **Figure 1.22**) and explored their antiviral properties.[81, 144, 145] They reported that 5-arylethynyl-2′-deoxyuridines with bulky aryl substituents (**1.190-1.194**) show potential antiviral activity against HSV-1. The 5-phenylethynyl-2′-deoxyuridine (**1.189**) was reported as inactive against HSV-1. Among the series, the anthracene labeled nucleoside (**1.194**) showed the highest activity against HSV-1. They observed that the introduction of a flexible spacer between aryl and triple bond (e.g. **1.193**) increases the cytotoxicity and significantly reduce the antiviral property. Thus, it can be concluded that for these compounds, the direct connection of the rigid ethynyl group to uracil is a crucial feature for antiviral activity.

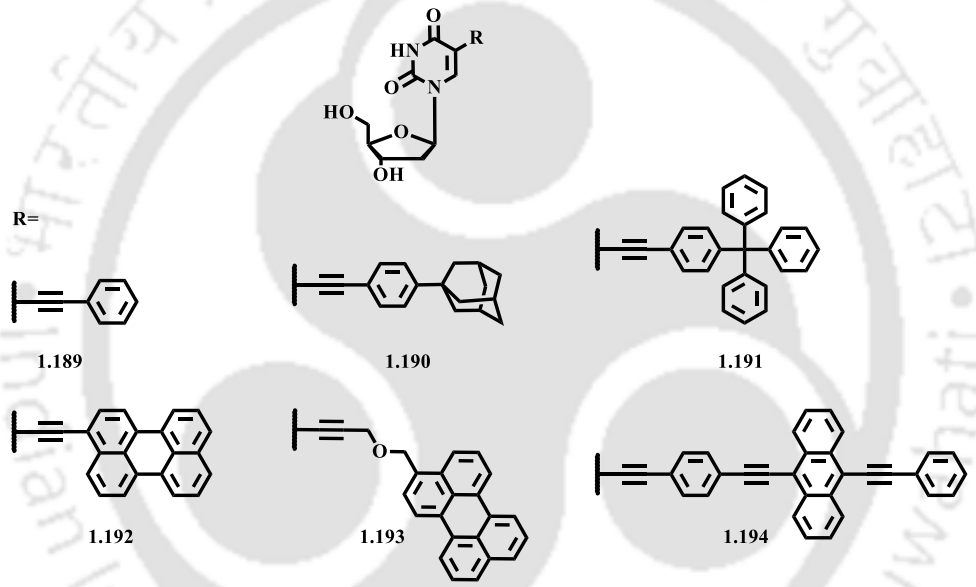

Figure 1.22. 5-arylethynyl-2′-deoxyuridines reported by Korshun and co-workers.

Following the success of 5-ethynyl-2'-deoxyuridine and its derivatives as an anticancer agent, Lee *et al*.[146] reported the synthesis of a series of isoxazole and triazole derivatives of 5-ethynyl-2'-deoxyuridine (**1.195-1.204**, **Figure 1.23**). Among the isoxazole nucleosides, the acetylated isoxazole nucleosides, (**1.197-1.199**) showed high potency against NUG-3 (stomach) and PC-3 (prostate) cancer cell lines, inhibiting 50% cancer growth rate at a concentration of 10 µM. Among these three nucleosides, **1.199** with the bulkiest group (tert-butyl) exhibited the greatest antioncogenic activity. The deacetylated isoxazole nucleosides along with other nucleosides with smaller substituents (**1.195**, **1.196**) were reported to show dramatically reduced anticancer activities. Among the triazole nucleosides, **1.201** was reported

as the most potent anticancer agent. Like isoxazole nucleosides, deacetylated triazole nucleosides displayed lower anticancer activity than their corresponding acetylated derivatives. The possible reason could be increased lipophilicity of the nucleosides due to acetyl groups. According to the authors, the triazole nucleosides exhibited lower anticancer activities than the isoxazole nucleosides. However, lower cytotoxicity was reported for triazole nucleosides in comparison to isoxazole nucleosides which suggested that triazole nucleosides are better drug candidates than isoxazole nucleosides.

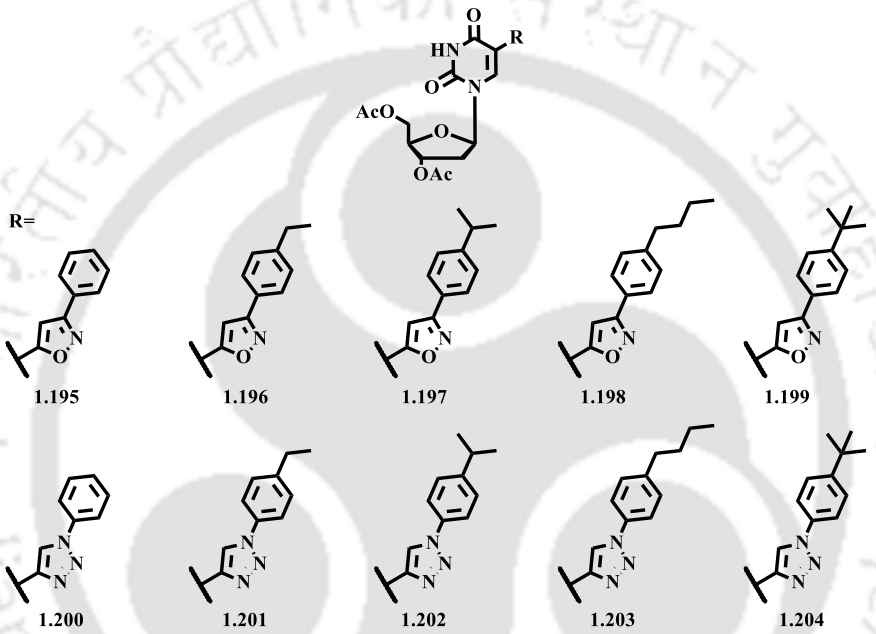

Figure 1.23. Isoxazole and triazole derivatives of 5-ethynyl-2'-deoxyuridine reported by Lee *et al.*

In 2010, Park *et al.*[147] synthesized 2'-deoxyuridine derivatives bearing perfluoroalkyltriazole moieties (**Figure 1.24**) and explored their anticancer properties. Among these analogs, **1.208** was reported as the most potent in inhibiting the cancer cell (PC-3, MDA-MB-231, ACHN) growth rate by more than 80% at a concentration of 10 µM. Interestingly, in this case, the acetylated congeners (acetyl protection on sugar hydroxyl groups) of these nucleosides exhibited decreased or non-enhanced activity in most cases. According to the authors, the fluorinated nucleoside analogs were sufficiently lipophilic by themselves due to which acetyl groups possibly remain ineffective in this case.

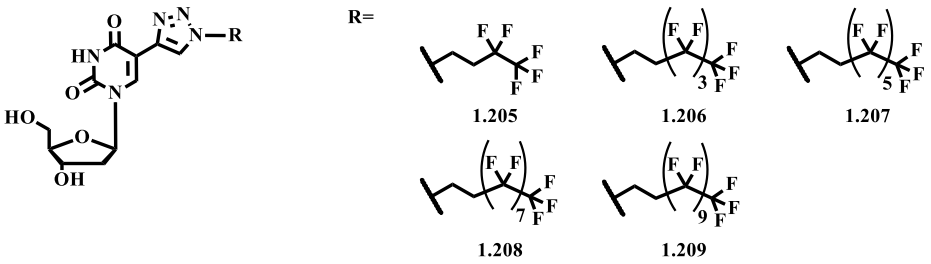

Figure 1.24. 5-perfluoroalkyltriazole -2′-deoxyuridines reported by Park *et al.*

Recently, Shmalenyuk *et al.*[148, 149] synthesized several C5-substituted uridines and explored their activity against tuberculosis (**Figure 1.25**). The selected nucleosides with long-chain alkyloxymethyl (**1.210-1.212**) and alkyltriazolidomethyl (**1.213-1.215**) substituents at C5-position of the nucleoside exhibited inhibitory activity against two Mycobacterium tuberculosis strains, H37Rv, and MDR MS-115. According to their report, all of these compounds inhibited the growth of the mycobacterium H37Rv by at least 99% at a concentration equal to or less than 20 µg mL^{-1}, except **1.210** (40 µg mL^{-1} for 99% inhibition). Among these compounds, **1.214** and **1.215** showed the highest inhibitory activities against both mycobacterium H37Rv and MDR MS-115. These two compounds inhibited the growth rate of both Mycobacterium tuberculosis strains by 99% at a concentration of 10 µg mL^{-1} in the assay.

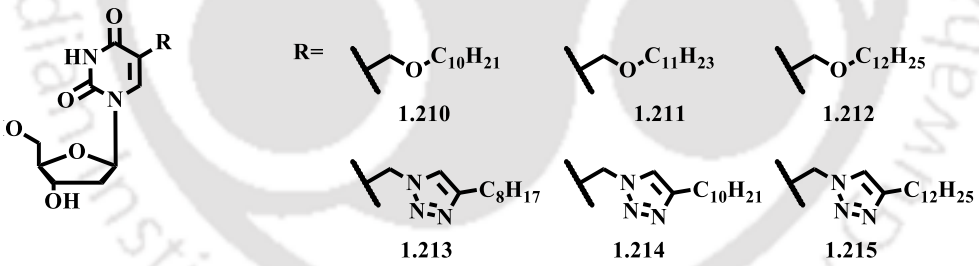

Figure 1.25. 5-substituted -2′-deoxyuridines with antituberculosis properties reported by Shmalenyuk *et al.*

1.7. Fluorescently Labeled 5-Substituted 2'-Deoxyuridines and Their Applications

Due to the lack of inherent emissive properties of the natural nucleobases, tremendous research efforts have been made towards the design and development of fluorescently labeled nucleosides. These fluorescent nucleosides find widespread applications in various research

fields of biochemical interest. The applications of a few 5-substituted fluorescent 2'-deoxyuridines are provided below.

1.7.1. Applications of 5-Substituted 2'-Deoxyuridines Directly Linked to Fluorophores

The utilization of nucleosides labeled with fluorophores via multiple C-C bonds in order to study molecular genetics is known for a long time. Oligonucleotides containing such types of extended fluorescent nucleosides found their applications significantly in the study of SNP detection, nucleic acid lesion and electron transfer process in DNA.[150-155] Fluorescent nucleosides can also be obtained by attaching fluorophores to the nucleobases via a single C-C bond, thereby extending the π-conjugation and installing modulated optical property in the nucleoside.[156-163] Many of these analogs form stable base pairs and show microenvironment sensitivity, when incorporated in oligonucleotides. Such types of fluorescent nucleosides analogs are listed in **Figure 1.26**.

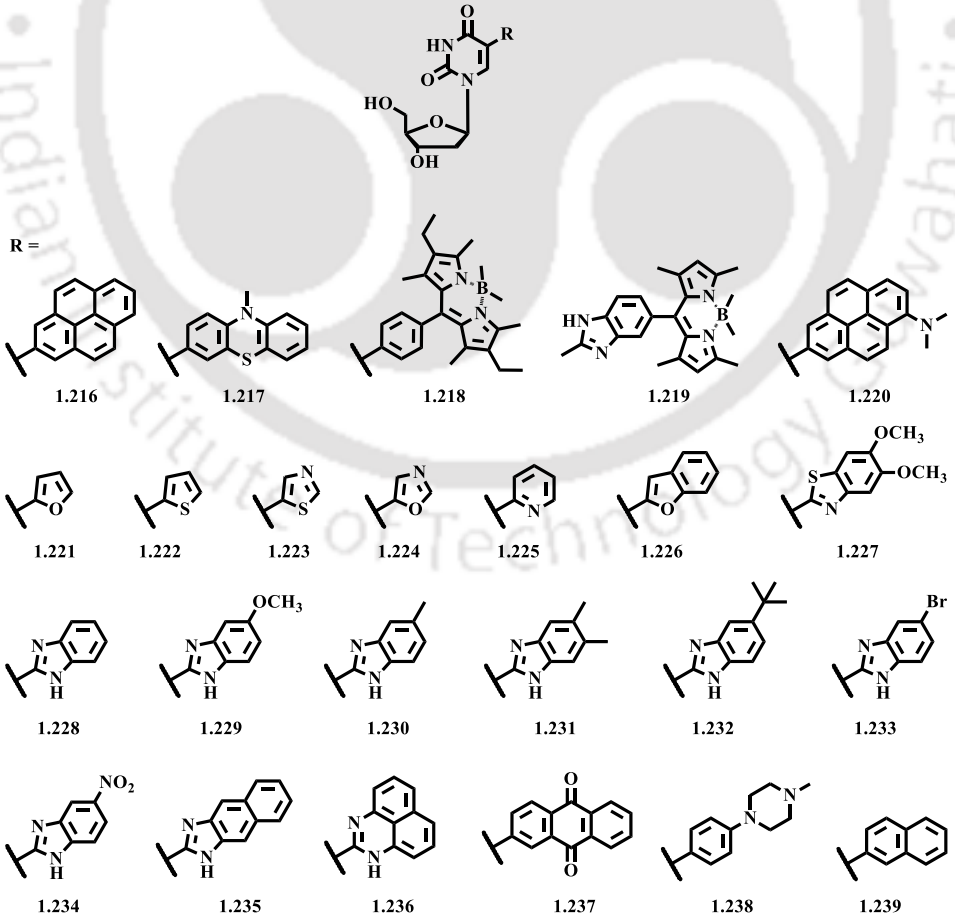

Figure 1.26. Examples of 5-substituted-2′-deoxyuridines directly linked to fluorophores.

One of the most representative examples of C5-substituted 2′-deoxyuridines directly linked to a fluorophore via a single C-C bond is pyrenyl modified 2'-deoxyuridine (**1.216**, **Figure 1.26**), which has been studied extensively for SNP detection and reductive electron transfer in DNA.[151, 164-166] A very distinguished study was reported by Wagenknecht and co-workers on single C-C bonded extended 2'-deoxyuridine analogs. In a DNA assay, they have incorporated a phenothiazine modified nucleoside, 5-(-10-methyl-phenothiazin-3-yl)-2'-deoxyuridine (**1.217**) into oligonucleotides and utilized the same for the study of the electron transfer process in DNA. In their investigation, the electron transfer is reported as highly sequence-dependent and occur more efficiently over T-A base pairs than over C-G base pairs.[167] In another study they have incorporated BODIPY, a dye as a fluorescent label into 2'-deoxyuridine (**1.218)** , the resulting nucleoside exhibited preferred Watson-Crick base pairing but showed low quantum yield.[150] They have also reported the incorporation of 6-N, N-dimethylaminopyrene-modified 2′-deoxyuridine (**1.220**) as an acceptor in a donor-DNA-acceptor system in order to study the DNA-mediated charge transfer processes.[168]

Tor *et al.* reported the synthesis and photophysical properties of five-membered heterocycle (furan, thiophene, oxazole, and thiazole) and pyridine modified 2'-deoxyuridines (**1.221-1.225**, **Figure 1.26**).[169-171] Among the 5-membered heterocyclic analogs, the furan-containing derivative (**1.221**) exhibited the highest emission quantum efficiency and microenvironment sensitivity. According to the authors, the oligonucleotides containing furan-modified 2'-deoxyuridine formed stable DNA duplexes. On the other hand, the pyridine-modified 2'-deoxyuridine displayed multiple sensing properties and thus highly sensitive to changes in polarity, viscosity, and acidity.[171] Recently, Srivatsan *et al.*[172] reported the synthesis of benzofuran modified 2'-deoxyuridine (**1.226**), which display enhanced fluorescence intensity when incorporated into human telomeric DNA and RNA oligonucleotide sequences. This emissive nucleoside has been utilized for the selective detection of DNA and RNA G-quadruplexes.

Matsuda *et al.*[159] reported the synthesis of 5-(5,6-dimethoxybenzothiazol-2-yl)-2'-deoxyuridine (**1.227**, **Figure 1.26**) and utilized for the selective detection of 5-formyl-2'-deoxyuridine which is an oxidized lesion of thymidine generated due to oxidative stress in DNA and speculated to cause carcinogenicity and aging of cells.[173] In another study, Zhou *et al.*[158] reported the synthesis of several highly fluorescent 5-benzimidazolyl-2'-deoxyuridines (**1.219**, **1.228-1.236**) from 5-formyl-2'-deoxyuridine and formation of these nucleosides can be utilized for the selective detection of 5-formyl-2'-deoxyuridine from a mixture of natural

nucleosides. The fluorescence emission quantum yields of these nucleosides were found to be sensitive to change in pH and organic solvents. Gothelf *et al.*[174] synthesized anthraquinone-modified 2'-deoxyuridine (**1.237**) labeled oligonucleotides and studied their electrochemical properties in order to explore the application of such modified bases in DNA assays.

Kim *et al.*[175] reported the synthesis of piperazinephenyl -bearing 2'-deoxyuridine, ^{PP}**U** (**1.238, Figure 1.26**) which impart cationic as well as high fluorescence property. The synthesized nucleotides containing ^{PP}**U** showed enhanced stability against enzymatic degradation and increased thermal stability than the unmodified ones. Furthermore, the fluorescent ^{PP}**U**-modified nucleotides can be delivered into the cytoplasm and their presence within the cytoplasm can be detected without tagging additional fluorophore. Such types of modified oligonucleotides can be very useful for monitoring the activity of oligonucleotides inside the cell.

Bag *et al.*[176] reported the synthesis of a 5-(2-naphthyl)-2'-deoxyuridine (**1.239, Figure 1.26**) labeled oligonucleotide probe for SNP detection. The naphthalene labeled oligonucleotide probe exhibited an enhanced fluorescence emission with a shift in wavelength upon hybridization with a target DNA where the naphthyl moiety lies opposite to adenine in the target DNA.

1.7.2. Applications of 5-Substituted 2'-Deoxyuridines Linked to Fluorophores via an Alkenyl Linker

2'-deoxyuridines containing alkenyl chains at the C5-position often utilized to tether highly fluorescent dyes and other bulky aromatics in order to synthesize highly functionalized fluorescent nucleotides. These alkenyl side chains often accompanied by polar amino or keto groups (acrylamides) possibly for the hydration of these chains by H_2O molecule in DNA grooves. Some recent examples of such types of nucleosides are shown in **Figure 1.27**. One of the most represented examples, a double thiazole orange labeled 2'-deoxyuridine (**1.240**) is reported by Okamoto and his co-workers.[177-186] The nucleotides labeled with this fluorescent nucleoside was reported as hybridization sensitive and therefore found to exhibit high fluorescence on hybridization with a target DNA. These fluorescent hybridized sensitive probes have been applied for RNA imaging[181-183] and monitoring,[178] fluorescent in situ hybridization (FISH) [184, 186] and detection of bacterial ribosomes.[177] Okamoto *et al.* also synthesized anthraquinone modified 2'-deoxyuridine (**1.241**) and incorporated into

oligonucleotides. The anthraquinone labeled oligonucleotide probes were applied in the investigation of photostimulated hole transport through DNA and photoelectrochemical SNP typing.[187, 188]

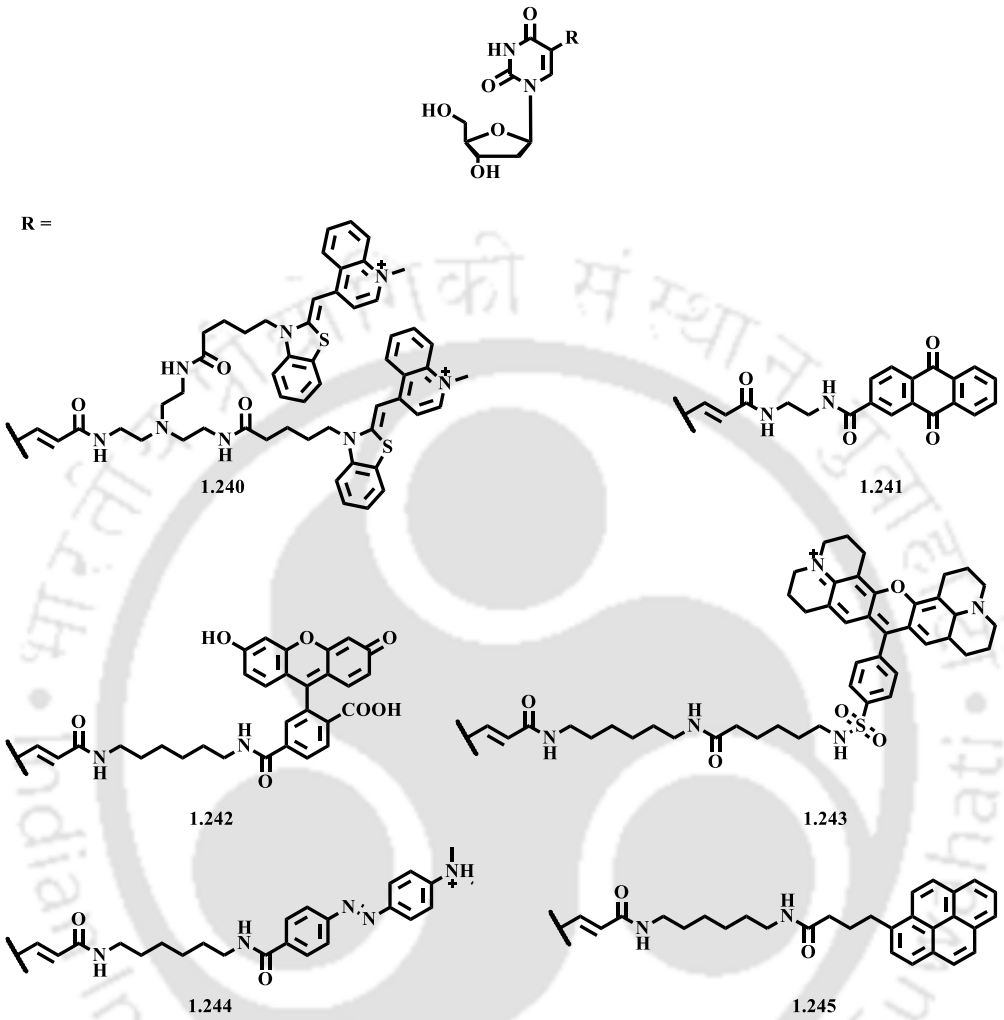

Figure 1.27. Selected examples of 5-substituted-2′-deoxyuridines linked to fluorophores via an alkenyl linker.

Modified 2'-deoxyuridines labeled with fluorescein (**1.242**) Texas red (**1.243**) and dabcyl (**1.244**) are also known.[189-191] Miyasaka *et al.* synthesized fluorescein modified 2'-deoxyuridine labeled oligonucleotides and explored their conformational dynamics in the single-stranded state.[189] Rindermann *et al.* synthesized oligonucleotides labeled with fluorescein and Texas red and explored their ability for the interpretation of fluorescence resonance energy transfer (FRET) process in DNA.[190] Toga *et al.* applied fluorescein and dabcyl labeled oligonucleotide probes for the detection of cellular nucleotide excision repair (NER) repair of damaged DNA.[191]

Yang *et al.*[192] synthesized pyrene labeled 2'-deoxyuridine (**1.245, Figure 1.27**) and incorporated into oligonucleotides. These pyrene labeled oligonucleotide probes have been applied for DNA detection utilizing competitive Host-Guest interaction strategy with the β-cyclodextrin polymer.

1.7.3. Applications of 5-Substituted 2'-Deoxyuridines Linked to Fluorophores via an Alkynyl Linker

As mentioned before, an alkynyl linker can provide rigid and linear structures to fluorophores for their incorporation in DNA. A common approach for the generation of fluorescent uridine nucleosides is based upon attachment of an ethynyl linker carrying a fluorophore at the C5-position of uracil. The Sonogashira coupling reaction is one of the most effective and frequently used methods for the synthesis of 5-alkynyl uridines. Some representative examples of modified fluorescent 2'-deoxyuridines containing ethynyl linker are shown in the scheme **Figure 1.28**.

Saito and co-workers represented some remarkable examples of such types of modified fluorescent 2'-deoxyuridines (**1.246-1.250**).[154, 193-195] These nucleosides belong to a distinct category of nucleosides called as base discriminating fluorescent (BDF) nucleosides and their corresponding oligonucleotide probes are called as BDF probes. One of the most important features of BDF probes is their change in fluorescence intensity depends on the BDF base itself and bases opposite to it on the complementary stand rather than hybridization. Saito *et al.* synthesized 1-pyrenoyl-labeled 2'-deoxyuridines ^{Py}**U** (**1.246**), ^{AMPy}**U** (**1.247**) and N,N-dimethylaminophenyl substituted 1-pyrenoyl-labeled 2'-deoxyuridine (**1.248**) in order to develope fluorescent oligonucleotide probes.[193-195] The oligonucleotide probes labeled with ^{Py}**U** and ^{AMPy}**U** have been applied for SNP detection. The ^{AMPy}**U** BDF probes reported as adenine base selective and thereby emit fluorescence only in presence of adenine opposite to the BDF base.[195] It was reported that the N, N-dimethylaminophenyl substituted 1-pyrenoyl-labeled 2'-deoxyuridine (**1.248**) exhibited dual fluorescence and the oligonucleotide probes containing this particular nucleoside have been applied to monitor DNA structures.[194] Such dual fluorescence emitting probes can be very useful for monitoring hybridization in DNA and RNA duplexes.

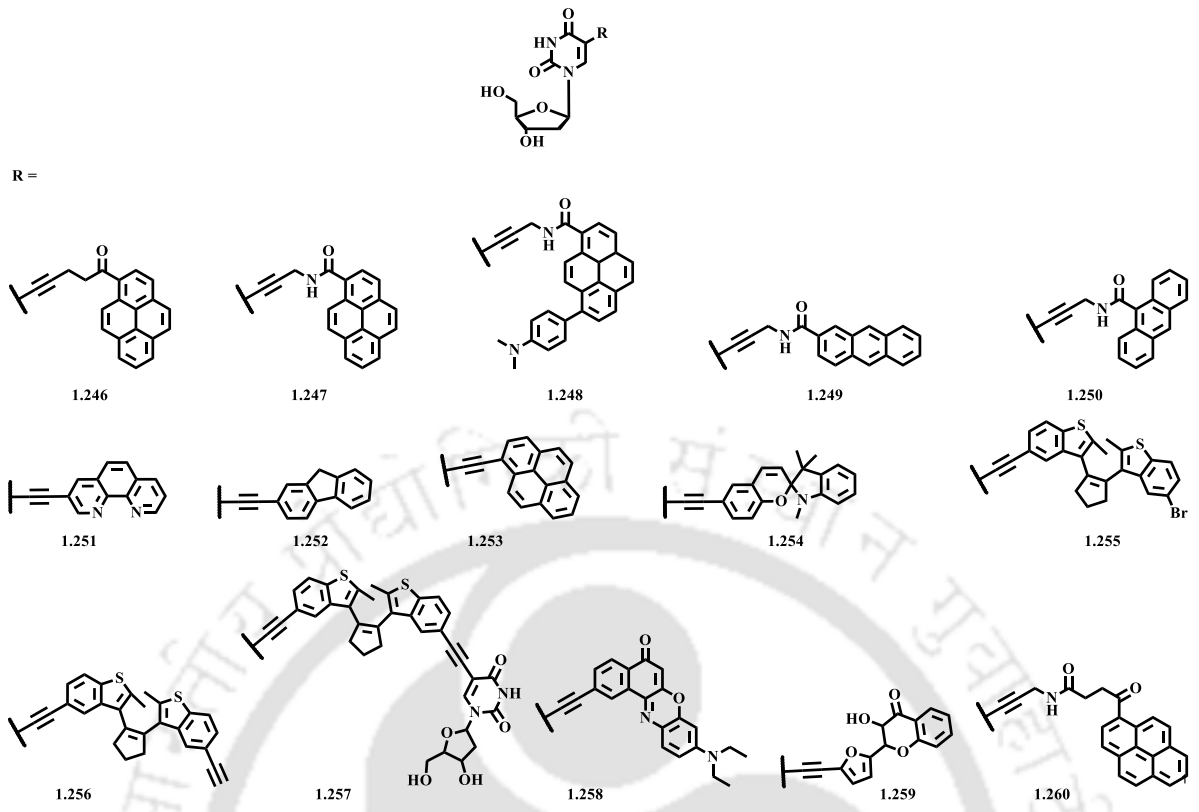

Figure 1.28. Selected examples of 5-substituted-2′-deoxyuridines linked to fluorophores via an alkynyl linker.

Saito *et al.* also synthesized 2- and 9-anthracenecarboxamide labeled 2'-deoxyuridines, $^{2\text{-Ant}}$**U** (**1.249**) and $^{9\text{-Ant}}$**U** (**1.250**) respectively and incorporated into oligonucleotides.[154] The authors studied the fluorescence behavior of the hybridized structures of these oligonucleotide probes with their target oligonucleotides. Based on observations, they reported that the probes containing $^{2\text{-Ant}}$**U** exhibit better fluorescence properties in response to change in solvent polarity and hence, is more suitable for DNA microenvironment study than the probes containing $^{9\text{-Ant}}$**U**. Also, $^{2\text{-Ant}}$**U** containing probes reported as adenine base selective and hence emit fluorescence only in presence of adenine in a target sequence opposite to BDF base.

Tor *et al.*[196] reported the synthesis of 1, 10-Phenanthroline labeled 2'-deoxyuridine (**1.251**, **Figure 1.28**) and incorporated into oligonucleotides. The synthesized fluorescent oligonucleotide probes have been applied for the detection of perfect and mismatched base pairing in DNA duplex and can be useful for SNP detection. However, these oligonucleotides labeled with phenanthroline exhibited a slight decrease in duplex stability than the unmodified ones. The authors further coordinated Ru^{II} and Os^{II} metals to the phenanthroline moiety of the

modified 2'-deoxyuridine for the generation of hybridization sensitive molecular beacon (MB) probes containing metals (Metallo beacons).[197, 198]

Kim *et al.* synthesized 2-ethynyl fluorene labeled (**1.252**) and 1-pyrenyl labeled (**1.253**) 2'-deoxyuridines and incorporated into oligonucleotides.[199-202] Several oligonucleotides containing these modified bases were found to serve as quencher-free molecular beacon (MB) probes. The synthesized oligonucleotide and MB probes have been applied to discriminate fully matched and one-base mismatched base pairing in DNA duplexes and in turn can be useful for SNP detection. The 1-pyrenyl labeled oligonucleotide probes also have been utilized for the detection of B-to-Z- DNA transition.[202]

Wagenknecht *et al.*[203, 204] reported the synthesis of 2'-deoxyuridines modified with spyropyran and diarylethenes (**1.254-1.257**, **Figure 1.28**), which are well-known for their photochromic behavior. As a representative example of diarylethene modified 2'-deoxyuridines, compound **1.255** was incorporated into oligonucleotides where the retention of the photochromic properties of the diarylethene moiety was observed and found to be independent of oligonucleotide sequences.[204] Recently, Wagenknecht *et al.* synthesized ethynyl Nile red labeled 2'-deoxyuridine (**1.258**) and applied for the study of supramolecular nature of DNA towards mixed non-covalent assemblies.[205] Mely *et al.* reported the synthesis of 2-furyl-3-hydroxychromone labeled 2'-deoxyuridine (**1.259**) which exhibit dual emissive behavior.[206] The synthetic oligonucleotide probes containing this particular nucleoside also inherited the dual emissive behavior and have been applied for the detection of SNPs, B conformer from A conformer of DNA and for monitoring DNA annealing.

Bag *et al.* have synthesized γ-oxo-pyrene carboxamide labeled solvatochromic 2'-deoxyuridine (**$^{oxo\text{-}Py}$U**, **1.260**, **Figure1.28**).[207] Upon incorporation into short oligonucleotides, the synthesized singly- and doubly-labeled fluorescent oligonucleotide probes were found to detect efficiently the base "A" and consecutive "AA" base of a target DNA sequences opposite to the labeled base via generation of an enhanced fluorescence signal. It was also demonstrated that the fluorescence of **$^{Oxo\text{-}Py}$U** is highly quenched by G-base, thus could be used for designing G-quenched molecular beacon for DNA detection. The probes also could be useful for discrimination of A/G or AA/GG allele as revealed from their fluorescence behavior.

1.8. Probing Biomolecular Microenvironment with Fluorescent Nucleosides

As a result of tremendous research effort, several fluorescent probes have been reported for probing biological microenvironment with a generation of a distinct and readable fluorescence signal. As for example, saccharide sensor, fructose sensor, fluorescence sensors for metal ions in living cells were developed and reported similar to a number of fluorescent nucleosides/fluorescently labeled nucleosides, fluorescent amino acids, *etc*., have appeared in the literature as biomolecular building blocks for probing of nucleic acids' /proteins' structures, dynamics, and functions. All these efforts are aimed at understanding the structure, dynamics, and functions of such biomolecular entity by studying the detectable signal generated from sensitive fluorescence techniques. All the research efforts are in success with the use of microenvironment sensitive solvatochromic fluorophores. Fluorophores with emission maxima that display sensitivity to solvent polarity, popularly known as solvatochromic fluorophores, are widely used in the study of biomolecular microenvironment surrounding the chromophore. Therefore, they are widely being used in the various research field of biochemical interest which includes: (a) In Carbohydrates Research[208-213]; (b) In Phospholipids and Fatty Acids Research[214-218]; (c) In Amino Acids and Protein Research[219-222]; (d) In Nucleic Acid Research. In this respect, we will restrict our discussion on the importance of fluorescent nucleosides for probing the biomolecules.

Nucleosides constitute an important class of biologically active molecules and are well-known for their antiviral, antibacterial and anticancer properties for more than 50 years. However, the number of nucleosides approved for clinical use as antiviral agents, drugs are limited due to issues such as poor resistance, poor bioavailability, and high cytotoxicity etc.[223] Another important factor is the poor cell membrane penetrability of the nucleosides due to their inability to recognize nucleoside transporter proteins.[224] The recognition of nucleosides by the nucleoside transfer proteins is highly specific and depends on the nucleobases present in a particular nucleoside. Thus, the understanding of protein-nucleoside interaction is critical for the development of new drugs. Therefore, the development of solvatochromic fluorescent nucleosides for probing biomolecules such as proteins could be highly useful not only for the understanding of protein-drug interactions but also for the development of new nucleoside-based drugs. In addition, the understanding of protein-drug interaction can be useful for the investigation of the structure and functions of proteins similar to nucleoside transporter proteins. Moreover, the nucleoside metabolism is critical for cellular survival and functions of

many enzymes depend directly or indirectly on nucleosides.[223] Thus, the development of fluorescent nucleosides is of paramount importance for the understanding of various biological processes and development of new chemotherapeutics. A few examples of nucleosides are depicted below which have been exploited for sensing the microenvironment of either BSA or various DNA.

Thus, Bag et al. recently reported the design and synthesis of a novel fused triazolyl-2-quinolinone (**FTQuon**) nucleoside (**1.261, Figure 1.29**) as a new generation of angularly widened unnatural nucleobase surrogate with two possible H-bonding faces, one H-bond acceptor and another donor.[225] They showed that this nucleoside exhibited good interaction property with BSA protein signaled via a switch on fluorescence response. The strong binding of the nucleoside probe occurs in the hydrophobic pocket of BSA as was evident from a steady state fluorescence anisotropy experiment and supported by docking study.

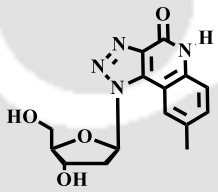

FTQuon
1.261

Figure 1.29. Structure of the triazolyl-2-quinolinone nucleoside, **FTQuon**.

They also have utilized their pyrene tetrazolyl unnatural fluorescent nucleoside, $^{TzPy}\mathbf{B}^{Do}$ (**1.262, Figure 1.30**) for sensing the DNA microenvironment and thereby in DNA detection.[226] They have demonstrated that the probe, $^{TzPy}\mathbf{B}^{Do}$ can be utilized as a versatile fluorescent light-up probe not only for label-free specific detection and discrimination of base mismatched base pairs but also for label-free recognition of abasic site and bulge DNA. Thus, it was demonstrated that the probe $^{TzPy}\mathbf{B}^{Do}$ exhibited enhanced fluorescence signals in presence of pyrimidine mismatch pairs (T/T) and purine mismatch pairs (C/C) in DNA. The probe also exhibited a strong enhanced fluorescence signal upon interaction with pyrimidine base bulge-out DNAs and abasic DNAs containing an abasic site opposite to pyrimidine bases. Thermal denaturation study revealed that the binding of these deformed DNA duplexes with the probe resulting in an increase in their thermal melting stability. As evident from the spectroscopic analysis, the probe is a minor groove binder and binds efficiently to the minor grove near the deformed site. Such types of versatile label-free fluorescent probes can be very useful for

recognition of various types of DNA lesions and also for the investigation of drug-DNA interaction in a simple and cost-effective way.

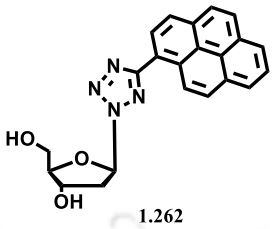

1.262

Figure 1.30. Structure of the tetrazolylpyrene unnatural fluorescent nucleoside, $^{TzPy}B^{Do}$.

The same pyrene tetrazolyl unnatural fluorescent nucleoside has also been utilized by them as a versatile fluorescent light-up probe for label-free detection of multimeric G-quadruplex DNA with high specificity.[227] It was demonstrated that the probe is able to discriminate between telomeric multimeric and monomeric G-quadruplexes in terms of fluorescence signal without affecting their conformation and thermal melting stability. The enhancement in the fluorescence signal of the probe was highly significant when it binds with multimeric H45 G-quadruplex. A strong intercalative binding interaction of the probe inside the TTA pocket connecting two G-quadruplex units of the multimeric H-45 G-quadruplex was explained by the authors which was also supported by a molecular docking study. Thus, such multimeric G-quadruplex selective light-up fluorescent probe can be very useful for designing and development of new G-quadruplex specific binders and new chemotherapeutics.

1.9. Summary and Future Prospect

From the literature report, we have seen that the C5-substituted 2'-deoxyuridine nucleosides constitute a special class of molecules which find diverse applications in the field of pharmaceutics and molecular genetics. Modifications at the C5-position of the pyrimidine nucleosides are highly exploited for the improvement of pharmacokinetics and physiological properties of nucleoside-based drugs. Many of the C5-substituted nucleosides find their applications in clinical research and have been discussed in **Section 1.6**. The diagnosis of the newly discovered diseases demand effective and safer drugs and therefore the C5-substituted nucleosides will always remain an interesting research area for application in chemotherapeutics and drug discovery.

The modification at the C5-position of a pyrimidine nucleoside is highly functional and can be utilized for the incorporation of diverse functional groups into DNA. Incorporation of a wide selection of biologically active molecules is possible via modification at C5-position without affecting the DNA duplex stability. In many cases, such modifications lead to enhanced DNA duplex stability (**Section 1.5**). Thus, the incorporation of functional groups with catalytic and electrostatic properties via C5-position can be utilized for the synthesis of stable functionalized DNA imparting such properties which can be useful for the interpretation of various processes of molecular genetics.

The applications of fluorescence-based techniques are rapidly growing in almost every field of science and technology due to their superior reliability, operational simplicity, and responsiveness than other molecular techniques. Since, the natural nucleosides shows weak emission properties, the development of fluorescent nucleosides is very crucial for the investigation of various biological events utilizing fluorescence-based techniques. Nucleosides can be modified to impart rich photophysical properties by attaching a known fluorophore with rich photophysical properties. These fluorophores are generally dyes and polyaromatic hydrocarbons. The C5-position of the pyrimidine nucleoside possibly the ideal site for incorporation of such large molecules without affecting the DNA stability, since the C5-position lies in the major groove of DNA. Thus, the C5-fluorescently labeled nucleosides are highly preferred for the development of fluorescent oligonucleotide probes which exhibit hybridization dependent emission response. In **Section 1.7**, we have discussed various types of fluorescent C5-substituted nucleosides and their applications. These fluorescent nucleosides have continuously aided researchers not only to gain insight into the structure and functions of biological macromolecules but also for the detection and diagnosis of DNA disorders such as SNP, Abasic sites etc.

From the literature, we have seen that most of the fluorescent nucleosides have been utilized as oligonucleotide probes for probing of the biological microenvironment. The examples of utilization of bare fluorescent nucleosides for probing biological microenvironment are rare. Incorporation of fluorescently labeled nucleosides into oligonucleotides for the development of fluorescent oligonucleotide probes is a tedious job and often depends on the size and chemical nature of the nucleosides. It is always desirable to develop fluorescent nucleosides which able to sense biological microenvironment on its own and deliver useful information in the form of highly distinguished emission signals. Therefore, the development of fluorescent nucleosides is very important in order to get insight into nucleoside/DNA and or protein interactions which definitely aid in the development of new chemotherapeutic drugs.

Moreover, understanding of such interactions can be very useful for the investigation of structure and functions of nucleic acids, nucleoside transporters and other similar proteins.

1.10. References

1. Franklin, R. E.; Gosling, R. G., Evidence for 2-chain helix in crystalline structure of sodium deoxyribonucleate. *Nature* **1953,** *172* (4369), 156-157.
2. Franklin, R. E.; Gosling, R. G., Molecular structure of nucleic acids. Molecular configuration in sodium thymonucleate. 1953. *Annals of the New York Academy of Sciences* **1995,** *758*, 16-17.
3. Jacobson, B., Hydration structure of deoxyribonucleic acid and its physicochemical properties. *Nature* **1953,** *172* (4380), 666-667.
4. Watson, J. D.; Crick, F. H., Molecular structure of nucleic acids; a structure for deoxyribose nucleic acid. *Nature* **1953,** *171* (4356), 737-738.
5. Watson, J. D.; Crick, F. H., The structure of DNA. *Cold Spring Harbor Symposia on Quantitative Biology* **1953,** *18*, 123-131.
6. Wilkins, M. H.; Seeds, W. E.; Stokes, A. R.; Wilson, H. R., Helical structure of crystalline deoxypentose nucleic acid. *Nature* **1953,** *172* (4382), 759-762.
7. Wilkins, M. H.; Stokes, A. R.; Wilson, H. R., Molecular structure of deoxypentose nucleic acids. *Nature* **1953,** *171* (4356), 738-740.
8. Brenner, S.; Jacob, F.; Meselson, M., An unstable intermediate carrying information from genes to ribosomes for protein synthesis. *Nature* **1961,** *190*, 576-581.
9. Watson, J. D.; Crick, F. H., Genetical implications of the structure of deoxyribonucleic acid. *Nature* **1953,** *171* (4361), 964-967.
10. Coverley, D.; Laskey, R. A., REGULATION OF EUKARYOTIC DNA REPLICATION. *Annual Review of Biochemistry* **1994,** *63* (1), 745-776.
11. Dounce, A. L., [Duplicating mechanism for peptide chain and nucleic acid synthesis]. *Enzymologia* **1952,** *15* (5), 251-258.
12. Kornberg, A., Biologic Synthesis of Deoxyribonucleic Acid. *Science* **1960,** *131* (3412), 1503.
13. Kornberg, R. D.; Lorch, Y., Chromatin Structure and Transcription. *Annual Review of Cell Biology* **1992,** *8* (1), 563-587.
14. Kozak, M., Regulation of translation in eukaryotic systems. *Annual Review of Cell Biology* **1992,** *8*, 197-225.
15. Nirenberg, M. W.; Matthaei, J. H., The dependence of cell-free protein synthesis in E. coli upon naturally occurring or synthetic polyribonucleotides. *Proceedings of the National Academy of Sciences of the United States of America* **1961,** *47* (10), 1588-1602.
16. Crick, F., Central dogma of molecular biology. *Nature* **1970,** *227* (5258), 561-563.
17. Crick, F. H., On protein synthesis. *Symposia of the Society for Experimental Biology* **1958,** *12*, 138-163.
18. Tooze, J.; Weiss, R., *Molecular biology of tumor viruses. RNA tumor viruses : text [Part 1], 1 [Part 1], 1*. 1984.
19. Cech, T. R.; Bass, B. L., Biological catalysis by RNA. *Annual Review of Biochemistry* **1986,** *55*, 599-629.
20. Sharp, P. A., Splicing of messenger RNA precursors. *Science* **1987,** *235* (4790), 766-771.
21. Cedar, H., DNA methylation and gene activity. *Cell* **1988,** *53* (1), 3-4.
22. Saenger, W., *Principles of nucleic acid structure*. Springer: New York; Berlin; Heidelberg; London; Paris; Tokyo; Hong Kong; Barcelona; Budapest, 1995.

23. Watson, J. D.; Crick, F. H. C., Molecular Structure of Nucleic Acids: A Structure for Deoxyribose Nucleic Acid. *Nature* **1953,** *171* (4356), 737-738.
24. Henry, A. A.; Romesberg, F. E., Beyond A, C, G and T: augmenting nature's alphabet. *Current Opinion in Chemical Biology* **2003,** *7* (6), 727-733.
25. Kool, E. T., Replacing the Nucleobases in DNA with Designer Molecules. *Accounts of Chemical Research* **2002,** *35* (11), 936-943.
26. Kool, E. T.; Morales, J. C.; Guckian, K. M., Mimicking the Structure and Function of DNA: Insights into DNA Stability and Replication. *Angewandte Chemie International Edition* **2000,** *39* (6), 990-1009.
27. Hirao, I.; Kimoto, M.; Mitsui, T.; Fujiwara, T.; Kawai, R.; Sato, A.; Harada, Y.; Yokoyama, S., An unnatural hydrophobic base pair system: site-specific incorporation of nucleotide analogs into DNA and RNA. *Nature Methods* **2006,** *3*, 729-735.
28. Leconte, A. M.; Chen, L.; Romesberg, F. E., Polymerase Evolution: Efforts toward Expansion of the Genetic Code. *Journal of the American Chemical Society* **2005,** *127* (36), 12470-12471.
29. Sismour, A. M.; Benner, S. A., The use of thymidine analogs to improve the replication of an extra DNA base pair: a synthetic biological system. *Nucleic Acids Research* **2005,** *33* (17), 5640-5646.
30. Soumpasis, D. M., A genetic switch: gene control and phage :Mark Ptashne, Blackwell Scientific Publications and Cell Press, Palo Alto, CA, 1986, 138 pp., $16.95. *Mathematical Biosciences* **1987,** *86* (2), 239-240.
31. Steitz, T. A., Structural studies of protein-nucleic acid interaction: the sources of sequence-specific binding. *Quarterly reviews of biophysics* **1990,** *23* (3), 205-280.
32. Abrams, M. J.; Murrer, B. A., Metal compounds in therapy and diagnosis. *Science* **1993,** *261* (5122), 725.
33. Lakowicz, J. R., *Principles of fluorescence spectroscopy*. Springer: New York, 2004.
34. Buscaglia, M.; Schuler, B.; Lapidus, L. J.; Eaton, W. A.; Hofrichter, J., Kinetics of Intramolecular Contact Formation in a Denatured Protein. *Journal of Molecular Biology* **2003,** *332* (1), 9-12.
35. Deniz, A. A.; Laurence, T. A.; Beligere, G. S.; Dahan, M.; Martin, A. B.; Chemla, D. S.; Dawson, P. E.; Schultz, P. G.; Weiss, S., Single-molecule protein folding: diffusion fluorescence resonance energy transfer studies of the denaturation of chymotrypsin inhibitor 2. *Proceedings of the National Academy of Sciences of the United States of America* **2000,** *97* (10), 5179-5184.
36. Krieger, F.; Fierz, B.; Bieri, O.; Drewello, M.; Kiefhaber, T., Dynamics of unfolded polypeptide chains as model for the earliest steps in protein folding. *Journal of Molecular Biology* **2003,** *332* (1), 265-274.
37. Lapidus, L. J.; Eaton, W. A.; Hofrichter, J., Measuring the rate of intramolecular contact formation in polypeptides. *Proceedings of the National Academy of Sciences* **2000,** *97* (13), 7220.
38. Schuler, B.; Lipman, E. A.; Eaton, W. A., Probing the free-energy surface for protein folding with single-molecule fluorescence spectroscopy. *Nature* **2002,** *419* (6908), 743-747.
39. Stryer, L.; Haugland, R. P., Energy transfer: a spectroscopic ruler. *Proceedings of the National Academy of Sciences of the United States of America* **1967,** *58* (2), 719-726.
40. Wang, X.; Bodunov, E. N.; Nau, W. M., Fluorescence quenching kinetics in short polymer chains: Dependence on chain length. *Optics and Spectroscopy* **2003,** *95* (4), 560-570.
41. Andréasson, J.; Holmén, A.; Albinsson, B., The Photophysical Properties of the Adenine Chromophore. *The Journal of Physical Chemistry B* **1999,** *103* (44), 9782-9789.

42. Daniels, M.; Hauswirth, W., Fluorescence of the purine and pyrimidine bases of the nucleic acids in neutral aqueous solution at 300 degrees K. *Science* **1971,** *171* (3972), 675-677.
43. Onidas, D.; Markovitsi, D.; Marguet, S.; Sharonov, A.; Gustavsson, T., Fluorescence Properties of DNA Nucleosides and Nucleotides: A Refined Steady-State and Femtosecond Investigation. *The Journal of Physical Chemistry B* **2002,** *106* (43), 11367-11374.
44. Anilkumar, R. K.; Irudaya, C., Recent Developments in the Synthesis and Applications of C5-Substituted Pyrimidine Nucleosides and Nucleotides. *Current Organic Chemistry* **2012,** *16* (17), 1996-2013.
45. Blanalt-Feidt, S.; Doronina, S. O.; Behr, J.-P., Synthesis of C-4 substituted pyrimidines exhibiting various H-bonding patterns. *Tetrahedron Letters* **1999,** *40* (34), 6229-6232.
46. Kögler, M.; De Jonghe, S.; Herdewijn, P., Synthesis of 6-aryl-2′-deoxyuridine nucleosides via a Liebeskind cross-coupling methodology. *Tetrahedron Letters* **2012,** *53* (2), 253-255.
47. Liang, Y.; Wnuk, F. S., Modification of Purine and Pyrimidine Nucleosides by Direct C-H Bond Activation. *Molecules* **2015,** *20* (3), 4874-4901.
48. Shih, Y.-C.; Chien, T.-C., Practical synthesis of 6-aryluridines via palladium(II) acetate catalyzed Suzuki–Miyaura cross-coupling reaction. *Tetrahedron* **2011,** *67* (21), 3915-3923.
49. Shimizu, T.; Kimura, T.; Funahashi, T.; Watanabe, K.; Ho, I. K.; Yamamoto, I., Synthesis of N3-substituted uridine and related pyrimidine nucleosides and their antinociceptive effects in mice. *Chemical and Pharmaceutical Bulletin* **2005,** *53* (3), 313-318.
50. Smith, W. S.; Sierzputowska-Gracz, H.; Sochacka, E.; Malkiewicz, A.; Agris, P. F., Chemistry and structure of modified uridine dinucleosides are determined by thiolation. *Journal of the American Chemical Society* **1992,** *114* (21), 7989-7997.
51. Sochacka, E.; Leszczynska, G.; Bartos, P.; Ebenryter-Olbinska, K.; Lodyga-Chruscinska, E.; Pawlak, J.; Nawrot, B.; Cypryk, M., C5-substituents of uridines and 2-thiouridines present at the wobble position of tRNA determine the formation of their keto-enol or zwitterionic forms - a factor important for accuracy of reading of guanosine at the 3′-end of the mRNA codons. *Nucleic Acids Research* **2017,** *45* (8), 4825-4836.
52. Cappellacci, L.; Petrelli, R.; Franchetti, P.; Vita, P.; Kusumanchi, P.; Kumar, M.; Jayaram, H. N.; Zhou, B.; Yen, Y.; Grifantini, M., Synthesis and biological activity of novel N6-substituted and 2,N6-disubstituted adenine ribo- and 3′-C-methyl-ribonucleosides as antitumor agents. *European Journal of Medicinal Chemistry* **2011,** *46* (5), 1499-1504.
53. Gayakhe, V.; Ardhapure, A. V.; Kapdi, A. R.; Sanghvi, Y. S.; Serrano, J. L.; Schulzke, C. C-C Bond Formation: Synthesis of C5 Substituted Pyrimidine and C8 Substituted Purine Nucleosides Using Water Soluble Pd-imidate Complex *Current Protocols in Nucleic Acid Chemistry* **2016**, 1.37.1-1.37.15.
54. Kokatla, H. P.; Lakshman, M. K., Two-step, one-pot synthesis of inosine, guanosine, and 2'-deoxyguanosine O6-ethers via intermediate O6-(benzotriazol-1-yl) derivatives. *Current Protocols in Nucleic Acid Chemistry* **2012,** *Chapter 1*, Unit1.26-Unit1.26.
55. Thomsen, N. M.; Vongsutilers, V.; Gannett, P., The Synthesis of C8-Aryl Purines, Nucleosides and Phosphoramidites. *Critical Reviews™ in Eukaryotic Gene Expression* **2011,** *21* (2), 155-176.
56. Tosh, D. K.; Finley, A.; Paoletta, S.; Moss, S. M.; Gao, Z.-G.; Gizewski, E. T.; Auchampach, J. A.; Salvemini, D.; Jacobson, K. A., In Vivo Phenotypic Screening for Treating Chronic Neuropathic Pain: Modification of C2-Arylethynyl Group of

Conformationally Constrained A3 Adenosine Receptor Agonists. *Journal of Medicinal Chemistry* **2014,** *57* (23), 9901-9914.
57. Seela, F.; Peng, X., Progress in 7-deazapurine - pyrrolo[2,3-d]pyrimidine - ribonucleoside synthesis. *Current Topics in Medicinal Chemistry* **2006,** *6* (9), 867-892.
58. Hobbs, F. W., Palladium-catalyzed synthesis of alkynylamino nucleosides. A universal linker for nucleic acids. *The Journal of Organic Chemistry* **1989,** *54* (14), 3420-3422.
59. Nauš, P.; Pohl, R.; Votruba, I.; Džubák, P.; Hajdúch, M.; Ameral, R.; Birkuš, G.; Wang, T.; Ray, A. S.; Mackman, R.; Cihlar, T.; Hocek, M., 6-(Het)aryl-7-Deazapurine Ribonucleosides as Novel Potent Cytostatic Agents. *Journal of Medicinal Chemistry* **2010,** *53* (1), 460-470.
60. Perlíková, P.; Pohl, R.; Votruba, I.; Shih, R.; Birkuš, G.; Cihlář, T.; Hocek, M., Phosphoramidate pronucleotides of cytostatic 6-aryl-7-deazapurine ribonucleosides. *Bioorganic & Medicinal Chemistry* **2011,** *19* (1), 229-242.
61. Sabat, N.; Smoleń, S.; Nauš, P.; Perlíková, P.; Cebová, M.; Poštová Slavětínská, L.; Hocek, M., Synthesis of 2,6-Substituted 7-(Het)aryl-7-deazapurine Nucleobases (2,4-Disubstituted 5-(Het)aryl-pyrrolo[2,3-d]pyrimidines). *Synthesis* **2017,** *49* (20), 4623-4650.
62. Seela, F.; Zulauf, M., Synthesis of 7-alkynylated 8-aza-7-deaza-2′-deoxyadenosines via the Pd-catalysed cross-coupling reaction. *Journal of the Chemical Society, Perkin Transactions 1* **1998,** (19), 3233-3240.
63. Zhao, H.; Leonard, P.; Guo, X.; Yang, H.; Seela, F., Silver-Mediated Base Pairs in DNA Incorporating Purines, 7-Deazapurines, and 8-Aza-7-deazapurines: Impact of Reduced Nucleobase Binding Sites and an Altered Glycosylation Position. *Chemistry – A European Journal* **2017,** *23* (23), 5529-5540.
64. Schweitzer, B. A.; Kool, E. T., Aromatic Nonpolar Nucleosides as Hydrophobic Isosteres of Pyrimidines and Purine Nucleosides. *The Journal of Organic Chemistry* **1994,** *59* (24), 7238-7242.
65. Chaudhuri, N. C.; Kool, E. T., An efficient method for the synthesis of aromatic C-nucleosides. *Tetrahedron Letters* **1995,** *36* (11), 1795-1798.
66. Guckian, K. M.; Morales, J. C.; Kool, E. T., Structure and Base Pairing Properties of a Replicable Nonpolar Isostere for Deoxyadenosine. *The Journal of Organic Chemistry* **1998,** *63* (26), 9652-9656.
67. Ren, X. F.; Schweitzer, B. A.; Sheils, C. J.; Kool, E. T., Formation of Stable DNA Loops by Incorporation of Nonpolar, Non-Hydrogen-Bonding Nucleoside Isosteres. *Angewandte Chemie International Edition* **1996,** *35* (7), 743-746.
68. Schweitzer, B. A.; Kool, E. T., Hydrophobic, Non-Hydrogen-Bonding Bases and Base Pairs in DNA. *Journal of the American Chemical Society* **1995,** *117* (7), 1863-1872.
69. Štambaský, J.; Hocek, M.; Kočovský, P., C-Nucleosides: Synthetic Strategies and Biological Applications. *Chemical Reviews* **2009,** *109* (12), 6729-6764.
70. Bag, S. S.; Talukdar, S.; Matsumoto, K.; Kundu, R., Triazolyl Donor/Acceptor Chromophore Decorated Unnatural Nucleosides and Oligonucleotides with Duplex Stability Comparable to That of a Natural Adenine/Thymine Pair. *The Journal of Organic Chemistry* **2013,** *78* (2), 278-291.
71. Teo, Y. N.; Kool, E. T., DNA-Multichromophore Systems. *Chemical Reviews* **2012,** *112* (7), 4221-4245.
72. Wojciechowski, F.; Lietard, J.; Leumann, C. J., 2-Pyrenyl-DNA: Synthesis, Pairing, and Fluorescence Properties. *Organic Letters* **2012,** *14* (20), 5176-5179.
73. Hawkins, M. E., Fluorescent pteridine nucleoside analogs: a window on DNA interactions. *Cell Biochemistry and Biophysics* **2001,** *34* (2), 257-281.

74. Hawkins, M. E., Fluorescent pteridine probes for nucleic acid analysis. *Methods in Enzymology* **2008,** *450*, 201-231.
75. Sinkeldam, R. W.; Greco, N. J.; Tor, Y., Fluorescent Analogs of Biomolecular Building Blocks: Design, Properties, and Applications. *Chemical Reviews* **2010,** *110* (5), 2579-2619.
76. Wilson, J. N.; Kool, E. T., Fluorescent DNA base replacements: reporters and sensors for biological systems. *Organic & Biomolecular Chemistry* **2006,** *4* (23), 4265-4274.
77. Rist, M. J.; Marino, J. P., Fluorescent Nucleotide Base Analogs as Probes of Nucleic Acid Structure, Dynamics and Interactions. *Current Organic Chemistry* **2002,** *6* (9), 775-793.
78. Srivatsan Seergazhi, G.; Sawant Anupam, A., Fluorescent ribonucleoside analogues as probes for investigating RNA structure and function. *Pure and Applied Chemistry*, **2010**, 83, 213-232.
79. Hall, K. B., 2-aminopurine as a probe of RNA conformational transitions. *Methods in Enzymology* **2009,** *469*, 269-285.
80. Cristofoli, W. A.; Wiebe, L. I.; De Clercq, E.; Andrei, G.; Snoeck, R.; Balzarini, J.; Knaus, E. E., 5-alkynyl analogs of arabinouridine and 2'-deoxyuridine: cytostatic activity against herpes simplex virus and varicella-zoster thymidine kinase gene-transfected cells. *Journal of Medicinal Chemistry* **2007,** *50* (12), 2851-2857.
81. Skorobogatyi, M. V.; Ustinov, A. V.; Stepanova, I. A.; Pchelintseva, A. A.; Petrunina, A. L.; Andronova, V. L.; Galegov, G. A.; Malakhov, A. D.; Korshun, V. A., 5-Arylethynyl-2'-deoxyuridines, compounds active against HSV-1. *Organic & Biomolecular Chemistry* **2006,** *4* (6), 1091-1096.
82. Guan, L.; van der Heijden, G. W.; Bortvin, A.; Greenberg, M. M., Intracellular detection of cytosine incorporation in genomic DNA by using 5-ethynyl-2'-deoxycytidine. *ChemBioChem* **2011,** *12* (14), 2184-2190.
83. Neef, A. B.; Luedtke, N. W., Dynamic metabolic labeling of DNA in vivo with arabinosyl nucleosides. *Proceedings of the National Academy of Sciences of the United States of America* **2011,** *108* (51), 20404-20409.
84. Salic, A.; Mitchison, T. J., A chemical method for fast and sensitive detection of DNA synthesis in vivo. *Proceedings of the National Academy of Sciences of the United States of America* **2008,** *105* (7), 2415-2420.
85. Kropinski, A. M.; Bose, R. J.; Warren, R. A., 5-(4-Aminobutylaminomethyl)uracil, an unusual pyrimidine from the deoxyribonucleic acid of bacteriophage phiW-14. *Biochemistry* **1973,** *12* (1), 151-157.
86. Takeda, T.; Ikeda, K.; Mizuno, Y.; Ueda, T., Synthesis and properties of deoxyoligonucleotides containing putrescinylthymine (nucleosides and nucleotides. LXXVI). *Chemical and Pharmaceutical Bulletin* **1987,** *35* (9), 3558-3567.
87. Hashimoto, H.; Nelson, M. G.; Switzer, C., Formation of chimeric duplexes between zwitterionic and natural DNA. *The Journal of Organic Chemistry* **1993,** *58* (16), 4194-4195.
88. Hashimoto, H.; Nelson, M. G.; Switzer, C., Zwitterionic DNA. *Journal of the American Chemical Society* **1993,** *115* (16), 7128-7134.
89. Nara, H.; Ono, A.; Matsuda, A., Nucleosides and Nucleotides. 135. DNA Duplex and Triplex formation and Resistance to Nucleolytic Degradation of Oligodeoxynucleotides Containing syn-Norspermidine at the 5-Position of 2'-Deoxyuridine. *Bioconjugate Chemistry* **1995,** *6* (1), 54-61.
90. Ito, T.; Ueno, Y.; Komatsu, Y.; Matsuda, A., Synthesis, thermal stability and resistance to enzymatic hydrolysis of the oligonucleotides containing 5-(N-aminohexyl)carbamoyl-2'-O-methyluridines. *Nucleic Acids Research* **2003,** *31* (10), 2514-2523.

91. Nakagawa, A.; Matsuda, A., Nucleosides and Nucleotides. 165. Chemical Ligation of Oligodeoxynucleotides Having a Mercapto Group at the 5-Position Of 2′-Deoxyuridine via a Disulfide Bond AU - Ueno, Yoshihito. *Nucleosides and Nucleotides* **1998,** *17* (1-3), 283-289.
92. Ozaki, H.; Mine, M.; Ogawa, Y.; Sawai, H., Effect of the terminal amino group of a linker arm and its length at the C5 position of a pyrimidine nucleoside on the thermal stability of DNA duplexes. *Bioorganic Chemistry* **2001,** *29* (4), 187-197.
93. Ozaki, H.; Mine, M.; Shinozuka, K.; Sawai, H., Effect of imino group of a linker arm at the C5 position of a pyrimidine nucleoside on the thermal stabilities of DNA/DNA and DNA/RNA duplexes. *Nucleosides, Nucleotides & Nucleic Acids* **2004,** *23* (1-2), 339-346.
94. Ozaki, H.; Nakamura, A.; Arai, M.; Endo, M.; Sawai, H., Novel C5-Substituted 2′-Deoxyuridine Derivatives Bearing Amino-Linker Arms: Synthesis, Incorporation into Oligodeoxyribonucleotides, and Their Hybridization Properties. *Bulletin of the Chemical Society of Japan* **1995,** *68* (7), 1981-1987.
95. Shinozuka, K.; Kohgo, S.; Ozaki, H.; Sawai, H., Multi-functionalization of oligodeoxynucleotide: a facile post-synthetic modification technique for the preparation of oligodeoxynucleotides with two different functional molecules. *Chemical Communications* **2000,** (1), 59-60.
96. Ohmichi, T.; Kuwahara, M.; Sasaki, N.; Hasegawa, M.; Nishikata, T.; Sawai, H.; Sugimoto, N., Nucleic acid with guanidinium modification exhibits efficient cellular uptake. *Angewandte Chemie International Edition* **2005,** *44* (41), 6682-6685.
97. Kuwahara, M.; Hanawa, K.; Ohsawa, K.; Kitagata, R.; Ozaki, H.; Sawai, H., Direct PCR amplification of various modified DNAs having amino acids: convenient preparation of DNA libraries with high-potential activities for in vitro selection. *Bioorganic & Medicinal Chemistry* **2006,** *14* (8), 2518-2526.
98. Kuwahara, M.; Nagashima, J.; Hasegawa, M.; Tamura, T.; Kitagata, R.; Hanawa, K.; Hososhima, S.; Kasamatsu, T.; Ozaki, H.; Sawai, H., Systematic characterization of 2'-deoxynucleoside- 5'-triphosphate analogs as substrates for DNA polymerases by polymerase chain reaction and kinetic studies on enzymatic production of modified DNA. *Nucleic Acids Research* **2006,** *34* (19), 5383-5394.
99. Nesbitt, S.; Hegg, L. A.; Fedor, M. J., An unusual pH-independent and metal-ion-independent mechanism for hairpin ribozyme catalysis. *Chemistry & Biology* **1997,** *4* (8), 619-630.
100. Sakthivel, K.; Barbas Iii, C. F., Expanding the Potential of DNA for Binding and Catalysis: Highly Functionalized dUTP Derivatives That Are Substrates for Thermostable DNA Polymerases. *Angewandte Chemie International Edition* **1998,** *37* (20), 2872-2875.
101. Hollenstein, M., Synthesis of Deoxynucleoside Triphosphates that Include Proline, Urea, or Sulfonamide Groups and Their Polymerase Incorporation into DNA. *Chemistry – A European Journal* **2012,** *18* (42), 13320-13330.
102. Ardhapure, A. V.; Sanghvi, Y. S.; Kapdi, A. R.; García, J.; Sanchez, G.; Lozano, P.; Serrano, J. L., Pd–imidate complexes as recyclable catalysts for the synthesis of C5-alkenylated pyrimidine nucleosides via Heck cross-coupling reaction. *RSC Advances* **2015,** *5* (31), 24558-24563.
103. Bhilare, S.; Gayakhe, V.; Ardhapure, A. V.; Sanghvi, Y. S.; Schulzke, C.; Borozdina, Y.; Kapdi, A. R., Novel water-soluble phosphatriazenes: versatile ligands for Suzuki–Miyaura, Sonogashira and Heck reactions of nucleosides. *RSC Advances* **2016,** *6* (87), 83820-83830.
104. Brazier, J. A.; Shibata, T.; Townsley, J.; Taylor, B. F.; Frary, E.; Williams, N. H.; Williams, D. M., Amino-functionalized DNA: the properties of C5-amino-alkyl

substituted 2'-deoxyuridines and their application in DNA triplex formation. *Nucleic Acids Research* **2005,** *33* (4), 1362-1371.
105. Kapdi, A. R.; Ardhapure, A.; Sanghvi, Y. S., Modulation of the Electronic Properties of Non-innocent (E,E)-Dibenzylideneacetone for Palladium(0)-Mediated Heck Alkenylation of 5-Iodo-2′-deoxyuridine and Scale-Up Studies. *Synthesis* **2015,** *47* (08), 1163-1169.
106. Lee, S. E.; Sidorov, A.; Gourlain, T.; Mignet, N.; Thorpe, S. J.; Brazier, J. A.; Dickman, M. J.; Hornby, D. P.; Grasby, J. A.; Williams, D. M., Enhancing the catalytic repertoire of nucleic acids: a systematic study of linker length and rigidity. *Nucleic Acids Research* **2001,** *29* (7), 1565-1573.
107. Ogino, M.; Taya, Y.; Fujimoto, K., Detection of methylcytosine by DNA photoligation via hydrophobic interaction of the alkyl group. *Organic & Biomolecular Chemistry* **2009,** *7* (15), 3163-3167.
108. Zhou, C.; Avins, J. L.; Klauser, P. C.; Brandsen, B. M.; Lee, Y.; Silverman, S. K., DNA-Catalyzed Amide Hydrolysis. *Journal of the American Chemical Society* **2016,** *138* (7), 2106-2109.
109. Froehler, B. C.; Wadwani, S.; Terhorst, T. J.; Gerrard, S. R., Oligodeoxynucleotides containing C-5 propyne analogs of 2′-deoxyuridine and 2′-deoxycytidine. *Tetrahedron Letters* **1992,** *33* (37), 5307-5310.
110. Wagner, R. W.; Matteucci, M. D.; Grant, D.; Huang, T.; Froehler, B. C., Potent and selective inhibition of gene expression by an antisense heptanucleotide. *Nature Biotechnology* **1996,** *14* (7), 840-844.
111. Wagner, R. W.; Matteucci, M. D.; Lewis, J. G.; Gutierrez, A. J.; Moulds, C.; Froehler, B. C., Antisense gene inhibition by oligonucleotides containing C-5 propyne pyrimidines. *Science* **1993,** *260* (5113), 1510-1513.
112. Barnes, T. W., 3rd; Turner, D. H., Long-range cooperativity in molecular recognition of RNA by oligodeoxynucleotides with multiple C5-(1-propynyl) pyrimidines. *Journal of the American Chemical Society* **2001,** *123* (18), 4107-4118.
113. Barnes, T. W., 3rd; Turner, D. H., Long-range cooperativity due to C5-propynylation of oligopyrimidines enhances specific recognition by uridine of ribo-adenosine over ribo-guanosine. *Journal of the American Chemical Society* **2001,** *123* (37), 9186-9187.
114. Kottysch, T.; Ahlborn, C.; Brotzel, F.; Richert, C., Stabilizing or Destabilizing Oligodeoxynucleotide Duplexes Containing Single 2′-Deoxyuridine Residues with 5-Alkynyl Substituents. *Chemistry – A European Journal* **2004,** *10* (16), 4017-4028.
115. Borsenberger, V.; Kukwikila, M.; Howorka, S., Synthesis and enzymatic incorporation of modified deoxyuridine triphosphates. *Organic & Biomolecular Chemistry* **2009,** *7* (18), 3826-3835.
116. Bhat, B.; Leonard, N. J.; Robinson, H.; Wang, A. H. J., Deoxyadenosine and Thymidine Bases Held Proximal and Distal by Means of a Covalently-Linked Dimensional Analogue of dA·dT: Intramolecular vs Intermolecular Hydrogen Bonding1. *Journal of the American Chemical Society* **1996,** *118* (44), 10744-10751.
117. Devadas, B.; Leonard, N. J., Synthesis of covalently-linked DNA/RNA cross sections. *Journal of the American Chemical Society* **1986,** *108* (16), 5012-5014.
118. Harwood, E. A.; Sigurdsson, S. T.; Edfeldt, N. B. F.; Reid, B. R.; Hopkins, P. B., Chemical Synthesis and Preliminary Structural Characterization of a Nitrous Acid Interstrand Cross-Linked Duplex DNA. *Journal of the American Chemical Society* **1999,** *121* (21), 5081-5082.
119. Murata, S.; Mizumura, Y.; Hino, K.; Ueno, Y.; Ichikawa, S.; Matsuda, A., Modular Bent DNAs: A New Class of Artificial DNAs with a Protein Binding Ability. *Journal of the American Chemical Society* **2007,** *129* (34), 10300-10301.

120. Nagatsugi, F.; Uemura, K.; Nakashima, S.; Maeda, M.; Sasaki, S., 2-Aminopurine derivatives with C6-substituted olefin as novel cross-linking agents and the synthesis of the corresponding β-phosphoramidite precursors. *Tetrahedron* **1997,** *53* (9), 3035-3044.
121. Noll, D. M.; Mason, T. M.; Miller, P. S., Formation and Repair of Interstrand Cross-Links in DNA. *Chemical Reviews* **2006,** *106* (2), 277-301.
122. Swenson, M. C.; Paranawithana, S. R.; Miller, P. S.; Kielkopf, C. L., Structure of a DNA Repair Substrate Containing an Alkyl Interstrand Cross-Link at 1.65 Å Resolution. *Biochemistry* **2007,** *46* (15), 4545-4553.
123. Wu, X.; Cooperman, B. S., Synthesis and biological activity of a bivalent nucleotide inhibitor of ribonucleotide reductase. *Bioorganic & Medicinal Chemistry Letters* **2000,** *10* (20), 2387-2389.
124. Velazquez, S.; Tunon, V.; Jimeno, M. L.; Chamorro, C.; De Clercq, E.; Balzarini, J.; Camarasa, M. J., Potential multifunctional inhibitors of HIV-1 reverse transcriptase. Novel [AZT]-[TSAO-T] and [d4T]-[TSAO-T] heterodimers modified in the linker and in the dideoxynucleoside region. *Journal of Medicinal Chemistry* **1999,** *42* (25), 5188-5196.
125. Mehl, R. A.; Begley, T. P., Mechanistic Studies on the Repair of a Novel DNA Photolesion: The Spore Photoproduct. *Organic Letters* **1999,** *1* (7), 1065-1066.
126. Sessler, J. L.; Jayawickramarajah, J.; Sathiosatham, M.; Sherman, C. L.; Brodbelt, J. S., Novel Guanosine−Cytidine Dinucleoside that Self-Assembles into a Trimeric Supramolecule. *Organic Letters* **2003,** *5* (15), 2627-2630.
127. Stanley, K.; Zemlicka, J., Simple models of nucleic acid interactions. 6. Synthesis and base-base interactions of 1-(adenosin-N6-yl)-2-(cytidin-N4-yl)ethane and 1-(adenosin-N6-yl)-2-(cytidin-N4-yl)butane. *The Journal of Organic Chemistry* **1980,** *45* (13), 2704-2708.
128. Crisp, G. T.; Jiang, Y.-L., Intramolecular hydrogen bonding of nucleobases. *Tetrahedron Letters* **2002,** *43* (17), 3157-3160.
129. Seela, F.; Sirivolu, V. R., Nucleosides and Oligonucleotides with Diynyl Side Chains: Base Pairing and Functionalization of 2′-Deoxyuridine Derivatives by the Copper(I)-Catalyzed Alkyne□Azide 'Click' Cycloaddition. *Helvetica Chimica Acta* **2007,** *90* (3), 535-552.
130. Sniady, A.; Sevilla, M. D.; Meneni, S.; Lis, T.; Szafert, S.; Khanduri, D.; Finke, J. M.; Dembinski, R., Synthesis and EPR Studies of 2′-Deoxyuridines with Alkynyl, Rodlike Linkages. *Chemistry – A European Journal* **2009,** *15* (31), 7569-7577.
131. Yang, H.; Seela, F., Circular DNA by "Bis-Click" Ligation: Template-Independent Intramolecular Circularization of Oligonucleotides with Terminal Alkynyl Groups Utilizing Bifunctional Azides. *Chemistry – A European Journal* **2016,** *22* (4), 1435-1444.
132. Prusoff, W. H.; Lin, T.-S.; Zucker, M., Potential targets for antiviral chemotherapy. *Antiviral Research* **1986,** *6* (6), 311-328.
133. Galasso, G. J.; Whitley, R. J.; Merigan, T. C., *Antiviral agents and viral diseases of man*. Raven Press: New York, **1997**.
134. De Clercq, E., Antivirals: Past, present and future. *Biochemical Pharmacology* **2013,** *85* (6), 727-744.
135. Black, D. J.; Livingston, R. B., Antineoplastic Drugs in 1990. *Drugs* **1990,** *39* (4), 489-501.
136. Wilman, D. E. V., *The chemistry of antitumor agents*. Blackie ; Chapman and Hall: Glasgow; New York, 1990.
137. Ninomiya, Y.; Miwa, M.; Eda, H.; Sahara, H.; Fujimoto, K.; Ishida, M.; Umeda, I.; Yokose, K.; Ishitsuka, H., Comparative antitumor activity and intestinal toxicity of 5'-

deoxy-5-fluorouridine and its prodrug trimethoxybenzoyl-5'-deoxy-5-fluorocytidine. *Japanese Journal of Cancer Research* **1990,** *81* (2), 188-195.
138. Sagi, J.; Szabolcs, A.; Szemzo, A.; Otvos, L., Modified polynucleotides. VII. Impaired integrity of a synthetic DNA containing the antiherpetic agent 5-isopropyl-2'-deoxyuridine. *Nucleic Acids Research* **1986,** *14* (8), 3449-3462.
139. Nomura, M.; Shuto, S.; Matsuda, A., Synthesis of the cyclic and acyclic acetal derivatives of 1-(3-C-Ethynyl-β-d-ribo-pentofuranosyl)cytosine, a potent antitumor nucleoside. Design of prodrugs to be selectively activated in tumor tissues via the bio-Reduction–Hydrolysis mechanism. *Bioorganic & Medicinal Chemistry* **2003,** *11* (11), 2453-2461.
140. Fan, X.; Zhang, X.; Zhou, L.; Keith, K. A.; Kern, E. R.; Torrence, P. F., 5-(Dimethoxymethyl)-2‘-Deoxyuridine: A Novel Gem Diether Nucleoside with Anti-Orthopoxvirus Activity. *Journal of Medicinal Chemistry* **2006,** *49* (11), 3377-3382.
141. El Safadi, Y.; Paillart, J.-C.; Laumond, G.; Aubertin, A.-M.; Burger, A.; Marquet, R.; Vivet-Boudou, V., 5-Modified-2′-dU and 2′-dC as Mutagenic Anti HIV-1 Proliferation Agents: Synthesis and Activity. *Journal of Medicinal Chemistry* **2010,** *53* (4), 1534-1545.
142. Meneni, S.; Ott, I.; Sergeant, C. D.; Sniady, A.; Gust, R.; Dembinski, R., 5-Alkynyl-2′-deoxyuridines: Chromatography-free synthesis and cytotoxicity evaluation against human breast cancer cells. *Bioorganic & Medicinal Chemistry* **2007,** *15* (8), 3082-3088.
143. Cristofoli, W. A.; Wiebe, L. I.; De Clercq, E.; Andrei, G.; Snoeck, R.; Balzarini, J.; Knaus, E. E., 5-Alkynyl Analogs of Arabinouridine and 2‘-Deoxyuridine: Cytostatic Activity against Herpes Simplex Virus and Varicella-Zoster Thymidine Kinase Gene-Transfected Cells. *Journal of Medicinal Chemistry* **2007,** *50* (12), 2851-2857.
144. Andronova, V. L.; Skorobogatyi, M. V.; Manasova, E. V.; Berlin, Y. A.; Korshun, V. A.; Galegov, G. A., Antiviral Activity of Some 2'-Deoxyuridine 5-Arylethynyl Derivatives. *Russian Journal of Bioorganic Chemistry* **2003,** *29* (3), 262-266.
145. Skorobogatyi, M. V.; Pchelintseva, A. A.; Petrunina, A. L.; Stepanova, I. A.; Andronova, V. L.; Galegov, G. A.; Malakhov, A. D.; Korshun, V. A., 5-Alkynyl-2′-deoxyuridines, containing bulky aryl groups: evaluation of structure–anti-HSV-1 activity relationship. *Tetrahedron* **2006,** *62* (6), 1279-1287.
146. Lee, Y.-S.; Park, S. M.; Kim, H. M.; Park, S.-K.; Lee, K.; Lee, C. W.; Kim, B. H., C5-Modified nucleosides exhibiting anticancer activity. *Bioorganic & Medicinal Chemistry Letters* **2009,** *19* (16), 4688-4691.
147. Park, S. M.; Yang, H.; Park, S.-K.; Kim, H. M.; Kim, B. H., Design, synthesis, and anticancer activities of novel perfluoroalkyltriazole-appended 2′-deoxyuridines. *Bioorganic & Medicinal Chemistry Letters* **2010,** *20* (19), 5831-5834.
148. Shmalenyuk, E. R.; Chernousova, L. N.; Karpenko, I. L.; Kochetkov, S. N.; Smirnova, T. G.; Andreevskaya, S. N.; Chizhov, A. O.; Efremenkova, O. V.; Alexandrova, L. A., Inhibition of Mycobacterium tuberculosis strains H37Rv and MDR MS-115 by a new set of C5 modified pyrimidine nucleosides. *Bioorganic & Medicinal Chemistry* **2013,** *21* (17), 4874-4884.
149. Shmalenyuk, E. R.; Karpenko, I. L.; Chernousova, L. N.; Chizhov, A. O.; Smirnova, T. G.; Andreevskaya, S. N.; Alexandrova, L. A., New 5-modified 2′-deoxyuridine derivatives: synthesis and antituberculosis activity. *Russian Chemical Bulletin* **2014,** *63* (5), 1197-1200.
150. Ehrenschwender, T.; Wagenknecht, H. A., 4,4-Difluoro-4-bora-3a,4a-diaza-s-indacene as a bright fluorescent label for DNA. *Journal of Organic Chemistry* **2011,** *76* (7), 2301-2304.
151. Grigorenko, N. A.; Leumann, C. J., Electron transfer through a stable phenanthrenyl pair in DNA. *Chemical Communications* **2008,** (42), 5417-5419.

152. Ikeda, S.; Kubota, T.; Wang, D. O.; Yanagisawa, H.; Umemoto, T.; Okamoto, A., Design and synthesis of caged fluorescent nucleotides and application to live-cell RNA imaging. *ChemBioChem* **2011,** *12* (18), 2871-2880.
153. Okamoto, A.; Sugizaki, K.; Yuki, M.; Yanagisawa, H.; Ikeda, S.; Sueoka, T.; Hayashi, G.; Wang, D. O., A nucleic acid probe labeled with desmethyl thiazole orange: a new type of hybridization-sensitive fluorescent oligonucleotide for live-cell RNA imaging. *Organic & Biomolecular Chemistry* **2013,** *11* (2), 362-371.
154. Saito, Y.; Motegi, K.; Bag, S. S.; Saito, I., Anthracene based base-discriminating fluorescent oligonucleotide probes for SNPs typing: synthesis and photophysical properties. *Bioorganic & Medicinal Chemistry* **2008,** *16* (1), 107-113.
155. Tainaka, K.; Tanaka, K.; Ikeda, S.; Nishiza, K.-i.; Unzai, T.; Fujiwara, Y.; Saito, I.; Okamoto, A., PRODAN-Conjugated DNA: Synthesis and Photochemical Properties. *Journal of the American Chemical Society* **2007,** *129* (15), 4776-4784.
156. Dierckx, A.; Diner, P.; El-Sagheer, A. H.; Kumar, J. D.; Brown, T.; Grotli, M.; Wilhelmsson, L. M., Characterization of photophysical and base-mimicking properties of a novel fluorescent adenine analogue in DNA. *Nucleic Acids Research* **2011,** *39* (10), 4513-4524.
157. Dumas, A.; Luedtke, N. W., Cation-mediated energy transfer in G-quadruplexes revealed by an internal fluorescent probe. *Journal of the American Chemical Society* **2010,** *132* (51), 18004-18007.
158. Guo, P.; Xu, X.; Qiu, X.; Zhou, Y.; Yan, S.; Wang, C.; Lu, C.; Ma, W.; Weng, X.; Zhang, X.; Zhou, X., Synthesis and spectroscopic properties of fluorescent 5-benzimidazolyl-2'-deoxyuridines 5-fdU probes obtained from o-phenylenediamine derivatives. *Organic and Biomolecular Chemistry* **2013,** *11* (10), 1610-1613.
159. Hirose, W.; Sato, K.; Matsuda, A., Selective detection of 5-formyl-2'-deoxyuridine, an oxidative lesion of thymidine, in DNA by a fluorogenic reagent. *Angewandte Chemie International Edition* **2010,** *49* (45), 8392-8394.
160. Kimoto, M.; Mitsui, T.; Harada, Y.; Sato, A.; Yokoyama, S.; Hirao, I., Fluorescent probing for RNA molecules by an unnatural base-pair system. *Nucleic Acids Research* **2007,** *35* (16), 5360-5369.
161. Krim, J.; Grunewald, C.; Taourirte, M.; Engels, J. W., Efficient microwave-assisted synthesis, antibacterial activity and high fluorescence of 5 benzimidazolyl-2'-deoxyuridines. *Bioorganic & Medicinal Chemistry* **2012,** *20* (1), 480-486.
162. Saito, Y.; Miyamoto, S.; Suzuki, A.; Matsumoto, K.; Ishihara, T.; Saito, I., Fluorescent nucleosides with 'on-off' switching function, pH-responsive fluorescent uridine derivatives. *Bioorganic & Medicinal Chemistry Letters* **2012,** *22* (8), 2753-2756.
163. Suzuki, A.; Takahashi, N.; Okada, Y.; Saito, I.; Nemoto, N.; Saito, Y., Naphthalene-based environmentally sensitive fluorescent 8-substituted 2'-deoxyadenosines: application to DNA detection. *Bioorganic & Medicinal Chemistry Letters* **2013,** *23* (3), 886-892.
164. Amann, N.; Wagenknecht, H.-A., Preparation of Pyrenyl-Modified Nucleosides via Suzuki-Miyaura Cross-Coupling Reactions. *Synlett* **2002,** *2002* (05), 0687-0691.
165. Kaden, P.; Mayer-Enthart, E.; Trifonov, A.; Fiebig, T.; Wagenknecht, H. A., Real-time spectroscopic and chemical probing of reductive electron transfer in DNA. *Angewandte Chemie International Edition* **2005,** *44* (11), 1636-1639.
166. Mayer-Enthart, E.; Wagenknecht, H. A., Structure-sensitive and self-assembled helical pyrene array based on DNA architecture. *Angewandte Chemie International Edition* **2006,** *45* (20), 3372-3375.

167. Wagner, C.; Wagenknecht, H.-A., Reductive Electron Transfer in Phenothiazine-Modified DNA Is Dependent on the Base Sequence. *Chemistry – A European Journal* **2005,** *11* (6), 1871-1876.
168. Ehrenschwender, T.; Liang, Y.; Unterreiner, A.-N.; Wagenknecht, H.-A.; Wolf, T. J. A., Fluorescence Quenching over Short Range in a Donor-DNA-Acceptor System. *ChemPhysChem* **2013,** *14* (6), 1197-1204.
169. Greco, N. J.; Tor, Y., Simple fluorescent pyrimidine analogues detect the presence of DNA abasic sites. *Journal of the American Chemical Society* **2005,** *127* (31), 10784-10785.
170. Greco, N. J.; Tor, Y., Furan Decorated Nucleoside Analogues as Fluorescent Probes: synthesis, photophysical evaluation and site-specific incorporation. *Tetrahedron* **2007,** *63* (17), 3515-3527.
171. Sinkeldam, R. W.; Marcus, P.; Uchenik, D.; Tor, Y., Multisensing emissive pyrimidine. *Chemphyschem* **2011,** *12* (12), 2260-2265.
172. Tanpure, A. A.; Srivatsan, S. G., Conformation-sensitive nucleoside analogues as topology-specific fluorescence turn-on probes for DNA and RNA G-quadruplexes. *Nucleic Acids Research* **2015,** *43* (22), e149.
173. Anensen, H.; Provan, F.; Lian, A. T.; Reinertsen, S. H.; Ueno, Y.; Matsuda, A.; Seeberg, E.; Bjelland, S., Mutations induced by 5-formyl-2'-deoxyuridine in Escherichia coli include base substitutions that can arise from mispairs of 5-formyluracil with guanine, cytosine and thymine. *Mutation Research* **2001,** *476* (1-2), 99-107.
174. Jacobsen, M. F.; Ferapontova, E. E.; Gothelf, K. V., Synthesis and electrochemical studies of an anthraquinone-conjugated nucleoside and derived oligonucleotides. *Organic & Biomolecular Chemistry* **2009,** *7* (5), 905-908.
175. Park, S. M.; Nam, S. J.; Jeong, H. S.; Kim, W. J.; Kim, B. H., The effects of the 4-(4-Methylpiperazine)phenyl group on nucleosides and oligonucleotides: cellular delivery, detection, and stability. *Chemistry – An Asian Journal* **2011,** *6* (2), 487-492.
176. Bag, S. S.; Pradhan, M. K.; Das, S. K.; Jana, S.; Bag, R., Wavelength shifting oligonucleotide probe for the detection of adenosine of a target DNA with enhanced fluorescence signal. *Bioorganic & Medicinal Chemistry Letters* **2014,** *24* (19), 4678-4681.
177. Guo, L.; Okamoto, A., Fluorescence-switching RNA for detection of bacterial ribosomes. *Chemical Communications* **2017,** *53* (68), 9406-9409.
178. Hayashi, G.; Yanase, M.; Takeda, K.; Sakakibara, D.; Sakamoto, R.; Wang, D. O.; Okamoto, A., Hybridization-sensitive fluorescent oligonucleotide probe conjugated with a bulky module for compartment-specific mRNA monitoring in a living cell. *Bioconjugate Chemistry* **2015,** *26* (3), 412-417.
179. Ikeda, S.; Kubota, T.; Kino, K.; Okamoto, A., Sequence Dependence of Fluorescence Emission and Quenching of Doubly Thiazole Orange Labeled DNA: Effective Design of a Hybridization-Sensitive Probe. *Bioconjugate Chemistry* **2008,** *19* (8), 1719-1725.
180. Ikeda, S.; Okamoto, A., Hybridization-sensitive on-off DNA probe: application of the exciton coupling effect to effective fluorescence quenching. *Chemistry – An Asian Journal* **2008,** *3* (6), 958-968.
181. Kubota, T.; Ikeda, S.; Okamoto, A., Intracellular mRNA imaging with a hybridization sensitive fluorescent nucleotide. *Nucleic Acids Symposium Series* **2008,** (52), 355-356.
182. Kubota, T.; Ikeda, S.; Yanagisawa, H.; Yuki, M.; Okamoto, A., Sets of RNA repeated tags and hybridization-sensitive fluorescent probes for distinct images of RNA in a living cell. *PloS one* **2010,** *5* (9), e13003.
183. Okamoto, A.; Sugizaki, K.; Yuki, M.; Yanagisawa, H.; Ikeda, S.; Sueoka, T.; Hayashi, G.; Wang, D. O., A nucleic acid probe labeled with desmethyl thiazole orange: a new

type of hybridization-sensitive fluorescent oligonucleotide for live-cell RNA imaging. *Organic & Biomolecular Chemistry* **2013,** *11* (2), 362-371.
184. Oomoto, I.; Suzuki-Hirano, A.; Umeshima, H.; Han, Y. W.; Yanagisawa, H.; Carlton, P.; Harada, Y.; Kengaku, M.; Okamoto, A.; Shimogori, T.; Wang, D. O., ECHO-liveFISH: in vivo RNA labeling reveals dynamic regulation of nuclear RNA foci in living tissues. *Nucleic Acids Research* **2015,** *43* (19), e126.
185. Shin, H. S.; Okamoto, A.; Sako, Y.; Kim, S. W.; Kim, S. Y.; Pack, C. G., Characterization of the triplet state of hybridization-sensitive DNA probe by using fluorescence correlation spectroscopy. *The Journal of Physical Chemistry A* **2013,** *117* (1), 27-33.
186. Wang, D. O.; Matsuno, H.; Ikeda, S.; Nakamura, A.; Yanagisawa, H.; Hayashi, Y.; Okamoto, A., A quick and simple FISH protocol with hybridization-sensitive fluorescent linear oligodeoxynucleotide probes. *RNA* **2012,** *18* (1), 166-175.
187. Okamoto, A.; Kamei, T.; Saito, I., DNA hole transport on an electrode: application to effective photoelectrochemical SNP typing. *Journal of the American Chemical Society* **2006,** *128* (2), 658-662.
188. Okamoto, A.; Kamei, T.; Tanaka, K.; Saito, I., Photostimulated Hole Transport through a DNA Duplex Immobilized on a Gold Electrode. *Journal of the American Chemical Society* **2004,** *126* (45), 14732-14733.
189. Kaji, T.; Ito, S.; Iwai, S.; Miyasaka, H., Nanosecond to Submillisecond Dynamics in Dye-Labeled Single-Stranded DNA, As Revealed by Ensemble Measurements and Photon Statistics at Single-Molecule Level. *The Journal of Physical Chemistry B* **2009,** *113* (42), 13917-13925.
190. Rindermann, J. J.; Akhtman, Y.; Richardson, J.; Brown, T.; Lagoudakis, P. G., Gauging the Flexibility of Fluorescent Markers for the Interpretation of Fluorescence Resonance Energy Transfer. *Journal of the American Chemical Society* **2011,** *133* (2), 279-285.
191. Toga, T.; Kuraoka, I.; Watanabe, S.; Nakano, E.; Takeuchi, S.; Nishigori, C.; Sugasawa, K.; Iwai, S., Fluorescence detection of cellular nucleotide excision repair of damaged DNA. *Scientific Reports* **2014,** *4*, 5578.
192. Liu, P.; Sun, S.; Guo, X.; Yang, X.; Huang, J.; Wang, K.; Wang, Q.; Liu, J.; He, L., Competitive host-guest interaction between beta-cyclodextrin polymer and pyrene-labeled probes for fluorescence analyses. *Analytical Chemistry* **2015,** *87* (5), 2665-2671.
193. Okamoto, A.; Tainaka, K.; Nishiza, K.; Saito, I., Monitoring DNA structures by dual fluorescence of pyrene derivatives. *Journal of the American Chemical Society* **2005,** *127* (38), 13128-13129.
194. Okamoto, A.; Tainaka, K.; Ochi, Y.; Kanatani, K.; Saito, I., Simple SNP typing assay using a base-discriminating fluorescent probe. *Molecular BioSystems* **2006,** *2* (2), 122-127.
195. Saito, Y.; Miyauchi, Y.; Okamoto, A.; Saito, I., Synthesis and properties of novel base-discriminating fluorescent (BDF) nucleosides: a highly polarity-sensitive fluorophore for SNP typing. *Tetrahedron Letters* **2004,** *45* (42), 7827-7831.
196. Hurley, D. J.; Seaman, S. E.; Mazura, J. C.; Tor, Y., Fluorescent 1,10-Phenanthroline-Containing Oligonucleotides Distinguish between Perfect and Mismatched Base Pairing. *Organic Letters* **2002,** *4* (14), 2305-2308.
197. Hurley, D. J.; Tor, Y., Ru(II) and Os(II) Nucleosides and Oligonucleotides: Synthesis and Properties. *Journal of the American Chemical Society* **2002,** *124* (14), 3749-3762.
198. Joshi, H. S.; Tor, Y., Metal-containing DNA hairpins as hybridization probes. *Chemical Communications* **2001,** (6), 549-550.

199. Hwang, G. T.; Seo, Y. J.; Kim, B. H., A highly discriminating quencher-free molecular beacon for probing DNA. *Journal of the American Chemical Society* **2004,** *126* (21), 6528-6529.
200. Hwang, G. T.; Seo, Y. J.; Kim, B. H., Pyrene-labeled deoxyuridine and deoxyadenosine: fluorescent discriminating phenomena in their oligonucleotides. *Tetrahedron Letters* **2005,** *46* (9), 1475-1477.
201. Hwang, G. T.; Seo, Y. J.; Kim, S. J.; Kim, B. H., Fluorescent oligonucleotide incorporating 5-(1-ethynylpyrenyl)-2′-deoxyuridine: sequence-specific fluorescence changes upon duplex formation. *Tetrahedron Letters* **2004,** *45* (18), 3543-3546.
202. Venkatesan, N.; Seo, Y.-J.; Bang, E.-K.; Park, S.-M.; Lee, Y.-S.; Kim, B.-H., Chemical Modification of Nucleic Acids toward Functional Nucleic Acid Systems. *Bulletin of the Korean Chemical Society* **2006,** *27* (5), 613-630.
203. Barrois, S.; Beyer, C.; Wagenknecht, H.-A., Covalent Modification of 2′-Deoxyuridine with Two Different Molecular Switches. *Synlett* **2012,** *23* (05), 711-716.
204. Barrois, S.; Wagenknecht, H. A., Diarylethene-modified nucleotides for switching optical properties in DNA. *Beilstein Journal of Organic Chemistry* **2012,** *8*, 905-914.
205. Ensslen, P.; Fritz, Y.; Wagenknecht, H. A., Mixed non-covalent assemblies of ethynyl nile red and ethynyl pyrene along oligonucleotide templates. *Organic and Biomolecular Chemistry* **2015,** *13* (2), 487-492.
206. Gavvala, K.; Barthes, N. P. F.; Bonhomme, D.; Dabert-Gay, A. S.; Debayle, D.; Michel, B. Y.; Burger, A.; Mély, Y., A turn-on dual emissive nucleobase sensitive to mismatches and duplex conformational changes. *RSC Advances* **2016,** *6* (90), 87142-87146.
207. Bag, S. S.; Kundu, R.; Matsumoto, K.; Saito, Y.; Saito, I., Singly and doubly labeled base-discriminating fluorescent oligonucleotide probes containing oxo-pyrene chromophore. *Bioorganic & Medicinal Chemistry Letters* **2010,** *20* (11), 3227-3230.
208. James, T. D.; Samankumara Sandanayake, K. R. A.; Shinkai, S., Chiral discrimination of monosaccharides using a fluorescent molecular sensor. *Nature* **1995,** *374* (6520), 345-347.
209. Mahal, L. K.; Yarema, K. J.; Bertozzi, C. R., Engineering chemical reactivity on cell surfaces through oligosaccharide biosynthesis. *Science* **1997,** *276* (5315), 1125-1128.
210. Scrafton, D. K.; Taylor, J. E.; Mahon, M. F.; Fossey, J. S.; James, T. D., "Click-fluors": Modular fluorescent saccharide sensors based on a 1,2,3-triazole ring. *Journal of Organic Chemistry* **2008,** *73* (7), 2871-2874.
211. Sun, X.; Zhai, W.; Fossey, J. S.; James, T. D., Boronic acids for fluorescence imaging of carbohydrates. *Chemical Communications* **2016,** *52* (17), 3456-3469.
212. Wang, Y. E.; Rong, R. X.; Chen, H.; Zhu, M. Y.; Wang, B. H.; Li, X. L., Synthesis of fluorescent bisboronic acid sensors and their recognition of mono-/oligo-saccharides. *Chinese Chemical Letters* **2017,** *28* (6), 1262-1267.
213. Yarema, K. J.; Mahal, L. K.; Bruehl, R. E.; Rodriguez, E. C.; Bertozzi, C. R., Metabolic delivery of ketone groups to sialic acid residues. Application To cell surface glycoform engineering. *Journal of Biological Chemistry* **1998,** *273* (47), 31168-31179.
214. Beld, J.; Cang, H.; Burkart, M. D., Visualizing the chain-flipping mechanism in fatty-acid biosynthesis. *Angewandte Chemie International Edition* **2014,** *53* (52), 14456-14461.
215. Faggiano, S.; Ronda, L.; Raboni, S.; Sartor, F.; Cavatorta, V.; Sgarbi, E.; Caivano, G.; Pertile, M.; Mozzarelli, A., Phospholipid components of the synthetic pulmonary surfactant CHF5633 probed by fluorescence spectroscopy. *International Journal of Pharmaceutics* **2018,** *553* (1-2), 290-297.

216. Ibrahim, H.; Jurcic, K.; Wang, J. S.; Whitehead, S. N.; Yeung, K. K., 1,6-Diphenyl-1,3,5-hexatriene (DPH) as a Novel Matrix for MALDI MS Imaging of Fatty Acids, Phospholipids, and Sulfatides in Brain Tissues. *Analytical Chemistry* **2017,** *89* (23), 12828-12836.
217. Obsil, T.; Amler, E.; Obsilova, V.; Pavlicek, Z., Effect of aminophospholipid glycation on order parameter and hydration of phospholipid bilayer. *Biophysical Chemistry* **1999,** *80* (3), 165-177.
218. Silva, J. P. N.; Oliveira, M. E. C. D. R.; Coutinho, P. J. G., Characterization of mixed DODAB/monoolein aggregates using Nile Red as a solvatochromic and anisotropy fluorescent probe. *Journal of Photochemistry and Photobiology A: Chemistry* **2009,** *203* (1), 32-39.
219. Bag, S. S.; De, S., Multipurpose isothiocyanyl alanine/lysine: Use as solvatochromic IR probes and in site specific labeling/ligation of short peptides. *Bioorganic & Medicinal Chemistry Letters* **2018,** *28* (8), 1404-1409.
220. Chen, L.; Li, J.; Du, L.; Li, M., Strategies in the design of small-molecule fluorescent probes for peptidases. *Medicinal Research Reviews* **2014,** *34* (6), 1217-1241.
221. Harkiss, A. H.; Sutherland, A., Recent advances in the synthesis and application of fluorescent alpha-amino acids. *Organic and Biomolecular Chemistry* **2016,** *14* (38), 8911-8921.
222. Krueger, A. T.; Imperiali, B., Fluorescent amino acids: modular building blocks for the assembly of new tools for chemical biology. *ChemBioChem* **2013,** *14* (7), 788-799.
223. Jordheim, L. P.; Durantel, D.; Zoulim, F.; Dumontet, C., Advances in the development of nucleoside and nucleotide analogues for cancer and viral diseases. *Nature Reviews Drug Discovery* **2013,** *12* (6), 447-464.
224. Johnson, Z. L.; Lee, J. H.; Lee, K.; Lee, M.; Kwon, D. Y.; Hong, J.; Lee, S. Y., Structural basis of nucleoside and nucleoside drug selectivity by concentrative nucleoside transporters. *eLife* **2014,** *3*, e03604.
225. Bag, S. S.; Das, S. K.; Gogoi, H., Design of a fused triazolyl 2-quinolinone unnatural nucleoside via tandem CuAAC-Ullmann coupling reaction and study of photophysical property. *Tetrahedron* **2018,** *74* (18), 2218-2229.
226. Bag, S. S.; Pradhan, M. K.; Talukdar, S., Trifunctional fluorescent unnatural nucleoside: Label free detection of T-T/C-C base mismatches, abasic site and bulge DNA. *Journal of Photochemistry and Photobiology B: Biology* **2017,** *173*, 165-169.
227. Bag, S. S.; Pradhan, M. K.; Talukdar, S., Tetrazolylpyrene unnatural nucleoside as a human telomeric multimeric G-quadruplex selective switch-on fluorescent sensor. *Organic & Biomolecular Chemistry* **2017,** *15* (48), 10145-10150.

Chapter 2

DESIGN, SYNTHESIS AND PHOTOPHYSICAL PROPERTIES OF FLUORESCENT C5-SUBSTITUTED 2′-DEOXYURIDINES

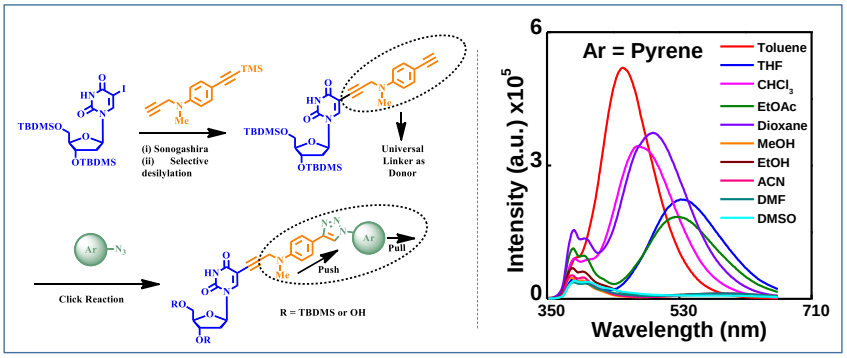

2.1. Introduction

The modified fluorescent nucleosides find extensive applications for exploring the structure, function, and dynamics of nucleic acids.[1-3] Particularly, the base modified fluorescently labeled nucleosides have many applications such as medical diagnostics, biological sciences, DNA sequencing, chemical and biochemical sensing processes, single nucleotide polymorphism (SNPs) typing.[4-10] It is a very indispensable research tool for understanding biological events associated with inter-biomolecular interactions, such as DNA-protein interactions, protein-protein interactions, drug-DNA and drug-protein interactions. Fluorescently labeled nucleosides/nucleotides that display a strong fluorescence signal upon hybridization with a target DNA can be used for the detection of single nucleotide polymorphism (SNPs typing).[1] In the previous chapter, we have mentioned and discussed numerous examples of 5-substituted uridine nucleosides which are modified in order to improve or generate usable photophysical properties within them. The fluorescently labeled nucleosides shown in **Figure 2.1** have been utilized for studying oligonucleotide dynamics (**2.01**), RNA-ligand binding interaction (**2.02**), SNPs detection (**2.03**) and in cell imaging (**2.04**). Many more solvatochromic fluorescent probes and fluorescently labeled biomolecular building blocks such as solvofluorochromic nucleosides/ amino acids have been successfully utilized for the sensing and detection of biomolecular microenvironment/biomolecules.[1, 11-13]

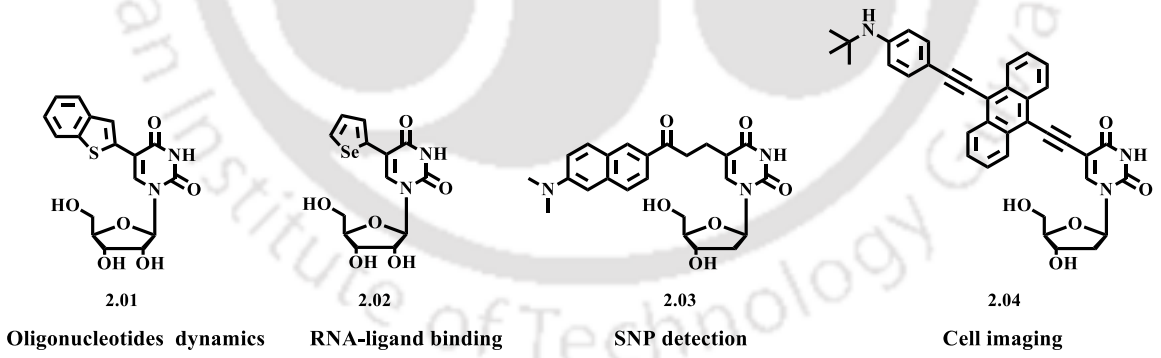

Figure 2.1. Few examples of 5-substituted fluorescent uridine nucleosides and their applications.[14-17]

Toward the synthesis of such type of modified nucleosides, transition-metal catalyzed coupling reactions play a significant role.[18] Palladium (Pd) and copper (Cu) are the two most significant and frequently used transition metals for the synthesis of modified and unnatural nucleosides. During the past two decades, Pd is perhaps the most widely used transition metal

in cross-coupling reactions. Some salient features of Pd chemistry are: (i) Pd complexes are inert to a variety of functional groups due to which chances of occurring unwanted side reactions are less, (ii) Pd catalyzed reactions often proceeds at ambient temperature within a couple of hours, (iii) low precatalyst loading (<1 mol%) is sufficient for the completion of reactions. The widespread applications of Pd chemistry in the field of nucleic acid chemistry are listed schematically in **Figure 2.2**. The Pd-catalyzed carbon-carbon bond formation has become one of the most common methods for modification of oligonucleotides.

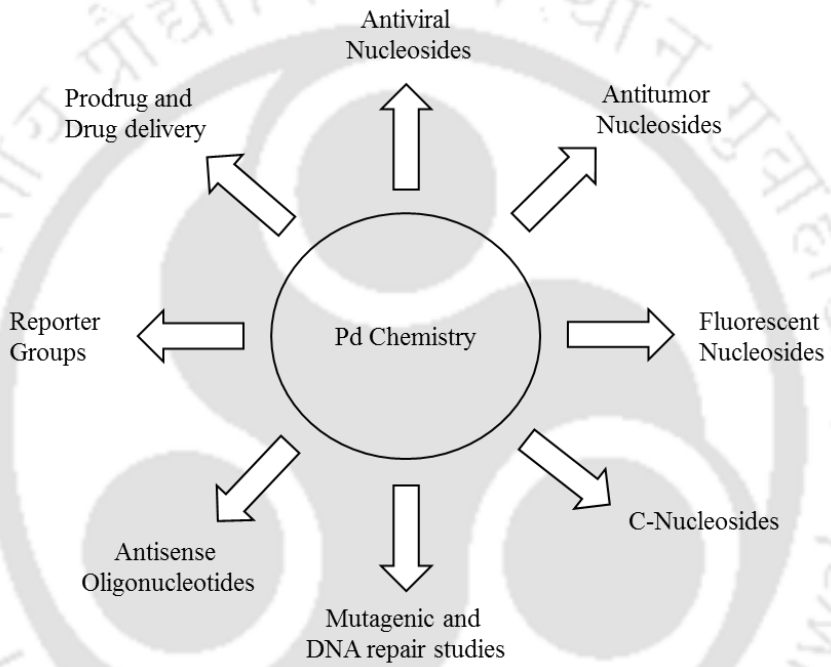

Figure 2.2. Applications of Pd chemistry in Nucleic acid chemistry

On the other hand, copper-catalyzed reactions are often utilized for the carbon-carbon and carbon-heteroatom bond formation. Some salient features of copper as a catalyst are (i) diverse functional group tolerance, (ii) cost-effective and, (iii) good associative property with heteroatom.[19, 20] As for example, copper-catalyzed Tandem or cascade reaction is a well-known method for the synthesis of heterocyclic molecules with significant biological importance.[21] Among the diverse heterocyclic molecules, 1, 2, 3-triazole heterocycles constitute a highly recognized class of biologically active molecules finding widespread applications in the field of chemical biology, medicinal chemistry, and material science.[22, 23] A triazole is a small structured molecule (five-membered ring with molecular formula $C_2H_3N_3$) having rich features

such as high metabolic stability, biocompatibility and H-bonding capability.[24-26] Many biologically active compounds containing triazole moiety find their applications as antibiotics, antiviral and antibacterial agents.[27] The triazole unit can be formed using Cu(I) catalyzed azide-alkyne cycloaddition reaction. This reaction is often called as click reaction which is utilized in a diversified way in nucleic acid chemistry.

Our work throughout this thesis will be utilizing Pd-catalyzed Sonogashira coupling reaction and click reaction for the synthesis of fluorescent molecules and nucleosides. Therefore, we will limit our discussions to these two reactions in the next sections.

2.2. Sonogashira Cross-Coupling Reaction

The Sonogashira coupling reaction is one of the soundest methodologies which was put forward by Kenkichi Sonogashira, Yasuo Tohda, and Nobue Hagihara in their 1975 publication.[28] The Sonogashira coupling reaction makes use of Palladium and copper as catalysts to couple an sp^2 and even sp^3 halide or triflate with a terminal alkyne under mild reaction conditions. Cassar, Dieck, and Heck reactions also afford the same reaction products, but these reactions required only copper as catalyst and the reaction conditions used by them were harsh, such as high temperatures.[29, 30] The high efficiency of the reagents, simple reaction setup and mild reaction conditions established the Sonogashira cross-coupling reaction as a highly useful reaction for a C-C bond formation between a terminal alkyne and an aryl or alkenyl halide. In brief Sonogashira cross-coupling reaction is the Pd (0)/Cu(I) catalyzed coupling reaction between an aryl halide and a terminal alkyne in the presence of base resulting in a conjugated alkynyl derivative. **Scheme 2.1** shows the classical Pd (0)/Cu(I) catalyzed Sonogashira cross-coupling reaction.

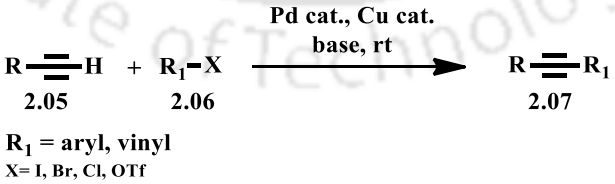

Scheme 2.1. Palladium, copper-catalyzed Sonogashira cross-coupling reaction.

2.2.1. Mechanism of Sonogashira Cross-Coupling Reaction

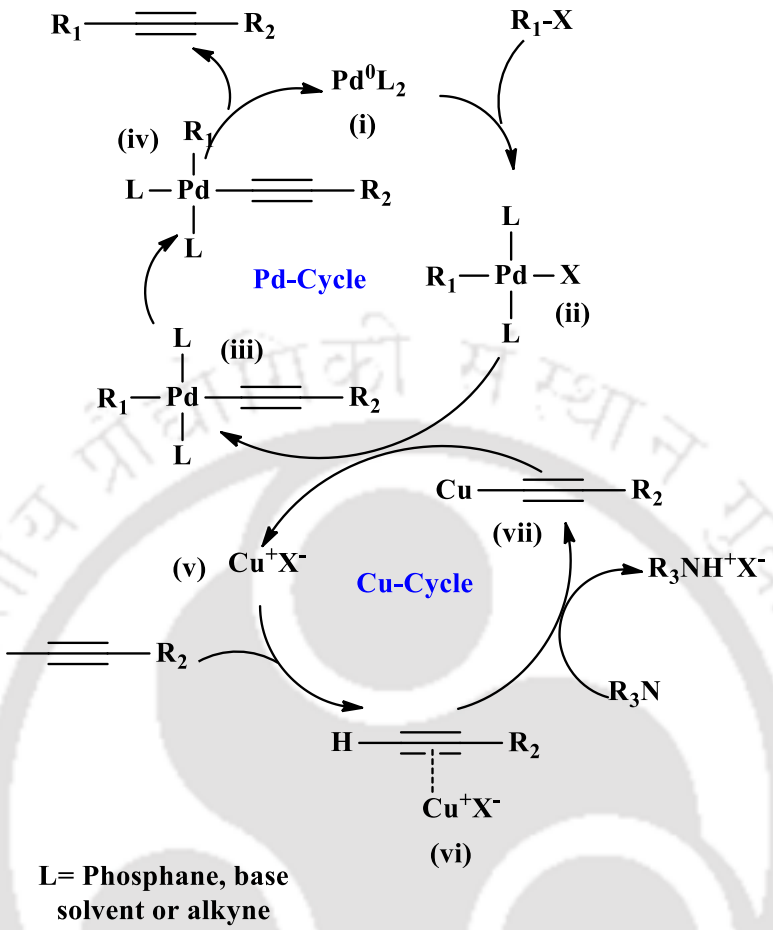

Figure 2.3. The supposed mechanism for Sonogashira Cross-Coupling.

The actual mechanism of Sonogashira coupling is not fully understood but the most accepted mechanism based on a palladium cycle and a copper cycle (**Figure 2.3**).[30] In the palladium catalyzed cycle, the pd^0L_2 complex (**i**) is catalytically active which reacts with aryl halide to form the intermediate oxidative addition complex $[Pd^{II}L_2R_1X]$ (**ii**). On the other hand in the copper cycle, the terminal alkyne in presence of a base reacts with Cu (I) (**v**) to form copper acetylide $[R_2\text{-}C{\equiv}C\text{-}Cu]$ complex (**vi**). Then the trans-metallation occurs between $[Pd^{II}L_2R_1X]$ and $[R_2\text{-}C{\equiv}C\text{-}Cu]$ complex (**ii** and **vi**, respectively) to form $[R_1Pd^{II}L_2C{\equiv}C\text{-}R_2]$ complex (**iii**), the orientation of both organic ligands are converted to cis from trans in a cis-trans isomerization (**iv**), which in turn followed by reductive elimination to forms the desired cross-coupled product $[R_1C{\equiv}CR_2]$.

Sonogashira cross-coupling reaction finds its applications in a wide range of research areas including natural product chemistry, medicinal chemistry, and material science. In the previous

chapter (**Section 1.5.3** and **Section 1.7.3**), we have discussed plenty of examples of modified nucleosides which have been synthesized utilizing Sonogashira cross-coupling reaction.

2.3. Click Chemistry

The green concept of click chemistry is one of the exciting methodologies first reported by K. B. Sharpless and his co-workers in 2001, which is a copper-catalyzed azide-alkyne 1,3-dipolar cycloaddition reaction (CuAAC) (**Scheme 2.2**). [23, 31-35] The products of classic Huisgen 1,3-dipolar cycloaddition are generally a mixture of both 1,4- and 1,5- disubstituted triazoles (regioisomers), but only 1,4-disubstituted triazoles are obtained from copper (I) catalyzed azide-alkyne cycloaddition reaction. The methods for generation of 1, 2, 3-triazole are shown in **Scheme 2.2** including the Cu(I)-catalyzed click reaction. The copper (I)-catalyzed reaction is a highly efficient reaction featuring simple reaction setup, a variety of functional group tolerance, mild reaction conditions, a wide range of selection of solvents including green solvent, water. The 1, 3-dipolar cycloaddition reaction of azides and terminal alkynes is a powerful and very robust transformation.[25, 35, 36] It finds various applications in host-guest chemistry, in metal coordination for sensing and detection of metal ions and in the generation of modulated solvatochromic fluorescent small organic molecules for possible application in sensing in chemical and biochemical research. The click reaction also finds its applications in biological research topics such as chemical ligation[37-39], labeling or modification of proteins[37-40], lipids[41], and nucleic acids.[42-46]

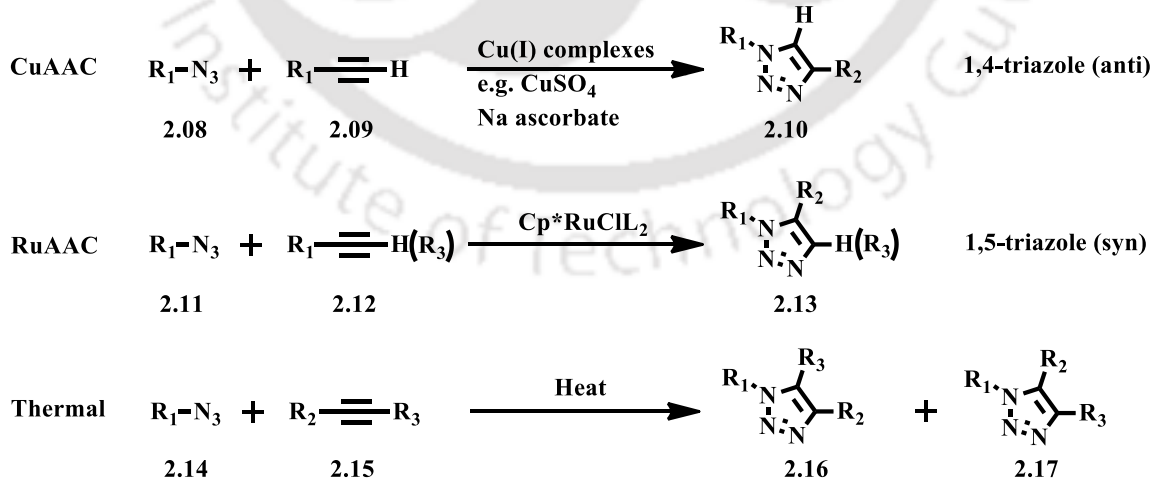

Scheme 2.2. Methods of 1, 2, 3-triazole synthesis.

Click chemistry can be utilized to synthesize highly fluorescent biomolecules and their mimics from nonfluorescent precursors.[46, 47] Researchers exploiting click chemistry to design highly fluorescent nucleic acids and proteins in order to study molecular genetics. Since the click product, the "triazole" unit is highly stable against enzymatic degradation, hydrolysis, and oxidation,[48] therefore, it is quite possible to impart these chemical properties into biologically active molecules with the help of click chemistry.

2.3.1. Mechanism of Copper-Catalyzed Azide-alkyne Cycloaddition Reaction

Fokin and Finn proposed a catalytic cyclic mechanism for CuAAC reaction based on density functional theory (DFT) calculations.[49] In the first step of the catalytic cycle, the terminal alkyne derivative displaces one ligand from copper metal to form Copper acetylide. In the second step, another ligand is displaced by the azide in order to bind with copper which leads to the formation of an uncommon six-membered copper (III) metallacycle in the third step. Then the ring contraction and protonolysis of the metallacycle lead to the formation of the triazole product and completes the catalytic cycle (**Figure 2.4**).

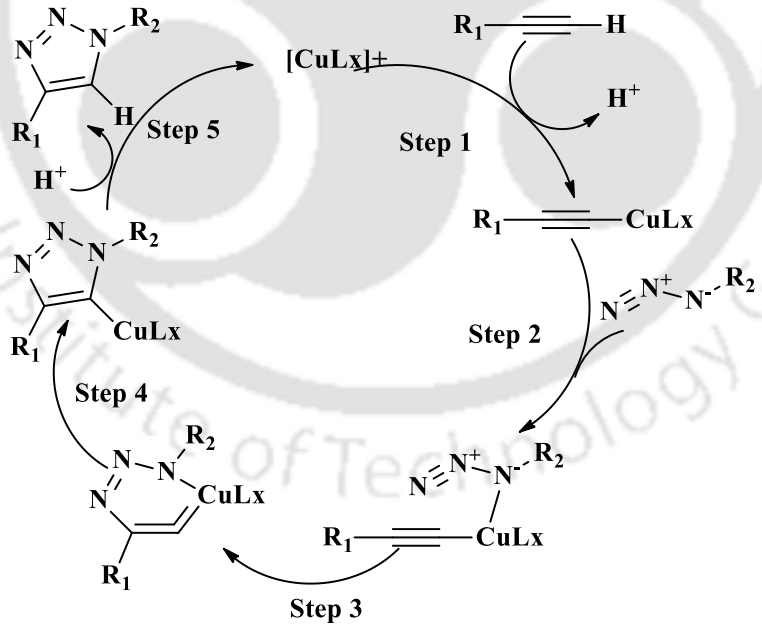

Figure 2.4. Supposed mechanism of copper-catalyzed azide-alkyne cycloaddition (CuAAC).

2.4. Click Chemistry as a Tool in Nucleic Acid Research for Generating Fluorescent Nucleosides

Understanding intercellular biological processes often depend on fluorescence-based tools and their ability to monitor biomolecules. Green fluorescent proteins (GFPs) and fluorescently labeled oligonucleotides often utilized to monitor biomolecules in biological system.[50-54] The generation of fluorescence by the "click" reaction can be used for the visualization of DNA in free solution or embedded in DNA-protein complexes and can also be used for labeling and visualization of biomolecules. The utilization of nucleosides, nucleotides, and oligonucleotides as substrates of click chemistry is well established for more than a decade.[42, 43] A comprehensive study was done by Seela and co-workers. A good example of their work is the incorporation of a pyrrolo dC analog of deoxycytidine with a terminal alkyne (**2.18**) into oligonucleotides (**Scheme 2.3**).[46] The terminal alkyne residues of oligonucleotides were selectively conjugated by the CuAAC reaction to the non-fluorescent 3-azido-7-hydroxycoumarin (**2.19**) to give strongly fluorescent 1,2,3-triazole conjugate (**2.20**). The fluorescence properties of oligonucleotides with these covalently linked coumarin-nucleobases displayed the expected pH-dependence of fluorescence intensity.

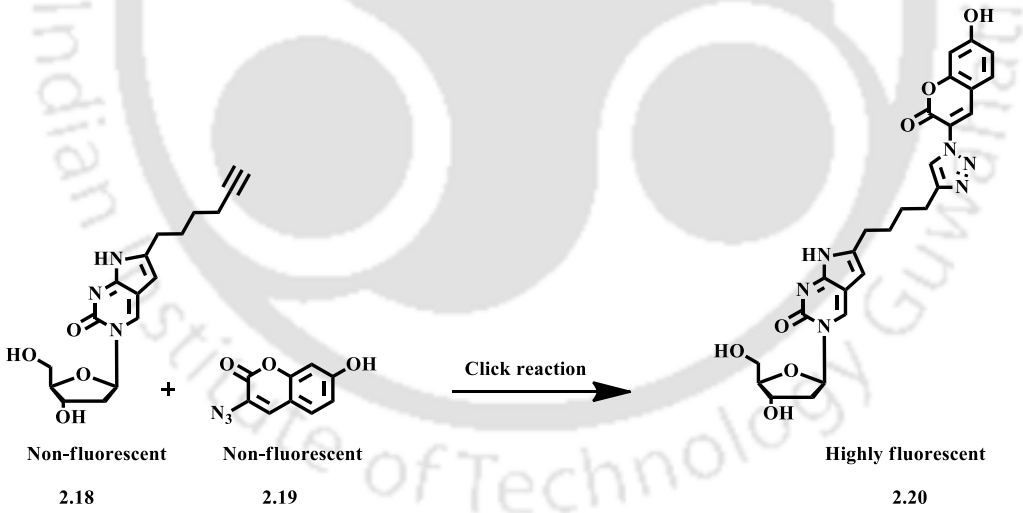

Scheme 2.3. Click chemistry to generate fluorescent nucleoside analogs from non-fluorescent precursors.

There are several examples of click chemistry mediated incorporation of fluorophores into DNA. The two basic methods utilized for this purpose are pre-synthetic and post-synthetic modifications of DNA. In this respect, we will discuss some recent examples of modifications at the DNA bases achieved via these two methods below.

2.4.1. Pre-Synthetic Modification of DNA

The term "pre-synthetic modification" denotes the desired modification on a nucleoside prior to the incorporation into DNA. In the field of the click reaction mediated synthesis of base modified fluorescent nucleosides/nucleotides, major contributions are done by Seela and co-workers. In 2012, they have reported two pyrrolo-dC (dC = deoxycytidine) click adducts (**2.21**, **2.22**, **Figure 2.5**) and incorporated into oligonucleotides for DNA mismatch detection.[55] According to the authors, the oligonucleotide probes containing these compounds were able to discriminate between matched and mismatched DNA base pairs.

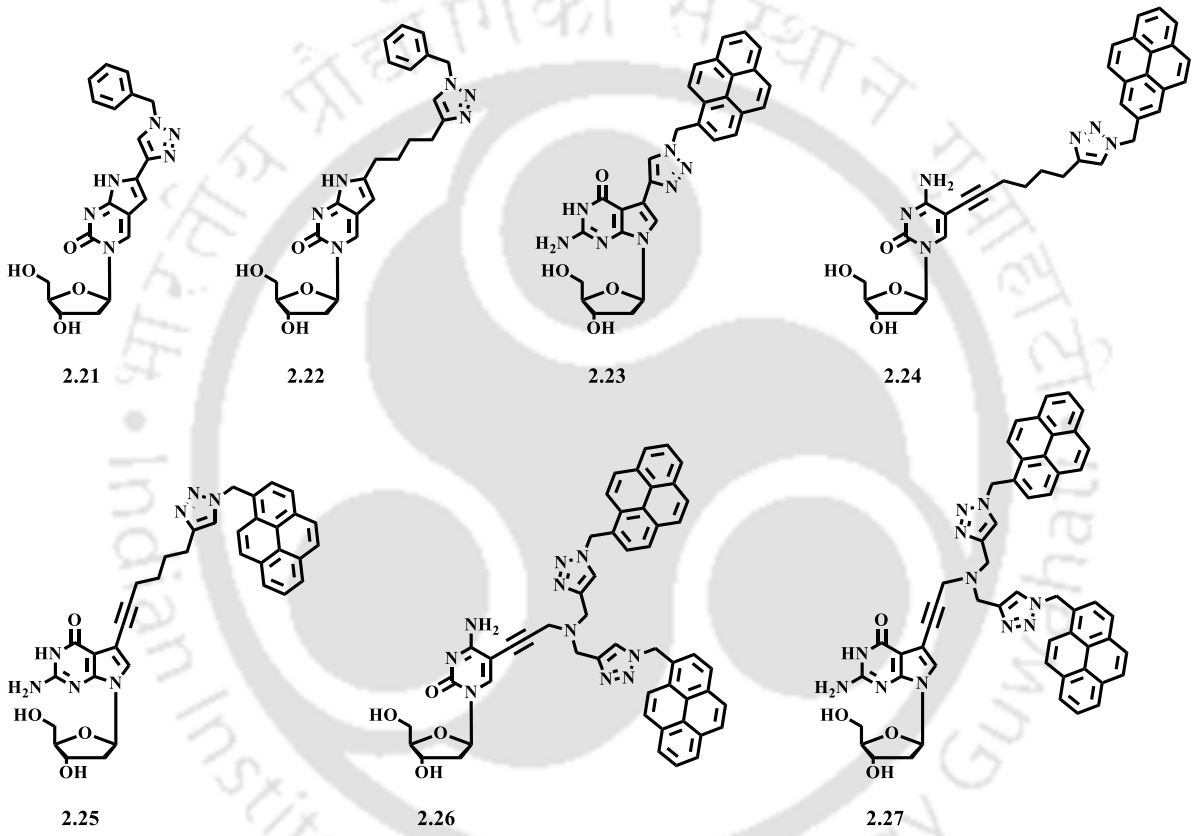

Figure 2.5. Fluorescent nucleoside click adducts reported by Seela and co-workers.

Seela and co-workers also reported several pyrene-labeled nucleosides (**2.23**-**2.27**, **Figure 2.5**) and incorporated into oligonucleotides.[56, 57] They have reported that the nucleoside **2.23** containing a short linker is destabilizing to the DNA duplex formation, while the nucleosides **2.24** and **2.25** with long linkers improve the DNA stability.[56]Also, the dC click conjugates (**2.24**, **2.26**) exhibited superior fluorescence emission properties than the 7-deazaguanosine derivatives (**2.23**, **2.25**, **2.27**), both in single-stranded and double-stranded DNA.[57]

2.4.2. Post-Synthetic Modification of DNA

Incorporation of fluorophores via pre-synthetic modification have certain limitations. For example, many fluorophores susceptible to decompositions under basic conditions and at deprotection step used during the solid-phase oligonucleotide synthesis or during the PCR process. Moreover, incorporation of bulky adducts into DNA can be difficult due to the steric hindrance. In these contexts, the post-synthetic modification is most probably the ideal method for DNA modification. The term "post-synthetic modification" denotes that the desired modification has been done on the DNA strand within a complex biological medium.[43, 58] In this respect, we will discuss a few examples in this section below.

In 2006, Carell *et al.* reported multiple post-synthetic labeling of alkyne-modified DNA.[59] They synthesized two modified uridine nucleosides (**2.28**, **2.29**, **Figure 2.6**) and incorporated into ODNs for the generation of ODNs bearing alkyne reporter groups in various densities. Afterward, they performed click reaction between the alkyne bearing duplexes of these ODNs and various azides (**2.19**, **2.30, 2.31**, **Figure 2.6**). A low conversion to products was reported for the ODNs containing the nucleoside with short alkyne linker (**2.28**), while complete high-density conversion was reported for ODNs containing the nucleoside with long flexible alkyne linker (**2.29**).

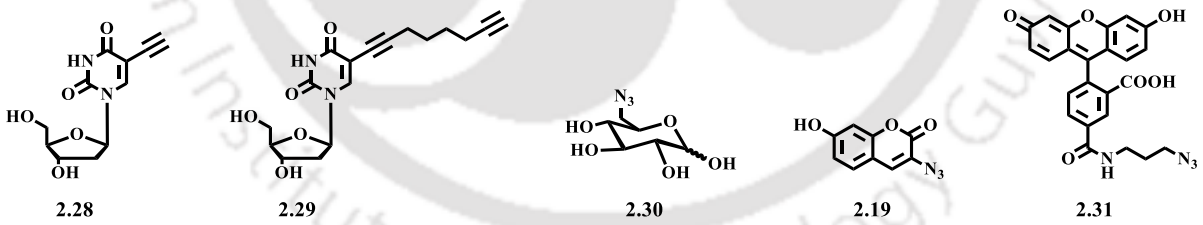

Figure 2.6. Alkyne bearing nucleosides and organic azides utilized by Carell *et al.* for post-modification of DNA.

In 2010, Seela *et al.* employed fluorogenic azides, 9-azidomethyl anthracene (**2.34**) and 3-azido-7-hydroxycoumarin (**2.19**) for post modification of ODNs containing octa-(1,7)-diynyl-8-aza-7-deaza-2′-deoxyadenosine (**2.32**, **Figure 2.7**).[44] According to the authors, the modified ODNs showed enhanced fluorescence emission as well as stability upon fully matched duplex formation. They have also compared the fluorescence emission properties of click compounds obtained by reaction between the free alkyne group of 8-aza-7deaza-2′-deoxyadenosine (**2.32**)

and 7-deaza-2′-deoxyadenosine (**2.33**) with both of the fluorogenic azides (**2.19**, **2.34**). It is interesting that the 8-aza-7-deaza-2′-deoxyadenosine click compounds did not exhibit fluorescence quenching in their analysis, while the 7-deaza-2′-deoxyadenosine click compounds exhibited quenched emission most possibly due to the charge transfer between the nucleobase and the fluorophore.

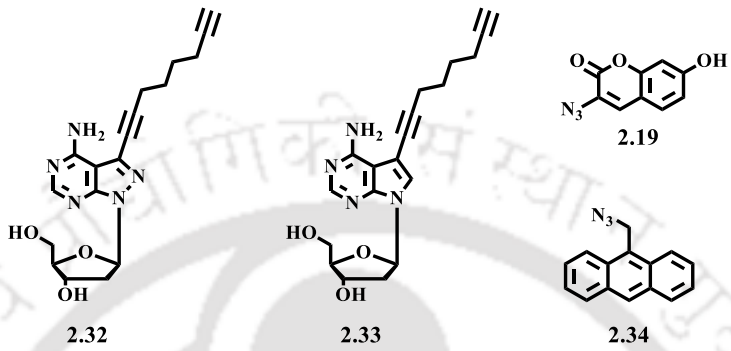

Figure 2.7. Alkyne bearing nucleosides, 8-aza-7deaza-2′-deoxyadenosine, 7-deaza-2′-deoxyadenosine and the fluorogenic azides utilized by Seela *et al.* for post-modification of DNA.

In 2010, Wagenknecht *et al.* reported successful incorporation of Nile Red dye into DNA post-synthetically (**Figure 2.8**).[60] For that purpose, they have utilized the *in-situ* generation of azide in the DNA by reaction with a nucleotide containing 5-iodo-2′-deoxyuridine with sodium azide, which was followed by a click with an ethynyl modified Nile Red (**2.35**) to yield the modified DNA.

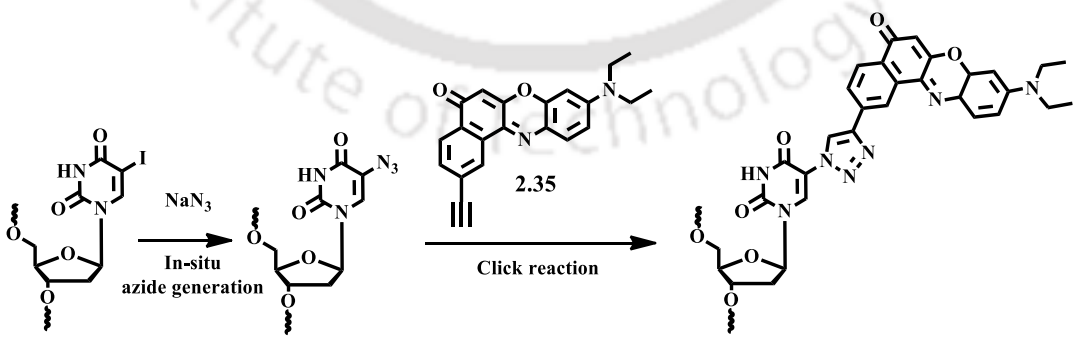

Figure 2.8. Schematic representation of post-synthetic incorporation of Nile Red dye into DNA reported by Wagenknecht *et al.*

The use of bioorthogonal chemical reporters in order to monitor biomolecules in living systems has drawn much attention among researchers lately.[61-65] Because of the unobtrusive nature of click substrates (azides and alkynes), click chemistry is a powerful candidate for generation of such reporters without perturbing the targets biological functions. However, performing Cu(I) catalyzed click reactions within live cells is not a safe practice even successful examples have been demonstrated.[66, 67] Copper ion impurities from the post-synthetic or in vivo modification can become a cytotoxic threat even when present in trace amounts. Hence, the development of copper-free "click" type reactions and alternatives for post-synthetic modification of nucleic acids is a current research topic in demand. Such types of reactions include strain-promoted[54, 68, 69] and other 1,3-dipolar cycloadditions,[70, 71] Diels-Alder reactions with normal[72] and inverse electron demand,[73, 74] reductive aminations,[75] thiol-ene additions[76, 77], and Suzuki-Miyaura-type coupling reactions.[78, 79]

2.5. Background

Polarity sensitive fluorescent molecules are ubiquitous for sensing of biomolecules and studying inter-biomolecular interactions inside a cell.[80-82] In particular sensing of the local microenvironment of DNA is highly important in connection with the detection of DNA mutations causing a deleterious effect on cellular survival, high throughput screening, and many other biotechnological applications.[83-85] All these events in DNA rely on novel fluorescent probe either as bare or unnatural fluorescent nucleosides or fluorescently labeled natural nucleosides.[1, 86-88] Though many such probe systems in relation to DNA have been reported but the probes suffer from fluorescence quenching by neighboring nucleobases or short wavelength emission or poor microenvironment sensitivity.[1, 86] Therefore, designing of novel emissive probes, particularly, fluorescent nucleosides with unique fluorescence properties, extreme sensitivity to change in DNA microenvironment and interactions are highly desirable. Among the three approaches, linking a fluorophore in nucleoside bases is the major approach to generate fluorescent nucleoside useable for DNA sensing.[1, 2, 83-91] As a result of tremendous research efforts, a large number of fluorescently labeled nucleosides and corresponding oligonucleotide probes have been designed and utilized to a variety of applications that include probing DNA hybridization,[92, 93] typing single nucleotide polymorphism (SNP),[7, 94, 95] and monitoring the interbiomolecular interaction,[96-98] to name a few. However, the majority of the reported environmentally sensitive fluorescent nucleosides

exhibited single band emission that senses the differences in micropolarity either by a change in emission intensity or wavelength.[17, 90, 99-102] Among these, Saito's ESF nucleosides[100, 103, 104](**1.224-1.228, Figure 1.27, Chapter 1)** are highly attractive for monitoring the micropolarity changes within DNA. However, often the majority of such probes suffer from several shortcomings such as poor microenvironment sensitivity and low quantum yields.[1, 83-88, 100, 103-105]

Therefore, to overcome these limitations, the concept of two-band emission would be more advantageous over commonly utilized single-band fluorescent probes/nucleosides.[106-108] Thus, recording a ratio of the intensities at two wavelengths would allow ratiometric sensing which is more advantageous than sensing based on single wavelength emission.[109, 110] Basically, ratiometric sensing results in an intrinsically calibrated emission response.[106-108] Ratiometric probing of DNA, though reported, but is based on labeling of DNA by two interacting dyes such as FRET pair or excimer/exciplex pair.[93, 95, 111, 112] However, labeling with two dyes is difficult, time-consuming as well as highly uneconomical.[93, 95, 106-110] On the contrary, a single fluorophore with dual emission property would be much more beneficial.[113-115] Highly increased dipole moment and dipole-dipole interactions in the excited state allow such fluorophores to be able to sense the changes in local micropolarity within a biomolecular microenvironment or in the cell.[80-82] Therefore, dual emissive fluorophores are very useful as a ratiometric probe because they offer facile and straightforward quantification of a biomolecular event through the ratio of their two bands. However, due to the scarcity of such fluorophores that display dual emissions and the difficulties in their syntheses, the phenomena of dual emission based sensing of biomolecular events are poorly explored, especially, in the field of DNA analysis.[116-119] With a poor literature reports and the unique ability for sensing the change in the microenvironment of DNA biomolecules, the design of dual emissive modified nucleosides that can control the equilibrium between two excited states at ambient temperature without changing the solvent properties is an unavoidable research area.

2.6. Aim and Objective

As a part of our continuous research efforts in the design of solvofluorochromic molecules/biomolecular building blocks, [120-124] we thought that it would be worthwhile to design dual emissive modified nucleosides. Based on our experience, literature reports and wider applicability we considered the design of C5 substituted uridines as model nucleoside probes useable for DNA analysis in the future.[45, 89, 120, 125-134] However, there is no report wherein C5 position of 2′-deoxyuridine is linked by an electron donor unit as a post-

synthetically modifiable functional group which effectively can generate a modulated fluorescence property of a fluorophore if attached at the terminus or the terminal alkyne can be reacted with a fluorophoric azide functionality. Previously, we have shown the "installation/modulation of fluorescence response" of various small fluorescent molecules and an interesting dual emission behavior from pyrene when attached to *N*,*N*-dimethylanilino triazole donor unit.[135] Inspired by our previous result and motivated by the importance of dual emitting probe for DNA analysis,[116-119] we thought that it would be worthwhile to generate a set of fluorescent 2'-deoxyuridine nucleosides which could show interesting intramolecular charge transfer property or dual emission. We further thought that attaching an electron donor phenylacetylene unit as a post-synthetically modifiable functional group at the C5-position of 2'-deoxyuridine would be beneficial to generate a set of fluorescent 2'-deoxyuridines with modulated fluorescence property of a fluorophore via azide-alkyne cycloaddition reaction.[45, 121-124, 129-134] Furthermore, the same nucleoside, if incorporated into DNA, can offer the opportunity of generating fluorescent oligonucleotide probes via post-synthetic click reaction with modulated fluorescence property. Following the aforementioned design logics the research was aimed as below:

(a) The design and synthesis of 5-(3-((4-ethynylphenyl)(methyl)amino)propynyl)-2'-deoxyuridine a possible post-synthetically modifiable nucleoside.

(b) Its application to generate a set of triazolyl fluorescent 2'-deoxyuridines generated via Sonogashira cross-coupling reaction and azide-alkyne cycloaddition reaction.

(c) Study of photophysical properties of a few such fluorescent 2'-deoxyuridines revealed interesting solvatochromic photophysical properties corroborating our design concept.

(d) Theoretical study to support the experimental photophysical properties of three fluorescent uridines by TDDFT calculation.

(e)

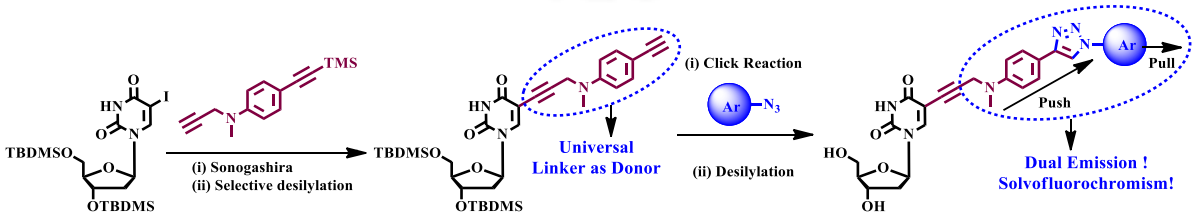

Scheme 2.4. The design concept of the dual emitting nucleoside.

2.7. Result and Discussion

The Design Concept

Our design involves the synthesis of a universal linker, 4-(Propynyl(methyl)amino)phenyl acetylene, and its incorporation into C5-position of 2′-deoxyuridine. The universal linker containing 2′-deoxyuridine can then undergo Huisgen 1, 3-dipolar cycloaddition reaction with donor-acceptor chromophore containing fluorogenic azides to afford the target fluorescent uridines. The donor aromatic substituted triazole moiety was thought to allow an intramolecular charge transfer (ICT) process from triazole-linked moiety to the fluorophoric units leading to solvatochromic fluorescence at a longer wavelength. Moreover, the fluorophores, such as pyrene, coupled electronically with donor aryltriazoles, could show dual fluorescence property or interesting modulated solvatochromic emission response (Figure 1). Thus, our design would ultimately lead to predetermined photophysical properties of the fluorophores and hence of the nucleoside. The dual fluorescent nucleosides having ratiometric fluorescence property could be utilized for DNA analysis if incorporated in a DNA for the generation of fluorescent oligonucleotide probes.

2.7.1. Synthesis of Fluorescently Labeled 2′-Deoxyuridines

The synthesis of fluorescently labeled 2′-deoxyuridines was achieved via Sonogashira coupling and 1,3-dipolar cycloaddition reaction. To generate a series of target fluorescent uridines, we first synthesized the universal linker containing uridine **2.43** (**Scheme 2.5)**. The synthesis was started from N-methylaniline (**2.36**) which was converted first to its *p*-iodo derivative (**2.37**). Afterward, the *p*-iodo derivative was allowed to undergo a Sonogashira coupling with trimethylsilylacetylene to afford compound **2.38,** which underwent propargylation to yield TMS- protected linker unit **2.39**. This linker unit was then coupled with bis-TBDMS-protected 5-iodo-2′-deoxyuridine (**2.41**) through its free propargyl end via a Sonogashira coupling to get compound **2.42**.[56] The TMS group was then deprotected to afford the bis-TBDMS-protected 5-iodo-2′-deoxyuridine containing donor-substituted phenylacetylene as universal linker **2.43** (S**cheme 2.5**).

Finally, the 1,3-Huisgen azide-alkyne cycloaddition reaction was carried out between the uridine containing the universal linker and various donor-acceptor-substituted fluorogenic aromatic azides (**A-G**, **Scheme 2.5b**) synthesized from the corresponding amines under click reaction condition to afford the target uridines **2.44A-G**, in bis-TBDMS-protected form and **2.45C**, **2.45E** and **2.45G** in desilylated form, in moderate to very good yields.[135] The final

products were purified by column chromatography and characterized by NMR and HRMS analysis. The structures of the synthesized nucleosides are shown in **Figure 2.9**.

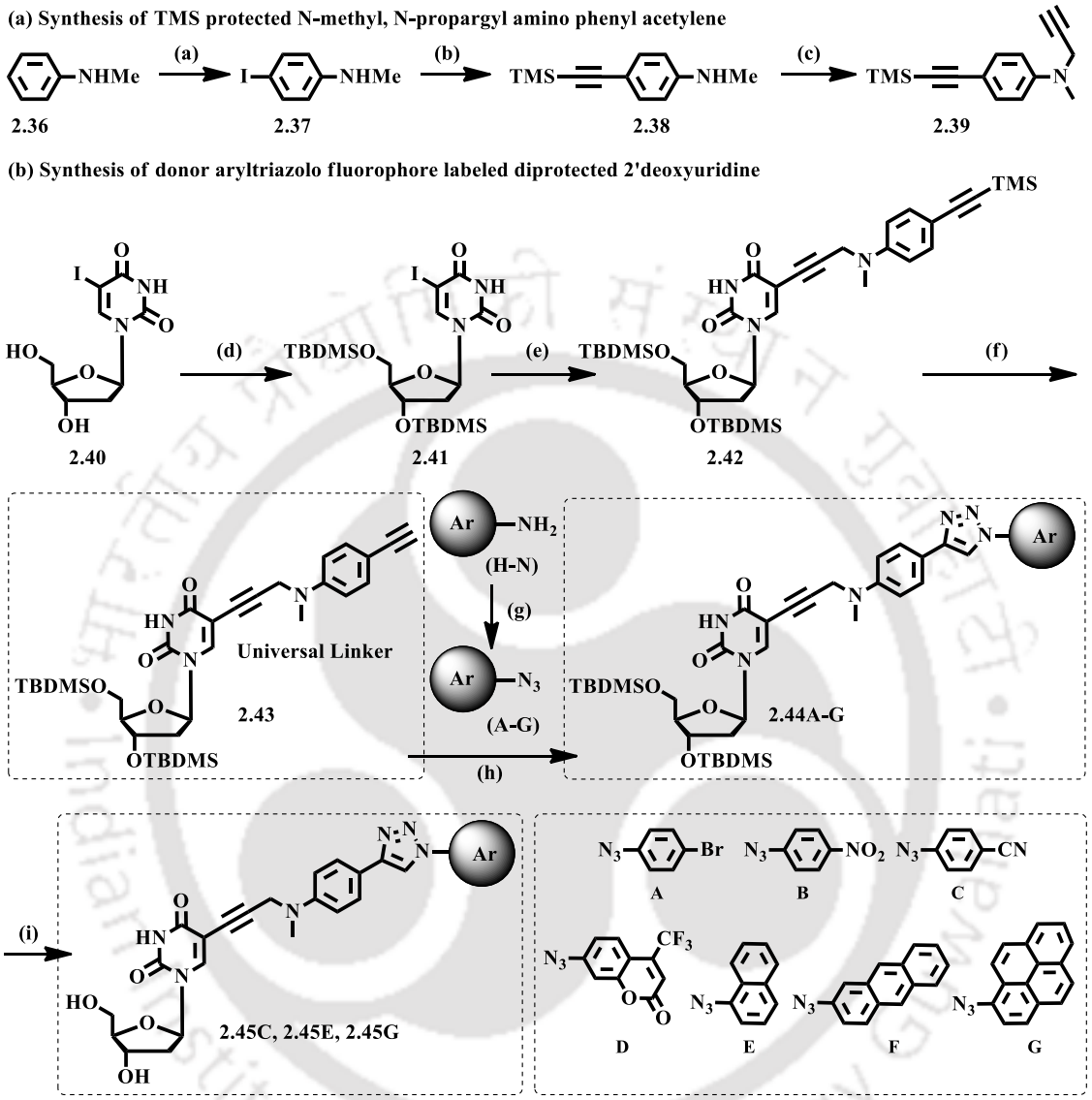

Reagents and condition: (a) I_2, pyridine:dioxan (1:1), 0 ^oC-rt, 22 h; (b) TMS-acetylene, $PdCl_2(PPh_3)_2$, CuI, benzene:$^nBuNH_2$, 80 ^oC, 7 h; (c) Propargylbromide, K_2CO_3, DMF, rt-50 ^oC, 15 h; (d) TBDMSCl, Imidazole, DMF, 0 ^oC-rt, 18 h; (e) 4, $PdCl_2(PPh_3)_2$, CuI, Et_3N, 55 ^oC, 7 h; (f) K_2CO_3, MeOH, rt, 4 h; (g) Arylamines(H-N), $NaNO_2$, NaN_3, HCl, H_2O; (h) Arylazides (A-G), t-BuOH:H_2O (1:1), $CuSO_4$, Sodium ascorbate, 70 ^oC , 12 h; (i) TBAF, THF, 1 h.

Scheme 2.5. (a) Synthesis of TMS protected N-methyl, N-propargyl amino phenylacetylene and (b) Synthesis of donor aryltriazolo fluorophore-labeled 2′-deoxyuridines and aromatic azides used in the synthesis.

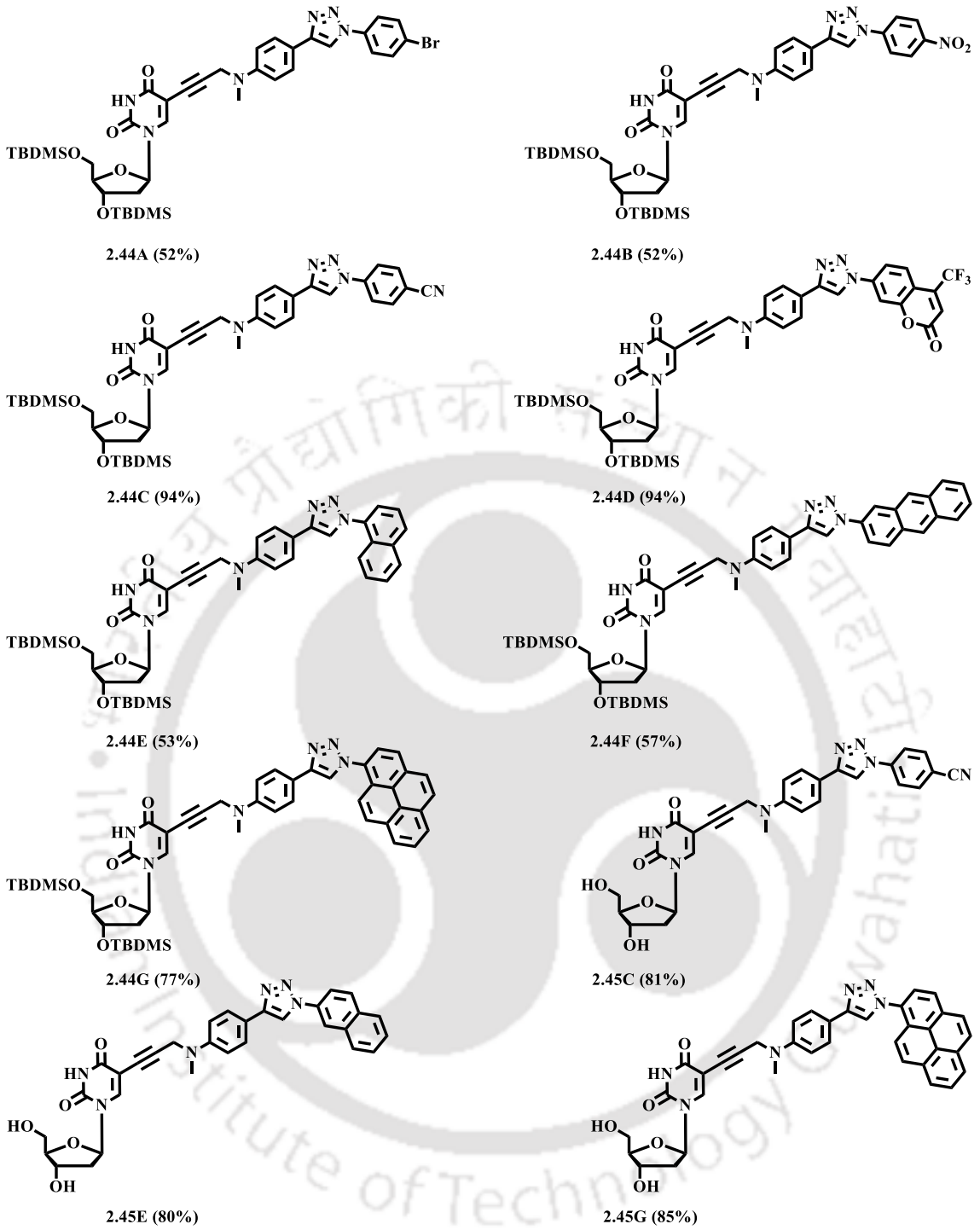

Figure 2.9. Structures of synthesized protected/deprotected fluorescent uridines.

2.7.2. Study of Photophysical Properties

After getting all the nucleosides in hands, we studied the photophysical properties of a few selected nucleosides in organic solvents of varying polarities to check the solvatochromic nature. The UV-visible spectra of all the compounds (10µm) were measured using a UV-visible

spectrophotometer with a cell of 1 cm path length at 25 °C and 1 mm slit width. All the sample solutions were prepared before an hour of the measurement. The excitation wavelengths for recording the emission spectra was at the maximum wavelength of absorbance (λ_{max}^{abs}) in each case. The fluorescence quantum yield (Φ_f) was determined using quinine sulfate as a reference with known $\Phi_f = 0.54$ in 0.1 molar solution in sulphuric acid.

From the UV-visible spectra, we observed that the solvent polarity had an only minor influence on the absorption properties of most of the fluorescent nucleosides. However, the fluorescence emission property was modulated enormously upon changing the polarity of the solvents. Thus, the analysis of absorption spectra of nitrobenzene containing nucleoside **2.44B** exhibited absorptions at around 290 and 365 nm in various organic solvents with very little solvatochromism (by 2-4 nm blue shift) (**Figure 2.10a**). Upon excitation at 365 nm, it exhibited weak structured emission at around 390 nm with almost similar intensity in all solvents except for EtOH, DMF, $CHCl_3$ and DMSO wherein enhanced intensity was observed (**Figure 2.10b**).

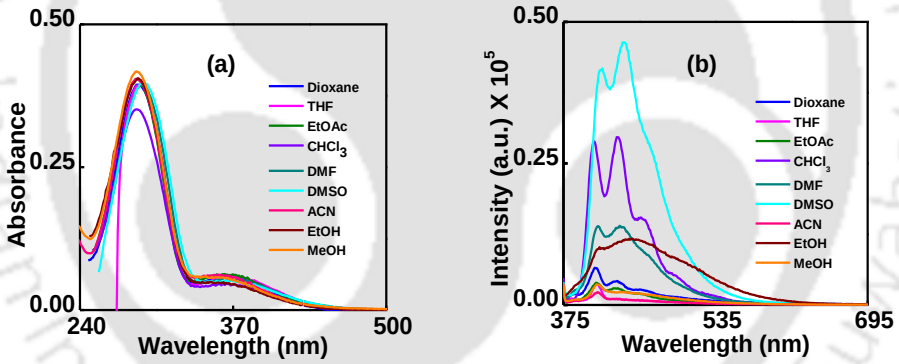

Figure 2.10. (a) UV-visible and (b) fluorescence emission spectra of nucleosides **2.44B** in various organic solvents (10 μM)

A similar absorption pattern with less solvatochromicity was shown by the trifluoromethyl coumarin containing nucleoside **2.44D** with absorption at 291nm and 375 nm. Excitation spectra at long wavelength (375 nm) showed very weak and broad emission at 445 nm (**Figure 2.11a, b**).

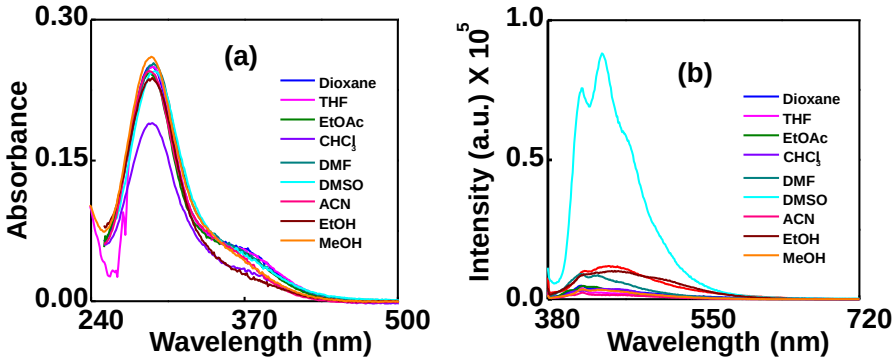

Figure 2.11. (a) UV-visible and (b) fluorescence emission spectra of nucleosides **2.44D** in various organic solvents (10 μM)

The UV-visible spectra of anthracene containing nucleoside **2.44F** revealed absorptions at around 290 nm and at three regions, 348, 367 and 386 nm in a regular pattern which is the vibronic absorption characteristic of anthracene (**Figure 2.12a**). In this case, also, negligible solvatochromicity was observed in the absorption spectra. However, upon excitation at 365 nm, interesting emissions have been observed. In the highly polar and protic solvents, only characteristic emissions of anthracene centered at 415 nm were observed and we characterized it as emission from a locally excited (LE) state (**Figure 2.12b**). On the other hand, in nonpolar solvents such as in dioxane and in moderately polar solvents such as $CHCl_3$, EtOAc and THF, a dual emission was observed. The additional band observed at higher wavelength region is characterized as emission from intramolecular charge transfer (ICT) state. The LE emission bands were observed at around 415-420 nm and solvatochromic ICT bands were observed at 490, 493, 534 and 543 nm in dioxane, $CHCl_3$, EtOAc, and THF respectively.

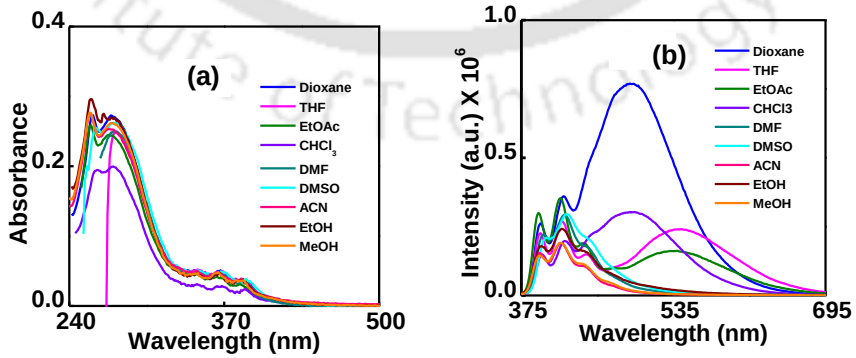

Figure 2.12. (a) UV-visible and (b) fluorescence emission spectra of nucleosides **2.44F** in various organic solvents. The concentration of the nucleoside was 10 μM.

The UV-visible spectra of nucleoside containing benzonitrile chromophore **2.45C** showed a short wavelength absorption at 288 nm and a long wavelength weak absorption centered at 346 nm in almost all solvents. Interestingly, upon excitation at long wavelength, the emission spectra showed a structureless, broad and strong solvent polarity dependant ICT emission (**Figure 2.13a, b**). A strong emission in dioxane at 471 nm was observed which experienced an 80 nm red shift with a gradual decrease in intensity when the polarity of the solvent increased to ACN/DMF (551 nm) (**Table 2.1**). In a polar protic solvent like methanol, almost no emission was observed which is possibly due to the fluorescence quenching event mediated via dipolar/H-bonding interaction.[113, 136]

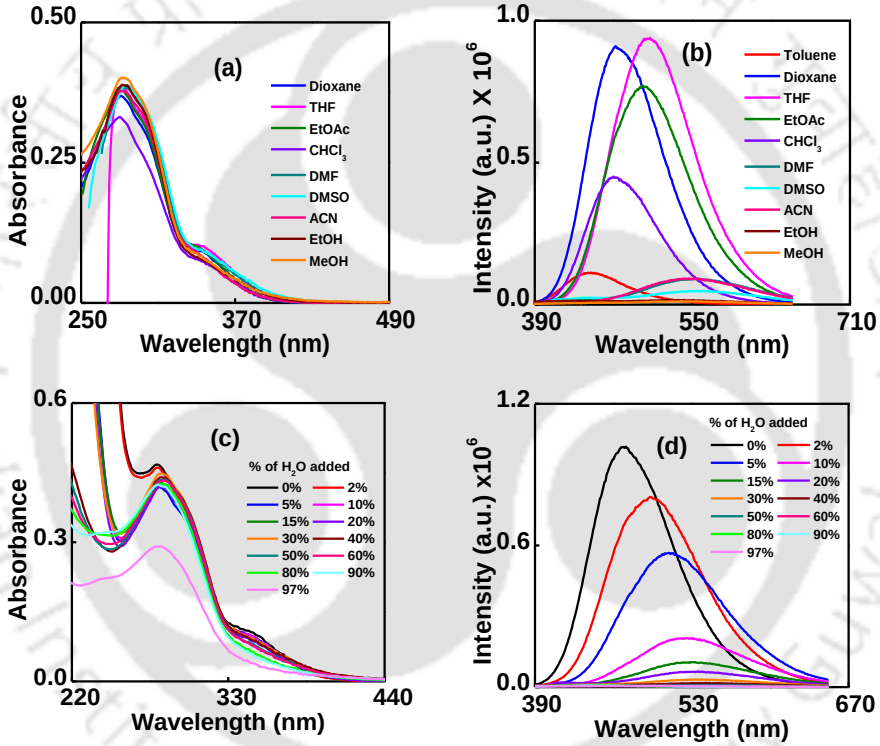

Figure 2.13. (a) UV-visible, (b) fluorescence emission spectra in various organic solvents for nucleoside **2.45C**. Dioxane-water titration: (c) UV-visible, (d) fluorescence emission spectra for the same. The concentration of the nucleoside **2.45C** was 10 µM.

Table 2.1. Summary table of photophysical properties of the nucleoside **2.45C**

Entry 2.45C	**Solvents**								
Prop.↓	**Diox.**	**$CHCl_3$**	**EtOAc**	**THF**	**DMSO**	**DMF**	**EtOH**	**ACN**	**MeOH**
Δf	0.021	0.148	0.201	0.21	0.265	0.275	0.29	0.305	0.309
λ_{max}^{abs} (nm)	281, 338	280, 335	280, 334	281, 341	286, 342	284, 339	282, 335	282, 331	282, 335
λ_{max}^{fl} (nm)	471	470	500	507	429, 535	551	429, 535	546	431, 539
Φ_f	0.34	0.21	0.27	0.29	0.04	0.04	0.02	0.04	0.008

Similar results were observed upon titration of a solution of the nucleoside **2.45C** in dioxane by water. A red shift in the emission of about 72 nm was observed in 30% water while decreased intensity along with a negligible shift in wavelength was observed up to 50% water. Beyond this, the addition of further water led to almost full quenching of fluorescence (**Figure 2.13c, d**). These features indicated an emission from an ICT state.[113, 135, 137-146] Fluorescence quantum yields revealed a similar trend as solvent polarity was increased (**Table 2.2**). The fluorescence lifetime for this nucleoside showed biexponential decay in all solvents following a similar trend as that was observed in steady-state emission upon changing the solvent polarity. As an example, in ACN the average lifetime and quantum yield were 1.75 ns and 0.04, respectively, while in dioxane the corresponding values were 2.83 ns and 0.34, respectively (**Table 2.2**). This may be because of the fluorescence quenching through nonradiative pathway via hydrogen bonding which is also supported from an increased nonradiative rate constant (K_{nr}) from 2.31 in dioxane to 5.46 in ACN (**Table 2.2**).[113]

Table 2.2. Summary table of fluorescence properties of the nucleoside **2.45C**

Entry 2.45C	**Solvents**						
Properties↓	**Dioxane**	**THF**	**ACN**	**$D_{95}W_5$**	**$D_{85}W_{15}$**	**$D_{80}W_{20}$**	**$D_{70}W_{30}$**
Δf	0.021	0.21	0.305	0.186	0.249	0.262	0.277
λ_{max}^{abs} (nm)	281,338	281,341	282,331	281, 336	282, 334	284, 335	283, 339
λ_{max}^{fl} (nm)	471	507	546	510	530	534	539
Φ_f	0.34	0.29	0.04	0.26	0.05	0.04	0.02
<τ> [ns]	2.83	2.97	1.75	2.4	2.29	1.68	1.45
k_f [10^8 s^{-1}]	1.22	0.98	0.25	1.08	0.24	0.23	0.13
k_{nr} [10^8 s^{-1}]	2.31	2.38	5.46	3.08	4.13	5.72	6.76
D_pW_q = Dioxane (D) and water (W) solvent mixture; p and q are the volume of each solvent.							

The nucleoside containing naphthalene fluorophore, **2.45E** showed structureless absorption at around 288 nm with little solvatochromicity as was revealed both from the spectra in various organic solvents as well as dioxane-water titration (**Figure 2.14a,c**). Only a slight increase in intensity was observed when polarity was increased. However, strong solvent dependent emission was observed for this nucleoside centering around 449 nm in dioxane when excited at 290 nm. A red shift of 80 nm was observed with an increase in intensity as we moved from dioxane to ACN (529 nm). On the other hand, in a polar protic solvent such as MeOH, the intensity and hence the quantum yields were decreased which might be because of an H-bonding effect (**Figure 2.14**, **Table 2.3**, **2.4**). A dioxane-water experiment revealed a red shift of 83 nm (449-532 nm) up to 50% dioxane-water mixture (**Table 2.4**). These results clearly indicated the features of an ICT emission. On addition of 30-60% water, another band at around 388 nm was observed with an increase in intensity. Beyond 70% water, the single band at 388 nm was prominent, which might be the emission from LE state (**Figure 2.14d**).

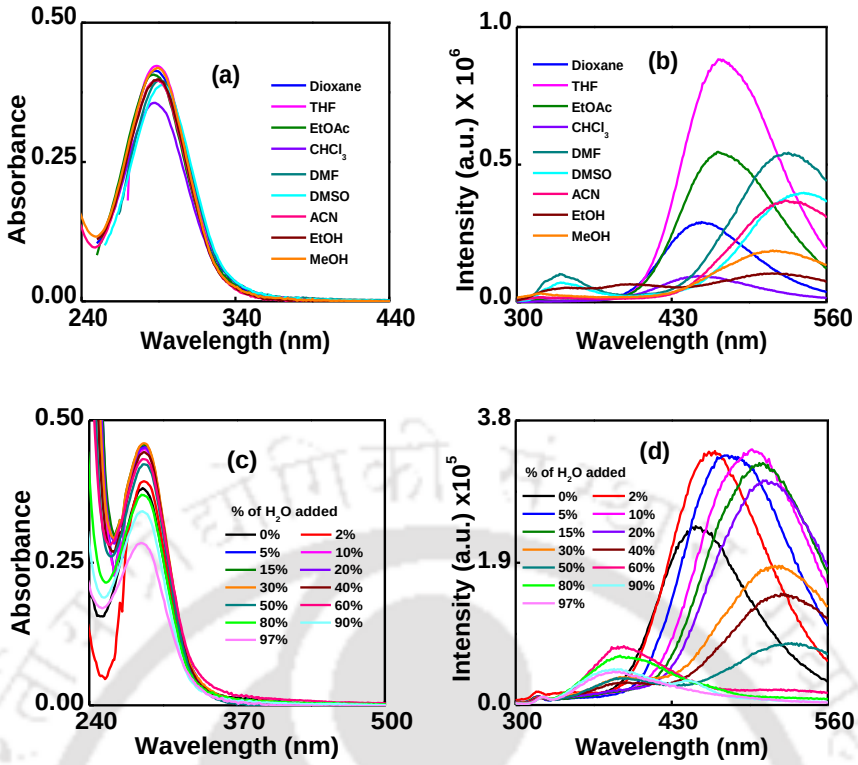

Figure 2.14. (a) UV-visible, (b) fluorescence emission spectra in various organic solvents for nucleoside **2.45E**. Dioxane-water titration: (c) UV-visible, (d) fluorescence emission spectra for same. The concentration of the nucleoside **2.45E** was 10 μM.

Table 2.3. Summary table of photophysical properties of the nucleoside **2.45E**

Entry 2.45E	**Solvents**								
Prop. ↓	**Diox**	**$CHCl_3$**	**EtOAc**	**THF**	**DMSO**	**DMF**	**EtOH**	**ACN**	**MeOH**
Δf	0.021	0.148	0.201	0.21	0.265	0.275	0.29	0.305	0.309
λ_{max}^{abs} (nm)	287	287	287	289	292	292	290	290	290
λ_{max}^{fl} (nm)	449	452	469	469	338, 541	338, 528	519	525	515
Φ_f	0.012	0.007	0.019	0.029	0.019	0.02	0.012	0.012	0.0008

Table 2.4. Summary table of fluorescence properties of the nucleoside **2.45E**

Entry 2.45E	**Solvents**							
Properties ↓	**Dioxane**	**THF**	**ACN**	**MeOH**	**$D_{95}W_5$**	**$D_{85}W_{15}$**	**$D_{70}W_{30}$**	**$D_{50}W_{50}$**
Δf	0.021	0.21	0.305	0.309	0.186	0.249	0.262	0.277
λ_{max}^{abs} (nm)	287	289	290	290	287	287	288	288
λ_{max}^{fl} (nm)	449	469	525	515	478	506	388, 518	388, 532
Φ_f	0.012	0.029	0.01	0.0008	0.018	0.017	0.01	0.005
<τ> [ns]	1.15	2.77	6.47	2.72	1.76	2.9	3.24	1.82
k_f [10^8 s^{-1}]	0.1	0.1	0.02	0.003	0.102	0.058	0.03	0.027
k_{nr} [10^8 s^{-1}]	8.59	3.50	1.53	3.67	5.58	3.39	3.05	5.47
D_pW_q = Dioxane (D) and water (W) solvent mixture; p and q are the volume of each solvent.								

The nucleoside containing pyrene fluorophore **2.45G** exhibited most interesting photophysics among the series of the synthesized nucleosides. This nucleoside showed slight blue-shifting (by 2-4 nm) in the absorption spectra when the polarity was increased from dioxane to methanol (**Figure 2.15a**). This nucleoside exhibited dual-emission behavior in low polar solvents like toluene, dioxane, chloroform, ethyl acetate, and THF. A red shift in the ICT band of about 84 nm (453-537 nm) with a decrease in intensity was observed when the solvent polarity was increased from toluene to THF (**Figure 2.15b**, **Table 2.5**). The LE band in these solvents consists of structured pyrene-like emission at 385 and 403 nm. However, in high polar solvents like ACN, EtOH and MeOH, only structured pyrene-like emission (LE emission) has been observed (**Figure 2.15b**). In a dioxane-water titration, we have revealed similar observation. In pure dioxane, the ICT emission at 487 nm was fully dominated over the LE emission. As the percentage of H_2O was increased up to 40%, the intensity of the ICT band gradually decreased with a strong red shift of 89 nm, while the intensity of LE emission increased gradually. Beyond this point, we observed only pure LE emission (**Figure 2.15d**). The fluorescence quantum yield of this nucleoside also followed a similar trend (**Table 2.6**).

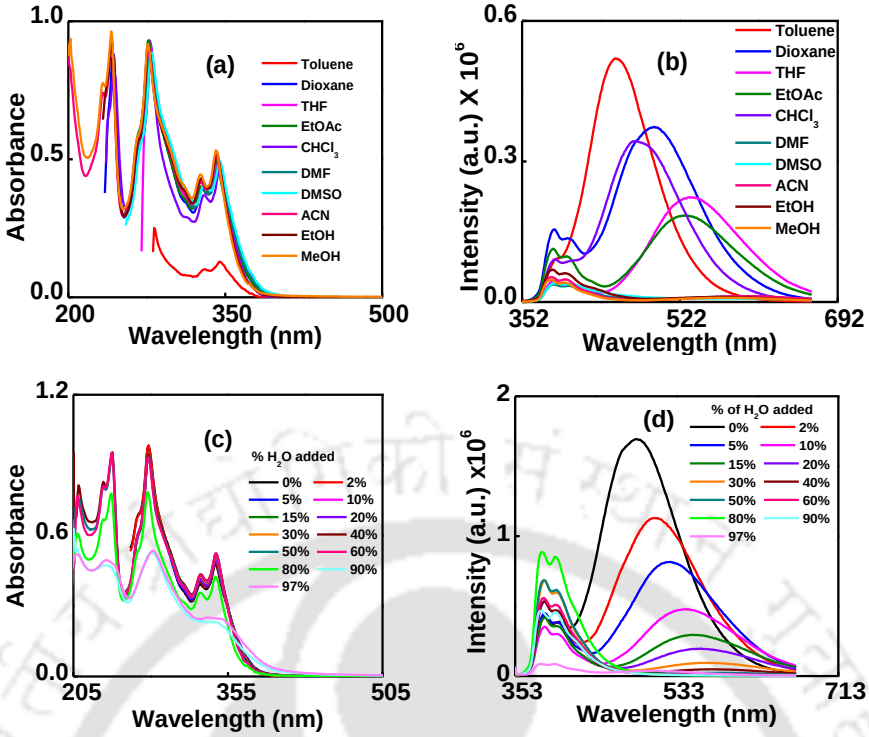

Figure 2.15. (a) UV-visible, (b) fluorescence emission spectra in various organic solvents for nucleoside **2.45G**. Dioxane-water titration: (c) UV-visible, (d) fluorescence emission spectra for same. The concentration of the nucleoside **2.45G** was 10 µM.

Furthermore, the values of τ_1 and τ_2 remain consistent while the relative contributions of the two lifetimes vary according to the observed wavelengths in dioxane and THF. Thus, the contribution from longer lifetime component τ_2 increased from 49% to 57% as the monitoring wavelength was changed from 400 to 495 nm in dioxane. The similar behavior was also observed in THF solvent. The decreased intensity of ICT band was reflected by the decreased lifetime from τ_1 = 0.13 (in dioxane) to τ_1 = 0.06 ns in THF (**Table 2.6**). We also observed a similar trend in a dioxane-water titration, the values of τ_1 and τ_2 were consistent while the relative contributions of the two lifetimes vary according to the observed wavelengths in the dioxane-water solvent mixture (**Table 2.6**).

Table 2.5. Summary table of photophysical properties of the nucleoside **2.45G**

Entry 2.45G	**Solvents**									
Properties ↓	**Toluene**	**Dioxane**	**$CHCl_3$**	**EtOAc**	**THF**	**DMSO**	**DMF**	**EtOH**	**ACN**	**MeOH**
Δf	0.013	0.021	0.148	0.201	0.21	0.265	0.275	0.29	0.305	0.309
λ_{max}^{abs} (nm)	282, 345	243, 278, 328, 343	244, 279, 345	245, 277, 326, 341	278, 343	280, 330, 346	278, 328, 344	241, 277, 326, 342	241, 276, 327, 341	241, 276, 326, 341
λ_{max}^{fl} (nm)	390, 453	387, 400, 494	387, 474	385, 401, 527	386, 403, 537	388, 406	386, 402,	385, 398,	384, 400,	382, 397
Φ_f	---	0.079	0.062	0.042	0.04	0.02	0.012	0.025	0.011	0.008

To interpret the photophysical properties in a more intuitive manner, we recorded the time-resolved fluorescence spectra of the pyrenyl nucleoside, **2.45G** in different solvents, which also supported the observation of steady-state fluorescence. Thus, we collected the lifetime data by monitoring both LE and ICT emissions with an excitation light of 337 nm which showed biexponential decays (**Table 2.6**). When we monitored the decay at LE emission (400 nm) in dioxane, the relative contribution of the longer lifetime component (τ_1 = 10.88 ns) was found to decrease from 49% to 39% as the solvent polarity increased (in THF, τ_1 = 7.13 ns), while the same was increased from 51% (τ_1 = 0.99 ns) to 61% (τ_1 = 0.66 ns) for the case of the shorter lifetime component. In methanol, the component contributing 49% showed a decay time τ_2 = 7.64 ns, while the other component contributing 51% showed a decay time τ_2 = 0.59 ns. These results suggest only a weak emission from LE state and no ICT emission which might be due to the nonradiative pathway followed by the chromophore in methanol (**Table 2.6**).

Table 2.6. Summary table of fluorescence properties of the nucleoside **2.45G**

Entry 2.45G		**Solvents**						
Properties ↓		**Dioxane**	**THF**	**ACN**	**$D_{95}W_5$**	**$D_{85}W_{15}$**	**$D_{70}W_{30}$**	**$D_{50}W_{50}$**
Δf		0.021	0.21	0.305	0.186	0.249	0.277	0.294
λ_{max}^{abs} (nm)		328, 343	343	327, 341	328 , 343	328 , 343	328 , 343	328, 343
λ_{max}^{fl} (nm)		387, 400, 494	386, 403, 533	384, 400, 590	386, 401, 526	386, 401, 550	386, 400, 570	385, 399, 580
LE	Φ_f	0.007	0.002	0.003	0.024	0.022	0.038	0.038
	τ_1[ns]	0.9 (51%)	0.6 (61%)	1.0 (42%)	1.5 (32%)	1.4 (29%)	1.8 (26%)	2.2 (21%)
	τ_2[ns]	10.8 (49%)	7.1 (39%)	11.7 (58%)	23.4 (68%)	26.8 (71%)	28.4 (74%)	29.3 (79%)
	k_f	0.012	0.006	0.004	0.015	0.011	0.017	0.016
	k_{nr}	1.68	3.13	1.37	0.60	0.50	0.44	0.41
ICT	Φ_f	0.054	0.035	0.002	0.027	0.01	0.003	0.0005
	τ_1[ns]	0.13 (43%)	0.06 (49%)	0.1 (40%)	0.3 (49%)	0.2 (56%)	0.1 (56%)	0.3 (92%)
	τ_2[ns]	1.3 (57%)	1.9 (51%)	1.4 (60%)	3.4 (51%)	1.3 (44%)	1.3 (44%)	1.31 (8%)
	k_f	0.71	0.35	0.021	0.14	0.15	0.05	0.013
	k_{nr}	12.44	9.55	10.73	5.23	15	15.82	25.63
k_f and k_{nr} in 10^8 s^{-1}; D_pW_q = Dioxane (D) and water (W) solvent mixture; p and q are the volume of each solvent.								

To gain insight into different solvatochromic behaviors of benzonitrile (**2.45C**), naphthyl (**2.45E**) and pyrenyl (**2.45G**) nucleosides, we studied the correlations of their absorption ($\tilde{\nu}_{max}^{abs}$) and fluorescence maxima ($\tilde{\nu}_{max}^{fl}$) with the solvent polarity function Δf (**Figure 2.16**). Thus, from the plots, it was clear that for all the cases, the $\tilde{\nu}_{abs}$ values apparently correlate linearly with Δf values. This indicated that the ground states of these fluorophoric nucleosides were moderately polar in nature. However, the $\tilde{\nu}_{fl}$ values for all the nucleosides showed a very good

linear correlation with Δ*f* for the whole range of the solvent polarity tested which indicates that the nature of the fluorescent states remained essentially unchanged in all the solvents for all the cases. However, due to modulation by the solvents, the spectral feature changes significantly. The highly polar nature of the fluorescence states of these nucleosides was evident from the high slopes of the $\tilde{\nu}_{fl}$ vs Δ*f* plots, indicating their possible ICT character (**Figure 2.16a-c**).[113, 135-146] Morever, a plot of Stokes' shift ($\Delta\tilde{\nu}$) in different solvents against solvent polarity parameter Δ*f* also showed a good linear correlation with Δ*f* with large slopes which also suggested that the fluorescence states are highly polar in nature (**Figure 2.16d**).

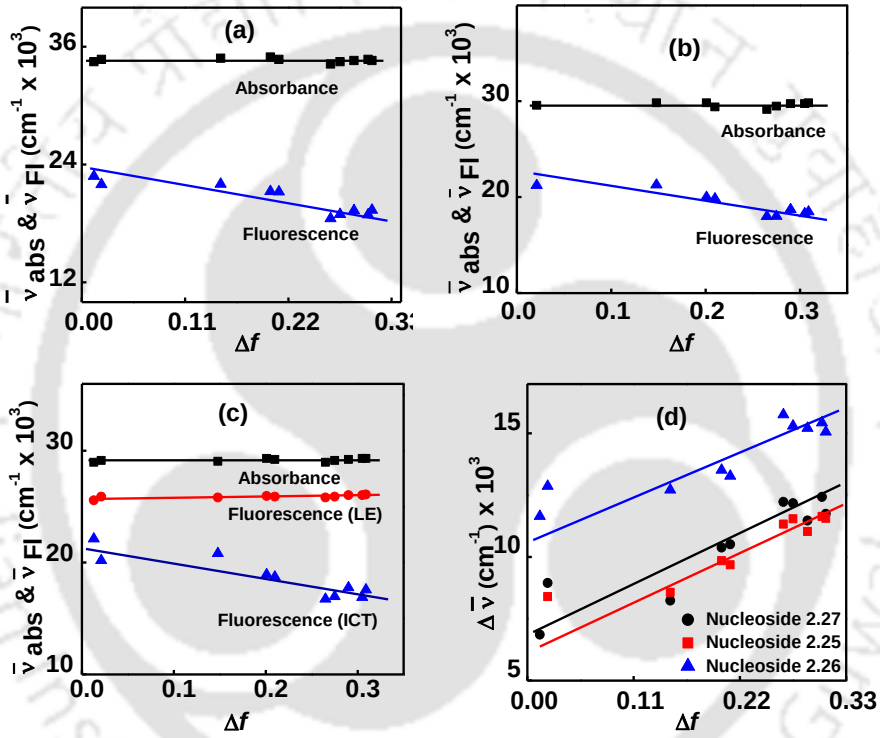

Figure 2.16. Plots of $\tilde{\nu}_{fl}$ and $\tilde{\nu}_{abs}$ values against Δ*f* for fluorescently labeled nucleoside **2.45C** (a), **2.45E** (b) and **2.45G** (c) ($\tilde{\nu}_{fl(ICT)}$ and $\tilde{\nu}_{abs}$ values) in different solvents. (d) plot of $\Delta\tilde{\nu}$ values against Δ*f* in different solvents for **2.45C**, **2.45E** and **2.45G**.

2.7.3. Theoretical Calculations

We next carried out a theoretical calculation to support the observed polarity-dependent emission and the ICT feature using the Gaussian 09 program package.[147] From the HOMO-LUMO overlap and transition oscillator strength, it is clear that the $S_0 \rightarrow S_1$ electronic transitions are fully allowed for all the three representative nucleosides indicating the reverse transition, *i.e.*, $S_0 \leftarrow S_1$, as fully allowed. Redistribution of electronic charge density was reflected from an

overlap in HOMO-LUMO supporting the solvatochromicity and intramolecular charge transfer emissions (**Figure 2.17-2.20**).[135, 148-152] As for example, except for coumarin (**2.44D**), the TDDFT calculations suggested the $S_0 \rightarrow S_1$ transitions with high configuration interaction (CI) values as the dominant orbital transitions in the low-lying singlet excited states of the studied nucleosides. Interestingly, the universal linker unit with the triazole at C5-position of 2′-deoxyuridine comprised the HOMO, while the aromatic fluorophoric unit irrespective of their substituents formed the LUMO in all the studied nucleosides supporting our designing concept. Except for the case of coumarin (**2.44D**), the triazole unit overlapped with the LUMO of the chromophore indicating a good electronic redistribution and ICT character (**Figure 2.17-2.20**).

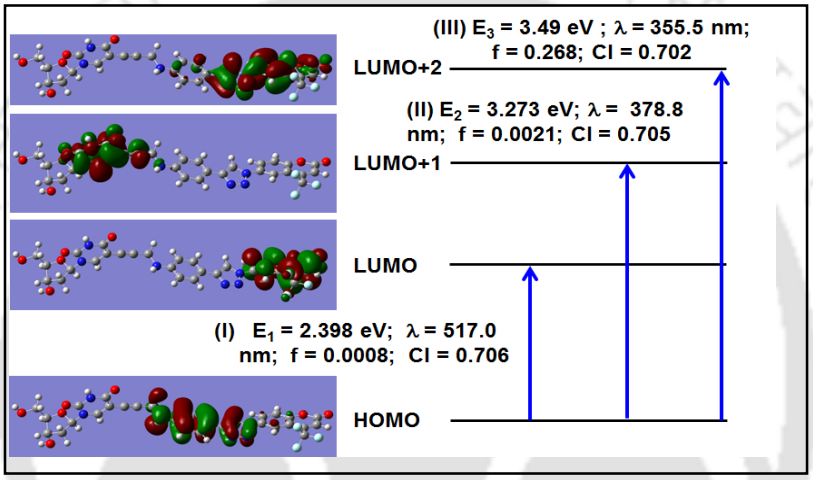

Figure 2.17. The possible transitions from TD-DFT calculation for the nucleoside containing coumarin (**2.44D**).

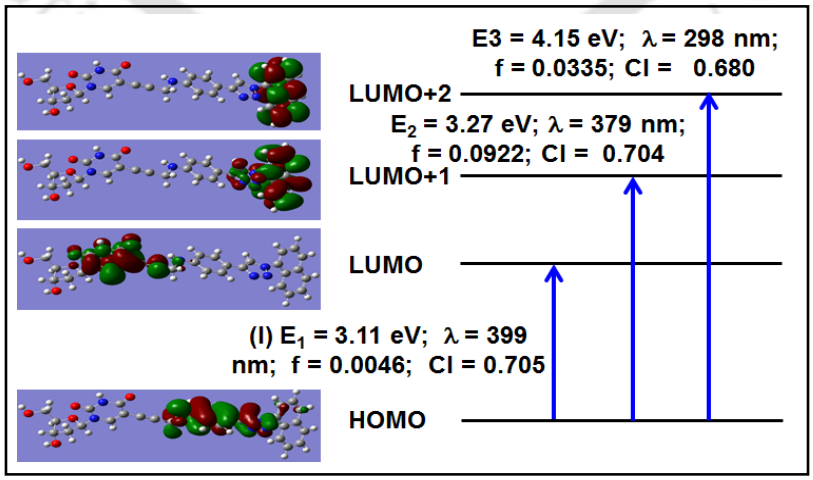

Figure 2.18. The possible transitions from TD-DFT calculation for the nucleoside containing naphthalene (**2.44E**).

Thus, the calculated excitation energy for the transition $S_0 \rightarrow S_1$ for pyrene (**2.45G**) and benzonitrile (**2.45E**) containing fluorescent nucleosides were found to be 436 nm (2.84 eV, f = 0.1299; CI = 0.704) (**Figure 2.19**); 407 nm (3.05ev, f = 0.217, CI = 0.705) (in vacuum) (**Figure 2.20**), respectively. These values co-related with the experimental results of 343 nm (Dioxane) and 346 nm (THF) respectively. Other two prominent transitions are at 414.8 nm (2.98 eV; f = 0.0006; CI = 0.703) and 348.8 nm (3.56 eV; f = 0.508; CI = 0.641) for pyrenyl nucleoside ((**Figure 2.19**) and at 376.4 nm (3.29 eV; f = 0.0010; CI = 0.705) and 315 nm (3.93 eV; f = 0.0551; CI = 0.702) for benzonitrile nucleoside (**Figure 2.20**). For the case of coumarin (**2.44D**) and naphthalene (**2.45E**) labeled nucleosides, along with weak $S_0 \rightarrow S_1$ transition (f = 0.0008/0.0046), the prominent transitions are observed from $S_0 \rightarrow S_2$ and $S_0 \rightarrow S_3$, respectively indicating the emissive states of these nucleosides as LE state (**Figure 2.17, 2.18**).

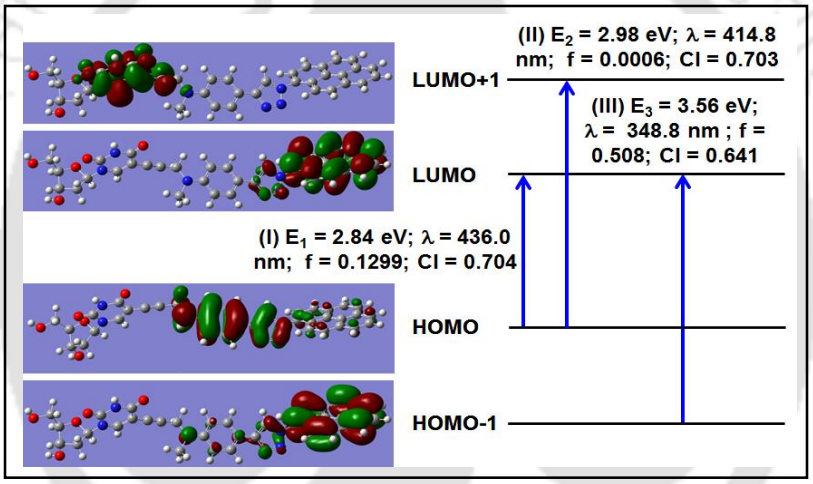

Figure 2.19. The possible transitions from TD-DFT calculation for the nucleoside containing pyrene (**2.45G**).

From the strong HOMO-LUMO mixing it is clear that the emissive state of benzonitrile (**2.45E**) is characterized by more significant electron redistribution, *i.e.*, ICT feature**.** The calculations rationalized the explanation of ICT origin of the solvent polarity dependency of the nucleosides emission (**Figure 2.20**). The pyrene nucleoside (**2.45G**) showed dual emission. The long wavelength band is highly sensitive to the polarity of the solvent i.e., ICT origin. Thus the dual emission comes from both LE and CT states. The transition from HOMO-1 to LUMO is closer to the experimental value with higher *f* value (*f* = 0.508) indicating that the S_2 state is populated well (**Figure 2.19**).

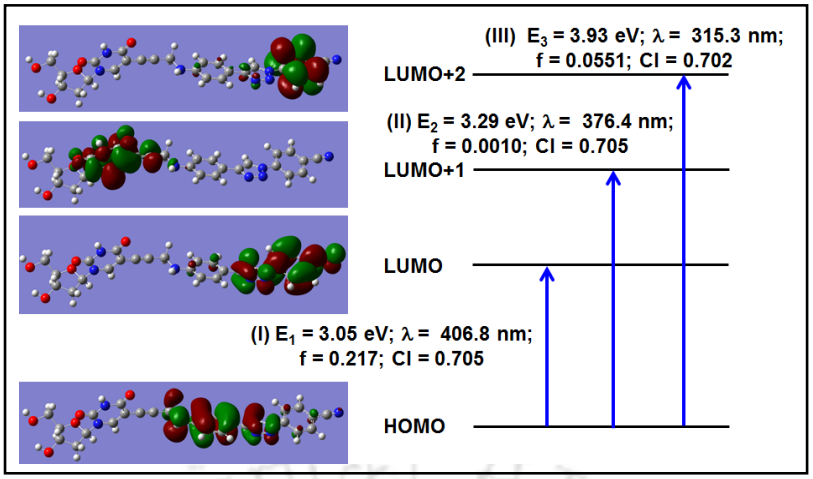

Figure 2.20. The possible transitions from TD-DFT calculation for the nucleoside containing benzonitrile (**2.45E**).

2.8. Conclusion

In conclusion, we have successfully synthesized few novel triazolyl donor and/or acceptor chromophore containing fluorescent nucleosides via Sonogashira coupling and click reaction which showed high solvatochromic properties in various solvents. The synthetic scheme was simple and most of the reagent, starting materials are easily available commercially at very low cost. The main importance of our work is the utilization of a simple donor phenylacetylene as linker to generate solvatochromic fluorescent nucleoside via click reaction with readily available fluorogenic aryl azides and hopefully all the experimental and theoretical results clearly showed that the fluorogenic aromatic azides having no substituent or electron withdrawing substituent, such as –CN, upon reaction with the universal donor phenylacetylene linker of the 2′-deoxyuridine under click reaction condition would able to generate interesting fluorescent nucleoside. Furthermore, the fluorophoric moieties in these nucleosides showed a direct correlation between the fluorescence intensities and the solvent polarity. All these results along with the fluorescence band-shape and quantum yields revealed a correlation between the D-A structure and the emissive states. The emissions from the nucleoside **2.45C**, **2.45E** and **2.45G** were originating from ICT states, indicated by their strong fluorescence emission with broad band-shapes, high quantum yield, and high solvofluorochromicity. In addition to that, the nucleoside **2.45G** exhibited solvent polarity independent LE emission originated from a non-polar $^1\pi$–π^* state. Therefore, the dual emission as was observed for nucleoside **2.45G**

indicated the presence of a mixed LE and CT state wherein the switching between these two states depends on the structure and the solvent polarity.

The strong polarity sensitive ICT emission from these nucleosides can be utilized in monitoring the change in micropolarity inside and outside a DNA duplex. Thus, these nucleosides would be useful in generating fluorescent oligonucleotide probes for DNA analysis. Furthermore, the sensing index derived from the intensity ratio between ICT and LE emission could be employed for the same. The dual emitting fluorescent pyrene containing nucleoside would impact greatly in nucleoside research as rare examples of such nucleosides exist in the literature. Furthermore, the donor phenylacetylene linker reported here is interesting and would find wide applications in generating fluorescent nucleosides or post-synthetically derived fluorescent oligonucleotide probes.

2.9. Experimental Section

2.9.1. General Experimental

All reactions were carried out under a nitrogen atmosphere in flame-dried glassware, using schlenk line. Organic extracts were dried over anhydrous sodium sulfate. Solvents were removed in a rotary evaporator under reduced pressure. Silica gel (60- 120 mesh size) was used for the column chromatography. Reactions were monitored by TLC on silica gel 60 F254 (0.25 mm). ^{1}H NMR spectra were recorded at 400 MHz or 600MHz and ^{13}C NMR spectra were recorded at 100 or at 150MHz (mentioned accordingly). Coupling constants (J value) were reported in Hertz. The chemical shifts were shown in ppm downfield from tetramethylsilane, using residual chloroform (δ = 7.26 in ^{1}H NMR, δ = 77.23 in ^{13}C NMR) or DMSO (δ = 2.5 in ^{1}H NMR, δ = 39.5 in ^{13}C NMR) as an internal standard. The NMR-FID files were processed in MestReNova v9.0 software. Mass spectra were recorded with a High-Resolution mass spectrometer (HRMS) and data analyzed by using the built-in software. IR spectra were recorded on KBr plate in an FT-IR spectrophotometer and reported in frequency of absorption (cm^{-1}). For dioxane-water titration experiments, water was taken from a Milli-Q purification system. For photophysical studies, all solutions were freshly prepared just before doing the experiments.

2.9.2. Synthesis and Characterizations

Synthesis of 4-iodo-N-methylaniline (2.37): This compound was synthesized following a modified literature procedure.[153] 3.95 g (13.84 mmol) of *N*-methylaniline (**2.36**) was taken in a round bottom (R.B.) flask and was dissolved in 20 ml of pyridine: dioxane (1:1). The resulting reaction mixture was cooled to 0 °C in an ice bath and half of the total 5.6 g (22.14 mmol) of I_2 was added to it. While maintaining the ice cooled condition, remaining half amount of I_2 was added after 2 hours. After stirring for about 3 hours, the ice bath was removed and the reaction mixture was stirred at room temperature for another 22 hours. After completion of the reaction, monitored by TLC, the reaction mixture was partitioned between ethyl acetate and water. The collected organic layer was washed with saturated sodium thiosulfate solution, water, and brine solution. After evaporation, the crude product was purified by column chromatography (Si-gel, Hex: EtOAc = 30:1) to obtain the 4-iodo-N-methylaniline **2.37** as a dark yellow liquid. Yield 92 % (7.97 g).^{1}H NMR ($CDCl_3$, 400 MHz): δ 7.4 (d, *J* = 8.4 Hz, 2H), 6.36 (d, *J* = 8.4 Hz, 2H), 3.71 (s, 1H), 2.767 (s, 3H); ^{13}C NMR ($CDCl_3$, 100MHz): δ 148.9, 137.8, 114.7, 77.7, 30.6.

Synthesis of N-methyl-4-((trimethylsilyl)ethynyl)aniline (2.38): This compound was synthesized following a modified literature procedure. 5 g (21.45 mmol) of 4-iodo-N-methylaniline (**2.37**) was taken in a dry R.B. and dissolved in 20 ml of dry benzene. To the above solution, 10 ml of dry n-butylamine was added and the resulting mixture was degassed for 10 minutes by bubbling N_2 through it. $PdCl_2(PPh_3)_2$ (0.45 g, 0.03 mmol) followed by CuI (0.04 g, 0.01 mmol), were added to the reaction mixture while continuing the degassing. Finally, trimethylsilylacetylene (3.16 g, 32.17 mmol) was added to the reaction mixture and it was refluxed (70-80 °C) under N_2 atmosphere for 7 hours. After completion of the reaction, the reaction mixture was partitioned between ethyl acetate and water. The collected organic layer was washed with an aqueous ammonium chloride solution, water, brine solution and dried over anhydrous Na_2SO_4. After evaporation, the crude product was purified by column chromatography (Si-gel, Hex: EtOAc = 30:1) to obtain product **2.38** as a reddish-brown liquid. Yield: 83% (3.62 g). IR (KBr): ῡ 3421, 2147, 1609, 1521cm^{-1}; ^{1}H NMR ($CDCl_3$, 400 MHz): δ 7.06 (d, *J* = 8.8 Hz, 2H), 6.23 (d, *J* = 8.8 Hz, 2H), 3.64 (s, 1H), 2.56 (s, 3H), 0.00 (s, 9H); ^{13}C NMR ($CDCl_3$, 100 MHz): δ 149.5, 133.4, 111.8, 106.6, 91.1, 30.4, 0.7; **+ESI-HRMS** calculated for $C_{12}H_{18}NSi$ **[M+H]**$^+$ 204.1203, found 204.1198.

Synthesis of N-methyl-N-(prop-2-yn-1-yl)-4-((trimethylsilyl)ethynyl)aniline (2.39): This

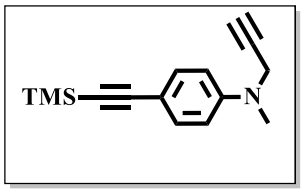

compound was synthesized following a modified literature procedure.[154] 2.5 g (12.29 mmol) of *N*-methyl-4-((trimethylsilyl)ethynyl)aniline (**2.38**) was taken in a R.B. and dissolved in 8 ml of dry DMF. K_2CO_3 (2.55 g, 18.44 mmol) was added to the mixture followed by propargylbromide (2.19 g, 18.44 mmol). The resulting reaction mixture was stirred at 50 °C for 15 hours under N_2 atmosphere. After completion of reaction, the reaction mixture was partitioned between ethyl acetate and water. Collected organic layer was washed with water, brine solution and dried over anhydrous Na_2SO_4. After evaporation, the product was purified by column chromatography (Si-gel, Hex: EtOAc = 30:1) and obtained as brown semi solid. Yield: 79 %(2.36g). IR (KBr): ῡ 3279, 2147, 1883, 1605, 1517cm^{-1}; ^{1}H NMR ($CDCl_3$, 400 MHz): δ 7.36 (d, *J* = 8.4 Hz, 2H), 6.71 (d, *J* = 8.4 Hz, 2H), 4.05 (d, *J* = 1.6 Hz, 2H), 2.98 (s, 3H), 2.17 (s, 2H), 0.2 (s, 9H); ^{13}C NMR ($CDCl_3$, 100 MHz): δ 148.9, 133.3, 113.4, 106.2, 91.9, 79.0, 72.3, 42.2, 38.5, 0.3; **+ESI-HRMS** calculated for $C_{15}H_{20}NSi$ **[M+H]**$^+$ 242.1360, found 242.1356.

Synthesis of 3′,5′-di-O-tert-butyldimethylsilyl-5-iodo-2′-deoxyuridine (2.41):This

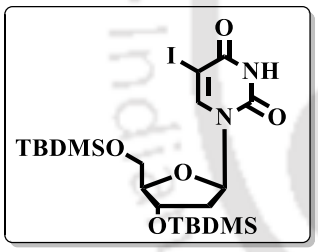

compound was synthesized following a modified literature procedure.[155] 4 g (11.23 mmol) of 5-iodo-2′-deoxyuridine (**2.40**) was taken in a dry R.B. and dissolved in dry DMF. The reaction mixture was vacuumed and filled with N_2. Imidazole (3.85 g, 56.49 mmol) was added to the reaction mixture and the clear reaction mixture was vacuumed one more time and filled with N_2. The above mixture was cooled to 0 °C in an ice bath and t-butyldimethylsilylchloride (5.08 g, 33.69 mmol) was added to the reaction mixture. The ice bath was removed after 1 hour and the resulting mixture was stirred at room temperature under N_2 for 18 hours. After completion of reaction, the reaction mixture was partitioned between ethyl acetate and water. Collected organic layer was washed with water, brine solution and dried over anhydrous Na_2SO_4. After evaporation, the product was purified by column chromatography (Si-gel, Hex: EtOAc = 5:1) and obtained as white foam. Yield: 96% (6.35 g). IR (KBr): ῡ 3457, 3184, 3062, 2954, 2931, 2857,1694, 1607cm^{-1}; ^{1}H NMR ($CDCl_3$, 600 MHz): δ 8.96 (s, 1H), 8.07 (s, 1H), 6.26 (t, *J* = 6.6 Hz, 1H), 4.38 (s, 1H), 3.97 (s, 1H), 3.88 (d, *J* = 11.4 Hz, 1H), 3.75 (d, *J* = 10.8 Hz, 1H), 2.31-2.28 (m, 1H), 2.00-1.96 (m, 1H), 0.93 (s, 9H), 0.88 (s, 9H), 0.14 (d, *J* = 6.6 Hz, 6H), (0.07) (d, *J* = 4.8 Hz, 6H); ^{13}C NMR ($CDCl_3$, 150 MHz): δ 160.2, 150.0, 144.6, 88.6, 86.0, 72.7, 68.5, 63.2, 42.2, 38.7, 26.3,

25.9, 18.7, 18.2, -4.4, -4.6, -4.9, -5.0; **+ESI-HRMS** calculated for $C_{21}H_{40}IN_2O_5Si_2$ **[M+H]** $^+$ 583.1515, found 583.1511.

Synthesis of 3′,5′-di-O-tert-butyldimethylsilyl-5-(3-((4-ethynylphenyl)(methyl)amino)propynyl)-2′-deoxyuridine (2.42):This compound was

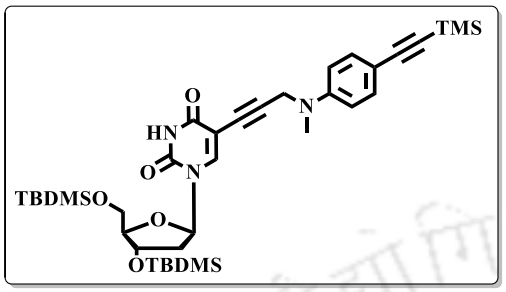

synthesized following a modified literature procedure.[156] 1.12 g (1.92 mmol) of 3′,5′-bis-*O*-tert-butyldimethylsilyl-5-iodo-2′-deoxyuridine (**2.41**) and *N*-methyl-*N*-(prop-2-yn-1-yl)-4-((trimethylsilyl)ethynyl)aniline (**2.39**) were taken in a dry R.B. and dissolved in 15 ml dry Et_3N. The resulting mixture was degassed by bubbling N_2 through it. After 10 minutes, $PdCl_2(PPh_3)_2$ (40.49 mg, 0.057 mmol) followed by CuI (3.66 mg, 0.019 mmol) were added to the above mixture while continuing the degassing. The resulting mixture was stirred at 55 °C for 7 hours. After completion, the reaction mixture was partitioned between ethyl acetate and water. Collected organic layer was washed with aqueous ammonium chloride, water, brine solution and dried over anhydrous Na_2SO_4. After evaporation, the product was purified by column chromatography (Si-gel, Hex: EtOAc = 3:1) and obtained as light brown foam. Yield: 78 % (783 mg). IR (KBr): ῡ 3451, 3047, 2954, 2930, 1714, 1688, 1609 cm^{-1}; ^1H NMR ($CDCl_3$, 600 MHz): δ 8.53 (s, 1H), 7.86 (s, 1H), 7.35 – 7.32 (m, 2H), 6.72 – 6.69 (m, 2H), 6.25 (dd, J = 7.5, 5.4 Hz, 1H), 4.38-4.36 (m, 1H), 4.25 (s, 2H), 3.96 (q, J = 2.4 Hz, 1H), 3.84 (dd, J = 11.4, 2.4 Hz, 1H), 3.73 (dd, J = 11.4, 2.4 Hz, 1H), 3.01 (s, 3H), 2.31 – 2.27 (m, 1H), 2.00 – 1.96 (m, 1H), 0.88 (s, 9H), 0.87 (s, 9H), 0.22 (s, 9H), 0.07 (s, 3H), 0.06 (s, 6H), 0.04 (s, 3H); ^{13}C NMR ($CDCl_3$, 150 MHz): δ 161.5, 149.2, 148.9, 142.4, 133.3, 113.1, 111.7, 106.3, 99.8, 91.7, 89.7, 88.5, 86.0, 77.2, 75.3, 72.6, 63.1, 43.0, 42.1, 38.4, 26.1, 25.8, 18.5, 18.1, 0.3, -4.5, -4.7, -5.2, -5.5; **+ESI-HRMS** calculated for $C_{36}H_{58}N_3O_5Si_3$ **[M+H]** $^+$ 696.3679, found 696.3672.

***Synthesis of 3′,5′-di-O-tert-butyldimethylsilyl-5-(3-((4-ethynylphenyl)(methyl)amino)propynyl)-2′-deoxyuridine(2.43)*:** This compound was

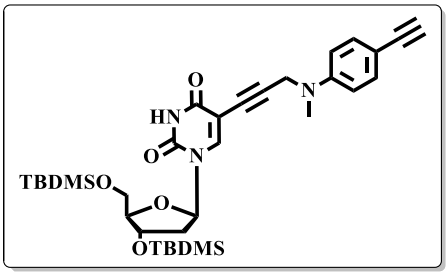

synthesised following a modified literature procedure.[157] 991 mg (1.42 mmol) of **(2.42)** was taken in a dry R.B. and dissolved in 10 ml dry methanol. Anhydrous K_2CO_3 (984g, 7.11 mmol) was added to the above solution and the resulting mixture was stirred for 4 hours at room temperature. After completion of reaction, the reaction mixture was partitioned between ethyl

acetate and water. Collected organic layer was washed with water, brine solution and dried over anhydrous Na_2SO_4. After evaporation, the product was purified by column chromatography (Si-gel, Hex: EtOAc = 4:1) and obtained as dark orange foam. Yield: 87% (773g). IR (KBr): $\tilde{\nu}$ 3312, 2954, 2928, 1712, 1685, 1609 cm^{-1}; ^1H NMR ($CDCl_3$, 600 MHz): δ 9.23 (s, 1H), 7.86 (s, 1H), 7.36 (d, *J* = 8.4 Hz, 2H), 6.72 (d, *J* = 9.0 Hz, 2H), 6.25 (t, *J* = 6.6 Hz, 2H), 4.36 (t, *J* = 2.4 Hz, 1H), 3.95 (s, 1H), 3.83 (d, *J* = 11.4 Hz, 1H), 3.72 (d, *J* = 11.4, 1H), 3.01 (s, 3H), 2.96 (s, 1H), 2.31-2.28 (m, 1H), 2.00-1.92 (m, 1H), 0.87 (s, 9H), 0.86 (s, 9H), 0.06 (s, 6H), 0.03 (s, 6H); **+APCI-HRMS** calculated for $C_{33}H_{50}N_3O_5Si_2$ **$[M+H]^+$** 624.3284, found 624.3299.

General Procedure for the Synthesis of Aryl Azides: An ice cold solution of sodium nitrite (3 eqv.) in water was added dropwise to a cold solution of arylamine (1 eqv.) in water and concentrated hydrochloric acid at 0 °C over 7 to10 min. The reaction mixture was slowly stirred for 1-2 min before an ice cold solution of sodium azide (6 eqv.) in water was added dropwise at 0 °C over 10 min. The mixture was stirred for 15 min. The resulting mixture was extracted with hexane. The organic layer was washed with water, followed by a brine solution, dried over anhydrous Na_2SO_4. After evaporation, the product was passed through a section of silica gel (60-120 mesh). Formation of the azides were confirmed from FT-IR study and yields were within 60%-80% in all cases. The produced azides were then immediately used for the next step without further purification.

General Procedure for Click Reaction: Alkyne (1 eqv.) and azide (1.5 eqv.) were suspended in a 1:1 water/*tert*-butanol mixture. Sodium ascorbate (0.05 eqv., freshly prepared in 1ml water) was added, followed by $CuSO_4.5H_2O$ (0.2eqv., freshly prepared in 1ml water). The reaction mixture was refluxed (70 °C) for 12 hours. The progress of the reaction was monitored by TLC. After completion of the reaction, *tert*-butanol was evaporated in a rotary evaporator and the reaction mixture was partitioned between ethyl acetate and water. The collected organic layer was washed with water, aqueous ammonium chloride, brine solution and dried over anhydrous Na_2SO_4. After evaporation, the product was purified by column chromatography.

General Procedure for Deprotection of Tertiarybutyldimethylsilyl Ether: To a solution of respective TBDMS protected nucleoside (1eqv.) in THF, a solution of tetra-*n*-butylammoniumfluoride (TBAF) (2.5 eqv.) in THF was added. The reaction mixture was stirred at room temperature for 1 hour. After completion of the reaction, the solvent was evaporated in a rotary evaporator and was partitioned between ethyl acetate and water. The

collected organic layer was washed with brine solution and dried over anhydrous Na_2SO_4. After evaporation, the crude material obtained was purified by column chromatography.

Synthesis of 3′,5′-di-O-tert-butyldimethylsilyl-5-(3-((4-(1-(4-bromophenyl)-triazolyl)phenyl)(methyl)amino)propynyl)-2′-deoxyuridine (2.44A): Using general procedure for click reaction, starting from 100 mg (0.16 mmol) of compound **2.43** and 47.5 mg of 1-azido-4-bromobenzene (0.24 mmol), the title compound was isolated by Si-gel column chromatography (Hex: EtOAc = 3:1) as yellow solid. Yield: 52% (68 mg); m.p. 138-140 °C. IR (KBr): ῡ 3423, 2928, 2856, 1717, 1688, 1618 cm^{-1}; ^1H NMR ($CDCl_3$, 600 MHz): δ 8.05 (s, 1H), 7.90 (s, 1H), 7.77 (d, *J* = 8.4 Hz, 2H), 6.90 (d, *J* = 8.4 Hz, 2H), 6.25 (t, *J* = 6.6 Hz, 2H), 4.36 (s,1H), 4.28 (s, 2H), 3.95 (s, 1H), 3.84 (d, *J* = 11.4 Hz, 1H), 3.72 (d, *J* = 11.4, 1H), 3.05 (s, 3H), 2.30-2.27 (m, 1H), 2.00-1.96 (m, 1H), 0.86 (s, 18H), 0.07 (s, 6H), 0.05 (s, 6H); ^{13}C NMR ($CDCl_3$, 150 MHz): δ 149.3, 149.1, 142.5, 136.3, 133.0, 122.2, 121.9, 119.7, 116.1, 114.1, 99.9, 90.1, 88.6, 86.1, 75.4, 72.6, 63.1, 43.3, 42.1, 38.7, 26.1, 25.9, -4.4, -4.6, -5.1, -5.4; **+ESI-HRMS** calculated for $C_{39}H_{54}BrN_6O_5Si_2$ **$[M+H]^+$** 821.2872, found 821.2873.

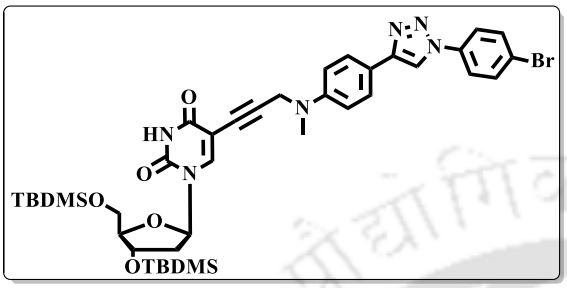

Synthesis of 3′,5′-di-O-tert-butyldimethylsilyl-5-(3-((4-(1-(4-nitrophenyl)-triazolyl)phenyl)(methyl)amino)propynyl)-2′-deoxyuridine(2.44B): Using general procedure for click reaction, starting from 100 mg (0.16 mmol) of compound **2.43** and 40 mg of 1-azido-4-nitrobenzene (0.24 mmol), the title compound was isolated by Si-gel column chromatography (Hex: EtOAc = 1:1) as rust brown solid. Yield: 52% (68 mg). IR (KBr): ῡ 3427, 2925, 1688, 1618, 1501 cm^{-1}; ^1H NMR ($CDCl_3$, 600 MHz): δ 9.39 (s, 1H), 8.36 (d, *J* = 8.4 Hz, 2H), 8.18 (s, 1H), 7.97 (d, *J* = 8.4 Hz, 2H), 7.95 (s, 1H), 7.75 (d, *J* = 8.4 Hz, 2H), 6.88 (d, *J* = 8.4 Hz, 2H), 6.26 (t, *J* = 6 Hz, 1H), 4.37 (s,1H), 4.25 (s, 2H), 3.95 (s, 1H), 3.87 (d, *J* = 10.8 Hz, 1H), 3.74 (d, *J* = 11.4, 1H), 3.03 (s, 3H), 2.30-2.28 (m, 1H), 2.01-1.97 (m, 1H), 0.89 (s, 9H), 0.87 (s, 9H), 0.1 (s, 6H), 0.06 (s, 6H); ^{13}C NMR ($CDCl_3$, 150 MHz): δ 162.1, 149.6, 149.5, 149.4, 147.0, 142.6, 141.4, 127.1, 125.6, 120.2, 119.1, 116.0, 114.1, 99.9, 90.0, 88.6,

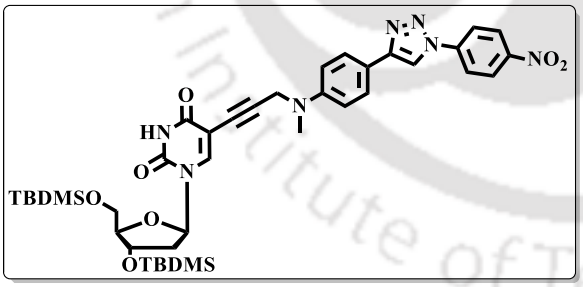

86.1, 75.7, 72.6, 63.1, 43.3, 42.2, 38.9, 26.2, 25.9, -4.5, -4.6, -5.2, -5.4; **+ESI-HRMS** calculated for $C_{39}H_{54}N_7O_7Si_2$ **[M+H]**$^+$ 788.3618, found 788.3617.

Synthesis of 3′,5′-di-O-tert-butyldimethylsilyl-5-(3-((4-(1-(4-cyanophenyl)-triazolyl)phenyl)(methyl)amino)propynyl)-2′-deoxyuridine(2.44C): Using general procedure for click reaction, starting from 100 mg (0.16 mmol) of compound **2.43** and 35 mg of 4-azidobenzonitrile (0.24 mmol), the title compound was isolated by Si-gel column chromatography (Hex: EtOAc = 2:1)as yellow solid. Yield: 94% (116 mg); m.p. 135-137 °C. IR (KBr): ῡ 3415, 2929, 2857, 1699, 1619, 1607 cm^{-1}; ^{1}H NMR ($CDCl_3$, 600 MHz): δ 9.39 (s, 1H), 8.36 (d, *J* = 8.4 Hz, 2H), 8.18 (s, 1H), 7.97 (d, *J* = 8.4 Hz, 2H), 7.95 (s, 1H), 7.75 (d, *J* = 8.4 Hz, 2H), 6.88 (d, *J* = 8.4 Hz, 2H), 6.26 (t, *J* = 6 Hz, 1H), 4.37 (s,1H), 4.25 (s, 2H), 3.95 (s, 1H), 3.87 (d, *J* = 10.8 Hz, 1H), 3.74 (d, *J* = 11.4, 1H), 3.03 (s, 3H), 2.30-2.28 (m, 1H), 2.01-1.97 (m, 1H), 0.89 (s, 9H), 0.87 (s, 9H), 0.1 (s, 6H), 0.06 (s, 6H); ^{13}C NMR ($CDCl_3$, 150 MHz): δ 162.1, 149.6, 149.5, 149.4, 147.0, 142.6, 141.4, 127.1, 125.6, 120.2, 119.1, 116.0, 114.1, 99.9, 90.0, 88.6, 86.1, 75.7, 72.6, 63.1, 43.3, 42.2, 38.9, 26.2, 25.9, -4.5, -4.6, -5.2, -5.4; **+ESI-HRMS** calculated for $C_{40}H_{54}N_7O_5Si_2$ **[M+H]**$^+$ 768.3719, found 768.3717.

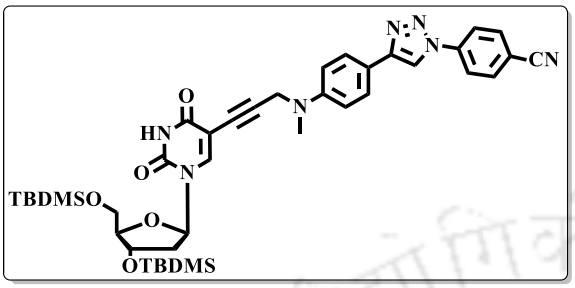

Synthesis of3′,5′-di-O-tert-butyldimethylsilyl-5-(3-(methyl(4-(1-(4-(trifluoromethyl)-7-coumarinyl)-triazolyl)phenyl)amino)propynyl)-2′-deoxyuridine(2.44D): Using general procedure for click reaction, starting from 100 mg (0.16 mmol) of compound **2.43** and 61 mg of 7-azido-4-trifluoromethylcoumarin (0.24 mmol), the title compound was isolated by Si-gel column chromatography (Hex: EtOAc =1:1)as yellow solid. Yield: 94% (132 mg); m.p. 227-230 °C. IR (KBr): ῡ 3425, 2955, 2929, 1720, 1686, 1617, 1607 cm^{-1}; ^{1}H NMR ($CDCl_3$, 600 MHz): δ 8.97 (s, 1H), 8.17 (s, 1H), 7.92 (s, 1H), 7.85 (d, *J* = 12.6 Hz, 3H), 7.77 (d, *J* = 7.2 Hz, 2H), 6.89 (d, *J* = 6.6 Hz, 2H), 6.83 (s, 1H), 6.25 (t, *J* = 6.6 Hz, 2H), 4.37 (s,1H), 4.26 (s, 2H), 3.95 (s, 1H), 3.85 (d, *J* = 11.4 Hz, 1H), 3.73 (d, *J* = 10.8, 1H), 3.04 (s, 3H), 2.30-2.28 (m, 1H), 2.01-1.98 (m, 1H), 0.88 (s, 9H), 0.87 (s, 9H), 0.08 (s, 6H), 0.06 (s, 6H); 13C NMR (CDCl3, 150 MHz): δ 161.8, 158.34, 155.3, 149.6, 149.5, 149.3, 142.5, 140.2, 127.1, 119.1, 116.4, 115.7,

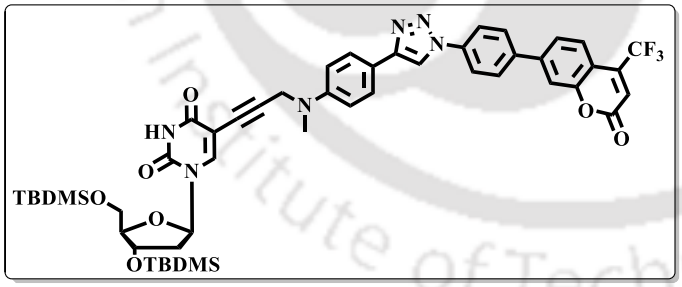

114.1, 113.1, 108.5, 99.9, 89.9, 88.1, 75.6, 72.6, 63.16, 43.3, 42.2, 38.7, 29.8, 26.2, 25.9, 18.5, 18.2, -4.4, -4.6, -5.1, -5.4; **+ESI-HRMS** calculated for $C_{43}H_{54}F_3N_6O_7Si_2$**[M+H]**$^+$ 879.3539, found 879.3531.

***Synthesis of 3′,5′-di-O-tert-butyldimethylsilyl-5-(3-((4-(1-(1-naphthyl)-triazolyl)phenyl)(methyl)amino)propynyl)-2′-deoxyuridine(2.44E)*:** Using general procedure

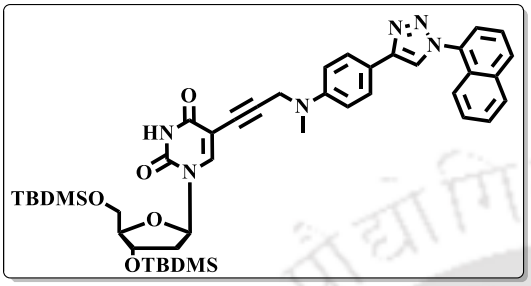

for click reaction, starting from 104 mg (0.166 mmol) of compound **2.43** and 1-azidonaphthalene (42.25 mg, 0.25 mmol), the title compound was isolated by Si-gel column chromatography (Hex: EtOAc = 2:1)as brown semi-solid. Yield: 53% (70 mg); m.p. 91-94 °C. IR (KBr): ῡ 3408, 2954, 2928, 2856, 1698, 1619 cm^{-1}; ^{1}H NMR ($CDCl_3$, 400 MHz): δ 8.95 (s, 1H), 8.03 (s, 2H), 7.96 (bs, 1H), 7.90 (s, 1H), 7.83 (bs, 2H), 7.69 (bs, 1H), 7.59 (m, 5H), 6.93 (bs, 2H), 6.25 (s, 1H), 4.37 (s, 1H), 4.29 (s, 2H), 3.95 (s, 1H), 3.84 (bs, 1H), 3.74-3.73 (m, 1H), 3.06 (s, 3H), 2.28-2.28 (m, 1H), 1.99 (bs, 1H), 0.87 (s, 18H), 0.06 (s, 12H); ^{13}C NMR ($CDCl_3$, 100 MHz): δ 161.9, 149.3, 148.2, 142.5, 134.3, 130.4, 128.4, 127.2, 127.0, 125.2, 123.7, 122.7, 121.2, 120.0, 114.2, 99.9, 90.1, 88.6, 86.1, 77.5, 77.2, 76.9, 63.1, 43.3, 42.1, 38.7, 26.1, 25.9, -4.4, -4.6, -5.1, -5.4; **+ESI-HRMS** calculated for $C_{43}H_{57}N_6O_5Si_2$ **[M+H]**$^+$ 793.3923, found 793.3925.

Synthesis of 3′,5′-di-O-tert-butyldimethylsilyl-5-(3-((4-(1-(2-anthrayl)-triazolyl)phenyl)(methyl)amino)propynyl)-2′-deoxyuridine(2.44F):Using general procedure

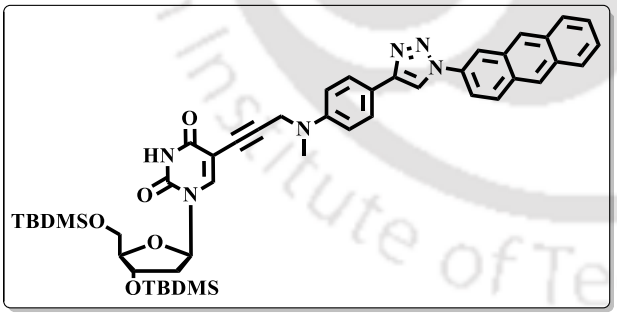

for click reaction, starting from 100 mg (0.16 mmol) of compound **2.43** and 53 mg of 2-azidoanthracene (0.24 mmol), the title compound was isolated by Si-gel column chromatography (Hex: EtOAc = 3:1)as yellow solid. Yield: 57% (77 mg); m.p. 204-208 °C. IR (KBr): ῡ 3406, 2953, 2928, 2856, 1699, 1619 cm^{-1}; ^{1}H NMR ($CDCl_3$, 600 MHz): δ 8.51 (s, 1H), 8.49 (s, 1H), 8.42 (s, 1H), 8.33 (s, 1H), 8.25 (s, 1H), 8.17 (d, *J* = 9.0 Hz, 1H), 8.03 (dd, *J* = 5.4, 3.6 Hz, 2H), 7.98 (dd, *J* = 9.0, 2.0 Hz, 1H), 7.91 (s, 1H), 7.84 (d, *J* = 8.4 Hz, 2H), 7.55 – 7.50 (m, 2H), 6.93 (d, *J* = 8.4 Hz, 2H), 6.25 (dd, *J* = 7.8, 6.0 Hz, 1H), 4.39 – 4.36 (m, 1H), 4.30 (s, 2H), 3.96 (d, *J* = 2.4 Hz, 1H), 3.85 (dd, *J* = 11.4, 2.4 Hz, 1H), 3.73 (dd, *J* = 11.4, 2.4 Hz, 1H), 3.07 (s, 3H), 2.31– 2.27 (m, 1H), 2.02 – 1.97 (m, 1H), 0.88 (s, 9H), 0.88 (s, 9H), 0.08 (d, *J* = 2.4 Hz, 6H), 0.06 (d, *J* = 4.8 Hz, 6H); ^{13}C NMR ($CDCl_3$, 150 MHz): δ 161.5,

149.3, 149.1, 142.4, 134.1, 132.6, 130.9, 130.7, 128.4, 128.2, 127.1, 127.0, 126.8, 126.4, 126.2, 119.9, 119.2, 117.8, 116.3, 114.1, 99.9, 88.5, 86.1, 77.1, 75.3, 72.6, 63.1, 43.3, 42.1, 38.7, 26.1, 25.8, 18.5, 18.1, -4.5, -4.7, -5.2, -5.46; **+ESI-HRMS** calculated for $C_{47}H_{59}N_6O_5Si_2$ **[M+H]** $^+$ 843.4080, found 843.4085.

Synthesis of 3′,5′-di-O-tert-butyldimethylsilyl-5-(3-((4-(1-(4-pyrenyl)-triazolyl)phenyl)(methyl)amino)propynyl)-2′-deoxyuridine (2.44G): Using general procedure for click reaction, starting from 100 mg (0.16 mmol) of compound **2.43** and 58 mg of 1-azidopyrene (0.24 mmol), the title compound was isolated by Si-gel column chromatography (Hex: EtOAc = 3:1) as pale yellow solid. Yield: 77% (107 mg); m.p. 135-138 °C. IR (KBr): ῦ 3423, 3046, 2954, 2928, 2856, 1699, 1619 cm^{-1}; ^{1}H NMR ($CDCl_3$, 600 MHz): δ 8.29 (dd, *J* = 6.0, 3 Hz, 2H), 8.26 (d, *J* = 6.6 Hz, 1H), 8.20 (d, *J* = 9.0 Hz, 1H), 8.16 (s, 1H), 8.16 (s, 1H), 8.14 (s, 1H), 8.13 – 8.08 (m, 2H), 7.96 (d, *J* = 9.0 Hz, 1H), 7.90 (d, *J* = 6.0 Hz, 2H), 7.88 (s, 1H), 6.96 (d, *J* = 9.0 Hz, 2H), 6.25 (dd, *J* = 7.8, 5.4 Hz, 1H), 4.38 (dt, *J* = 5.4, 2.4 Hz, 1H), 4.31 (s, 2H), 3.96 (q, *J* = 2.4 Hz, 1H), 3.86 (dd, *J* = 11.4, 2.4 Hz, 1H), 3.74 (dd, *J* = 11.4, 1.8 Hz, 1H), 3.08 (s, 3H), 2.32 – 2.27 (m, 1H), 2.03 – 1.97 (m, 1H), 0.90 (s, 9H), 0.88 (s, 9H), 0.09 (d, *J* = 3.0 Hz, 6H), 0.07 (d, *J* = 4.8 Hz, 6H); ^{13}C NMR ($CDCl_3$, 150 MHz): δ 161.4, 149.3, 149.1, 148.3, 142.4, 132.3, 131.3, 130.8, 130.8, 129.7, 129.0, 127.2, 127.1, 126.9, 126.5, 126.38, 126.2, 125.2, 124.9, 124.36, 123.5, 121.6, 121.5, 120.1, 114.2, 99.9, 90.1, 88.6, 86.1, 77.4, 77.1, 76.9, 75.3, 72.6, 63.1, 43.3, 42.1, 38.7, 26.1, 25.8, 18.5, 18.1, -4.5, -4.7, -5.2, -5.4; **+ESI-HRMS** calculated for $C_{49}H_{59}N_6O_5Si_2$ **[M+H]** $^+$ 867.4080, found 867.4082.

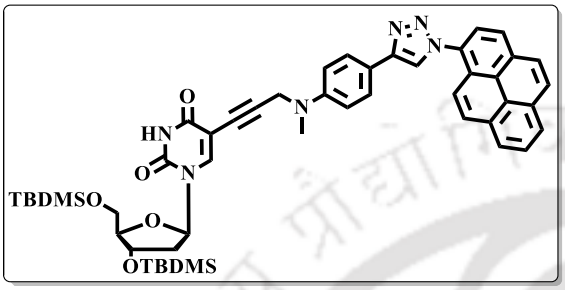

Synthesis of 5-(3-((4-(1-(4-cyanophenyl)-triazolyl)phenyl)(methyl)amino)propynyl)-2′-deoxyuridine (2.45C): Using general procedure for TBDMS deprotection, starting from 230 mg (0.3 mmol) of nucleoside **2.44C**, the title compound was isolated by Si-gel column chromatography ($CHCl_3$: MeOH = 10:1) as orange-yellow solid. Yield: 81% (130 mg); m.p. 178-181 °C. IR (KBr): ῦ 3426, 3056, 2925, 2837, 2229, 1714, 1607, 1619 cm^{-1}; ^{1}H NMR (DMSO-d6, 600 MHz): δ 11.54 (s, 1H), 9.23 (s, 1H), 8.15 – 8.12 (m, 3H), 8.09 (d, *J* = 9.0 Hz, 2H), 7.74 (d, *J* = 9.0 Hz, 2H), 6.95 (d, *J* = 9.0 Hz, 2H), 6.04 (t, *J* = 6.6 Hz, 1H), 5.21 (d, *J* = 4.2 Hz, 1H), 5.06 (t, *J* = 5.0 Hz, 1H), 4.34 (s, 2H), 4.20 – 4.15 (m, 1H), 3.74 (q, *J*

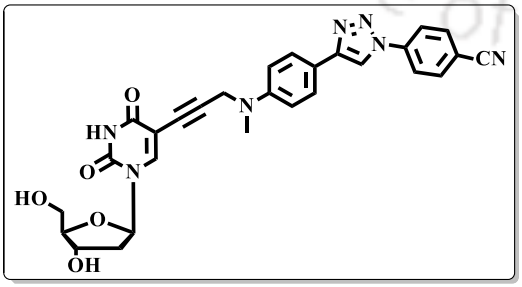

= 3.6 Hz, 1H), 3.59 – 3.53 (m, 1H), 3.54 – 3.49 (m, 1H), 2.95 (s, 3H); ^{13}C NMR (DMSO-d6, 150 MHz): δ 161.5, 149.4, 149.1, 148.3, 143.7, 139.6, 134.3, 126.4, 120.2, 118.8, 118.2, 117.9, 113.9, 110.8, 98.1, 88.6, 87.6, 84.8, 76.1, 70.1, 60.9, 42.1, 40.2, 40.1, 38.0; **+ESI-HRMS** calculated for $C_{28}H_{26}N_7O_5$**[M+H]**$^+$ 540.1990, found 540.1990.

***Synthesis of 5-(3-((4-(1-(naphthayl)-triazolyl)phenyl)(methyl)amino)propynyl)-2′-deoxyuridine(2.45E*)**: Using general procedure for TBDMS deprotection, starting from 94 mg

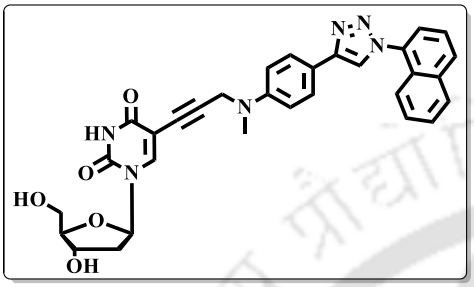

(0.12 mmol) of **2.44E**, the title compound was isolated by Si-gel column chromatography ($CHCl_3$: MeOH = 20:1)as pale yellow solid. Yield: 80% (53 mg); m.p. 152-155 °C. IR (KBr): ῡ 3417, 3059, 2922, 2851, 1691, 1618cm^{-1}; ^{1}H NMR (600 MHz, DMSO-d6): δ 11.61 (s, 1H), 8.96 (s, 1H), 8.21 (d, *J* = 8.4 Hz, 1H), 8.18 (s, 1H), 8.14 (d, *J* = 7.8 Hz, 1H), 7.83 (d, *J* = 8.7 Hz, 2H), 7.80 (d, *J* = 7.0 Hz, 1H), 7.75 – 7.70 (m, 1H), 7.70 – 7.59 (m, 3H), 6.99 (d, *J* = 9.0 Hz, 2H), 6.08 (t, *J* = 6.6 Hz, 1H), 5.25 (d, *J* = 4.2 Hz, 1H), 5.12 (t, *J* = 5.0 Hz, 1H), 4.39 (s, 2H), 4.22 (p, *J* = 4.2 Hz, 1H), 3.78 (q, *J* = 3.2 Hz, 1H), 3.63 – 3.58 (m, 1H), 3.58 – 3.53 (m, 1H), 2.99 (s, 3H); ^{13}C NMR (DMSO-d6, 150 MHz): δ 172.2, 161.6, 149.5, 148.9, 147.1, 143.7, 133.7, 133.5, 130.2, 128.4, 128.1, 127.9, 127.2, 126.4, 125.5, 123.8, 122.6, 122.2, 119.5, 114.1, 98.2, 88.7, 87.6, 84.8, 79.2, 76.2, 70.1, 60.9, 45.7, 42.3, 40.2, 40.1, 38.1; **+ESI-HRMS** calculated for $C_{31}H_{29}N_6O_5$ **[M+H]**$^+$ 565.2194 , found 565.2203.

Synthesis of 5-(3-((4-(1-(pyrenyl)triazolyl)phenyl)(methyl)amino)propynyl)-2′-deoxyuridine (2.45G):Using general procedure for TBDMS deprotection, starting from 158 mg (0.18 mmol) of **2.44G**, the title compound was isolated by Si-gel column chromatography ($CHCl_3$: MeOH = 20:1) as light brown solid. Yield: 85% (99 mg); m.p. 217-220 °C. IR (KBr): ῡ 3420, 3054, 2924, 2851, 1691, 1618cm^{-1}; ^{1}H NMR (DMSO-d6, 600 MHz): δ 11.60 (s, 1H), 9.10 (s, 1H), 8.52 (d, *J* = 8.4 Hz, 1H), 8.46 (d, *J* = 7.2 Hz, 1H), 8.42 (d, *J* = 7.8 Hz, 1H), 8.40 – 8.33 (m, 3H), 8.30 (d, *J* = 9.0 Hz, 1H), 8.22 – 8.17 (m, 2H), 7.93 – 7.87 (m, 3H), 7.01 (d, *J* = 8.4 Hz, 2H), 6.09 (t, *J* = 6.6 Hz, 1H), 5.25 (d, *J* = 4.2 Hz, 1H), 5.12 (t, *J* = 4.8 Hz, 1H), 4.40 (s, 2H), 4.22 (p, *J* = 4.2 Hz, 1H), 3.79 (q, *J* = 3.6 Hz, 1H), 3.64 – 3.59 (m, 1H), 3.59 – 3.54 (m, 1H), 3.01 (s, 3H); ^{13}C NMR (DMSO-d6, 150 MHz): δ 161.6, 149.5, 148.9, 147.3, 143.7, 131.7, 130.7, 130.5, 130.2, 129.7, 128.86, 127.2, 127.2, 126.6, 126.4, 126.2, 125.4, 125.2, 124.1, 123.8, 123.4, 123.0, 121.2,

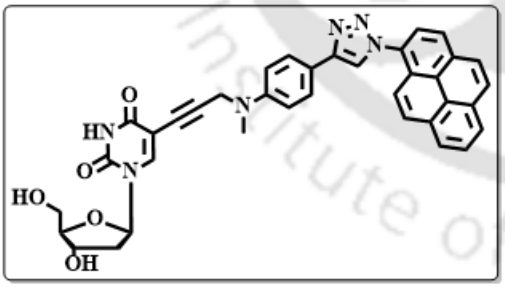

119.5, 114.1, 98.2, 88.7, 87.6, 84.8, 79.2, 76.2, 70.1, 60.9, 42.3, 40.1, 40.1, 39.5, 38.1; **+ESI-HRMS** calculated for $C_{37}H_{31}N_6O_5$ **[M+H]**$^+$ 639.2350, found 639.2313.

2.9.3. Photophysical Studies of the Synthesized Nucleosides

UV-visible Measurements: All the *UV* –visible spectra of the nucleosides (10 μM) were measured in different solvents using Shimadzu UV-2550 UV–Visible spectrophotometer with a quartz cell of 1 cm path length. The measurements were carried out in absorbance mode. The absorbance values of the sample solutions were measured in the wavelength regime of 200–550 nm. All the sample solutions were prepared just before doing the experiment.

Fluorescence Experiments: All fluorescence experiments were performed using Fluoromax 4 spectrophotometer with a cell of 1 cm path length at 298 K. All the sample solutions were prepared as described in UV measurement experiments. The excitation wavelengths for all the cases were set at the excitation maxima of each sample in each solvent and emission spectra were measured in the wavelength regime of 300–700 nm with an integration time of 0.2 sec. All the sample solutions were prepared just before doing the experiment. Fluorescence emissions were collected exciting the samples at the wavelength corresponding to their absorption maxima. The fluorescence quantum yields (Φ_f) were determined using quinine sulfate as a reference with the known Φ_f(0.55) in 0.1 molar solution in sulfuric acid. The following equation was used to calculate the quantum yield,

$$\Phi_S = \Phi_R \frac{Fl_S^{Area}}{Fl_R^{Area}} \frac{Abs_R}{Abs_S} \frac{n_S^2}{n_R^2}$$

where, Φ_R is the quantum yield of standard reference, Fl_S^{Area} (sample) and Fl_R^{Area} (reference) are the integrated emission peak areas, Abs_S (sample) and Abs_R (reference) are the absorbances at the excitation wavelength, and n_S (sample) and n_R (reference) are the refractive indices of the solutions.

The fluorescence lifetime experiment was carried out using a time-resolved fluorescence spectrophotometer at 25 °C using a 1 cm path length cell. 290 and 337 nm LED were used as excitation light source. The lifetime data were calculated by software with a fixed fitting range. The time-correlated single photon counting (TCSPC) method was used to calculate the lifetime data.

2.9.4. Theoretical Calculation

The ground state structures of the fluorophores were optimized using density functional theory (DFT)[147] with B3LYP functional and 6-31G (d) basis set. The excited state related calculations were carried out with the time-dependent density functional theory (TD-DFT) with the optimized structure of the ground state (B3LYP/6-31G(d)). There are no imaginary frequencies in frequency analysis of all the calculated structures, therefore each calculated structure is a local energy minimum.

2.9.5. B3LYP/6-31G* Optimized Structure and Cartesian Coordinates of the Synthesized Compounds

2.9.5.1. Cartesian Coordinates for Coumarin-Based Nucleoside

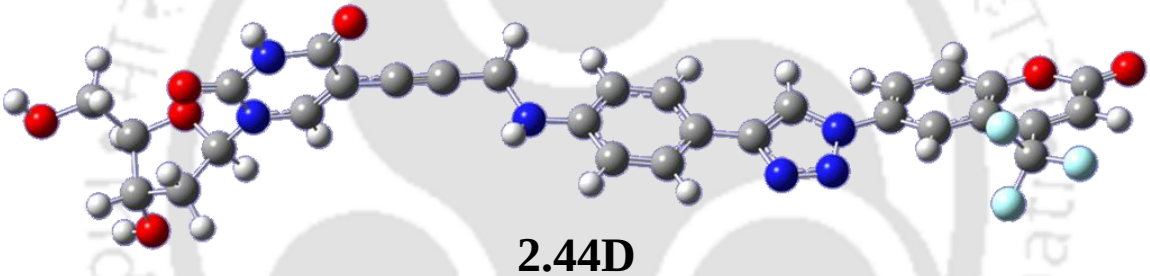

2.44D

E(RB3LYP) = -2311.60304067 a.u.;

Imaginary Freq. = 0; Dipole Moment = 8.2017

Standard orientation:

Center Number	Atomic Number	Atomic Type	Coordinates (Angstroms) X	Y	Z
1	6	0	-11.809880	-0.818242	1.927374
2	6	0	-10.669458	0.183734	1.757772
3	8	0	-10.578638	-1.363393	-0.039804
4	6	0	-11.895325	-1.467549	0.531842
5	6	0	-12.911671	-0.814530	-0.400043
6	8	0	-14.197766	-1.126933	0.130022
7	6	0	-9.750297	-0.557508	0.776436
8	6	0	-7.550169	-0.010441	-0.163787
9	7	0	-8.890400	0.285541	-0.077628
10	6	0	-9.458422	1.280719	-0.891610
11	6	0	-6.662697	0.643213	-0.966111
12	7	0	-8.542997	1.937675	-1.692479
13	6	0	-7.157689	1.731562	-1.825750
14	8	0	-10.644478	1.565364	-0.894811
15	6	0	-4.112075	-0.000223	-1.031246

16	6	0	-2.691425	-0.331816	-1.092992
17	8	0	-6.499766	2.412389	-2.589565
18	7	0	-1.952128	0.301980	-0.005485
19	6	0	-5.286631	0.294518	-0.996929
20	6	0	4.655550	-0.716484	-0.231698
21	7	0	5.853979	-0.347089	0.305202
22	7	0	4.391305	0.820405	1.351122
23	6	0	-0.567098	0.231087	0.059572
24	6	0	0.132345	1.092710	0.930288
25	6	0	1.509982	1.023352	1.050358
26	6	0	2.258345	0.090492	0.308788
27	6	0	1.561691	-0.765436	-0.553809
28	6	0	0.177572	-0.701617	-0.686114
29	6	0	3.715247	0.037071	0.445103
30	8	0	-11.391377	-1.751317	2.921693
31	7	0	5.665585	0.594111	1.271315
32	6	0	7.159725	-0.797702	-0.012078
33	6	0	8.247373	0.027632	0.253248
34	6	0	9.549366	-0.404436	-0.052703
35	6	0	9.719536	-1.672633	-0.644069
36	6	0	8.625790	-2.497848	-0.907588
37	6	0	7.348539	-2.066253	-0.583427
38	6	0	10.757054	0.370233	0.181382
39	6	0	11.965998	-0.124958	-0.161340
40	6	0	12.122745	-1.441935	-0.775883
41	8	0	10.948880	-2.158318	-0.983458
42	6	0	10.661925	1.742725	0.813873
43	8	0	13.168118	-1.942559	-1.108486
44	1	0	-12.760754	-0.344736	2.198977
45	1	0	-11.030663	1.111952	1.318078
46	1	0	-10.176717	0.390566	2.709618
47	1	0	-12.145227	-2.532097	0.625987
48	1	0	-12.770457	-1.226104	-1.409834
49	1	0	-12.731116	0.265959	-0.453560
50	1	0	-14.858789	-0.654844	-0.390495
51	1	0	-9.051541	-1.195488	1.330028
52	1	0	-7.218445	-0.822668	0.471869
53	1	0	-8.938195	2.666512	-2.274963
54	1	0	-2.571350	-1.421759	-1.020395
55	1	0	-2.297994	-0.042155	-2.083150
56	1	0	-2.351382	1.177915	0.301774
57	1	0	4.575672	-1.421888	-1.041425
58	1	0	-0.423971	1.819565	1.517061
59	1	0	2.031010	1.695391	1.723505
60	1	0	2.102242	-1.502912	-1.141244
61	1	0	-0.317289	-1.383225	-1.368566
62	1	0	-12.080441	-2.423726	3.007785
63	1	0	8.070871	0.994674	0.702591
64	1	0	8.798909	-3.471843	-1.350296
65	1	0	6.501154	-2.719989	-0.756078
66	1	0	12.880438	0.429465	0.001570
67	9	0	11.869630	2.313074	0.968787
68	9	0	10.081357	1.674180	2.029457
69	9	0	9.912477	2.571032	0.054974

2.9.5.2. Optimized Structure and Cartesian Coordinates for Benzonitrile-Based Nucleoside

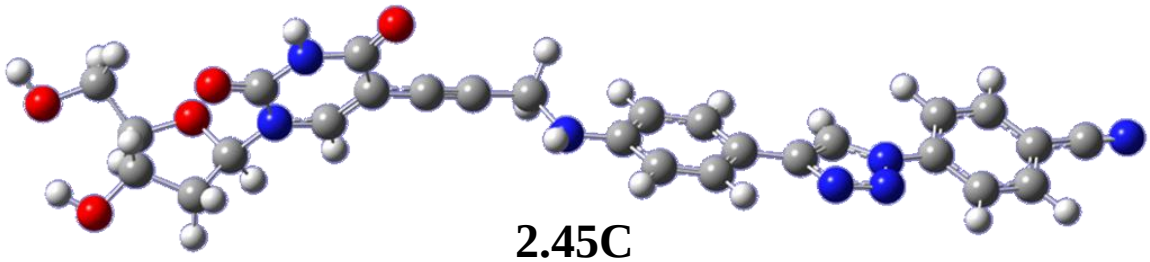

2.45C

E(RB3LYP) = -1802.04346057 a.u.;

Imaginary Freq. = 0; Dipole Moment = 8.8454 Debye

Standard orientation:

Center Number	Atomic Number	Atomic Type	Coordinates (Angstroms) X	Y	Z
1	6	0	-9.875323	-0.638301	1.238866
2	6	0	-8.475262	-0.440231	1.827580
3	8	0	-8.283842	-1.601954	-0.257705
4	6	0	-9.640356	-1.736191	0.184475
5	6	0	-10.567515	-1.624810	-1.014374
6	8	0	-11.890742	-1.719900	-0.479898
7	6	0	-7.512724	-0.954732	0.734754
8	6	0	-5.306089	-0.158485	-0.018084
9	7	0	-6.657425	0.065138	0.087984
10	6	0	-7.252941	1.179766	-0.523290
11	6	0	-4.434194	0.673386	-0.656309
12	7	0	-6.354761	2.017757	-1.156978
13	6	0	-4.960276	1.891360	-1.296269
14	8	0	-8.450373	1.405645	-0.492471
15	6	0	-1.858479	0.151531	-0.787203
16	6	0	-0.424347	-0.107101	-0.879098
17	8	0	-4.317713	2.733080	-1.894975
18	7	0	0.305690	0.584320	0.179103
19	6	0	-3.044577	0.389793	-0.723646
20	6	0	6.942826	-0.214031	-0.042086
21	7	0	8.134866	0.263599	0.422840
22	7	0	6.643232	1.527390	1.305468
23	6	0	1.692792	0.582974	0.217157
24	6	0	2.365643	1.499436	1.052316
25	6	0	3.746819	1.499052	1.147022
26	6	0	4.525584	0.584769	0.413403
27	6	0	3.855764	-0.322299	-0.417950
28	6	0	2.468143	-0.329447	-0.522934
29	6	0	5.984709	0.600643	0.527673
30	8	0	-10.790112	-1.039313	2.242179
31	7	0	7.920889	1.330375	1.246679
32	6	0	9.450971	-0.182327	0.161593
33	6	0	10.486953	0.195368	1.026731
34	6	0	11.781334	-0.238484	0.778447
35	6	0	12.056792	-1.061174	-0.327924

36	6	0	11.012536	-1.432566	-1.189560
37	6	0	9.717231	-0.990442	-0.950435
38	6	0	13.392352	-1.516103	-0.577085
39	7	0	14.476241	-1.887117	-0.780145
40	1	0	-10.204562	0.280543	0.743545
41	1	0	-8.270212	0.591566	2.113455
42	1	0	-8.383485	-1.071230	2.716731
43	1	0	-9.782289	-2.711966	0.673073
44	1	0	-10.391561	-0.657788	-1.504513
45	1	0	-10.366315	-2.426421	-1.738778
46	1	0	-12.520122	-1.499648	-1.176856
47	1	0	-6.794816	-1.664506	1.162093
48	1	0	-4.950677	-1.065987	0.455656
49	1	0	-6.769043	2.833956	-1.591616
50	1	0	-0.247072	-1.187959	-0.790645
51	1	0	-0.067951	0.184046	-1.882797
52	1	0	-0.131995	1.443350	0.481858
53	1	0	6.872165	-1.076510	-0.682345
54	1	0	1.785596	2.212776	1.632541
55	1	0	4.246967	2.211989	1.793317
56	1	0	4.421217	-1.038755	-1.007885
57	1	0	1.994417	-1.047109	-1.182941
58	1	0	-11.624302	-1.206499	1.777792
59	1	0	10.261529	0.824479	1.878160
60	1	0	12.586289	0.050507	1.445105
61	1	0	11.222243	-2.058221	-2.050006
62	1	0	8.924909	-1.259435	-1.639248

2.9.5.3. Optimized Structure and Cartesian Coordinates for Naphthalene-Based Nucleoside

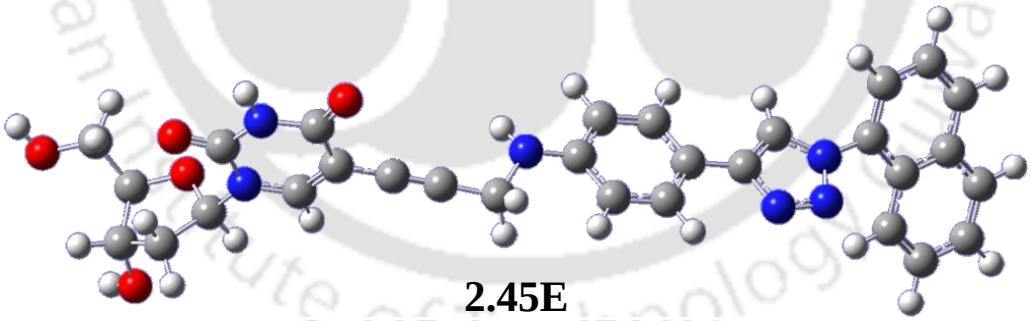

2.45E

E(RB3LYP) = -1863.44380538 a.u.;

Imaginary Freq. = 0; Dipole Moment = 6.2310 Debye

Standard orientation:

Center Number	Atomic Number	Atomic Type	Coordinates (Angstroms) X	Y	Z
1	6	0	-9.882133	2.309619	-0.571192
2	6	0	-9.134052	1.143082	-1.213140
3	8	0	-8.164577	1.574273	0.909670

4	6	0	-9.457144	2.206879	0.907001
5	6	0	-10.420433	1.408311	1.780041
6	8	0	-11.602862	2.196765	1.894299
7	6	0	-7.838680	1.115931	-0.388961
8	6	0	-5.806247	-0.250113	-0.561132
9	7	0	-7.153770	-0.187715	-0.291750
10	6	0	-7.840194	-1.312607	0.196451
11	6	0	-5.043708	-1.374066	-0.444114
12	7	0	-7.052626	-2.442923	0.306795
13	6	0	-5.683413	-2.613667	0.029142
14	8	0	-9.024939	-1.316130	0.487330
15	6	0	-2.480012	-1.385849	-1.038224
16	6	0	-1.059070	-1.387982	-1.375335
17	8	0	-5.149099	-3.694263	0.189166
18	7	0	-0.228254	-1.395380	-0.176421
19	6	0	-3.659692	-1.372561	-0.762287
20	6	0	6.319796	-0.369116	0.649612
21	7	0	7.527907	-0.291174	0.023975
22	7	0	6.115740	-0.716705	-1.533621
23	6	0	1.142250	-1.189587	-0.247173
24	6	0	1.862561	-0.892417	0.928050
25	6	0	3.236670	-0.715281	0.893896
26	6	0	3.958931	-0.825195	-0.307260
27	6	0	3.240186	-1.120726	-1.473973
28	6	0	1.860549	-1.299159	-1.452607
29	6	0	5.411469	-0.640191	-0.356799
30	8	0	-9.389264	3.499965	-1.183445
31	7	0	7.379934	-0.515553	-1.312186
32	1	0	-10.970979	2.229912	-0.672793
33	1	0	-9.685217	0.212434	-1.088655
34	1	0	-8.946387	1.325377	-2.272930
35	1	0	-9.349408	3.210175	1.338825
36	1	0	-10.612638	0.427914	1.327428
37	1	0	-9.943043	1.236945	2.755589
38	1	0	-12.264171	1.677443	2.367297
39	1	0	-7.097345	1.787382	-0.837706
40	1	0	-5.362936	0.680402	-0.894962
41	1	0	-7.538240	-3.264540	0.647047
42	1	0	-0.838915	-0.516523	-2.016985
43	1	0	-0.835517	-2.278413	-1.979954
44	1	0	-0.683709	-1.029271	0.646898
45	1	0	6.217770	-0.205216	1.709666
46	1	0	1.329236	-0.805862	1.871596
47	1	0	3.754728	-0.484764	1.820920
48	1	0	3.780776	-1.208728	-2.410183
49	1	0	1.346918	-1.530785	-2.379021
50	1	0	-9.813525	4.253831	-0.752132
51	6	0	8.808211	-0.102016	0.624038
52	6	0	9.706576	0.891773	0.123162
53	6	0	9.135780	-0.882336	1.713883
54	6	0	9.411388	1.743096	-0.976025
55	6	0	10.967169	1.041052	0.793903
56	6	0	10.375135	-0.713915	2.368423
57	1	0	8.438677	-1.641901	2.051906
58	6	0	10.322500	2.686099	-1.395330
59	1	0	8.468425	1.627348	-1.494718
60	6	0	11.883006	2.021223	0.325326
61	6	0	11.272347	0.223483	1.914261
62	1	0	10.615305	-1.339249	3.222375
63	6	0	11.570952	2.826296	-0.744710

64	1	0	10.080911	3.327701	-2.237318
65	1	0	12.837515	2.124038	0.834395
66	1	0	12.231167	0.353363	2.408399
67	1	0	12.279841	3.571900	-1.092226

2.9.5.4. Optimized Structure and Cartesian Coordinates for Pyrene-Based Nucleoside

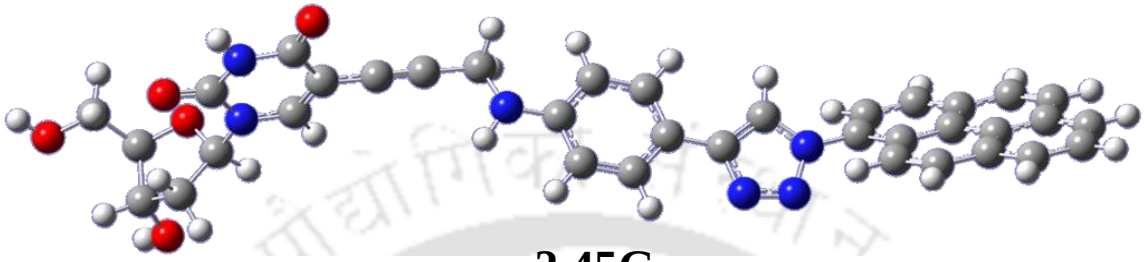

2.45G

E(RB3LYP) = -2093.32737330 a.u.;

Imaginary Freq = 0; Dipole Moment = 4.2695 Debye

Standard orientation:

Center Number	Atomic Number	Atomic Type	Coordinates (Angstroms) X	Y	Z
1	6	0	-11.381849	-1.862549	1.464406
2	6	0	-10.339772	-0.771881	1.704254
3	8	0	-10.277749	-1.369589	-0.591253
4	6	0	-11.529316	-1.852813	-0.070343
5	6	0	-12.670488	-0.978403	-0.581329
6	8	0	-13.877129	-1.633005	-0.195896
7	6	0	-9.449528	-0.915001	0.461510
8	6	0	-7.379216	0.221462	-0.209421
9	7	0	-8.731015	0.300233	0.031064
10	6	0	-9.442670	1.478300	-0.252702
11	6	0	-6.613334	1.249377	-0.673471
12	7	0	-8.651110	2.509232	-0.722706
13	6	0	-7.266049	2.535587	-0.972161
14	8	0	-10.645328	1.604089	-0.091650
15	6	0	-4.023415	0.985782	-1.058916
16	6	0	-2.587706	0.827180	-1.272902
17	8	0	-6.731422	3.543677	-1.392585
18	7	0	-1.834976	1.095802	-0.051696
19	6	0	-5.216073	1.101890	-0.879807
20	6	0	4.691244	-0.335243	-0.442350
21	7	0	5.820482	-0.570098	0.283289
22	7	0	4.275915	-0.245363	1.736655
23	6	0	-0.488345	0.774283	0.050283
24	6	0	0.120466	0.719903	1.321185
25	6	0	1.468304	0.431801	1.455888
26	6	0	2.275637	0.183990	0.330490
27	6	0	1.668869	0.240364	-0.930805
28	6	0	0.314439	0.527630	-1.078627
29	6	0	3.698378	-0.123981	0.496462

30	6	0	13.151612	0.296452	-0.014051
31	8	0	-10.814949	-3.083604	1.935714
32	7	0	5.540244	-0.518474	1.616789
33	6	0	7.113418	-0.915356	-0.208142
34	6	0	8.268574	-0.234851	0.237282
35	6	0	9.529325	-0.630505	-0.314514
36	6	0	9.602544	-1.673548	-1.288647
37	6	0	8.419093	-2.306280	-1.697759
38	6	0	7.194281	-1.935006	-1.160025
39	6	0	8.240536	0.840000	1.192131
40	6	0	9.386266	1.463911	1.580367
41	6	0	10.668359	1.083092	1.060780
42	6	0	10.726672	0.027653	0.102124
43	6	0	11.988782	-0.364270	-0.441276
44	6	0	12.024654	-1.422521	-1.411864
45	6	0	10.885111	-2.045519	-1.817652
46	6	0	11.857891	1.715079	1.457470
47	6	0	13.084348	1.323363	0.925403
48	1	0	-12.341758	-1.654037	1.951608
49	1	0	-10.806437	0.211643	1.728544
50	1	0	-9.788324	-0.944496	2.630404
51	1	0	-11.683776	-2.874370	-0.440844
52	1	0	-12.588397	0.030695	-0.159378
53	1	0	-12.578983	-0.891522	-1.673559
54	1	0	-14.616516	-1.058428	-0.428115
55	1	0	-8.660766	-1.652747	0.650262
56	1	0	-6.931598	-0.741441	0.005753
57	1	0	-9.150425	3.367923	-0.922631
58	1	0	-2.266524	1.520564	-2.063079
59	1	0	-2.388577	-0.189827	-1.654773
60	1	0	-2.371249	0.984380	0.796577
61	1	0	4.703696	-0.308351	-1.519459
62	1	0	-0.481401	0.910951	2.206492
63	1	0	1.919899	0.390335	2.441086
64	1	0	2.257066	0.050753	-1.824740
65	1	0	-0.111020	0.563885	-2.075308
66	1	0	14.110972	-0.002647	-0.427410
67	1	0	-11.440141	-3.795222	1.743187
68	1	0	8.467025	-3.105145	-2.431955
69	1	0	6.286317	-2.448882	-1.458141
70	1	0	7.289214	1.132955	1.616645
71	1	0	9.342861	2.273496	2.303820
72	1	0	12.987782	-1.716294	-1.820407
73	1	0	10.925234	-2.843212	-2.554358
74	1	0	11.810952	2.518075	2.187909
75	1	0	13.994474	1.822875	1.243847

2.10. ^{1}H and ^{13}C NMR Spectra of Few Selected Nucleosides

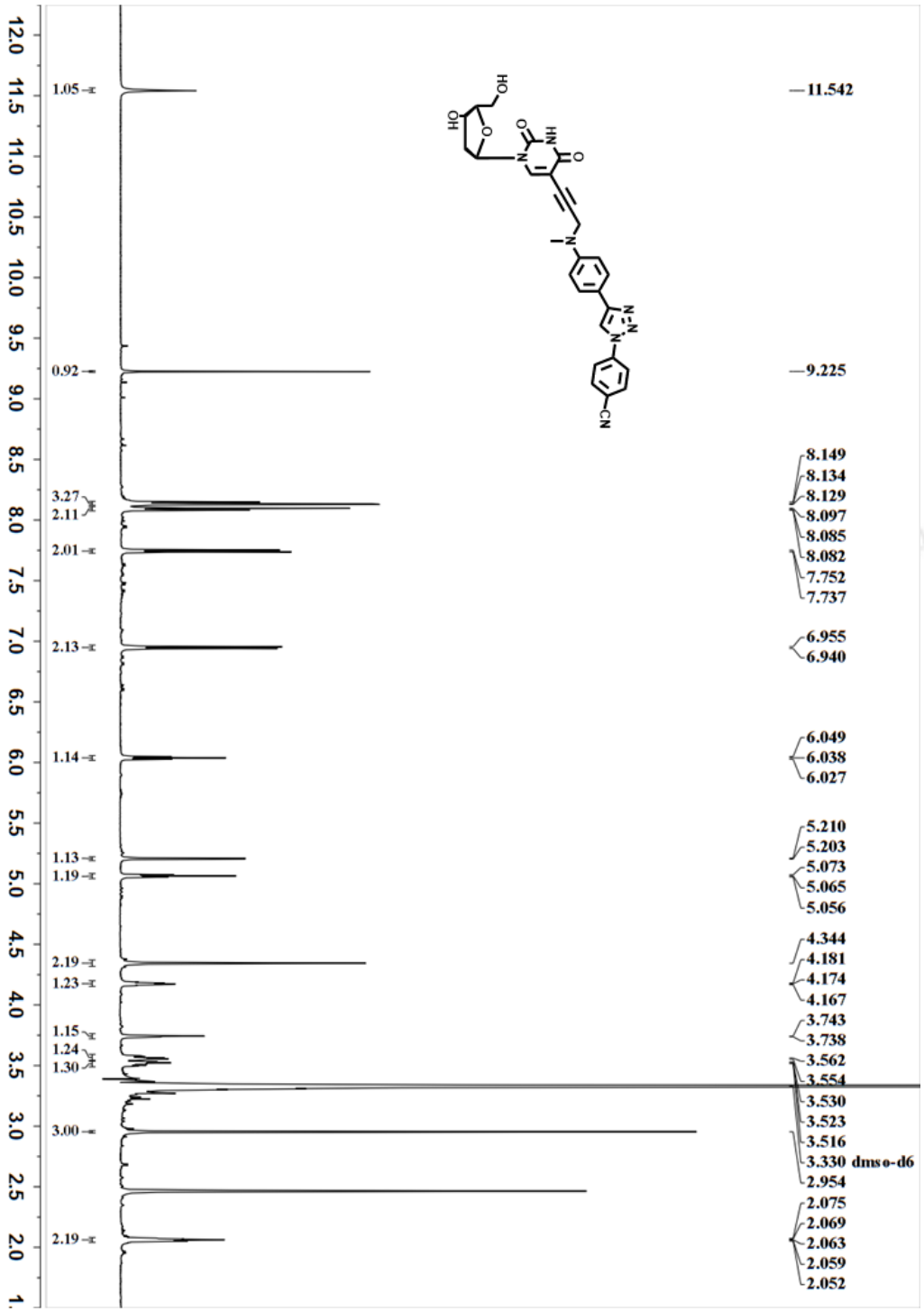

Figure 2.21: ^{1}H NMR spectra of synthesized compound **2.45C**

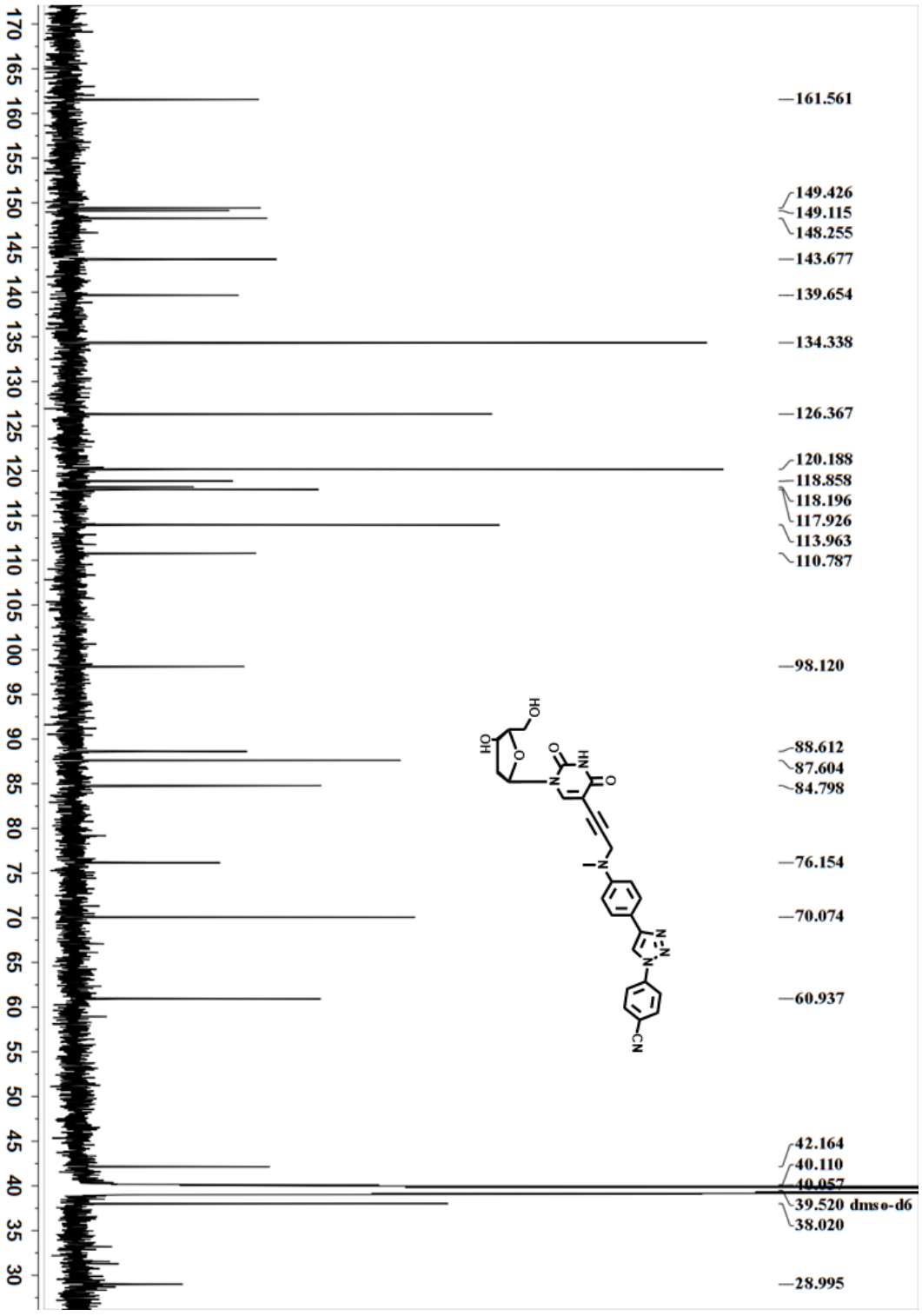

Figure 2.22: ^{13}C NMR spectra of synthesized compound **2.45C**

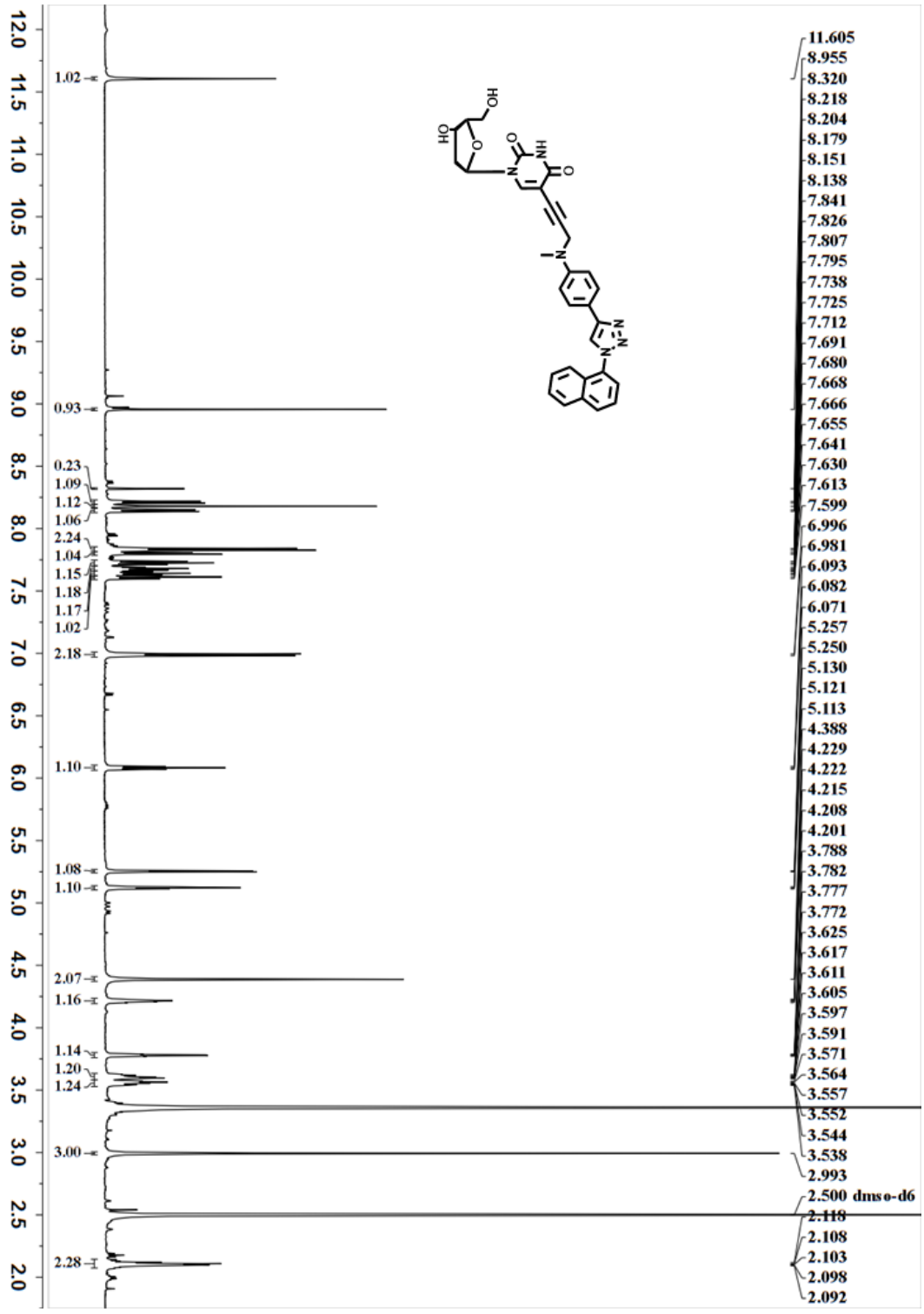

Figure 2.23: ^{1}H NMR spectra of synthesized compound **2.45E**

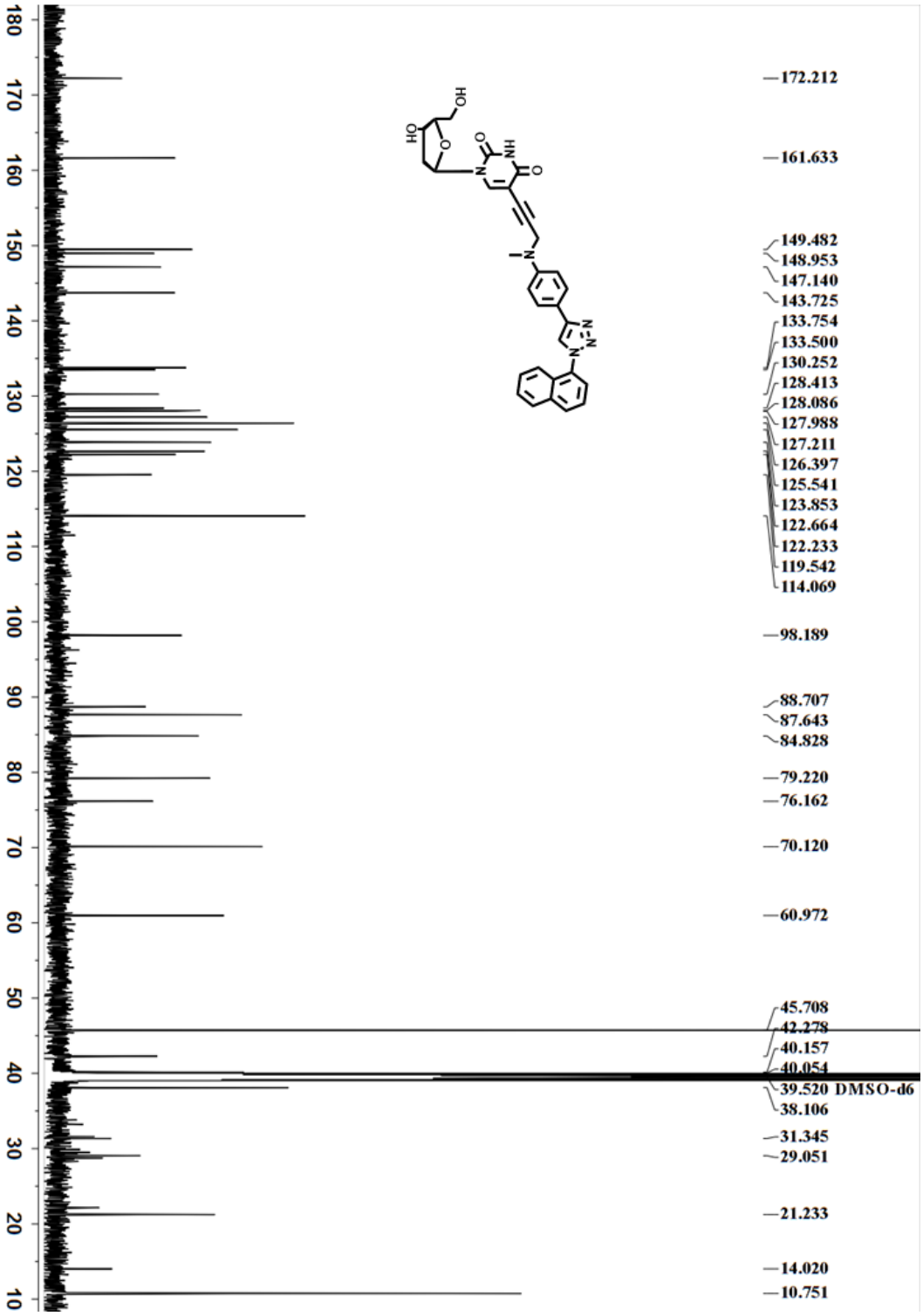

Figure 2.24: ^{13}C NMR spectra of synthesized compound **2.45E**

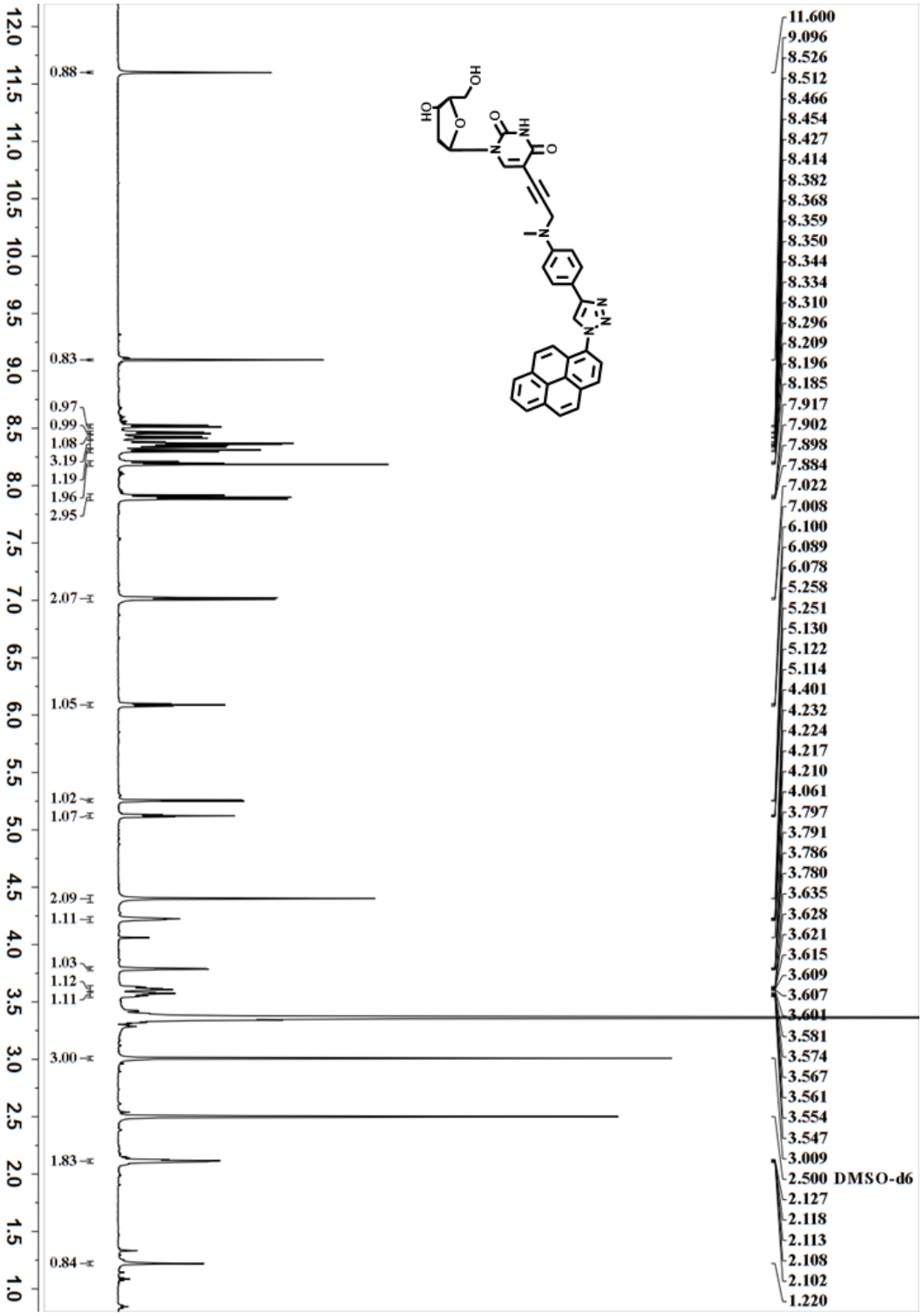

Figure 2.25: ^{1}H NMR spectra of synthesized compound **2.45G**

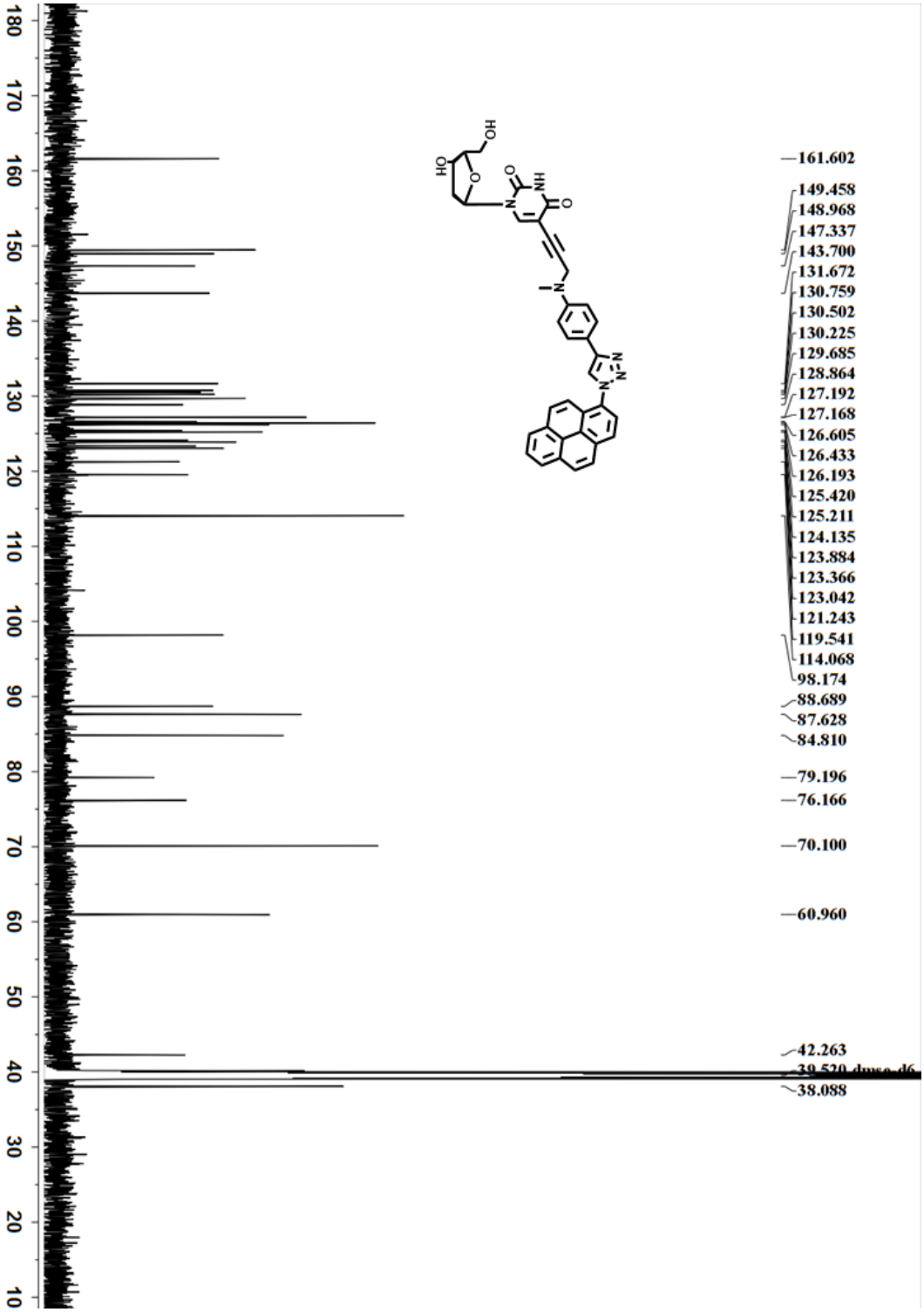

Figure 2.26: ^{13}C NMR spectra of synthesized compound **2.45G**

2.11. References

1. Sinkeldam, R. W.; Greco, N. J.; Tor, Y., Fluorescent Analogs of Biomolecular Building Blocks: Design, Properties, and Applications. *Chemical Reviews* **2010,** *110* (5), 2579-2619.
2. Tanpure, A. A.; Pawar, M. G.; Srivatsan, S. G., Fluorescent Nucleoside Analogs: Probes for Investigating Nucleic Acid Structure and Function. *Israel Journal of Chemistry* **2013,** *53* (6-7), 366-378.
3. Xu, W.; Chan, K. M.; Kool, E. T., Fluorescent nucleobases as tools for studying DNA and RNA. *Nature Chemistry* **2017,** *9*, 1043.
4. Cekan, P.; Sigurdsson, S. T., Single base interrogation by a fluorescent nucleotide: each of the four DNA bases identified by fluorescence spectroscopy. *Chemical Communications* **2008,** (29), 3393-3395.
5. Miyata, K.; Tamamushi, R.; Ohkubo, A.; Taguchi, H.; Seio, K.; Santa, T.; Sekine, M., Synthesis and Properties of a New Fluorescent Bicyclic 4-N-Carbamoyldeoxycytidine Derivative. *Organic Letters* **2006,** *8* (8), 1545-1548.
6. Mizuta, M.; Seio, K.; Miyata, K.; Ohkubo, A.; Taguchi, H.; Sekine, M., A Pyrimidopyrimidoindole Nucleoside (dC PPI): Photophysical Properties and Thermal Stability of the Modified Dna Duplexes. *Nucleosides, Nucleotides and Nucleic Acids* **2007,** *26* (10-12), 1335-1338.
7. Okamoto, A.; Tainaka, K.; Saito, I., Clear Distinction of Purine Bases on the Complementary Strand by a Fluorescence Change of a Novel Fluorescent Nucleoside. *Journal of the American Chemical Society* **2003,** *125* (17), 4972-4973.
8. Okamoto, A.; Tainaka, K.; Saito, I., Synthesis and properties of a novel fluorescent nucleobase, naphthopyridopyrimidine. *Tetrahedron Letters* **2003,** *44* (36), 6871-6874.
9. Okamoto, A.; Tanaka, K.; Fukuta, T.; Saito, I., Design of Base-Discriminating Fluorescent Nucleoside and Its Application to T/C SNP Typing. *Journal of the American Chemical Society* **2003,** *125* (31), 9296-9297.
10. Saito, Y.; Miyauchi, Y.; Okamoto, A.; Saito, I., Synthesis and properties of novel base-discriminating fluorescent (BDF) nucleosides: a highly polarity-sensitive fluorophore for SNP typing. *Tetrahedron Letters* **2004,** *45* (42), 7827-7831.
11. Brauns, E. B.; Madaras, M. L.; Coleman, R. S.; Murphy, C. J.; Berg, M. A., Measurement of Local DNA Reorganization on the Picosecond and Nanosecond Time Scales. *Journal of the American Chemical Society* **1999,** *121* (50), 11644-11649.
12. Hawkins, M. E. J. C. B.; Biophysics, Fluorescent pteridine nucleoside analogs. *Cell Biochemistry and Biophysics* **2001,** *34* (2), 257-281.
13. Jeong, H. S.; Kang, S.; Lee, J. Y.; Kim, B. H., Probing specific RNA bulge conformations by modified fluorescent nucleosides. *Organic & Biomolecular Chemistry* **2009,** *7* (5), 921-925.
14. Pawar, M. G.; Nuthanakanti, A.; Srivatsan, S. G., Heavy Atom Containing Fluorescent Ribonucleoside Analog Probe for the Fluorescence Detection of RNA-Ligand Binding. *Bioconjugate Chemistry* **2013,** *24* (8), 1367-1377.
15. Pawar, M. G.; Srivatsan, S. G., Environment-Responsive Fluorescent Nucleoside Analogue Probe for Studying Oligonucleotide Dynamics in a Model Cell-like Compartment. *The Journal of Physical Chemistry B* **2013,** *117* (46), 14273-14282.
16. Saito, Y.; Miyamoto, S.; Suzuki, A.; Matsumoto, K.; Ishihara, T.; Saito, I., Fluorescent nucleosides with ‘on–off’ switching function, pH-responsive fluorescent uridine derivatives. *Bioorganic & Medicinal Chemistry Letters* **2012,** *22* (8), 2753-2756.

17. Tainaka, K.; Tanaka, K.; Ikeda, S.; Nishiza, K.-i.; Unzai, T.; Fujiwara, Y.; Saito, I.; Okamoto, A., PRODAN-Conjugated DNA: Synthesis and Photochemical Properties. *Journal of the American Chemical Society* **2007,** *129* (15), 4776-4784.
18. Liang, Y.; Wnuk, S. F., Modification of Purine and Pyrimidine Nucleosides by Direct C-H Bond Activation. *Molecules* **2015,** *20* (3), 4874-4901.
19. Beletskaya, I. P.; Cheprakov, A. V., Copper in cross-coupling reactions: The post-Ullmann chemistry. *Coordination Chemistry Reviews* **2004,** *248* (21), 2337-2364.
20. Do, H.-Q.; Khan, R. M. K.; Daugulis, O., A General Method for Copper-Catalyzed Arylation of Arene C−H Bonds. *Journal of the American Chemical Society* **2008,** *130* (45), 15185-15192.
21. Liu, Y.; Wan, J.-P., Tandem reactions initiated by copper-catalyzed cross-coupling: A new strategy towards heterocycle synthesis. *Organic & Biomolecular Chemistry* **2011,** *9* (20), 6873-6894.
22. Agalave, S. G.; Maujan, S. R.; Pore, V. S., Click Chemistry: 1,2,3-Triazoles as Pharmacophores. *Chemistry – An Asian Journal* **2011,** *6* (10), 2696-2718.
23. Meldal, M.; Tornøe, C. W., Cu-Catalyzed Azide−Alkyne Cycloaddition. *Chemical Reviews* **2008,** *108* (8), 2952-3015.
24. Finn, M. G.; Fokin, V. V., Click chemistry: function follows form. *Chemical Society Reviews* **2010,** *39* (4), 1231-1232.
25. Kolb, H. C.; Finn, M. G.; Sharpless, K. B., Click Chemistry: Diverse Chemical Function from a Few Good Reactions. *Angewandte Chemie International Edition* **2001,** *40* (11), 2004-2021.
26. Wu, P.; Feldman, A. K.; Nugent, A. K.; Hawker, C. J.; Scheel, A.; Voit, B.; Pyun, J.; Fréchet, J. M. J.; Sharpless, K. B.; Fokin, V. V., Efficiency and Fidelity in a Click-Chemistry Route to Triazole Dendrimers by the Copper(I)-Catalyzed Ligation of Azides and Alkynes. *Angewandte Chemie International Edition* **2004,** *43* (30), 3928-3932.
27. Tron, G. C.; Pirali, T.; Billington, R. A.; Canonico, P. L.; Sorba, G.; Genazzani, A. A., Click chemistry reactions in medicinal chemistry: Applications of the 1,3-dipolar cycloaddition between azides and alkynes. *Medicinal Research Reviews* **2008,** *28* (2), 278-308.
28. Sonogashira, K.; Tohda, Y.; Hagihara, N., A convenient synthesis of acetylenes: catalytic substitutions of acetylenic hydrogen with bromoalkenes, iodoarenes and bromopyridines. *Tetrahedron Letters* **1975,** *16* (50), 4467-4470.
29. Cassar, L., Synthesis of aryl- and vinyl-substituted acetylene derivatives by the use of nickel and palladium complexes. *Journal of Organometallic Chemistry* **1975,** *93* (2), 253-257.
30. Chinchilla, R.; Nájera, C., The Sonogashira Reaction: A Booming Methodology in Synthetic Organic Chemistry. *Chemical Reviews* **2007,** *107* (3), 874-922.
31. Huisgen, R., Kinetics and reaction mechanisms: selected examples from the experience of forty years. *Pure and Applied Chemistry* **1989,** *61* (4), 613-628.
32. Huisgen, R.; Szeimies, G.; Möbius, L., 1.3-Dipolare Cycloadditionen, XXXII. Kinetik der Additionen organischer Azide an CC-Mehrfachbindungen. *Chemische Berichte* **1967,** *100* (8), 2494-2507.
33. Tornøe, C. W.; Christensen, C.; Meldal, M., Peptidotriazoles on Solid Phase: [1,2,3]-Triazoles by Regiospecific Copper(I)-Catalyzed 1,3-Dipolar Cycloadditions of Terminal Alkynes to Azides. *The Journal of Organic Chemistry* **2002,** *67* (9), 3057-3064.
34. Fischler, M.; Sologubenko, A.; Mayer, J.; Clever, G.; Burley, G.; Gierlich, J.; Carell, T.; Simon, U., Chain-like assembly of gold nanoparticles on artificial DNA templates via 'click chemistry'. *Chemical Communications* **2008,** (2), 169-171.

35. Rostovtsev, V. V.; Green, L. G.; Fokin, V. V.; Sharpless, K. B., A Stepwise Huisgen Cycloaddition Process: Copper(I)-Catalyzed Regioselective "Ligation" of Azides and Terminal Alkynes. *Angewandte Chemie International Edition* **2002,** *41* (14), 2596-2599.
36. Kolb, H. C.; Sharpless, K. B., The growing impact of click chemistry on drug discovery. *Drug Discovery Today* **2003,** *8* (24), 1128-1137.
37. Bock, V. D.; Hiemstra, H.; van Maarseveen, J. H., CuI-Catalyzed Alkyne–Azide "Click" Cycloadditions from a Mechanistic and Synthetic Perspective. *European Journal of Organic Chemistry* **2006,** *2006* (1), 51-68.
38. Briehn, C. A.; Schiedel, M.-S.; Bonsen, E. M.; Schuhmann, W.; Bäuerle, P., Single-Compound Libraries of Organic Materials: From the Combinatorial Synthesis of Conjugated Oligomers to Structure–Property Relationships. *Angewandte Chemie International Edition* **2001,** *40* (24), 4680-4683.
39. Sawa, M.; Hsu, T.-L.; Itoh, T.; Sugiyama, M.; Hanson, S. R.; Vogt, P. K.; Wong, C.-H., Glycoproteomic probes for fluorescent imaging of fucosylated glycans <em>in vivo</em&gt. *Proceedings of the National Academy of Sciences* **2006,** *103* (33), 12371.
40. Evans, C. E.; Lovell, P. A., Click chemistry as a route to surface functionalization of polymer particles dispersed in aqueous media. *Chemical Communications* **2009,** (17), 2305-2307.
41. Dirks, A. J.; Cornelissen, J. J. L. M.; Nolte, R. J. M., Monitoring Protein−Polymer Conjugation by a Fluorogenic Cu(I)-Catalyzed Azide−Alkyne 1,3-Dipolar Cycloaddition. *Bioconjugate Chemistry* **2009,** *20* (6), 1129-1138.
42. Anilkumar, R. K.; Irudaya, C., Click Chemistry Based Functionalizations of Nucleoside, Nucleotide and Nucleic Acids. *Current Organic Chemistry* **2013,** *17* (19), 2164-2191.
43. El-Sagheer, A. H.; Brown, T., Click chemistry with DNA. *Chemical Society Reviews* **2010,** *39* (4), 1388-1405.
44. Seela, F.; Pujari, S. S., Azide−Alkyne "Click" Conjugation of 8-Aza-7-deazaadenine-DNA: Synthesis, Duplex Stability, and Fluorogenic Dye Labeling. *Bioconjugate Chemistry* **2010,** *21* (9), 1629-1641.
45. Seela, F.; Shaikh, K. I., Oligonucleotides containing 7-propynyl-7-deazaguanine: synthesis and base pair stability. *Tetrahedron* **2005,** *61* (10), 2675-2681.
46. Seela, F.; Sirivolu, V. R.; Chittepu, P., Modification of DNA with Octadiynyl Side Chains: Synthesis, Base Pairing, and Formation of Fluorescent Coumarin Dye Conjugates of Four Nucleobases by the Alkyne−Azide "Click" Reaction. *Bioconjugate Chemistry* **2008,** *19* (1), 211-224.
47. Sivakumar, K.; Xie, F.; Cash, B. M.; Long, S.; Barnhill, H. N.; Wang, Q., A Fluorogenic 1,3-Dipolar Cycloaddition Reaction of 3-Azidocoumarins and Acetylenes. *Organic Letters* **2004,** *6* (24), 4603-4606.
48. Holub, J. M.; Kirshenbaum, K., Tricks with clicks: modification of peptidomimetic oligomers via copper-catalyzed azide-alkyne [3 + 2] cycloaddition. *Chemical Society Reviews* **2010,** *39* (4), 1325-1337.
49. Liang, L.; Astruc, D., The copper(I)-catalyzed alkyne-azide cycloaddition (CuAAC) "click" reaction and its applications. An overview. *Coordination Chemistry Reviews* **2011,** *255* (23), 2933-2945.
50. Hoffman, R. M., Live cell imaging in live animals with fluorescent proteins. *Methods in Enzymology* **2012,** *506*, 197-224.
51. Kulkarni, G.; Wadsworth, W. G., Hitting the sweet spot. *Nature methods* **2012,** *9* (5), 451, 453.
52. Kurishita, Y.; Kohira, T.; Ojida, A.; Hamachi, I., Organelle-Localizable Fluorescent Chemosensors for Site-Specific Multicolor Imaging of Nucleoside Polyphosphate

Dynamics in Living Cells. *Journal of the American Chemical Society* **2012,** *134* (45), 18779-18789.
53. Prescher, J. A.; Contag, C. H., Guided by the light: visualizing biomolecular processes in living animals with bioluminescence. *Current Opinion in Chemical Biology* **2010,** *14* (1), 80-9.
54. Zayas, J.; Annoual, M.; Das, J. K.; Felty, Q.; Gonzalez, W. G.; Miksovska, J.; Sharifai, N.; Chiba, A.; Wnuk, S. F., Strain Promoted Click Chemistry of 2- or 8-Azidopurine and 5-Azidopyrimidine Nucleosides and 8-Azidoadenosine Triphosphate with Cyclooctynes. Application to Living Cell Fluorescent Imaging. *Bioconjugate Chemistry* **2015,** *26* (8), 1519-1532.
55. Ming, X.; Seela, F., A Nucleobase-Discriminating Pyrrolo-dC Click Adduct Designed for DNA Fluorescence Mismatch Sensing. *Chemistry – A European Journal* **2012,** *18* (31), 9590-9600.
56. Ingale, S. A.; Seela, F., Nucleoside and oligonucleotide pyrene conjugates with 1,2,3-triazolyl or ethynyl linkers: synthesis, duplex stability, and fluorescence changes generated by the DNA-dye connector. *Tetrahedron* **2014,** *70* (2), 380-391.
57. Mei, H.; Ingale, S. A.; Seela, F., Pyrene and bis-pyrene DNA nucleobase conjugates: excimer and monomer fluorescence of linear and dendronized cytosine and 7-deazaguanine click adducts. *Tetrahedron* **2013,** *69* (23), 4731-4742.
58. Gramlich, P. M. E.; Wirges, C. T.; Manetto, A.; Carell, T., Postsynthetic DNA Modification through the Copper-Catalyzed Azide–Alkyne Cycloaddition Reaction. *Angewandte Chemie International Edition* **2008,** *47* (44), 8350-8358.
59. Gierlich, J.; Burley, G. A.; Gramlich, P. M. E.; Hammond, D. M.; Carell, T., Click Chemistry as a Reliable Method for the High-Density Postsynthetic Functionalization of Alkyne-Modified DNA. *Organic Letters* **2006,** *8* (17), 3639-3642.
60. Beyer, C.; Wagenknecht, H.-A., In situ azide formation and "click" reaction of nile red with DNA as an alternative postsynthetic route. *Chemical Communications* **2010,** *46* (13), 2230-2231.
61. Griffin, B. A.; Adams, S. R.; Tsien, R. Y., Specific covalent labeling of recombinant protein molecules inside live cells. *Science* **1998,** *281* (5374), 269-72.
62. Kho, Y.; Kim, S. C.; Jiang, C.; Barma, D.; Kwon, S. W.; Cheng, J.; Jaunbergs, J.; Weinbaum, C.; Tamanoi, F.; Falck, J.; Zhao, Y., A tagging-via-substrate technology for detection and proteomics of farnesylated proteins. *Proceedings of the National Academy of Sciences of the United States of America* **2004,** *101* (34), 12479.
63. Link, A. J.; Vink, M. K. S.; Tirrell, D. A., Presentation and Detection of Azide Functionality in Bacterial Cell Surface Proteins. *Journal of the American Chemical Society* **2004,** *126* (34), 10598-10602.
64. Prescher, J. A.; Bertozzi, C. R., Chemistry in living systems. *Nature Chemical Biology* **2005,** *1* (1), 13-21.
65. Zhang, Z.; Smith, B. A. C.; Wang, L.; Brock, A.; Cho, C.; Schultz, P. G., A New Strategy for the Site-Specific Modification of Proteins in Vivo. *Biochemistry* **2003,** *42* (22), 6735-6746.
66. Hong, V.; Steinmetz, N. F.; Manchester, M.; Finn, M. G., Labeling Live Cells by Copper-Catalyzed Alkyne−Azide Click Chemistry. *Bioconjugate Chemistry* **2010,** *21* (10), 1912-1916.
67. Li, S.; Wang, L.; Yu, F.; Zhu, Z.; Shobaki, D.; Chen, H.; Wang, M.; Wang, J.; Qin, G.; Erasquin, U. J.; Ren, L.; Wang, Y.; Cai, C., Copper-catalyzed click reaction on/in live cells. *Chemical Science* **2017,** *8* (3), 2107-2114.
68. Merkel, M.; Arndt, S.; Ploschik, D.; Cserép, G. B.; Wenge, U.; Kele, P.; Wagenknecht, H.-A., Scope and Limitations of Typical Copper-Free Bioorthogonal Reactions with

DNA: Reactive 2′-Deoxyuridine Triphosphates for Postsynthetic Labeling. *The Journal of Organic Chemistry* **2016,** *81* (17), 7527-7538.
69. Stubinitzky, C.; Cserép, G. B.; Bätzner, E.; Kele, P.; Wagenknecht, H.-A., 2′-Deoxyuridine conjugated with a reactive monobenzocyclooctyne as a DNA building block for copper-free click-type postsynthetic modification of DNA. *Chemical Communications* **2014,** *50* (76), 11218-11221.
70. Gutsmiedl, K.; Wirges, C. T.; Ehmke, V.; Carell, T., Copper-Free "Click" Modification of DNA via Nitrile Oxide−Norbornene 1,3-Dipolar Cycloaddition. *Organic Letters* **2009,** *11* (11), 2405-2408.
71. Singh, I.; Vyle, J. S.; Heaney, F., Fast, copper-free click chemistry: a convenient solid-phase approach to oligonucleotide conjugation. *Chemical Communications* **2009,** (22), 3276-3278.
72. Borsenberger, V.; Howorka, S., Diene-modified nucleotides for the Diels–Alder-mediated functional tagging of DNA. *Nucleic Acids Research* **2009,** *37* (5), 1477-1485.
73. Bußkamp, H.; Batroff, E.; Niederwieser, A.; Abdel-Rahman, O. S.; Winter, R. F.; Wittmann, V.; Marx, A., Efficient labelling of enzymatically synthesized vinyl-modified DNA by an inverse-electron-demand Diels–Alder reaction. *Chemical Communications* **2014,** *50* (74), 10827-10829.
74. Rieder, U.; Luedtke, N. W., Alkene–Tetrazine Ligation for Imaging Cellular DNA. *Angewandte Chemie International Edition* **2014,** *53* (35), 9168-9172.
75. Raindlová, V.; Pohl, R.; Hocek, M., Synthesis of Aldehyde-Linked Nucleotides and DNA and Their Bioconjugations with Lysine and Peptides through Reductive Amination. *Chemistry – A European Journal* **2012,** *18* (13), 4080-4087.
76. Dadová, J.; Orság, P.; Pohl, R.; Brázdová, M.; Fojta, M.; Hocek, M., Vinylsulfonamide and Acrylamide Modification of DNA for Cross-linking with Proteins. *Angewandte Chemie International Edition* **2013,** *52* (40), 10515-10518.
77. Dadová, J.; Orság, P.; Pohl, R.; Brázdová, M.; Fojta, M.; Hocek, M., Vinylsulfonamide and Acrylamide Modification of DNA for Cross-linking with Proteins. *Angewandte Chemie International Edition* **2013,** *125* (40), 10709-10712.
78. Fukazawa, A.; Karasawa, T.; Zhang, H.; Minemura, K.; Camacho, C.; Wang, J.; Irle, S.; Yamaguchi, S., Photochemical Double 5-exo Cyclization of Alkenyl-Substituted Dithienylacetylenes: Efficient Synthesis of Diarylated Dithienofulvalenes. *Angewandte Chemie International Edition* **2013,** *125* (40), 10713-10717.
79. Lercher, L.; McGouran, J. F.; Kessler, B. M.; Schofield, C. J.; Davis, B. G., DNA modification under mild conditions by Suzuki-Miyaura cross-coupling for the generation of functional probes. *Angewandte Chemie International Edition* **2013,** *52* (40), 10553-10558.
80. Amaro, M.; Šachl, R.; Jurkiewicz, P.; Coutinho, A.; Prieto, M.; Hof, M., Time-resolved fluorescence in lipid bilayers: selected applications and advantages over steady state. *Biophysical Journal* **2014,** *107* (12), 2751-2760.
81. Loving, G. S.; Sainlos, M.; Imperiali, B., Monitoring protein interactions and dynamics with solvatochromic fluorophores. *Trends in Biotechnology* **2010,** *28* (2), 73-83.
82. Wu, F.-Y.; Xiang, Y.-L.; Wu, Y.-M.; Xie, F.-Y., Study of interaction of a fluorescent probe with DNA. *Journal of Luminescence* **2009,** *129* (11), 1286-1291.
83. McCarthy, J. J.; Hilfiker, R., The use of single-nucleotide polymorphism maps in pharmacogenomics. *Nature Biotechnology* **2000,** *18* (5), 505-508.
84. Okamoto, A.; Kanatani, K.; Saito, I., Pyrene-Labeled Base-Discriminating Fluorescent DNA Probes for Homogeneous SNP Typing. *Journal of the American Chemical Society* **2004,** *126* (15), 4820-4827.

85. Sholokh, M.; Improta, R.; Mori, M.; Sharma, R.; Kenfack, C.; Shin, D.; Voltz, K.; Stote, R. H.; Zaporozhets, O. A.; Botta, M.; Tor, Y.; Mély, Y., Tautomers of a Fluorescent G Surrogate and Their Distinct Photophysics Provide Additional Information Channels. *Angewandte Chemie International Edition* **2016,** *55* (28), 7974-7978.
86. Wilhelmsson, L. M., Fluorescent nucleic acid base analogues. *Quarterly reviews of Biophysics* **2010,** *43* (2), 159-83.
87. Su, X.; Xiao, X.; Zhang, C.; Zhao, M., Nucleic Acid Fluorescent Probes for Biological Sensing. *Applied Spectroscopy* **2012,** *66* (11), 1249-1261.
88. Wilson, J. N.; Kool, E. T., Fluorescent DNA base replacements: reporters and sensors for biological systems. *Organic & Biomolecular Chemistry* **2006,** *4* (23), 4265-4274.
89. Dziuba, D.; Pohl, R.; Hocek, M., Polymerase synthesis of DNA labelled with benzylidene cyanoacetamide-based fluorescent molecular rotors: fluorescent light-up probes for DNA-binding proteins. *Chemical Communications* **2015,** *51* (23), 4880-4882.
90. Kanamori, T.; Ohzeki, H.; Masaki, Y.; Ohkubo, A.; Takahashi, M.; Tsuda, K.; Ito, T.; Shirouzu, M.; Kuwasako, K.; Muto, Y.; Sekine, M.; Seio, K., Controlling the Fluorescence of Benzofuran-Modified Uracil Residues in Oligonucleotides by Triple-Helix Formation. *ChemBioChem* **2015,** *16* (1), 167-176.
91. Tokugawa, M.; Masaki, Y.; Canggadibrata, J. C.; Kaneko, K.; Shiozawa, T.; Kanamori, T.; Grøtli, M.; Wilhelmsson, L. M.; Sekine, M.; Seio, K., 7-(Benzofuran-2-yl)-7-deazadeoxyguanosine as a fluorescence turn-ON probe for single-strand DNA binding protein. *Chemical Communications* **2016,** *52* (19), 3809-3812.
92. Guo, J.; Ju, J.; Turro, N. J., Fluorescent hybridization probes for nucleic acid detection. *Analytical and Bioanalytical Chemistry* **2012,** *402* (10), 3115-3125.
93. Holzhauser, C.; Wagenknecht, H.-A., In-Stem-Labeled Molecular Beacons for Distinct Fluorescent Color Readout. *Angewandte Chemie International Edition* **2011,** *50* (32), 7268-7272.
94. Furukawa, K.; Hattori, M.; Ohki, T.; Kitamura, Y.; Kitade, Y.; Ueno, Y., Nucleic acid probe containing fluorescent tricyclic base-linked acyclonucleoside for detection of single nucleotide polymorphisms. *Bioorganic & Medicinal Chemistry* **2012,** *20* (1), 16-24.
95. Kolpashchikov, D. M., Binary Probes for Nucleic Acid Analysis. *Chemical Reviews* **2010,** *110* (8), 4709-4723.
96. Dai, N.; Kool, E. T., Fluorescent DNA-based enzyme sensors. *Chemical Society Reviews* **2011,** *40* (12), 5756-5770.
97. Riedl, J.; Ménová, P.; Pohl, R.; Orság, P.; Fojta, M.; Hocek, M., GFP-like Fluorophores as DNA Labels for Studying DNA–Protein Interactions. *The Journal of Organic Chemistry* **2012,** *77* (18), 8287-8293.
98. Riedl, J.; Pohl, R.; Ernsting, N. P.; Orság, P.; Fojta, M.; Hocek, M., Labelling of nucleosides and oligonucleotides by solvatochromic 4-aminophthalimide fluorophore for studying DNA–protein interactions. *Chemical Science* **2012,** *3* (9), 2797-2806.
99. Okamoto, A.; Tainaka, K.; Fujiwara, Y., Nile Red Nucleoside: Design of a Solvatofluorochromic Nucleoside as an Indicator of Micropolarity around DNA. *The Journal of Organic Chemistry* **2006,** *71* (9), 3592-3598.
100. Saito, Y.; Suzuki, A.; Okada, Y.; Yamasaka, Y.; Nemoto, N.; Saito, I., An environmentally sensitive fluorescent purine nucleoside that changes emission wavelength upon hybridization. *Chemical Communications* **2013,** *49* (50), 5684-5686.
101. Weber, G.; Farris, F. J., Synthesis and spectral properties of a hydrophobic fluorescent probe: 6-propionyl-2-(dimethylamino)naphthalene. *Biochemistry* **1979,** *18* (14), 3075-3078.

102. Weinberger, M.; Berndt, F.; Mahrwald, R.; Ernsting, N. P.; Wagenknecht, H.-A., Synthesis of 4-Aminophthalimide and 2,4-Diaminopyrimidine C-Nucleosides as Isosteric Fluorescent DNA Base Substitutes. *The Journal of Organic Chemistry* **2013,** *78* (6), 2589-2599.
103. Shinohara, Y.; Matsumoto, K.; Kugenuma, K.; Morii, T.; Saito, Y.; Saito, I., Design of environmentally sensitive fluorescent 2′-deoxyguanosine containing arylethynyl moieties: Distinction of thymine base by base-discriminating fluorescent (BDF) probe. *Bioorganic & Medicinal Chemistry Letters* **2010,** *20* (9), 2817-2820.
104. Suzuki, A.; Saito, M.; Katoh, R.; Saito, Y., Synthesis of 8-aza-3,7-dideaza-2′-deoxyadenosines possessing a new adenosine skeleton as an environmentally sensitive fluorescent nucleoside for monitoring the DNA minor groove. *Organic & Biomolecular Chemistry* **2015,** *13* (27), 7459-7468.
105. Dziuba, D.; Pospíšil, P.; Matyašovský, J.; Brynda, J.; Nachtigallová, D.; Rulíšek, L.; Pohl, R.; Hof, M.; Hocek, M., Solvatochromic fluorene-linked nucleoside and DNA as color-changing fluorescent probes for sensing interactions. *Chemical Science* **2016,** *7* (9), 5775-5785.
106. Demchenko, A. P., The Concept of λ-Ratiometry in Fluorescence Sensing and Imaging. *Journal of Fluorescence* **2010,** *20* (5), 1099-1128.
107. Demchenko, A. P., Practical aspects of wavelength ratiometry in the studies of intermolecular interactions. *Journal of Molecular Structure* **2014,** *1077*, 51-67.
108. Xu, L.; He, M.-L.; Yang, H.-B.; Qian, X., A simple fluorescent probe for Cd2+ in aqueous solution with high selectivity and sensitivity. *Dalton Transactions* **2013,** *42* (23), 8218-8222.
109. Nandhikonda, P.; Heagy, M. D., Dual Fluorescent N-Aryl-2,3- naphthalimides: Applications in Ratiometric DNA Detection and White Organic Light-Emitting Devices. *Organic Letters* **2010,** *12* (21), 4796-4799.
110. Srikun, D.; Miller, E. W.; Domaille, D. W.; Chang, C. J., An ICT-Based Approach to Ratiometric Fluorescence Imaging of Hydrogen Peroxide Produced in Living Cells. *Journal of the American Chemical Society* **2008,** *130* (14), 4596-4597.
111. Socher, E.; Bethge, L.; Knoll, A.; Jungnick, N.; Herrmann, A.; Seitz, O., Low-Noise Stemless PNA Beacons for Sensitive DNA and RNA Detection. *Angewandte Chemie International Edition* **2008,** *47* (49), 9555-9559.
112. Teo, Y. N.; Kool, E. T., DNA-Multichromophore Systems. *Chemical Reviews* **2012,** *112* (7), 4221-4245.
113. Grabowski, Z. R.; Rotkiewicz, K.; Rettig, W., Structural Changes Accompanying Intramolecular Electron Transfer: Focus on Twisted Intramolecular Charge-Transfer States and Structures. *Chemical Reviews* **2003,** *103* (10), 3899-4032.
114. Rettig, W., Charge Separation in Excited States of Decoupled Systems—TICT Compounds and Implications Regarding the Development of New Laser Dyes and the Primary Process of Vision and Photosynthesis. *Angewandte Chemie International Edition in English* **1986,** *25* (11), 971-988.
115. Weigel, W.; Rettig, W.; Dekhtyar, M.; Modrakowski, C.; Beinhoff, M.; Schlüter, A. D., Dual Fluorescence of Phenyl and Biphenyl Substituted Pyrene Derivatives. *The Journal of Physical Chemistry A* **2003,** *107* (31), 5941-5947.
116. Barthes, N. P. F.; Karpenko, I. A.; Dziuba, D.; Spadafora, M.; Auffret, J.; Demchenko, A. P.; Mély, Y.; Benhida, R.; Michel, B. Y.; Burger, A., Development of environmentally sensitive fluorescent and dual emissive deoxyuridine analogues. *RSC Advances* **2015,** *5* (42), 33536-33545.
117. Dziuba, D.; Postupalenko, V. Y.; Spadafora, M.; Klymchenko, A. S.; Guérineau, V.; Mély, Y.; Benhida, R.; Burger, A., A Universal Nucleoside with Strong Two-Band

Switchable Fluorescence and Sensitivity to the Environment for Investigating DNA Interactions. *Journal of the American Chemical Society* **2012,** *134* (24), 10209-10213.
118. Gavvala, K.; Barthes, N. P. F.; Bonhomme, D.; Dabert-Gay, A. S.; Debayle, D.; Michel, B. Y.; Burger, A.; Mély, Y., A turn-on dual emissive nucleobase sensitive to mismatches and duplex conformational changes. *RSC Advances* **2016,** *6* (90), 87142-87146.
119. Okamoto, A.; Tainaka, K.; Nishiza, K.-i.; Saito, I., Monitoring DNA Structures by Dual Fluorescence of Pyrene Derivatives. *Journal of the American Chemical Society* **2005,** *127* (38), 13128-13129.
120. Bag, S. S.; Kundu, R.; Matsumoto, K.; Saito, Y.; Saito, I., Singly and doubly labeled base-discriminating fluorescent oligonucleotide probes containing oxo-pyrene chromophore. *Bioorganic & Medicinal Chemistry Letters* **2010,** *20* (11), 3227-3230.
121. Bag, S. S.; Pradhan, M. K.; Das, S. K.; Jana, S.; Bag, R., Wavelength shifting oligonucleotide probe for the detection of adenosine of a target DNA with enhanced fluorescence signal. *Bioorganic & Medicinal Chemistry Letters* **2014,** *24* (19), 4678-4681.
122. Bag, S. S.; Talukdar, S.; Anjali, S. J., Regioselective and stereoselective route to N2-β-tetrazolyl unnatural nucleosides via SN2 reaction at the anomeric center of Hoffer's chlorosugar. *Bioorganic & Medicinal Chemistry Letters* **2016,** *26* (8), 2044-2050.
123. Bag, S. S.; Talukdar, S.; Kundu, R.; Saito, I.; Jana, S., Dual door entry to exciplex emission in a chimeric DNA duplex containing non-nucleoside–nucleoside pair. *Chemical Communications* **2014,** *50* (7), 829-832.
124. Bag, S. S.; Talukdar, S.; Matsumoto, K.; Kundu, R., Triazolyl Donor/Acceptor Chromophore Decorated Unnatural Nucleosides and Oligonucleotides with Duplex Stability Comparable to That of a Natural Adenine/Thymine Pair. *The Journal of Organic Chemistry* **2013,** *78* (2), 278-291.
125. Bandy, T. J.; Brewer, A.; Burns, J. R.; Marth, G.; Nguyen, T.; Stulz, E., DNA as supramolecular scaffold for functional molecules: progress in DNA nanotechnology. *Chemical Society Reviews* **2011,** *40* (1), 138-148.
126. Ensslen, P.; Gärtner, S.; Glaser, K.; Colsmann, A.; Wagenknecht, H.-A., A DNA–Fullerene Conjugate as a Template for Supramolecular Chromophore Assemblies: Towards DNA-Based Solar Cells. *Angewandte Chemie International Edition* **2016,** *55* (5), 1904-1908.
127. Liang, Y.; Gloudeman, J.; Wnuk, S. F., Palladium-Catalyzed Direct Arylation of 5-Halouracils and 5-Halouracil Nucleosides with Arenes and Heteroarenes Promoted by TBAF. *The Journal of Organic Chemistry* **2014,** *79* (9), 4094-4103.
128. Saito, Y.; Bag, S. S.; Kusakabe, Y.; Nagai, C.; Matsumoto, K.; Mizuno, E.; Kodate, S.; Suzuka, I.; Saito, I., Dual-labeled oligonucleotide probe for sensing adenosinevia FRET: A novel alternative to SNPs genotyping. *Chemical Communications* **2007,** (21), 2133-2135.
129. Agrofoglio, L. A.; Gillaizeau, I.; Saito, Y., Palladium-Assisted Routes to Nucleosides. *Chemical Reviews* **2003,** *103* (5), 1875-1916.
130. Barnes, T. W.; Turner, D. H., Long-Range Cooperativity in Molecular Recognition of RNA by Oligodeoxynucleotides with Multiple C5-(1-Propynyl) Pyrimidines. *Journal of the American Chemical Society* **2001,** *123* (18), 4107-4118.
131. He, J.; Seela, F., Propynyl groups in duplex DNA: stability of base pairs incorporating 7-substituted 8-aza-7-deazapurines or 5-substituted pyrimidines. *Nucleic acids research* **2002,** *30* (24), 5485-5496.

132. Ingale, S. A.; Leonard, P.; Yang, H.; Seela, F., 5-Nitroindole oligonucleotides with alkynyl side chains: universal base pairing, triple bond hydration and properties of pyrene "click" adducts. *Organic & Biomolecular Chemistry* **2014,** *12* (42), 8519-8532.
133. Meščić, A.; Harej, A.; Klobučar, M.; Glavač, D.; Cetina, M.; Pavelić, S. K.; Raić-Malić, S., Discovery of New Acid Ceramidase-Targeted Acyclic 5-Alkynyl and 5-Heteroaryl Uracil Nucleosides. *ACS Medicinal Chemistry Letters* **2015,** *6* (11), 1150-1155.
134. Wagner, R. W.; Matteucci, M. D.; Lewis, J. G.; Gutierrez, A. J.; Moulds, C.; Froehler, B. C., Antisense gene inhibition by oligonucleotides containing C-5 propyne pyrimidines. *Science* **1993,** *260* (5113), 1510.
135. Bag, S. S.; Kundu, R., Installation/Modulation of the Emission Response via Click Reaction. *The Journal of Organic Chemistry* **2011,** *76* (9), 3348-3356.
136. Badger, G. M.; Walker, I. S., 24. Polynuclear heterocyclic systems. Part IX. n-π*-Transitions in the spectra of aromatic aza-hydrocarbons. *Journal of the Chemical Society* **1956,** (0), 122-126.
137. Benniston, A. C.; Harriman, A.; Lawrie, D. J.; Mayeux, A., The photophysical properties of a pyrene–thiophene–terpyridine conjugate and of its zinc(ii) and ruthenium(ii) complexes. *Physical Chemistry Chemical Physics* **2004,** *6* (1), 51-57.
138. Benniston, A. C.; Harriman, A.; Lawrie, D. J.; Mayeux, A.; Rafferty, K.; Russell, O. D., A general purpose reporter for cations: absorption, fluorescence and electrochemical sensing of zinc(ii). *Dalton Transactions* **2003,** (24), 4762-4769.
139. Kim, J.; Lee, M., Excited-State Photophysics and Dynamics of a Hemicyanine Dye in AOT Reverse Micelles. *The Journal of Physical Chemistry A* **1999,** *103* (18), 3378-3382.
140. Strehmel, B.; Seifert, H.; Rettig, W., Photophysical Properties of Fluorescence Probes. 2. A Model of Multiple Fluorescence for Stilbazolium Dyes Studied by Global Analysis and Quantum Chemical Calculations. *The Journal of Physical Chemistry B* **1997,** *101* (12), 2232-2243.
141. Yang, S.-W.; Elangovan, A.; Hwang, K.-C.; Ho, T.-I., Electronic Polarization Reversal and Excited State Intramolecular Charge Transfer in Donor/Acceptor Ethynylpyrenes. *The Journal of Physical Chemistry B* **2005,** *109* (35), 16628-16635.
142. Albinsson, B., Dual Fluorescence from N6,N6-Dimethyladenosine. *Journal of the American Chemical Society* **1997,** *119* (27), 6369-6375.
143. Chen, X.; Zhao, Y.; Cao, Z., Theoretical study on the dual fluorescence of 2-(4-cyanophenyl)-N,N-dimethylaminoethane and its deactivation pathway. *The Journal of Chemical Physics* **2009,** *130* (14), 144307.
144. Pham, T. H. N.; Clarke, R. J., Solvent Dependence of the Photochemistry of the Styrylpyridinium Dye RH421. *The Journal of Physical Chemistry B* **2008,** *112* (20), 6513-6520.
145. Shim, T.; Lee, M. H.; Kim, D.; Ouchi, Y., Comparison of Photophysical Properties of the Hemicyanine Dyes in Ionic and Nonionic Solvents. *The Journal of Physical Chemistry B* **2008,** *112* (7), 1906-1912.
146. Thiagarajan, V.; Selvaraju, C.; Malar, E. J. P.; Ramamurthy, P., A Novel Fluorophore with Dual Fluorescence: Local Excited State and Photoinduced Electron-Transfer-Promoted Charge-Transfer State. *ChemPhysChem* **2004,** *5* (8), 1200-1209.
147. Frisch, M. J. T., G. W.; Schlegel, H. B.; Scuseria, G. E.; Robb, M. A.; Cheeseman, J. R.; Scalmani, G.; Barone, V.; Mennucci, B.; Petersson, G. A.; Nakatsuji, H.; Caricato, M.; Li, X.; Hratchian, H. P.; Izmaylov, A. F.; Bloino, J.; Zheng, G.; Sonnenberg, J. L.; Hada, M.; Ehara, M.; Toyota, K.; Fukuda, R.; Hasegawa, J.; Ishida, M.; Nakajima, T.; Honda, Y.; Kitao, O.; Nakai, H.; Vreven, T.; Montgomery, J. A., Jr.; Peralta, J. E.; Ogliaro, F.; Bearpark, M.; Heyd, J. J.; Brothers, E.; Kudin, K. N.; Staroverov, V. N.; Kobayashi, R.;

Normand, J.; Raghavachari, K.; Rendell, A.; Burant, J. C.; Iyengar, S. S.; Tomasi, J.; Cossi, M.; Rega, N.; Millam, J. M.; Klene, M.; Knox, J. E.; Cross, J. B.; Bakken, V.; Adamo, C.; Jaramillo, J.; Gomperts, R.; Stratmann, R. E.; Yazyev, O.; Austin, A. J.; Cammi, R.; Pomelli, C.; Ochterski, J. W.; Martin, R. L.; Morokuma, K.; Zakrzewski, V. G.; Voth, G. A.; Salvador, P.; Dannenberg, J. J.; Dapprich, S.; Daniels, A. D.; Farkas, Ö.; Foresman, J. B.; Ortiz, J. V.; Cioslowski, J.; Fox, D. J., *Gaussian 09 (Gaussian, Inc., Wallingford CT, 2009)* **2009**.

148. Bag, S. S.; Jana, S.; Pradhan, M. K., Synthesis, photophysical properties of triazolyl-donor/acceptor chromophores decorated unnatural amino acids: Incorporation of a pair into Leu-enkephalin peptide and application of triazolylperylene amino acid in sensing BSA. *Bioorganic & Medicinal Chemistry* **2016,** *24* (16), 3579-3595.
149. Bucevicius, J.; Skardziute, L.; Dodonova, J.; Kazlauskas, K.; Bagdziunas, G.; Jursenas, S.; Tumkevicius, S., 2,4-Bis(4-aryl-1,2,3-triazol-1-yl)pyrrolo[2,3-d]pyrimidines: synthesis and tuning of optical properties by polar substituents. *RSC Advances* **2015,** *5* (48), 38610-38622.
150. Fromherz, P., Monopole-Dipole Model for Symmetrical Solvatochromism of Hemicyanine Dyes. *The Journal of Physical Chemistry* **1995,** *99* (18), 7188-7192.
151. Ji, L.; Lorbach, A.; Edkins, R. M.; Marder, T. B., Synthesis and Photophysics of a 2,7-Disubstituted Donor–Acceptor Pyrene Derivative: An Example of the Application of Sequential Ir-Catalyzed C–H Borylation and Substitution Chemistry. *The Journal of Organic Chemistry* **2015,** *80* (11), 5658-5665.
152. Nagarajan, N.; Velmurugan, G.; Venuvanalingam, P.; Renganathan, R., Tunable single and dual emission behavior of imidazole fluorophores based on D-π-A architecture. *Journal of Photochemistry and Photobiology A: Chemistry* **2014,** *284*, 36-48.
153. Monnereau, C.; Blart, E.; Odobel, F., A cheap and efficient method for selective para-iodination of aniline derivatives. *Tetrahedron Letters* **2005,** *46* (32), 5421-5423.
154. Tayama, E.; Sugai, S., A facile method for the stereoselective preparation of (1E,3E)-4-substituted-1-amino-1,3-dienes via 1,4-elimination. *Tetrahedron Letters* **2007,** *48* (35), 6163-6166.
155. Heinrich, D.; Wagner, T.; Diederichsen, U., Synthesis and DNA Incorporation of an Ethynyl-Bridged Cytosine C-Nucleoside as Guanosine Surrogate. *Organic Letters* **2007,** *9* (25), 5311-5314.
156. Semioshkin, A.; Ilinova, A.; Lobanova, I.; Bregadze, V.; Paradowska, E.; Studzińska, M.; Jabłońska, A.; Lesnikowski, Z. J., Synthesis of the first conjugates of 5-ethynyl-2′-deoxyuridine with closo-dodecaborate and cobalt-bis-dicarbollide boron clusters. *Tetrahedron* **2013,** *69* (37), 8034-8041.
157. Reddy, M. R.; Shibata, N.; Kondo, Y.; Nakamura, S.; Toru, T., Design, Synthesis, and Spectroscopic Investigation of Zinc Dodecakis(trifluoroethoxy)phthalocyanines Conjugated with Deoxyribonucleosides. *Angewandte Chemie International Edition* **2006,** *45* (48), 8163-8166.

Chapter 3

STUDIES ON THE INTERACTION OF TRIAZOLYLPYRENE-LABELED FLUORESCENT 2'-DEOXYURIDINE AND UNNATURAL TETRAZOLYLPYRENE NUCLEOSIDES WITH BSA

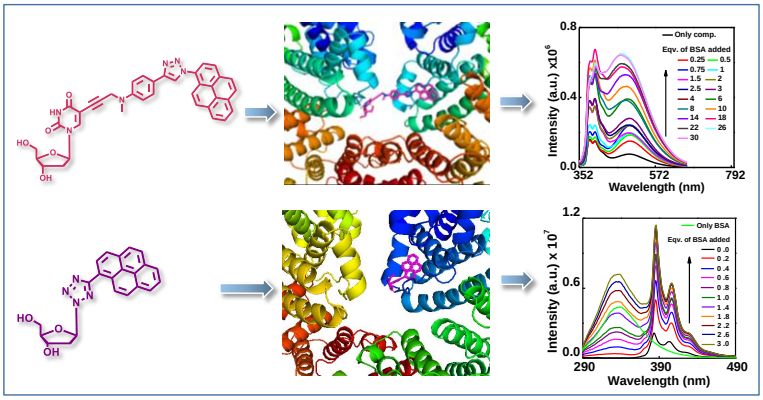

3.1. Introduction

3.1.1. Protein-Ligand Interaction

Protein-ligand interactions are of paramount importance for all processes taking place in living organisms. Molecular signal transmission derived from protein-ligand interactions is essential for almost all forms of life to exist. These interactions regulate the states and functions of proteins which are important for regulation of biological functions. [1-4] On the other hand, understanding the nature of drug-protein interaction or small molecule-protein interaction is of paramount importance for the development of new chemotherapeutics for several diseases and has led to the foundation of chemical biology.

The mechanism of molecular recognition and binding of a ligand to a protein is a complex process and not fully understood. Molecular recognition is a process in which biological macromolecules undergo specific interaction with each other or with various ligands to form a complex.[5] Two most important characteristics of the molecular recognition process are (i) specificity, which enables high specific recognition between two binding partners from rest of the less specific partners and (ii) affinity, which determines the non-replaceable effect of a specific binding partner interacting with high affinity even present in low concentration than the other less specific partners which are present in high concentrations.[6] In order to get more insight into the protein-ligand interaction, understanding of kinetic and thermodynamical factors such as Gibbs free energy, enthalpy and entropy of a protein-ligand-solvent system is very important. For example, in analogy with any spontaneous process, the change in Gibbs free energy of a protein-ligand-solvent system should be negative for binding to occur.[2]

There are three proposed protein-ligand binding models found in the literature which have been used to explain protein-ligand interactions. These are "lock-and-key",[7] "induced fit"[8] and "conformational selection" [9-12] and are depicted in **Scheme 3.1**.

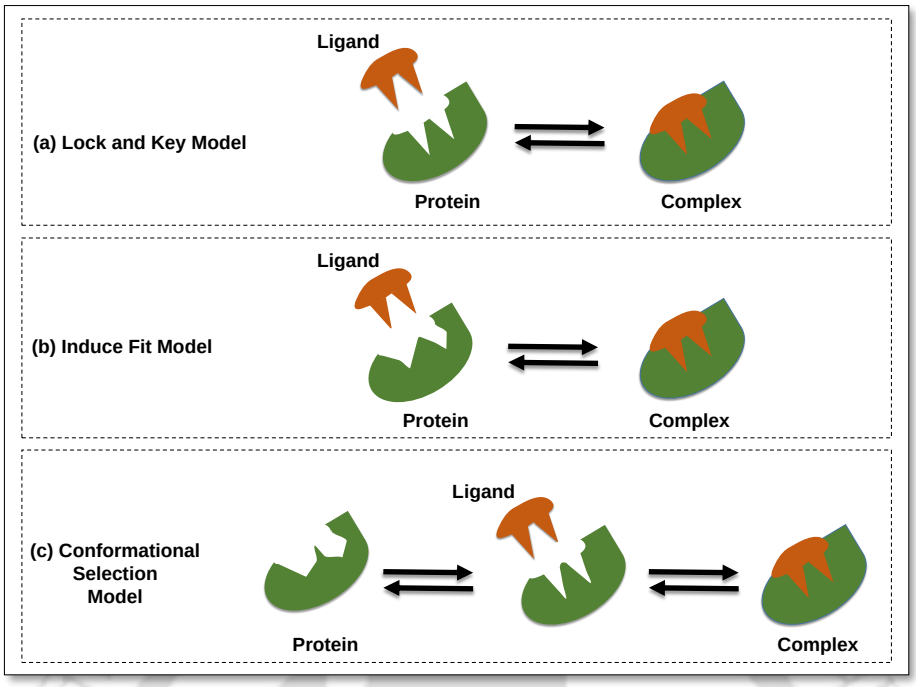

Scheme 3.1. Schematic representation of protein-ligand binding models.

The lock-and-key model (**Scheme 3.1a**) demands both protein and ligands should have a rigid structure and perfectly matched binding sites for a binding to occur between them.[7] Thus, according to this model, a ligand resembles a key which can be inserted in the binding site (keyhole) of a protein having correct shape and size (the lock). However, this model fails to explain the binding interaction exists between a protein and a ligand where their shapes at the binding sites do not match at all.

The induce fit model considers the protein binding sites as flexible regions which get induced for a conformational change while interacting with specific ligands (**Scheme 3.1b**).[8] Since the induce fit model only considers the conformational flexibility of the protein binding site, the cases where a protein undergo only a slight change in its conformation after binding with a ligand can be well-explained by using this mod.0el.

Both the lock-and-key model and induce fit model assume the protein molecule as a single and stable conformer but it is experimentally proven that most of the proteins are inherently dynamic and can adopt several conformations.[13-15] This leads to the conformational selection model (**Scheme 3.1c**) which presumes that the proteins exist as an ensemble of infinite conformational states or substates. According to this model, the various conformational states are always in equilibrium with different population distributions and the ligand selectively

binds to the most fitting conformational state due to which the equilibrium shifted towards that particular conformation of the protein. The most practical binding model through which most of the protein-ligand binding interactions are taking place is a subject of debate for a long time and extensive research has been done to examine the validity of all the three models.[9, 16-18] However, the conformational selection model seems to be more realistic by taking account of inherent protein flexibility as well as the population shift and redistribution of the conformational states.

3.1.2. Bovine Serum Albumin (BSA): Highly Recognized Protein Model

The study of specific interaction with small molecule/drug is central to understand the functions of many proteins. Serum albumins are the major soluble transport proteins found in blood plasma.[19-21] They are mainly associated with transportation of a wide variety of compounds including fatty acids, bilirubin, bile salts, metal ions, hormones etc.[22-27] Extensive research has been carried out to investigate the structure, functions as well as their interactions with other biomolecules, drugs and biologically active molecules. Among various serum albumins, bovine serum albumin is one of the frequently used protein models because of its high availability and structural homology with human serum albumin (HSA). [19-21, 28] The protein sequence of BSA exhibits 75% identity and 87% similarity with HSA. BSA has a heart-shaped structure with three domains I, II, III. Each domain consists of two sub-domains IA, IB; IIA, IIB and IIIA, IIIB. There are two primary binding sites present in BSA known as site-I and site-II from which the specific physiological activity of a ligand initiated upon binding.[29, 30] Their locations are detected in the hydrophobic pockets of subdomain IIA and IIB respectively.[31, 32] Extensive experimental and theoretical studies revealed that the site-I is governed predominantly by hydrophobic interactions during a drug binding event whereas the interaction at site-II is combinatory interaction of hydrophobic, hydrogen bonding and electrostatic interactions.[33, 34] The structures of BSA and HSA and their various homologous domains and subdomains are shown in **Figure 3.1**.

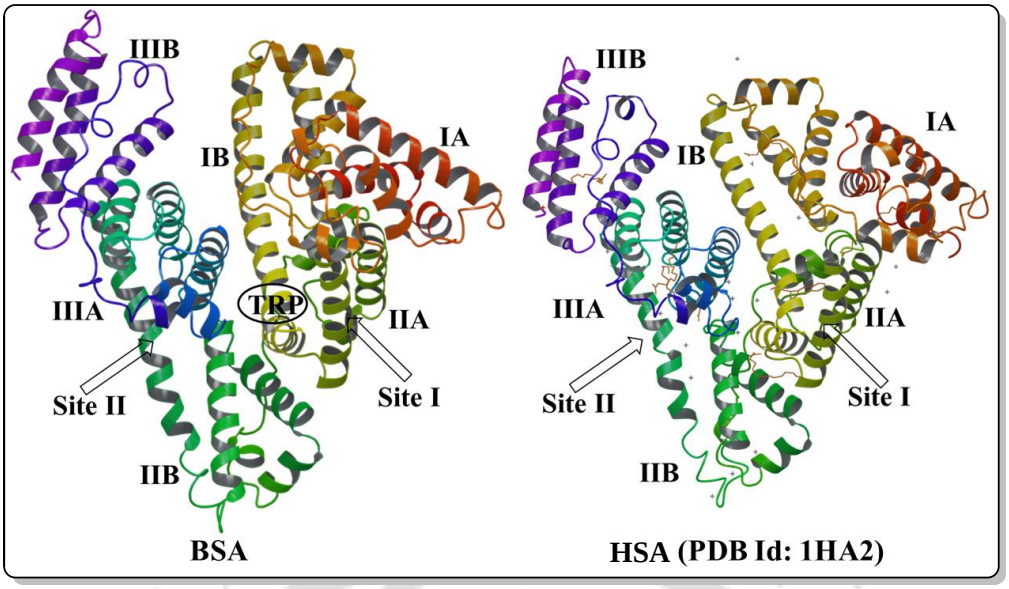

Figure 3.1: Structure of BSA and HSA and their various homologous domains.

3.2. Some Recent Small Molecule Probes of BSA

To gain insight into structure, functions and binding interactions of BSA with drugs and small fluorescent molecules, fluorescence-based techniques have been frequently utilized. The protein binding ability of a variety of small molecules, drugs, chromophores has been studied by utilizing their fluorescence photophysical properties.[35-40] In 2015, Li *et al.* reported a 1,2, 5-triphenylpyrole (TPP) derivative, **3.01** (**Figure 3.2**) and utilized it for the quantification of BSA and HSA without isolation from serum.[41] The compound showed aggregation induced emission property (AIE) and found to correlate linearly with both BSA and HSA over a wide range of concentration (2.18-70 µg/mL for BSA) with an enhancement of fluorescence signal. It was reported that the interactions occurred between the compound and BSA are mainly hydrophobic and hydrogen bonding. Malathi *et al.* designed and synthesized a benzimidazoquinoline derivative, **3.02** for sensing of BSA and metal ions.[42] It was reported that this compound also showed AIE properties and strong binding interaction with BSA due to a FRET process from the BSA to the probe. An enhancement of AIE (AIEE) of the probe was observed in the presence of BSA. Cell viability assay for both of the compounds (**3.01**, **3.02**) indicated low cytotoxicity and in-vivo experiments suggested their future application in cell imaging. Yang *et al.* reported two red-NIR (red to near-infrared) probes (**3.03** and **3.04**) for the quantitative and qualitative detection of both BSA and HSA.[43] These two probes showed differential recognition towards BSA and HSA in terms of fluorescence intensity even though

these two proteins have structural homology. The compound **3.03** showed strong fluorescence in the presence of HSA, while **3.04** being highly selective towards BSA showed a strong fluorescence upon interaction with BSA. Docking study revealed that the active binding site of **3.04** was located in between subdomains II and IIA of BSA and binding interaction mainly depend upon hydrogen bonding interaction. On the other hand, the binding site of **3.03** was located within the site I of HSA and binding interactions were mainly hydrophobic and π-π stacking.

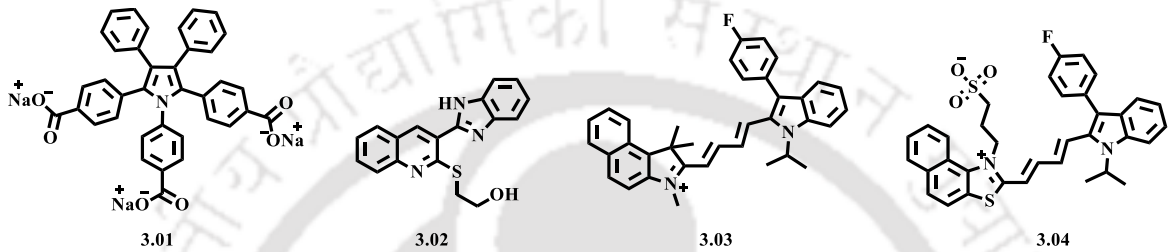

Figure 3.2. Examples of various molecular probes for BSA.

Polyaromatic hydrocarbons (PAH) constitute a class of highly fluorescent molecules with strong photophysical properties. Thus, these molecules and their derivatives often utilized as fluorescent probes in various investigations related to proteins. For example, Wang *et al.* studied diketopyrrolopyrrole (DPP)-anthracenone conjugates for sensing of BSA.[44, 45] One representative example of their work is the compound **3.05** (**Figure 3.3**) which exhibited enhanced fluorescence emission upon binding with BSA.[44] It was reported that this compound exhibits amphiphilic character due to its structure and undergoes complexation with BSA via electrostatic and hydrophobic interactions. Densil *et al.* reported three anthracene-derived Schiff base compounds, **3.06-3.08** as BSA sensing probes.[46] It was reported that these compounds are low toxic and AIE active and exhibit strong emission upon binding with BSA with an enhancement in their fluorescence signal. The binding interactions of all the three compounds with BSA were found to be mainly hydrogen bonding and hydrophobic interaction. Ali *et al.* reported a phenanthrene-pyrene fluorescent conjugate (**3.09**) for probing BSA. Association of this compound with BSA caused both static and dynamic quenching of BSA fluorescence.[47] Experimental and molecular docking study revealed the location of the binding site within the subdomain IIA of BSA. Singh *et al.* reported a perylenediimide-benzimidazolium derived fluorescent probe (**3.10**), which showed selective detection of BSA

and HSA among other proteins and inorganic ions.[48] This compound exhibited AIE characteristics and underwent complex formation with BSA with an enhancement in its fluorescence signal. This compound is reported as low cytotoxic and finds applications in detection of HSA in blood serum, urine samples and cell imaging in HeLa cells.

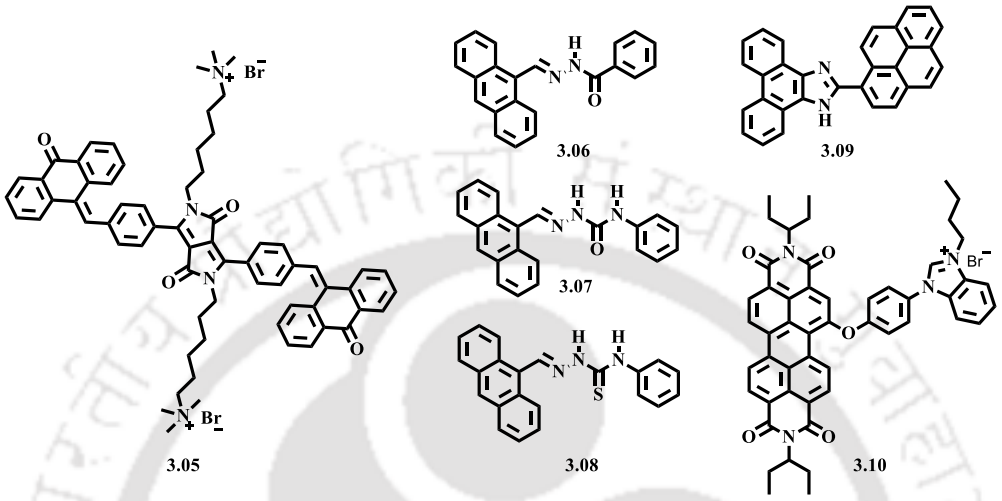

Figure 3.3. PAH derived fluorescent probes for BSA.

Synthetic dyes find widespread applications in the field proteins analysis such as characterization of protein folding, protein surface-hydrophobicity sensing, and detection of protein aggregation etc.[49-55] Superior fluorescence emission properties of synthetic and natural dyes established themselves as powerful components of fluorescent tools. As for an example, Jurek *et al.* investigated binding interactions of a few amino-substituted squaraine dyes with BSA.[56] Two representative examples of their work are **3.11** and **3.12** (**Figure 3.4**). Both of the compounds showed efficient binding interaction with binding constants 45.5×10^4 and 37.3×10^4, respectively. Reis *et al.* also reported several squaraine dye derivatives for the detection of BSA and HSA.[57] A few examples (**3.13-3.15**) of their work are shown in **Figure 3.4**. Authors reported low solubility of these compounds in aqueous media which led to poor fluorescence emission. However, significant enhancement in fluorescence intensity was observed in the presence of BSA and HSA, which indicated a strong interaction between these compounds and BSA/HSA. Onganer *et al.* studied the photophysical and biophysical impact of coumarin 35 dye (**3.16**) on BSA.[58, 59] A strong interaction between the coumarin 35 dye with BSA was reported leading to a significant enhancement in the fluorescence signal the probe. The authors also studied the influence of certain metal cations on the binding interactions between the

Coumarin 35 dye and BSA. The binding constant of the BSA-coumarin35 complex was found to be increased in the presence of metal ions and was highest in the presence of Sn^{4+} ions. Qian *et al.* investigated boron-dipyrromethene (BODIPY)-triphenylamine derivatives (**3.17** and **3.18**) for sensing of BSA.[60] These fluorescent compounds with AIE properties showed efficient association with BSA with an enhancement in their fluorescence signal. Vodyanova *et al.* also reported several BODIPY derivatives which can be utilized as fluorescence light-up probes for the detection of BSA.[61] Some representative examples of their work are shown in **Figure 3.4** (**3.19-3.21**).

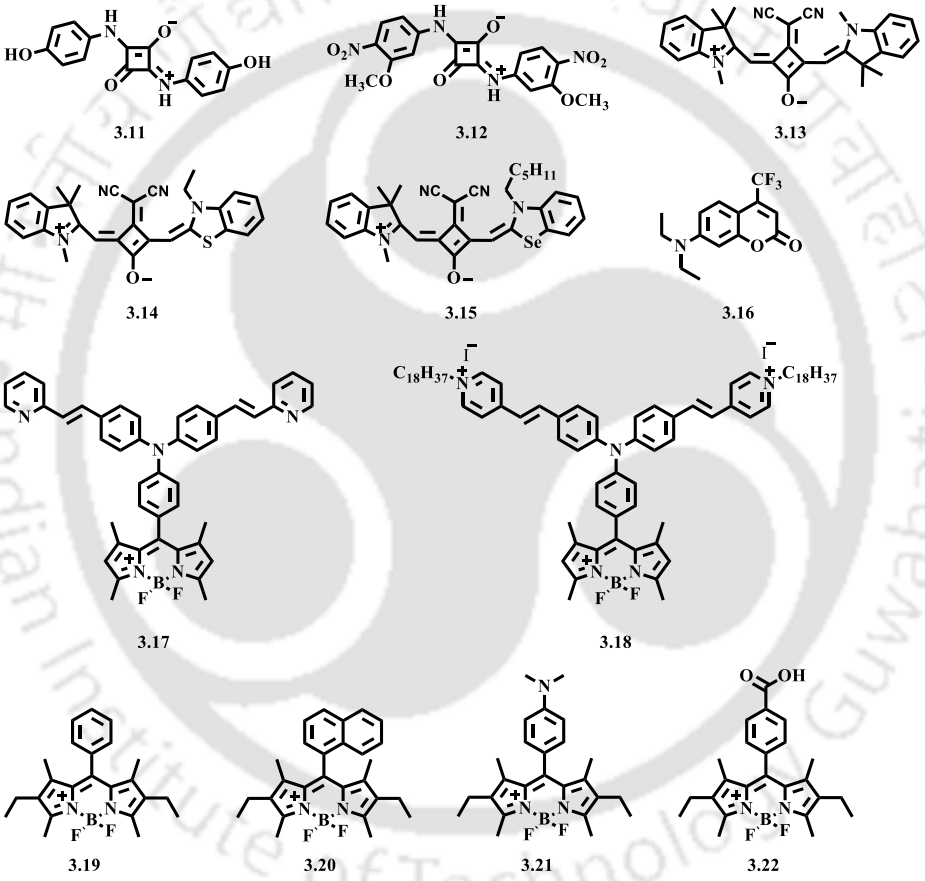

Figure 3.4. Fluorescent probes derived from various dyes for BSA detection.

Our research group also contributed towards the detection and sensing of BSA.[62, 63] As representative examples, two recent fluorescent molecules (**3.23** and **3.24**) reported by our research group are shown in **Figure 3.5**. Both the compounds exhibited strong fluorescence signals upon binding with BSA and therefore can be utilized as light-up fluorescent probes for the detection of BSA. Experimental results and molecular docking study indicated that the

binding interactions in both cases are mainly due to hydrophobic and electrostatic interactions in the hydrophobic pocket of BSA.

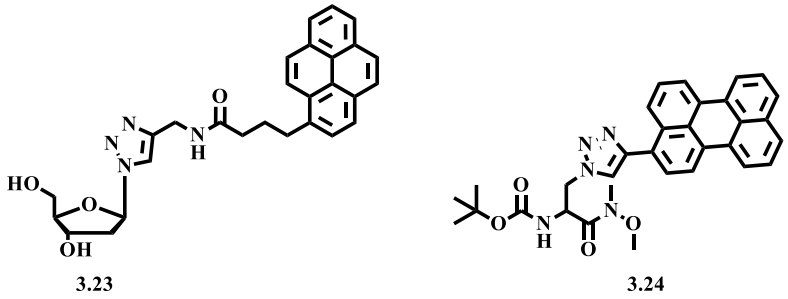

Figure 3.5. Fluorescent molecules reported by our research group for sensing of BSA.

3.3. Protein-Nucleic Acid Interactions

The existence of proteins with DNA as a complex structure was first recognized in the late 19th century.[64] Since then, researchers applied numerous synthetic, organic, and biochemical approaches in vitro and in vivo in order to get an insight into fundamental outcomes of protein-nucleic acid interactions. After tremendous research efforts, it has been established that the existence of protein-nucleic acid interactions is crucial for a variety of biological processes to occur. For example, the initiation and regulation of biological processes such as translation, transcription, DNA replication and RNA translocation depend directly or indirectly on the protein-nucleic acid interactions.[65] Understanding of these fundamental biological processes continuously aiding researchers to get insights into cell biology, origin and mechanism of various diseases, which ultimately aiding in the development of new chemotherapeutics.

The forces involved in protein-nucleic acid interactions are electrostatic (salt bridges), hydrophobic and hydrogen bonding.[66] The degree of contribution of these forces are different for the formation of a non-covalent protein-nucleic acid complex and therefore, the overall affinity and stability towards the complex formation depends on the sum of many favorable and unfavorable interactions. Although modes of interactions are similar, many proteins showed specific binding with a particular nucleic acid sequence or structure. For example, specific protein-DNA interactions are generally mediated via insertion of a protein α-helix motif into the major groove of the DNA, where the motif interacts with a specific base sequence through H-bonds and salt bridges.[67-69] On the other hand, protein-RNA interactions are more like protein-protein interactions due to the flexibility of RNA molecules for the formation of a

variety of surfaces and folding.[66] Therefore, protein-DNA recognition is more specific than the protein-RNA recognition.

3.4. Nucleoside as Drug: Nucleoside-Protein Interaction

Nucleosides and nucleobase analogs constitute the largest class of compounds possessing potential antiviral properties.[70, 71] Due to high antiviral properties and favorable pharmacokinetics, many of these compounds have been used for the inhibition and treatment of various chronic diseases including HIV, hepatitis, and herpes. In chapter 1 (**Section 1.6.**), we have listed several examples of modified nucleoside analogs and discussed their medicinal properties and clinical use.

Most of the nucleosides and nucleoside-based drugs are hydrophilic in nature and very few of them are able to diffuse through the cell membrane, however very slowly.[72] Therefore, to exert their potential effects, these drug molecules have to rely on certain transporter agents for transportation across the cell membrane which are collectively known as nucleoside transporters (NTs).[73] These transporters are basically a class of membrane proteins and are of types in humans: concentrative nucleoside transporters (CNTs) and equilibrative nucleoside transporters (ENTs).[72-74] These nucleoside transporters transport a wide range of nucleoside-derived drugs across the cell membrane.[75-80] Both NT families are divided into several subtypes and each subtypes transport different types of nucleosides.[72-80] Therefore, it can be concluded that the recognition of nucleosides by the nucleoside transfer proteins is highly specific.

The mechanism of protein-nucleoside interaction is difficult to understand and believed to be accompanied by a series of induce fit processes, which require a change in conformations of proteins, in the ligands or in both.[81, 82] A direct interaction of nucleotide's/nucleoside's bases were reported while NT proteins bind with DNA or RNA.[81] Selvaraj *et al.* also demonstrated that proteins are able to discriminate nucleobases in terms of their noncovalent interactions.[83, 84] Several structural analysis revealed that weak noncovalent interactions including van der Waal interactions, aromatic stacking interactions are very important for the stabilization of protein-nucleoside interaction.[85, 86] Using these ideas, John *et al.* demonstrated that nucleosides can be designed to get specifically recognized by NTs for their efficient transportation across the cell membrane.[87] Such evidence provides proof that the understanding of protein-nucleoside interaction is very crucial for the design and development of new drugs. Moreover,

the study of protein-nucleoside interaction can be very helpful in the investigation of the structure and function of proteins structurally similar to the nucleoside transporter proteins.

3.5. Background

From the literature study, it is clear that the protein-ligand interactions are of paramount importance for all processes taking place in living organisms. These interactions regulate the states and functions of proteins which are important for the regulation of many biological functions. The study of the interaction of proteins with drugs and small molecules with rich photophysical properties contributed significantly in the field of pharmacology.[88-91] These protein-drug binding events are mostly dependent on the microenvironment and dynamics of protein structure. A small molecule with unique photophysical properties can interact to the microenvironment exceptionally and bear information related to biological protein-ligand binding sites and events. Such information is highly significant for drug discovery and many other research topics.[92-95] However, a large number of experimental trials are required to gain insight into the properties and functions of a particular protein and develop such smart molecules accordingly. Moreover, these experimental trials are a lot of time consuming and unsafe when done in vitro. Therefore, highly abundant proteins like serum albumins often used as models in order to investigate protein-small molecule interactions in vivo, which ultimately assist in designing biologically active compounds. Therefore, aqueous complexation studies of synthetic molecules with serum albumins such as bovine serum albumin (BSA) gain significant research interest during the last decade.

3.6. Objective

With the above background and the observed photophysical properties of our previously reported (**Chapter 1 and Chapter 2**) pyrene-labeled fluorescent probes, **2.45G** and **1.262** (**Figure 3.6**), we envisaged that these nucleosides might offer some interesting binding interactions with a biomolecule such as a model protein BSA. Thus we framed our objective to study the following:

(a) Studies on the interaction of our previously reported pyrene-labeled nucleoside **2.45G** with BSA via the study of UV-visible and fluorescence photophysical property.

(b) Studies on the interaction of our previously reported tetrazolylpyrene unnatural nucleoside **1.262** with BSA.

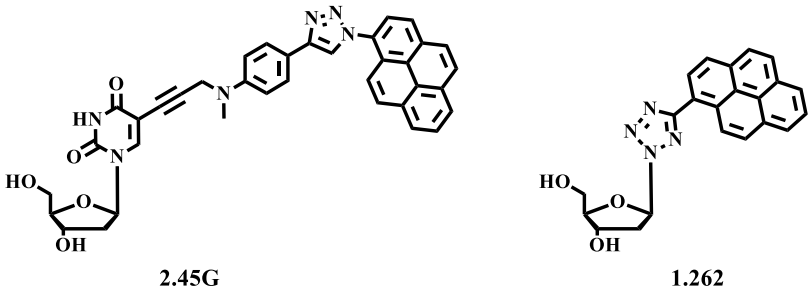

Figure 3.6. Structures of pyrene-labeled nucleosides.

3.7. Result and Discussion

In order to investigate the binding interaction of our probes towards BSA, we have studied the UV-visible and fluorescence spectroscopy in aqueous phosphate buffer (pH = 7.0) at 298 K. At first, we want to highlight the spectral properties of the probes in various organic solvents.

3.7.1. UV-visible and Fluorescence Photophysical Properties of Pyrene-Labeled Nucleosides

We have extensively discussed the photophysical properties of the triazolylpyrene nucleoside **2.45G** in **Chapter 2**. Therefore, here we only provide a brief summary of the photophysical properties of the nucleoside in various organic solvents. Thus, the triazolylpyrene nucleoside **2.45G** showed characteristic pyrene absorption at around 343 nm in dioxane which experienced a slight blue-shifting (by 2-4 nm) when the polarity was increased from dioxane to methanol (**Figure 3.7a**). This nucleoside exhibited dual-emission behavior in low polar solvents like toluene, dioxane, chloroform, ethyl acetate, and THF. A red shift in the ICT band of about 84 nm (453-537 nm) with a decrease in intensity was observed when the solvent polarity was increased from toluene to THF (**Figure 3.7b**). The LE band in these solvents consisted of structured pyrene-like emission at 385 and 403 nm. However, in high polar solvents like ACN, EtOH and MeOH, only structured pyrene-like emission (LE emission) was observed.

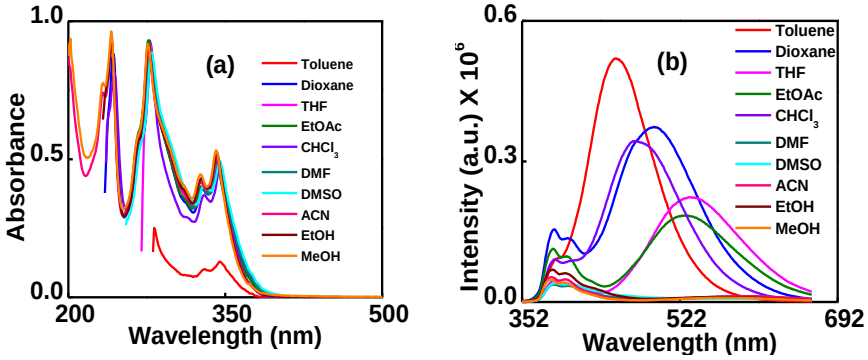

Figure 3.7. (a) UV-visible, (b) fluorescence emission spectra in various organic solvents for nucleoside **2.45G**

The absorption spectra of tetrazolylpyrene nucleoside **1.262** revealed a structureless absorption at 354 nm in dioxane which experienced a strong blue shift (by 8-9 nm) when the solvent polarity was increased from dioxane to methanol (**Figure 3.8a**). Upon excitation at 350 nm, the emission spectra revealed two structured emissions at around 385 and 406 nm which experienced a slight red shift (by 2-3 nm) with almost no change in intensities when the solvent polarity was increased from dioxane to $CHCl_3$ (**Figure 3.8b**).

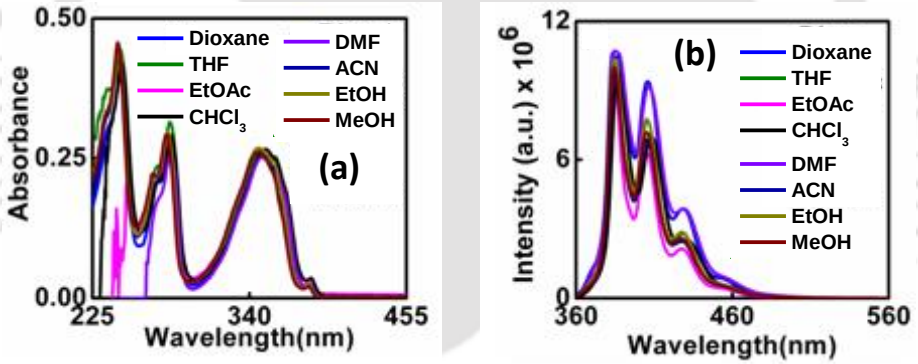

Figure 3.8. (a) UV-visible, (b) fluorescence emission spectra in various organic solvents for nucleoside **1.262.**

3.7.2. Theoretical Calculations

In **Chapter 2**, we have shown the TDDFT calculation for the triazolylpyrene nucleoside **2.45G**. In this chapter, we studied the TDDFT calculation for the tetrazolylpyrene nucleoside, **1.262** in order to examine the effect of solvent polarity on its absorption and emission property using Gaussian 09 program package.[96] Thus, from the HOMO-LUMO overlap and transition oscillator strength (f) of the tetrazolylpyrene nucleoside, it was clear that the electronic transition from S_0 to S_1 or other possible electronic transitions are feasible. So the reverse transition i.e., $S_0 \leftarrow S_1$ was also fully allowed that revealed the fluorophoric nature of the

nucleoside. Solvatochromicity and intramolecular charge transfer emissions were also explained by redistribution of electronic charge density between HOMO-LUMO (**Figure 3.9**).[62, 97-100] From the TDDFT calculations, it was clear that the dominant orbital transition in the low-lying singlet excited states of the studied nucleoside is the $S_0 \rightarrow S_1$ transition having the highest configuration interaction (CI) value. Thus, the calculated excitation energy for the transition from $S_0 \rightarrow S_1$ of the tetrazolylpyrene found to be 367nm (3.89 ev, f = 0.48, CI = 0.68) (in vacuum). The experimental observations in low polar solvents from UV-visible spectra correlated well with the theoretical calculation in the gas phase. Thus, the absorption of the tetrazolylpyrene nucleoside was found to be 354 nm in dioxane.

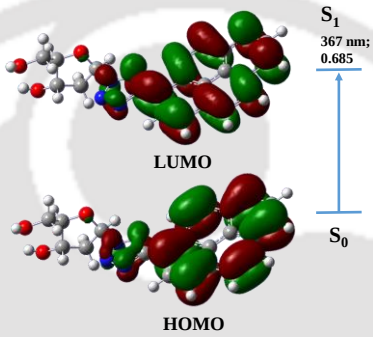

Figure 3.9. The HOMO-LUMO transition from TD-DFT calculation for the tetrazolylpyrene nucleoside **1.262**.

3.7.3. Study of UV-visible and Fluorescence Photophysical Properties of Triazolylpyrene-Labeled Nucleoside 2.45G in presence of BSA

The UV-visible spectra in phosphate buffer revealed that the probe nucleoside **2.45G** exhibited very weak, broad and structureless short and long wavelength absorptions at around 283 and 351 nm. The characteristic pyrenyl absorption was not present in contrary to that in the organic solvent. Upon gradual addition of BSA to a solution of the probe, the absorption bands experienced strong hyperchromicity and hypsochromic shift of 5-7 nm along with the appearance of characteristic pyrenyl bands at around 345 and 329 nm (**Figure 3.10a**). This indicated a strong binding interaction of the probe in the hydrophobic region of BSA.

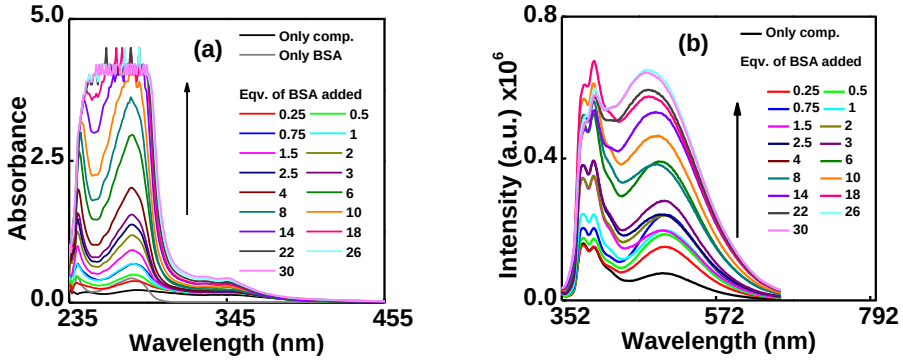

Figure 3.10. (a) UV-visible spectra of **2.45G** in the absence or in the presence of BSA. (b) fluorescence emission titration spectra of **2.45G** in the absence or in the presence of BSA (λ_{ex} = 342 nm).The probe concentration [**2.45G**] =10μM.

To gain further insight, we performed a fluorescence titration in the buffer. We observed that the probe showed dual emission, LE (at 381, 398 and 427 nm) band characteristic of pyrene and ICT band at 501 nm. Interestingly, the nucleoside **2.45G** retained its dual emitting property in all the concentration of BSA. It showed a regularly increased intensity in both the LE and ICT bands when excited at 343 nm upon the gradual addition of an increasing amount of BSA (**Figure 3.10b**). The quantum yield variations also followed the same trend. (**Table 3.1**). While position and shape of the LE band remained unaltered, peak broadenings and blue shifts were the major results of ICT bands with increasing concentration of BSA similar to what was observed in organic solvents or in dioxane-water titration experiments of the probe. All these observations clearly suggested the accommodation of the fluorophoric pyrenyl moiety of the probe inside the hydrophobic pocket of BSA. Therefore, even in the BSA microenvironment, the probe **2.45G** behaved as a system of dual emitting switch-on fluorescent probe.

Table 3.1. Summary of the photophysical property of **2.45G** in the absence and in the presence of various concentrations of BSA in phosphate buffer (2% DMF)

Properties ↓		**Only Comp.**	**1eqv. BSA**	**10eqv. BSA**	**22 eqv. BSA**	**30 eqv. BSA**
λ_{max}^{abs} (nm)		282, 344	279, 344	279 , 345	345	345
λ_{max}^{fl} (nm)		382, 397, 498	382, 397, 499	383, 397, 487	385, 398, 477	398, 472
LE	Φ_f	0.0025	0.006	0.008	0.009	0.007
ICT	Φ_f	0.003	0.006	0.012	0.014	0.015

Next, we plotted the LE, ICT fluorescence intensity and the I_{LE}/I_{ICT} ratio (I_{398}/I_{500}) against the equivalent concentration of BSA added to clearly demonstrate the fluorescence behavior of the ratiometric fluorescent pyrenyl nucleoside probe. Thus, from the plot in **Figure 3.11a,** it is clear that the intensity of both the LE and ICT bands increased up to 14 equivalent of BSA with respect to 10 μM probe concentration. Further addition of BSA does not induce a notable change in both LE and ICT bands. The same plot for ratio LE/ICT vs. equivalent concentration of BSA added shows that the LE/ICT values decreased or ICT/LE increases exponentially indicating that the probe nucleoside **2.45G** functions as a good ratiometric BSA sensor (**Figure 3.11b**).[96] Ratiometric fluorescence sensing offers increased signal-to-noise ratio leading to more reliable quantification compared to that by using a probe of emission at a wavelength.[97-101] Furthermore, ratiometric fluorescence is more reliable compared to absolute fluorescence intensity in demonstrating sensing events because the ratios do not suffer from simultaneous drifts or fluctuations of individual signals.[102-104] Therefore, the probe nucleoside 10G could find wide applications in ratiometric sensing in chemistry, biology and in materials sciences.[96-104]

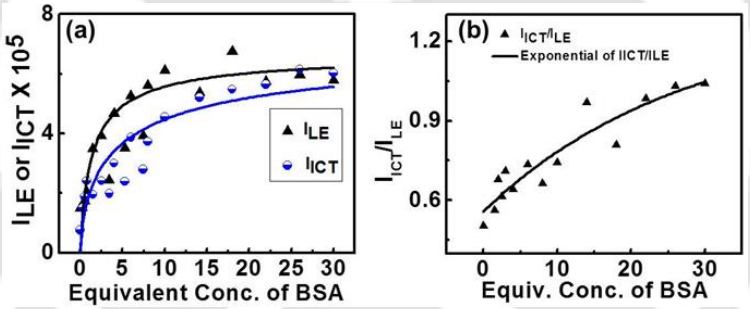

Figure 3.11. (a) The plot of the intensity of LE or ICT and of (b) LE/ICT vs. equivalent concentration of BSA added. The probe concentration [**2.45G**] =10μM.

To quantify the stoichiometry between the fluorophore (**2.45G**) and the BSA protein, the absorption measurement was carried out for Job's plot. For this purpose, an equal concentration of probe (**2.45G**) and BSA protein solutions was prepared separately in phosphate buffer. Then, the fluorophore and the BSA protein were mixed in different fractions of volume maintaining the total volume of the mixture at 3 mL. All the solutions were mixed well and kept for some time in room temperature. Then the absorbance spectra of the solutions of different composition of fluorophore and BSA protein were recorded. To calculate the Probe-BSA protein complexation ratio, [Probe-BSA protein] vs. Xprobe were plotted, where [Probe -BSA protein] = ΔA x Xprobe, {ΔA = (A-A0)}; and Xprobe is the mole fraction of probe, {Xprobe

= [probe]/([probe] + [BSA])}. The Job's plot (**Figure 3.12**) showed the point of maximum at the mole fraction of ~0.50 of the probe, which clearly indicated a 1:1 stoichiometry of the probe to BSA in the complex.

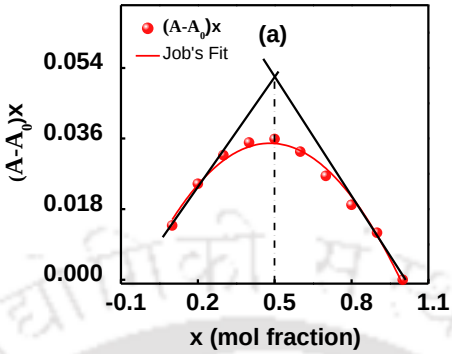

Figure 3.12. (a) Absorption Job's plot of the probe, **2.45G** in presence of BSA protein indicates a 1:1 stoichiometry of the probe to BSA in the complex.

3.7.4. Study of UV-visible and Fluorescence Photophysical Properties of Tetrazolylpyrene-Labeled Nucleoside 1.262 in presence of BSA

The UV-visible spectra of the fluorescent nucleoside **1.262** in phosphate buffer also exhibited very weak, broad and structureless short and long wavelength absorptions at around 278 and 348 nm. Upon gradual addition of BSA to a solution of the probe, the absorption bands exhibited a strong hyperchromicity with a negligible shifting in wavelength (1-2 nm) (**Figure 3.13a**). Upon addition of just 0.2 equivalent of BSA, we observed an increase of absorbance from 0.15 to 0.19 at around 345 nm. Beyond this point, a slow and steady increase in absorbance was observed leading to almost saturation upon addition of 3 equivalent of BSA. The observed hyperchromicity indicated a strong binding interaction of the nucleoside **1.262** in the hydrophobic region of BSA (**Figure 3.13a**). Upon excitation at 350 nm, this nucleoside showed two sharp emissions at around 383, 403 and a broad emission band centering around 426 nm. Upon gradual addition of an increasing amount of BSA, the emission intensity of the nucleoside gradually increased with a red shift of 2-3 nm at all the three emission bands. The intensity of emission almost reached saturation upon addition of 3 equivalent of BSA (**Figure 3.13b,c)**. Thus, both the UV and fluorescence observations indicated a strong interaction between the probe and the hydrophobic pocket of BSA.

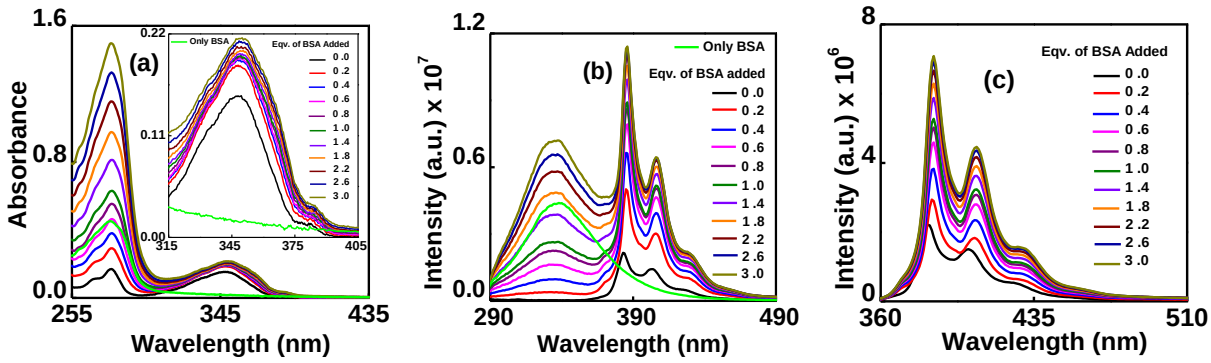

Figure 3.13. (a) UV-visible, (b) fluorescence emission spectra (λ_{ex} = 280 nm), (c) fluorescence emission spectra (λ_{ex} = 350 nm) of **1.262** in absence or in presence of BSA (λ_{ex} = 350 nm).The probe concentration [**1.262**] =10µM.

3.7.4.1. Steady State Anisotropy Study

To get into more insight into the binding events of the fluorophoric nucleoside **1.262** with BSA, we examined the steady-state fluorescence anisotropy. The steady-state fluorescence anisotropy study can explain the nature of the surrounding environment of the probe and its interaction with protein in a much clear way than the steady-state fluorescence.[105] Experimentally, the anisotropy/polarization is determined from measurements of fluorescence intensities parallel and perpendicular with respect to the plane of linearly polarized excitation light and is expressed in terms of fluorescence anisotropy (r) or polarization (P). In an aqueous medium, the small molecules are weakly polarized due to the rapid tumbling motion. However, when they bind with protein, the rotational motion of the probe molecules would restrict by the binding protein and thereby the fluorescence polarization would increase. Thus, upon binding with BSA the probe moves from the free aqueous environment to a rigid protein environment. The anisotropy experiment also reflects our expected result. With increasing concentration of BSA, the free motion of the probe is restricted by the rigid environment of the BSA protein and thus anisotropy values increases. Thus, the protein bound probe experiences a more rigid environment compared to its free aqueous environment and we observed a change in anisotropy value (r_0) from 0.003 in the free buffer to 0. 15 in 1 equivalent of BSA (**Figure 3.14**). At the same time, the polarization value changes from 0.005 in the free buffer to 0.21 in 1 equivalent of BSA. Thus, from the above observations, it is evident that the probe is involved in tight binding inside the hydrophobic pocket of BSA and experiences a highly restricted rotational motion.[106-109]

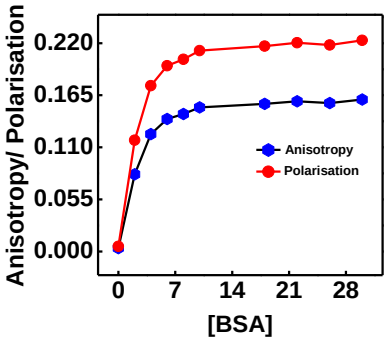

Figure 3.14. Steady-state fluorescence anisotropy and polarisation change of nucleoside **1.262** in presence of various concentrations of BSA at 298K. [**1.262**] = 10 μM and [BSA] = 0, 2, 4, 6, 8, 10, 14, 18, 22, and 26 μM. λ_{ex} = 350 nm.

3.7.5. Determination of Protein–Probe Binding Constant

The binding constants (*K*) of the protein-probe complexes of both of the nucleosides were determined spectroscopically by well-known Benesi-Hildebrand plot (**Figure 3.15**) using the following equation 1,

$$\frac{1}{(I - I_0)} = \frac{1}{(I_\infty - I_0)} + \frac{1}{(I_\infty - I_0)K[BSA]} \quad \ldots\ldots\ldots\ldots\ldots\ldots (1)$$

where I_0, I and I_α are the emission intensities of nucleosides in the absence of BSA, and in the presence of intermediate and at an infinite concentration of BSA, respectively. From the slope (linear region's data points) of the plot of $1/(I - I_0)$ *vs.* 1/[BSA] the binding constant *K* was determined, which was found to be 1.0 x 10^4 M^{-1} and 1.16 x 10^5 M^{-1} for the nucleosides **2.45G** and **1.262** respectively. Next, the free energy of binding (ΔG) was calculated using equation 2, which was found to be -5.5 kcal/mol and -6.9 kcal/mol for the nucleosides **2.45G** and **1.262**, respectively.

$$\Delta G = -RT \ln K \quad \ldots\ldots\ldots\ldots\ldots\ldots\ldots (2)$$

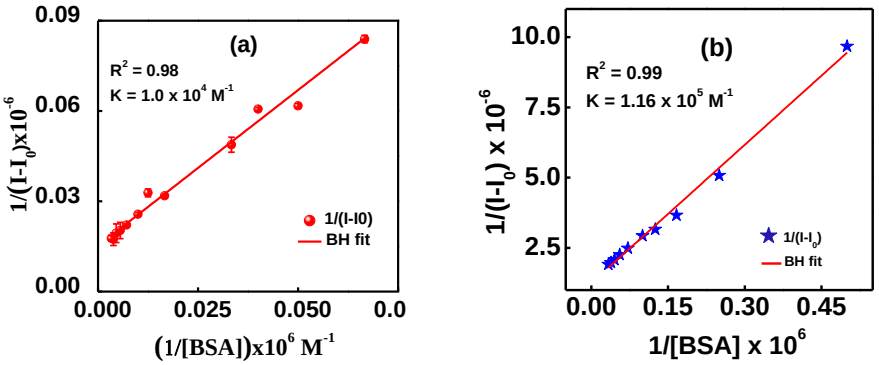

Figure 3.15. Benesi–Hildebrand plots of nucleosides **2.45G** (a) and **1.262** (b) in the presence of an increasing concentration of BSA at 298K.

3.7.6. Circular Dichroism (CD) Study

CD experiment was also carried out to get insight into possible structural perturbation of BSA in the presence of our probes. BSA exhibits two negative bands in the far UV region at 208 and 222 nm characteristics of α-helices. The α-helix content of free BSA is within the range (56.8 %) observed in other studies.[29, 110-115] Thus, an investigation of CD spectra of BSA in the presence and absence of the probes also revealed the same band position. However, a slight increase in % of α-helicity in presence of both of the probes was observed that can be attributed to conformational adjustments on the complex formation (**Figure 3.16a,b**).[114]

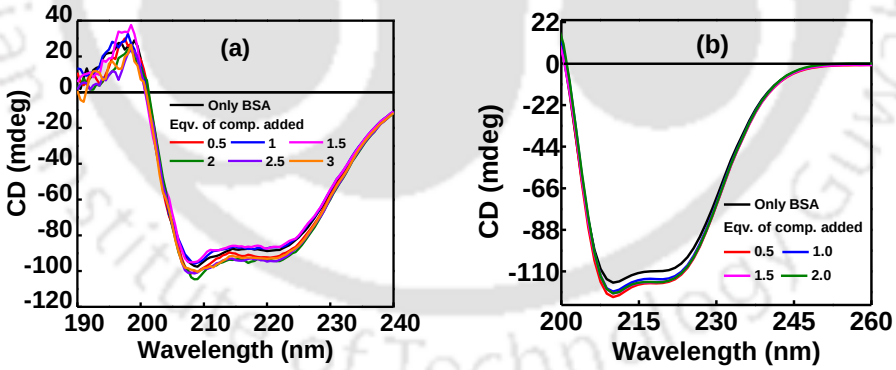

Figure 3.16. CD spectra of BSA in presence and absence of probes (a) **2.45G**, (b) **1.262**.

3.7.7. Molecular Docking Study

Docking calculations were carried out using Autodock 4.2.[116, 117] The amino acid sequence of BSA protein was observed from the NCBI website, http://www.ncbi.nlm.nih.gov/protein/CAA76847.1. The 3D model of the BSA protein was built using the 3D structure 1AO6 chain 'A' as a template using the ESyPred3D[118] web server.

This template shares 72.4% identities with the BSA sequence. Following is the BSA sequence which was used to generate the 3D model.

>gi|3336842|emb|CAA76847.1| bovine serum albumin [Bos taurus]

MKWVTFISLLLLFSSAYSRGVFRRDTHKSEIAHRFKDLGEEHFKGLVLIAFSQYLQQC
PFDEHVKLVNELTEFAKTCVADESHAGCEKSLHTLFGDELCKVASLRETYGDMADC
CEKQEPERNECFLSHKDDSPDLPKLKPDPNTLCDEFKADEKKFWGKYLYEIARRHPY
FYAPELLYYANKYNGVFQECCQAEDKGACLLPKIETMREKVLTSSARQRLRCASIQK
FGERALKAWSVARLSQKFPKAEFVEVTKLVTDLTKVHKECCHGDLLECADDRADL
AKYICDNQDTISSKLKECCDKPLLEKSHCIAEVEKDAIPENLPPLTADFAEDKDVCKN
YQEAKDAFLGSFLYEYSRRHPEYAVSVLLRLAKEYEATLEECCAKDDPHACYSTVF
DKLKHLVDEPQNLIKQNCDQFEKLGEYGFQNALIVRYTRKVPQVSTPTLVEVSRSLG
KVGTRCCTKPESERMPCTEDYLSLILNRLCVLHEKTPVSEKVTKCCTESLVNRRPCFS
ALTPDETYVPKAFDEKLFTFHADICTLPDTEKQIKKQTALVELLKHKPKATEEQLKTV
MENFVAFVDKCCAADDKEACFAVEGPKLVVSTQTALA

3.7.7.1. Molecular Docking Study of Triazolylpyrene-Labeled Nucleoside

From the docking study, it is revealed that the dual emitting pyrenyl nucleoside **2.45G** binds to both the chains of BSA. As revealed from the docking pose in **Figure 3.17**, the Leu115, Pro117, Asp118, Leu122, Lys136, Glu140, Ile141 and Tyr137 residues of chain B was involved in hydrophobic interactions mostly with the chromophoric phenyl triazolyl pyrenyl unit.[62, 119]

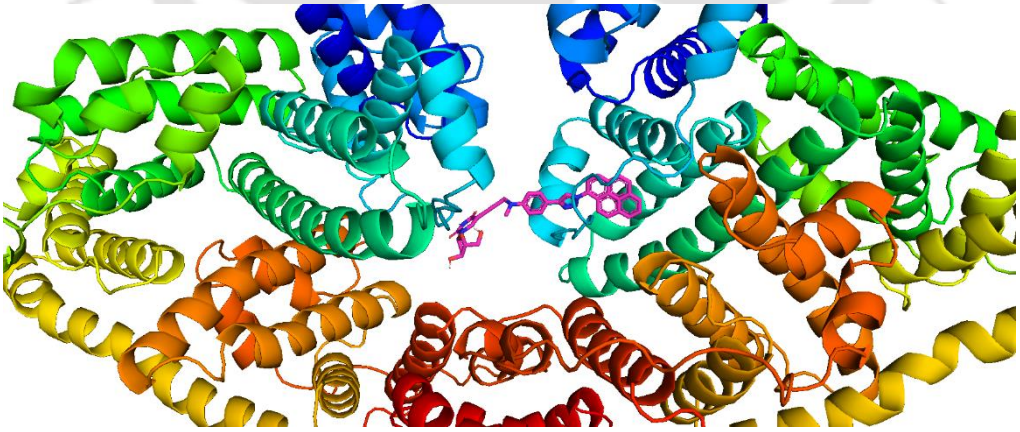

Figure 3.17. Docking pose of the nucleoside **2.45G** inside the hydrophobic pocket of BSA.

Table 3.2. The energy of **2.45G** - BSA complex obtained from Autodock4.

Interaction Energy	kcal/mol
Estimated Free Energy of Binding	-10.18
Final Intermolecular Energy	-13. 16
vdW + Hbond + desolv Energy	-12.89
Electrostatic Energy	-0.27
Final Total Internal Energy	-2.20
Torsional Free Energy	+2.98
Unbound System's Energy	-2.20

The number of distinct conformational clusters from the docking analysis was found to be 10 out of 10 runs with rmsd-tolerance of 2.0 Å. The clustering histogram is depicted in **Table 3.3**. **Figure 3.18** represents the number of multi-member conformational cluster and found that all are single cluster out of 10 runs. The docking pose of the triazolylpyrene nucleoside **2.45G** showed the conformation of the compound having binding energy with BSA as -9.2 kcal/mol. The binding energy of this conformer is close to the lowest energy conformer as was revealed from the histogram (**Figure 3.18**).

Table 3.3. Clustering histogram

Cluster Rank	**Lowest Binding Energy**	**Run**	**Mean Binding Energy**	**Number In Cluster**
1	-10.68	2	-10.68	1
2	-10.42	10	-10.42	1
3	-10.18	3	-10.18	1
4	-9.58	9	-9.58	1
5	-9.20	5	-9.20	1
6	-8.99	4	-8.99	1
7	-8.81	6	-8.81	1
8	-8.74	7	-8.74	1
9	-7. 47	1	-7.47	1
10	-7.30	8	-7.30	1

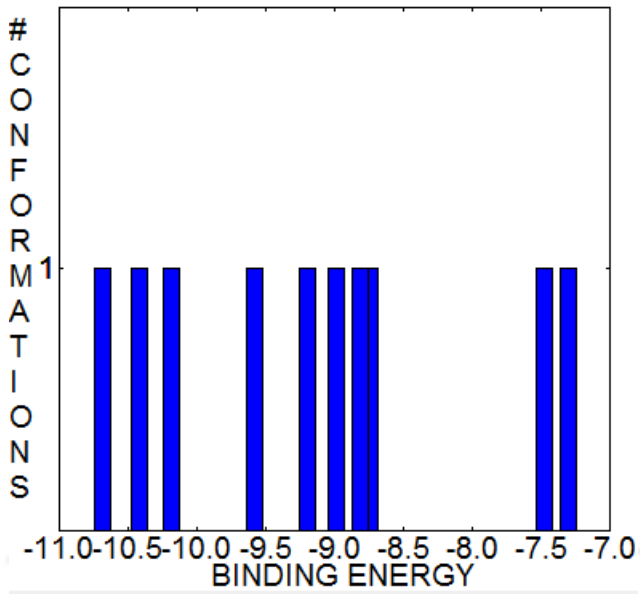

Figure 3.18. Histogram showing the number of multi-member conformational clusters.

The triazolylpyrene nucleoside **2.45G** involved in various types of interactions with BSA protein as is shown in **Figure 3.19** below and Table 3.4. The residues Pro, Leu, Asp, Tyr, Glu, and Isoleucine of BSA protein hydrophobically interacted with **2.45.G**. Hydrogen bonding interactions were also evident between Asp, Lys, Glu residues of BSA and triazole nitrogen/ carbonyl and hydroxyl units of the nucleoside **2.45G**. (**Figure 3.19, Table 3.4**).

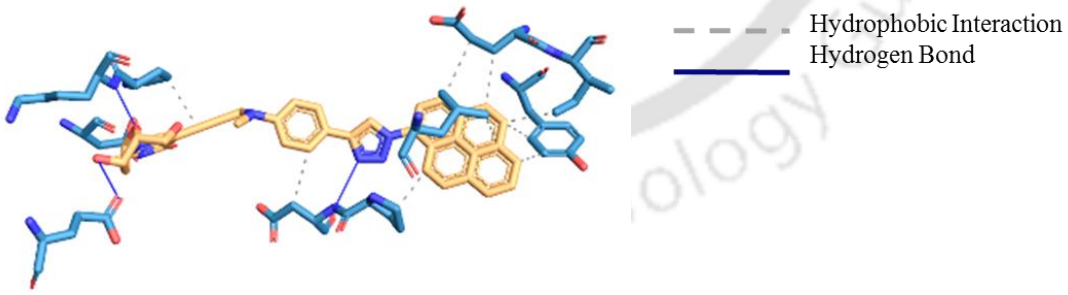

Figure 3.19. Graphically shown the interaction of **2.45G** in BSA protein.

Table 3.4. Different interactions of **2.45G** in the hydrophobic pocket of BSA

Hydrophobic Interactions				Hydrogen Bonds				
Index	**Residue**	**AA**	**Distance**	**Residue**	**AA**	**Distance H-A**	**Distance D-A**	**Donor Angle**
1	113A	PRO	3.43	111A	ASP	3.21	4.05	141.55
2	115B	LEU	3.65	114A	LYS	1.69	2.69	167.88
3	115B	LEU	3.52	118B	ASP	2.23	3.11	143.46
4	117B	PRO	3.25	519A	GLU	2.33	2.93	119.46
5	118B	ASP	3.59					
6	137B	TYR	3.31					
7	137B	TYR	3.13					
8	140B	GLU	3.80					
9	140B	GLU	3.30					
10	141B	ILE	3.14					

3.7.7.2. Molecular Docking Study of Tetrazolylpyrene-Labeled Nucleoside

From the docking study, it is revealed that the tetrazolylpyrene-labeled nucleoside **1.262** binds to the A chain of BSA. As revealed from the docking pose in **Figure 3.20**, the Leu115, Lys116, Pro117, Leu122, Lys136 and Tyr137 and Tyr160 residues of chain A were involved in hydrophobic interactions with the chromophoric pyrenyl unit.

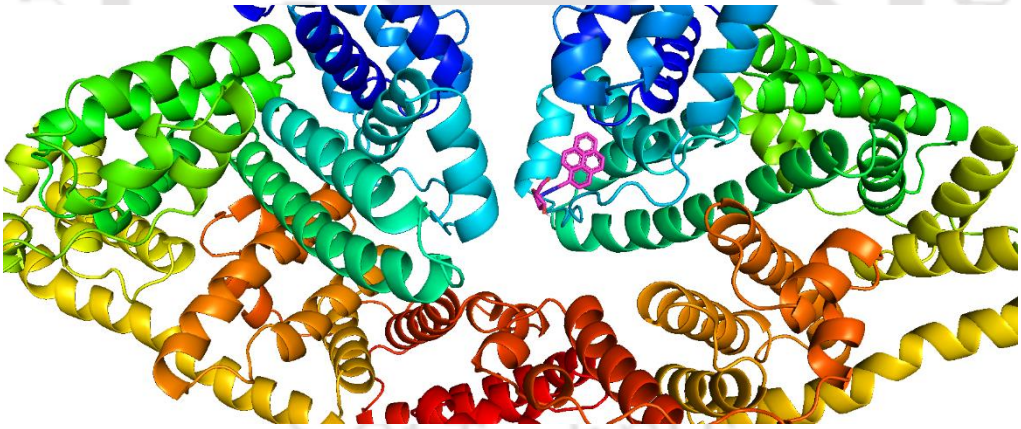

Figure 3.20. Docking pose of the nucleoside **1.262** inside the hydrophobic pocket of BSA.

Table 3.5. The energy of **1.262** - BSA complex obtained from Autodock4.

Interaction Energy	kcal/mol
Estimated Free Energy of Binding	-9.11
Final Intermolecular Energy	-10.60
vdW + Hbond + desolv Energy	-10.64
Electrostatic Energy	+0.04
Final Total Internal Energy	-2.23
Torsional Free Energy	+1.49
Unbound System's Energy	-2.33

The number of distinct conformational clusters from the docking analysis was found to be 8 out of 10 runs with rmsd-tolerance of 2.0 Å. The clustering histogram is depicted in **Table 3.6**. **Figure 3.21** represents the number of multi-member conformational cluster and found 1 out of 10 runs. The docking pose of the tetrazolylpyrene nucleoside **1.262** showed the conformation of the compound having binding energy with BSA as -9.09 kcal/mol supporting the experimental result of free energy of binding (-6.9 Kcal/mol). The binding energy of this conformer is close to the lowest energy conformer as was revealed from the histogram (**Table 3.6**, **Figure 3.21**).

Table 3.6. Clustering histogram

Cluster Rank	**Lowest Binding Energy**	**Run**	**Mean Binding Energy**	**Number In Cluster**
1	-9.11	5	-9.09	3
2	-9.10	3	-9.10	1
3	-8.83	2	-8.83	1
4	-8.72	9	-8.72	1
5	-8.69	1	-8.69	1
6	-8.45	4	-8.45	1
7	-8.26	10	-8.26	1
8	-8.02	8	-8.02	1

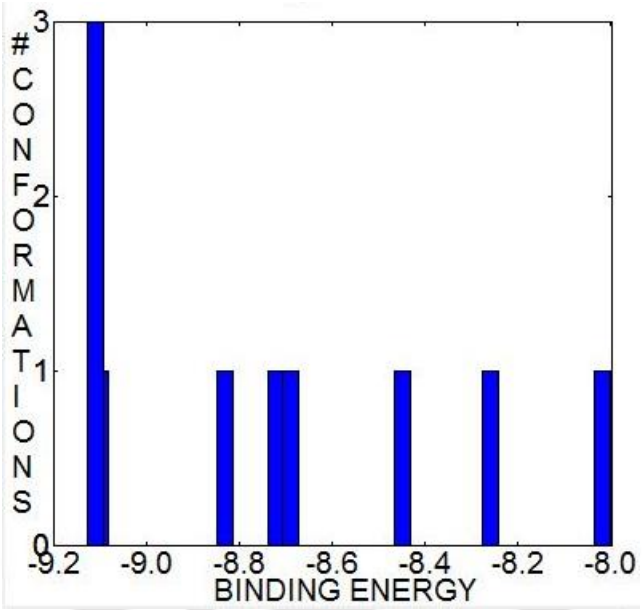

Figure 3.21. Histogram showing the number of multi-member conformational clusters.

The tetrazolylpyrene nucleoside **1.262** involved in various types of interactions with BSA protein as is shown in **Figure 3.22** below. The residue Leu, Lys, Pro and Tyrosine of BSA protein hydrophobically interacted with **1.262**. Hydrogen bonding interactions were also evident between Lys and Asp residues of BSA and triazole nitrogen/ hydroxyl units of the nucleoside **1.262**. The pyrene moiety of **1.262** involved in π-stacking interaction with phenylalanine residue of BSA. (**Figure 3.22, Table 3.7**).

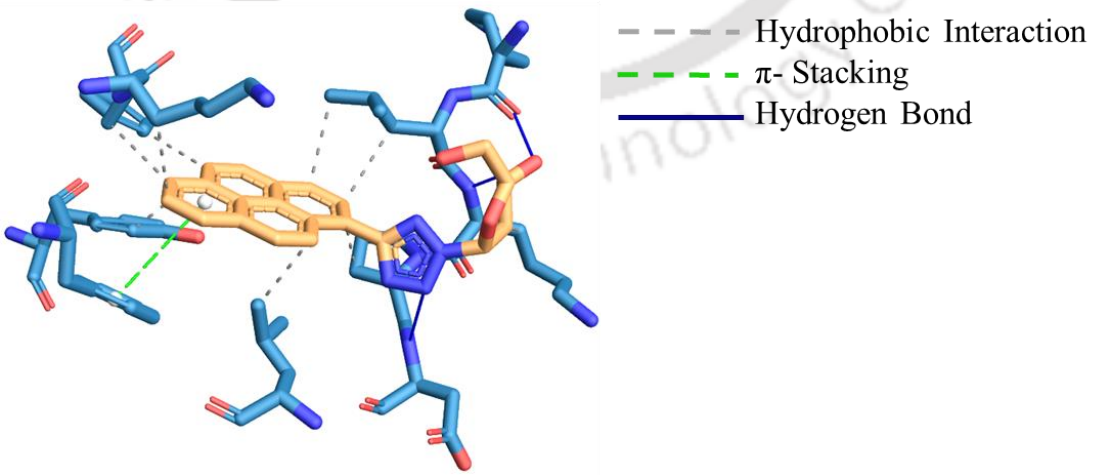

Figure 3.22. Graphically shown the interaction of **1.262** in BSA protein.

Table 3.7. Different interaction of **1.262** in the hydrophobic pocket of BSA

Hydrophobic Interactions				**Hydrogen Bonds**				
Index	**Residue**	**AA**	**Distance**	**Residue**	**AA**	**Distance H-A**	**Distance D-A**	**Donor Angle**
1	115A	LEU	3.38	114A	LYS	2.02	2.84	141.40
2	115A	LEU	3.47	116A	LYS	2.48	3.42	153.54
3	116A	LYS	3.36	118A	ASP	2.29	3.22	151.26
4	117A	PRO	3.52					
5	117A	PRO	3.16					
6	122A	LEU	3.25					
7	136A	LYS	3.22					
8	137A	TYR	3.44					
9	137A	TYR	3.61					
10	160A	TYR	3.71					
π-Stacking								
Index	**Residue**	**AA**	**Distance**	**Angle**	**Offset**	**Type**		
1	133A	PHE	4.46	25.93	1.70	P (Pyrene ring)		

3.8. Conclusion

In conclusion, we have successfully shown that our click chemistry derived triazolyl and tetrazolyl fluorophoric nucleosides **2.45G** and **1.262**, respectively serves as a versatile fluorescent light-up probe for BSA protein detection in the aqueous media. The enhancement in fluorescence intensity of both of the fluorophores upon addition of BSA indicates spontaneous complexation with BSA with a high binding constant, $K = 1.0 \times 10^4\ M^{-1}$ and $1.16 \times 10^5\ M^{-1}$ for the nucleosides **2.45G** and **1.262** respectively. The dual emitting nucleoside **2.45G** was efficient to interact with BSA via a switch on fluorescence and was able to retain its photophysical property in the biomolecular microenvironment. As the ratiometric fluorescence sensing is highly advantageous compared to a single wavelength emission, the ratiometric fluorescent nucleoside probe **2.45G** would find wide future application in chemistry, biology and in material sciences.

3.9. Experimental Section

3.9.1. Materials

BSA, Na_2HPO_4, and $NaH_2PO_4.H_2O$ (for preparation of phosphate buffer) were purchased from Merck, India and used without further purification. Water was obtained from a Milli-Q purification system. All experiments were performed with freshly prepared solutions. The probe molecule **2.45G** was synthesized and purified according to the procedure described in

Chapter 2 and the probe molecule **1.262** was synthesized and purified following a literature procedure.[120] We recrystallized the column purified material in the methanol-ethylacetate solvent mixture, dried under vacuum, again characterized and used for the study.

3.9.2. Preparation of BSA Solution

The BSA solution was prepared in Milli-Q water and the concentration was measured from UV-visible spectra using molar absorption coefficient (ε) of 43,800 M^{-1} cm^{-1} at 280 nm.[121]

3.9.3. Preparation of Nucleoside Solution

The nucleosides in pure form were dissolved in DMF for the preparation of the stock solution. Then dilutions were made by adding phosphate buffer and Milli-Q water in order to obtain experimental samples with desired concentrations. The percentage of DMF in the experimental samples was maintained at 2-3% with respect to the total volume of the experimental samples.

3.9.4. Photophysical Study

3.9.4.1. UV-Visible Study

The UV–Visible absorbance measurements were performed using Shimadzu UV-2550 UV–Visible spectrophotometer with a cell of 1 cm path length at 298 K. All the UV-Visible studies were carried out in 20 mM phosphate buffer of pH 7.0 at 298 K. 2-3 % DMF was used to solubilize the probe. The measurements were taken in absorbance mode and the absorbance values of the sample solutions were measured in the wavelength regime of 200–600 nm. All the experiments were carried out with freshly prepared sample solutions.

3.9.4.2. Fluorescence Study

The steady-state fluorescence emission and steady-state anisotropy experiments were performed using Fluoromax 4 spectrophotometer at 298 K with quartz cell of 1 cm path length. The slit width was 3 nm and the integration time was 0.2 sec. All the fluorescence studies were carried out in 20 mM phosphate buffer of pH 7.0 at 298 K. 2-3 % DMF was used to solubilize the probe. The excitation wavelength for the probe **2.45G** was set at 342 nm, and emission spectra were measured in the wavelength regime of 350–675 nm. The excitation wavelength for the probe **1.262** was set at 280/350 nm and emission spectra were measured in the wavelength regime of 290–690 nm. The steady-state fluorescence emission spectra were

recorded using an excitation slit of 3.0 nm, emission slit 3.0. The fluorescence anisotropy (*r*) was calculated using the following equation-

$$r = \frac{(I_{VV} - I_{VH}G)}{(I_{VV} + 2I_{VH}G)};\ G = \frac{I_{HV}}{I_{HH}}$$

where I_{VV} and I_{VH} are the emission intensities when the excitation polarizer is vertically oriented and the emission polarizer is oriented vertically and horizontally respectively. *G* is the correction factor. The terms I_{HV} and I_{HH} are the emission intensities when the excitation polarization is horizontally oriented and the emission polarization is oriented vertically and horizontally, respectively.

3.9.4.3. Circular Dichroism (CD) Study

CD spectra were recorded with JASCO CD J-810 spectropolarimeter. The data were collected as an average of 5 scans with a scan speed of 100 nm/min using a quartz cell with 1mm path length within the wavelength regime of 190–260 nm at 298 k. The spectral data were analyzed with the spectra manager software.

3.9.5. Molecular Docking

The docking study was performed using AutoDock 4.2 program.[117, 122] At first, we optimized the ligands (**2.45G** and **1.262**) at B3Lyp/6-31G* level of theory using the G09 program package.[123] To test the accuracy of the docking results, the docking process was repeated three times. The AutoDock tools (ADT) were utilized for charges and addition of polar hydrogens as well as for setting the other parameters. AutoGrid 4.0 and AutoDock 4.0 were used to produce grid maps. A grid box to a size of 126 × 126 × 126 with 0.378 Å spacing was generated. The centre grid box for x-, y- and z centres were 37.396, 34.903; 30.567, 24.015; and 98.389, 98.782 with offsets 13.582, 19.528; 6.753, 10.515; and 74.575, 82.282 for the probes **2.45G** and **1.262** respectively. In the prescriptive grid box, we calculated the complex conformation with a flexible molecular docking method. The Lamarckian genetic algorithm (LGA) [122] was chosen to carry out a flexible molecular docking of the probes to the BSA and to calculate the complex conformation. The other items used were in the default settings. Further, intermolecular-hydrophobic, polar and hydrogen bond interactions were analyzed using PyMOL.[124, 125]

3.9.6. TDDFT Calculations

The ground state structure of the tetrazolylpyrene nucleoside, **1.262** was optimized using density functional theory (DFT) [96] with B3LYP functional and 6-31G (d) basis set. The excited state related calculations were carried out with the time-dependent density functional theory (TD-DFT) with the optimized structure of the ground state (B3LYP/6-31G(d)). There are no imaginary frequencies in frequency analysis of the calculated structure, therefore the calculated structure is a local energy minimum.

3.9.7. B3LYP/6-31G* Optimized Structure and Cartesian Coordinates of the Tetrazolylpyrene Nucleoside 1.262

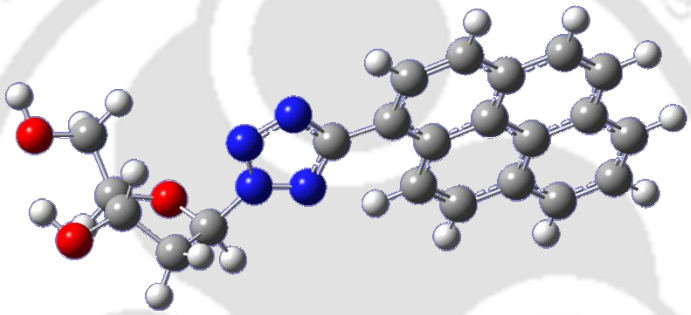

E(RB3LYP) = -1293.83516597 a.u.

Standard orientation:

Center Number	Atomic Number	Atomic Type	Coordinates (Angstroms) X	Y	Z
1	7	0	0.935739	0.275636	-0.199543
2	6	0	0.234438	1.431591	-0.081612
3	6	0	-1.095945	1.533885	0.003262
4	7	0	2.246400	0.543185	-0.258720
5	7	0	2.331583	1.864384	-0.175944
6	7	0	1.083733	2.431892	-0.064899
7	6	0	5.640430	-0.077645	-0.938150
8	6	0	4.243995	-0.032169	-1.544310
9	6	0	3.326817	-0.397338	-0.384637
10	8	0	4.135709	-0.408276	0.777920
11	6	0	5.437466	-0.769838	0.403115
12	1	0	4.011821	0.987296	-1.925915
13	8	0	6.512538	-0.814635	-1.751810
14	1	0	4.131206	-0.719234	-2.412641
15	1	0	6.095550	0.932779	-0.834452
16	1	0	2.878951	-1.402608	-0.550638

17	6	0	6.451777	-0.275135	1.425850
18	1	0	5.574853	-1.872562	0.341317
19	8	0	7.186836	-1.362192	1.919481
20	6	0	-1.885118	0.374768	-0.027441
21	6	0	-3.291614	0.492000	0.062793
22	6	0	-3.888807	1.768355	0.182578
23	6	0	-3.072443	2.908667	0.210537
24	6	0	-1.685737	2.792048	0.121466
25	6	0	-4.102721	-0.669456	0.033198
26	6	0	-5.509141	-0.552139	0.123515
27	6	0	-6.083838	0.720471	0.241699
28	6	0	-5.284063	1.866026	0.270828
29	6	0	-1.310497	-0.897927	-0.145708
30	6	0	-2.110290	-2.043387	-0.175039
31	6	0	-3.505528	-1.945811	-0.086588
32	6	0	-4.321852	-3.086084	-0.114382
33	6	0	-5.708559	-2.969464	-0.025312
34	6	0	-6.298426	-1.711387	0.092810
35	1	0	7.412825	-0.925371	-1.497986
36	1	0	7.143090	0.449986	0.941150
37	1	0	5.918400	0.223869	2.265669
38	1	0	7.858679	-1.222260	2.564868
39	1	0	-3.530451	3.904408	0.303697
40	1	0	-1.056136	3.693779	0.144446
41	1	0	-7.177157	0.818886	0.312302
42	1	0	-5.755106	2.855728	0.364169
43	1	0	-0.217141	-0.996296	-0.216392
44	1	0	-1.639339	-3.033086	-0.268420
45	1	0	-3.863826	-4.081920	-0.207341
46	1	0	-6.338196	-3.871242	-0.048210
47	1	0	-7.392928	-1.627199	0.162558

3.10. References

1. Becker, W.; Bhattiprolu, K. C.; Gubensäk, N.; Zangger, K., Investigating Protein–Ligand Interactions by Solution Nuclear Magnetic Resonance Spectroscopy. *ChemPhysChem* **2018,** *19* (8), 895-906.
2. Du, X.; Li, Y.; Xia, Y.-L.; Ai, S.-M.; Liang, J.; Sang, P.; Ji, X.-L.; Liu, S.-Q., Insights into Protein–Ligand Interactions: Mechanisms, Models, and Methods. *International Journal of Molecular Sciences* **2016,** *17* (2).
3. Held, M.; Metzner, P.; Prinz, J.-H.; Noé, F., Mechanisms of Protein-Ligand Association and Its Modulation by Protein Mutations. *Biophysical Journal* **2011,** *100* (3), 701-710.
4. Williams, M. A., Protein–Ligand Interactions: Fundamentals. In *Protein-Ligand Interactions: Methods and Applications*, Williams, M. A.; Daviter, T., Eds. Humana Press: Totowa, NJ, 2013; pp 3-34.
5. Janin, J., Protein-protein recognition. *Progress in Biophysics and Molecular Biology* **1995,** *64* (2), 145-166.

6. Koshland, D. E., Application of a Theory of Enzyme Specificity to Protein Synthesis. *Proceedings of the National Academy of Sciences* **1958,** *44* (2), 98.
7. Fischer, E., Einfluss der Configuration auf die Wirkung der Enzyme. *Berichte der Deutschen Chemischen Gesellschaft* **1894,** *27* (3), 2985-2993.
8. Koshland, D. E., Application of a Theory of Enzyme Specificity to Protein Synthesis. *Proceedings of the National Academy of Sciences of the United States of America* **1958,** *44* (2), 98-104.
9. Csermely, P.; Palotai, R.; Nussinov, R., Induced fit, conformational selection and independent dynamic segments: an extended view of binding events. *Trends in Biochemical Sciences* **2010,** *35* (10), 539-546.
10. Ma, B.; Kumar, S.; Tsai, C.-J.; Nussinov, R., Folding funnels and binding mechanisms. *Protein Engineering, Design and Selection* **1999,** *12* (9), 713-720.
11. Tobi, D.; Bahar, I., Structural changes involved in protein binding correlate with intrinsic motions of proteins in the unbound state. *Proceedings of the National Academy of Sciences of the United States of America* **2005,** *102* (52), 18908-18913.
12. Tsai, C.-J.; Kumar, S.; Ma, B.; Nussinov, R., Folding funnels, binding funnels, and protein function. *Protein Science* **1999,** *8* (6), 1181-1190.
13. Bu, Z.; Callaway, D. J. E., Chapter 5 - Proteins MOVE! Protein dynamics and long-range allostery in cell signaling. In *Advances in Protein Chemistry and Structural Biology*, Donev, R., Ed. Academic Press: 2011; Vol. 83, pp 163-221.
14. Fraser, J. S.; Clarkson, M. W.; Degnan, S. C.; Erion, R.; Kern, D.; Alber, T., Hidden alternative structures of proline isomerase essential for catalysis. *Nature* **2009,** *462* (7273), 669-673.
15. Fraser, J. S.; van den Bedem, H.; Samelson, A. J.; Lang, P. T.; Holton, J. M.; Echols, N.; Alber, T., Accessing protein conformational ensembles using room-temperature X-ray crystallography. *Proceedings of the National Academy of Sciences* **2011,** *108* (39), 16247.
16. Boehr, D. D.; Nussinov, R.; Wright, P. E., The role of dynamic conformational ensembles in biomolecular recognition. *Nature Chemical Biology* **2009,** *5*, 789-796.
17. Changeux, J.-P.; Edelstein, S., Conformational selection or induced fit? 50 years of debate resolved. *F1000 Biology Reports* **2011,** *3*, 19-19.
18. Nussinov, R.; Ma, B.; Tsai, C.-J., Multiple conformational selection and induced fit events take place in allosteric propagation. *Biophysical Chemistry* **2014,** *186*, 22-30.
19. Bai, H.; Qian, J.; Tian, H.; Pan, W.; Zhang, L.; Zhang, W., Fluorescent polarity probes for identifying bovine serum albumin: Amplification effect of para-substituted benzene. *Dyes and Pigments* **2014,** *103*, 1-8.
20. Mirapurkar, S.; Nagvekar, U. H.; Sivaprasad, N., Polyreactivity of Monoclonal Antibodies Produced Against Thyroid Stimulating Hormone (hTSH). *Journal of Immunoassay and Immunochemistry* **2007,** *28* (2), 119-126.
21. Rezende, J. d. P.; Ferreira, G. M. D.; Ferreira, G. M. D.; da Silva, L. H. M.; do Carmo Hepanhol da Silva, M.; Pinto, M. S.; Pires, A. C. d. S., Polydiacetylene/triblock copolymer nanosensor for the detection of native and free bovine serum albumin. *Materials Science and Engineering: C* **2017,** *70*, 535-543.
22. Barnett, J. P.; Blindauer, C. A.; Kassaar, O.; Khazaipoul, S.; Martin, E. M.; Sadler, P. J.; Stewart, A. J., Allosteric modulation of zinc speciation by fatty acids. *Biochimica et Biophysica Acta (BBA) - General Subjects* **2013,** *1830* (12), 5456-5464.
23. Bartalena, L.; Robbins, J., Thyroid Hormone Transport Proteins. *Clinics in Laboratory Medicine* **1993,** *13* (3), 583-598.

24. Malarkani, K.; Sarkar, I.; Selvam, S., Denaturation studies on bovine serum albumin–bile salt system: Bile salt stabilizes bovine serum albumin through hydrophobicity. *Journal of Pharmaceutical Analysis* **2018,** *8* (1), 27-36.
25. Trauner, M.; Boyer, J. L., Bile Salt Transporters: Molecular Characterization, Function, and Regulation. *Physiological Reviews* **2003,** *83* (2), 633-671.
26. van der Vusse, G. J., Albumin as Fatty Acid Transporter. *Drug Metabolism and Pharmacokinetics* **2009,** *24* (4), 300-307.
27. Zucker, S. D.; Goessling, W., Mechanism of hepatocellular uptake of albumin-bound bilirubin11Preliminary reports of this work have been published in abstract form (W. Goessling, S.D. Zucker, Hepatology 26 (1997) 385A). *Biochimica et Biophysica Acta (BBA) - Biomembranes* **2000,** *1463* (2), 197-208.
28. Mandeville, J. S.; Tajmir-Riahi, H. A., Complexes of Dendrimers with Bovine Serum Albumin. *Biomacromolecules* **2010,** *11* (2), 465-472.
29. Jisha, V. S.; Arun, K. T.; Hariharan, M.; Ramaiah, D., Site-Selective Interactions: Squaraine Dye−Serum Albumin Complexes with Enhanced Fluorescence and Triplet Yields. *The Journal of Physical Chemistry B* **2010,** *114* (17), 5912-5919.
30. Larsen, M. T.; Kuhlmann, M.; Hvam, M. L.; Howard, K. A., Albumin-based drug delivery: harnessing nature to cure disease. *Molecular and Cellular Therapies* **2016,** *4* (1), 3.
31. Jana, S.; Ghosh, S.; Dalapati, S.; Guchhait, N., Exploring structural change of protein bovine serum albumin by external perturbation using extrinsic fluorescence probe: spectroscopic measurement, molecular docking and molecular dynamics simulation. *Photochemical & Photobiological Sciences* **2012,** *11* (2), 323-332.
32. Sardar, P. S.; Samanta, S.; Maity, S. S.; Dasgupta, S.; Ghosh, S., Energy transfer photophysics from serum albumins to sequestered 3-hydroxy-2-naphthoic acid, an excited state intramolecular proton-transfer probe. *The Journal of Physical Chemistry B* **2008,** *112* (11), 3451-3461.
33. Jiménez, M. C.; Miranda, M. A.; Vayá, I., Triplet Excited States as Chiral Reporters for the Binding of Drugs to Transport Proteins. *Journal of the American Chemical Society* **2005,** *127* (29), 10134-10135.
34. Lhiaubet-Vallet, V.; Sarabia, Z.; Boscá, F.; Miranda, M. A., Human Serum Albumin-Mediated Stereodifferentiation in the Triplet State Behavior of (S)- and (R)-Carprofen. *Journal of the American Chemical Society* **2004,** *126* (31), 9538-9539.
35. Lee, C. Y.; Kim, H. Y.; Kim, S.; Park, K. S.; Park, H. G., A simple and sensitive detection of small molecule–protein interactions based on terminal protection-mediated exponential strand displacement amplification. *Analyst* **2018,** *143* (9), 2023-2028.
36. Lee, M. M.; Peterson, B. R., Quantification of Small Molecule–Protein Interactions using FRET between Tryptophan and the Pacific Blue Fluorophore. *ACS Omega* **2016,** *1* (6), 1266-1276.
37. Li, S.; Li, Y.; Yu, H.; Wu, Z.; Jiang, J.; Yu, R.; Wang, Y., Fluorescence amplification detection via terminal protection of small molecule–protein interactions. *RSC Advances* **2015,** *5* (129), 107179-107184.
38. Liu, X.-Y.; Shi, L.; Ding, Z.; Long, Y.-T., New insight into the application of GFP chromophore inspired derivatives: a F− fluorescent chemodosimeter. *RSC Advances* **2014,** *4* (96), 53557-53560.
39. Sonu, V. K.; Islam, M. M.; Gurung, A. B.; Bhattacharjee, A.; Mitra, S., Serum albumin interaction with xanthine drugs at nano-bio interfaces: A combined multi-spectroscopic and molecular modelling approach. *Journal of Molecular Liquids* **2017,** *242*, 919-927.

40. Svendsen, A.; Kiefer, H. V.; Pedersen, H. B.; Bochenkova, A. V.; Andersen, L. H., Origin of the Intrinsic Fluorescence of the Green Fluorescent Protein. *Journal of the American Chemical Society* **2017,** *139* (25), 8766-8771.
41. Li, W.; Chen, D.; Wang, H.; Luo, S.; Dong, L.; Zhang, Y.; Shi, J.; Tong, B.; Dong, Y., Quantitation of Albumin in Serum Using "Turn-on" Fluorescent Probe with Aggregation-Enhanced Emission Characteristics. *ACS Applied Materials & Interfaces* **2015,** *7* (47), 26094-26100.
42. Manikandan, I.; Chang, C.-H.; Chen, C.-L.; Sathish, V.; Li, W.-S.; Malathi, M., Aggregation induced emission enhancement (AIEE) characteristics of quinoline based compound — A versatile fluorescent probe for pH, Fe(III) ion, BSA binding and optical cell imaging. *Spectrochimica Acta Part A: Molecular and Biomolecular Spectroscopy* **2017,** *182*, 58-66.
43. Liu, C.; Yang, W.; Gao, Q.; Du, J.; Luo, H.; Liu, Y.; Yang, C., Differential recognition and quantification of HSA and BSA based on two red-NIR fluorescent probes. *Journal of Luminescence* **2018,** *197*, 193-199.
44. Wang, L.; Yang, L.; Cao, D., Probes based on diketopyrrolopyrrole and anthracenone conjugates with aggregation-induced emission characteristics for pH and BSA sensing. *Sensors and Actuators B: Chemical* **2015,** *221*, 155-166.
45. Wang, L.; Yang, L.; Zhu, L.; Cao, D.; Li, L., Synthesis, characterization and fluorescence "turn-on" detection of BSA based on the cationic poly(diketopyrrolopyrrole-co-ethynylfluorene) through deaggregating process. *Sensors and Actuators B: Chemical* **2016,** *231*, 733-743.
46. Densil, S.; Chang, C.-H.; Chen, C.-L.; Mathavan, A.; Ramdass, A.; Sathish, V.; Thanasekaran, P.; Li, W.-S.; Rajagopal, S., Aggregation-induced emission enhancement of anthracene-derived Schiff base compounds and their application as a sensor for bovine serum albumin and optical cell imaging. *Luminescence* **2018,** *33* (4), 780-789.
47. Sasmal, M.; Bhowmick, R.; Musha Islam, A. S.; Bhuiya, S.; Das, S.; Ali, M., Domain-Specific Association of a Phenanthrene–Pyrene-Based Synthetic Fluorescent Probe with Bovine Serum Albumin: Spectroscopic and Molecular Docking Analysis. *ACS Omega* **2018,** *3* (6), 6293-6304.
48. Singh, P.; Mittal, L. S.; Kaur, S.; Kaur, S.; Bhargava, G.; Kumar, S., Self-assembled small molecule based fluorescent detection of serum albumin proteins: Clinical detection and cell imaging. *Sensors and Actuators B: Chemical* **2018,** *255*, 478-489.
49. Dorh, N.; Zhu, S.; Dhungana, K. B.; Pati, R.; Luo, F.-T.; Liu, H.; Tiwari, A., BODIPY-Based Fluorescent Probes for Sensing Protein Surface-Hydrophobicity. *Scientific Reports* **2015,** *5*, 18337.
50. Hawe, A.; Sutter, M.; Jiskoot, W., Extrinsic Fluorescent Dyes as Tools for Protein Characterization. *Pharmaceutical Research* **2008,** *25* (7), 1487-1499.
51. Lindhoud, S.; Westphal, A. H.; Visser, A. J. W. G.; Borst, J. W.; van Mierlo, C. P. M., Fluorescence of Alexa fluor dye tracks protein folding. *PLoS One* **2012,** *7* (10), e46838.
52. Oshinbolu, S.; Shah, R.; Finka, G.; Molloy, M.; Uden, M.; Bracewell, D. G., Evaluation of fluorescent dyes to measure protein aggregation within mammalian cell culture supernatants. *Journal of Chemical Technology & Biotechnology* **2018,** *93* (3), 909-917.
53. Ryzhova, O.; Vus, K.; Trusova, V.; Kirilova, E.; Kirilov, G.; Gorbenko, G.; Kinnunen, P., Novel benzanthrone probes for membrane and protein studies. *Methods and Applications in Fluorescence* **2016,** *4* (3), 034007.
54. Taylor, C. G.; Meisl, G.; Horrocks, M. H.; Zetterberg, H.; Knowles, T. P. J.; Klenerman, D., Extrinsic Amyloid-Binding Dyes for Detection of Individual Protein Aggregates in Solution. *Analytical Chemistry* **2018,** *90* (17), 10385-10393.

55. Yu, Y.; Huang, Y.; Hu, F.; Jin, Y.; Zhang, G.; Zhang, D.; Zhao, R., Self-Assembled Nanostructures Based on Activatable Red Fluorescent Dye for Site-Specific Protein Probing and Conformational Transition Detection. *Analytical Chemistry* **2016,** *88* (12), 6374-6381.
56. Jurek, K.; Kabatc, J.; Kostrzewska, K., Fluorescent amino-substituted squaraine probes for bovine serum albumin. *Coloration Technology* **2017,** *133* (2), 170-177.
57. Martins, T. D.; Pacheco, M. L.; Boto, R. E.; Almeida, P.; Farinha, J. P. S.; Reis, L. V., Synthesis, characterization and protein-association of dicyanomethylene squaraine dyes. *Dyes and Pigments* **2017,** *147*, 120-129.
58. Bayraktutan, T.; Onganer, Y., Spectral-luminescent study of coumarin 35 as fluorescent "light-up" probe for BSA and DNA monitoring. *Dyes and Pigments* **2017,** *142*, 62-68.
59. Bayraktutan, T.; Onganer, Y., Biophysical influence of coumarin 35 on bovine serum albumin: Spectroscopic study. *Spectrochimica Acta Part A: Molecular and Biomolecular Spectroscopy* **2017,** *171*, 90-96.
60. Li, Q.; Wang, C.; Qian, Y., BODIPY-Triphenylamine with conjugated pyridines and a quaternary pyridium salt: Synthesis, aggregation-induced red emission and interaction with bovine serum albumin. *Journal of Photochemistry and Photobiology A: Chemistry* **2017,** *346*, 311-317.
61. Vodyanova, O. S.; Kochergin, B. A.; Usoltsev, S. D.; Marfin, Y. S.; Rumyantsev, E. V.; Aleksakhina, E. L.; Tomilova, I. K., BODIPY dyes in bio environment: Spectral characteristics and possibilities for practical application. *Journal of Photochemistry and Photobiology A: Chemistry* **2018,** *350*, 44-51.
62. Bag, S. S.; Jana, S.; Pradhan, M. K., Synthesis, photophysical properties of triazolyl-donor/acceptor chromophores decorated unnatural amino acids: Incorporation of a pair into Leu-enkephalin peptide and application of triazolylperylene amino acid in sensing BSA. *Bioorganic & Medicinal Chemistry* **2016,** *24* (16), 3579-3595.
63. Bag, S. S.; Talukdar, S.; Das, S. K.; Pradhan, M. K.; Mukherjee, S., Donor/acceptor chromophores-decorated triazolyl unnatural nucleosides: synthesis, photophysical properties and study of interaction with BSA. *Organic & Biomolecular Chemistry* **2016,** *14* (22), 5088-5108.
64. Tan, S.; Nagai, K., Protein–nucleic interactions: 'I have a cunning plan…'. *Current Opinion in Structural Biology* **2013,** *23* (1), 90-92.
65. Delong, R. K.; Zhou, Q., Experiment 7 - Investigating Protein: Nucleic Acid Interactions by Electrophoretic Mobility Shift Assay (EMSA). In *Introductory Experiments on Biomolecules and their Interactions*, Delong, R. K.; Zhou, Q., Eds. Academic Press: Boston, **2015**, 67-72.
66. Correll, C. C.; Rice, P. A., Chapter 1 Introduction. In *Protein-Nucleic Acid Interactions: Structural Biology*, The Royal Society of Chemistry: **2008**; pp 1-12.
67. Garvie, C. W.; Wolberger, C., Recognition of Specific DNA Sequences. *Molecular Cell* **2001,** *8* (5), 937-946.
68. Luscombe, N. M.; Austin, S. E.; Berman, H. M.; Thornton, J. M., An overview of the structures of protein-DNA complexes. *Genome Biology* **2000,** *1* (1), reviews001.1.
69. Rohs, R.; Jin, X.; West, S. M.; Joshi, R.; Honig, B.; Mann, R. S., Origins of Specificity in Protein-DNA Recognition. *Annual Review of Biochemistry* **2010,** *79* (1), 233-269.
70. Eyer, L.; Nencka, R.; de Clercq, E.; Seley-Radtke, K.; Růžek, D., Nucleoside analogs as a rich source of antiviral agents active against arthropod-borne flaviviruses. *Antiviral Chemistry and Chemotherapy* **2018,** *26*, 1-28.
71. Jordheim, L. P.; Durantel, D.; Zoulim, F.; Dumontet, C., Advances in the development of nucleoside and nucleotide analogues for cancer and viral diseases. *Nature Reviews Drug Discovery* **2013,** *12*, 447.

72. Pastor-Anglada, M.; Pérez-Torras, S., Nucleoside transporter proteins as biomarkers of drug responsiveness and drug targets. *Frontiers in Pharmacology* **2015,** *6*, 13.
73. Johnson, Z. L.; Lee, J.-H.; Lee, K.; Lee, M.; Kwon, D.-Y.; Hong, J.; Lee, S.-Y., Structural basis of nucleoside and nucleoside drug selectivity by concentrative nucleoside transporters. *eLife* **2014,** *3*, e03604.
74. Pastor-Anglada, M.; Pérez-Torras, S., Who Is Who in Adenosine Transport. *Frontiers in Pharmacology* **2018,** *9*, 627.
75. Bhutia, Y. D.; Hung, S. W.; Patel, B.; Lovin, D.; Govindarajan, R., CNT1 Expression Influences Proliferation and Chemosensitivity in Drug-Resistant Pancreatic Cancer Cells. *Cancer Research* **2011**.
76. Doehring, A.; Hofmann, W. P.; Schlecker, C.; Zeuzem, S.; Sarrazin, C.; Berg, T.; Müller, T.; Herrmann, E.; Geisslinger, G.; Lötsch, J., Role of nucleoside transporters SLC28A2/3 and SLC29A1/2 genetics in ribavirin therapy: protection against anemia in patients with chronic hepatitis C. *Pharmacogenet Genomics* **2011,** *21* (5), 289-296.
77. Farré, X.; Guillén-Gómez, E.; Sánchez, L.; Hardisson, D.; Plaza, Y.; Lloberas, J.; Casado, F. J.; Palacios, J.; Pastor-Anglada, M., Expression of the nucleoside-derived drug transporters hCNT1, hENT1 and hENT2 in gynecologic tumors. *International Journal of Cancer* **2004,** *112* (6), 959-966.
78. Maréchal, R.; Mackey, J. R.; Lai, R.; Demetter, P.; Peeters, M.; Polus, M.; Cass, C. E.; Young, J.; Salmon, I.; Devière, J.; Van Laethem, J.-L., Human Equilibrative Nucleoside Transporter 1 and Human Concentrative Nucleoside Transporter 3 Predict Survival after Adjuvant Gemcitabine Therapy in Resected Pancreatic Adenocarcinoma. *Clinical Cancer Research* **2009,** *15* (8), 2913.
79. Rabascio, C.; Laszlo, D.; Andreola, G.; Saronni, L.; Radice, D.; Rigacci, L.; Fabbri, A.; Frigeri, F.; Calabrese, L.; Billio, A.; Bertolini, F.; Martinelli, G., Expression of the human concentrative nucleotide transporter 1 (hCNT1) gene correlates with clinical response in patients affected by Waldenström's Macroglobulinemia (WM) and small lymphocytic lymphoma (SLL) undergoing a combination treatment with 2-chloro-2′-deoxyadenosine (2-CdA) and Rituximab. *Leukemia Research* **2010,** *34* (4), 454-457.
80. Rau, M.; Stickel, F.; Russmann, S.; Manser, C. N.; Becker, P. P.; Weisskopf, M.; Schmitt, J.; Dill, M. T.; Dufour, J.-F.; Moradpour, D.; Semela, D.; Müllhaupt, B.; Geier, A., Impact of genetic SLC28 transporter and ITPA variants on ribavirin serum level, hemoglobin drop and therapeutic response in patients with HCV infection. *Journal of Hepatology* **2013,** *58* (4), 669-675.
81. Guallar, V.; Borrelli, K. W., A binding mechanism in protein–nucleotide interactions: Implication for U1A RNA binding. *Proceedings of the National Academy of Sciences of the United States of America* **2005,** *102* (11), 3954.
82. Williamson, J. R., Induced fit in RNA–protein recognition. *Nature Structural Biology* **2000,** *7*, 834.
83. Usha, S.; Selvaraj, S., Structure-wise discrimination of cytosine, thymine, and uracil by proteins in terms of their nonbonded interactions. *Journal of Biomolecular Structure and Dynamics* **2014,** *32* (10), 1686-1704.
84. Usha, S.; Selvaraj, S., Structure-wise discrimination of adenine and guanine by proteins on the basis of their nonbonded interactions. *Journal of Biomolecular Structure and Dynamics* **2015,** *33* (7), 1474-1492.
85. Jones, S.; Daley, D. T.; Luscombe, N. M.; Berman, H. M.; Thornton, J. M., Protein-RNA interactions: a structural analysis. *Nucleic Acids Research* **2001,** *29* (4), 943-954.
86. Nobeli, I.; Laskowski, R. A.; Valdar, W. S.; Thornton, J. M., On the molecular discrimination between adenine and guanine by proteins. *Nucleic Acids Research* **2001,** *29* (21), 4294-4309.

87. Johnson, Z. L.; Cheong, C.-G.; Lee, S.-Y., Crystal structure of a concentrative nucleoside transporter from Vibrio cholerae at 2.4 Å. *Nature* **2012,** *483*, 489.
88. Beljaars, L.; Molema, G.; Schuppan, D.; Geerts, A.; De Bleser, P. J.; Weert, B.; Meijer, D. K.; Poelstra, K., Successful targeting to rat hepatic stellate cells using albumin modified with cyclic peptides that recognize the collagen type VI receptor. *The Journal of Biological Chemistry* **2000,** *275* (17), 12743-12751.
89. Kragh-Hansen, U., Molecular aspects of ligand binding to serum albumin. *Pharmacological Reviews* **1981,** *33* (1), 17-53.
90. Kurtzhals, P.; Havelund, S.; Jonassen, I.; Kiehr, B.; Larsen, U. D.; Ribel, U.; Markussen, J., Albumin binding of insulins acylated with fatty acids: characterization of the ligand-protein interaction and correlation between binding affinity and timing of the insulin effect in vivo. *Biochemical journal* **1995,** *312 (Pt 3)* (Pt 3), 725-731.
91. Sheffield, W. P., Modification of clearance of therapeutic and potentially therapeutic proteins. *Current Drug Targets - Cardiovascular & Hematological Disorders* **2001,** *1* (1), 1-22.
92. Abou-Zied, O. K.; Al-Shihi, O. I. K., Characterization of Subdomain IIA Binding Site of Human Serum Albumin in its Native, Unfolded, and Refolded States Using Small Molecular Probes. *Journal of the American Chemical Society* **2008,** *130* (32), 10793-10801.
93. Cohen, B. E.; McAnaney, T. B.; Park, E. S.; Jan, Y. N.; Boxer, S. G.; Jan, L. Y., Probing Protein Electrostatics with a Synthetic Fluorescent Amino Acid. *Science* **2002,** *296* (5573), 1700.
94. Er, J. C.; Vendrell, M.; Tang, M. K.; Zhai, D.; Chang, Y.-T., Fluorescent Dye Cocktail for Multiplex Drug-Site Mapping on Human Serum Albumin. *ACS Combinatorial Science* **2013,** *15* (9), 452-457.
95. Royer, C. A., Probing Protein Folding and Conformational Transitions with Fluorescence. *Chemical Reviews* **2006,** *106* (5), 1769-1784.
96. M. J. Frisch, G. W. T., H. B. Schlegel, G. E. Scuseria, M. A. Robb, J. R. Cheeseman, G. Scalmani, V. Barone, B. Mennucci, G. A. Petersson, H. Nakatsuji, M. Caricato, X. Li, H. P. Hratchian, A. F. Izmaylov, J. Bloino, G. Zheng, J. L. Sonnenberg, M. Hada, M. Ehara, K. Toyota, R. Fukuda, J. Hasegawa, M. Ishida, T. Nakajima, Y. Honda, O. Kitao, H. Nakai, T. Vreven, J. A. Montgomery, Jr., J. E. Peralta, F. Ogliaro, M. Bearpark, J. J. Heyd, E. Brothers, K. N. Kudin, V. N. Staroverov, R. Kobayashi, J. Normand, K. Raghavachari, A. Rendell, J. C. Burant, S. S. Iyengar, J. Tomasi, M. Cossi, N. Rega, J. M. Millam, M. Klene, J. E. Knox, J. B. Cross, V. Bakken, C. Adamo, J. Jaramillo, R. Gomperts, R. E. Stratmann, O. Yazyev, A. J. Austin, R. Cammi, C. Pomelli, J. W. Ochterski, R. L. Martin, K. Morokuma, V. G. Zakrzewski, G. A. Voth, P. Salvador, J. J. Dannenberg, S. Dapprich, A. D. Daniels, Ö. Farkas, J. B. Foresman, J. V. Ortiz, J. Cioslowski, and D. J. Fox, Gaussian 09. *Gaussian, Inc., Wallingford CT* **2009**.
97. Bag, S. S.; Kundu, R., Installation/Modulation of the Emission Response via Click Reaction. *The Journal of Organic Chemistry* **2011,** *76* (9), 3348-3356.
98. Bucevicius, J.; Skardziute, L.; Dodonova, J.; Kazlauskas, K.; Bagdziunas, G.; Jursenas, S.; Tumkevicius, S., 2,4-Bis(4-aryl-1,2,3-triazol-1-yl)pyrrolo[2,3-d]pyrimidines: synthesis and tuning of optical properties by polar substituents. *RSC Advances* **2015,** *5* (48), 38610-38622.
99. Fromherz, P., Monopole-Dipole Model for Symmetrical Solvatochromism of Hemicyanine Dyes. *The Journal of Physical Chemistry* **1995,** *99* (18), 7188-7192.
100. Nagarajan, N.; Velmurugan, G.; Venuvanalingam, P.; Renganathan, R., Tunable single and dual emission behavior of imidazole fluorophores based on D-π-A architecture. *Journal of Photochemistry and Photobiology A: Chemistry* **2014,** *284*, 36-48.

101. Nakamura, A.; Tsukiji, S., Ratiometric fluorescence imaging of nuclear pH in living cells using Hoechst-tagged fluorescein. *Bioorganic & Medicinal Chemistry Letters* **2017,** *27* (14), 3127-3130.
102. Demchenko, A. P., The Concept of λ-Ratiometry in Fluorescence Sensing and Imaging. *Journal of Fluorescence* **2010,** *20* (5), 1099-1128.
103. Doussineau, T.; Schulz, A.; Lapresta-Fernandez, A.; Moro, A.; Körsten, S.; Trupp, S.; Mohr, G. J., On the Design of Fluorescent Ratiometric Nanosensors. *Chemistry – A European Journal* **2010,** *16* (34), 10290-10299.
104. Fan, J.; Hu, M.; Zhan, P.; Peng, X., Energy transfer cassettes based on organic fluorophores: construction and applications in ratiometric sensing. *Chemical Society Reviews* **2013,** *42* (1), 29-43.
105. Feng, Y.; Cheng, J.; Zhou, L.; Zhou, X.; Xiang, H., Ratiometric optical oxygen sensing: a review in respect of material design. *Analyst* **2012,** *137* (21), 4885-4901.
106. Lee, M. H.; Kim, J. S.; Sessler, J. L., Small molecule-based ratiometric fluorescence probes for cations, anions, and biomolecules. *Chemical Society Reviews* **2015,** *44* (13), 4185-4191.
107. Deniz, A. A.; Laurence, T. A.; Dahan, M.; Chemla, D. S.; Schultz, P. G.; Weiss, S., RATIOMETRIC SINGLE-MOLECULE STUDIES OF FREELY DIFFUSING BIOMOLECULES. *Annual Review of Physical Chemistry* **2001,** *52* (1), 233-253.
108. Wu, C.; Zheng, J.; Huang, C.; Lai, J.; Li, S.; Chen, C.; Zhao, Y., Hybrid Silica–Nanocrystal–Organic Dye Superstructures as Post-Encoding Fluorescent Probes. *Angewandte Chemie International Edition* **2007,** *46* (28), 5393-5396.
109. Wu, P.; Hou, X.; Xu, J.-J.; Chen, H.-Y., Ratiometric fluorescence, electrochemiluminescence, and photoelectrochemical chemo/biosensing based on semiconductor quantum dots. *Nanoscale* **2016,** *8* (16), 8427-8442.
110. Yengo, C. M.; Berger, C. L., Fluorescence anisotropy and resonance energy transfer: powerful tools for measuring real time protein dynamics in a physiological environment. *Current Opinion in Pharmacology* **2010,** *10* (6), 731-737.
111. Bhattacharya, B.; Nakka, S.; Guruprasad, L.; Samanta, A., Interaction of Bovine Serum Albumin with Dipolar Molecules: Fluorescence and Molecular Docking Studies. *The Journal of Physical Chemistry B* **2009,** *113* (7), 2143-2150.
112. Hazra, P.; Chakrabarty, D.; Chakraborty, A.; Sarkar, N., Probing protein-surfactant interaction by steady state and time-resolved fluorescence spectroscopy. *Biochemical and Biophysical Research Communications* **2004,** *314* (2), 543-549.
113. Maity, S. S.; Samanta, S.; Sardar, P. S.; Pal, A.; Dasgupta, S.; Ghosh, S., Fluorescence, anisotropy and docking studies of proteins through excited state intramolecular proton transfer probe molecules. *Chemical Physics* **2008,** *354* (1), 162-173.
114. Paul, B. K.; Guchhait, N., Modulation of Prototropic Activity and Rotational Relaxation Dynamics of a Cationic Biological Photosensitizer within the Motionally Constrained Bio-environment of a Protein. *The Journal of Physical Chemistry B* **2011,** *115* (34), 10322-10334.
115. Aggarwal, B. B.; Kumar, A.; Bharti, A. C., Anticancer potential of curcumin: preclinical and clinical studies. *Anticancer Research* **2003,** *23* (1a), 363-398.
116. Chauhan, D. P., Chemotherapeutic potential of curcumin for colorectal cancer. *Current Pharmaceutical Design* **2002,** *8* (19), 1695-1706.
117. Jana, S.; Dalapati, S.; Ghosh, S.; Guchhait, N., Binding interaction between plasma protein bovine serum albumin and flexible charge transfer fluorophore: A spectroscopic study in combination with molecular docking and molecular dynamics simulation. *Journal of Photochemistry and Photobiology A: Chemistry* **2012,** *231* (1), 19-27.

118. Ojha, B.; Das, G., Artificial amphiphilic scaffolds for the selective sensing of protein based on hydrophobicity. *Chemical Communications* **2010,** *46* (12), 2079-2081.
119. Sahoo, B. K.; Ghosh, K. S.; Dasgupta, S., Investigating the binding of curcumin derivatives to bovine serum albumin. *Biophysical Chemistry* **2008,** *132* (2-3), 81-88.
120. Tong, H.; Hong, Y.; Dong, Y.; Häußler, M.; Lam, J. W. Y.; Li, Z.; Guo, Z.; Guo, Z.; Tang, B. Z., Fluorescent "light-up" bioprobes based on tetraphenylethylene derivatives with aggregation-induced emission characteristics. *Chemical Communications* **2006,** (35), 3705-3707.
121. Bikadi, Z.; Hazai, E., Application of the PM6 semi-empirical method to modeling proteins enhances docking accuracy of AutoDock. *Journal of Cheminformatics* **2009,** *1* (1), 15.
122. Morris, G. M.; Huey, R.; Lindstrom, W.; Sanner, M. F.; Belew, R. K.; Goodsell, D. S.; Olson, A. J., AutoDock4 and AutoDockTools4: Automated docking with selective receptor flexibility. *Journal of Computational Chemistry* **2009,** *30* (16), 2785-2791.
123. Lambert, C.; Leonard, N.; De Bolle, X.; Depiereux, E., ESyPred3D: Prediction of proteins 3D structures. *Bioinformatics* **2002,** *18* (9), 1250-1256.
124. Uppuluri, K. B.; Ayaz Ahmed, K. B.; Jothi, A.; Veerappan, A., Spectrofluorimetric and molecular docking investigation on the interaction of 6-azauridine, a pyrimidine nucleoside antimetabolite, with serum protein. *Journal of Molecular Liquids* **2016,** *219*, 602-607.
125. Bag, S. S.; Talukdar, S.; Anjali, S. J., Regioselective and stereoselective route to N2-β-tetrazolyl unnatural nucleosides via SN2 reaction at the anomeric center of Hoffer's chlorosugar. *Bioorganic & Medicinal Chemistry Letters* **2016,** *26* (8), 2044-2050.
126. Pace, C. N.; Vajdos, F.; Fee, L.; Grimsley, G.; Gray, T., How to measure and predict the molar absorption coefficient of a protein. *Protein Science* **1995,** *4* (11), 2411-2423.
127. Morris, G. M.; Goodsell, D. S.; Halliday, R. S.; Huey, R.; Hart, W. E.; Belew, R. K.; Olson, A. J., Automated docking using a Lamarckian genetic algorithm and an empirical binding free energy function. *Journal of Computational Chemistry* **1998,** *19* (14), 1639-1662.
128. Singh, P.; Talwar, P., Exploring putative inhibitors of Death Associated Protein Kinase 1 (DAPK1) via targeting Gly-Glu-Leu (GEL) and Pro-Glu-Asn (PEN) substrate recognition motifs. *Journal of Molecular Graphics and Modelling* **2017,** *77*, 153-167.
129. Vijesh, A. M.; Isloor, A. M.; Telkar, S.; Arulmoli, T.; Fun, H.-K., Molecular docking studies of some new imidazole derivatives for antimicrobial properties. *Arabian Journal of Chemistry* **2013,** *6* (2), 197-204.

Chapter 4

SYNTHESIS AND STUDIES ON THE PHOTOPHYSICAL/BIOPHYSICAL PROPERTIES OF TRIAZOLYLFLUORENE-LABELED 2′-DEOXYURIDINES

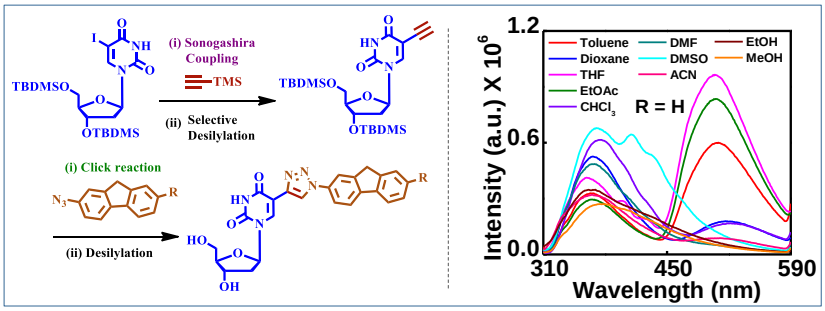

4.1. Introduction

Fluorene is a rigid, planar molecule containing two benzene rings fused by a five-member ring. Its structural features are its planar structure and delocalized π-electrons throughout the structure. Fluorene can be utilized as a spacer via aromatic coupling at the C2 and C7 positions, which could be helpful for the design and synthesis of fluorescent compounds. Also, the C-H functionalization at the C9 position of the fluorene is highly facile. For such structural features, fluorene can be utilized as building blocks for the synthesis of various organic molecules including dyes, polymers etc. Many of these molecules have been explored for their applications in cell imaging and detection of explosives. Organic dyes comprised of fluorene derivatives are widely used for the manufacturing of organic light-emitting diodes (OLEDs), polymeric materials with superconductivity and various optoelectronic devices.[1] Many of the potent antimalarial and antiviral drugs contains fluorene derivatives. Fluorenes exhibit distinct absorption and emission properties at longer wavelengths. Features such as high quantum efficiency, high photostability and low cytotoxicity have marked fluorenes as an important class of compounds in biophysical and biomedical research.[2-8]

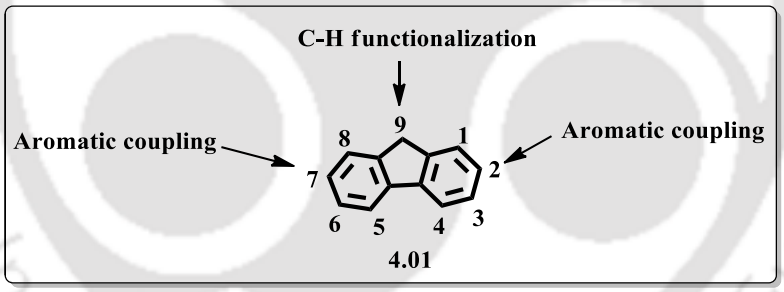

Figure 4.1. Chemical structure of fluorene.

4.2. Fluorene Derivatives and Their Applications

Due to its rigid structure, a fluorene molecule can be efficiently modified to a highly fluorescent molecule with stable structure both in the ground and in the excited state. Development of such fluorenes usually features large emission shifts, high response and stronger fluorescence intensity and hence many of them find numerous applications in various fields of chemistry as fluorescent probes. Few applications of fluorene derivatives are depicted below.

4.2.1. Fluorene Analogues as Metal Ion Sensor

In 2010, Belfield *et al.* reported a fluorenyl macrocycle (**4.02**, **Figure 4.2**) and studied its photophysical, photochemical, two-photon absorption and metal ion sensing properties in various organic and aqueous media.[9] The compound **4.02** showed highly selective and sensitive detection of Zn^{+2} in THF and H_2O/ACN mixture as revealed from both absorption and fluorescence spectra. A gradual increase in the intensity in both absorption and emission signals of the fluorenyl probe was reported on the gradual increase in the concentration of Zn^{+2} ions. Also, this fluorophore provided good photostability and ratiometric fluorescence detection of Zn^{+2} ions, which can be very useful for various bioassays in vivo.

Very recently, Feng *et al*. also reported a fluorescent conjugated polymer probe consists of fluorene, quinolone and benzothiazole units (**4.03**, **Figure 4.2**) for the selective detection of Zn^{2+} among other cations in ethanol.[10] The authors described a ratiometric analysis of the fluorescence signal of the probe in the presence of Zn^{2+} ions in ethanol. The detection limit of the probe for Zn^{+2} ions was reported up to 10^{-8} mol/L.

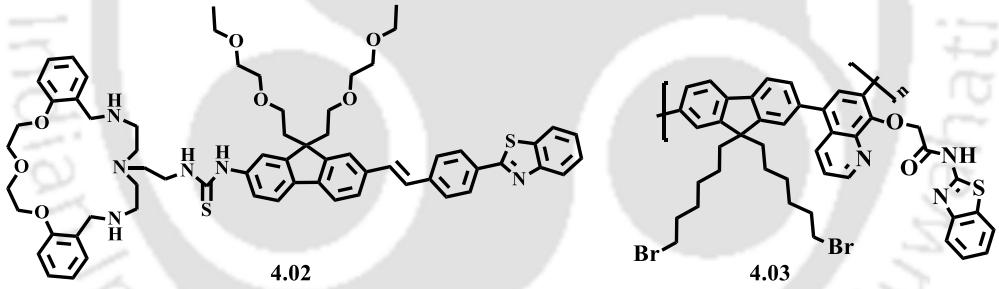

Figure 4.2. Examples of fluorene analogs utilized as Zn^{2+} ion sensor.

In 2013, Ibrahimova *et al*.[11] reported a series of fluorene-based conjugated copolymers **4.04-4.07**, **Figure 4.3**) and studied their optical, electronic and metal sensing properties. It was demonstrated that all of these polymers were able to sense Fe^{3+}ions in THF. The sensing of Fe^{3+} ions is based on the quenching in their fluorescence signal in the presence of Fe^{3+} ions and as per suggested, the backbone of these polymers binds with Fe^{3+} ions forming a ferrocene-like complex. Among the series, the polymer **4.05** showed the highest sensitivity towards Fe^{3+} ions with a high quantum efficiency ($K_{sv} = 3.28 \times 10^6\ M^{-1}$). According to the authors, the polymer **4.05** can be utilized for selective detection of Fe^{3+} ions in organic solvents as well as in aqueous solutions when converted to its salt.

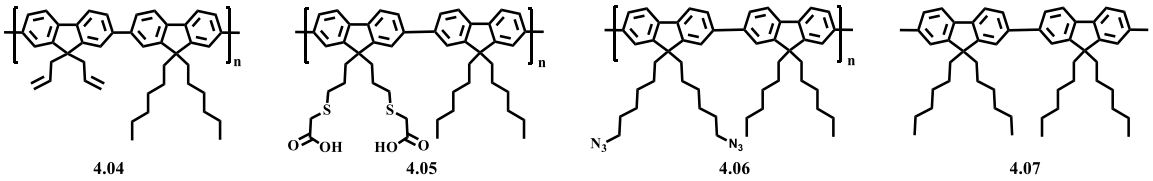

Figure 4.3. Examples of fluorene analogs utilized as Fe^{3+} ion sensor.

In 2016, Koner *et al*. reported a chiral fluorescent molecule synthesized via condensation of a fluorene unit with L-leucine (**4.08**, **Figure 4.4**).[12] This fluorescent probe has been utilized for the selective detection of Cu^{2+} ions following a fluorescence turn-off mechanism. The metal complex of the compound **4.08** with Cu^{2+} has been isolated, characterized and further utilized for the selective detection of Cr^{3+} ion following a fluorescence turn-on mechanism even at the picomolar level of concentration.

In 2017, Carlos *et al.* reported a fluorene derived Schiff-base (**4.09**, **Figure 4.4**) and utilized for selective detection of Cu^{2+} ions in DMSO.[13] According to the authors, the complexation of this compound with Cu^{2+} led to quenching of its fluorescence signal due to the photoinduced electron transfer from copper (II) orbitals center to the fluorophore.

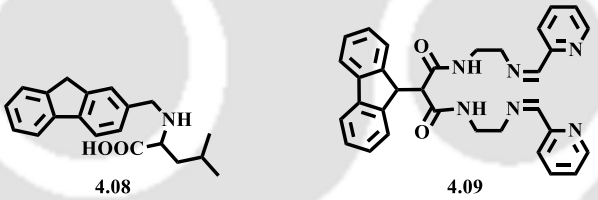

Figure 4.4. Examples of fluorene analogs utilized as Cu^{2+} ion sensor.

In 2014, Bera *et al.* reported a salicylaldehyde appended fluorene-based chemodosimeter (**4.10**, **Figure 4.5**) which had been utilized for selective detection of cyanide ions.[14] It was reported that the compound **4.10** is a weak emitter in ACN due to the excited state intramolecular proton transfer (ESIPT), which follows a nonradiative pathway. In the presence of cyanide ions, the formyl group of the compound **4.10** generates a cyanoalkoxide anion that exchanges a phenolic proton, which inhibits the ESIPT leading to strong fluorescence emission.

Very recently, Dong *et al*., have reported a fluorescent probe where a fluorene group is conjugated to a hemicyanine group (**4.11**, **Figure 4.5**).[15] This probe has been utilized for

selective detection of cyanide ions among the other anions. According to the authors, this probe is highly selective towards cyanide ions with a significant change in colorimetric as well as fluorometric signals in aqueous solution. These changes were explained on the basis of restriction of intramolecular charge transfer (ICT) within the molecule in the presence of cyanide ions.

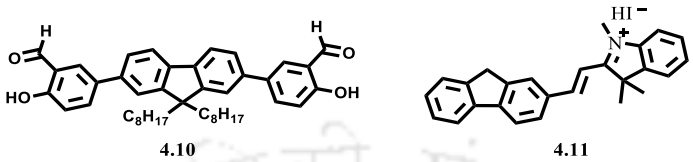

4.10 **4.11**

Figure 4.5. Fluorene analogs utilized as CN^- ion sensor by Dong *et al*.

Liu *et al.* developed a quencher-free functional nucleic acid (FNA)-based biosensor (**4.12**, **Figure 4.6**) for selective detection of Pb^{2+} metal ions.[16] This fluorescence sensor composed of a G-rich DNA sequence as a recognition probe and conjugated fluorene. The concept of Pb^{2+} ion detection based on the inhibition of the conjugated fluorene aggregates which caused the quenching of fluorescence following the aggregation-caused quenching (ACQ) phenomenon. In the presence of Pb^{2+} ions, inhibition of aggregation of conjugated fluorenes taking place which resulted in fluorescence enhancement of the probe.

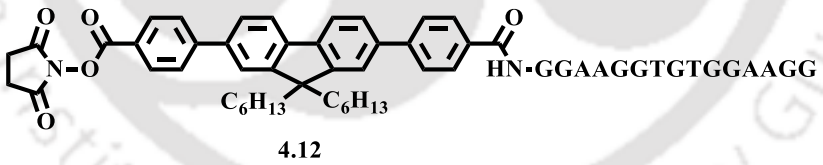

4.12

Figure 4.6. Conjugated fluorene labeled DNA utilized as Pb^{2+} ion sensor by Liu *et al*.

4.2.2. Fluorene Analogues Utilized for Cell Imaging

In 2010, Yao *et al*. synthesized several donor-acceptor-donor type fluorene derivatives for lysosomal imaging.[17] Four representative examples (**4.13**-**4.16**) of their work are shown in **Figure 4.7**. These probes were encapsulated in Pluronic F 128 NF micelles for cellular uptake and their interaction with cells was investigated by confocal and two-photon fluorescence imaging. High lysosomal selectivity by these probes has been reported on the basis of colocalization experiments with Lysotracker Red.

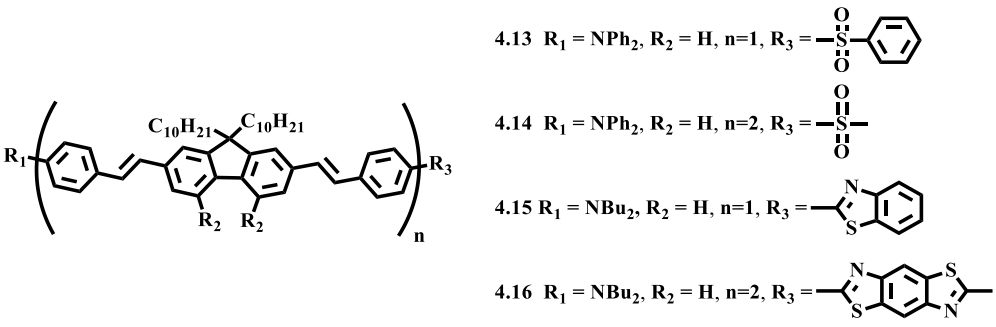

Figure 4.7. Donor-acceptor-donor type fluorene derivatives for lysosomal imaging by Yao *et al*.

In 2012, Liu *et al*. reported two fluorene derived amphiphilic conjugated polyelectrolytes (**4.17**, **4.18**, **Figure 4.8**) and utilized for imaging of HT-29 cancer cells.[18] These polyelectrolytes contain long polyethylene glycol (PEG) chains incorporated into polymeric fluorene chains via click reaction. According to the authors, these polyelectrolytes are low cytotoxic, highly soluble in water due to long PEG side chains and formed nanoparticles in water. From the Cell imaging study, it was reported that the nanoparticles of **4.17** showed brighter images than nanoparticles of **4.18.** Moreover, the polyelectrolyte **4.18** was further modified to yield polyelectrolyte **4.19**, the nanoparticles of which had been reported as highly efficient and highly specific nanoprobes for cellular imaging of HT-29 cancer cells.

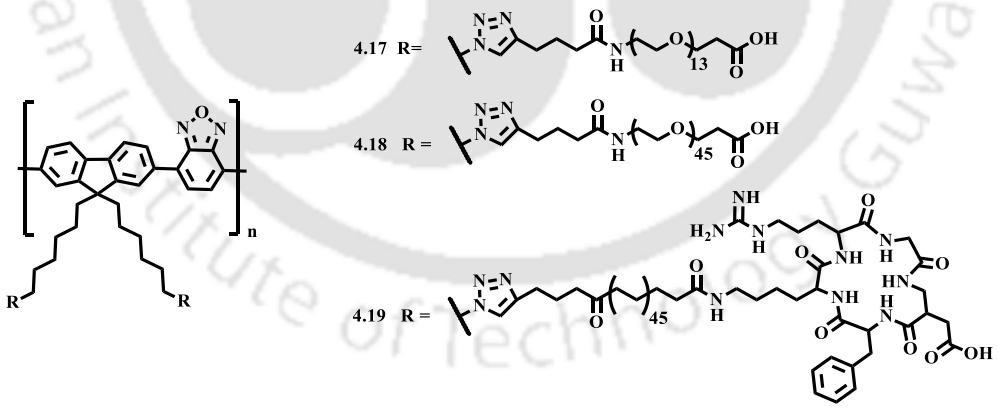

Figure 4.8. Fluorene derived polyelectrolytes for HT-29 cancer cell imaging by Liu *et al*.

In 2012, Aparicio-Ixta *et al.* reported the utilization of a fluorene-based monomer and its cross-conjugated polymer (**4.20**, **4.21**, **Figure 4.9**) for cell imaging in HeLa cells.[19] These materials had been encapsulated into silica nanoparticles to provide biocompatibility and incubated with HeLa cells to carry out two-photon imaging. It was demonstrated that the silver

nanoparticles loaded with **4.20** and **4.21** penetrated into the cells and reversibly stained the cytoplasm.

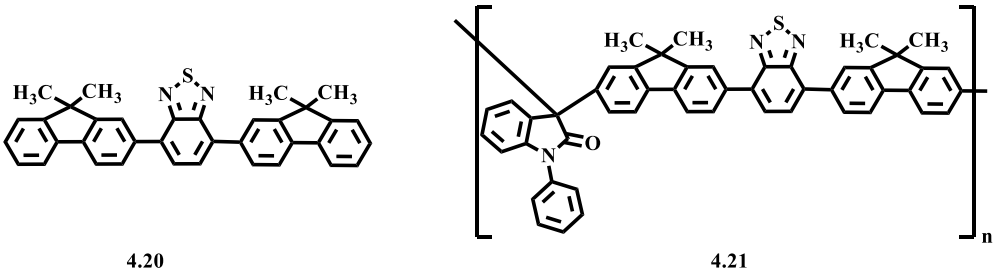

4.20 **4.21**

Figure 4.9. Fluorene derived monomer and its polymer for cell imaging by Aparicio-Ixa *et al*.

In 2014, Guo *et al.* reported utilization of a quencher-free fluorene-based DNA probe (**4.22**, **Figure 4.10**) for imaging normal human liver cells HL-7702.[20] The cell imaging ability of the probe was demonstrated through the "ON-OFF" fluorescence switching induced due to pH change. It was reported that the probe emits fluorescence when its terminal carboxylic group is in the deprotonated state (basic and neutral pH), while protonated carboxylic group (acidic pH) causes quenching of fluorescence. It was demonstrated that the fluorene-based DNA probe **4.22** efficiently penetrated cells and stained cytoplasm at an extracellular buffer solution of pH 8.

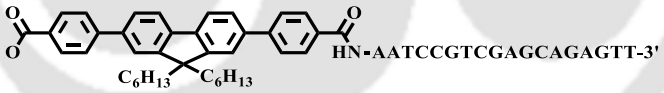

4.22

Figure 4.10. Fluorene derived DNA probe for cell imaging by Guo *et al*.

In 2016, Liu *et al.* developed highly fluorescent conjugated polymer nanoparticles (CPNs) via encapsulation of Rhodamine B dye molecules within a fluorene-based polymer, poly[(9,9-dioctylfluorenyl-2,7-diyl)-co-fluorenone] (**4.23**, **Figure 4.11**).[21] There was a significant improvement of fluorescence properties reported for Rhodamine B dye molecules owing to an efficient FRET from the fluorene polymer to the dye molecules. These CPNs were successfully utilized for cellular imaging in HeLa cells.

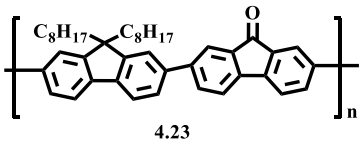

4.23

Figure 4.11. Fluorene-based polymer for cell imaging by Liu *et al*.

In 2016, Xiao *et al.* reported the utilization of a fluorescent dye (**4.24**, **Figure 4.12**) consists of spirobifluorene and triphenylamine for selective detection of Ag+ ions and cell imaging of living 293T cells.[22] It was demonstrated utilizing two-photon microscopy that the cells treated with the dye **4.24** showed bright fluorescence.

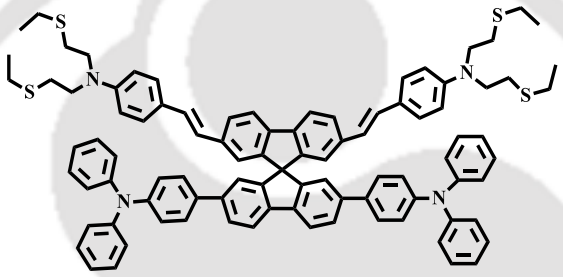

4.24

Figure 4.12. Spirobifluorene derivative for cell imaging by Xiao *et al*.

In 2017, Burger *et al.* reported three fluorescent fluorene probes (**4.25**-**4.27**, **Figure 4.13**) based on push-pull strategy and studied their photostability and applications for cell imaging utilizing HeLa cells.[23] It was demonstrated that the probe **4.27** is highly useful for the imaging of the plasma membrane at the outer leaflet, whereas the probe **4.25** can be utilized equally for the imaging of both plasma membranes and cytoplasm.

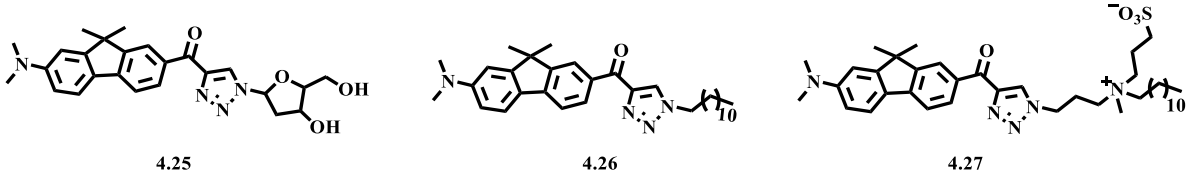

In 2017, Belfield and co-workers reported fluorenyl-loaded quatsome fluorescent nanoprobes and utilized for cell imaging in an epithelial colorectal carcinoma cell line, HCT 116.[24] The fluorenyl unit (**4.28**, **Figure 4.14**) is a hydrophobic fluorene derivative which is stably dispersed in aqueous media with the help of quatsomes. These fluorescent nanoprobes reported as lysosome selective and can be very useful for lysosomal –addressed drug delivery.

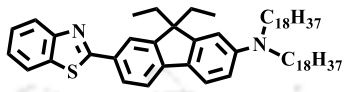

4.28

Figure 4.14. Fluorene analog utilized for cell imaging by Belfield and coworkers.

4.2.3. Fluorene Analogues Utilized for Detection of Explosives

Polyfluorenes consist of a class of highly recognized conjugated polymers and dendrimers with highly emissive fluorescence properties which are often utilized as probes for fluorescent-based explosives detection.[25-28] In 2010, Yang *et al*. reported utilization of a silafluorene-fluorene conjugated polymer (**4.29**, **Figure 4.15**) coated on hollow silica nanoparticles for aqueous TNT and RDX detection.[29] It was demonstrated that the fluorescence emission intensity of the nanoparticles coated with **4.29** experienced quenching in presence of TNT and RDX explosives in aqueous environments. It was suggested that the LUMO of the explosive analytes matches with the energy of the fluorene polymer, which might be due to the coadsorption of the explosive analytes on the silica in close proximity to the polymer and therefore resulting in the quenching of fluorescence.

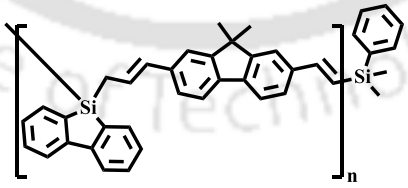

4.29

Figure 4.15. Fluorene-based polymer utilized for detection of TNT and RDX explosives by Yang *et al*.

In 2012, Leng *et al*. reported a fluorene-based conjugated polymer (**4.30**, **Figure 4.16**) containing phenylene and bulky adamantine moieties as side groups and utilized for the

detection of 2,4-dinitrotoluene (DNT) vapor.[30] It was demonstrated that the fluorescence emission intensity of the polymer film of the **4.30** gradually decreases over time upon exposure to DNT vapor. It was suggested that the incorporation of rigid three-dimensional structures of adamantine moieties and phenylene groups could effectively suppress the interchain interactions within the polymer and provide cavities for rapid diffusion of explosive DNT molecule into films resulting in the increased fluorescence quenching efficiency.

In 2015, Wang *et al.* reported several fluorene analogs containing adamantine moieties.[31] Two examples (**4.31**, **4.32**) of their work are shown in **Figure 4.16**. These conjugated polymers had been utilized for the detection of TNT vapor.[31] According to the authors, the fluorescence emission intensities of these fluorescent polymers experienced quenching in the presence of TNT vapor due to the photoinduced electron transfer. It was demonstrated that being decorated with dibenzothiophene-S,S-dioxide units, the polymer **4.32** exhibited more efficient quenching efficiency than the polymer **4.31**. It was explained that the dibenzothiophene-S,S-dioxide units could increase the polarity and reduce the π-π stacking of the polymers chains, which ultimately provide more contact sites for explosive analytes and therefore resulting in the high quenching efficiency for the polymer **4.32**.

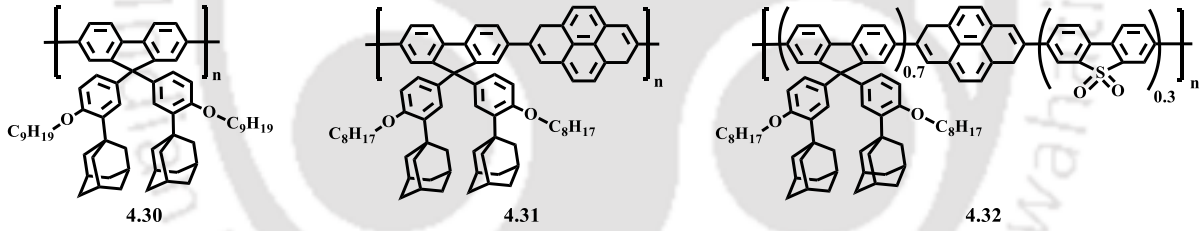

Figure 4.16. Fluorene-based polymers containing adamantine moieties utilized for detection of explosives.

In 2014, Mallet *et al*. reported the utilization of two fluorene derivatives (**4.33**, **4.34 Figure 4.17**) for detection of 2,6-dinitrotoluene.[32] It was demonstrated that the fluorescence emission intensities of these fluorophores were experienced quenching in the presence of nitrotoluene analytes, which is most possibly due to the photoinduced electron transfer from the fluorophores to the nitroaromatics.

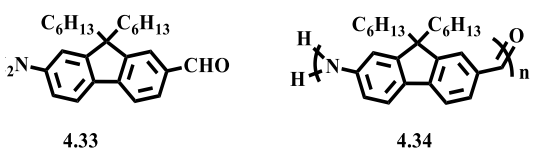

Figure 4.17. Fluorene analogs utilized for detection of nitrotoluenes by Mallet *et al*.

In 2014, Chen *et al*. reported the utilization of an 8-pyrenyl-substituted fluorene dimer (**4.35**, **Figure 4.18**) for the detection of nitrate ester explosives.[33] It was demonstrated that being highly sensitive to the vapor of nitroglycerin, the fluorescence emission of the compound **4.35** was almost quenched by 90% upon exposure to a saturate vapor of nitroglycerin for about 50 seconds. The detection limit for nitroglycerin is reported as low as femtogram level (0.5×10^{-15} g/cm^2). According to the authors, such high and rapid sensitivity of the compound **4.35** attributed to its high molar extinction coefficient, larger steric hindrance, higher area-to-volume ratio and marching energy levels with nitrate esters.

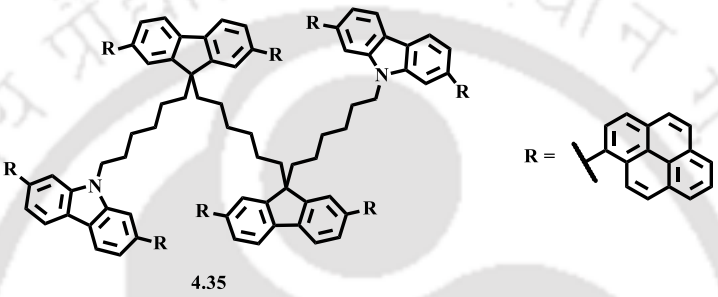

Figure 4.18. Fluorene analog utilized for detection of nitroglycerin by Chen *et al*.

In 2015, Cheng *et al.* reported three borate endcapped pyrenyl-fluorene copolymers (**4.36**-**4.38 Figure 4.19**) for the detection of vapor of peroxide explosives.[34] The detection strategy was based on a deboronation reaction in presence of peroxide which ultimately resulting in fluorescence quenching in the polymer. In their analysis, the hyperbranched polymer (**4.38**) showed the highest sensitivity towards H_2O_2 vapor which has greater steric environment, more external borate ester groups, higher HOMO level and higher fluorescence quantum yield than the other two linear copolymers (**4.36**, **4.37**).

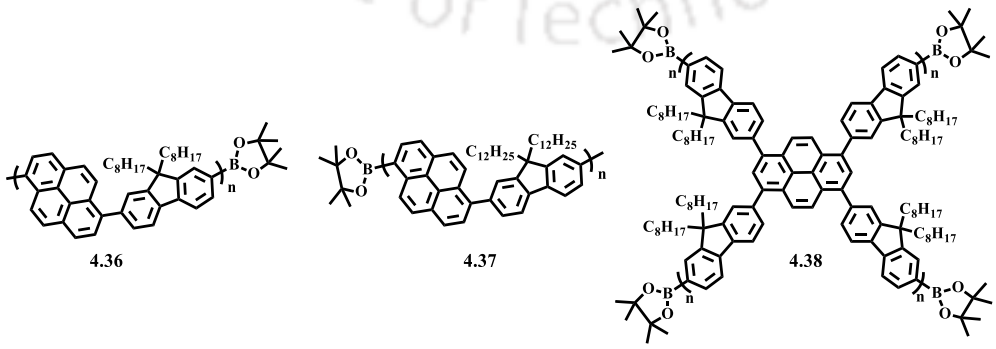

Figure 4.19. Borate endcapped pyrenyl-fluorene copolymers utilized for detection of peroxide explosives by Cheng *et al*.

In 2016, Ni *et al.* reported a fluorene derivative, 4,4′-(9,9-dimethylfluorene-2,7-diyl)dibenzoic acid (**4.39**, **Figure 4.20**) for the detection of 2,4,6-trinitrophenol (TNP) in ACN.[35] It was demonstrated that the fluorene analog **4.39** in ACN exhibited high quenching efficiency of about 98% in the presence of TNP analytes. It was suggested that such high quenching efficiency attributed to the π-π interaction and hydrogen bonding between **4.39** and TNP analytes.

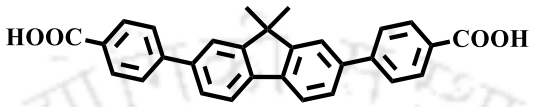

4.39

Figure 4.20. Fluorene analog utilized for detection of TNP by Ni *et al*.

4.3. Nucleosides containing Fluorene Derivatives

In 2013, Kool *et al.* reported several oligodeoxyfluorosides (ODFs) including ODFs (**4.41**, **4.42**, **Figure 4.21**) containing fluorene dye monomers (**4.40**) for labeling of proteins via HaloTag methodology.[36] In a HaloTag method, a simple haloalkane is conjugated to the desired label and fuse to a protein of interest.[37] The authors reported nine different ODFs containing the HaloTag domain **4.43** and investigated to the enzymatic self-conjugation of these ODF-HaloTag ligands to surface and interior proteins of HeLa cells. It was demonstrated that these ODF-HaloTag ligands capable of genetically encoded protein labeling on the surface as well as in the interior of cells. Most of the ODF-HaloTag ligands were found to increase in brightness or change in color upon conjugation to proteins. Utilizing these features, the authors demonstrated the imaging of protein localization in HeLa cells.

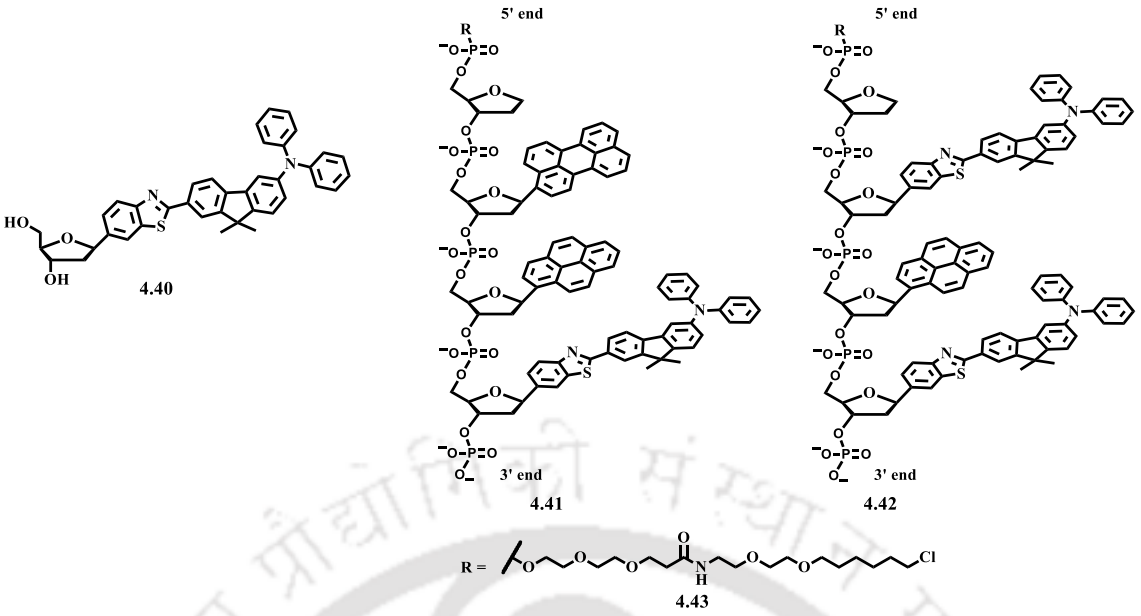

Figure 4.21. Fluorene-based ODF-HaloTag ligands utilized for protein labeling by Kool *et al*.

Hwang and coworkers presented several works related to fluorescent nucleosides containing fluorene moieties.[38-42] For example, they have reported two 2′-deoxyuridines, $\mathbf{U^{FL}}$ and $\mathbf{U^{FO}}$ (**4.44**, **4.47**, **Figure 4.22**) containing 2-ethynylfluorene and 2-ethynyl-9-fluorenone units respectively and incorporated into ODNs (**4.45**, **4.46**, **4.48**-**4.51**, **Figure 4.22**) in order to develop molecular beacon probes (MBs) for quencher-free SNP typing.[39, 41] It was demonstrated that the MBs **4.45** and hairpin **4.46** containing fluorophore $\mathbf{U^{FL}}$ were able to distinguish between their target and one base-mismatched (A/C) DNA sequences. It was reported that these quencher-free MBs exhibited strong fluorescence upon hybridization with their fully matched target DNA while quenching of fluorescence of the MBs taking place upon hybridization with mismatched target DNAs. Similarly, in case of ODN probes (**4.48**-**4.51**, **Figure 4.22)** containing the fluorophore **4.47**, the emission of strong fluorescence was reported upon hybridization with fully matched target DNAs, where the fluorophore was opposite to adenine (A).

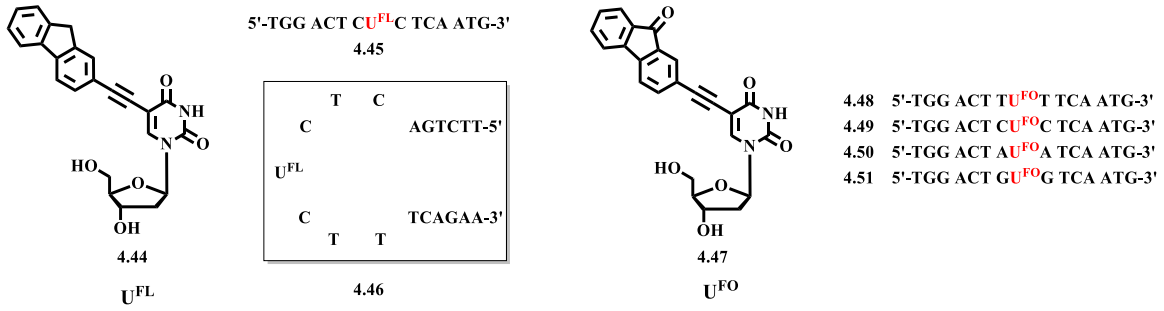

Figure 4.22. Fluorene-labeled 2′-deoxyuridines and ODNs reported by Hwang *et al*.

In 2014, Hwang *et al.* also reported the incorporation of same fluorene moieties i.e. 2-ethynylfluorene and 2-ethynyl-9-fluorenone units in 2′-deoxyguanosine and developed two fluorescent guanosine nucleosides (**4.52**, **4.53 Figure 4.23**).[43] They have investigated the photophysical properties of these nucleosides and reported that both of the nucleosides exhibited solvent-dependent fluorescence emission. It was demonstrated that the nucleoside **4.52** exhibited an excimer emission in nonpolar solvents which can be useful for investigations of various biological binding events and dynamics.

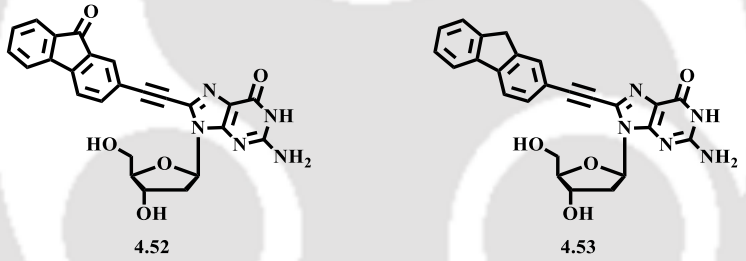

Figure 4.23. Fluorene-labeled 2′-deoxyguanidines reported by Hwang *et al*.

In 2016, Hwang *et al.* reported two more 2′-deoxyuridines (**4.54**, **4.55, Figure 4.24**) containing 2-aminofluorene and 2-dimethylaminofluorene units and studied their photophysical properties.[44] It was reported that these nucleosides exhibited pH-sensitive fluorescence emissions. It was demonstrated that both of the nucleosides exhibited enhanced fluorescence intensities upon acidification which is possibly due to the influence of their protonated forms in the acidic environment. Utilizing this feature, the authors also demonstrated cell imaging in HeLa cells using these two nucleosides.

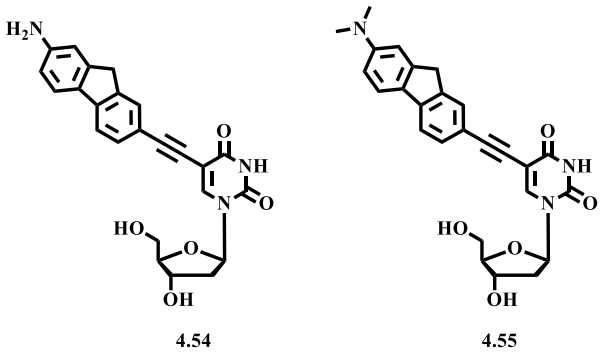

Figure 4.24. Fluorene-labeled 2′-deoxyuridines reported by Hwang *et al*.

In 2016, Hocek *et al.* reported a 2′-deoxycytidine analog, **dC^{FL}** (**4.56 Figure 4.25**) containing a push-pull fluorene fluorophore.[45] It was reported that the **dC^{FL}** showed high solvofluorochromicity and retained high quantum yields in high polar solvents including water. It was demonstrated that the triphosphate of **dC^{FL}** is well-recognized by DNA polymerases for the synthesis of fluorene-labeled DNA probe, **DNA^{FL}** (**4.57**). According to the authors, the probe **DNA^{FL}** exhibited significant color change even visible to the naked eye upon hybridization with DNA binding protein p53 and lipids. Such DNA probes can be useful for the investigation of DNA-protein interactions or DNA-lipid interactions.

Figure 4.25. Examples of nucleosides containing fluorene derivatives.

4.4. Background

In the second chapter, we have briefly discussed the importance of fluorescently labeled nucleosides in various research fields. During the past decade, modified nucleosides have gained a wide range of applications in medicinal chemistry and chemical biology. Considerable attention has been devoted on new fluorescent nucleosides as probes of DNA structure and as potential chemotherapeutic agents. From the literature report, it is clear that fluorescent fluorene derivatives find numerous applications in biochemistry research. However, nucleoside chemistry based on fluorene derivatives are still less explored and there are very few examples of fluorene containing nucleosides available in the literature. Therefore, the design and synthesis of fluorene labeled nucleosides might extend our vision in the field of molecular genetics. Furthermore, incorporation of an electron deficient passive linker such as triazole to the fluorene scaffold might install modulated photophysical properties which in turn might lead to the generation of highly sensitive fluorescent probes for the investigation of various biological events. Triazoles are metabolically inert and can easily associate with biological targets through hydrogen bonding and dipole interactions.[9-11] Therefore, the synthesis of triazolyl fluorene decorated nucleosides with novel photophysical property is an interesting topic of research.

4.5. Objective

Our current research interests focus on the synthesis of fluorescent small molecules and biomolecular building blocks via azide-alkyne cycloaddition reaction. In the second chapter, we have shown that the triazole ring introduces modulated photophysical properties to the generated fluorophores and building blocks. With the above literature report, the background and our previous research efforts, herein, we planned to synthesize fluorescent nucleosides electronically conjugated with a fluorene and a triazolyl moiety by utilizing Sonogashira cross-coupling and copper-catalyzed click chemistry. We envisaged that these nucleosides might offer some interesting photophysical properties and binding interaction with DNAs/proteins. Thus, we framed our total work plan as follows:

(a) Synthesis of fluorene labeled C5-substituted 2′-deoxyuridines via Sonogashira cross-coupling reaction and copper-catalyzed click chemistry (**Scheme 4.1**).

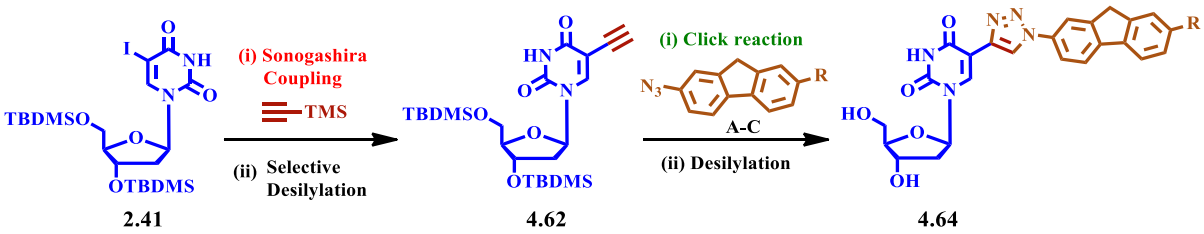

Scheme 4.1. Graphical representation of the synthesis of triazolylfluorene labeled 2′-deoxyuridines.

(b) Study of photophysical properties of synthesized fluorene modified 2′-deoxyuridines.

(c) Investigation of the interaction of a triazolylfluorene nucleoside with ctDNA

4.6. Result and Discussion

4.6.1. Synthesis of Fluorene-Labeled Nucleosides

The synthesis of fluorene labeled 2′-deoxyuridines was achieved via Sonogashira coupling and 1,3-dipolar cycloaddition reaction. To generate a series of target fluorescent uridines, we first synthesized 2-aminofluorene derivative. The synthesis was started from 2-aminofluorene (**4.58**) which was converted to 7-bromo-2-aminofluorene (**4.59**) (**Scheme 4.2**). Then this bromo fluorene derivative was further converted to 7-cyano-2-aminofluorenes (**4.60**). Afterward, corresponding azides (**A-C**) were prepared from these three 2-aminofluorenes (**4.58-4.60**). In the next step, we have synthesized TBDMS protected 5-ethynyl-2′-deoxyuridine (**4.62**). For this purpose, the synthesis was started from 5-iodo-2′-deoxyuridine (**2.32**) which was converted first to its TBDMS protected derivative (**2.33**). Afterward, the TBDMS protected 5-iodo-2′-deoxyuridine was allowed to undergo a Sonogashira coupling with trimethylsilylacetylene to afford compound **4.61**, which underwent selective desilylation to yield compound **4.62**. Finally, the 1,3-Huisgen azide-alkyne cycloaddition reaction was carried out between the uridine containing the ethynyl linker and various fluorene azides (**A-C**, **Figure 4.26a**) under click reaction condition to afford the target uridines **4.63A-C** in bis-TBDMS-protected form and **4.64A** and **4.64B** in desilylated form, in very good yields. The final products were purified by column chromatography and characterized by NMR and HRMS analysis.

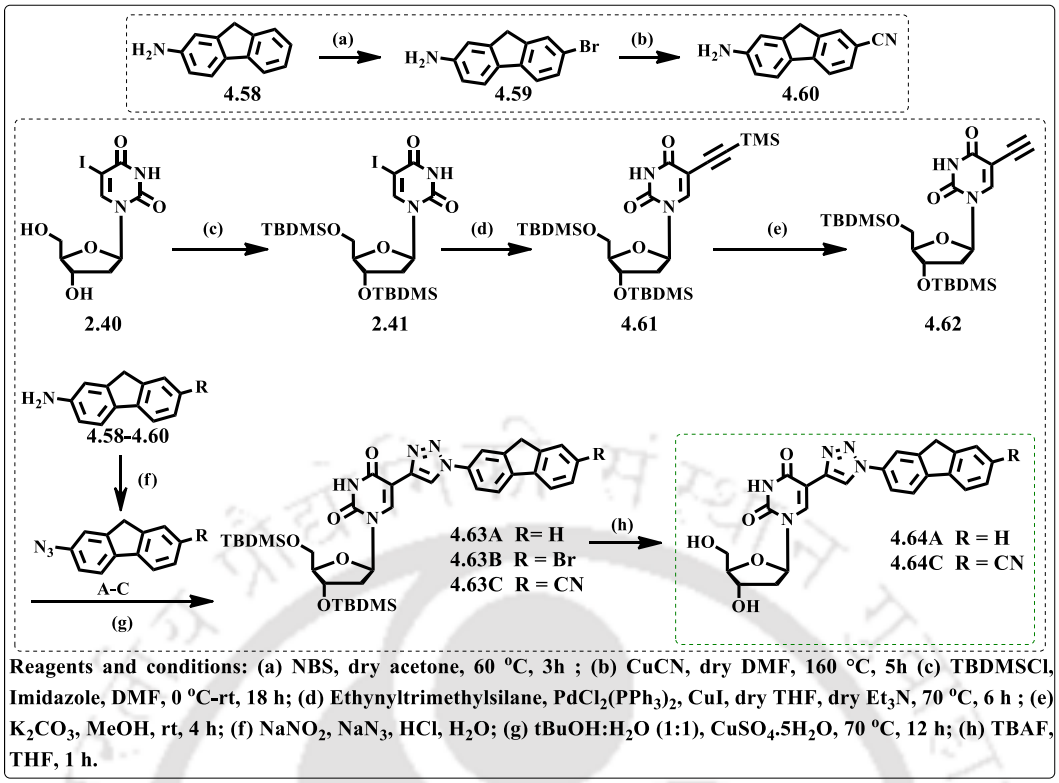

Scheme 4.2. Synthesis of fluorene labeled 2′-deoxyuridines.

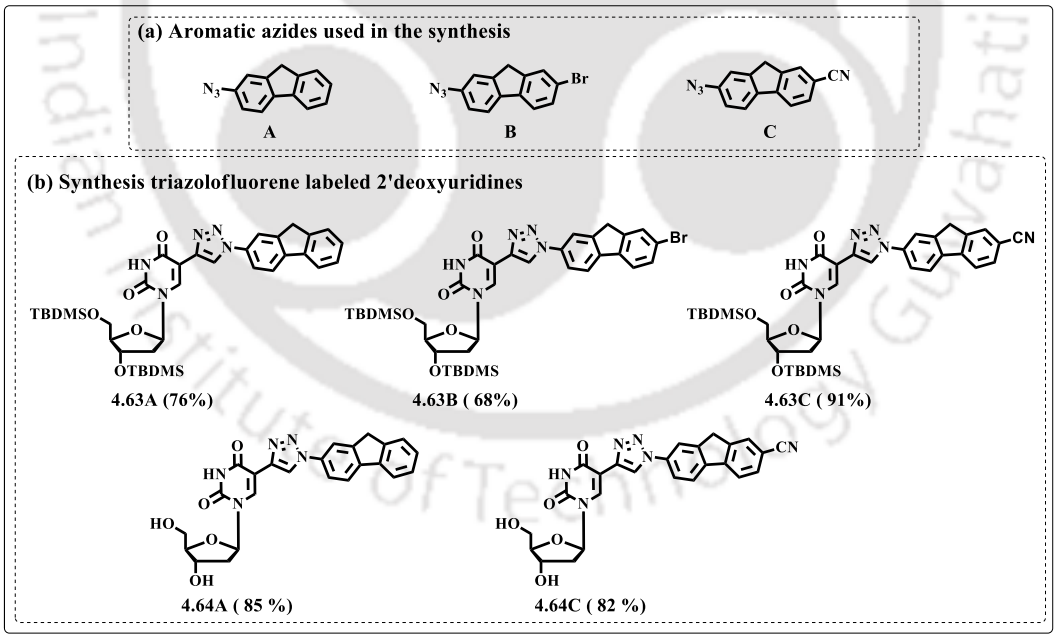

Figure 4.26. (a) Aromatic azides used in the synthesis, (b) Structures of synthesized protected/deprotected triazolylfluorene labeled 2′-deoxyuridines.

4.6.2. Study of Photophysical Properties

After getting all the nucleosides in hands, we studied the photophysical properties of a few selected nucleosides in organic solvents of varying polarities to check their solvatochromic nature. The UV-visible spectra of all the compounds (10 µm) were measured using a UV-visible spectrophotometer with a cell of 1 cm path length at 25 °C and 1 mm slit width. All the sample solutions were prepared before an hour of the measurement. The excitation wavelengths for recording the emission spectra was at the maximum wavelength of absorbance (λ_{max}^{abs}) in each case. The fluorescence quantum yield (Φf) was determined using quinine sulfate as a reference with known Φf = 0.54 in 0.1 molar solution in sulphuric acid.

From the UV-visible spectra of **4.63B**, we observed that the solvent polarity had only minor influence on the absorption properties of the nucleoside. Therefore, the absorption spectra of the nucleoside **4.63B** exhibited structureless and broad absorptions at around 286 and 300 nm in various organic solvents with very little solvatochromism at 286 nm (by 4-6 nm blue shift) (**Figure 4.27a, Table 4.1**). Upon excitation at 300 nm, it exhibited a single emission at around 371 nm with almost similar intensity in toluene, THF, EtOAc and ACN solvents except for MeOH, DMF, EtOH, DMSO, dioxane and $CHCl_3$ wherein enhanced intensity was observed. A red shift of about 5-6 nm was observed in the case of EtOH, MeOH and $CHCl_3$ (**Figure 4.27b, Table 4.1**).

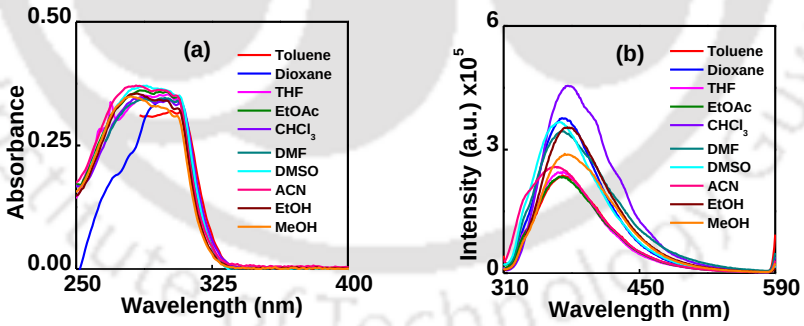

Figure 4.27. (a) UV-visible, (b) fluorescence emission spectra in various organic solvents for nucleoside **4.63B**. The concentration of the nucleoside was 10 µM.

Table 4.1. Summary table of photophysical properties of the nucleoside **4.63B**

Entry 4.63B	**Solvents**									
Properties ↓	**Toluene**	**Dioxane**	**$CHCl_3$**	**EtOAc**	**THF**	**DMSO**	**DMF**	**EtOH**	**ACN**	**MeOH**
Δf	0.013	0.021	0.148	0.201	0.21	0.265	0.275	0.29	0.305	0.309
λ_{max}^{abs} (nm)	305	300	286, 300	286, 300	286, 300	286, 300	300	283, 300	282, 298	280, 298
λ_{max}^{fl} (nm)	371	371	377	371	371	367	371	376	363	376
Φ_f	0.004	0.006	0.007	0.004	0.004	0.006	0.006	0.006	0.005	0.005

Next, the photophysical property of the compound **4.64A** in organic solvents was measured in order to get a comparative picture of it with our synthesized nucleoside **4.64C**. From the UV-visible spectra, it is clear that the nucleoside **4.64A** containing triazolylfluorene exhibited structureless broad absorption maxima centering at around 300 nm in various organic solvents (**Figure 4.28a**). The solvent polarity had an only minor influence on the absorption properties of this nucleoside. Upon excitation at 300 nm, this nucleoside showed a dual emission. In highly polar and protic solvents, only characteristic emissions from a locally excited state were observed. On the other hand, in nonpolar solvents such as in toluene, dioxane and in moderately polar solvents such as $CHCl_3$, EtOAc and THF, a dual emission was observed (**Figure 4.28b**). The additional band observed at higher wavelength region is characterized as emission from intramolecular charge transfer (ICT) state. The LE emission bands were observed at around 360-376 nm and solvatochromic ICT bands were observed at 504, 506, 507, 520 and 524 nm in THF, EtOAc, toluene, dioxane and $CHCl_3$ respectively (**Table 4.2**).

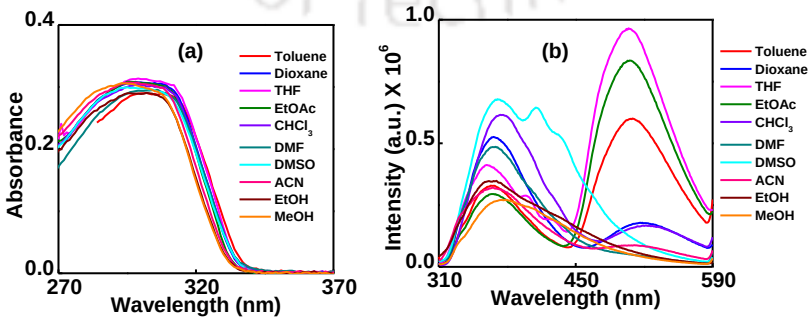

Figure 4.28. (a) UV-visible, (b) fluorescence emission spectra in various organic solvents for the nucleoside **4.64A**. The concentration of the nucleoside was 10 µM.

Table 4.2. Summary table of photophysical properties of the nucleoside **4.64A**

Entry 4.63A	**Solvents**									
Properties ↓	**Toluene**	**Dioxane**	**$CHCl_3$**	**EtOAc**	**THF**	**DMSO**	**DMF**	**EtOH**	**ACN**	**MeOH**
Δf	0.013	0.021	0.148	0.201	0.21	0.265	0.275	0.29	0.305	0.309
λ_{max}^{abs} (nm)	300	300	300	300	300	300	300	300	300	300
λ_{max}^{fl} (nm)	365, 507	366, 520	375, 524	365, 506	360 504	370	366	365	366, 509	376

In order to gain more insight into the dual emissive behavior of the nucleoside **4.64A**, we investigated its photophysical properties in a THF-water titration experiment. Therefore, from the absorption spectra, it is revealed that addition of H_2O in THF has a negligible effect on absorbance and almost no change in absorption maxima was observed till 80% of H_2O (**Figure 4.29a**). Upon addition of 90% and 97% of H_2O, a significant decrease in the absorbance accompanied by a blue shift of about 9 nm and 16 nm respectively was observed. Upon excitation at 300 nm, the intensity of the ICT band greatly decreased on addition of just 2% H_2O in THF with a red shift of about 9 nm (**Figure 4.29b**). Addition of 10% H_2O led to almost full quenching of ICT emission and we observed only LE emission on addition of H_2O up to 90%. On addition of 97% H_2O, we observed a single emission at around 517 nm which is the characteristic emission peak of the compound in water. On the other hand, the emission from the LE state increased gradually up to 20% of H_2O with a red shift of about 5 nm. Beyond, 30% H_2O, the intensity of the LE emission gradually decreased and almost quenched at 97% H_2O.

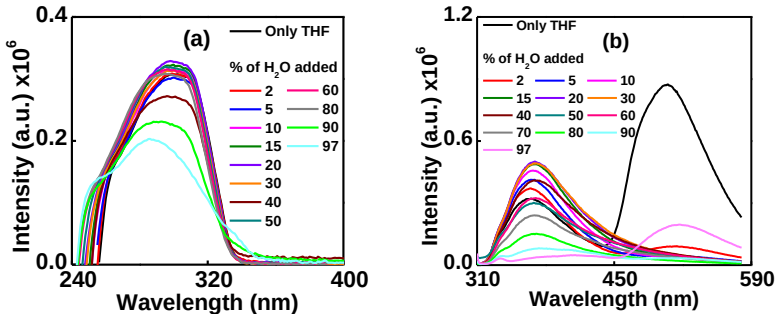

Figure 4.29. (a) UV-visible, (b) fluorescence emission spectra in THF-water mixtures for nucleoside **4.64A**. The concentration of the nucleoside was 10 µM.

The UV-visible spectra of cyanofluorenyl nucleoside **4.64C** showed a short wavelength absorption at around 260 nm and a broad absorption band centered around 290 nm in almost all solvents (**Figure 4.30a**). Almost no shifting in absorption maxima was observed in the spectra except in DMF. However, higher absorbance was observed at 260 nm for dioxane, THF and ACN compared to the rest of the organic solvents. Upon excitation at 300 nm, this nucleoside exhibited dual-emission behavior in low polar solvents like toluene, dioxane and in moderately polar solvent chloroform (**Figure 4.30b**). In other moderately polar solvents like THF, EtOAc and DMF, we observed a hybrid emission structure possibly resulting from the overlapping of LE and ICT emissions. In DMSO and other high polar solvents like ACN, MeOH and EtOH, we observed only LE emission at around 438, 450, 439 and 446 nm respectively. The LE emission bands were observed at around 404-430 nm and solvatochromic ICT bands observed at around 500, 508, 513 nm in dioxane, toluene and $CHCl_3$ respectively (**Table 4.3**).

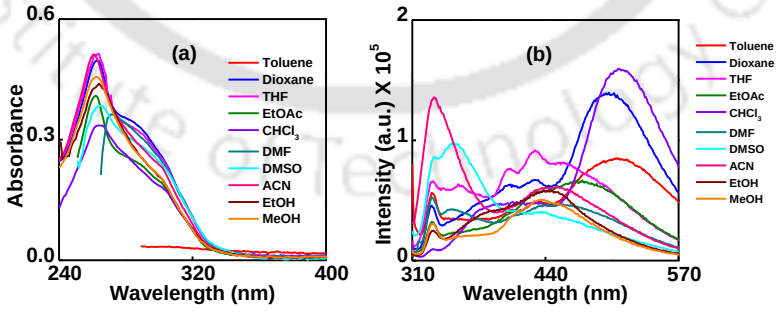

Figure 4.30. (a) UV-visible, (b) fluorescence emission spectra in various organic solvents for nucleoside **4.64C**. The concentration of the nucleoside was 10 µM.

Table 4.3. Summary table of photophysical properties of the nucleoside **4.64C**

Prop. ↓	**Solvents**								
	Diox	**$CHCl_3$**	**EtOAc**	**THF**	**DMSO**	**DMF**	**EtOH**	**ACN**	**MeOH**
Δf	0.021	0.148	0.201	0.21	0.265	0.275	0.29	0.305	0.309
λ_{max}^{abs} (nm)	263, 290, 304	263, 290	263, 290, 301	263, 290, 304	264, 290	272	263, 302	261, 302	263, 302
λ_{max}^{fl} (nm)	403, 429, 500	409, 508	473	403, 430, 456	453	350, 438	446	447	438
Φ_f	0.008	0.01	0.004	0.007	0.007	0.004	0.004	0.006	0.002

In order to gain more insight into the dual emissive behavior of the nucleoside **4.64C**, we investigated its photophysical properties in a dioxane-water titration experiment. Therefore, from the absorption spectra, it is revealed that the addition of H_2O in dioxane has a negligible effect on absorbance and almost no change in absorption maxima was observed throughout all of the dioxane-water mixtures. Only a slight low absorbance was observed upon addition of 97% H_2O in dioxane (**Figure 4.31a**). Upon excitation at 300nm, we observed a similar emission pattern as shown by the nucleoside **4.64A**. The intensity of the ICT band greatly decreased upon addition of just 2% H_2O in dioxane with a blue shift of about 11 nm (**Figure 4.31b**). Addition of 10% H_2O led to almost full quenching of ICT emission and beyond that we observed only LE emission. On the other hand, the emission from the LE state increased gradually on addition of H_2O up to 5%. Beyond this point, the intensity of the LE emission gradually decreased.

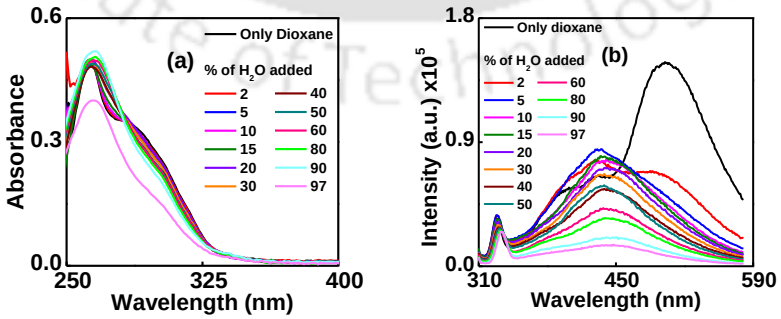

Figure 4.31. (a) UV-visible, (b) fluorescence emission spectra in dioxane-water mixtures for nucleoside **4.64C**. The concentration of the nucleoside was 10 µM.

4.6.3. Theoretical Calculations

Next, we studied the TDDFT calculation in order to examine the effect of solvent polarity on the absorption and emission property of synthesized nucleosides using Gaussian 09 program package .[46] Thus, from the HOMO-LUMO overlap and transition oscillator strength (f) of the fluorene labeled nucleosides it was clear that the electronic transition from S_o to S_1 or other possible electronic transitions are feasible (**Figure 4.32-4.33**). So the reverse transition *i.e.*, $S_0 \leftarrow S_1$ was also fully allowed that revealed the fluorophoric nature of the synthesized nucleosides. Solvatochromicity and intramolecular charge transfer emissions were also explained by redistribution of electronic charge density between HOMO-LUMO in nucleosides **4.64A** and **4.64C** (**Figure 4.33**).[47-51]

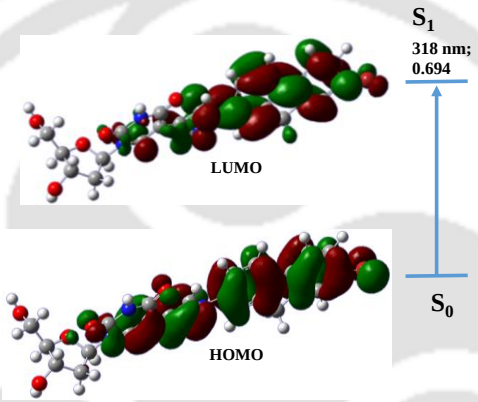

Figure 4.32. Diagram of HOMO-LUMO of **4.63B** calculated at B3LYP//6-31G* level of theory using Gaussian 09 program package.

From the TDDFT calculations, it was clear that the dominant orbital transition in the low-lying singlet excited states of the studied nucleosides is the $S_0 \rightarrow S_1$ transition having the highest configuration interaction (CI) value. Thus, the calculated excitation energy for the transition from $S_0 \rightarrow S_1$ of bromofluorenyl nucleoside (**4.63B, Figure 4.32**), fluorenyl nucleoside (**4.64A, Figure 4.33a**) and cyanofluorenyl nucleoside (**4.64C, Figure 4.33b**) were found to be 318 (3.89 ev, f = 1.17, CI = 0.69); 310 nm (3.99 ev, f = 0.92; CI = 0.70) and 336 nm (3.69 ev, f = 0.70, CI = 0.70) (in vacuum), respectively. The experimental observations in low polar solvents from UV-visible spectra correlated well with the theoretical calculation in the gas phase. Thus, the absorptions of bromofluorenyl nucleoside (**4.63B**), cyanofluorenyl nucleoside (**4.64C**) and fluorenyl nucleoside (**4.64A**) were found to be 305 nm in cyclohexane, 304 nm in dioxane and 300 nm in toluene respectively.

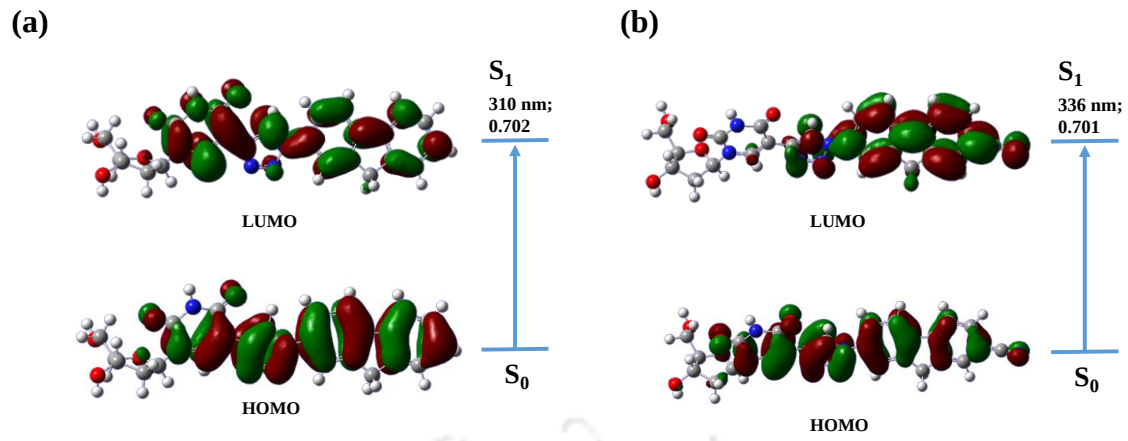

Figure 4.33. Diagram of HOMO-LUMO of (a) **4.64A** and (b) **4.64C** calculated at B3LYP//6-31G* level of theory using Gaussian 09 program package.

The emission spectra for fluorenyl nucleoside (**4.64A**) and cyanofluorenyl nucleoside (**4.64C**) showed solvatochromic effect and bathochromic shift due to electronic charge redistribution between uridine nucleus and fluorenyltriazole/cyanofluorenyltriazole moieties which was also reflected from their individual HOMO-LUMO diagrams. However, the emissive states of both the fluorenyl (**4.64A**) and cyanofluorenyl nucleosides (**4.64C**) were characterized with more significant electron redistribution, *i.e.*, ICT feature as was supported from the calculated results of HOMO−LUMO distribution. These results correlated well with the experimental observation.

4.6.4. Study of Interaction of Nucleoside 4.64C with ctDNA

Finally, we explored the novel cyanofluorenyl nucleoside **4.64C** as a possible probe for studying the interaction with ctDNA. We envisaged that the cyanofluorenyl nucleoside **4.64C** would sense the ctDNA via the generation of an enhanced fluorescence signal.

4.6.4.1. Study of UV-visible and Fluorescence Photophysical Properties of Cyanofluorenyl Triazolyl Nucleoside (4.64C) in Presence of ctDNA

The UV-visible absorption of the nucleoside **4.64C** in phosphate buffer showed an absorption band at around 264 nm and a weak broad band at around 315 nm (**Figure 4.34a**). Addition of an increasing concentration of ctDNA to the probe solution, no significant change was observed around 300 nm, while higher absorbance was observed around 262 nm which is obvious due to the increase in the concentration of ctDNA (λ_{max} = 260 nm).

Upon excitation at 320 nm in phosphate buffer, nucleoside **4.64C** showed extremely weak emission at 551 nm (**Figure 4.34b**,**c**). Upon gradual addition of an increasing amount of ctDNA, the emission intensity of the probe **4.64C** gradually increased and reached maximum upon addition of 0.5 equivalent of ctDNA with a blue shift of about 3nm. Further increase in the concentration of the ctDNA resulted in a gradual decrease in emission intensity at 551 nm. The increase in the emission intensity of the nucleoside upon addition of ctDNA indicated a strong interaction between the probe and ctDNA.

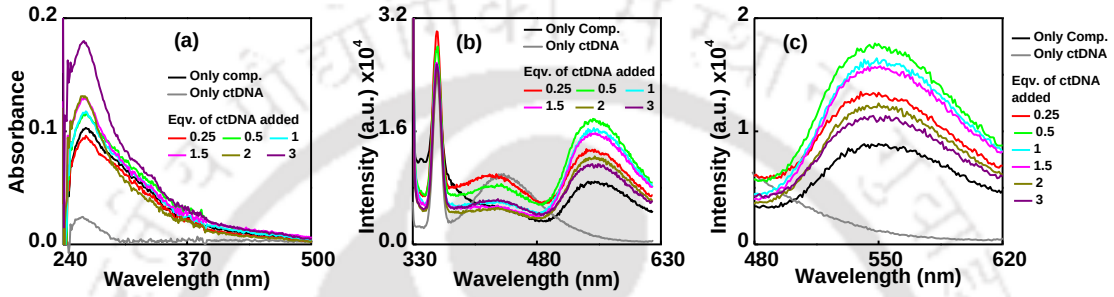

Figure 4.34. (a) UV-visible, (b) fluorescence emission spectra (λ_{ex} = 320 nm) and (c) an enlarged section of the fluorescence emission spectra (λ_{ex} = 320 nm) of the nucleoside **4.64C** in absence or in presence of ctDNA. The probe concentration was 10 μM.

4.6.4.2. Determination of Binding Constant

The binding constant (*K*) of the complex was determined spectroscopically for the nucleoside **4.64C** by well-known Benesi-Hildebrand plot (**Figure 4.35**) using the following equation 1,

$$\frac{1}{(I-I_0)} = \frac{1}{(I_\infty - I_0)} + \frac{1}{(I_\infty - I_0)K[\text{ctDNA}]} \quad \ldots\ldots\ldots\ldots\ldots (1)$$

where I_0, I and I_α are the emission intensities of the nucleoside in the absence of ctDNA, and in the presence of intermediate and at an infinite concentration of ctDNA, respectively. From the slope (linear region's data points) of the plot of $1/(I - I_0)$ *vs.* 1/[ctDNA], the binding constant *K* was determined, which was found to be 1.5 x 10^4 M^{-1} for the nucleoside **4.64C**. Next, the free energy of binding (ΔG) was calculated using equation 2, which was found to be -5.7 kcal/mol.

$$\Delta G = -RT \ln K \quad \ldots\ldots\ldots\ldots\ldots\ldots\ldots\ldots\ldots\ldots\ldots\ldots\ldots\ldots (2)$$

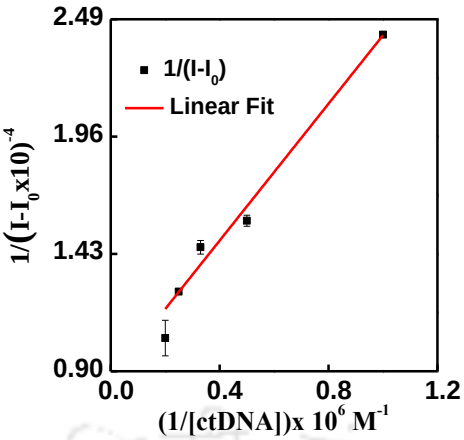

Figure 4.35. Benesi–Hildebrand plots of nucleosides **4.64C** in the presence of an increasing concentration of ctDNA at 298 K.

4.6.4.3. Molecular Docking

To support, the binding event of the probe **4.64C** with ctDNA, we carried out a docking study using AutoDock 4.2 software [52, 53] and Gaussian[46] optimized geometry of the probe. The structure of B-DNA dodecamer d(CGCGAATTCGCG)$_2$ used for docking was downloaded from the protein data bank (http://www.rcsb.org./pdb, PDB ID: 1BNA). Next, the probe, **4.64C**, was optimized with B3LYP functional and 6-31G (d,p) basis set with Gaussian 09 program package.[46] Finally, the docking study was carried to get insight into the binding event with flexible molecular docking method and the full DNA was under the grid map. From the docking study, we find that the probe encompasses the minor groove involving π-π-stacking and H-bonding interaction (**Figure 4.36**). Thus, the docking study supported our experimental observation.

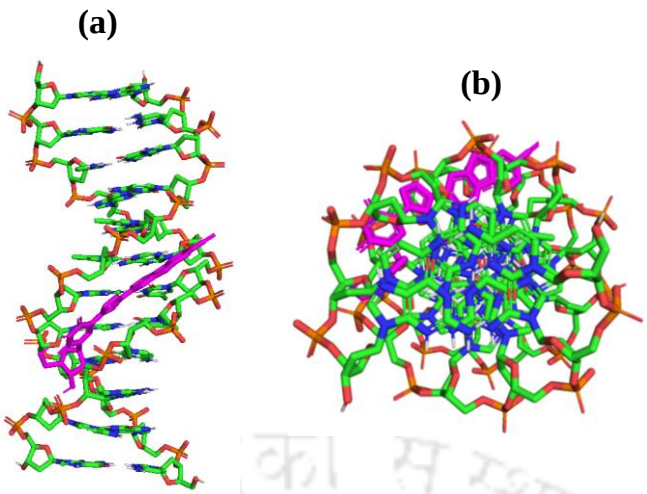

Figure 4.36. Docked structure of the complex of ctDNA and the probe, **4.64C**. (a) Side view and (b) bottom view

4.7. Conclusion

In conclusion, we have successfully synthesized three novel triazolylfluorenyl labeled fluorescent nucleosides via Sonogashira coupling and click reaction. The synthetic scheme was simple and most of the reagent, starting materials are easily available commercially at very low cost. The main importance of our work is the modulation of the photophysical properties of 2′-deoxyuridine by labeling with fluorescent fluorene moiety via a triazole spacer. The nucleosides **4.64A** and **4.64C** showed dual emissive properties in various organic solvents. The nucleoside **4.64C** is able to sense ctDNA as a fluorescent light up probe in aqueous media. Thus, these nucleosides would be useful in generating fluorescent oligonucleotide probes for DNA analysis. The dual emitting fluorene nucleosides would impact greatly in nucleoside research as rare examples of such nucleosides exist in the literature.

4.8. Experimental Section

4.8.1. General Experimental

All reactions were carried out under a nitrogen atmosphere in flame-dried glassware, using schlenk line. Organic extracts were dried over anhydrous sodium sulfate. Solvents were removed in a rotary evaporator under reduced pressure. Silica gel (60- 120 mesh size) was used for the column chromatography. Reactions were monitored by TLC on silica gel 60 F254 (0.25 mm). ^{1}H NMR spectra were recorded at 600MHz and ^{13}C NMR spectra were recorded at 150MHz. Coupling constants (*J* value) were reported in Hertz. The chemical shifts were shown

in ppm downfield from tetramethylsilane, using residual chloroform (δ = 7.26 in ^{1}H NMR, δ = 77.23 in ^{13}C NMR) or DMSO (δ = 2.5 in ^{1}H NMR, δ = 39.5 in ^{13}C NMR) as an internal standard. All the NMR-FID files were processed in MestReNova v9.0 software. Mass spectra were recorded with a High-Resolution mass spectrometer (HRMS) and data analyzed by using the built-in software. IR spectra were recorded on KBr plate in an FT-IR spectrophotometer and reported in the frequency of absorption (cm^{-1}). For dioxane-water titration experiments, water was taken from a Milli-Q purification system. For photophysical studies, all solutions were prepared before 1 hour of experiments done.

4.8.2. Synthesis and Characterizations

Synthesis of 2-amino-7-bromofluorene (4.59): This compound was synthesized following

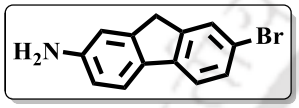

a standard literature procedure.[54] N-bromosuccinimide (707 mg, 3.97 mmol) was added to a solution of 2-aminofluorene (**4.58**) (600mg, 3.31 mmol) in 15 ml of dry acetone under nitrogen atmosphere. The resulting reaction mixture was stirred at 60 °C for 3 hours. The completion of the reaction was monitored by TLC. After completion of the reaction, the reaction mixture was cooled to room temperature and ice water was added. Then the reaction mixture was partitioned between ethyl acetate and water. The collected organic layer was washed with water, and brine solution. After evaporation, the crude product was purified by column chromatography (Si-gel, Hex: EtOAc = 5:1) to obtain the 2-amino-7-bromofluorene **4.59** as a brown solid. Yield 81 % (700 mg). ^{1}H NMR (600 MHz, $CDCl_3$) δ 7.81 (s, 1H), 7.60 (d, *J* = 7.6 Hz, 1H), 7.46 (d, *J* = 7.4 Hz, 1H), 7.32 (t, *J* = 7.4 Hz, 1H), 7.22 (t, *J* = 7.4 Hz, 1H), 6.96 (s, 1H), 4.14 (s, 2H), 3.78 (s, 2H); **+ESI-HRMS** calculated for $C_{13}H_{10}BrN$ **[M+H]$^+$** 260.0069, found 260.0065.

Synthesis of 2-amino-7-cyanofluorene (4.60): This compound was synthesized following

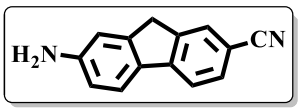

a standard literature procedure.[55] 258 mg of CuCN (2.88 mmol) was added to a solution of 2-amino-7-bromofluorene, **4.59** (500mg, 1.92mmol) in 10 ml DMF. The resulting mixture was refluxed for 5 hours. After completion of the reaction, the reaction mixture was partitioned between ethyl acetate and water. The collected organic layer was washed with water, brine solution and dried over anhydrous Na_2SO_4. After evaporation, the crude product was purified by column chromatography (Si-gel, Hex: EtOAc = 5:1) to obtain the desired product **4.60** as a reddish-brown solid. Yield: 86% (340 mg). ^{1}H NMR (600 MHz, $CDCl_3$) δ 7.75 (s, 1H), 7.63 (d, *J* = 7.6 Hz, 1H), 7.47 (d, *J* = 7.5 Hz, 1H), 7.35 (t, *J* = 7.5 Hz, 1H), 7.29 – 7.23 (m, 1H), 6.92 (s, 1H), 4.45 (s, 2H), 3.87 (s, 2H);

^{13}C NMR (151 MHz, $CDCl_3$) δ 150.57, 148.97, 141.84, 140.36, 133.10, 127.26, 126.59, 125.08, 123.19, 119.31, 112.02, 94.93, 77.16, 37.28; **+ESI-HRMS** calculated for $C_{14}H_{10}N_2$ **[M+H]**$^+$ 207.0917, found 207.0915.

Synthesis of 3',5'-di-O-tert-butyldimethylsilyl-5-iodo-2'-deoxyuridine (2.33):This compound was synthesised following a modified literature procedure.[56] 4 g (11.23 mmol) of 5-iodo-2'-deoxyuridine (**2.32**) was taken in a dry R.B. and dissolved in dry DMF. The reaction mixture was vacuumed and filled with N_2. Imidazole (3.85 g, 56.49 mmol) was added to the reaction mixture and the clear reaction mixture was vacuumed one more time and filled with N_2. The above mixture was cooled to 0°C in an ice bath and t-butyldimethylsilylchloride (5.08 g, 33.69 mmol) was added to the reaction mixture. The ice bath was removed after 1 hour and the resulting mixture was stirred at room temperature under N_2 for 18 hours. After completion of reaction, the reaction mixture was partitioned between ethyl acetate and water. Collected organic layer was washed with water, brine solution and dried over anhydrous Na_2SO_4. After evaporation, the product was purified by column chromatography (Si-gel, Hex: EtOAc = 5:1) and obtained as white foam. Yield: 96% (6.35 g). IR (KBr): ῡ 3457, 3184, 3062, 2954, 2931, 2857,1694, 1607cm^{-1}; ^{1}H NMR ($CDCl_3$, 600 MHz): δ 8.96 (s, 1H), 8.07 (s, 1H), 6.26 (t, *J* = 6.6 Hz, 1H), 4.38 (s, 1H), 3.97 (s, 1H), 3.88 (d, *J* = 11.4 Hz, 1H), 3.75 (d, *J* = 10.8 Hz, 1H), 2.31-2.28 (m, 1H), 2.00-1.96 (m, 1H), 0.93 (s, 9H), 0.88 (s, 9H), 0.14 (d, *J* = 6.6 Hz, 6H), (0.07) (d, *J* = 4.8 Hz, 6H); ^{13}C NMR ($CDCl_3$, 150 MHz): δ 160.2, 150.0, 144.6, 88.6, 86.0, 72.7, 68.5, 63.2, 42.2, 38.7, 26.3, 25.9, 18.7, 18.2, -4.4, -4.6, -4.9, -5.0; **+ESI-HRMS** calculated for $C_{21}H_{40}IN_2O_5Si_2$ **[M+H]** $^+$ 583.1515, found 583.1511.

Synthesis of 3',5'-di-O-tert-butyldimethylsilyl-5-trimethylsilylethynyl-2'-deoxyuridine (4.61):This compound was synthesised following a modified literature procedure.[57] 1.5 g (2.57 mmol) of 3',5'-bis-*O*-tert-butyldimethylsilyl-5-iodo-2'-deoxyuridine (**2.33**) was taken in a dry R.B. and dissolved in 30 ml dry 1:1 THF/Et_3N. The resulting mixture was degassed by bubbling N_2 through it. After 10 minutes, $PdCl_2(PPh_3)_2$ (54.22 mg, 0.08 mmol) followed by CuI (4.9 mg, 0.026 mmol) were added to the above mixture while continuing the degassing. Then degassing was stopped and added trimethylsilylacetylene (379.4 mg, 3.86 mmol). The resulting mixture was stirred at 55 °C for 7 hours. After completion, the reaction mixture was partitioned between ethyl

acetate and water. Collected organic layer was washed with aqueous ammonium chloride, water, brine solution and dried over anhydrous Na_2SO_4. After evaporation, the product was purified by column chromatography (Si-gel, Hex: EtOAc = 5:1) and obtained as white foam. Yield: 80 % (1.14 g). IR (KBr): ṽ 3173, 3051, 2955, 2858, 2167, 1722, 1684, 1419, 1253, 1131, 841 cm^{-1}; ^1H NMR (600 MHz, $CDCl_3$) δ 8.32 (s, 1H), 7.97 (s, 1H), 6.28 (dd, *J* = 7.8, 5.8 Hz, 1H), 4.42 – 4.38 (m, 1H), 3.98 (d, *J* = 2.0 Hz, 1H), 3.90 (dd, *J* = 11.4, 2.1 Hz, 1H), 3.76 (dd, *J* = 11.4, 1.9 Hz, 1H), 2.30 (ddd, *J* = 13.1, 5.7, 2.2 Hz, 1H), 2.01 (ddd, *J* = 13.3, 7.8, 5.9 Hz, 1H), 1.61 (d, *J* = 8.2 Hz, 2H), 0.93 (s, 9H), 0.89 (s, 9H), 0.21 (s, 9H), 0.14 (d, *J* = 7.9 Hz, 6H), 0.08 (d, *J* = 5.2 Hz, 6H); **+ESI-HRMS** calculated for $C_{26}H_{48}N_2O_5Si_3$ **[M+H]** $^+$ 553.2944, found 553.2943.

***Synthesis of 3',5'-di-O-tert-butyldimethylsilyl-5-ethynyl-2'-deoxyuridine (4.62)*:** This

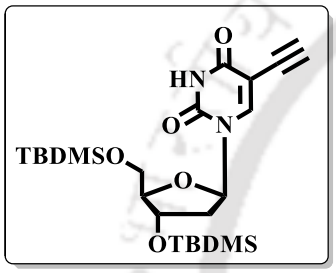

compound was synthesized following a modified literature procedure.[58] 746 mg (1.35 mmol) of **(4.61)** was taken in a dry R.B. and dissolved in 25 ml dry methanol. Anhydrous K_2CO_3 (932 mg, 6.75 mmol) was added to the above solution and the resulting mixture was stirred for 2 hours at room temperature. After completion of reaction, the reaction mixture was partitioned between ethyl acetate and water. Collected organic layer was washed with water, brine solution and dried over anhydrous Na_2SO_4. After evaporation, the product was purified by column chromatography (Si-gel, Hex: EtOAc = 4:1) and obtained as dark orange foam. Yield: 70% (455 mg). IR (KBr): ṽ 3480, 3315, 3248, 2930, 2857, 2117, 1714, 1624, 1462, 1279, 1255, 1116, 837, 779 cm^{-1}; ^1H NMR (600 MHz, $CDCl_3$) δ 8.45 (s, 1H), 8.11 (s, 1H), 6.29 (dd, *J* = 7.5, 5.8 Hz, 1H), 4.40 (dt, *J* = 5.6, 2.7 Hz, 1H), 3.98 (q, *J* = 2.3 Hz, 1H), 3.91 (dd, *J* = 11.5, 2.3 Hz, 1H), 3.76 (dd, *J* = 11.5, 2.1 Hz, 1H), 3.17 (s, 1H), 2.32 (ddd, *J* = 13.2, 5.9, 2.8 Hz, 1H), 2.17 (s, 1H), 2.02 (ddd, *J* = 13.2, 7.5, 5.8 Hz, 1H), 0.93 (s, 9H), 0.89 (s, 9H), 0.13 (d, *J* = 5.9 Hz, 6H), 0.08 (d, *J* = 4.8 Hz, 6H); **+APCI-HRMS** calculated for $C_{23}H_{40}N_2O_5Si_2$ **[M+H]**$^+$ 481.2549, found 481.2543.

General Procedure for the Synthesis of Aryl Azides: An ice cold solution of sodium nitrite (3 eqv.) in water was added dropwise to a cold solution of arylamine (1 eqv.) in water and hydrochloric acid at 0°C over 7 to10 min. The reaction mixture was slowly stirred for 1-2 minutes before an ice cold solution of sodium azide (6 eqv.) in water was added dropwise at 0°C over 10 min. The mixture was stirred for 30 min and allowed to stand overnight. The resulting mixture was extracted with hexane. The organic layer was washed with water, followed by a brine solution, dried over anhydrous Na_2SO_4. After evaporation, the product was

passed through a section of silica gel (60-120 mesh). Formation of the azides was confirmed from IR study and yields were within 60%-80% in all cases. The produced azides were then immediately used for the next step without further purification.

General Procedure for Click Reaction: Alkyne (1 eqv.) and azide (1.5 eqv.) were suspended in a 1:1 water/*tert*-butanol mixture. Sodium ascorbate (0.05 eqv., freshly prepared in 1ml water) was added, followed by $CuSO_4.5H_2O$ (0.2eqv., freshly prepared in 1ml water). The reaction mixture was refluxed (75 °C) for 12 hours. The progress of the reaction was monitored by TLC. After completion of the reaction, *tert*-butanol was evaporated in a rotary evaporator and the reaction mixture was partitioned between ethyl acetate and water. The collected organic layer was washed with water, aqueous ammonium chloride, brine solution and dried over anhydrous Na_2SO_4. After evaporation, the product was purified by column chromatography.

General Procedure for Deprotection of Tertiarybutyldimethylsilyl Ether: To a solution of respective TBDMS protected nucleoside (1eqv.) in THF, a solution of tetra-*n*-butylammoniumfluoride (TBAF) (2.5 eqv.) in THF was added. The reaction mixture was stirred at room temperature for 1 hour. After completion of the reaction, the solvent was evaporated in a rotary evaporator and was partitioned between ethyl acetate and water. The collected organic layer was washed with brine solution and dried over anhydrous Na_2SO_4. After evaporation, the crude material obtained was purified by column chromatography.

Synthesis of 3',5'-di-O-tert-butyldimethylsilyl-5-(2-triazolylfluorenyl)-2'-deoxyuridine (4.63A): Using general procedure for click reaction, starting from 120 mg (0.25 mmol) of compound **4.62** and 78 mg of 2-azidofluorene (0.375 mmol), the title compound was isolated by Si-gel column chromatography (Hex: EtOAc = 3:1) as yellow solid. Yield: 76% (130 mg); m.p. 230-232 °C. IR (KBr): ῡ 3417, 2928, 2856, 1718, 1468, 1255, 1032, 837 cm^{-1}; ^1H NMR (600 MHz, $CDCl_3$) δ 8.68 (s, 1H), 8.64 (s, 1H), 7.98 (dd, *J* = 1.9, 0.8 Hz, 1H), 7.89 (d, *J* = 8.2 Hz, 1H), 7.82 (d, *J* = 7.6 Hz, 1H), 7.78 (dd, *J* = 8.1, 2.0 Hz, 1H), 7.58 (dt, *J* = 7.5, 1.1 Hz, 1H), 7.42 (td, *J* = 7.4, 1.1 Hz, 1H), 7.36 (td, *J* = 7.4, 1.2 Hz, 1H), 6.37 (dd, *J* = 8.0, 5.8 Hz, 1H), 5.30 (s, 1H), 4.48 (dt, *J* = 5.8, 2.3 Hz, 1H), 4.05 (td, *J* = 3.7, 2.2 Hz, 1H), 4.00 (s, 2H), 3.89 (dd, *J* = 11.1, 4.0 Hz, 1H), 3.84 (dd, *J* = 11.2, 3.5 Hz, 1H), 2.40 (ddd, *J* = 13.2, 5.8, 2.3 Hz, 1H), 2.20 (ddd, *J* = 13.6, 8.1, 5.9 Hz, 1H), 0.92 (s, 9H), 0.88 (s,

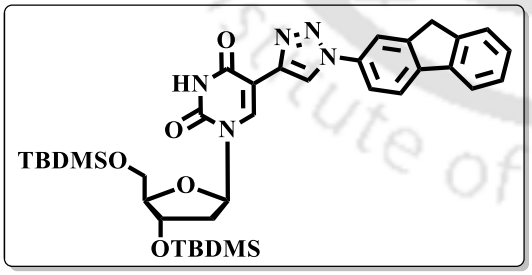

9H), 0.13 (s, 3H), 0.12 – 0.10 (m, 9H); ^{13}C NMR (151 MHz, $CDCl_3$) δ 161.15, 149.50, 144.89, 143.64, 142.39, 140.58, 139.79, 136.72, 135.82, 127.55, 127.23, 125.32, 120.80, 120.41, 120.32, 119.58, 117.64, 106.00, 88.62, 86.34, 77.16, 72.95, 66.00, 63.41, 53.57, 41.46, 37.21, 26.14, 25.92, 15.41, -4.51, -4.64, -5.18, -5.37; **+ESI-HRMS** calculated for $C_{36}H_{49}N_5O_5Si_2$ **[M+H]$^+$** 688.3345, found 688.3340.

Synthesis of 3',5'-di-O-tert-butyldimethylsilyl-5-(2-triazolyl-7-bromo-fluorenyl)-2'-deoxyuridine (4.63B): Using general procedure for click reaction, starting from 120 mg (0.25 mmol) of compound **4.62** and 107 mg of 2-azido-7-bromofluorene (0.375 mmol), the title compound was isolated by Si-gel column chromatography (Hex: EtOAc = 3:1) as yellow solid. Yield: 68% (130 mg); m.p. 189-190 °C.

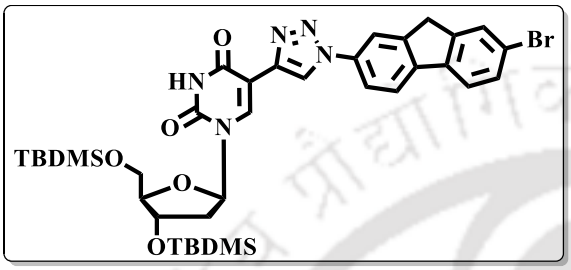

IR (KBr): ῦ 3455, 2953, 2929, 2856, 1685, 1639, 1468, 1256, 1105, 1030, 836, 778 cm^{-1}; ^{1}H NMR (600 MHz, $CDCl_3$) δ 8.86 – 8.73 (m, 1H), 8.67 (s, 1H), 8.57 (s, 1H), 8.11 (s, 1H), 7.85 – 7.80 (m, 1H), 7.67 (d, *J* = 1.1 Hz, 1H), 7.62 – 7.57 (m, 1H), 7.43 (dtd, *J* = 22.2, 7.4, 1.2 Hz, 2H), 6.39 (dd, *J* = 8.0, 5.7 Hz, 1H), 4.49 (dt, *J* = 5.9, 2.3 Hz, 1H), 4.07 – 4.03 (m, 1H), 3.94 (s, 2H), 3.90 (dd, *J* = 11.2, 3.8 Hz, 1H), 3.84 (dd, *J* = 11.2, 3.3 Hz, 1H), 2.39 (ddd, *J* = 13.3, 5.8, 2.2 Hz, 1H), 2.22 – 2.18 (m, 1H), 0.91 (s, 9H), 0.88 (s, 9H), 0.15 – 0.08 (m, 12H); ^{13}C NMR (151 MHz, $CDCl_3$) δ 161.13, 149.54, 145.14, 144.10, 143.39, 139.34, 138.94, 136.75, 134.45, 128.49, 127.47, 125.49, 124.88, 124.82, 124.61, 120.90, 117.86, 106.06, 88.64, 86.27, 72.94, 63.36, 41.55, 36.83, 26.17, 25.92, 18.59, 18.18, -4.52, -4.65, -5.19, -5.40; **+ESI-HRMS** calculated for $C_{36}H_{48}BrN_5O_5Si_2$ **[M+H]$^+$** 766.2450, found 766.2447.

Synthesis of 3',5'-di-O-tert-butyldimethylsilyl-5-(2-triazolyl-7-cyano-fluorenyl)-2'-deoxyuridine (4.63C): Using general procedure for click reaction, starting from 120 mg (0.25 mmol) of compound **4.62** and 87 mg of 2-azido-7-cyanofluorene (0.375 mmol), the title compound was isolated by Si-gel column chromatography (Hex: EtOAc = 2:1) as yellow solid. Yield: 91% (162 mg). m.p. 219-220 °C.

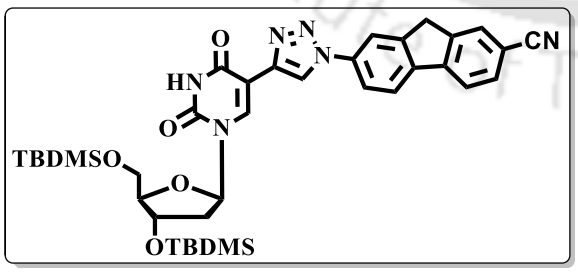

IR (KBr): ῦ 3470, 3417, 2930, 2857, 2229, 1693, 1463, 1256, 1106, 1030, 837, 779 cm^{-1}; ^{1}H NMR (600 MHz, $CDCl_3$) δ 8.77 (s, 1H), 8.68 (s, 1H), 8.18 (s, 1H), 7.90 (s, 1H), 7.86 (d, *J* = 7.4 Hz, 1H), 7.63 (d, *J* = 7.2 Hz, 1H), 7.51 – 7.44 (m, 2H), 6.38 (dd, *J* = 7.9, 5.8 Hz, 1H), 4.50 – 4.46 (m, 1H), 4.08 (s, 2H), 4.06 (d, *J* = 2.4 Hz, 1H), 3.90 (dd, *J* = 11.2, 3.7 Hz, 1H), 3.84 (dd, *J* = 11.2, 3.2 Hz, 1H), 2.43 – 2.37 (m, 1H), 2.18 (ddd, *J* = 13.5, 7.9, 5.9 Hz, 1H), 0.91 (s, 9H),

0.88 (s, 9H), 0.13 (s, 3H), 0.12 (s, 3H), 0.11 (s, 3H), 0.10 (s, 3H); ^{13}C NMR (151 MHz, $CDCl_3$) δ 161.01, 149.61, 149.48, 143.55, 143.51, 140.04, 138.65, 137.12, 136.90, 129.08, 127.82, 125.57, 125.08, 122.92, 122.56, 121.09, 116.17, 106.63, 105.65, 88.70, 86.35, 77.16, 72.97, 66.00, 63.39, 41.63, 37.67, 26.14, 25.92, 18.60, 18.17, 15.41, -4.51, -4.65, -5.19, -5.3; **+ESI-HRMS** calculated for $C_{37}H_{48}N_6O_5Si_2$ **[M+H]$^+$** 713.3297, found 713.3295.

Synthesis of 5-(2-triazolylfluorenyl)-2'-deoxyuridine (4.64A): Using general procedure for

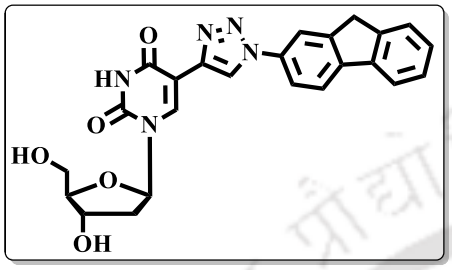

TBDMS deprotection, starting from 100 mg (0.145 mmol) of compound **4.63A**, the title compound was isolated by Si-gel column chromatography ($CHCl_3$: MeOH = 10:1) as yellow solid. Yield: 85% (57 mg); m.p. over 300 °C. IR (KBr): ῡ 3427, 2925, 1704, 1673, 1467, 1276, 1098, 1052, 871, 768 cm^{-1}; 1H NMR (600 MHz, DMSO-d6) δ 11.74 (d, J = 2.6 Hz, 1H), 8.90 (dq, J = 6.3, 1.7 Hz, 1H), 8.67 (d, J = 1.7 Hz, 1H), 8.22 – 8.14 (m, 1H), 8.14 – 8.06 (m, 1H), 8.04 – 7.93 (m, 2H), 7.70 – 7.61 (m, 1H), 7.42 (q, J = 6.9 Hz, 1H), 7.37 (tdd, J = 8.7, 4.6, 2.2 Hz, 1H), 6.26 (td, J = 6.8, 3.7 Hz, 1H), 5.31 (dt, J = 4.2, 1.2 Hz, 1H), 5.07 (t, J = 4.9 Hz, 1H), 4.31 (tq, J = 5.7, 2.8, 2.1 Hz, 1H), 4.07 – 4.02 (m, 2H), 3.88 (dt, J = 5.2, 1.9 Hz, 1H), 3.63 (q, J = 4.8 Hz, 2H), 2.23 (t, J = 5.4 Hz, 2H); 13C NMR (151 MHz, DMSO) δ 161.13, 149.70, 144.72, 143.49, 141.42, 140.03, 139.98, 136.76, 135.25, 127.34, 127.00, 125.27, 121.04, 120.51, 120.11, 119.08, 117.16, 104.79, 87.71, 84.89, 79.18, 70.65, 61.41, 36.67.; **+ESI-HRMS** calculated for $C_{24}H_{21}N_5O_5$ **[M+H]$^+$** 460.1615, found 460.1609.

Synthesis of 5-(2-triazolyl-7-cyano-fluorenyl)-2'-deoxyuridine (4.64C): Using general

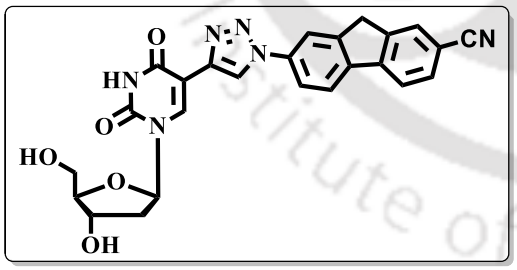

procedure for TBDMS deprotection, starting from 100 mg (0.14 mmol) of compound **4.63C**, the title compound was isolated by Si-gel column chromatography ($CHCl_3$: MeOH = 7:1) as yellow solid. Yield: 82% (56 mg). m.p. over 300°C. IR (KBr): ῡ 3416, 2925, 2826, 2228, 1703, 1680, 1340, 1277, 1103, 1085, 867 cm^{-1}; ^{1}H NMR (600 MHz, DMSO-d6) δ 11.80 (s, 1H), 9.00 (s, 1H), 8.76 (s, 1H), 8.63 (s, 1H), 8.07 (s, 1H), 8.02 – 7.99 (m, 1H), 7.77 – 7.71 (m, 2H), 7.51 (td, *J* = 7.4, 0.9 Hz, 1H), 6.26 (t, *J* = 6.8 Hz, 1H), 5.34 (d, *J* = 4.1 Hz, 1H), 5.13 (t, *J* = 4.8 Hz, 1H), 4.33 – 4.29 (m, 1H), 3.88 (q, *J* = 3.6 Hz, 1H), 3.68 – 3.59 (m, 2H), 2.27 – 2.19 (m, 2H); ^{13}C NMR (151 MHz, DMSO) δ 190.64, 161.09, 149.72, 144.11, 141.95, 140.06, 138.94, 137.55, 137.10, 136.34, 133.43, 130.98, 126.86, 124.85, 122.90, 122.74, 120.81, 115.78, 111.97, 104.38, 87.78, 84.99, 70.73, 61.42, 40.21.; **+ESI-HRMS** calculated for $C_{25}H_{20}N_6O_5$ **[M+H]$^+$** 485.1568, found 485.1561.

4.8.3. Photophysical Studies of the Nucleosides

UV-visible Measurements: The UV–Visible absorbance measurements were performed using Shimadzu UV-2550 UV–Visible spectrophotometer with a cell of 1 cm path length at 298 K. The measurements were carried out in absorbance mode. The absorbance values of the sample solutions were measured in the wavelength regime of 200–550 nm. All the sample solutions were prepared just before doing the experiment.

Fluorescence Experiments: All the sample solutions were prepared as described in UV measurement experiments. Fluorescence spectra were obtained using Fluoromax 4 spectrophotometer at 25 °C using a 1 cm path length cell. The excitation wavelengths for all the cases were set at the excitation maxima of each sample in each solvent and emission spectra were measured in the wavelength regime of 300–700 nm with an integration time of 0.2 sec. All the sample solutions were prepared just before doing the experiment. Fluorescence emissions were collected exciting the samples at the wavelength corresponding to their absorption maxima. The fluorescence quantum yields (Φ_f) were determined using quinine sulfate as a reference with the known Φ_f (0.55) in 0.1 molar solution in sulfuric acid. The following equation was used to calculate the quantum yield,

$$\Phi_S = \Phi_R \frac{Fl_S^{Area}}{Fl_R^{Area}} \frac{Abs_R}{Abs_S} \frac{n_S^2}{n_R^2}$$

where, Φ_R is the quantum yield of standard reference, Fl_S^{Area} (sample) and Fl_R^{Area} (reference) are the integrated emission peak areas, Abs_S (sample) and Abs_R (reference) are the absorbances at the excitation wavelength, and n_S (sample) and n_R (reference) are the refractive indices of the solutions.

4.8.4. Studies on the Interaction of Nucleoside 4.64C with ctDNA

Materials: Calf thymus DNA was purchased from Sigma (USA) and used without further purification. Na_2HPO_4 and $NaH_2PO_4.H_2O$ (for preparation of phosphate buffer) were purchased from Merck, India. Water was obtained from a Milli-Q purification system. All experiments were performed with freshly prepared solutions. The probe molecule was recrystallized in the methanol-ethylacetate solvent mixture, dried under vacuum, again characterized and used for the study.

Preparation of ct-DNA Solution: The purity of ct-DNA was checked by UV-visible spectroscopy by measuring the ratio of absorbances at 260 nm to 280 nm which was found to be 1.9 indicating that the ct-DNA is sufficiently free of protein.[59] The concentration of ct-DNA was measured from UV-visible spectra using the molar absorption coefficient (ε) of 6600 M^{-1} cm^{-1} at 260 nm.

UV-Visible Study: The UV–Visible absorbance measurements were performed using Shimadzu UV-2550 UV–Visible spectrophotometer with a cell of 1 cm path length at 298 K. All the UV-Visible studies were carried out in 50 mM phosphate buffer of pH 7.0 containing 100 mM NaCl solution at 298 K. 2-3 % DMF was used to solubilize the probe. The measurements were taken in absorbance mode and the absorbance values of the sample solutions were measured in the wavelength regime of 200–600 nm. All the experiments were carried out by freshly prepared sample solutions.

Fluorescence Study: All fluorescence and steady-state anisotropy experiments were performed using Fluoromax 4 spectrophotometer with a cell of 1 cm path length at 298 K. All the fluorescence studies were carried out in 50 mM phosphate buffer of pH 7.0 containing 100 mM NaCl solution at 298 K. 2-3 % DMF was used to solubilize the probe. The excitation wavelength for the probe (**4.64C**) was set at 320 nm, and emission spectra were measured in the wavelength regime of 330–620 nm.

4.8.5. Molecular Docking

Docking calculations were carried out using Autodock 4.2.[52, 53] To test the accuracy of the docking results, the docking process was repeated three times. The AutoDock tools (ADT) were utilized for charges and polar hydrogens addition as well as for setting the other parameters. Auto Grid 4.0 and AutoDock 4.0 were used to produce grid maps. A grid box to a size of 66 × 68 × 116 with 0.375 Å spacing was generated. The centre grid box for x-, y- and z centres were 14.780, 20.976 and 8.807 with offsets 2.405, 8.226 and -12.943, respectively. In the prescriptive grid box, we calculated the complex conformation with flexible molecular docking method. The Lamarckian genetic algorithm (LGA)[52] was chosen to carry out a flexible molecular docking to examine the docking of the nucleoside **4.64C** to the ctDNA and to calculate the complex conformation. The other items used were the default settings. A total of 10 conformations from each docking were obtained and the least binding energy was considered as the best-docked conformation.

4.8.6. Theoretical Calculations

The ground state structures of the synthesized nucleosides were optimized using density functional theory (DFT)[46] with B3LYP functional and 6-31G (d) basis set. The excited state related calculations were carried out with the time-dependent density functional theory (TD-DFT) with the optimized structure of the ground state (B3LYP/6-31G(d)). There are no imaginary frequencies in frequency analysis of all the calculated structures, therefore each calculated structure is a local energy minimum.

4.8.7. B3LYP/6-31G* Optimized Structure and Cartesian Coordinates of the Synthesized Compounds

4.8.7.1. Optimized Structure and Cartesian Coordinates for Bromofluorenyl-Based Nucleoside

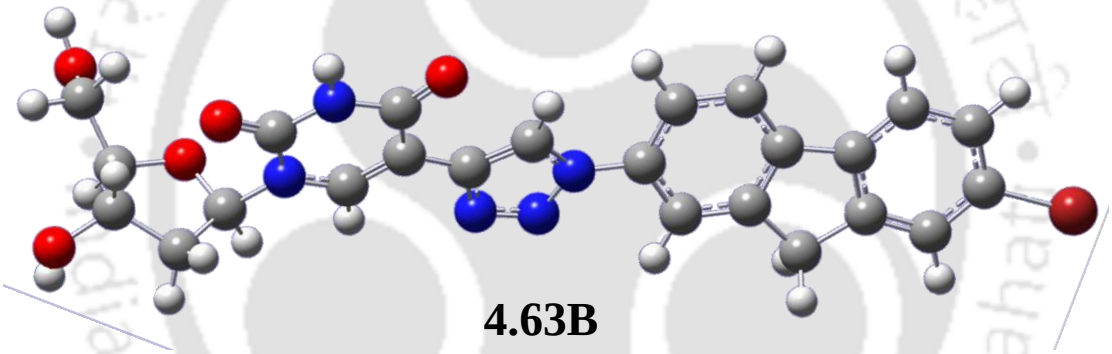

4.63B

E(RB3LYP) = -4148.21329725 a.u.

Standard orientation:

Center Number	Atomic Number	Atomic Type	Coordinates (Angstroms) X	Y	Z
1	6	0	8.886496	-0.817366	-0.766827
2	6	0	7.556194	-1.288743	-1.383924
3	8	0	7.225040	-0.910836	0.948722
4	6	0	8.644384	-0.994494	0.746452
5	8	0	10.042238	-1.486637	-1.235032
6	6	0	9.352543	0.040447	1.595891
7	8	0	9.266452	-0.351268	2.958157
8	6	0	6.522163	-1.145851	-0.250127
9	6	0	3.163417	0.515193	-0.337231
10	6	0	4.173931	-0.392432	-0.269604
11	7	0	5.504473	-0.084877	-0.435881
12	6	0	5.916696	1.235171	-0.644184
13	7	0	4.874261	2.143335	-0.709655
14	6	0	3.496833	1.917351	-0.575302
15	8	0	2.707378	2.849894	-0.657586
16	8	0	7.082999	1.571204	-0.773585
17	6	0	1.771984	0.112579	-0.170996

18	7	0	1.419493	-1.196916	0.039904
19	7	0	0.129661	-1.286658	0.150876
20	7	0	-0.382381	-0.031537	0.011019
21	6	0	0.618991	0.870053	-0.192366
22	6	0	-1.784453	0.184416	0.086663
23	6	0	-2.651391	-0.888204	-0.164873
24	6	0	-4.016699	-0.661617	-0.085999
25	6	0	-4.524448	0.617647	0.226189
26	6	0	-3.650597	1.678038	0.474167
27	6	0	-2.277076	1.456168	0.411234
28	6	0	-5.156351	-1.633989	-0.307209
29	6	0	-6.379195	-0.767492	-0.088375
30	6	0	-5.988254	0.553445	0.225063
31	6	0	-7.719697	-1.109109	-0.158635
32	6	0	-8.687044	-0.114930	0.088580
33	6	0	-8.296757	1.201466	0.401429
34	6	0	-6.948789	1.538915	0.470286
35	1	0	9.043804	0.236019	-0.998142
36	1	0	7.639161	-2.347110	-1.657330
37	1	0	7.282024	-0.733104	-2.280978
38	1	0	8.989352	-1.995128	1.057711
39	1	0	9.963854	-2.423596	-1.005715
40	1	0	8.878992	1.014865	1.410436
41	1	0	10.398557	0.090165	1.252079
42	1	0	9.622982	0.365385	3.497232
43	1	0	5.925044	-2.059763	-0.153665
44	1	0	3.950851	-1.435988	-0.079793
45	1	0	5.154655	3.103979	-0.867688
46	1	0	0.471583	1.922170	-0.357571
47	1	0	-2.238882	-1.859879	-0.408888
48	1	0	-4.024099	2.665955	0.725512
49	1	0	-1.589368	2.264906	0.630924
50	1	0	-5.117718	-2.475374	0.396566
51	1	0	-5.135758	-2.069078	-1.314644
52	1	0	-8.036292	-2.119203	-0.398466
53	1	0	-9.060105	1.949080	0.587753
54	1	0	-6.656949	2.556368	0.711647
55	35	0	-10.543153	-0.556369	-0.001373

4.8.7.2. Optimized Structure and Cartesian Coordinates for Fluorenyl-Based Nucleoside

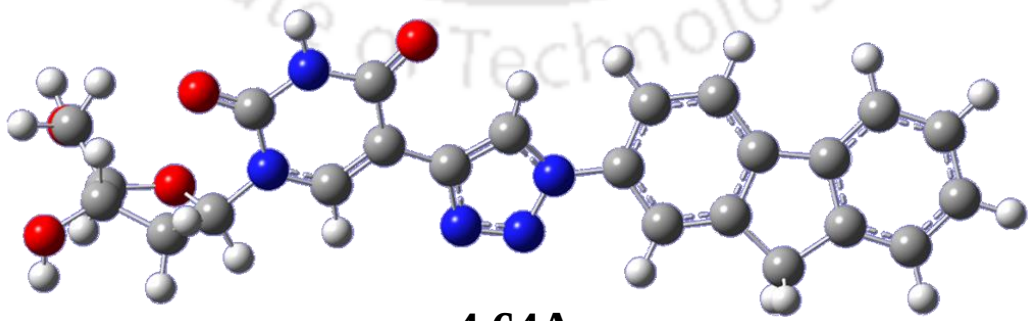

4.64A

E(RB3LYP) = -1577.11055584 a.u.

Standard orientation:

Center Number	Atomic Number	Atomic Type	Coordinates (Angstroms) X	Y	Z
1	6	0	7.413123	-0.702233	-0.754479
2	6	0	6.096178	-1.228787	-1.355102
3	8	0	5.758345	-0.802155	0.968184
4	6	0	7.178905	-0.843107	0.763936
5	8	0	8.587108	-1.351616	-1.206044
6	6	0	7.853046	0.239819	1.580788
7	8	0	7.783742	-0.114680	2.954349
8	6	0	5.059982	-1.086662	-0.223175
9	6	0	1.653641	0.472042	-0.345404
10	6	0	2.690559	-0.402974	-0.255936
11	7	0	4.012272	-0.061242	-0.433888
12	6	0	4.385252	1.263375	-0.678537
13	7	0	3.316757	2.138252	-0.766378
14	6	0	1.946029	1.876279	-0.622561
15	8	0	1.131028	2.783884	-0.728728
16	8	0	5.541514	1.630076	-0.819472
17	6	0	0.275086	0.032057	-0.164334
18	7	0	-0.035445	-1.280648	0.083191
19	7	0	-1.323065	-1.406450	0.201556
20	7	0	-1.873089	-0.173171	0.028536
21	6	0	-0.901681	0.752529	-0.203257
22	6	0	-3.282655	0.005124	0.102269
23	6	0	-4.121119	-1.085394	-0.167729
24	6	0	-5.492144	-0.895480	-0.091082
25	6	0	-6.035266	0.365476	0.236610
26	6	0	-5.188754	1.443095	0.502310
27	6	0	-3.808566	1.257916	0.442467
28	6	0	-6.606836	-1.892930	-0.330101
29	6	0	-7.853516	-1.061894	-0.103668
30	6	0	-7.499273	0.262732	0.228963
31	6	0	-9.190539	-1.434115	-0.182125
32	6	0	-10.177441	-0.476058	0.073948
33	6	0	-9.826640	0.837727	0.404045
34	6	0	-8.486107	1.217839	0.484011
35	1	0	7.540043	0.348093	-1.016337
36	1	0	6.209930	-2.291033	-1.601036
37	1	0	5.804066	-0.705090	-2.265604
38	1	0	7.558640	-1.821870	1.103225
39	1	0	8.535701	-2.283165	-0.948744
40	1	0	7.345442	1.191249	1.368563
41	1	0	8.896144	0.315755	1.232773
42	1	0	8.106297	0.633536	3.471439
43	1	0	4.490091	-2.014770	-0.101860
44	1	0	2.498060	-1.447020	-0.037645
45	1	0	3.568393	3.102013	-0.951120
46	1	0	-1.085411	1.793907	-0.397803
47	1	0	-3.683084	-2.042924	-0.423962
48	1	0	-5.588708	2.417473	0.766019
49	1	0	-3.141947	2.080324	0.677393
50	1	0	-6.546305	-2.743673	0.361281
51	1	0	-6.569096	-2.313488	-1.343567
52	1	0	-9.470182	-2.452720	-0.437949
53	1	0	-10.605641	1.568705	0.599797

54	1	0	-8.220331	2.239539	0.740372
55	1	0	-11.225583	-0.754365	0.016187

4.8.7.3. Optimized Structure and Cartesian Coordinates for Cyanofluorenyl-Based Nucleoside

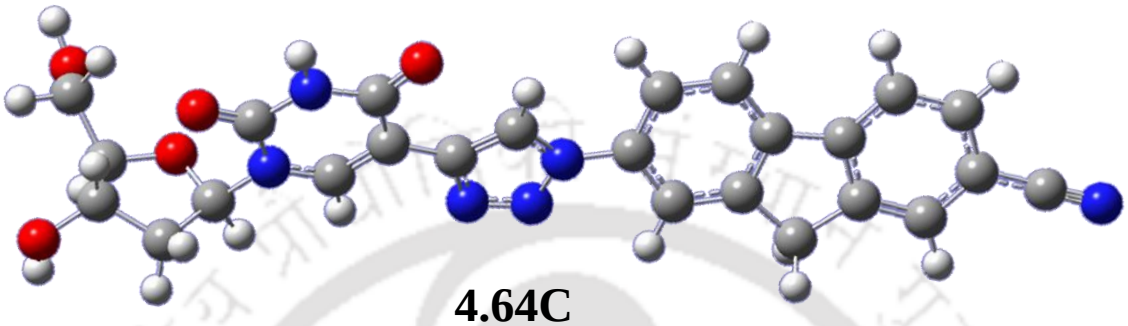

4.64C

E(RB3LYP) = -1669.35253833 a.u.;

Standard orientation:

Center Number	Atomic Number	Atomic Type	Coordinates (Angstroms) X	Y	Z
1	6	0	-5.413557	-2.901219	0.726647
2	6	0	-4.355913	-1.805922	0.608018
3	8	0	-6.343275	-1.025621	-0.306236
4	6	0	-6.540075	-2.424951	-0.175052
5	8	0	-4.903762	-4.160769	0.285374
6	6	0	-7.927441	-2.710591	0.368288
7	8	0	-8.905471	-2.333855	-0.602156
8	6	0	-4.941391	-0.821659	-0.411577
9	6	0	-2.523596	1.983373	-0.047016
10	6	0	-3.115167	0.777912	-0.216105
11	7	0	-4.448882	0.556956	-0.226002
12	6	0	-5.313066	1.620736	-0.094677
13	7	0	-4.755213	2.865076	0.085710
14	6	0	-3.415125	3.161426	0.129889
15	8	0	-3.024130	4.306711	0.301957
16	8	0	-6.515888	1.513959	-0.128745
17	6	0	-1.058562	2.130021	-0.024539
18	7	0	-0.353207	3.266302	0.087136
19	7	0	0.913851	2.920673	0.077172
20	7	0	1.095796	1.595136	-0.030915
21	6	0	-0.157063	1.072203	-0.100759
22	6	0	2.342127	0.892598	-0.055122
23	6	0	3.558889	1.597081	0.032522
24	6	0	4.763426	0.896308	0.016253
25	6	0	4.756807	-0.499843	-0.084363
26	6	0	3.571517	-1.225725	-0.177002
27	6	0	2.373452	-0.513584	-0.161803
28	6	0	6.160078	1.469602	0.102672
29	6	0	6.948837	0.180526	0.038580

30	6	0	6.138549	-0.957028	-0.068570
31	6	0	8.333265	0.035589	0.074767
32	6	0	8.881267	-1.255598	0.004075
33	6	0	8.053232	-2.385089	-0.099862
34	6	0	6.664644	-2.247211	-0.137597
35	6	0	10.306685	-1.429965	0.038728
36	7	0	11.474109	-1.578243	0.066020
37	1	0	-5.742245	-3.022762	1.784287
38	1	0	-3.363839	-2.204601	0.296624
39	1	0	-4.233499	-1.297304	1.594014
40	1	0	-6.435958	-2.881645	-1.189558
41	1	0	-4.687088	-4.091813	-0.628692
42	1	0	-8.129467	-2.135438	1.299274
43	1	0	-8.060668	-3.796291	0.576935
44	1	0	-9.747868	-2.359398	-0.182263
45	1	0	-4.648919	-1.144454	-1.442542
46	1	0	-2.493445	-0.116232	-0.361386
47	1	0	-5.399710	3.636908	0.194622
48	1	0	-0.352384	0.001925	-0.190178
49	1	0	3.578952	2.694444	0.117201
50	1	0	3.580563	-2.323445	-0.256126
51	1	0	1.449460	-1.105927	-0.232783
52	1	0	6.323319	1.997829	1.068425
53	1	0	6.384044	2.125712	-0.767771
54	1	0	8.979174	0.923180	0.157453
55	1	0	8.496178	-3.393124	-0.152725
56	1	0	6.007522	-3.126218	-0.218565

4.9. ^{1}H and ^{13}C NMR Spectra of Few Selected Nucleosides

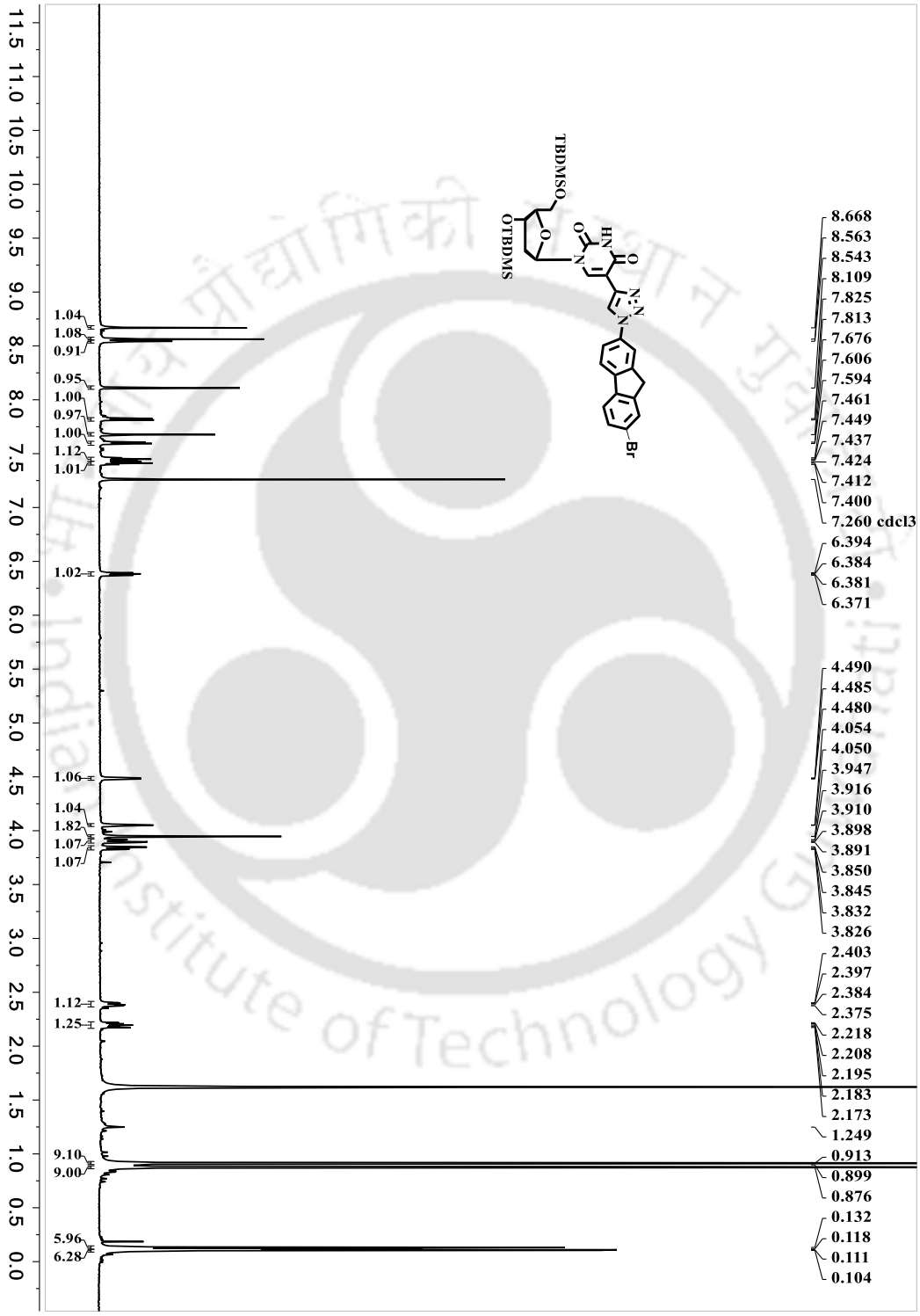

Figure 4.37. ^{1}H NMR spectra of synthesized compound **4.63B**

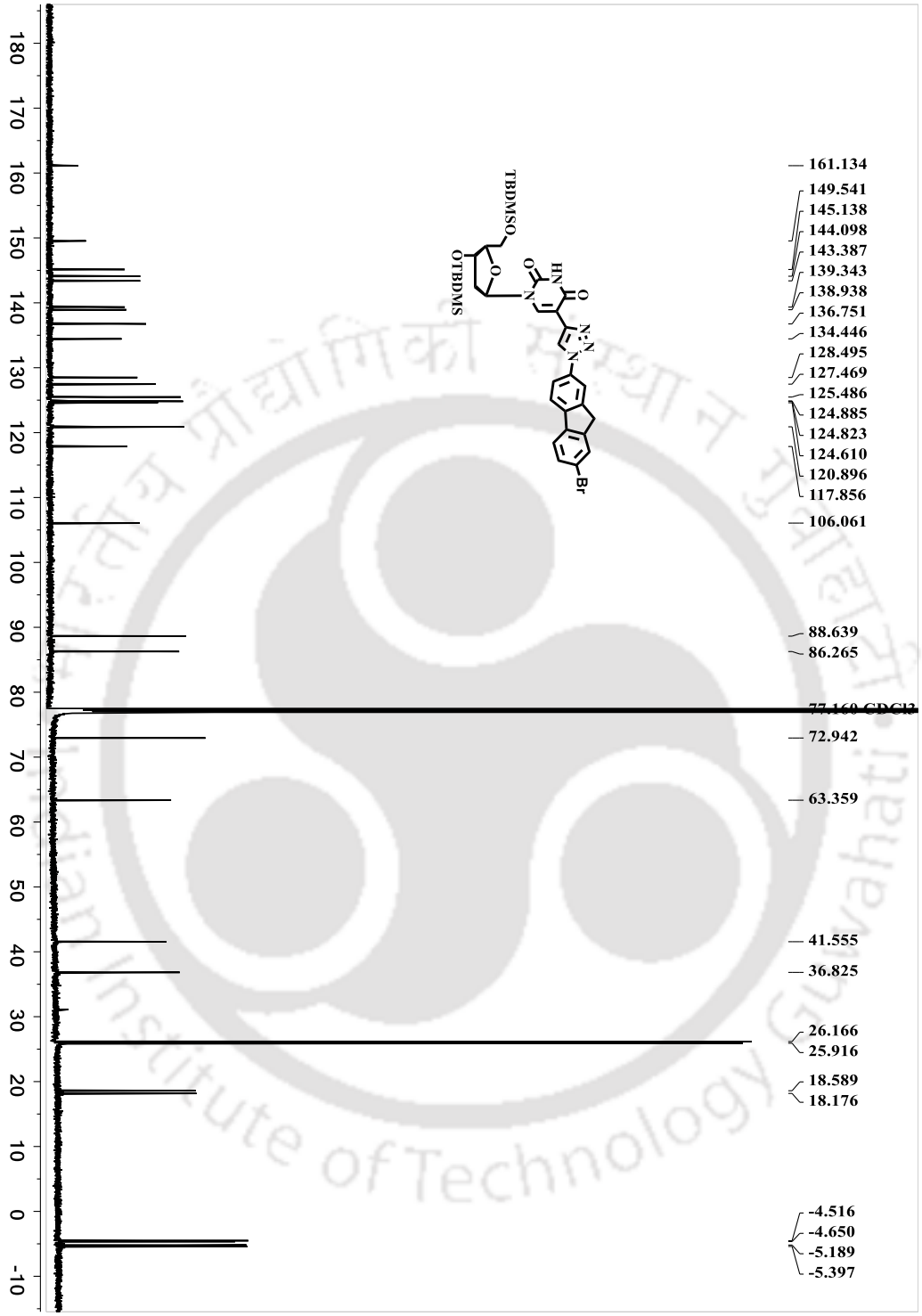

Figure 4.38: ^{13}C NMR spectra of synthesized compound **4.63B**

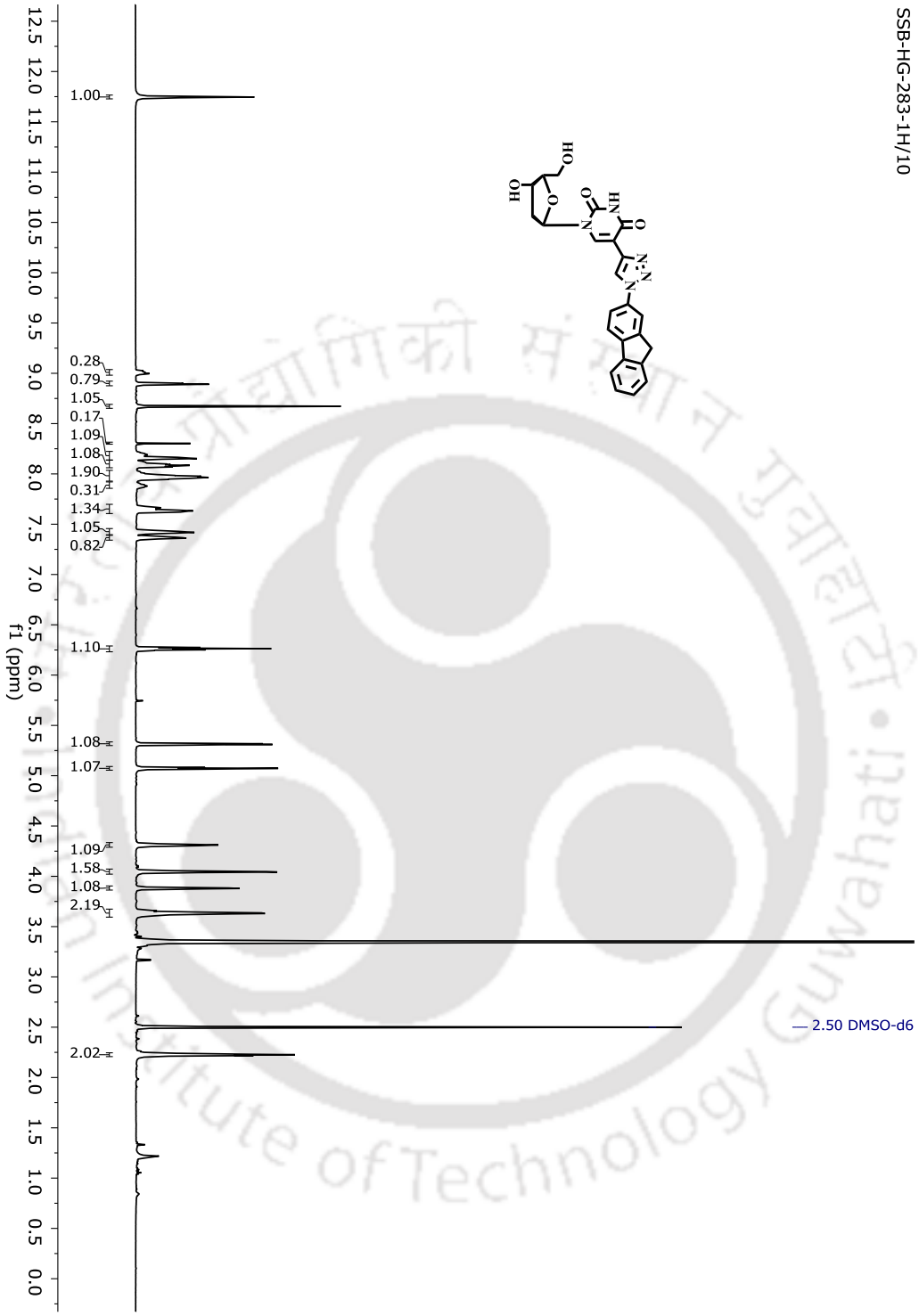

Figure 4.39: ^{1}H NMR spectra of synthesized compound **4.64A**

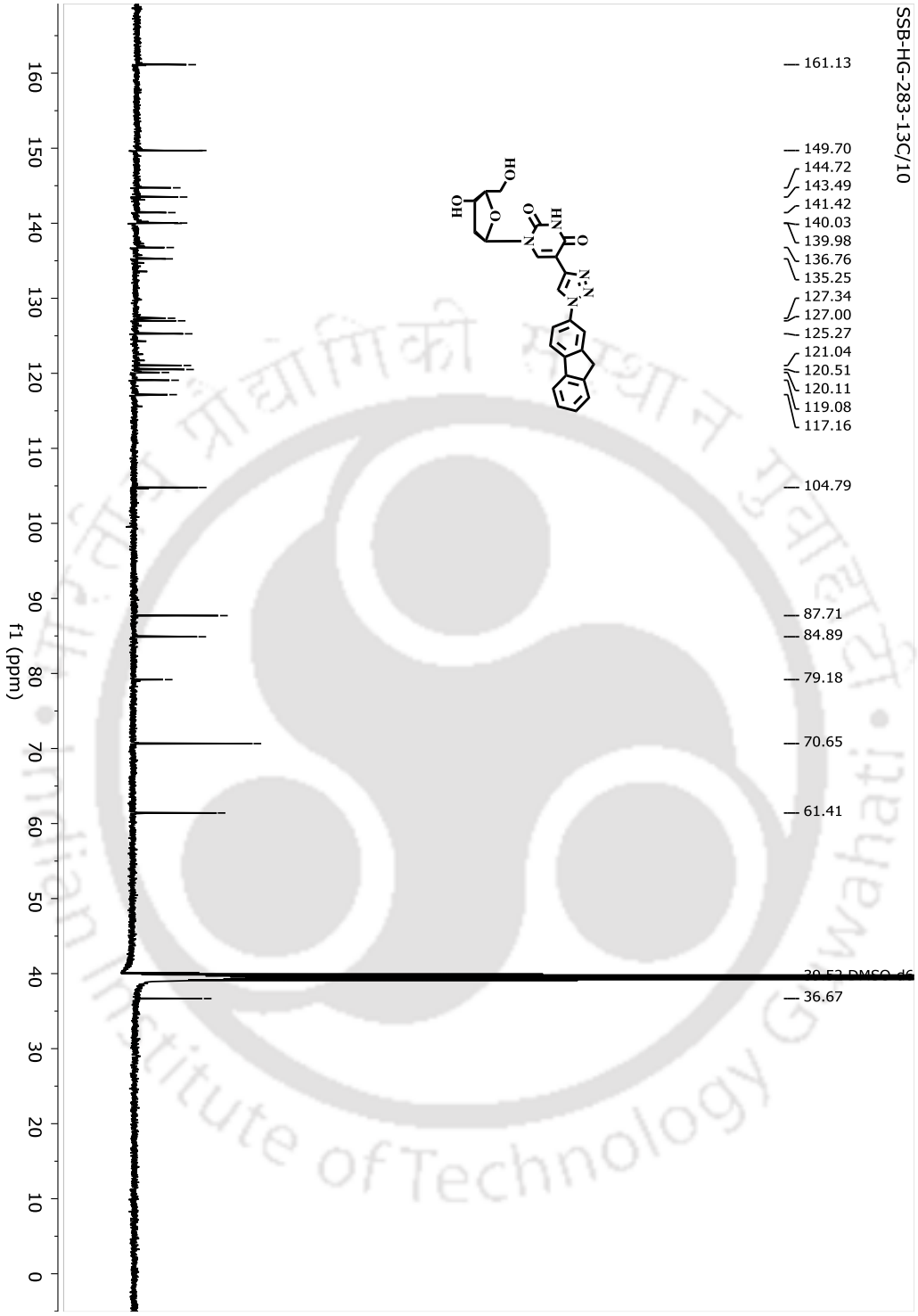

Figure 4.40: ^{13}C NMR spectra of synthesized compound **4.64A**

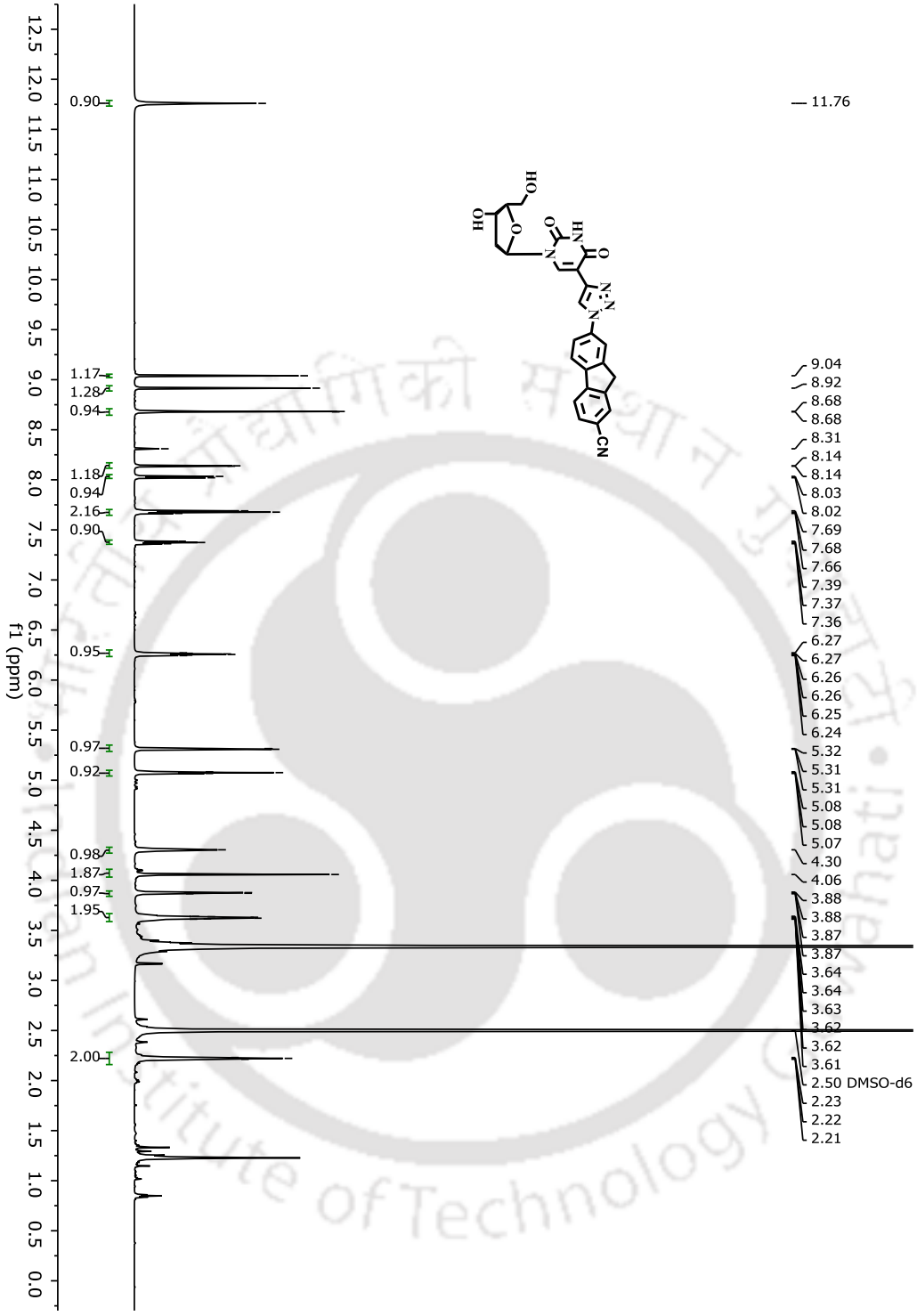

Figure 4.41: ^{1}H NMR spectra of synthesized compound **4.64A**

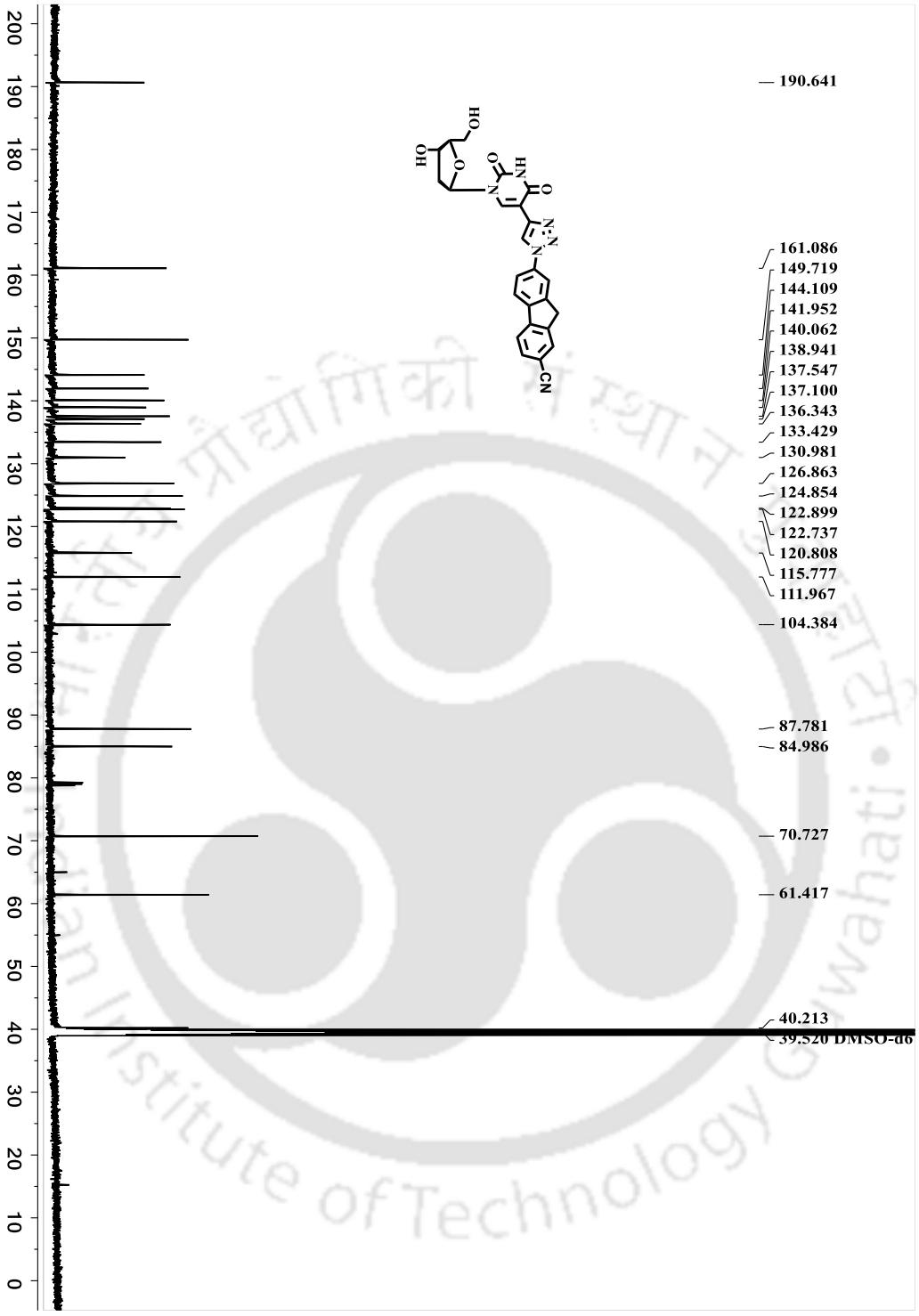

Figure 4.42: ^{13}C NMR spectra of synthesized compound **4.64C**

4.10. References

1. Kurdyukova, I. V.; Ishchenko, A. A., Organic dyes based on fluorene and its derivatives. *Russian Chemical Reviews* **2012,** *81* (3), 258-290.
2. Hernández, F. E.; Belfield, K. D.; Cohanoschi, I.; Balu, M.; Schafer, K. J., Three- and four-photon absorption of a multiphoton absorbing fluorescent probe. *Applied Optics* **2004,** *43* (28), 5394-5398.
3. Oar, M. A.; Serin, J. M.; Dichtel, W. R.; Fréchet, J. M. J.; Ohulchanskyy, T. Y.; Prasad, P. N., Photosensitization of Singlet Oxygen via Two-Photon-Excited Fluorescence Resonance Energy Transfer in a Water-Soluble Dendrimer. *Chemistry of Materials* **2005,** *17* (9), 2267-2275.
4. Rathore, K.; Lim, C. S.; Lee, Y.; Cho, B. R., Dual-color imaging of cytosolic and mitochondrial zinc ions in live tissues with two-photon fluorescent probes. *Organic & Biomolecular Chemistry* **2014,** *12* (21), 3406-3412.
5. Reinhardt, B. A.; Brott, L. L.; Clarson, S. J.; Dillard, A. G.; Bhatt, J. C.; Kannan, R.; Yuan, L.; He, G. S.; Prasad, P. N., Highly Active Two-Photon Dyes: Design, Synthesis, and Characterization toward Application. *Chemistry of Materials* **1998,** *10* (7), 1863-1874.
6. Yao, S.; Belfield, K. D., Two-Photon Fluorescent Probes for Bioimaging (Eur. J. Org. Chem. 17/2012). *European Journal of Organic Chemistry* **2012,** *2012* (17), 3199-3217.
7. Yue, X.; Yanez, C. O.; Yao, S.; Belfield, K. D., Selective Cell Death by Photochemically Induced pH Imbalance in Cancer Cells. *Journal of the American Chemical Society* **2013,** *135* (6), 2112-2115.
8. Zhang, H.; Fan, J.; Dong, H.; Zhang, S.; Xu, W.; Wang, J.; Gao, P.; Peng, X., Fluorene-derived two-photon fluorescent probes for specific and simultaneous bioimaging of endoplasmic reticulum and lysosomes: group-effect and localization. *Journal of Materials Chemistry B* **2013,** *1* (40), 5450-5455.
9. Belfield, K. D.; Bondar, M. V.; Frazer, A.; Morales, A. R.; Kachkovsky, O. D.; Mikhailov, I. A.; Masunov, A. E.; Przhonska, O. V., Fluorene-Based Metal-Ion Sensing Probe with High Sensitivity to Zn2+ and Efficient Two-Photon Absorption. *The Journal of Physical Chemistry B* **2010,** *114* (28), 9313-9321.
10. Diao, H.; Guo, L.; Liu, W.; Feng, L., A novel polymer probe for Zn(II) detection with ratiometric fluorescence signal. *Spectrochimica Acta Part A: Molecular and Biomolecular Spectroscopy* **2018,** *196*, 274-280.
11. Ibrahimova, V.; Eda Kocak, M.; Önal, A. M.; Tuncel, D., Optical and electronic properties of fluorene-based copolymers and their sensory applications. *Journal of Polymer Science Part A: Polymer Chemistry* **2013,** *51* (4), 815-823.
12. Dey, G.; Venkateswarulu, M.; Vivekananthan, V.; Pramanik, A.; Krishnan, V.; Koner, R. R., Sub-Picomolar Recognition of Cr3+ through Bioinspired Organic–Inorganic Ensemble Utilization. *ACS Sensors* **2016,** *1* (6), 663-669.
13. dos Santos Carlos, F.; Nunes, M. C.; De Boni, L.; Machado, G. S.; Nunes, F. S., A novel fluorene-derivative Schiff-base fluorescent sensor for copper(II) in organic media. *Journal of Photochemistry and Photobiology A: Chemistry* **2017,** *348*, 41-46.
14. Bera, M. K.; Chakraborty, C.; Singh, P. K.; Sahu, C.; Sen, K.; Maji, S.; Das, A. K.; Malik, S., Fluorene-based chemodosimeter for "turn-on" sensing of cyanide by hampering ESIPT and live cell imaging. *Journal of Materials Chemistry B* **2014,** *2* (29), 4733-4739.

15. Li, L.; Zan, M.; Qie, X.; Miao, P.; Yue, J.; Chang, Z.; Wang, Z.; Bai, F.-Q.; Zhang, H.-X.; Ferri, J. K.; Dong, W.-F., A highly selective fluorescent probe for cyanide ion and its detection mechanism from theoretical calculations. *Talanta* **2018,** *185*, 1-6.
16. Li, Q.; Jia, Y.; Feng, Z.; Liu, F., A highly sensitive and selective fluorescent probe without quencher for detection of Pb2+ ions based on aggregation-caused quenching phenomenon. *RSC Advances* **2018,** *8* (68), 38929-38934.
17. Yao, S.; Ahn, H.-Y.; Wang, X.; Fu, J.; Van Stryland, E. W.; Hagan, D. J.; Belfield, K. D., Donor−Acceptor−Donor Fluorene Derivatives for Two-Photon Fluorescence Lysosomal Imaging. *The Journal of Organic Chemistry* **2010,** *75* (12), 3965-3974.
18. Liu, J.; Ding, D.; Geng, J.; Liu, B., PEGylated conjugated polyelectrolytes containing 2,1,3-benzoxadiazole units for targeted cell imaging. *Polymer Chemistry* **2012,** *3* (6), 1567-1575.
19. Aparicio-Ixta, L.; Ramos-Ortiz, G.; Pichardo-Molina, J. L.; Maldonado, J. L.; Rodríguez, M.; Tellez-Lopez, V. M.; Martinez-Fong, D.; Zolotukhin, M. G.; Fomine, S.; Meneses-Nava, M. A.; Barbosa-García, O., Two-photon excited fluorescence of silica nanoparticles loaded with a fluorene-based monomer and its cross-conjugated polymer: their application to cell imaging. *Nanoscale* **2012,** *4* (24), 7751-7759.
20. Guo, J.; Han, L.; Bao, X.; Du, Z.; Wang, T.; Yang, R., Multiple Logic Functions Based on Small Molecular Fluorene Derivatives and Their Application in Cell Imaging. *The Journal of Physical Chemistry C* **2014,** *118* (18), 9368-9376.
21. Liu, Y.; Wang, H.; Tao, P.; Liu, X.; Liu, Y.; Dong, Q.; Liang, W.; Zhao, Q.; Wong, W.-Y.; Xu, B., Poly[(9,9-dioctyl-fluorenyl-2,7-diyl)-co-fluorenone]-based orange fluorescence probe for cellular imaging. *Tetrahedron* **2016,** *72* (18), 2287-2292.
22. Xiao, H.; Zhang, Y.; Zhang, W.; Li, S.; Xu, R., Two novel dyes containing spirobifluorene and triphenylamine: Synthesis, one- and two-photon excited fluorescence and applications as probes for silver ions, water and cell imaging. *Sensors and Actuators B: Chemical* **2016,** *233*, 469-475.
23. Shaya, J.; Collot, M.; Bénailly, F.; Mahmoud, N.; Mély, Y.; Michel, B. Y.; Klymchenko, A. S.; Burger, A., Turn-on Fluorene Push–Pull Probes with High Brightness and Photostability for Visualizing Lipid Order in Biomembranes. *ACS Chemical Biology* **2017,** *12* (12), 3022-3030.
24. Liu, X.; Ardizzone, A.; Sui, B.; Anzola, M.; Ventosa, N.; Liu, T.; Veciana, J.; Belfield, K. D., Fluorenyl-Loaded Quatsome Nanostructured Fluorescent Probes. *ACS Omega* **2017,** *2* (8), 4112-4122.
25. Sun, X.; Wang, Y.; Lei, Y., Fluorescence based explosive detection: from mechanisms to sensory materials. *Chemical Society Reviews* **2015,** *44* (22), 8019-8061.
26. Zhang, Y.; Fu, Y.-Y.; Zhu, D.-F.; Xu, J.-Q.; He, Q.-G.; Cheng, J.-G., Recent advances in fluorescence sensor for the detection of peroxide explosives. *Chinese Chemical Letters* **2016,** *27* (8), 1429-1436.
27. Shaw, P. E.; Chen, S. S. Y.; Wang, X.; Burn, P. L.; Meredith, P., High-Generation Dendrimers with Excimer-like Photoluminescence for the Detection of Explosives. *The Journal of Physical Chemistry C* **2013,** *117* (10), 5328-5337.
28. Cavaye, H.; Shaw, P. E.; Wang, X.; Burn, P. L.; Lo, S.-C.; Meredith, P., Effect of Dimensionality in Dendrimeric and Polymeric Fluorescent Materials for Detecting Explosives. *Macromolecules* **2010,** *43* (24), 10253-10261.
29. Yang, J.; Aschemeyer, S.; Martinez, H. P.; Trogler, W. C., Hollow silica nanospheres containing a silafluorene–fluorene conjugated polymer for aqueous TNT and RDX detection. *Chemical Communications* **2010,** *46* (36), 6804-6806.

30. Leng, H.; Wu, W., Synthesis of a novel fluorene-based conjugated polymer with pendent bulky caged adamantane moieties and its application in the detection of trace DNT explosives. *Reactive and Functional Polymers* **2012,** *72* (3), 206-211.
31. Wang, Y.; Gao, Y.; Chen, L.; Fu, Y.; Zhu, D.; He, Q.; Cao, H.; Cheng, J.; Zhang, R.; Zheng, S.; Yan, S., Fluorescent diphenylfluorene-pyrenyl copolymer with dibenzothiophene-S,S-dioxide and adamantane units for explosive vapor detection. *RSC Advances* **2015,** *5* (7), 4853-4860.
32. Mallet, C.; Bolduc, A.; Bishop, S.; Gautier, Y.; Skene, W. G., Unusually high fluorescence quantum yield of a homopolyfluorenylazomethine – towards a universal fluorophore. *Physical Chemistry Chemical Physics* **2014,** *16* (44), 24382-24390.
33. Chen, L.; Gao, Y.; Wang, Y.; He, C.; Zhu, D.; He, Q.; Cao, H.; Cheng, J., Femtogram Level Detection of Nitrate Ester Explosives via an 8-Pyrenyl-Substituted Fluorene Dimer Bridged by a 1,6-Hexanyl Unit. *ACS Applied Materials & Interfaces* **2014,** *6* (11), 8817-8823.
34. Chen, L.; Gao, Y.; Fu, Y.; Zhu, D.; He, Q.; Cao, H.; Cheng, J., Borate ester endcapped fluorescent hyperbranched conjugated polymer for trace peroxide explosive vapor detection. *RSC Advances* **2015,** *5* (38), 29624-29630.
35. Ni, J. C.; Yan, J.; Zhang, L. J.; Shang, D.; Du, N.; Li, S.; Zhao, J. X.; Wang, Y.; Xing, Y. H., Bifunctional fluorescent quenching detection of 2,4,6-trinitrophenol (TNP) and acetate ions via 4,4′-(9,9-dimethyl-9H-fluorene-2,7-diyl)dibenzoic acid. *Tetrahedron Letters* **2016,** *57* (45), 4978-4982.
36. Singh, V.; Wang, S.; Kool, E. T., Genetically Encoded Multispectral Labeling of Proteins with Polyfluorophores on a DNA Backbone. *Journal of the American Chemical Society* **2013,** *135* (16), 6184-6191.
37. Los, G. V.; Encell, L. P.; McDougall, M. G.; Hartzell, D. D.; Karassina, N.; Zimprich, C.; Wood, M. G.; Learish, R.; Ohana, R. F.; Urh, M.; Simpson, D.; Mendez, J.; Zimmerman, K.; Otto, P.; Vidugiris, G.; Zhu, J.; Darzins, A.; Klaubert, D. H.; Bulleit, R. F.; Wood, K. V., HaloTag: A Novel Protein Labeling Technology for Cell Imaging and Protein Analysis. *ACS Chemical Biology* **2008,** *3* (6), 373-382.
38. Cho, Y. H.; Woo, K. S.; Hwang, T. G., Synthesis and Photophysical Study of 2′-Deoxyuridines Labeled with Fluorene Derivatives. *Molecules* **2012,** *17* (10).
39. Hwang, G. T.; Seo, Y. J.; Kim, B. H., A Highly Discriminating Quencher-Free Molecular Beacon for Probing DNA. *Journal of the American Chemical Society* **2004,** *126* (21), 6528-6529.
40. Lee, J.; Cho, H. Y.; Hwang, G. T., Highly Efficient Quencher-Free Molecular Beacon Systems Containing 2-Ethynyldibenzofuran- and 2-Ethynyldibenzothiophene-Labeled 2′-Deoxyuridine Units. *ChemBioChem* **2013,** *14* (11), 1353-1362.
41. Ryu, J. H.; Heo, J. Y.; Bang, E.-K.; Hwang, G. T.; Kim, B. H., Quencher-free linear beacon systems containing 2-ethynylfluorenone-labeled 2′-deoxyuridine units. *Tetrahedron* **2012,** *68* (1), 72-78.
42. Ryu, J. H.; Seo, Y. J.; Hwang, G. T.; Lee, J. Y.; Kim, B. H., Triad base pairs containing fluorene unit for quencher-free SNP typing. *Tetrahedron* **2007,** *63* (17), 3538-3547.
43. Kim, M. J.; Seo, Y.; Hwang, G. T., Synthesis and photophysical properties of 2′-deoxyguanosine derivatives labeled with fluorene and fluorenone units: toward excimer probes. *RSC Advances* **2014,** *4* (23), 12012-12017.
44. Lee, J. W.; Son, Y.-s.; Lee, J.-Y.; Kim, M. H.; Woo, S.-K.; Lee, K. C.; Lee, Y. J.; Hwang, G. T., pH-sensitive fluorescent deoxyuridines labeled with 2-aminofluorene derivatives. *Tetrahedron* **2016,** *72* (36), 5595-5601.
45. Dziuba, D.; Pospíšil, P.; Matyašovský, J.; Brynda, J.; Nachtigallová, D.; Rulíšek, L.; Pohl, R.; Hof, M.; Hocek, M., Solvatochromic fluorene-linked nucleoside and DNA as

color-changing fluorescent probes for sensing interactions. *Chemical Science* **2016,** *7* (9), 5775-5785.

46. M. J. Frisch, G. W. T., H. B. Schlegel, G. E. Scuseria, M. A. Robb, J. R. Cheeseman, G. Scalmani, V. Barone, B. Mennucci, G. A. Petersson, H. Nakatsuji, M. Caricato, X. Li, H. P. Hratchian, A. F. Izmaylov, J. Bloino, G. Zheng, J. L. Sonnenberg, M. Hada, M. Ehara, K. Toyota, R. Fukuda, J. Hasegawa, M. Ishida, T. Nakajima, Y. Honda, O. Kitao, H. Nakai, T. Vreven, J. A. Montgomery, Jr., J. E. Peralta, F. Ogliaro, M. Bearpark, J. J. Heyd, E. Brothers, K. N. Kudin, V. N. Staroverov, R. Kobayashi, J. Normand, K. Raghavachari, A. Rendell, J. C. Burant, S. S. Iyengar, J. Tomasi, M. Cossi, N. Rega, J. M. Millam, M. Klene, J. E. Knox, J. B. Cross, V. Bakken, C. Adamo, J. Jaramillo, R. Gomperts, R. E. Stratmann, O. Yazyev, A. J. Austin, R. Cammi, C. Pomelli, J. W. Ochterski, R. L. Martin, K. Morokuma, V. G. Zakrzewski, G. A. Voth, P. Salvador, J. J. Dannenberg, S. Dapprich, A. D. Daniels, Ö. Farkas, J. B. Foresman, J. V. Ortiz, J. Cioslowski, and D. J. Fox, Gaussian 09. *Gaussian, Inc., Wallingford CT* **2009**.
47. Bag, S. S.; Jana, S.; Pradhan, M. K., Synthesis, photophysical properties of triazolyl-donor/acceptor chromophores decorated unnatural amino acids: Incorporation of a pair into Leu-enkephalin peptide and application of triazolylperylene amino acid in sensing BSA. *Bioorganic & Medicinal Chemistry* **2016,** *24* (16), 3579-3595.
48. Bag, S. S.; Kundu, R., Installation/Modulation of the Emission Response via Click Reaction. *The Journal of Organic Chemistry* **2011,** *76* (9), 3348-3356.
49. Bucevicius, J.; Skardziute, L.; Dodonova, J.; Kazlauskas, K.; Bagdziunas, G.; Jursenas, S.; Tumkevicius, S., 2,4-Bis(4-aryl-1,2,3-triazol-1-yl)pyrrolo[2,3-d]pyrimidines: synthesis and tuning of optical properties by polar substituents. *RSC Advances* **2015,** *5* (48), 38610-38622.
50. Fromherz, P., Monopole-Dipole Model for Symmetrical Solvatochromism of Hemicyanine Dyes. *The Journal of Physical Chemistry* **1995,** *99* (18), 7188-7192.
51. Nagarajan, N.; Velmurugan, G.; Venuvanalingam, P.; Renganathan, R., Tunable single and dual emission behavior of imidazole fluorophores based on D-π-A architecture. *Journal of Photochemistry and Photobiology A: Chemistry* **2014,** *284*, 36-48.
52. Morris, G. M.; Goodsell, D. S.; Halliday, R. S.; Huey, R.; Hart, W. E.; Belew, R. K.; Olson, A. J., Automated docking using a Lamarckian genetic algorithm and an empirical binding free energy function. *Journal of Computational Chemistry* **1998,** *19* (14), 1639-1662.
53. Morris, G. M.; Huey, R.; Lindstrom, W.; Sanner, M. F.; Belew, R. K.; Goodsell, D. S.; Olson, A. J., AutoDock4 and AutoDockTools4: Automated docking with selective receptor flexibility. *Journal of Computational Chemistry* **2009,** *30* (16), 2785-2791.
54. Chandrasekharam, M.; Rajkumar, G.; Srinivasa Rao, C.; Suresh, T.; Yella Reddy, P.; Yum, J.-H.; Khaja Nazeeruddin, M.; Graetzel, M., A molecularly engineered fluorene-substituted Ru-complex for efficient mesoscopic dye-sensitized solar cells. *Advances in Natural Sciences: Nanoscience and Nanotechnology* **2011,** *2* (3), 035016.
55. Omer, K. M.; Ku, S.-Y.; Chen, Y.-C.; Wong, K.-T.; Bard, A. J., Electrochemical Behavior and Electrogenerated Chemiluminescence of Star-Shaped D−A Compounds with a 1,3,5-Triazine Core and Substituted Fluorene Arms. *Journal of the American Chemical Society* **2010,** *132* (31), 10944-10952.
56. Heinrich, D.; Wagner, T.; Diederichsen, U., Synthesis and DNA Incorporation of an Ethynyl-Bridged Cytosine C-Nucleoside as Guanosine Surrogate. *Organic Letters* **2007,** *9* (25), 5311-5314.
57. Semioshkin, A.; Ilinova, A.; Lobanova, I.; Bregadze, V.; Paradowska, E.; Studzińska, M.; Jabłońska, A.; Lesnikowski, Z. J., Synthesis of the first conjugates of 5-ethynyl-2′-

deoxyuridine with closo-dodecaborate and cobalt-bis-dicarbollide boron clusters. *Tetrahedron* **2013,** *69* (37), 8034-8041.

58. Reddy, M. R.; Shibata, N.; Kondo, Y.; Nakamura, S.; Toru, T., Design, Synthesis, and Spectroscopic Investigation of Zinc Dodecakis(trifluoroethoxy)phthalocyanines Conjugated with Deoxyribonucleosides. *Angewandte Chemie International Edition* **2006,** *45* (48), 8163-8166.
59. Reichmann, M. E.; Rice, S. A.; Thomas, C. A.; Doty, P., A Further Examination of the Molecular Weight and Size of Desoxypentose Nucleic Acid. *Journal of the American Chemical Society* **1954,** *76* (11), 3047-3053.

Chapter 5

STUDIES ON THE AGGREGATION INDUCED FLUORESCENCE EMISSION PROPERTY OF PYRENYLAMIDO TRIAZOLYL AROMATIC AMINO ACID AND ITS INTERACTION WITH SHORT ABASIC DNAs

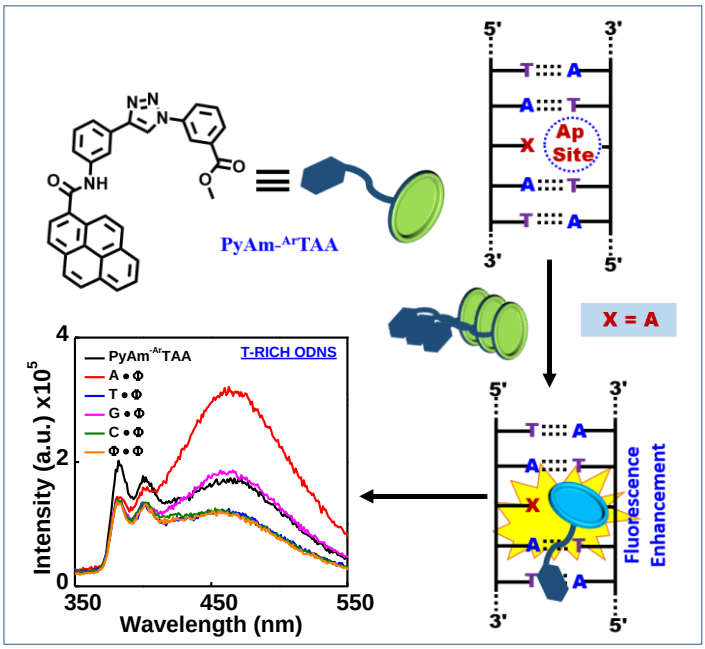

5.1. Introduction: Aggregation-Induced Emission

Biological processes are essential for life to exist in organisms. These processes are recognized as a series of biochemical reactions, events which are vital for normal physiological functions of a living organism. The investigation of various biological processes demands fast, sensitive and reliable techniques. One of the most suitable and popular methods fulfilling these features is the fluorescence-based techniques. The development of fluorescent molecules and techniques has a great impact on unraveling the structure and functions of biomolecules. Successful implementation of these techniques often relies on the fluorophores with high photostability, large Stokes shift, high quantum efficiency, and high signal-to-noise ratio. However, many organic fluorophores experience aggregation-caused quenching (ACQ) effect due to π-π stacking when present in high concentration or in the condensed phase.[1-4] The quenching of fluorescence on aggregation is most probably due to the decay of aggregates in the excited states via non-radiative pathways. Due to the possible detrimental effect of ACQ phenomenon, it is often recommended to utilize fluorophores at low concentration in fluorometric assays. The use of dilute solutions have certain drawbacks such as weak emissions which ultimately lead to poor fluorescence signal, low signal-to-noise ratio and poor sensitivity of the fluorescence tools.[5-7] In the worst case, ACQ might happen in very dilute solutions also. For example, in a bioassay, the concentration of small fluorophores can increase locally due to their accumulation in the hydrophobic cavities of biomolecules leading to ACQ.[8-10] Thus, ACQ phenomenon is a serious threat for the applications of fluorophores in various research fields.

In 2001, Tang and co-workers described an unusual property of a silole, 1-methyl-1,2,3,4,5-pentaphenylsilole (MPPS) (**5.01 Figure 5.1**) which is non-fluorescent in solutions but exhibits strong fluorescence emission on aggregation.[11] They coined this phenomenon as aggregation-induced emission (AIE) and molecules exhibiting this unique property is generally called as AIEgens. They have reported several silole fluorophores which exhibited AIE effect similar to MPPS (**Figure 5.1**).[12]

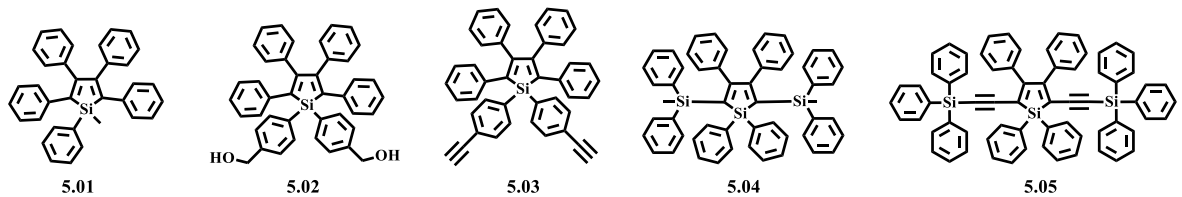

Figure 5.1. Examples of silole fluorophores reported by Tang and co-workers.

The effect of AIE is totally opposite to that of the ACQ. This phenomenon has the potential to break the limitations set by the ACQ effect in various research areas. In bioassays and experiments, implementation of AIE fluorophores not only would allow us to take advantages of aggregation but also to use these fluorophores in any concentration for the development of light up fluorescent probes for the investigation of biological processes. The family of AIE fluorophores is not limited to siloles. There are numerous examples of AIE fluorophores present in literature and many of them have been designed and synthesized based on scaffolds tetraphenylethylene (TPE), hexaphenylsilole (HPS) and distyrylanthracene.[13, 14]

The mechanism of AIE is not fully understood and depends on many factors including restriction of intramolecular rotation (RIR),[15-17] restriction of intramolecular vibrations (RIV),[18, 19] restriction of intramolecular motion (RIM),[18] intramolecular charge transfer (ICT),[20] twisted intramolecular charge transfer (TICT),[12, 21-23] and J-aggregate formation.[24] Upon aggregation, these factors most probably restrict the non-radiative decay of these fluorophores from their excited states which in turn favor strong radiative decay resulting in high photostability, large Stokes shift and hence high signal to noise ratio. AIE molecules find widespread applications in various research areas such as sensors, organic light-emitting diodes (OLEDs), bioimaging etc.[21, 23, 25-28] Use of AIE molecules as fluorescent probes in biomedical science is definitely going to have a great impact on the better understanding of biological processes and development of new drugs candidates, therapies, etc. Recent years, AIE probes have drawn much attention from researchers and a lot of works have been reviewed. Some recent examples of AIE probes used for investigation of various biological processes and diagnosis of diseases have been shown in **Figure 5.2**.[29-40]

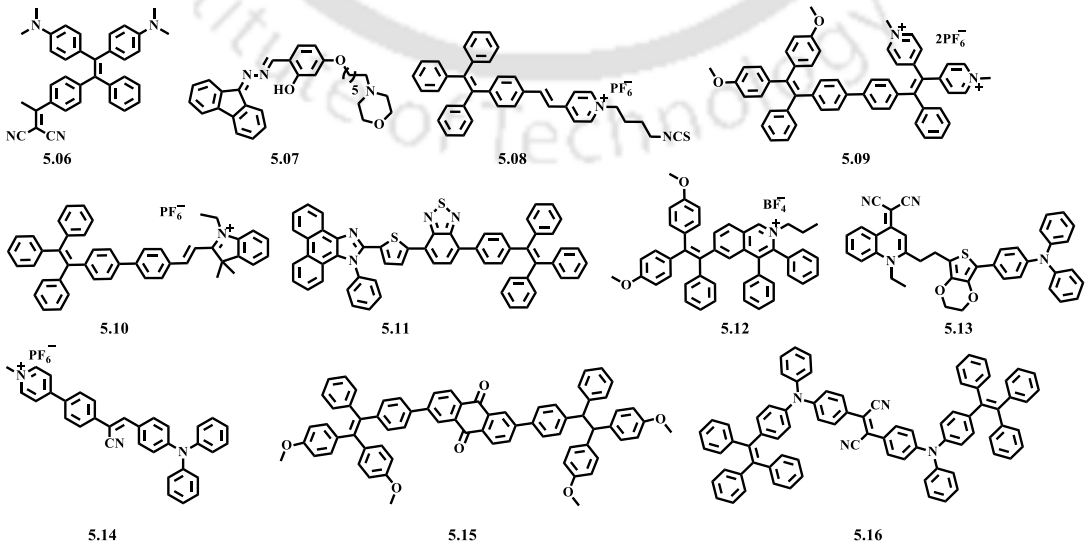

Figure 5.2. Examples of AIE probes used in biomedical chemistry.

5.1.1. Study to Prove Aggregation-Induced Emission

UV-Visible and Fluorescence Titration Study: AIE molecules are generally non-fluorescent in a solvent wherein the dissolution is high. However, they exhibit strong fluorescence emission on aggregation in a poor solubilizing solvent or in the solid state. Therefore, titration of AIE molecules dissolved in a particular solvent where the dissolution of organic molecules is poor such as water is often utilized to induce aggregation.[12, 15, 41-43] The formation of aggregates i.e. the AIE characteristic of a particular molecule would be observable from the UV-visible and fluorescence spectroscopic study. According to the literature, the formation of aggregations in water often is indicated by the appearance of extended absorption bands and the level-off tails in the visible region. This is due to the Mie scattering caused by the nanosized particles.[41, 44] Water is a poor solvent for luminogens and ordinary organic fluorescent molecules exhibit quenched fluorescence in the presence of water due to ACQ effect. In a particular organic solvent-water titration of a luminogen, a strong emission observed in the presence of high water percentage indicate AIE characteristics.[12]

Variable Temperature Fluorescence Study: It is reported that the restriction of intramolecular rotation (RIR) plays a major role in AIE.[15-17]According to the literature, the RIR in AIE molecules makes them highly emissive most possibly by blocking nonradiative pathways in their excited state.[15] Therefore, RIR dependent AIE molecules should exhibit high emission in conditions such as high viscosity, low temperature where intramolecular rotation is restricted. Therefore, an increase in temperature of an AIE system should accompany a decrease in fluorescence emission intensity due to the disaggregation process within the system.[45] Thus, the variable temperature fluorescence emission study of an AIE molecule in a high viscous solvent such as glycerol is a common practice for a demonstration of its AIE property.[12, 14, 42]

CD Spectroscopic Measurement: Circular dichroism (CD) spectroscopy is widely used for the study of chirality of small as well as large biological molecules. It is known that chirality can be achieved even from achiral molecules by a crystallization process where a restriction to their conformational flexibility and rotation is imposed.[21] Thus AIE molecules can obtain chiral structures in the solid state. Therefore, an achiral AIE molecule which is CD inactive in the solution can become CD active in solid state due to the acquired chirality via RIR/RIV process. For example, the bisethynylated TPE derivative (**5.17**, **Figure 5.3**) is CD active in the solid state whereas completely CD inactive in solution.[21] The crystal structure of TPE derivative

(5.17) revealed the formation of atropisomeric crystals of its cis-isomer due to which strong cotton effects were observed in its solid-state CD spectrum. Therefore, AIE property of a molecule can be checked by using CD spectroscopy implying that it can form atropisomeric crystals under suitable conditions.

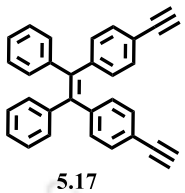

5.17

Figure 5.3. The structure of a bisethynylated TPE derivative.

5.1.2. Various Types of Probes Showing Aggregation-Induced Emission

The research interest in AIE systems is growing exponentially in recent years due to their widespread applications in various research areas. A large number of AIE molecules or AIEgens have been developed and published since the discovery of AIE phenomena. AIE family constitutes diverse structured molecules ranging from pure hydrocarbons to heteroatomic compounds, from small molecules to macromolecules and from organic to inorganic or organometallics. A brief description of various types of AIE probes has been discussed below.

Pure Hydrocarbon-Based AIEgens: The AIEgens containing only hydrocarbons in their chemical structures are belong to this category. This category is a very important class of AIEgens which provides simpler structural systems when compared to other AIEgens with heteroatoms. Due to the simple structures of this type of AIEgens, the study of their chemical, photophysical properties are relatively easier and therefore, their mechanism of action in an experimental sample is easily predictable. Moreover, these AIEgens can be utilized as building blocks for the synthesis of macromolecular AIEgens. For example, tetraphenylethylene (TPE) (**5.18**, **Figure 5.4**) is extensively used for the mechanistic studies and macromolecules construction.[46-51] Some of the examples of this type of AIEgens are shown in **Figure 5.4**.

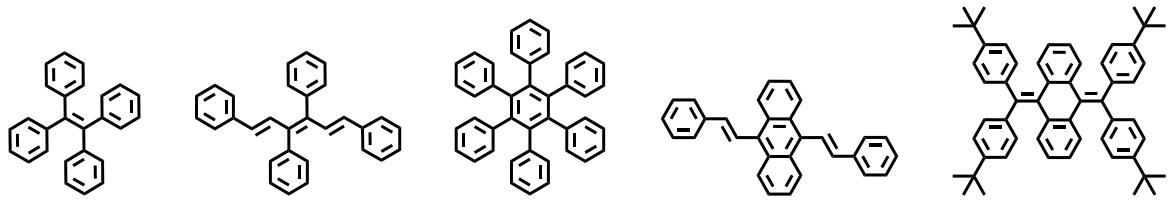

5.18 **5.19** **5.20** **5.21** **5.22**

Figure 5.4. Examples of pure hydrocarbon-based AIEgens.[52-55]

Heteroatom-Containing AIEgens: The application of pure hydrocarbon AIEgens is limited in various research areas due to their limited number and variations. Incorporation of heteroatoms in an AIE system provides the possibility to construct a variety of AIEgens and thus expand the scope of AIEgens. Since, a large number of heteroatoms available for incorporation in an organic system, this class of AIEgens consists of molecules with great structural diversity. For example, such type of AIEgens includes molecules derived from pentacyclics,[56-61] boron compounds,[62-66] Schiff bases,[17, 67, 68] nitrile compounds[69-73] and miscellaneous compounds containing oxygen, nitrogen, sulfur and phosphorous.[74-80] Incorporation of heteroatoms is definitely beneficial for the development of AIEgens with new properties. For example, incorporation of oxygen and nitrogen atoms enables processes like intramolecular hydrogen bonding and ESIPT, which might be associated with RIR to provide excellent AIE properties.[81-84] Some examples of such types of AIEgens are shown in **Figure 5.5**.

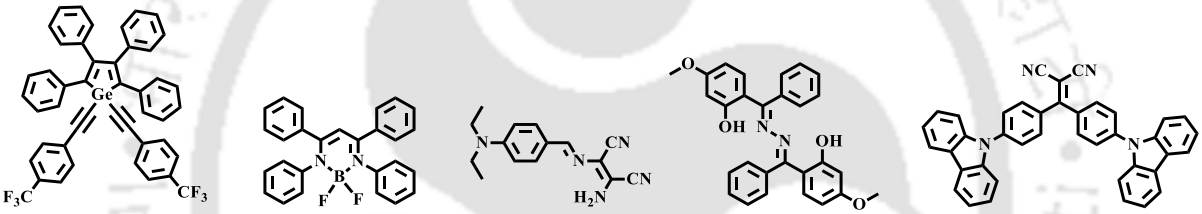

5.23 5.24 5.25 5.26 5.27

Figure 5.5. Examples of heteroatom-containing AIEgens.[56, 67, 71, 85, 86]

Macromolecular AIEgens: After the successful development of small structured AIEgens, construction of macromolecules with AIE properties become one of the interesting topics in AIE research. Small AIEgens have several shortcomings. As for example, the possibilities like adjustment of molecular structure, topology, morphology, and functionalities are sometimes harder to realize or achieve in small AIEgens when compared to macromolecular AIEgens.[14, 23] In addition, macromolecular AIEgens can be processed by simpler processes like spin-coating or static coating in comparison to tedious processes like vacuum vapor deposition utilized for processing of small AIEgens.[14] Therefore, AIE macromolecules could be a better platform for AIE research than other small AIEgens. Macromolecular AIEgens include various types of polymer systems such as main-chain polymers, [87-90] side-chain polymers, [91-96] and hyperbranched polymers, [97-100] as well as dendrimer systems [60, 101-104] and metal-organic frameworks (MOFs).[105-107] Some examples of macromolecular AIEgens are shown in **Figure 5.6**.

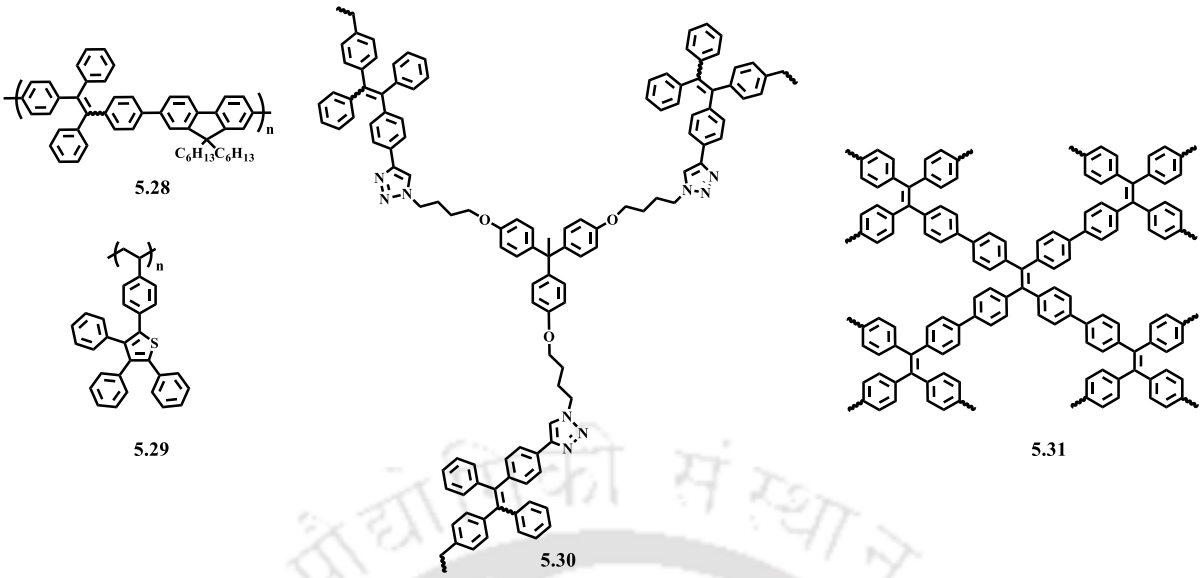

Figure 5.6. Examples of macromolecular AIEgens.[91, 99, 100, 108]

Metal Complex AIEgens: Metal complexes find widespread applications in the field of stoichiometry, catalysis, and optoelectronics.[109-111] There are many examples of metal complexes showing AIE properties are reported in the literature.[3, 12, 21] The presence of metals in an AIE complex system provides the possibility to take the advantages of metallic properties. As for example, by incorporating transition metals, phosphorescence can be easily accessed via minimization of intersystem crossing to triplet excited states.[111] Thus, the incorporation of metals into AIEgens could be highly beneficial for the development of new AIEgens with rich luminescent properties. There are several examples of metal complex AIEgens having metal ions with coordination number 2 (Au, Ag, Cu), [112-115] coordination number 4 (Cu, Zn, Pd, Pt), [116-120] Coordination number 6 (Ru, Re, Ir) [121-128] and coordination number 8 (Os) [129] are reported in the literature. Some examples of metal-complex AIEgens are shown in **Figure 5.7**.

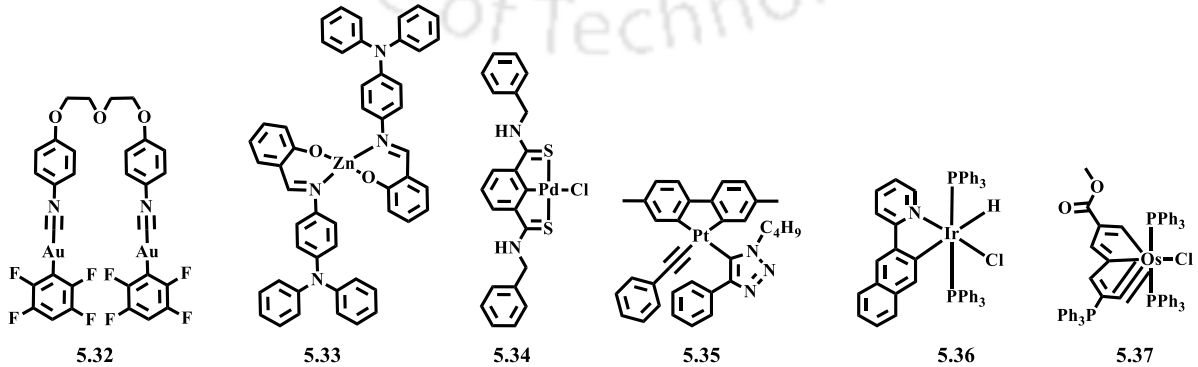

Figure 5.7. Examples of metal complex AIEgens.[117, 119, 121, 129, 130]

5.1.3. Applications of Probes Showing Aggregation-Induced Emission

5.1.3.1. Introduction

Luminescence and luminescent materials find widespread applications in the field of optoelectronics, chemical, and biological science.[12, 131-134] However, the practical applications of many traditional luminogens are limited due to the detrimental effect of ACQ phenomena. AIEgens defy the limit bound by the ACQ effect and expand the applications of luminescence to a great extent in various research fields. From the literature, we have seen that AIEgens constitute a diverse class of molecules. In this sense, the applications of AIEgens are unlimited. The rich features such as high brightness, exceptional photostability, high biocompatibility, efficient cellular uptake, and retention make AIEgens superior candidates for various optical, chemical and biological applications than other traditional luminogens.

5.1.3.2. Types of Applications

From the discovery of AIE to till date, tremendous research efforts have been carried out to demonstrate the possible applications of AIE in a wide range of research fields. In this context, we briefly outline the different types of applications of AIEgens below.

In Optoelectronic Devices: The AIEgens are promising candidates for the development of OLEDs due to their highly emissive property in the solid state. Despite the fact that there are several examples of OLEDs derived from traditional luminogens are found in the literature, many of them are poor blue light emitters.[135, 136] To address this limitation, several highly efficient blue emitters have been reported utilizing TPE as a building block.[137-140] AIEgens-derived red and near-infrared emitters are also known.[141, 142] AIEgens also have been utilized for the synthesis of light-emitting liquid crystals (LELCs).[143-146] Besides OLEDs and LELCs, AIEgens are successfully employed for the construction of materials with optical properties such as circularly polarized luminescence (CPL) [147-150] and optical waveguide effect.[151-153] CPL provides information related to the chirality of materials in the excited state. The chiral materials with efficient CPL have been utilized for biosensing and optoelectronic applications including stereoscopic optical information processing, display, and storage.[154-156] The utilization of CPL materials derived from AIEgens can be highly beneficial for such types of applications. A few examples of AIEgens utilized in optoelectronic devices are shown in **Figure 5.8** below.

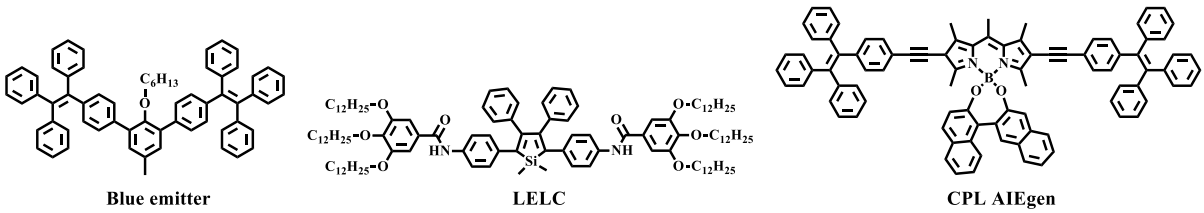

Figure 5.8. Examples of AIEgens utilized in optoelectronics.[138, 144, 150]

As Biological Probes: In biological areas, AIE probes are mainly utilized for sensing of biological molecules and imaging of cells. AIE effect and low background are two main merits of AIEgens due which they are promising candidates for the monitoring and sensing of various biological processes and molecules.[157-160] Taking advantages of these features, a variety of AIEgens has been successfully utilized for the sensing of small biological molecules such as monosaccharides,[161-164] amino acids,[165-167] amines,[168, 169] adenosine triphosphate[170-175] and biothiols.[176-180] In case of biological macromolecules also, diverse AIEgen systems have been established for detection and investigation of various chemical and physical properties of polysaccharides,[181-184] DNAs,[185-188] proteins,[189-193] enzymes[194-198] and lipids.[199, 200]

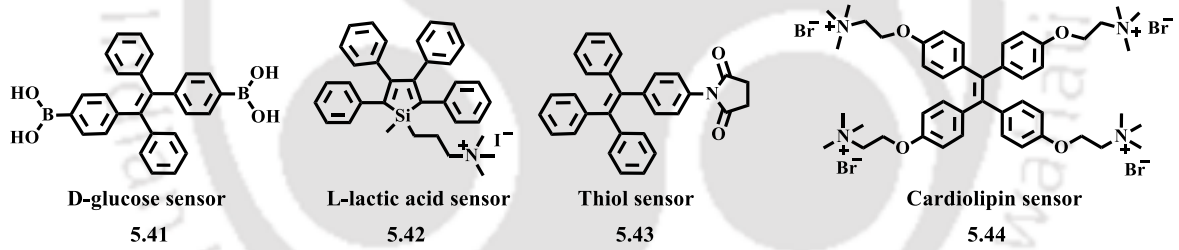

Figure 5.9. Examples of AIEgen sensors for biomolecules.[162, 176, 199, 201]

In the field of bio-imaging, AIE-based systems show superior features when compared to conventional organic dyes and luminogens in terms of molar absorptivity, brightness, photobleaching resistance, biocompatibility and blinking.[3, 23, 202] By considering these advantages, AIEgens have a high potential for imaging at the subcellular, cellular and tissue levels. Various forms of AIEgen systems including small AIEgens, [203-208] polymeric AIEgens, [95, 209, 210] and AIE dots [211-215] have been utilized successfully for imaging in biological systems.

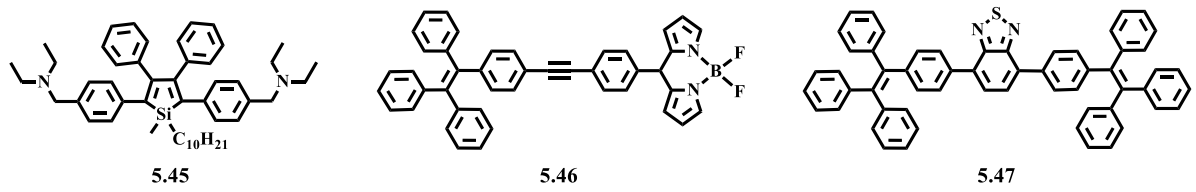

Figure 5.10. Examples of AIEgens utilized in biological imaging.[204, 208, 212]

As Chemical Sensors: AIEgen systems find widespread applications as chemical sensor including detection, recognition, and visualization of various chemical species. For example, AIEgen systems have been successfully utilized for the detection of various ions,[216-220] gas,[221-223] explosives[88, 224-227] and various hazardous species such as melamine and gamma-ray radiation.[228, 229] In addition, AIEgen systems also have been utilized for pH sensing,[185, 230-232] chiral recognition,[233-236] conformation probing,[237-240] viscosity evaluation,[241, 242] self-assembly monitoring,[243-247] fingerprint visualization[248, 249] and morphology visualization.[250-252] As chemical sensors, a great advantage of AIEgen systems over conventional organic luminogens is their high quantum efficiency in aqueous media. Detection of toxic metals and explosives in aqueous media are highly demanded research topics[253, 254] in terms of human health as well as environmental protection and AIEgen systems definitely have the potential to excel in these research areas.

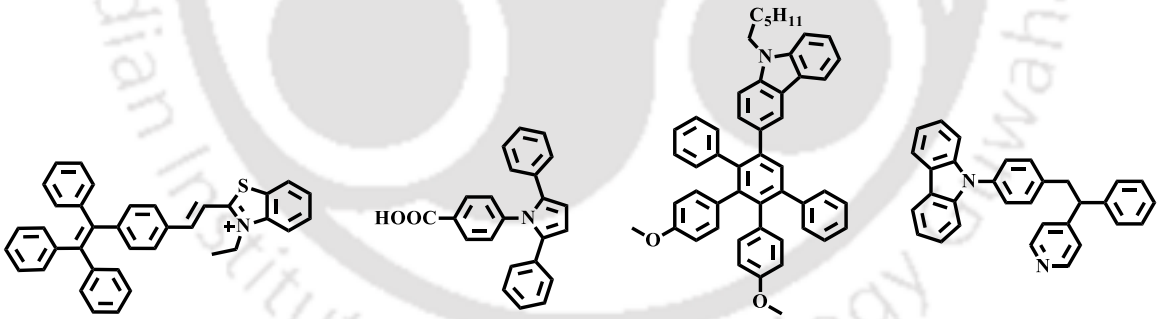

Figure 5.11. Examples of AIEgens utilized as chemical sensors.[220, 222, 225, 255]

5.2. Applications of Probes Showing Aggregation-Induced Emission in DNA Research

The nucleic acids (DNA and RNA) and proteins being the most important biological macromolecules are crucial for all forms of life to exist. Therefore, the investigation of their structures and functions is a topic of great importance. In this context, a vast number of fluorophores and fluorescence techniques have been reported in the literature. Despite the successful implementation of various conventional fluorophores, a large number of AIEgen systems have been established as fluorescent probes for DNA recognition,[185-188, 256] labeling,[257] quantification,[258] visualization [259] and monitoring of conformational changes.[260, 261] These AIEgen systems have shown superior features than conventional fluorophores in many respects. Applying the AIE effect, it is quite possible to prepare highly fluorescent DNA with a high degree of labeling. For example, in 2012, Yu *et al.*[257] have successfully demonstrated the labeling of DNA with the degree of labeling (DOL) up to the theoretical limit by enzymatically incorporating a silole isothiocyanate (**5.52**, **Figure 5.12**) labeled nucleotide **5.53** via nick translation, PCR or random priming.

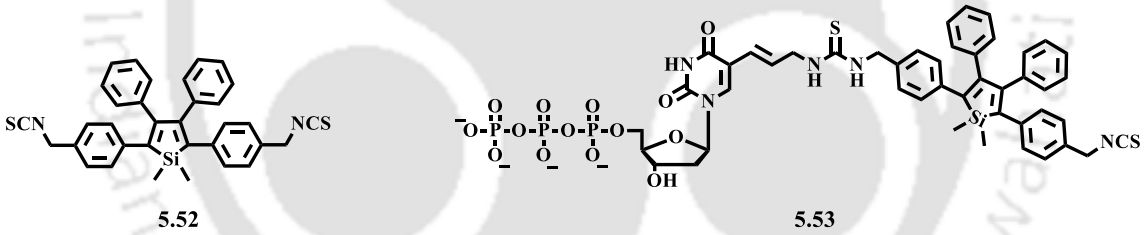

Figure 5.12. Silole isothiocyanate AIEgen and its nucleotide reported by Yu *et al*.

In 2013, Li *et al.* reported a tetraphenylethene labeled single-stranded oligonucleotide (**5.54, Figure 5.13**) as fluorescence light-up probe for the homogeneous detection of specific complementary DNA in solution.[262] It was reported that the probe **5.54**, is tolerant of high ionic strength which enables its applicability to hybridization conditions. A strong fluorescence turn-on effect was reported when the probe hybridized with its complementary ssDNA than other ssDNAs containing mismatch bases. Such types of probes can be highly useful for SNP detection.

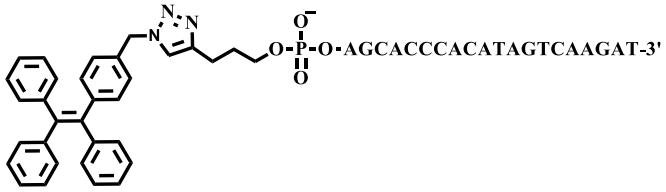

5.54

Figure 5.13. TPE labeled oligonucleotide probe reported by Li *et al*.

In 2014, Wang et al. reported a perylene-functionalized polycation (**5.55**, **Figure 5.14**) which exhibited AIE property.[263] The synthesized polycation undergoes complexation with polyanion ssDNA to form a complex. Thus, this molecule can be utilized as a light-up probe for the detection of DNA hybridization. A significant enhancement in the fluorescence emission of the probe due to the AIE effect was reported when it interacts with a noncomplementary ssDNA. On the other hand, a little change in the fluorescence emission intensity of the probe was observed upon addition of the complementary ssDNA most possibly due to the combined effects of AIE and duplex-quenching resulting from the intercalation of perylene into the duplex.

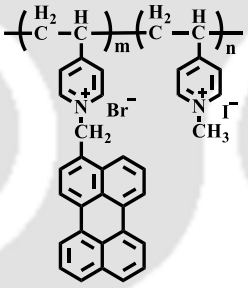

5.55

Figure 5.14. Perylene-functionalized polycation reported by Wang *et al*.

In 2016, Wang et al. utilized three cationic distyrylanthracene (DSA) derivatives (**5.56-5.58**, **Figure 5.15**) in combination with graphene oxide (GO) as fluorescent probes for label-free DNA sensing.[264] The strategy behind this work is based on the different affinity of GO with ssDNA and dsDNA and high quenching ability of GO to the fluorescent molecules. The authors have demonstrated that the DSA derivatives exhibit enhanced fluorescence on complexation with an ssDNA aptamer **5.59 (Figure 5.15)**. In any **DSA-5.59** complex system, the addition of GO results in quenching of fluorescence due to the fluorescence resonance transfer from the DSA to GO. After that, the addition of the ssODN complementary to the **5.59**

resulted fully matched duplex due to which displacement of the **DSA-5.59** complex occurs from the surface of GO. As a result, the fluorescence of the **DSA-5.59** complex is recovered. On the other hand, mismatched ssODNs failed to hybridize with **5.59** due to the mismatched base pairs and therefore, as a result, no recovery in fluorescence intensity has been observed in these cases as the **DSA-5.59** complex remained absorbed at the surface of the GO.

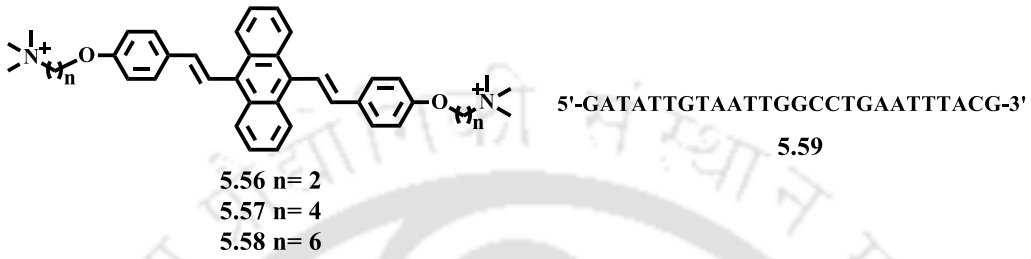

Figure 5.15. Distyrylanthracene derivatives and ssDNA aptamer utilized by Wang *et al* for DNA sensing.

In 2018, Wang *et al*. reported a novel cationic AIEgen, (E)-TPEDEPy-DBz (**5.60**, **Figure 5.16**), which exhibited solvatochromism and mechanoluminochromism characteristics.[186] Thus, it was reported that the emissions of the probe are yellow-greenish and red-orange in the crystalline state and amorphous state, respectively, which were switchable from one to other by applying simple processes such as grinding and fuming treatments. This AIEgen has been utilized as a light-up fluorescent probe for the detection of DNA in Tris–HCl buffer solution. Upon binding with DNAs, a significant enhancement in the fluorescence signal of the probe was reported which is found to be applicable to a variety of DNA samples from different species. The enhanced fluorescence signal was explained on the basis of binding of the probe molecules to the DNA chains which led to the *in situ* formation of aggregates of probe molecules.

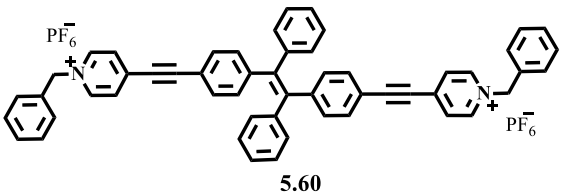

Figure 5.16. The structure of (E)-TPEDEPy-DBz reported by Wang *et al.* for DNA detection.

Very recently, Hiremath *et al.* reported a water-soluble aggregation-induced emission (AIE)-active probe TPE-diBuS (**5.61**, **Figure 5.17**) containing long chains with sulfonate groups which showed selective light-up fluorescence response towards Al^{3+} ions under organic solvent-free conditions.[265] The high selectivity of the probe towards Al^{3+} was explained on the basis of a strong affinity of sulfonate groups with $Al^{3+}$and increased fluorescence intensity of the probe was due to the formation of aggregates of the probe in presence of Al^{3+} ions. The authors utilized the highly emissive feature of the probe-Al^{3+} ensemble and exploited its possible application in DNA tracking by investigating its interaction with ctDNA. Thus, upon gradual addition of increasing concentrations of ctDNA, an exponential decrease in the fluorescence signal of the probe-Al^{3+} ensemble was reported. The quenching of the fluorescence signal was explained on the basis of displacement of Al^{3+} from the probe-Al^{3+} ensemble to DNA due to the higher affinity of the Al^{3+} towards phosphate groups present in DNA backbone than the sulfonate groups. Thus, such types of systems can be highly useful for DNA tracking in terms of fluorescence response.

5.61

Figure 5.17. The structure of TPE-diBuS reported by Hiremath *et al.* for DNA tracking.

In the literature, several efforts have also been reported regarding the utilization of AIEgens for probing the formation of the G-quadruplex DNA.[260, 261, 266] A G-quadruplex is a single-stranded DNA (ssDNA) with guanine (G)-rich repeated sequences forming a secondary four-stranded structure with the help of Hoogsteen hydrogen bonds. In a series of experiments, researchers utilized TPE based AIEgens with varying alkyl units (**5.62-5.64**, **Figure 5.18**) in the side chains for the investigation of structural effects of these molecules on G-quadruplex formation in terms of fluorescence response.[260, 261, 266] The cationic charge on the side chains of these AIE probes is a useful feature for binding with negatively charged DNA via electrostatic forces.

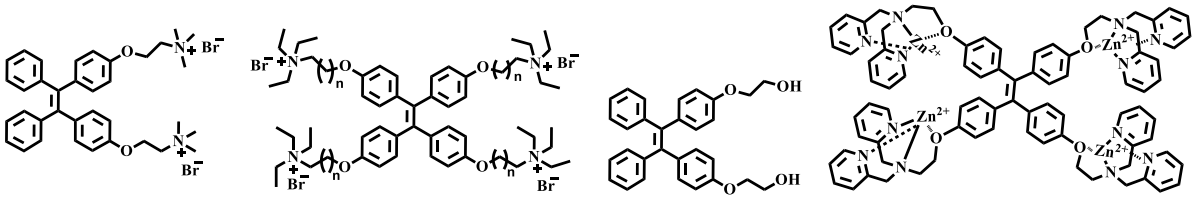

Figure 5.18. Examples of AIEgens systems utilized in DNA research.

The TPE derived AIE probe **5.65** (**Figure 5.18**) has been utilized for the detection of nucleic acids in gel matrix on basis of hydrogen bonding interactions between the probe and the phosphate backbone of DNA strands.[267] In addition to the electrostatic and hydrogen bonding interactions, DNA detection by utilizing AIE probe capable of coordination interaction (**5.66**, **Figure 5.18**) with DNA had also been reported.[188]

5.3. Applications of Fluorescent Probes in Abasic DNA Detection

5.3.1. Abasic DNA: Its Structure, Generation and Reactivity

An abasic site or an AP site (Φ) is a form of DNA lesion which is most common and frequently occurred in genomic DNA.[268, 269] It is produced due to the cleavage of the glycosidic bond between the deoxyribose sugar and the nucleobase which results in the loss of a purine or a pyrimidine base leaving behind the deoxyribose sugar in the DNA strand (**Figure 5.19**). An abasic site can occur spontaneously either due to the action of exogenous agents or as a result of repair of modified or abnormal bases by cell's base excision repair (BER).[270-274] A spontaneous depurination process can alone generate abasic sites in large scale as much as 10,000 abasic sites per cycle.[275, 276] The formation of AP sites can cause DNA mutation and thus if left unrepaired by BER, it may lead to deleterious phenomena such as cancer, apoptosis, and cellular senescence.[277, 278] An abasic site being chemically unstable can lead to strand breakage which may ultimately lead to cell death. Structurally, DNAs containing abasic sites show deviation from their regular structure due to the discontinuity occurred as a result of abasic site formation.[279, 280]

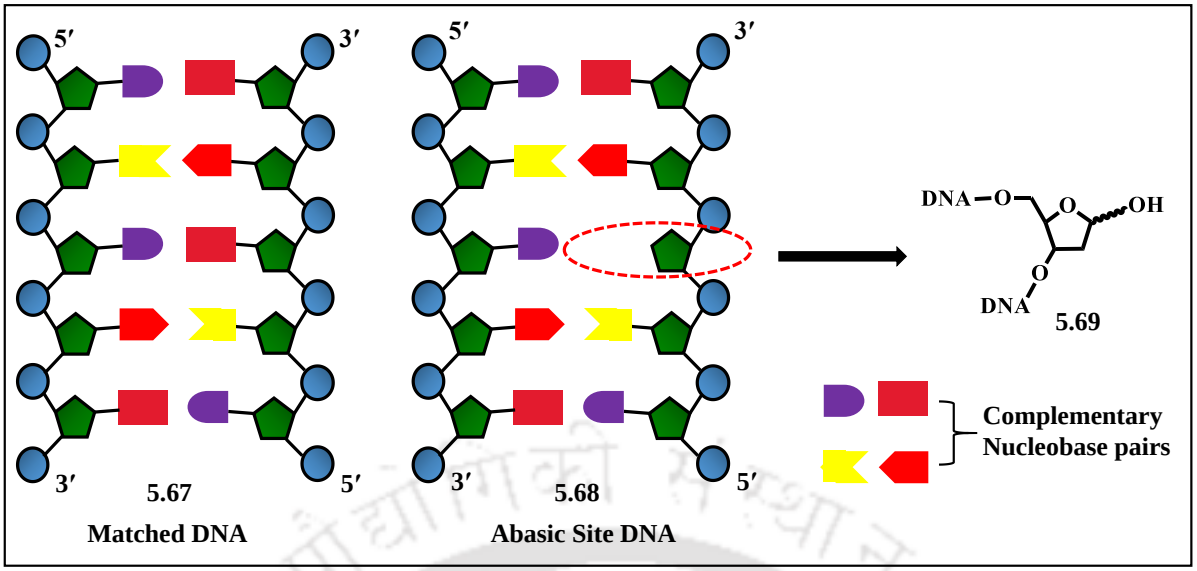

Figure 5.19. Schematic representation of an abasic site in DNA.

The biological implications of abasic sites are diverse, therefore numerous efforts have been made in order to understand the chemistry and enzymology of abasic DNA. In this regard, the experimental techniques often rely upon the study of synthetic abasic DNAs. It is well known that the abasic sites occurred in DNA as a result of hydrolytic cleavage of the N-glycosidic bond. Therefore, the basic strategy for preparation of synthetic abasic DNAs or oligonucleotides is the labilization of N-glycosidic bond by developing a positive charge on the nucleobase with the help of chemical modification or other factors.[281-283] Towards this end, various efficient synthetic methods have been developed for the synthesis of oligonucleotides containing abasic sites at the desired positions. Among these, the most common method is the incorporation of unnatural or modified deoxynucleoside precursors into oligonucleotides by utilizing automated DNA/RNA synthesizer.[284-288] Moreover, several abasic site analogs were reported in the literature which are chemically stable and mimic both the cyclic and the open-chain forms of the deoxyribose moiety.[289-292] The structures of natural and synthetic models of abasic sites are shown in **Figure 5.20**.

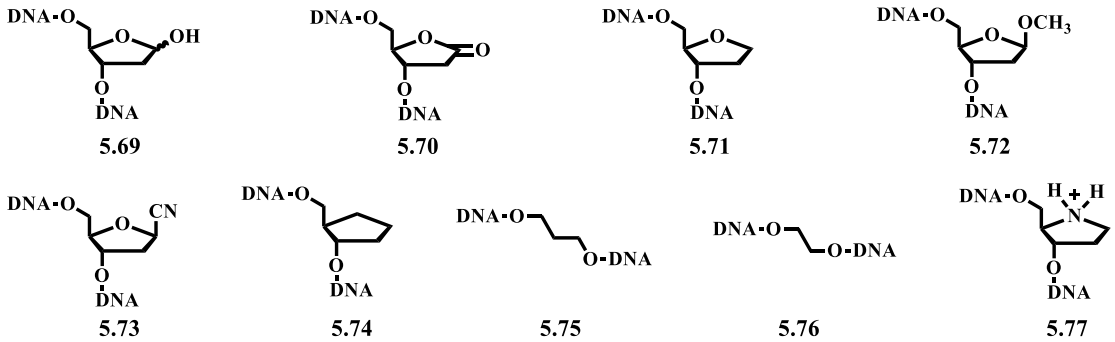

Figure 5.20. Examples of abasic site structures and their analogs.

The characterization of the structure of the abasic sites has been done by NMR spectroscopy analysis of oligodeoxynucleotides containing abasic sites labeled with ^{17}O and ^{13}C isotopes.[293-295] The abasic sites in a typical cell exist as a mixture of α- and β-hemiacetal anomers (40:60 ratio) in equilibrium with a minor ring-opened aldehydic form which is less than 1% of total sites.[295] The existence of the aldehydic form makes the abasic site highly sensitive to alkaline conditions and thus undergoes a β-elimination reaction leading to the formation of an α,β-unsaturated aldehyde.[296, 297] The δ-elimination cleavage of the AP sites has also been proposed and believed to follow β-elimination cleavage of the abasic sites during the enzymatic repair of damaged DNA.[298]

The impact of abasic sites on the conformation and duplex stability of DNA has been investigated by several research groups. In this regard, various physicochemical and spectroscopic means such as high-field NMR spectroscopy, calorimetry, and thermal denaturation experiment have been approached to examine the properties of the abasic site containing oligonucleotides.[299-302] All of these research efforts have revealed that the DNA containing abasic sites show reduced stability even B-form of the DNA is retained. Therefore, DNAs containing abasic sites suffer a thermodynamic destabilization of about 3-11 Kcal/mol when compared to a native DNA duplex.[269, 303] The magnitude of destabilization is dependent on the sequence context and type of unpaired base complementary to the abasic site. In general, abasic sites containing purines as flanking bases and as well as complementary bases show more stability than those with pyrimidines.[304] The unpaired base complementary to an abasic site can obtain extrahelical or intrahelical conformation depending upon its type and that of the surrounding bases.[299, 305-307] The conformations of unpaired purines are often intrahelical. On

the other hand, in case of unpaired pyrimidines, an equilibrium of extrahelical and intrahelical forms exist unless flanking bases are pyrimidines which favor extrahelical conformation.

When an abasic site is formed, it destabilizes the DNA locally.[306, 307] Under normal condition, the cell quickly and efficiently repairs the abasic site defect through BER machinery in order to prevent any serious damage to the cell. However, as a result of suppression or disabling of these repair mechanism, the formation of abasic sites can occur which may lead to deleterious consequences such as single nucleotide polymorphism (SNPs), block transcription, inhibition of DNA replication and generation of topoisomerase poisons.[280, 308, 309] Because of the tremendous biological implication, estimation of abasic site is a topic great of research interest which might provide a quantitative measure of DNA damage done by various mutagens or genotoxic compounds. Moreover, the recognition of the abasic sites is critical for evaluation of DNA damage and screening of various drugs as potential anticancer agents.[310] Therefore, detection and stabilization of abasic sites is very important for the development of new drugs and diagnostics. After tremendous research efforts, several molecules which recognizes abasic sites specifically by exhibiting a cleavage activity and the mimicking action of AP nucleases have been reported in the literature. The design and synthesis of molecules which target and bind specifically to the abasic sites are also reported. In this contexts, we will briefly discuss some examples of small molecules utilized for the detection and stabilization of abasic sites below.

5.3.2. Stabilization of Abasic Site by Non-Nucleosidic Base Surrogates

As revealed from the previous section, several small molecule intercalators have been found to recognize and stabilize an abasic site. The stabilization of an abasic site relies mainly on the adjustment of the probe molecule within the gap created by the abasic site. The molecules with good intercalating property and volume comparable to a natural **A:T** pair, in general, are expected to cover the full space along the abasic site which in turn involve in an inter-/intrastrand π-π stacking interaction with the bases of the abasic DNA duplex leading to stabilization of the abasic DNA. Research efforts toward the expanding of the genetic alphabet and searching for DNA based materials have evolved several new nucleosidic as well as non-nucleosidic base surrogates out of which many of them have been found having intercalation property with similar size as that of a natural **A:T** pair. Therefore, with this concept of abasic duplex stabilization, many of the designed fluorescent nucleosidic and non-nucleosidic base surrogates have been exploited for fluorimetric sensing as well as stabilization of abasic DNA.

In this section, the abasic duplex stabilization by a few of the designer non-nucleosidic base surrogates has been discussed. Next section will be devoted to the stabilization by few reported nucleosidic base surrogates. The aromatic stacking in an abasic DNA can be maintained by placing extended aromatic residues as a nucleobase surrogate opposite to the abasic site which ultimately may lead to the stabilization of the abasic DNA. Such aromatic building blocks are very interesting and might display greater advantage for stabilizing abasic site with high specificity over free intercalators.

Towards this end, Häner *et al.* have designed and synthesized few non-nucleosidic base-surrogates and studied their abasic site stabilization properties. They have incorporated various derivatives of phenanthrene-3,6-dicarboxamide with flexible aliphatic linkers (**5.78**, **Figure 5.21**) opposite to an abasic site by standard phosphoramidite chemistry and examined the duplex stability of the corresponding abasic DNAs.[311, 312] The flexible aliphatic linkers constitute the methylene groups and varied in length. It has been observed from the thermal denaturation experiment that the incorporation of the phenanthrene with a tetramethylene linker at opposite to the abasic site led to a significant stabilization of the abasic DNA duplex. Later on, Häner and co-workers have analyzed the effect of 2,9-disubstituted 1,10-phenanthroline (**5.79**) and 1,8-disubstituted pyrene (**5.80**) building blocks on the stability of DNA duplexes containing an abasic site.[313] Thermal denaturation experiment revealed that both of the building blocks provided a significant stabilization to the abasic DNA duplexes. The authors also investigated the influence of the chain length of the aliphatic linkers in both cases. Thus, in the pyrene series, the T_m varies within a narrow range of approximately 1 °C on increasing methylene groups from two to five in both linker arms. Thus, the stabilization of abasic DNA by pyrene derivatives remains relatively insensitive to changes of the linker length. However, in the phenanthroline series, a strong influence of the linker length on the thermal melting stability has been observed which is reflected by an increased T_m value of about 4.2 °C as the linker length is increased from 2 to 5. Thus, 1,10-phenanthroline-2,9-dicarboxamide bearing two pentamethylene linkers showed the highest stabilization of the abasic site in the duplexes. The observed stabilization is explained on basis of the stacking interactions between polyaromatic systems and the adjacent base pairs.

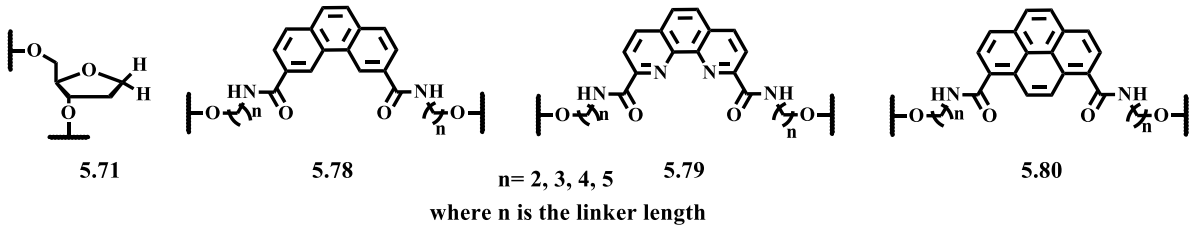

Figure 5.21. Abasic site structures containing non-nucleosidic base surrogates reported by Häner *et al.*

Stabilization of abasic site with oligonucleotide (ODN) modified with 9-amino-6-chloro-2-methoxyacridine (ACMA) (**5.81**, **Figure 5.22**) has been demonstrated by Shimidzu *et al.*[314] The thermodynamic studies indicated that the duplexes containing the acridine derivative opposite to an abasic site are more stable by about 11.2 °C as compared to that of duplexes containing abasic site opposite natural bases. The UV- visible and fluorescence spectroscopic investigation revealed that acridine is selectively intercalated along the abasic site in the duplex.

Tanaka *et al.* have studied the interactions of the intercalating agent, 9-amino-6-chloro-2-methoxyacridine (ACMA) with tri- and pentamethylene linker at three types of abasic sites of the DNA helix *i.e.* abasic frameshift, apurinic (purine base missing) and apyrimidinic (pyrimidine base missing) (**Figure 5.22**).[315] It has been elucidated through the thermal denaturation experiment that the ACMA with the pentamethylene linker and apyrimidinic site is the most stable system. The UV-visible and the fluorescence experiments have revealed that ACMA selectively intercalated to the apyrimidinic site rather than the frameshift abasic site (**Figure 5.23**).

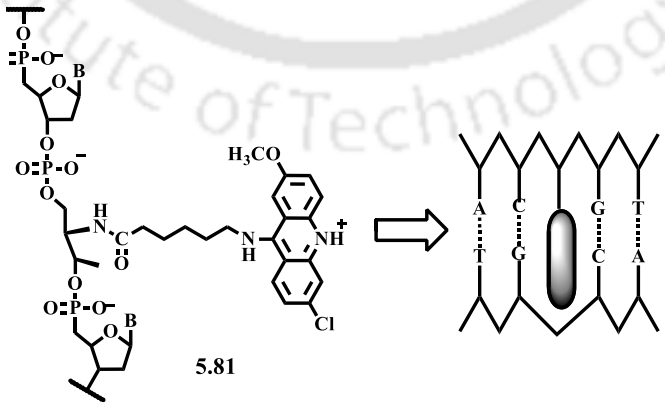

Figure 5.22: Structure of oligonucleotide (ODN) modified with 9-amino-6-chloro-2-methoxyacridine (ACMA) and its intercalation in a DNA duplex.

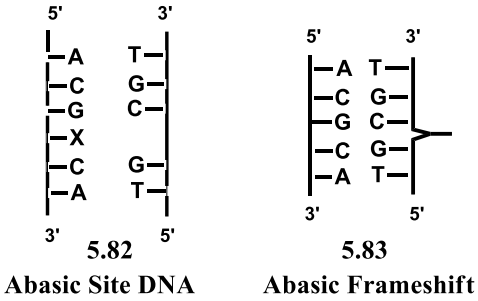

Figure 5.23: Structure of the abasic site and abasic frameshift site in DNA.

5.3.3. Targeting Abasic Site with Nucleosidic Base Surrogates

The abasic sites are known to destabilize DNA when paired opposite to natural bases.[316] It has already been discussed in the previous section that many non-nucleosidic aromatic base surrogates are able to stabilize abasic DNA via intercalation and aromatic stacking along the abasic site. Stabilization of abasic sites has also been reported using complementary oligonucleotides carrying modified nucleosides. The idea behind using the deoxyribose-derived nucleosidic base surrogates is to cause as little change as possible to the sugar-phosphate backbone. In this context, deoxyribose-derived extended aromatic residues have been placed opposite to the abasic site which can maintain the aromatic stacking throughout the duplex as a substitute of the missing nucleobase. For example, deoxyribofuranosides carrying 1-pyrene and 2-pyrene (**Figure 5.24** and **Figure 5.25**) have been used for the stabilization Absic DNAs as these pyrene nucleoside analogs are sterically large enough to fit well against an abasic site.

The first example of stabilization of an abasic site by nucleosidic base surrogate has been reported by Kool *et al*. *via* the synthesis of 1-pyrenyl C-nucleoside (**5.84**, **Figure 5.24**).[317-320] It has been observed that 1-pyrenyl C-nucleoside stabilizes an abasic duplex well. However, the pyrene/abasic duplexes are found to slightly less stable than the natural A:T pair. The thermal denaturation experiments also revealed that the pyrene selectively paired against an abasic site as compared to the natural bases since the replacement of the central pyrene-abasic pair with P-X pair (P = pyrene and X = A. T, C, G) destabilized the DNA duplex relative to P-Φ pair.

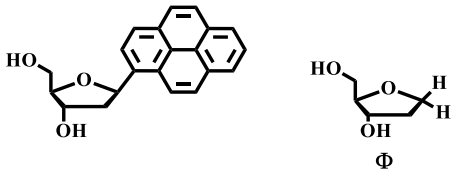

Figure 5.24: Structure of 1-pyrenyl C-nucleoside and an abasic site.

A similar experiment relating the stabilization of the abasic site has been carried out by Leumann *et al.* with 2-pyrenyl-C-nucleoside (**5.85**, **Figure 5.25**).[321] The synthesis of 2-pyrenyl C-nucleoside has been carried out in order to maximize π-π stacking interactions and to minimize conformational isomerism around the *C*-glycosidic bond. From the thermal denaturation study, it is observed that a duplex containing 2-pyrene residue opposite to an abasic site has led to a minor decrease in its thermal stability as compared to the duplex containing a natural A:T base pair. Duplexes containing two or three intrastacked pyrene residues paired against two or three abasic sites (**5.86**) showed a gradual decrease in thermal stability.

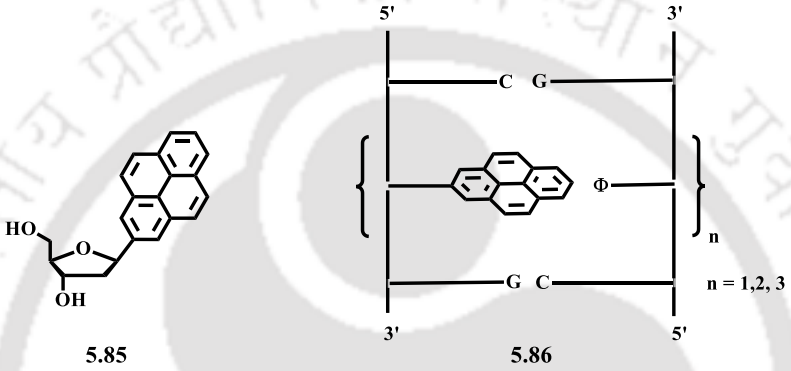

Figure 5.25: Structure of 2-pyrenyl C-nucleoside and illustration of intrastacked pyrene residues.

The results obtained by pairing 1-pyrene deoxynucleoside and 2-pyrene deoxynucleoside opposite to an abasic site are thus comparable demonstrating that both the pyrene nucleosides stabilize an abasic site well. Pyrene was chosen to be paired against the abasic site as it occupies an area (220 $Å^2$) which is very close to the area covered by a natural A:T pair (269 $Å^2$). The pairing selectivity of pyrene with the abasic nucleoside over the natural bases can be justified on the basis of its large surface area and strong stacking ability which is nearly twice that of natural adenine. The model study also suggests that an aromatic building block replaces the missing base by intercalation into the cavity resulting from loss of a nucleobase.

Hence, from the above literature reports it is clear that the DNA duplexes containing abasic sites can be stabilized by incorporating extended aromatic residues opposite to the abasic site. In this regard, we have also demonstrated the stabilization of an abasic site containing DNA duplex utilizing a novel triazolylphenanthrene nucleoside, $^{Tphen}\mathbf{B}_{DO}$ (**5.87**, **Figure 5.26**).[322] Thus, from the thermal denaturation study, it is revealed that the DNA duplexes containing triazolylphenanthrene nucleoside opposite to the abasic site are more stable than the all other duplexes containing natural bases (A,T,G,C) opposite to the abasic site. Interestingly, the

stabilization of the duplex $^{Tphen}B_{DO}$- Φ is found to be almost equal to that of the control A-T pair. Such a significant stabilization is most probably attributed to its high stacking propensity and large surface area (248 $Å^2$), which is comparable to that of the natural A-T pair (273 $Å^2$). A strong intercalative interaction between the $^{Tphen}B_{DO}$ and the abasic site is revealed from UV-visible spectroscopy, fluorescence anisotropy, and CD spectroscopy.

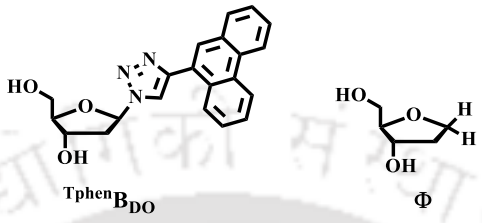

$^{Tphen}B_{DO}$ Φ

5.87 **5.71**

Figure 5.26: Structure of triazolylphenanthrene nucleoside and abasic site.

5.3.4. Label-Free Detection of Abasic Site

A most common and suited method for the detection of abasic sites and other DNA disorders such as SNP, base mismatches, etc. is the utilization of fluorescent probes as a fluorescent signal transducer. Such fluorescent probes include oligonucleotide probes covalently labeled with one or several fluorophores [323-326] and non-oligonucleotide small fluorophores capable of selective recognition of AP sites with a target-base-dependent 'turn-on' or 'turn-off' emission response.[327-329] The utilization of later class of fluorophores is simpler, less time consuming, cost-effective and less laborious than the fluorescently labeled oligonucleotide probes. Such features favored these fluorescent probes as ideal candidates for detection of abasic sites, SNPs and DNA base mismatches and introduced the term 'label-free' DNA detection.

In label-free approach, fluorescent ligands are not covalently attached to the nucleic acid backbone but it interacts noncovalently with DNA through a number of binding modes such as intercalation, groove-binding, end-stacking or electrostatic interactions. The fluorescent molecules used in label-free DNA detection are in general non-emissive or weakly emissive in aqueous solution, due to quenching by solvent-solute interactions. However, they show fluorescence enhancement upon binding to defined DNA structures due to the protection of their excited states within the hydrophobic interior of the oligonucleotide.[330] The specific binding of these fluorophores with DNA allows them to enter into the intrahelical hydrophobic environment of the DNA and hence less exposed to the polar solvent surroundings.

Our research interest in this chapter deals with the label-free interaction of our molecule with abasic DNA. Therefore, we want to discuss a few examples as below of abasic DNA detection achieved via a label-free approach.

Sato and co-workers reported several cyanine dye conjugates as DNA abasic site-binding ligands and studied their applications as fluorescent probes. Three recent examples of their work, **ATMND-TO** (**5.88**), **DMP-BO** (**5.89**) and **DML-Lys-TO** (**5.90**) are shown in **Figure 5.27**.[331, 332] According to the authors, these conjugates are capable of intercalation and exhibited enhanced fluorescence emission upon binding to an abasic DNA. The fluorescence intensities of these conjugates were found to be much higher upon binding with AP site-containing DNA duplexes than the fully-matched DNA duplexes. Moreover, the intensity of fluorescence emission of these conjugates is nucleobase selective and depends on the target nucleobases present opposite to the AP site. For example, **ATMND-TO** exhibited high light-up emission response in the presence of C and T opposite to the AP site. On the other hand, the emission responses of **DMP-BO** and **DML-Lys-TO** are G-selective and A-selective respectively.

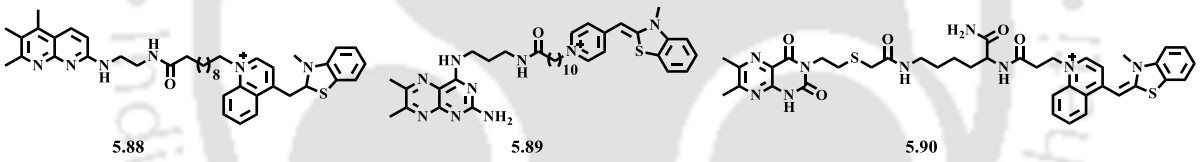

5.88 **5.89** **5.90**

Figure 5.27: Structure of cyanine dye conjugates reported by Sato and co-workers.

In 2015, Wu *et al.*, reported a fluorophore, 9-dicyanovinyljulolidine (**5.91**, **Figure 5.28**) capable of binding to AP sites selectively.[333] This fluorophore is reported as environment-selective and exhibits enhanced fluorescence signal only when the flanking base is guanine. According to the authors, the enhancement in the fluorescence signal is most probably due to the comparable electron energy levels of the fluorophore in the excited state and the flanking guanine base.

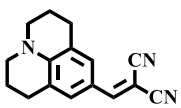

5.91

Figure 5.28: Structure of 9-dicyanovinyljulolidine reported by Wu *et al*.

In 2016, Shao *et al.*[334] investigated several isoquinoline alkaloids for recognition and detection of AP sites. Among these alkaloids, palmatine (**5.92**, **Figure 5.29**) is reported as the most efficient fluorophore for recognition of AP sites with an enhancement in its fluorescence signal in presence of all AP site flanking base sequences. However, stronger binding affinity and stronger enhancement in fluorescence signal are reported when the flanking bases are pyrimidines rather than purines.

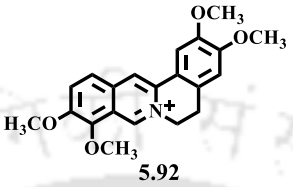

5.92

Figure 5.29: Structure of palmatine.

In 2018, Ni *et al.*[330] reported a 1H-benzo[e]indolium based fluorescent probe (**5.93**, **Figure 5.30**) for selective detection of AP sites. According to the authors, the fluorophore **5.93** is non-fluorescent in aqueous solution but exhibits strong fluorescence signal only when a triplex-forming oligonucleotide (TFO) binds to the DNA containing the AP sites. Inhibition of the non-radiative twist relaxation process in the excited state of the fluorophore due to the TFO binding is most probably the reason behind the enhanced fluorescence signal. Such types of fluorophores can be very useful for the selective detection of triplexes containing AP sites.

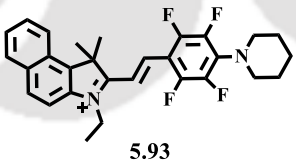

5.93

Figure 5.30: 1H-benzo[e]indolium based fluorescent probe reported by Ni *et al*.

Recently, our research group has also contributed to this area. We have reported an unnatural tetrazolylpyrene nucleoside (**1.262**, **Figure 5.31**) capable of label-free detection of DNA abasic site, T-T/C-C base mismatches and bulge DNA as a fluorescent light-up probe.[335] We have studied the UV-visible, fluorescence and thermal denaturation of several 13 mer DNA sequences (**5.94-5.97**, **Figure 5.31**) in the presence of the tetrazolylpyrene nucleoside. From the fluorescence study, we observed a significant enhancement in the fluorescence signal of the probe upon binding with the abasic DNAs where the AP site is paired against C or T and

flanking bases surrounding the AP site are pyrimidines. Very less or almost no enhancement in fluorescence signal was observed for abasic DNAs containing purines as flanking base pairs surrounding the AP site. Thermal denaturation study also revealed that the tetrazolylpyrene nucleoside stabilizes the DNA duplexes significantly where the abasic site is opposite to C and T and flanking bases are pyrimidines. The failure of the tetrazolylpyrene probe to detect AP sites surrounded by purines as flanking bases is most probably attributed to the large size of the purines which makes the probe unfit at the AP site.

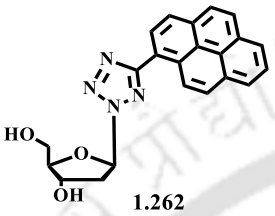

1.262

5.94 5'-CGCAATXTAACGC-3' [X = A, G, C, T]
5.95 5'-GCGTTAYATTGCG-3' [Y= A, G, C, T, Φ]
5.96 5'-CGCAACXCAACGC-3' [X = A, G, C, T]
5.97 5'-GCGTTGYGTTGCG-3' [Y=A, G, C, T, Φ]

Figure 5.31. Structure of tetrazolylpyrene nucleoside and ODN sequences utilized in the study.

Though there is no report of particular AIE probe for the detection of abasic DNA, few probes are there to target DNA and DNA lesion such as single nucleotide polymorphism typing. We already have furnished (**Section 5.2**, above) few examples of DNA detection via the use of AIE probe. Herein we want to highlight one literature report to target SNPs by using an AIE probe. Thus in 2017, Tian et al. utilized an AIE active DSA derivative (**5.98**, **Figure 5.32**) along with water-soluble carbon nanotubes (CNTs) for SNP detection on the basis of a fluorescence quenching effect.[336] It was reported that the AIE probe **5.98** forms aggregates on interaction with DNA leading to the emission of a strong fluorescence signal in solution. Strong interaction between the DNA and the probe to form a complex was reported as a result of a combined effect of intercalation, electrostatic interactions and hydrophobic interactions. The authors demonstrated that the complex between a fully matched natural DNA and the probe exhibits strong fluorescence emission even in the presence of a strong quencher such as CNTs. On the other hand, the complex between a mutated DNA and the probe showed significantly quenched fluorescence in the presence of CNTs. It was explained that the interaction of the probe is weaker with mutated DNA due to which some aggregates hauled out from the mutated DNA and get absorbed on the CNTs and consequently get quenched. Therefore, from this example, it can be realized that DNA abnormalities such as SNP can be detected using AIE probes.

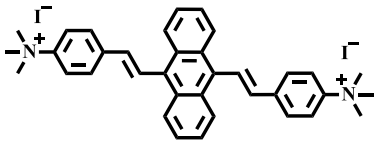

5.98

Figure 5.32. Structure of DSA derivative reported by Tian *et al.* for SNP detection.

5.4. Background

The development of fluorescent molecules with the ability to recognize DNA sequence alteration via the generation of highly specific fluorescence signal are of recent attraction in biology, bioorganic and medicinal chemistry. In particular, sensing of DNA lesions is crucial for reliable disease diagnosis and the design of new chemotherapeutics. DNA lesions are the sites of sequence alteration or damage in the base-pairing or in the structure of DNA. The most commonly encountered DNA lesions are abasic DNA, mismatched DNA, base modified DNA, single-strand breaks, double-strand breaks, and intrastrand cross-linked DNA. Out of all DNA lesions, however, an abasic site [AP or Φ] DNA is a most frequent and can lead to deleterious mutations. The local destabilization in DNA by an AP site provides a clue to the base excision repair (BER) machinery to repair it.

However, as mentioned above, the suppression or prohibition of these repair mechanism is often met with dreadful outcomes. As for example abasic sites can cause single nucleotide polymorphisms (SNPs), block transcription, inhibit DNA replication and can act as potent topoisomerase poisons. Thus, if left unrepaired it becomes dangerous to cellular survival. Therefore, the AP sites in the genomic DNA has profound implications for genome integrity. Because of the tremendous biological implication estimating the abasic site is of great research interest which might help in the quantitative determination of the exposure of DNA to various mutagenic or genotoxic substances. Moreover, recognition of the AP site is crucial in assessing DNA damage and screening antitumor/antioxidant drugs that can target a cancer cell. Therefore, sensing of abasic DNA is crucial for reliable disease diagnosis and the design of new chemotherapeutics.

From the literature report, we observed that AIE probes find numerous applications in the various research fields ranging from material science to biomedical chemistry. Features like high photostability, large Stokes shift, high quantum yield and usability in any concentration make AIE probes powerful candidates as fluorescent probes for investigations of structure and functions of biomolecules. The development of AIE probes for detection of DNA lesions will greatly impact in research for new diagnostics and chemotherapeutics.

5.5. Objective

Over the years, many platforms have been developed for the detection and stabilization of DNA abasic site. However, no single protocol can meet all research needs. Thus, fluorescent oligonucleotide probes containing non-nucleosidic base surrogates have been utilized for AP site recognition and stabilization. Similarly, fluorometric sensing, as well as stabilization of an abasic DNA, has also been achieved with the use of nucleosidic base surrogates. However, these methods require preparation of modified fluorescent DNA probes which in turn need complicated probe design and high cost analysis. Therefore, the best alternative strategy is to employ a ligand/ molecule which can fit within the gap created by the AP site. Therefore, the label-free detection of AP site is very much desirable to offer simple and low-cost strategy. The molecules having a comparable volume of an A: T pair and good intercalating property are, in general, the suitable candidates to cover the gap space created by an AP site and thus, are capable of sensing and stabilizing AP DNA via inter-/intrastrand π-π stacking interaction.

In the context, the fluorescence photophysical property of our recently developed EtOH sensor, pyrenylamido aromatic triazolo amino acid scaffold, **PyAm-^{Ar}TAA**, (**5.99**, **Figure 5.33a**) in the water attracted us as it generated a broad emission at 465 nm which might possibly be an aggregated pyrene emission.[23] We envisaged that the origin of this emission is a result of aggregation in water or in buffer. Thus, we also thought that the pyrene moiety of **PyAm-^{Ar}TAA** might aggregate near the Ap site pointing rest part of the molecule toward minor groove. The aggregated state of the probe would face more hydrophobic microenvironment leading to enhanced emission.

We envisaged that the probe would preferentially bind the groove near the deformed abasic site (Ap) via H-bonding/stacking interaction through the **^{Ar}TAA** scaffold unit and the pyrenylamido unit (**PyAm**) would possibly engage in intercalative stacking interaction with the base opposite to the abasic site (Ap) and other bases alongside the Ap site. We also hypothesized that adenine base (A) unit opposite to the abasic site would offer better stacking with the **PyAm** unit of the bare probe which would ultimately result in an enhanced fluorescence signal. Practically, we applied our simple, cost-effective just "Mix & Read" strategy and found that the probe, **PyAm-^{Ar}TAA**, alongside the Ap site responded well with an enhanced fluorescence signal in presence of A base opposite to Ap site in a duplex with A/T-flanking base next to the Ap site (**Figure 5.33a**). On the other hand, the Ap site opposite to base G or C led to a diminished fluorescence emission from the aggregated probe molecule

which might be because of quenching of fluorescence emission via electron transfer from opposite base G or C.

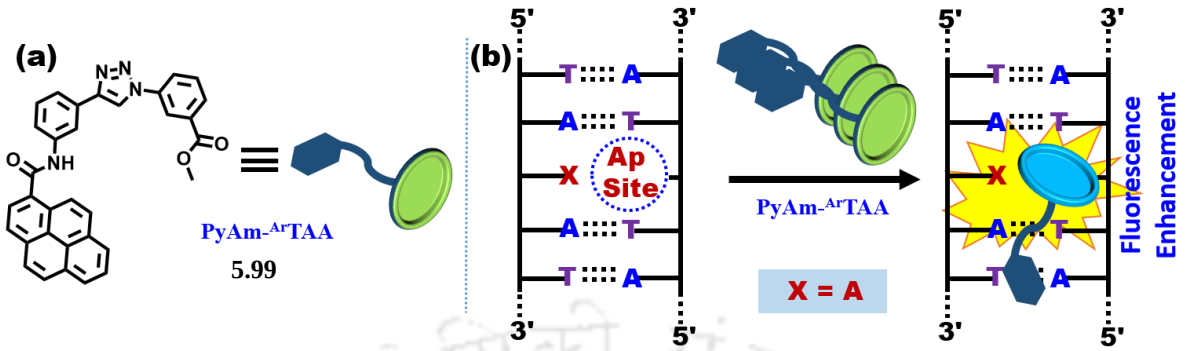

Figure 5.33. (a) The chemical structure of the AIE probe and (b) the schematics of the concept of binding of the probe **PyAm-^{Ar}TAA** to abasic site opposite to A base (X = A).

With this concept and idea, we framed our objective as follows:

(a) Photophysical studies on the AIE properties of pyrenylamido triazolyl aromatic amino acid scaffold (**PyAm-^{Ar}TAA**, **Figure 5.33**) previously reported by our research group.

(b) Utilization of **PyAm-^{Ar}TAA** probe for sensing of DNA abasic site.

5.6. Result and Discussion

5.6.1. Study on Photophysical Properties of PyAm-^{Ar}TAA

Following the above ideas and our objective, we initially studied the photophysical property of the probe, pyrenylamido aromatic triazolo amino acid scaffold, **PyAm-^{Ar}TAA**, in various organic and aqueous solvents. Thus, with an increase in solvent polarity the long wavelength absorption band at 344 nm (in the least polar solvent dioxane) experienced a hypsochromic shift in wavelength and hypochromic effect in absorbance (**Figure 5.34a**). In particular, a 5 nm shift was observed when the solvent polarity was changed from dioxane to TFE. On the other hand, in water, the structureless broad absorption band at 328 nm is the result with very low comparable absorption. In glycerol, the absorption becomes low with no hypsochromic shift. However, in sodium phosphate buffer, the effect is again more prominent than water. Thus, both in water and in aqueous buffer the short wavelength absorption band experienced a large bathochromic shift of 12 nm when compared with dioxane.

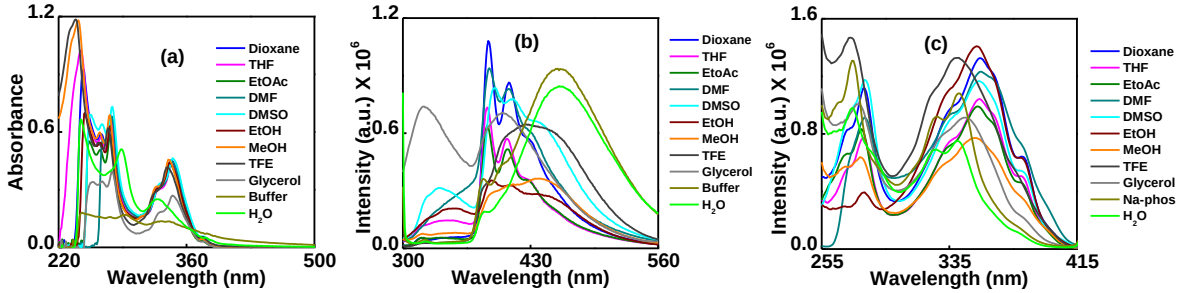

Figure 5.34. (a) UV-visible, (b) fluorescence emission and (c) fluorescence excitation spectra in organic solvents for **PyAm-^{Ar}TAA**. The concentration of the fluorophore was 10 µM.

Next, we studied the fluorescence photophysical property. Thus, upon excitation at 290 nm the probe molecule emitted at 335 nm corresponding to the emission from the scaffold amino acid **^{Ar}TAA** and pyrenyl structured band at 387, 405, 430 nm in dioxane (**Figure 5.34b**). As the polarity increases, the intensity of scaffold emission increases at the expense of pyrenyl emission. In DMSO and Ethanol, along with the low intense pyrenyl band, the probe showed a new emission, at around 443-448 nm. However, in MeOH and TFE a structureless broad emission appeared at 431-440 nm. In glycerol, both the pyrenyl emission and the scaffold emission increases. However, a completely new situation arose in water and in aqueous buffer leading to a prominent emission at 462 nm with negligible or no emission from monomeric pyrene unit or scaffold. The probe showed only pyrenyl structural emission when excited at 342 nm in low polar solvents like dioxane, THF, EtOAc, and DMF. However, similar to the earlier observation, in polar solvents, the monomeric pyrenyl emission decreased and aggregation induced enhanced (AIE) emission (AIEE) at around 455-475 nm appeared. In water and phosphate buffer the AIE emission became most prominent similar to the earlier observation when the probe was excited at scaffold's absorption (290 nm) (**Figure 5.34b**). The excitation spectra also showed a prominent hypsochromic shift with strong hypochromic effect (**Figure 5.34c**). All these observations from both UV-visible and fluorescence indicated the aggregation effect of the probe

In dilute solution, in general, the classical pyrene derivatives exhibit good fluorescence emission, however, aggregation-caused quenching (ACQ) is observed when the concentration was very high. To ascertain the fact of aggregation we recorded the photophysical spectra in dioxane solutions and dioxane/H_2O mixtures as well as measured the absorbance and fluorescence at various concentrations of the probe. Thus, a tremendously decreased absorbance with blue shift was the result when a dioxane solution of the probe was titrated with

an increasing amount of water (**Figure 5.35a**). A significant effect was observed in the case of 40:60 dioxane: water mixture.

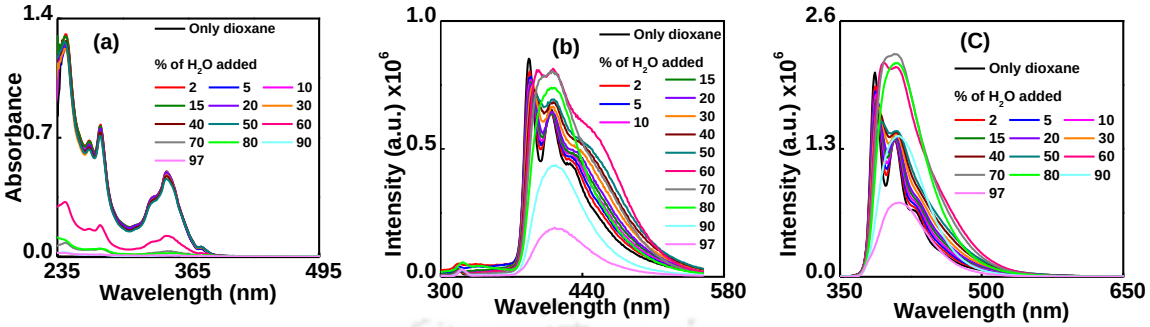

Figure 5.35. (a) UV-visible, (b) fluorescence emission spectra (λ_{ex} = 290 nm), (c) fluorescence emission spectra (λ_{ex} = 340 nm) of **PyAm-^{Ar}TAA** in various dioxane-H_2O mixtures.

Upon excitation at 290 nm, the pyrenyl emission at 410 nm of the probe solution in dioxane was found to be increased along with the incremental emission at 462 nm as the volume % of water increased up to 60% (**Figure 5.35b**). The emission from the scaffold moiety was remained negligible but gradually enhanced and shifted to a long wavelength region. Upon excitation at 340 nm also, we observed similar emission pattern (**Figure 5.35c**). All such observations reflected the aggregation of the probe.

After that, we investigated the absorption and emission properties of **PyAm-^{Ar}TAA** in different concentrations in phosphate buffer (**Figure 5.36**). Thus, a plot of absorbance vs. concentration of the probe reflected a nonlinearity for a range of concentration from 10 μM to 120 μM (**Figure 5.36 d**). A nonlinear fitting for the emission at 380 nm (**Figure 5.36 e**) and sigmoidal growth curve fitting for the emission at 480 nm (**Figure 5.36 f**) were observed when emission spectra were recorded at both the excitation wavelengths of 290 and 340 nm with an increase in probe concentration from 10-120 μM. Therefore, it is clear that the probe under investigation showed AIE effect in both water and buffer.

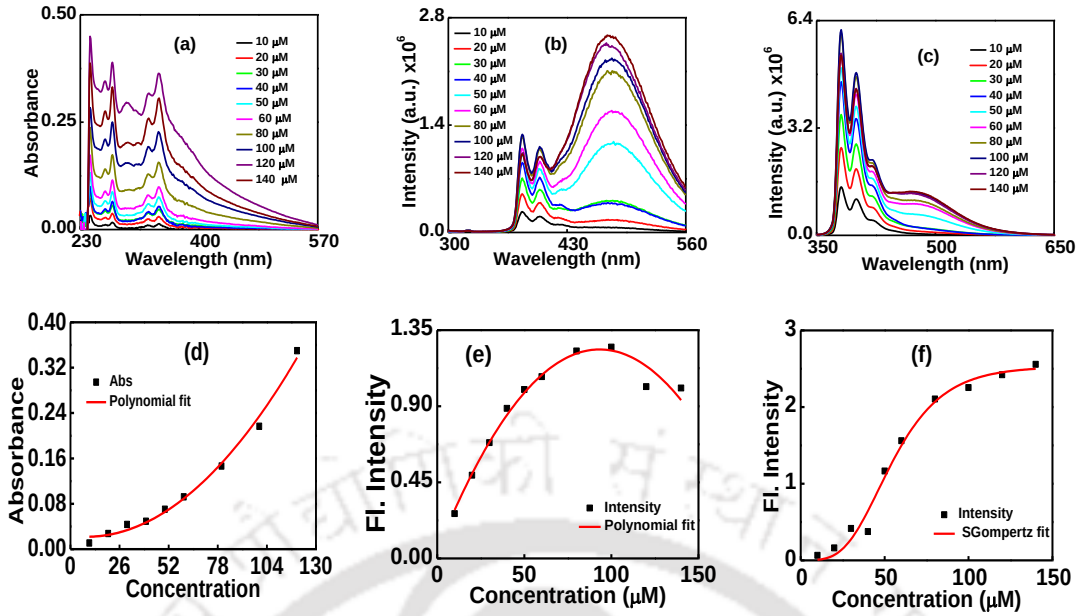

Figure 5.36. (a) UV-visible, (b) fluorescence emission spectra (λ_{ex} = 290 nm), (c) fluorescence emission spectra (λ_{ex} = 340 nm) of **PyAm-^{Ar}TAA** in increasing concentrations in phosphate buffer, (d) absorbance vs concentration plot, (e) a fluorescence intensity vs concentration plot at 380 nm, (f) fluorescence intensity vs concentration plot at 480 nm.

5.6.1.2. Variable Temperature Experiment of PyAm-^{Ar}TAA

To gain further insight into the AIE properties of **PyAm-^{Ar}TAA**, we studied the fluorescence emission properties of the fluorophore at different temperatures within the range 20 °C to 70 ° (**Figure 5.37**). Thus, upon excitation at both 290 nm and 340, we observed that the fluorescence intensity of the fluorophore gradually decreases with a gradual increase in the system temperature (**Figure 5.37**). The variable temperature fluorescence also indicated the aggregation enhanced emission from the probe. High temperatures generally destroy the aggregates resulting in quenching of fluorescence of an AIE molecule. Therefore, from these observations, it is clear that the probe under investigation showed AIE effect in both water and buffer.

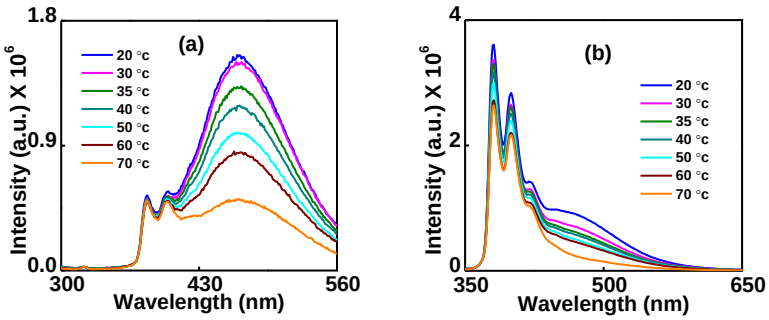

Figure 5.37. Variable temperature fluorescence emission spectra of **PyAm-^{Ar}TAA** (a) at 290 nm, (b) at 340 nm. [**PyAm-^{Ar}TAA]** = 60 µM in phosphate buffer.

5.6.2. Interaction of PyAm-^{Ar}TAA with Short Abasic DNAs

5.6.2.1. Spectral Studies of PyAm-^{Ar}TAA with Short Abasic DNAs

In order to investigate the abasic site recognition and detection ability of **PyAm-^{Ar}TAA**, we studied the interaction of the probe with short 13-mer DNA duplexes containing an abasic site opposite to all four natural bases and having both A/T and C/G flanking base pairs utilizing UV-visible and fluorescence spectroscopy. For this purpose, we mixed the probe (10 µM) with the DNA duplex (2.5 µM) in phosphate buffer (50mM sodium phosphate and 100mM NaCl in water, pH = 7.0) at room temperature and followed a "Mix & Read" strategy which does not need annelation and relies on read out of the fluorescence signal from the probe. The DNA sequences used in this study are tabulated (**Table 5.1**).

Table 5.1. DNA sequences used in this study

ODNs	T-A flanking base sequences	ODNs	C-G flanking base sequences
1.	5'-CGCAAT **A** TAACGC-3'	8.	5'-CGCAAC **A** CAACGC-3'
2.	5'-CGCAAT **G** TAACGC-3'	9.	5'-CGCAAC **G** CAACGC-3'
3.	5'-CGCAAT **C** TAACGC-3'	10.	5'-CGCAAC **C** CAACGC-3'
4.	5'-CGCAAT **T** TAACGC-3'	11.	5'-CGCAAC **T** CAACGC-3'
5.	5'-GCGTTA **Φ** ATTGCG-3'	12.	5'-GCGTTG **Φ** GTTGCG-3'
6.	5'-GCGTTA **T** ATTGCG-3'	13.	5'-GCGTTG **T** GTTGCG-3'
7.	5'-GCGTTA **C** ATTGCG-3'	14.	5'-GCGTTG **C** GTTGCG-3'

Thus, the analysis of UV-visible spectra of the DNA duplexes containing T-A flanking base pairs at the abasic site (ODNs 1-7) revealed that the probe experienced a blue shift in amidopyrenyl unit (**PyAm**) from 337 nm to 330 nm along with strong hyperchromism in presence of abasic site opposite to base **A** [ODN 1●5 (**A●Φ** duplex)]. However, the scaffold unit (**^{Ar}TAA**) of the probe exhibited a strong bathochromic shift from 294 to 304 nm along

with hyperchromism. On the other hand, for all other duplexes, the absorption remained the same (**Figure 5.38** and **Table 5.1**). These observations indicated that the scaffold unit (**^{Ar}TAA**) of the probe, **PyAm-^{Ar}TAA**, possibly involved in intercalative stacking interaction alongside the gap created by the abasic site opposite of base **A** compared to any other opposite bases [ODN 2-5●5 (**G/C/T/Φ●Φ** duplex DNAs] or matched duplexes (ODN 1●6 and ODN 2●7) in T-A flanking base sequences. On the other hand, the amidopyrenyl unit (**PyAm**) possibly involved in stacking interaction alongside the minor groove.

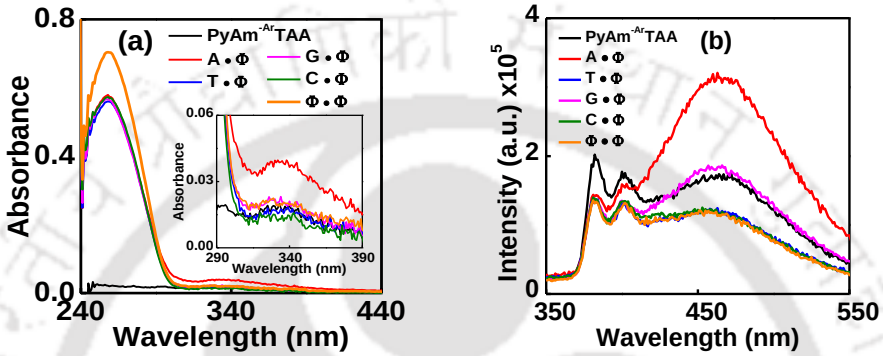

Figure 5.38. (a) UV-visible absorption spectra and (b) Fluorescence emission spectra (λ_{ex} = 340 nm) of **PyAm-^{Ar}TAA** in absence or in presence of ODN 1-5●5 (**A/G/C/T/Φ●Φ** duplex). [**PyAm-^{Ar}TAA**] =10μM.

Upon excitation at the amidopyrenyl unit (**PyAm**) (340 nm) an enhancement of aggregation induced emission (AIEE) fluorescence compared to probe's monomer emission was observed at 470 nm in presence of duplex ODN 1●5 (**A●Φ** duplex). A two-fold increase in fluorescence intensity compared to the bare probe was calculated in the presence of A-Φ abasic DNA [ODN 1●5 (**A●Φ** duplex)]. The same emission from the duplex DNA containing abasic site opposite to another purine base G [ODN 2●5 (**G●Φ** duplex)] was found to be similar to that of the bare probe. However, for the case of pyrimidine bases opposite of abasic site [ODN 3-4●5 (**C/T●Φ** duplexes)], the duplexes showed quenched emission (**Figure 5.38b**). Therefore, the probe was efficient in sensing the abasic site opposite of **A** base (**Figure 5.38b**).

In case of DNA duplexes containing G-C as flanking base pairs, (ODNs 8-14), the UV-visible spectra revealed that the probe experienced a slight hyperchromism in amidopyrenyl unit (PyAm) at 337 nm with almost no shifting in wavelength in presence of DNA duplexes containing abasic site opposite to base **A** and **T** [ODN 8●12 and 11●12 (**A●Φ** duplex and **T●Φ** respectively)] (**Figure 5.39a**). On the other hand, the probe experienced a strong

hypochromism with a bathochromic shift from 337 to 342 nm in presence of DNA duplexes containing abasic site opposite to base **G** and **C** [ODN 9●12 and 10●12 (**A●Φ** duplex and **T●Φ** respectively)].

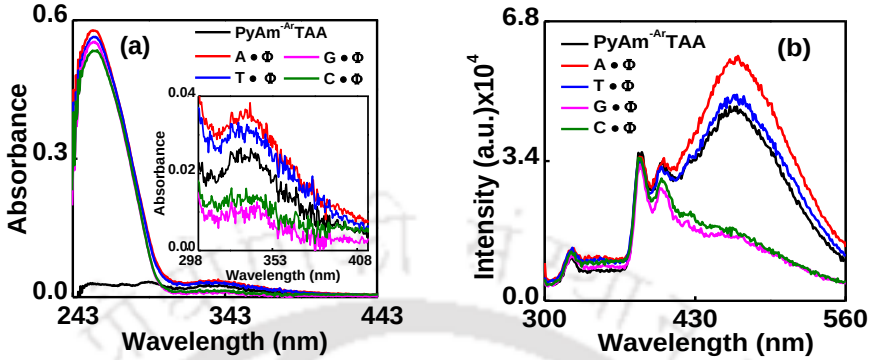

Figure 5.39. (a) UV-visible absorption spectra and (b) Fluorescence emission spectra (λ_{ex} = 340 nm) of **PyAm-^{Ar}TAA** in absence or in presence of ODN 8-11●12 (**A/G/C/T●Φ**duplex). [**PyAm-^{Ar}TAA**] =10µM.

Upon excitation at the amidopyrenyl unit (**PyAm**) (340 nm), we observed an enhanced aggregation induced emission (AIEE) fluorescence at 470 nm in case of ODN 8●12 (**A●Φ** duplex) but very less significant when compared to that of the duplex ODN 1●5. In case of the ODN 11●12 (**T●Φ** duplex) where the abasic site is opposite to T, the emission observed was found to be similar to that of the bare probe. However, in rest of the cases [ODN 9-10●12 (**G/C●Φ** duplexes)], the duplexes showed significant quenched emission in comparison to the bare probe. (**Figure 5.39b**).

5.6.2.2. Titration Study of PyAm-^{Ar}TAA with ODN 1●5

A titration experiment was next carried out to investigate the association between the probe and the duplex abasic DNA, ODN 1●5 (**A●Φ** duplex) wherein we observed a distinctive enhancement of emission. Thus, the absorbance of the amidopyrenyl unit (**PyAm**) of the probe at 340 nm, **PyAm-^{Ar}TAA**, gradually increased as the concentration of ODN 1●5 increased (**Figure 5.40a**) which was also supported from the excitation spectra. When excited at the scaffold, **^{Ar}TAA** (280 nm) or at **PyAm** (340 nm) the emission at around 455-460 nm was found to increase gradually with a slight blue shift (**Figure 5.40b**). At some concentration of DNAs the observed irregularities is probably because of the different mode of binding of the two units, **^{Ar}TAA** and **PyAm**, of the probe. We also observed that the thermal melting temperature of the

abasic duplex [ODN 1●5 (**A●Φ** duplex)] gradually increased from 33.7 °C to 35.5 °C upon addition of the probe. All these observations suggested an intercalative stacking interaction of the amidopyrenyl unit (**PyAm**) of the probe along the abasic site opposite of base **A** leaving the hairpin-shaped scaffold unit (**^{Ar}TAA**) possibly in the groove.

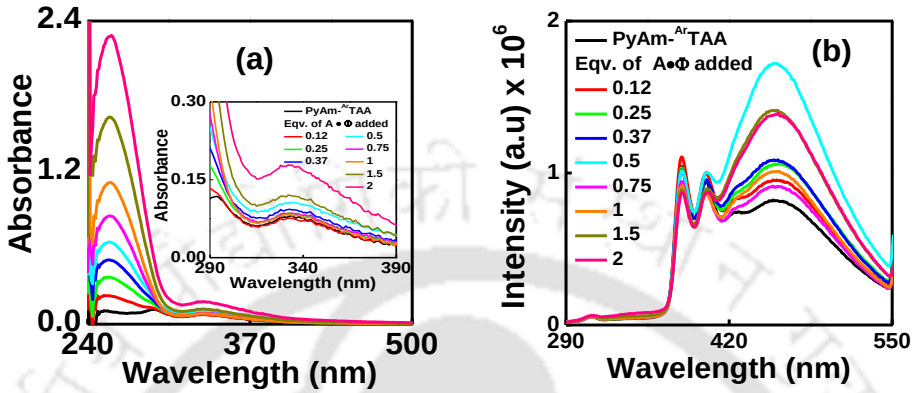

Figure 5.40. (a) UV-visible and (b) fluorescence ((λ_{ex} = 280 nm) titration spectra when the probe solution (10 μM) was titrated with increasing concentration of abasic duplex DNA, ODN 1●5 (**A●Φ** duplex).

5.6.2.3. Determination of A●Φ–Probe Binding Constant

The binding constant (*K*) of the **A●Φ**–probe complex was determined spectroscopically by Benesi-Hildebrand plot (**Figure 5.41**) using the following equation 1,

$$\frac{1}{(I - I_0)} = \frac{1}{(I_\infty - I_0)} + \frac{1}{(I_\infty - I_0)K[\text{DNA}]} \quad \ldots\ldots\ldots\ldots\ldots (1)$$

where I_0, I and I_α are the emission intensities of **PyAm-^{Ar}TAA** in the absence of DNA, and in the presence of intermediate and at an infinite concentration of DNA, respectively. From the slope (linear region's data points) of the plot of $1/(I - I_0)$ *vs.* 1/[DNA], the binding constant *K* was determined, which was found to be 2.5 x 10^5 M^{-1}. Next, the free energy of binding (ΔG) was calculated using equation 2, which was found to be -7.4 kcal/mol.

$$\Delta G = -RT \ln K \quad \ldots\ldots\ldots\ldots\ldots\ldots\ldots\ldots\ldots\ldots\ldots\ldots\ldots\ldots (2)$$

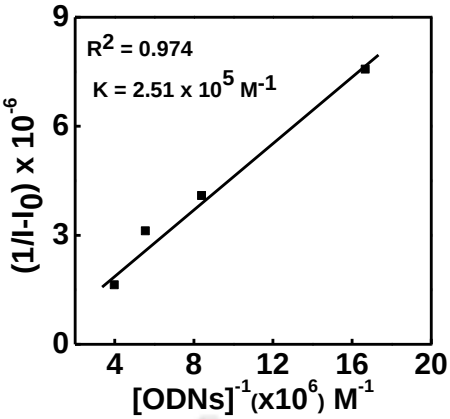

Figure 5.41. Benesi–Hildebrand plots of the probe **PyAm-^{Ar}TAA** in the presence of an increasing concentration of **A●Φ** duplex at 298K.

5.6.2.4. Circular Dichroism (CD) Study

CD experiment was also carried out to get insight into possible structural perturbation of **A●Φ** duplex in the presence of **PyAm-^{Ar}TAA**. Thus, from the CD spectra, we observed that the helicity of the duplex remained unchanged throughout the experimental conditions. Moreover, the helicity of the scaffold is reflected as positive cotton effect with absorption at 250nm (-ve) and at 280 nm (+ ve) (**Figure 5.42**). However, as the concentration of **PyAm-^{Ar}TAA** increased, the induced CD (ICD) was also found to be increased reflecting a strong binding event without perturbing the B-form of the abasic DNA.

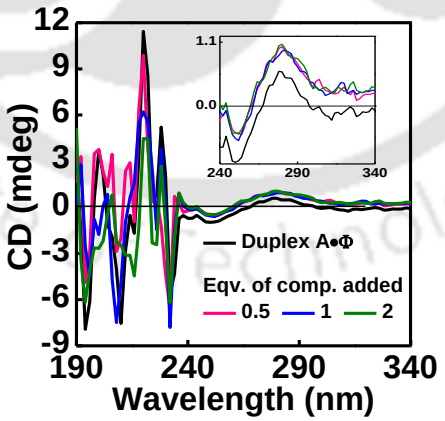

Figure 5.42. CD spectra of **A●Φ** duplex in presence and absence of **PyAm-^{Ar}TAA**.

5.6.2.5. Molecular Docking Study of ODN 1●5 with PyAm-^{Ar}TAA

To support, the binding event of the probe with abasic duplex ODN 1●5 (**A●Φ** duplex), we carried out docking study using AutoDock 4.2 software[337, 338] and AMBER* energy minimized

geometry[339, 340] of **A●Φ** duplex and Gaussian[341] optimized geometry of the probe. The conformations of abasic duplex ODN 1●5 (**A●Φ** duplex) was minimized with the AMBER* force field using Schrödinger Macro Model software (Maestro, version 9.0). A conjugate gradient minimization scheme [PRCG (Polak-Ribiere Conjugate Gradient)] that uses the Polak-Ribiere first derivative method with restarts every 3N iterations were employed for the minimization of the B-form **A●Φ** duplex. The AMBER* minimized structure of the abasic duplex paired against **A** showed a gap alongside the abasic site. Next, the probe, **PyAm-^{Ar}TAA**, was optimized with B3LYP functional and 6-31G (d,p) basis set with Gaussian 09 program package.[341] Finally, the docking study was carried to get insight into the abasic site binding event alongside the groove with flexible molecular docking method and the full DNA was under the grid map. From the docking study, we find that the probe encompasses the minor groove extending the amidopyrenyl unit to the gap created at the abasic site and the scaffold unit remained on the groove site involving π-π-stacking and H-bonding interaction (**Figure 5.43**). Thus, the docking study supported our experimental observation.

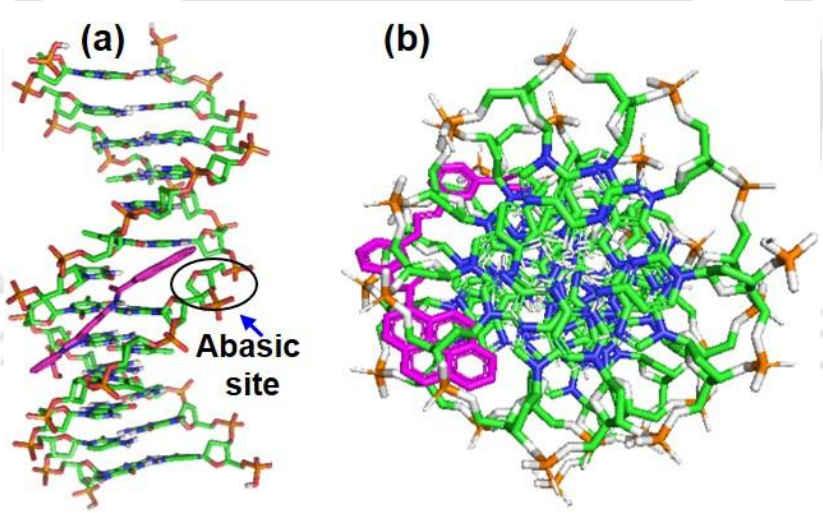

Figure 5.43. Docked structure of the complex of abasic DNA [ODN 1●5 (**A●Φ** duplex)] and the probe, **PyAm-^{Ar}TAA**. (a) Side view and (b) top view

5.7. Conclusion

In conclusion, we have successfully demonstrated that the bare fluorescent pyrenylamido aromatic triazolo amino acid scaffold, **PyAm-^{Ar}TAA** showed AIE characteristics. On interaction with short abasic DNAs, it exhibited significant hyperchromism in the UV-visible

spectra and enhanced fluorescence signal in the emission spectra when the abasic site was opposite to base adenine (**A**). These observations indicated that the scaffold unit (**^{Ar}TAA**) of the probe, **PyAm-^{Ar}TAA**, possibly involved in intercalative stacking interaction alongside the gap created by the abasic site opposite of base **A (A●Φ** duplex**).** A strong interaction of the probe, **PyAm-^{Ar}TAA** with **A●Φ** duplex was also indicated by a binding constant of 2.5× 10^5 M^{-1} calculated from Benesi-Hilderbrand plot. A CD spectrometry study revealed a negligible effect on the conformation of the **A●Φ** duplex in presence of the probe, **PyAm-^{Ar}TAA**. Therefore, The label-free fluorescent light-up sensing of abasic DNAs based on our fluorescent probe would be very useful and might find future applications for the detection and targeting of other DNA lesions with "Just Mix & Read Strategy" which is a less laborious, simple and cost-effective method.

5.8. Experimental Section

5.8.1. Materials

Na_2HPO_4 and $NaH_2PO_4.H_2O$ (for preparation of phosphate buffer) were purchased from Merck, India and used without further purification. Oligonucleotides sequences were purchased from Integrated DNA Technologies (IDT). Water was obtained from a Milli-Q purification system. All experiments were performed with freshly prepared solutions. The probe molecule **PyAm-^{Ar}TAA** was synthesized and purified according to our previously reported literature procedure.[342] We recrystallized the column purified material in the methanol-ethylacetate solvent mixture, dried under vacuum, again characterized and used for the study.

5.8.2. Preparation of Abasic DNA Solutions

The concentrations of the ODNs stock solutions were determined by applying Beer-Lambert equation 3 as shown below:

$$A_{260} = \log I/I_0 = \varepsilon_{260} \times c \times l \quad \ldots\ldots\ldots\ldots\ldots\ldots\ldots\ldots\ldots\ldots \quad (3)$$

Where, A_{260} is the absorbance of the ODN at 260 nm which is determined from the intensity of the transmitted light (I) compared to the intensity of the emerging light (I_0), ε_{260} is the algebraic sum of extinction-coefficients of the individual nucleosides at 260 nm (for natural nucleosides, ε_{260} is calculated with oligo analyzer), c is the concentration of ODN and l is the path length of the light through the sample.

After the concentrations of individual ODNs determined, the ODNs are mixed with their complementary ODNs in equimolar concentrations to obtain the corresponding DNA duplexes (2.5 μM) in phosphate buffer (50mM sodium phosphate and 100mM NaCl in water, pH = 7.0).

5.8.3. Photophysical Study

5.8.3.1. UV-Visible Study

The UV–Visible absorbance measurements were performed using Shimadzu UV-2550 UV–Visible spectrophotometer with quartz cell of 1 cm path length at 298 K. All the UV-Visible studies were carried out in 50 mM phosphate buffer of pH 7.0 at 298 K. 2-3 % DMF was used to solubilize the probe. The measurements were taken in absorbance mode and the absorbance values of the sample solutions were measured in the wavelength regime of 200–600 nm. The concentrations of ODNs were 2.5 μM in 50mM sodium phosphate buffer (pH = 7.0) containing 100 mM NaCl. All the experiments were carried out with freshly prepared sample solutions.

5.8.3.2. Fluorescence Study

All fluorescence and steady-state fluorescence experiments were performed using Fluoromax 4 spectrophotometer with quartz cell of 1 cm path length at 298 K. The slit width was set at 3 nm and the integration time was 0.2 sec. All the fluorescence studies were carried out in 50 mM phosphate buffer of pH 7.0 at 298 K. 2-3 % DMF was used to solubilize the probe. The excitation wavelength for probe **PyAm-^{Ar}TAA** was set at 290nm, the absorption maxima of the amino acid scaffold **^{Ar}TAA** nm and at 342 nm, the absorption maxima of the amidopyrenyl unit (**PyAm**). The emission spectra were measured in the wavelength regime of 300–680 nm.

5.8.4. Molecular Docking

Docking calculations were carried out using Autodock 4.2.[337, 338] To test the accuracy of the docking results, the docking process was repeated three times. The AutoDock tools (ADT) were utilized for charges and polar hydrogens addition as well as for setting the other parameters. Auto Grid 4.0 and AutoDock 4.0 were used to produce grid maps. A grid box to a size of 70 × 64 × 106 with 0.375 Å spacing was generated. The centre grid box for x-, y- and z centres were -0.953, 3.033 and 20.114 with offsets -14.078, -8.967 and 0.239, respectively. In the prescriptive grid box, we calculated the complex conformation with flexible molecular

docking method. The Lamarckian genetic algorithm (LGA) [337] was chosen to carry out a flexible molecular docking of the **PyAm-^{Ar}TAA** to the **A●Φ** duplex and to calculate the complex conformation. The other items used were the default settings. A total of 10 conformations from each docking were obtained and the least binding energy was considered as the best-docked conformation.

5.8.5. B3LYP/6-31G* Optimized Structure and Cartesian Coordinates of PyAm-^{Ar}TAA

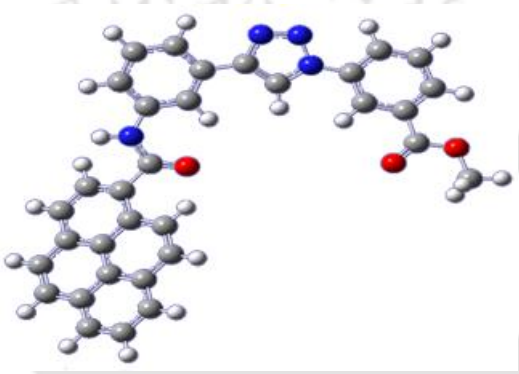

E(RB+HF-LYP)= -1715.3694 a.u.

Standard orientation

Center Number	Atomic Number	Atomic Type	Coordinates (Angstroms) X	Y	Z
1	6	0	6.184107	2.216060	0.254274
2	6	0	5.840746	-0.171483	0.147853
3	6	0	5.344200	1.123324	0.012241
4	1	0	4.321652	1.315223	-0.292514
5	6	0	7.521339	2.010760	0.613908
6	1	0	8.166312	2.862355	0.795715
7	6	0	7.177561	-0.385638	0.507334
8	1	0	7.544029	-1.400791	0.601669
9	6	0	8.008795	0.709180	0.731487
10	1	0	9.045316	0.542220	1.009114
11	6	0	2.064217	-3.383776	-0.444835
12	6	0	0.870940	-2.691548	-0.191523
13	1	0	0.875678	-1.645629	0.078687
14	6	0	-0.358347	-3.353145	-0.292814
15	6	0	2.027418	-4.740416	-0.798903
16	1	0	2.956608	-5.264307	-0.992573
17	6	0	0.800279	-5.391854	-0.898747
18	1	0	0.766467	-6.442417	-1.173896
19	6	0	-0.387730	-4.711438	-0.649121
20	1	0	-1.341173	-5.229973	-0.728761
21	6	0	5.592991	3.577362	0.095455

22	6	0	5.980006	5.896971	0.211552
23	1	0	5.150008	6.065053	0.902719
24	1	0	5.632768	6.072404	-0.810008
25	1	0	6.818759	6.551202	0.450572
26	6	0	-1.859003	-1.411095	0.291347
27	8	0	6.485780	4.559117	0.348112
28	8	0	4.440066	3.789766	-0.224570
29	8	0	-0.983909	-0.556984	0.404311
30	6	0	3.353845	-2.689893	-0.343077
31	6	0	3.639035	-1.374985	-0.029199
32	1	0	3.013803	-0.538899	0.238811
33	7	0	4.996134	-1.290461	-0.081477
34	7	0	-1.597800	-2.723392	-0.049840
35	1	0	-2.409261	-3.303969	-0.211536
36	7	0	5.530766	-2.500637	-0.413517
37	7	0	4.547398	-3.331096	-0.567958
38	6	0	-3.319925	-1.128586	0.518194
39	6	0	-4.095663	-2.063475	1.219911
40	6	0	-3.914557	0.078247	0.064937
41	6	0	-5.442930	-1.846696	1.477615
42	1	0	-3.623832	-2.962534	1.607531
43	6	0	-5.309094	0.293003	0.313980
44	6	0	-3.191768	1.089492	-0.662201
45	6	0	-6.076119	-0.679191	1.028213
46	1	0	-6.014376	-2.581808	2.038485
47	6	0	-5.947848	1.484748	-0.148443
48	6	0	-3.808113	2.221028	-1.102725
49	1	0	-2.134354	0.941686	-0.836764
50	6	0	-7.470580	-0.432836	1.269089
51	6	0	-7.337771	1.702443	0.102581
52	6	0	-5.200750	2.466095	-0.865115
53	1	0	-3.238643	2.969938	-1.648003
54	6	0	-8.073645	0.703939	0.826633
55	1	0	-8.037852	-1.181585	1.816451
56	6	0	-7.941439	2.881528	-0.362459
57	6	0	-5.846889	3.630629	-1.311353
58	1	0	-9.130497	0.876191	1.015598
59	6	0	-7.202225	3.834054	-1.061831
60	1	0	-8.998808	3.045440	-0.169443
61	1	0	-5.273827	4.376431	-1.856680
62	1	0	-7.686251	4.740832	-1.414006

5.9. References

1. Chen, C.-T., Evolution of Red Organic Light-Emitting Diodes: Materials and Devices. *Chemistry of Materials* **2004,** *16* (23), 4389-4400.
2. Jakubiak, R.; Collison, C. J.; Wan, W. C.; Rothberg, L. J.; Hsieh, B. R., Aggregation Quenching of Luminescence in Electroluminescent Conjugated Polymers. *The Journal of Physical Chemistry A* **1999,** *103* (14), 2394-2398.
3. Mei, J.; Hong, Y.; Lam, J. W. Y.; Qin, A.; Tang, Y.; Tang, B. Z., Aggregation-Induced Emission: The Whole Is More Brilliant than the Parts. *Advanced Materials* **2014,** *26* (31), 5429-5479.

4. Thomas, S. W.; Joly, G. D.; Swager, T. M., Chemical Sensors Based on Amplifying Fluorescent Conjugated Polymers. *Chemical Reviews* **2007,** *107* (4), 1339-1386.
5. Borisov, S. M.; Wolfbeis, O. S., Optical Biosensors. *Chemical Reviews* **2008,** *108* (2), 423-461.
6. Geddes, C. D.; Lakowicz, J.R., Advanced Concepts in Fluorescence Sensing Part A: Small Molecule Sensing. Springer **2014**.
7. Thompson, R. B., Fluorescence sensors and biosensors. Taylor & Francis **2006**.
8. Domaille, D. W.; Que, E. L.; Chang, C. J., Synthetic fluorescent sensors for studying the cell biology of metals. *Nature Chemical Biology* **2008,** *4*, 168.
9. Giepmans, B. N. G.; Adams, S. R.; Ellisman, M. H.; Tsien, R. Y., The Fluorescent Toolbox for Assessing Protein Location and Function. *Science* **2006,** *312* (5771), 217-224.
10. Jares-Erijman, E. A.; Jovin, T. M., FRET imaging. *Nature Biotechnology* **2003,** *21*, 1387-1395.
11. Luo, J.; Xie, Z.; Lam, J. W. Y.; Cheng, L.; Chen, H.; Qiu, C.; Kwok, H. S.; Zhan, X.; Liu, Y.; Zhu, D.; Tang, B. Z., Aggregation-induced emission of 1-methyl-1,2,3,4,5-pentaphenylsilole. *Chemical Communications* **2001,** (18), 1740-1741.
12. Hong, Y.; Lam, J. W. Y.; Tang, B. Z., Aggregation-induced emission: phenomenon, mechanism and applications. *Chemical Communications* **2009,** (29), 4332-4353.
13. Chen, S.; Chen, Q.; Li, Q.; An, J.; Sun, P.; Ma, J.; Gao, H., Biodegradable Synthetic Antimicrobial with Aggregation-Induced Emissive Luminogens for Temporal Antibacterial Activity and Facile Bacteria Detection. *Chemistry of Materials* **2018,** *30* (5), 1782-1790.
14. Mei, J.; Leung, N. L. C.; Kwok, R. T. K.; Lam, J. W. Y.; Tang, B. Z., Aggregation-Induced Emission: Together We Shine, United We Soar! *Chemical Reviews* **2015,** *115* (21), 11718-11940.
15. Chen, J.; Law, C. C. W.; Lam, J. W. Y.; Dong, Y.; Lo, S. M. F.; Williams, I. D.; Zhu, D.; Tang, B. Z., Synthesis, Light Emission, Nanoaggregation, and Restricted Intramolecular Rotation of 1,1-Substituted 2,3,4,5-Tetraphenylsiloles. *Chemistry of Materials* **2003,** *15* (7), 1535-1546.
16. Li, Y.; Li, F.; Zhang, H.; Xie, Z.; Xie, W.; Xu, H.; Li, B.; Shen, F.; Ye, L.; Hanif, M.; Ma, D.; Ma, Y., Tight intermolecular packing through supramolecular interactions in crystals of cyano substituted oligo(para-phenylene vinylene): a key factor for aggregation-induced emission. *Chemical Communications* **2007,** (3), 231-233.
17. Yu, Z.; Duan, Y.; Cheng, L.; Han, Z.; Zheng, Z.; Zhou, H.; Wu, J.; Tian, Y., Aggregation induced emission in the rotatable molecules: the essential role of molecular interaction. *Journal of Materials Chemistry* **2012,** *22* (33), 16927-16932.
18. Leung, N. L. C.; Xie, N.; Yuan, W.; Liu, Y.; Wu, Q.; Peng, Q.; Miao, Q.; Lam, J. W. Y.; Tang, B. Z., Restriction of Intramolecular Motions: The General Mechanism behind Aggregation-Induced Emission. *Chemistry – A European Journal* **2014,** *20* (47), 15349-15353.
19. Gu, Y.; Wang, K.; Dai, Y.; Xiao, G.; Ma, Y.; Qiao, Y.; Zou, B., Pressure-Induced Emission Enhancement of Carbazole: The Restriction of Intramolecular Vibration. *The Journal of Physical Chemistry Letters* **2017,** *8* (17), 4191-4196.
20. Gao, B.-R.; Wang, H.-Y.; Hao, Y.-W.; Fu, L.-M.; Fang, H.-H.; Jiang, Y.; Wang, L.; Chen, Q.-D.; Xia, H.; Pan, L.-Y.; Ma, Y.-G.; Sun, H.-B., Time-Resolved Fluorescence Study of Aggregation-Induced Emission Enhancement by Restriction of Intramolecular Charge Transfer State. *The Journal of Physical Chemistry B* **2010,** *114* (1), 128-134.
21. Hong, Y.; Lam, J. W. Y.; Tang, B. Z., Aggregation-induced emission. *Chemical Society Reviews* **2011,** *40* (11), 5361-5388.

22. Hu, R.; Lager, E.; Aguilar-Aguilar, A.; Liu, J.; Lam, J. W. Y.; Sung, H. H. Y.; Williams, I. D.; Zhong, Y.; Wong, K. S.; Peña-Cabrera, E.; Tang, B. Z., Twisted Intramolecular Charge Transfer and Aggregation-Induced Emission of BODIPY Derivatives. *The Journal of Physical Chemistry C* **2009,** *113* (36), 15845-15853.
23. Hu, R.; Leung, N. L. C.; Tang, B. Z., AIE macromolecules: syntheses, structures and functionalities. *Chemical Society Reviews* **2014,** *43* (13), 4494-4562.
24. Kaiser, T. E.; Wang, H.; Stepanenko, V.; Würthner, F., Supramolecular Construction of Fluorescent J-Aggregates Based on Hydrogen-Bonded Perylene Dyes. *Angewandte Chemie International Edition* **2007,** *46* (29), 5541-5544.
25. Chi, Z.; Zhang, X.; Xu, B.; Zhou, X.; Ma, C.; Zhang, Y.; Liu, S.; Xu, J., Recent advances in organic mechanofluorochromic materials. *Chemical Society Reviews* **2012,** *41* (10), 3878-3896.
26. Ding, D.; Li, K.; Liu, B.; Tang, B. Z., Bioprobes Based on AIE Fluorogens. *Accounts of Chemical Research* **2013,** *46* (11), 2441-2453.
27. Liu, J.; Lam, J. W. Y.; Tang, B. Z., Aggregation-induced Emission of Silole Molecules and Polymers: Fundamental and Applications. *Journal of Inorganic and Organometallic Polymers and Materials* **2009,** *19* (3), 249.
28. Wang, M.; Zhang, G.; Zhang, D.; Zhu, D.; Tang, B. Z., Fluorescent bio/chemosensors based on silole and tetraphenylethene luminogens with aggregation-induced emission feature. *Journal of Materials Chemistry* **2010,** *20* (10), 1858-1867.
29. Cai, X.; Bandla, A.; Mao, D.; Feng, G.; Qin, W.; Liao, L.-D.; Thakor, N.; Tang, B. Z.; Liu, B., Biocompatible Red Fluorescent Organic Nanoparticles with Tunable Size and Aggregation-Induced Emission for Evaluation of Blood–Brain Barrier Damage. *Advanced Materials* **2016,** *28* (39), 8760-8765.
30. Feng, G.; Wu, W.; Xu, S.; Liu, B., Far Red/Near-Infrared AIE Dots for Image-Guided Photodynamic Cancer Cell Ablation. *ACS Applied Materials & Interfaces* **2016,** *8* (33), 21193-21200.
31. Gao, M.; Chen, J.; Lin, G.; Li, S.; Wang, L.; Qin, A.; Zhao, Z.; Ren, L.; Wang, Y.; Tang, B. Z., Long-Term Tracking of the Osteogenic Differentiation of Mouse BMSCs by Aggregation-Induced Emission Nanoparticles. *ACS Applied Materials & Interfaces* **2016,** *8* (28), 17878-17884.
32. Gu, X.; Zhao, E.; Zhao, T.; Kang, M.; Gui, C.; Lam, J. W. Y.; Du, S.; Loy, M. M. T.; Tang, B. Z., A Mitochondrion-Specific Photoactivatable Fluorescence Turn-On AIE-Based Bioprobe for Localization Super-Resolution Microscope. *Advanced Materials* **2016,** *28* (25), 5064-5071.
33. Gui, C.; Zhao, E.; Kwok, R. T. K.; Leung, A. C. S.; Lam, J. W. Y.; Jiang, M.; Deng, H.; Cai, Y.; Zhang, W.; Su, H.; Tang, B. Z., AIE-active theranostic system: selective staining and killing of cancer cells. *Chemical Science* **2017,** *8* (3), 1822-1830.
34. Kang, M.; Gu, X.; Kwok, R. T. K.; Leung, C. W. T.; Lam, J. W. Y.; Li, F.; Tang, B. Z., A near-infrared AIEgen for specific imaging of lipid droplets. *Chemical Communications* **2016,** *52* (35), 5957-5960.
35. Leung, C. W. T.; Wang, Z.; Zhao, E.; Hong, Y.; Chen, S.; Kwok, R. T. K.; Leung, A. C. S.; Wen, R.; Li, B.; Lam, J. W. Y.; Tang, B. Z., A Lysosome-Targeting AIEgen for Autophagy Visualization. *Advanced Healthcare Materials* **2016,** *5* (4), 427-431.
36. Lo, C. Y.-W.; Chen, S.; Creed, S. J.; Kang, M.; Zhao, N.; Tang, B. Z.; Elgass, K. D., Novel super-resolution capable mitochondrial probe, MitoRed AIE, enables assessment of real-time molecular mitochondrial dynamics. *Scientific Reports* **2016,** *6*, 30855.
37. Shao, A.; Xie, Y.; Zhu, S.; Guo, Z.; Zhu, S.; Guo, J.; Shi, P.; James, T. D.; Tian, H.; Zhu, W.-H., Far-Red and Near-IR AIE-Active Fluorescent Organic Nanoprobes with

Enhanced Tumor-Targeting Efficacy: Shape-Specific Effects. *Angewandte Chemie International Edition* **2015,** *54* (25), 7275-7280.

38. Yu, C. Y. Y.; Xu, H.; Ji, S.; Kwok, R. T. K.; Lam, J. W. Y.; Li, X.; Krishnan, S.; Ding, D.; Tang, B. Z., Mitochondrion-Anchoring Photosensitizer with Aggregation-Induced Emission Characteristics Synergistically Boosts the Radiosensitivity of Cancer Cells to Ionizing Radiation. *Advanced Materials* **2017,** *29* (15), 1606167.
39. Zhang, W.; Kwok, R. T. K.; Chen, Y.; Chen, S.; Zhao, E.; Yu, C. Y. Y.; Lam, J. W. Y.; Zheng, Q.; Tang, B. Z., Real-time monitoring of the mitophagy process by a photostable fluorescent mitochondrion-specific bioprobe with AIE characteristics. *Chemical Communications* **2015,** *51* (43), 9022-9025.
40. Zhang, Y.; Chang, K.; Xu, B.; Chen, J.; Yan, L.; Ma, S.; Wu, C.; Tian, W., Highly efficient near-infrared organic dots based on novel AEE fluorogen for specific cancer cell imaging. *RSC Advances* **2015,** *5* (46), 36837-36844.
41. Hwang, T. G.; Kim, J. Y.; Namgoong, J. W.; Lee, J. M.; Yuk, S. B.; Kim, S. H.; Kim, J. P., Aggregation induced emission of diketopyrrolopyrrole (DPP) derivatives for highly fluorescent red films. *Photochemical & Photobiological Sciences* **2019**.
42. Tong, H.; Hong, Y.; Dong, Y.; Häußler, M.; Lam, J. W. Y.; Li, Z.; Guo, Z.; Guo, Z.; Tang, B. Z., Fluorescent "light-up" bioprobes based on tetraphenylethylene derivatives with aggregation-induced emission characteristics. *Chemical Communications* **2006,** (35), 3705-3707.
43. Zou, Q.; Tao, F.; Wu, H.; Yu, W. W.; Li, T.; Cui, Y., A new carbazole-based colorimetric and fluorescent sensor with aggregation induced emission for detection of cyanide anion. *Dyes and Pigments* **2019,** *164*, 165-173.
44. Tang, B. Z.; Geng, Y.; Lam, J. W. Y.; Li, B.; Jing, X.; Wang, X.; Wang, F.; Pakhomov, A. B.; Zhang, X. X., Processible Nanostructured Materials with Electrical Conductivity and Magnetic Susceptibility: Preparation and Properties of Maghemite/Polyaniline Nanocomposite Films. *Chemistry of Materials* **1999,** *11* (6), 1581-1589.
45. Datta, S.; Bhattacharya, S., Evidence of aggregation induced emission enhancement and keto-enol-tautomerism in a gallic acid derived salicylideneaniline gel. *Chemical Communications* **2012,** *48* (6), 877-879.
46. Bhosale, R. S.; Aljabri, M.; La, D. D.; Bhosale, S. V.; Jones, L. A.; Bhosale, S. V., Tetraphenylethene Derivatives: A Promising Class of AIE Luminogens—Synthesis, Properties, and Applications. In *Principles and Applications of Aggregation-Induced Emission*, Tang, Y.; Tang, B. Z., Eds. Springer International Publishing: Cham, 2019; pp 223-264.
47. Chen, S.; Qiu, R.; Yu, Q.; zhang, X.; Wei, M.; Dai, Z., Boranil dyes bearing tetraphenylethene: Synthesis, AIE/AIEE effect properties, pH sensitive properties and application in live cell imaging. *Tetrahedron Letters* **2018,** *59* (27), 2671-2678.
48. Chen, T.; Chen, Z.-Q.; Gong, W.-L.; Li, C.; Zhu, M.-Q., Ultrasensitive water sensors based on fluorenone-tetraphenylethene AIE luminogens. *Materials Chemistry Frontiers* **2017,** *1* (9), 1841-1846.
49. Mahendran, V.; Pasumpon, K.; Thimmarayaperumal, S.; Thilagar, P.; Shanmugam, S., Tetraphenylethene–2-Pyrone Conjugate: Aggregation-Induced Emission Study and Explosives Sensor. *The Journal of Organic Chemistry* **2016,** *81* (9), 3597-3602.
50. Ooyama, Y.; Sagisaka, R.; Enoki, T.; Tsunoji, N.; Ohshita, J., Tetraphenylethene– and diphenyldibenzofulvene–anthracene-based fluorescence sensors possessing photo-induced electron transfer and aggregation-induced emission enhancement characteristics for detection of water. *New Journal of Chemistry* **2018,** *42* (16), 13339-13350.

51. Ooyama, Y.; Sugino, M.; EnoKi, T.; Yamamoto, K.; Tsunoji, N.; Ohshita, J., Aggregation-induced emission (AIE) characteristic of water-soluble tetraphenylethene (TPE) bearing four sulfonate salts. *New Journal of Chemistry* **2017,** *41* (12), 4747-4749.
52. Banal, J. L.; White, J. M.; Ghiggino, K. P.; Wong, W. W. H., Concentrating Aggregation-Induced Fluorescence in Planar Waveguides: A Proof-of-Principle. *Scientific Reports* **2014,** *4*, 4635.
53. He, J.; Xu, B.; Chen, F.; Xia, H.; Li, K.; Ye, L.; Tian, W., Aggregation-Induced Emission in the Crystals of 9,10-Distyrylanthracene Derivatives: The Essential Role of Restricted Intramolecular Torsion. *The Journal of Physical Chemistry C* **2009,** *113* (22), 9892-9899.
54. Hu, R.; Lam, J. W. Y.; Liu, Y.; Zhang, X.; Tang, B. Z., Aggregation-Induced Emission of Tetraphenylethene–Hexaphenylbenzene Adducts: Effects of Twisting Amplitude and Steric Hindrance on Light Emission of Nonplanar Fluorogens. *Chemistry – A European Journal* **2013,** *19* (18), 5617-5624.
55. Shimizu, M.; Tatsumi, H.; Mochida, K.; Shimono, K.; Hiyama, T., Synthesis, Crystal Structure, and Photophysical Properties of (1E,3E,5E)-1,3,4,6-Tetraarylhexa-1,3,5-trienes: A New Class of Fluorophores Exhibiting Aggregation-Induced Emission. *Chemistry – An Asian Journal* **2009,** *4* (8), 1289-1297.
56. Bandrowsky, T. L.; Carroll, J. B.; Braddock-Wilking, J., Synthesis, Characterization, and Crystal Structures of 1,1-Disubstituted-2,3,4,5-tetraphenylgermoles That Exhibit Aggregation-Induced Emission. *Organometallics* **2011,** *30* (13), 3559-3569.
57. Feng, X.; Tong, B.; Shen, J.; Shi, J.; Han, T.; Chen, L.; Zhi, J.; Lu, P.; Ma, Y.; Dong, Y., Aggregation-Induced Emission Enhancement of Aryl-Substituted Pyrrole Derivatives. *The Journal of Physical Chemistry B* **2010,** *114* (50), 16731-16736.
58. Fukazawa, A.; Ichihashi, Y.; Yamaguchi, S., Intense fluorescence of 1-aryl-2,3,4,5-tetraphenylphosphole oxides in the crystalline state. *New Journal of Chemistry* **2010,** *34* (8), 1537-1540.
59. Lai, C.-T.; Hong, J.-L., Aggregation-Induced Emission in Tetraphenylthiophene-Derived Organic Molecules and Vinyl Polymer. *The Journal of Physical Chemistry B* **2010,** *114* (32), 10302-10310.
60. Shiraishi, K.; Kashiwabara, T.; Sanji, T.; Tanaka, M., Aggregation-induced emission of dendritic phosphole oxides. *New Journal of Chemistry* **2009,** *33* (8), 1680-1684.
61. Tracy, H. J.; Mullin, J. L.; Klooster, W. T.; Martin, J. A.; Haug, J.; Wallace, S.; Rudloe, I.; Watts, K., Enhanced Photoluminescence from Group 14 Metalloles in Aggregated and Solid Solutions. *Inorganic Chemistry* **2005,** *44* (6), 2003-2011.
62. Cheng, X.; Li, D.; Zhang, Z.; Zhang, H.; Wang, Y., Organoboron Compounds with Morphology-Dependent NIR Emissions and Dual-Channel Fluorescent ON/OFF Switching. *Organic Letters* **2014,** *16* (3), 880-883.
63. Galer, P.; Korošec, R. C.; Vidmar, M.; Šket, B., Crystal Structures and Emission Properties of the BF2 Complex 1-Phenyl-3-(3,5-dimethoxyphenyl)-propane-1,3-dione: Multiple Chromisms, Aggregation- or Crystallization-Induced Emission, and the Self-Assembly Effect. *Journal of the American Chemical Society* **2014,** *136* (20), 7383-7394.
64. Kokado, K.; Chujo, Y., Emission via Aggregation of Alternating Polymers with o-Carborane and p-Phenylene−Ethynylene Sequences. *Macromolecules* **2009,** *42* (5), 1418-1420.
65. Kokado, K.; Chujo, Y., Multicolor Tuning of Aggregation-Induced Emission through Substituent Variation of Diphenyl-o-carborane. *The Journal of Organic Chemistry* **2011,** *76* (1), 316-319.
66. Yan, W.; Hong, C.; Long, G.; Yang, Y.; Liu, Z.; Bian, Z.; Chen, Y.; Huang, C., Synthesis, crystal structures and photophysical properties of novel boron-containing

derivatives of phenalene with bright solid-state luminescence. *Dyes and Pigments* **2014,** *106*, 197-204.

67. Han, T.; Hong, Y.; Xie, N.; Chen, S.; Zhao, N.; Zhao, E.; Lam, J. W. Y.; Sung, H. H. Y.; Dong, Y.; Tong, B.; Tang, B. Z., Defect-sensitive crystals based on diaminomaleonitrile-functionalized Schiff base with aggregation-enhanced emission. *Journal of Materials Chemistry C* **2013,** *1* (44), 7314-7320.
68. Liu, G.; Yang, M.; Wang, L.; Zheng, J.; Zhou, H.; Wu, J.; Tian, Y., Schiff base derivatives containing heterocycles with aggregation-induced emission and recognition ability. *Journal of Materials Chemistry C* **2014,** *2* (15), 2684-2691.
69. Cao, Y.; Xi, W.; Wang, L.; Wang, H.; Kong, L.; Zhou, H.; Wu, J.; Tian, Y., Reversible piezofluorochromic nature and mechanism of aggregation-induced emission-active compounds based on simple modification. *RSC Advances* **2014,** *4* (47), 24649-24652.
70. Shao, A.; Guo, Z.; Zhu, S.; Zhu, S.; Shi, P.; Tian, H.; Zhu, W., Insight into aggregation-induced emission characteristics of red-emissive quinoline-malononitrile by cell tracking and real-time trypsin detection. *Chemical Science* **2014,** *5* (4), 1383-1389.
71. Tian, G.; Huang, W.; Cai, S.; Zhou, H.; Li, B.; Wang, Q.; Su, J., Small molecules based on diphenylamine and carbazole with large two-photon absorption cross sections and extraordinary AIEE properties. *RSC Advances* **2014,** *4* (73), 38939-38942.
72. Zhao, X.; Xue, P.; Wang, K.; Chen, P.; Zhang, P.; Lu, R., Aggregation-induced emission of triphenylamine substituted cyanostyrene derivatives. *New Journal of Chemistry* **2014,** *38* (3), 1045-1051.
73. Zheng, Z.; Yu, Z.; Yang, M.; Jin, F.; Zhang, Q.; Zhou, H.; Wu, J.; Tian, Y., Substituent Group Variations Directing the Molecular Packing, Electronic Structure, and Aggregation-Induced Emission Property of Isophorone Derivatives. *The Journal of Organic Chemistry* **2013,** *78* (7), 3222-3234.
74. Han, T.; Zhang, Y.; Feng, X.; Lin, Z.; Tong, B.; Shi, J.; Zhi, J.; Dong, Y., Reversible and hydrogen bonding-assisted piezochromic luminescence for solid-state tetraaryl-buta-1,3-diene. *Chemical Communications* **2013,** *49* (63), 7049-7051.
75. Namitharan, K.; Pitchumani, K., Cascade synthesis of bis-N-sulfonylcyclobutenes via Cu(i)/Lewis acid-catalyzed (3 + 2)/(2 + 2) cycloadditions: observation of aggregation-induced emission enhancement from restricted C=N photoisomerization. *Organic & Biomolecular Chemistry* **2012,** *10* (15), 2937-2941.
76. Nandakumar, A.; Perumal, P. T., Tetrasubstituted Olefinic Xanthene Dyes: Synthesis via Pd-Catalyzed 6-exo-dig Cyclization/C–H Activation of 2-Bromobenzyl-N-propargylamines and Solid State Fluorescence Properties. *Organic Letters* **2013,** *15* (2), 382-385.
77. Natarajan, P., Luminescence of triarylphosphines and their application to detection of elemental chlorine in aqueous solution. *Analytical Methods* **2014,** *6* (8), 2432-2435.
78. Shimizu, M.; Asai, Y.; Takeda, Y.; Yamatani, A.; Hiyama, T., Twisting strategy applied to N,N-diorganoquinacridones leads to organic chromophores exhibiting efficient solid-state fluorescence. *Tetrahedron Letters* **2011,** *52* (32), 4084-4089.
79. Shimizu, M.; Takeda, Y.; Higashi, M.; Hiyama, T., 1,4-Bis(alkenyl)-2,5-dipiperidinobenzenes: Minimal Fluorophores Exhibiting Highly Efficient Emission in the Solid State. *Angewandte Chemie International Edition* **2009,** *48* (20), 3653-3656.
80. Zhang, X.; Lu, X.; Zhen, Y.; Liu, J.; Dong, H.; Zhao, G.; He, P.; Wang, Z.; Jiang, L.; Hu, W., Synthesis and aggregation-induced emissions of thienyl substituted cyclobutene derivatives. *Journal of Materials Chemistry C* **2014,** *2* (26), 5083-5086.
81. Beppu, T.; Kawata, S.; Aizawa, N.; Pu, Y.-J.; Abe, Y.; Ohba, Y.; Katagiri, H., 2,6-Bis(arylsulfonyl)anilines as Fluorescent Scaffolds through Intramolecular Hydrogen

Bonds: Solid-State Fluorescence Materials and Turn-On-Type Probes Based on Aggregation-Induced Emission. *ChemPlusChem* **2014,** *79* (4), 536-545.

82. Mutai, T.; Tomoda, H.; Ohkawa, T.; Yabe, Y.; Araki, K., Switching of Polymorph-Dependent ESIPT Luminescence of an Imidazo[1,2-a]pyridine Derivative. *Angewandte Chemie International Edition* **2008,** *47* (49), 9522-9524.
83. Shen, Y.-T.; Li, C.-H.; Chang, K.-C.; Chin, S.-Y.; Lin, H.-A.; Liu, Y.-M.; Hung, C.-Y.; Hsu, H.-F.; Sun, S.-S., Synthesis, Optical, and Mesomorphic Properties of Self-Assembled Organogels Featuring Phenylethynyl Framework with Elaborated Long-Chain Pyridine-2,6-Dicarboxamides. *Langmuir* **2009,** *25* (15), 8714-8722.
84. Tang, W.; Xiang, Y.; Tong, A., Salicylaldehyde Azines as Fluorophores of Aggregation-Induced Emission Enhancement Characteristics. *The Journal of Organic Chemistry* **2009,** *74* (5), 2163-2166.
85. Wei, R.; Song, P.; Tong, A., Reversible Thermochromism of Aggregation-Induced Emission-Active Benzophenone Azine Based on Polymorph-Dependent Excited-State Intramolecular Proton Transfer Fluorescence. *The Journal of Physical Chemistry C* **2013,** *117* (7), 3467-3474.
86. Yoshii, R.; Hirose, A.; Tanaka, K.; Chujo, Y., Boron Diiminate with Aggregation-Induced Emission and Crystallization-Induced Emission-Enhancement Characteristics. *Chemistry – A European Journal* **2014,** *20* (27), 8320-8324.
87. Chan, C. Y. K.; Tseng, N.-W.; Lam, J. W. Y.; Liu, J.; Kwok, R. T. K.; Tang, B. Z., Construction of Functional Macromolecules with Well-Defined Structures by Indium-Catalyzed Three-Component Polycoupling of Alkynes, Aldehydes, and Amines. *Macromolecules* **2013,** *46* (9), 3246-3256.
88. Hu, R.; Maldonado, J. L.; Rodriguez, M.; Deng, C.; Jim, C. K. W.; Lam, J. W. Y.; Yuen, M. M. F.; Ramos-Ortiz, G.; Tang, B. Z., Luminogenic materials constructed from tetraphenylethene building blocks: Synthesis, aggregation-induced emission, two-photon absorption, light refraction, and explosive detection. *Journal of Materials Chemistry* **2012,** *22* (1), 232-240.
89. Shi, J.; Wu, Y.; Sun, S.; Tong, B.; Zhi, J.; Dong, Y., Tunable fluorescence conjugated copolymers consisting of tetraphenylethylene and fluorene units: From aggregation-induced emission enhancement to dual-channel fluorescence response. *Journal of Polymer Science Part A: Polymer Chemistry* **2013,** *51* (2), 229-240.
90. Yao, B.; Mei, J.; Li, J.; Wang, J.; Wu, H.; Sun, J. Z.; Qin, A.; Tang, B. Z., Catalyst-Free Thiol–Yne Click Polymerization: A Powerful and Facile Tool for Preparation of Functional Poly(vinylene sulfide)s. *Macromolecules* **2014,** *47* (4), 1325-1333.
91. Chien, R.-H.; Lai, C.-T.; Hong, J.-L., Enhanced Aggregation Emission of Vinyl Polymer Containing Tetraphenylthiophene Pendant Group. *The Journal of Physical Chemistry C* **2011,** *115* (13), 5958-5965.
92. Dong, W.; Fei, T.; Palma-Cando, A.; Scherf, U., Aggregation induced emission and amplified explosive detection of tetraphenylethylene-substituted polycarbazoles. *Polymer Chemistry* **2014,** *5* (13), 4048-4053.
93. Ma, C.; Ling, Q.; Xu, S.; Zhu, H.; Zhang, G.; Zhou, X.; Chi, Z.; Liu, S.; Zhang, Y.; Xu, J., Preparation of Biocompatible Aggregation-Induced Emission Homopolymeric Nanoparticles for Cell Imaging. *Macromolecular Bioscience* **2014,** *14* (2), 235-243.
94. Wang, T.; Cai, Y.; Wang, Z.; Guan, E.; Yu, D.; Qin, A.; Sun, J.; Tang, B. Z.; Gao, C., Decomposition-Assembly of Tetraphenylethylene Nanoparticles With Uniform Size and Aggregation-Induced Emission property. *Macromolecular Rapid Communications* **2012,** *33* (18), 1584-1589.

95. Wang, Z.; Chen, S.; Lam, J. W. Y.; Qin, W.; Kwok, R. T. K.; Xie, N.; Hu, Q.; Tang, B. Z., Long-Term Fluorescent Cellular Tracing by the Aggregates of AIE Bioconjugates. *Journal of the American Chemical Society* **2013,** *135* (22), 8238-8245.
96. Yuan, W. Z.; Zhao, H.; Shen, X. Y.; Mahtab, F.; Lam, J. W. Y.; Sun, J. Z.; Tang, B. Z., Luminogenic Polyacetylenes and Conjugated Polyelectrolytes: Synthesis, Hybridization with Carbon Nanotubes, Aggregation-Induced Emission, Superamplification in Emission Quenching by Explosives, and Fluorescent Assay for Protein Quantitation. *Macromolecules* **2009,** *42* (24), 9400-9411.
97. Hu, R.; Lam, J. W. Y.; Liu, J.; Sung, H. H. Y.; Williams, I. D.; Yue, Z.; Wong, K. S.; Yuen, M. M. F.; Tang, B. Z., Hyperbranched conjugated poly(tetraphenylethene): synthesis, aggregation-induced emission, fluorescent photopatterning, optical limiting and explosive detection. *Polymer Chemistry* **2012,** *3* (6), 1481-1489.
98. Hu, X.-M.; Chen, Q.; Zhou, D.; Cao, J.; He, Y.-J.; Han, B.-H., One-step preparation of fluorescent inorganic–organic hybrid material used for explosive sensing. *Polymer Chemistry* **2011,** *2* (5), 1124-1128.
99. Wang, J.; Mei, J.; Yuan, W.; Lu, P.; Qin, A.; Sun, J.; Ma, Y.; Tang, B. Z., Hyperbranched polytriazoles with high molecular compressibility: aggregation-induced emission and superamplified explosive detection. *Journal of Materials Chemistry* **2011,** *21* (12), 4056-4059.
100. Xu, Y.; Chen, L.; Guo, Z.; Nagai, A.; Jiang, D., Light-Emitting Conjugated Polymers with Microporous Network Architecture: Interweaving Scaffold Promotes Electronic Conjugation, Facilitates Exciton Migration, and Improves Luminescence. *Journal of the American Chemical Society* **2011,** *133* (44), 17622-17625.
101. Arseneault, M.; Leung, N. L. C.; Fung, L. T.; Hu, R.; Morin, J.-F.; Tang, B. Z., Probing the dendritic architecture through AIE: challenges and successes. *Polymer Chemistry* **2014,** *5* (20), 6087-6096.
102. Chen, Y.; Lv, Y.; Han, Y.; Zhu, B.; Zhang, F.; Bo, Z.; Liu, C.-Y., Dendritic Effect on Supramolecular Self-Assembly: Organogels with Strong Fluorescence Emission Induced by Aggregation. *Langmuir* **2009,** *25* (15), 8548-8555.
103. Huang, G.; Ma, B.; Chen, J.; Peng, Q.; Zhang, G.; Fan, Q.; Zhang, D., Dendron-Containing Tetraphenylethylene Compounds: Dependence of Fluorescence and Photocyclization Reactivity on the Dendron Generation. *Chemistry – A European Journal* **2012,** *18* (13), 3886-3892.
104. Zeng, Y.; Li, P.; Liu, X.; Yu, T.; Chen, J.; Yang, G.; Li, Y., A "breathing" dendritic molecule—conformational fluctuation induced by external stimuli. *Polymer Chemistry* **2014,** *5* (20), 5978-5984.
105. Shustova, N. B.; McCarthy, B. D.; Dincă, M., Turn-On Fluorescence in Tetraphenylethylene-Based Metal–Organic Frameworks: An Alternative to Aggregation-Induced Emission. *Journal of the American Chemical Society* **2011,** *133* (50), 20126-20129.
106. Wei, Z.; Gu, Z.-Y.; Arvapally, R. K.; Chen, Y.-P.; McDougald, R. N.; Ivy, J. F.; Yakovenko, A. A.; Feng, D.; Omary, M. A.; Zhou, H.-C., Rigidifying Fluorescent Linkers by Metal–Organic Framework Formation for Fluorescence Blue Shift and Quantum Yield Enhancement. *Journal of the American Chemical Society* **2014,** *136* (23), 8269-8276.
107. Zhang, M.; Feng, G.; Song, Z.; Zhou, Y.-P.; Chao, H.-Y.; Yuan, D.; Tan, T. T. Y.; Guo, Z.; Hu, Z.; Tang, B. Z.; Liu, B.; Zhao, D., Two-Dimensional Metal–Organic Framework with Wide Channels and Responsive Turn-On Fluorescence for the Chemical Sensing of Volatile Organic Compounds. *Journal of the American Chemical Society* **2014,** *136* (20), 7241-7244.

108. He, B.; Ye, S.; Guo, Y.; Chen, B.; Xu, X.; Qiu, H.; Zhao, Z., Aggregation-enhanced emission and efficient electroluminescence of conjugated polymers containing tetraphenylethene units. *Science China Chemistry* **2013,** *56* (9), 1221-1227.
109. Santos, M. A., Chemistry and applications of metal complexes. *Dalton Transactions* **2013,** *42* (17), 5957-5959.
110. Turel, I., Special Issue: Practical Applications of Metal Complexes. *Molecules* **2015,** *20* (5).
111. Xu, H.; Chen, R.; Sun, Q.; Lai, W.; Su, Q.; Huang, W.; Liu, X., Recent progress in metal–organic complexes for optoelectronic applications. *Chemical Society Reviews* **2014,** *43* (10), 3259-3302.
112. Fujisawa, K.; Okuda, Y.; Izumi, Y.; Nagamatsu, A.; Rokusha, Y.; Sadaike, Y.; Tsutsumi, O., Reversible thermal-mode control of luminescence from liquid-crystalline gold(i) complexes. *Journal of Materials Chemistry C* **2014,** *2* (18), 3549-3555.
113. Jia, X.; Li, J.; Wang, E., Supramolecular self-assembly of morphology-dependent luminescent Ag nanoclusters. *Chemical Communications* **2014,** *50* (67), 9565-9568.
114. Liang, J.; Chen, Z.; Yin, J.; Yu, G.-A.; Liu, S. H., Aggregation-induced emission (AIE) behavior and thermochromic luminescence properties of a new gold(i) complex. *Chemical Communications* **2013,** *49* (34), 3567-3569.
115. Xin, X.-L.; Chen, M.; Ai, Y.-b.; Yang, F.-l.; Li, X.-L.; Li, F., Aggregation-Induced Emissive Copper(I) Complexes for Living Cell Imaging. *Inorganic Chemistry* **2014,** *53* (6), 2922-2931.
116. Chen, Z.; Wong, K. M.-C.; Kwok, E. C.-H.; Zhu, N.; Zu, Y.; Yam, V. W.-W., Electrogenerated Chemiluminescence of Platinum(II) Alkynyl Terpyridine Complex with Peroxydisulfate as Coreactant. *Inorganic Chemistry* **2011,** *50* (6), 2125-2132.
117. Honda, H.; Ogawa, Y.; Kuwabara, J.; Kanbara, T., Emission Behavior of Secondary Thioamide-Based Cationic Pincer Platinum(II) Complexes in the Aggregate State. *European Journal of Inorganic Chemistry* **2014,** *2014* (11), 1865-1869.
118. Kuwabara, J.; Ogawa, Y.; Taketoshi, A.; Kanbara, T., Enhancement of the photoluminescence of a thioamide-based pincer palladium complex in the crystalline state. *Journal of Organometallic Chemistry* **2011,** *696* (6), 1289-1293.
119. Li, Y.; Tsang, D. P.-K.; Chan, C. K.-M.; Wong, K. M.-C.; Chan, M.-Y.; Yam, V. W.-W., Synthesis of Unsymmetric Bipyridine–PtII–Alkynyl Complexes through Post-Click Reaction with Emission Enhancement Characteristics and Their Applications as Phosphorescent Organic Light-Emitting Diodes. *Chemistry – A European Journal* **2014,** *20* (42), 13710-13715.
120. Xie, Y.-Z.; Shan, G.-G.; Li, P.; Zhou, Z.-Y.; Su, Z.-M., A novel class of Zn(II) Schiff base complexes with aggregation-induced emission enhancement (AIEE) properties: Synthesis, characterization and photophysical/electrochemical properties. *Dyes and Pigments* **2013,** *96* (2), 467-474.
121. Alam, P.; Das, P.; Climent, C.; Karanam, M.; Casanova, D.; Choudhury, A. R.; Alemany, P.; Jana, N. R.; Laskar, I. R., Facile tuning of the aggregation-induced emission wavelength in a common framework of a cyclometalated iridium(iii) complex: micellar encapsulated probe in cellular imaging. *Journal of Materials Chemistry C* **2014,** *2* (28), 5615-5628.
122. Alam, P.; Karanam, M.; Bandyopadhyay, D.; Choudhury, A. R.; Laskar, I. R., Aggregation-Induced Emission Activity in Iridium(III) Diimine Complexes: Investigations of Their Vapochromic Properties. *European Journal of Inorganic Chemistry* **2014,** *2014* (23), 3710-3719.

123. Chen, Y.; Xu, W.-C.; Kou, J.-F.; Yu, B.-L.; Wei, X.-H.; Chao, H.; Ji, L.-N., Aggregation-induced emission of ruthenium(II) polypyridyl complex [Ru(bpy)2(pzta)]2+. *Inorganic Chemistry Communications* **2010,** *13* (10), 1140-1143.
124. Howarth, A. J.; Patia, R.; Davies, D. L.; Lelj, F.; Wolf, M. O.; Singh, K., Elucidating the Origin of Enhanced Phosphorescence Emission in the Solid State (EPESS) in Cyclometallated Iridium Complexes. *European Journal of Inorganic Chemistry* **2014,** *2014* (23), 3657-3664.
125. Huang, K.; Wu, H.; Shi, M.; Li, F.; Yi, T.; Huang, C., Reply to comment on 'aggregation-induced phosphorescent emission (AIPE) of iridium(iii) complexes': origin of the enhanced phosphorescence. *Chemical Communications* **2009,** (10), 1243-1245.
126. Quartapelle Procopio, E.; Mauro, M.; Panigati, M.; Donghi, D.; Mercandelli, P.; Sironi, A.; D'Alfonso, G.; De Cola, L., Highly Emitting Concomitant Polymorphic Crystals of a Dinuclear Rhenium Complex. *Journal of the American Chemical Society* **2010,** *132* (41), 14397-14399.
127. Sathish, V.; Ramdass, A.; Lu, Z.-Z.; Velayudham, M.; Thanasekaran, P.; Lu, K.-L.; Rajagopal, S., Aggregation-Induced Emission Enhancement in Alkoxy-Bridged Binuclear Rhenium(I) Complexes: Application as Sensor for Explosives and Interaction with Microheterogeneous Media. *The Journal of Physical Chemistry B* **2013,** *117* (46), 14358-14366.
128. Zhao, Q.; Li, L.; Li, F.; Yu, M.; Liu, Z.; Yi, T.; Huang, C., Aggregation-induced phosphorescent emission (AIPE) of iridium(iii) complexes. *Chemical Communications* **2008,** (6), 685-687.
129. Zhu, C.; Li, S.; Luo, M.; Zhou, X.; Niu, Y.; Lin, M.; Zhu, J.; Cao, Z.; Lu, X.; Wen, T.; Xie, Z.; Schleyer, P. v. R.; Xia, H., Stabilization of anti-aromatic and strained five-membered rings with a transition metal. *Nature Chemistry* **2013,** *5*, 698.
130. Liang, J.; Chen, Z.; Xu, L.; Wang, J.; Yin, J.; Yu, G.-A.; Chen, Z.-N.; Liu, S. H., Aggregation-induced emission-active gold(i) complexes with multi-stimuli luminescence switching. *Journal of Materials Chemistry C* **2014,** *2* (12), 2243-2250.
131. Agbaria, R. A.; Oldham, P. B.; McCarroll, M.; McGown, L. B.; Warner, I. M., Molecular Fluorescence, Phosphorescence, and Chemiluminescence Spectrometry. *Analytical Chemistry* **2002,** *74* (16), 3952-3962.
132. Kitai, A. H., Luminescent materials and applications. John Wiley: Chichester, 2008.
133. Lakowicz, J. R., Topics in fluorescence spectroscopy. Vol. 3, Vol. 3. **2002**.
134. Roda, A., Luminescence provides powerful performance in practical applications: Report on the XIII International Symposium on Luminescence Spectrometry – Analytical Luminescence: New Diagnostic Tools in Life Science, Food Safety and Cultural Heritage, Bologna, Italy, 7–11 September 2008. *TrAC Trends in Analytical Chemistry* **2009,** *28* (1), 10-12.
135. Saragi, T. P. I.; Spehr, T.; Siebert, A.; Fuhrmann-Lieker, T.; Salbeck, J., Spiro Compounds for Organic Optoelectronics. *Chemical Reviews* **2007,** *107* (4), 1011-1065.
136. Wu, K. C.; Ku, P. J.; Lin, C. S.; Shih, H. T.; Wu, F. I.; Huang, M. J.; Lin, J. J.; Chen, I. C.; Cheng, C. H., The Photophysical Properties of Dipyrenylbenzenes and Their Application as Exceedingly Efficient Blue Emitters for Electroluminescent Devices. *Advanced Functional Materials* **2008,** *18* (1), 67-75.
137. Huang, J.; Sun, N.; Dong, Y.; Tang, R.; Lu, P.; Cai, P.; Li, Q.; Ma, D.; Qin, J.; Li, Z., Similar or Totally Different: The Control of Conjugation Degree through Minor Structural Modifications, and Deep-Blue Aggregation-Induced Emission Luminogens for Non-Doped OLEDs. *Advanced Functional Materials* **2013,** *23* (18), 2329-2337.
138. Huang, J.; Sun, N.; Yang, J.; Tang, R.; Li, Q.; Ma, D.; Qin, J.; Li, Z., Benzene-cored fluorophors with TPE peripheries: facile synthesis, crystallization-induced blue-shifted

emission, and efficient blue luminogens for non-doped OLEDs. *Journal of Materials Chemistry* **2012,** *22* (24), 12001-12007.

139. Huang, J.; Yang, X.; Wang, J.; Zhong, C.; Wang, L.; Qin, J.; Li, Z., New tetraphenylethene-based efficient blue luminophors: aggregation induced emission and partially controllable emitting color. *Journal of Materials Chemistry* **2012,** *22* (6), 2478-2484.
140. Zhao, Z.; Chan, C. Y. K.; Chen, S.; Deng, C.; Lam, J. W. Y.; Jim, C. K. W.; Hong, Y.; Lu, P.; Chang, Z.; Chen, X.; Lu, P.; Kwok, H. S.; Qiu, H.; Tang, B. Z., Using tetraphenylethene and carbazole to create efficient luminophores with aggregation-induced emission, high thermal stability, and good hole-transporting property. *Journal of Materials Chemistry* **2012,** *22* (10), 4527-4534.
141. Du, X.; Qi, J.; Zhang, Z.; Ma, D.; Wang, Z. Y., Efficient Non-doped Near Infrared Organic Light-Emitting Devices Based on Fluorophores with Aggregation-Induced Emission Enhancement. *Chemistry of Materials* **2012,** *24* (11), 2178-2185.
142. Li, H.; Chi, Z.; Zhang, X.; Xu, B.; Liu, S.; Zhang, Y.; Xu, J., New thermally stable aggregation-induced emission enhancement compounds for non-doped red organic light-emitting diodes. *Chemical Communications* **2011,** *47* (40), 11273-11275.
143. Chen, Y.; Lin, J.; Yuan, W.; Yu, Z.; Lam, J. W.; Tang, B. Z., 1-((12-Bromododecyl)oxy)-4-((4-(4-pentylcyclohexyl)phenyl)ethynyl) benzene: Liquid crystal with aggregation-induced emission characteristics. *Science China Chemistry* **2013,** *56* (9), 1191-1196.
144. Wan, J.-H.; Mao, L.-Y.; Li, Y.-B.; Li, Z.-F.; Qiu, H.-Y.; Wang, C.; Lai, G.-Q., Self-assembly of novel fluorescent silole derivatives into different supramolecular aggregates: fibre, liquid crystal and monolayer. *Soft Matter* **2010,** *6* (14), 3195-3201.
145. Yoon, S.-J.; Kim, J. H.; Kim, K. S.; Chung, J. W.; Heinrich, B.; Mathevet, F.; Kim, P.; Donnio, B.; Attias, A.-J.; Kim, D.; Park, S. Y., Mesomorphic Organization and Thermochromic Luminescence of Dicyanodistyrylbenzene-Based Phasmidic Molecular Disks: Uniaxially Aligned Hexagonal Columnar Liquid Crystals at Room Temperature with Enhanced Fluorescence Emission and Semiconductivity. *Advanced Functional Materials* **2012,** *22* (1), 61-69.
146. Yuan, W. Z.; Yu, Z.-Q.; Lu, P.; Deng, C.; Lam, J. W. Y.; Wang, Z.; Chen, E.-Q.; Ma, Y.; Tang, B. Z., High efficiency luminescent liquid crystal: aggregation-induced emission strategy and biaxially oriented mesomorphic structure. *Journal of Materials Chemistry* **2012,** *22* (8), 3323-3326.
147. Liu, J.; Su, H.; Meng, L.; Zhao, Y.; Deng, C.; Ng, J. C. Y.; Lu, P.; Faisal, M.; Lam, J. W. Y.; Huang, X.; Wu, H.; Wong, K. S.; Tang, B. Z., What makes efficient circularly polarised luminescence in the condensed phase: aggregation-induced circular dichroism and light emission. *Chemical Science* **2012,** *3* (9), 2737-2747.
148. Xue, S.; Meng, L.; Wen, R.; Shi, L.; Lam, J. W.; Tang, Z.; Li, B. S.; Tang, B. Z., Unexpected aggregation induced circular dichroism, circular polarized luminescence and helical assembly from achiral hexaphenylsilole (HPS). *RSC Advances* **2017,** *7* (40), 24841-24847.
149. Zhang, S.; Sheng, Y.; Wei, G.; Quan, Y.; Cheng, Y.; Zhu, C., Aggregation-induced circularly polarized luminescence of an (R)-binaphthyl-based AIE-active chiral conjugated polymer with self-assembled helical nanofibers. *Polymer Chemistry* **2015,** *6* (13), 2416-2422.
150. Zhang, S.; Wang, Y.; Meng, F.; Dai, C.; Cheng, Y.; Zhu, C., Circularly polarized luminescence of AIE-active chiral O-BODIPYs induced via intramolecular energy transfer. *Chemical Communications* **2015,** *51* (43), 9014-9017.

151. Gu, X.; Yao, J.; Zhang, G.; Yan, Y.; Zhang, C.; Peng, Q.; Liao, Q.; Wu, Y.; Xu, Z.; Zhao, Y.; Fu, H.; Zhang, D., Polymorphism-Dependent Emission for Di(p-methoxylphenyl)dibenzofulvene and Analogues: Optical Waveguide/Amplified Spontaneous Emission Behaviors. *Advanced Functional Materials* **2012,** *22* (23), 4862-4872.
152. Shi, C.; Guo, Z.; Yan, Y.; Zhu, S.; Xie, Y.; Zhao, Y. S.; Zhu, W.; Tian, H., Self-Assembly Solid-State Enhanced Red Emission of Quinolinemalononitrile: Optical Waveguides and Stimuli Response. *ACS Applied Materials & Interfaces* **2013,** *5* (1), 192-198.
153. Zhao, N.; Li, M.; Yan, Y.; Lam, J. W. Y.; Zhang, Y. L.; Zhao, Y. S.; Wong, K. S.; Tang, B. Z., A tetraphenylethene-substituted pyridinium salt with multiple functionalities: synthesis, stimuli-responsive emission, optical waveguide and specific mitochondrion imaging. *Journal of Materials Chemistry C* **2013,** *1* (31), 4640-4646.
154. Chen, S. H.; Katsis, D.; Schmid, A. W.; Mastrangelo, J. C.; Tsutsui, T.; Blanton, T. N., Circularly polarized light generated by photoexcitation of luminophores in glassy liquid-crystal films. *Nature* **1999,** *397* (6719), 506-508.
155. Montali, A.; Bastiaansen, C.; Smith, P.; Weder, C., Polarizing energy transfer in photoluminescent materials for display applications. *Nature* **1998,** *392* (6673), 261-264.
156. Peeters, E.; Christiaans, M. P. T.; Janssen, R. A. J.; Schoo, H. F. M.; Dekkers, H. P. J. M.; Meijer, E. W., Circularly Polarized Electroluminescence from a Polymer Light-Emitting Diode. *Journal of the American Chemical Society* **1997,** *119* (41), 9909-9910.
157. Hu, F.; Liu, B., Organelle-specific bioprobes based on fluorogens with aggregation-induced emission (AIE) characteristics. *Organic & Biomolecular Chemistry* **2016,** *14* (42), 9931-9944.
158. Liang, J.; Tang, B. Z.; Liu, B., Specific light-up bioprobes based on AIEgen conjugates. *Chemical Society Reviews* **2015,** *44* (10), 2798-2811.
159. Mei, J.; Huang, Y.; Tian, H., Progress and Trends in AIE-Based Bioprobes: A Brief Overview. *ACS Applied Materials & Interfaces* **2018,** *10* (15), 12217-12261.
160. Shi, J.; Li, Y.; Li, Q.; Li, Z., Enzyme-Responsive Bioprobes Based on the Mechanism of Aggregation-Induced Emission. *ACS Applied Materials & Interfaces* **2018,** *10* (15), 12278-12294.
161. Hu, F.; Huang, Y.; Zhang, G.; Zhao, R.; Zhang, D., A highly selective fluorescence turn-on detection of hydrogen peroxide and d-glucose based on the aggregation/deaggregation of a modified tetraphenylethylene. *Tetrahedron Letters* **2014,** *55* (8), 1471-1474.
162. Liu, Y.; Deng, C.; Tang, L.; Qin, A.; Hu, R.; Sun, J. Z.; Tang, B. Z., Specific Detection of d-Glucose by a Tetraphenylethene-Based Fluorescent Sensor. *Journal of the American Chemical Society* **2011,** *133* (4), 660-663.
163. Shen, X.; Shi, Y.; Peng, B.; Li, K.; Xiang, J.; Zhang, G.; Liu, Z.; Chen, Y.; Zhang, D., Fluorescent Polymeric Micelles with Tetraphenylethylene Moieties and Their Application for the Selective Detection of Glucose. *Macromolecular Bioscience* **2012,** *12* (11), 1583-1590.
164. Zhang, L.; Zhang, Z.-Y.; Liang, R.-P.; Li, Y.-H.; Qiu, J.-D., Boron-Doped Graphene Quantum Dots for Selective Glucose Sensing Based on the "Abnormal" Aggregation-Induced Photoluminescence Enhancement. *Analytical Chemistry* **2014,** *86* (9), 4423-4430.
165. Liu, H.; Wang, X.; Xiang, Y.; Tong, A., Fluorescence turn-on detection of cysteine over homocysteine and glutathione based on "ESIPT" and "AIE". *Analytical Methods* **2015,** *7* (12), 5028-5033.

166. Tong, J.; Wang, Y.; Mei, J.; Wang, J.; Qin, A.; Sun, J. Z.; Tang, B. Z., A 1,3-Indandione-Functionalized Tetraphenylethene: Aggregation-Induced Emission, Solvatochromism, Mechanochromism, and Potential Application as a Multiresponsive Fluorescent Probe. *Chemistry – A European Journal* **2014,** *20* (16), 4661-4670.
167. Zhang, W.; Gao, N.; Cui, J.; Wang, C.; Wang, S.; Zhang, G.; Dong, X.; Zhang, D.; Li, G., AIE-doped poly(ionic liquid) photonic spheres: a single sphere-based customizable sensing platform for the discrimination of multi-analytes. *Chemical Science* **2017,** *8* (9), 6281-6289.
168. Alam, P.; Leung, N. L. C.; Su, H.; Qiu, Z.; Kwok, R. T. K.; Lam, J. W. Y.; Tang, B. Z., A Highly Sensitive Bimodal Detection of Amine Vapours Based on Aggregation Induced Emission of 1,2-Dihydroquinoxaline Derivatives. *Chemistry – A European Journal* **2017,** *23* (59), 14911-14917.
169. Nakamura, M.; Sanji, T.; Tanaka, M., Fluorometric Sensing of Biogenic Amines with Aggregation-Induced Emission-Active Tetraphenylethenes. *Chemistry – A European Journal* **2011,** *17* (19), 5344-5349.
170. Jiang, G.; Zhu, W.; Chen, Q.; Shi, A.; Wu, Y.; Zhang, G.; Li, X.; Li, Y.; Fan, X.; Wang, J., A new tetraphenylethylene based AIE sensor with light-up and tunable measuring range for adenosine triphosphate in aqueous solution and in living cells. *Analyst* **2017,** *142* (23), 4388-4392.
171. Ma, H.; Yang, M.; Zhang, C.; Ma, Y.; Qin, Y.; Lei, Z.; Chang, L.; Lei, L.; Wang, T.; Yang, Y., Aggregation-induced emission (AIE)-active fluorescent probes with multiple binding sites toward ATP sensing and live cell imaging. *Journal of Materials Chemistry B* **2017,** *5* (43), 8525-8531.
172. Ma, K.; Wang, H.; Li, H.; Wang, S.; Li, X.; Xu, B.; Tian, W., A label-free aptasensor for turn-on fluorescent detection of ATP based on AIE-active probe and water-soluble carbon nanotubes. *Sensors and Actuators B: Chemical* **2016,** *230*, 556-558.
173. Noguchi, T.; Shiraki, T.; Dawn, A.; Tsuchiya, Y.; Ngoc Lien, L. T.; Yamamoto, T.; Shinkai, S., Nonlinear fluorescence response driven by ATP-induced self-assembly of guanidinium-tethered tetraphenylethene. *Chemical Communications* **2012,** *48* (65), 8090-8092.
174. Zhang, Y.; Li, Y.; Su, C.; Barboiu, M., Dynameric Frameworks with Aggregation-Induced Emission for Selective Detection of Adenosine Triphosphate. *ChemPlusChem* **2018,** *83* (6), 506-513.
175. Zhao, M.; Wang, M.; Liu, H.; Liu, D.; Zhang, G.; Zhang, D.; Zhu, D., Continuous On-Site Label-Free ATP Fluorometric Assay Based on Aggregation-Induced Emission of Silole. *Langmuir* **2009,** *25* (2), 676-678.
176. Li, X.; Zhang, X.; Chi, Z.; Chao, X.; Zhou, X.; Zhang, Y.; Liu, S.; Xu, J., Simple fluorescent probe derived from tetraphenylethylene and benzoquinone for instantaneous biothiol detection. *Analytical Methods* **2012,** *4* (10), 3338-3343.
177. Liu, Y.; Yu, Y.; Lam, J. W. Y.; Hong, Y.; Faisal, M.; Yuan, W. Z.; Tang, B. Z., Simple Biosensor with High Selectivity and Sensitivity: Thiol-Specific Biomolecular Probing and Intracellular Imaging by AIE Fluorogen on a TLC Plate through a Thiol–Ene Click Mechanism. *Chemistry – A European Journal* **2010,** *16* (28), 8433-8438.
178. Peng, L.; Zhou, Z.; Wei, R.; Li, K.; Song, P.; Tong, A., A fluorescent probe for thiols based on aggregation-induced emission and its application in live-cell imaging. *Dyes and Pigments* **2014,** *108*, 24-31.
179. Yuan, Y.; Kwok, R. T. K.; Feng, G.; Liang, J.; Geng, J.; Tang, B. Z.; Liu, B., Rational design of fluorescent light-up probes based on an AIE luminogen for targeted intracellular thiol imaging. *Chemical Communications* **2014,** *50* (3), 295-297.

180. Zhang, R.; Yuan, Y.; Liang, J.; Kwok, R. T. K.; Zhu, Q.; Feng, G.; Geng, J.; Tang, B. Z.; Liu, B., Fluorogen–Peptide Conjugates with Tunable Aggregation-Induced Emission Characteristics for Bioprobe Design. *ACS Applied Materials & Interfaces* **2014,** *6* (16), 14302-14310.
181. Gao, Y.; Wei, K.; Li, J.; Li, Y.; Hu, J., A facile four-armed AIE fluorescent sensor for heparin and protamine. *Sensors and Actuators B: Chemical* **2018,** *277*, 408-414.
182. Li, S.; Gao, M.; Wang, S.; Hu, R.; Zhao, Z.; Qin, A.; Tang, B. Z., Light up detection of heparin based on aggregation-induced emission and synergistic counter ion displacement. *Chemical Communications* **2017,** *53* (35), 4795-4798.
183. Yang, S.; Gao, T.; Dong, J.; Xu, H.; Gao, F.; Chen, Q.; Gu, Y.; Zeng, W., A novel water-soluble AIE-based fluorescence probe with red emission for the sensitive detection of heparin in aqueous solution and human serum samples. *Tetrahedron Letters* **2017,** *58* (37), 3681-3686.
184. Zheng, J.; Ye, T.; Chen, J.; Xu, L.; Ji, X.; Yang, C.; He, Z., Highly sensitive fluorescence detection of heparin based on aggregation-induced emission of a tetraphenylethene derivative. *Biosensors and Bioelectronics* **2017,** *90*, 245-250.
185. Lu, H.; Xu, B.; Dong, Y.; Chen, F.; Li, Y.; Li, Z.; He, J.; Li, H.; Tian, W., Novel Fluorescent pH Sensors and a Biological Probe Based on Anthracene Derivatives with Aggregation-Induced Emission Characteristics. *Langmuir* **2010,** *26* (9), 6838-6844.
186. Wang, Z.; Gu, Y.; Liu, J.; Cheng, X.; Sun, J. Z.; Qin, A.; Tang, B. Z., A novel pyridinium modified tetraphenylethene: AIE-activity, mechanochromism, DNA detection and mitochondrial imaging. *Journal of Materials Chemistry B* **2018,** *6* (8), 1279-1285.
187. Xu, X.; Yan, S.; Zhou, Y.; Huang, R.; Chen, Y.; Wang, J.; Weng, X.; Zhou, X., A novel aggregation-induced emission fluorescent probe for nucleic acid detection and its applications in cell imaging. *Bioorganic & Medicinal Chemistry Letters* **2014,** *24* (7), 1654-1656.
188. Zhu, Z.; Xu, L.; Li, H.; Zhou, X.; Qin, J.; Yang, C., A tetraphenylethene-based zinc complex as a sensitive DNA probe by coordination interaction. *Chemical Communications* **2014,** *50* (53), 7060-7062.
189. Hong, Y.; Feng, C.; Yu, Y.; Liu, J.; Lam, J. W. Y.; Luo, K. Q.; Tang, B. Z., Quantitation, Visualization, and Monitoring of Conformational Transitions of Human Serum Albumin by a Tetraphenylethene Derivative with Aggregation-Induced Emission Characteristics. *Analytical Chemistry* **2010,** *82* (16), 7035-7043.
190. Hong, Y.; Meng, L.; Chen, S.; Leung, C. W. T.; Da, L.-T.; Faisal, M.; Silva, D.-A.; Liu, J.; Lam, J. W. Y.; Huang, X.; Tang, B. Z., Monitoring and Inhibition of Insulin Fibrillation by a Small Organic Fluorogen with Aggregation-Induced Emission Characteristics. *Journal of the American Chemical Society* **2012,** *134* (3), 1680-1689.
191. Sathish, V.; Babu, E.; Ramdass, A.; Lu, Z.-Z.; Velayudham, M.; Thanasekaran, P.; Lu, K.-L.; Rajagopal, S., Alkoxy bridged binuclear rhenium (I) complexes as a potential sensor for β-amyloid aggregation. *Talanta* **2014,** *130*, 274-279.
192. Sun, B.; Yang, X.; Ma, L.; Niu, C.; Wang, F.; Na, N.; Wen, J.; Ouyang, J., Design and Application of Anthracene Derivative with Aggregation-Induced Emission Charateristics for Visualization and Monitoring of Erythropoietin Unfolding. *Langmuir* **2013,** *29* (6), 1956-1962.
193. Wang, Z.; Ma, K.; Xu, B.; Li, X.; Tian, W., A highly sensitive "turn-on" fluorescent probe for bovine serum albumin protein detection and quantification based on AIE-active distyrylanthracene derivative. *Science China Chemistry* **2013,** *56* (9), 1234-1238.

194. Peng, L.; Zhang, G.; Zhang, D.; Wang, Y.; Zhu, D., A direct continuous fluorometric turn-on assay for monoamine oxidase B and its inhibitor-screening based on the abnormal fluorescent behavior of silole. *Analyst* **2010,** *135* (7), 1779-1784.
195. Shi, H.; Kwok, R. T. K.; Liu, J.; Xing, B.; Tang, B. Z.; Liu, B., Real-Time Monitoring of Cell Apoptosis and Drug Screening Using Fluorescent Light-Up Probe with Aggregation-Induced Emission Characteristics. *Journal of the American Chemical Society* **2012,** *134* (43), 17972-17981.
196. Wang, M.; Gu, X.; Zhang, G.; Zhang, D.; Zhu, D., Convenient and Continuous Fluorometric Assay Method for Acetylcholinesterase and Inhibitor Screening Based on the Aggregation-Induced Emission. *Analytical Chemistry* **2009,** *81* (11), 4444-4449.
197. Xie, H.; Zeng, F.; Wu, S., Ratiometric Fluorescent Biosensor for Hyaluronidase with Hyaluronan As Both Nanoparticle Scaffold and Substrate for Enzymatic Reaction. *Biomacromolecules* **2014,** *15* (9), 3383-3389.
198. Yu, C.; Wu, Y.; Zeng, F.; Li, X.; Shi, J.; Wu, S., Hyperbranched Polyester-Based Fluorescent Probe for Histone Deacetylase via Aggregation-Induced Emission. *Biomacromolecules* **2013,** *14* (12), 4507-4514.
199. Leung, C. W. T.; Hong, Y.; Hanske, J.; Zhao, E.; Chen, S.; Pletneva, E. V.; Tang, B. Z., Superior Fluorescent Probe for Detection of Cardiolipin. *Analytical Chemistry* **2014,** *86* (2), 1263-1268.
200. Shi, J.; Tian, Y.; Guo, B.; Wu, Y.; Jing, J.; Zhang, R.; Zhang, X., An AIEgen-based fluorescent probe for highly selective and specific imaging of lipid droplets in L02 and HepG2 cells. *Sensors and Actuators B: Chemical* **2019,** *284*, 545-552.
201. Shen, X.; Zhang, G.; Zhang, D., A New Fluorometric Turn-On Detection of l-Lactic Acid Based on the Cascade Enzymatic and Chemical Reactions and the Abnormal Fluorescent Behavior of Silole. *Organic Letters* **2012,** *14* (7), 1744-1747.
202. Kwok, R. T. K.; Leung, C. W. T.; Lam, J. W. Y.; Tang, B. Z., Biosensing by luminogens with aggregation-induced emission characteristics. *Chemical Society Reviews* **2015,** *44* (13), 4228-4238.
203. Chen, S.; Hong, Y.; Liu, Y.; Liu, J.; Leung, C. W. T.; Li, M.; Kwok, R. T. K.; Zhao, E.; Lam, J. W. Y.; Yu, Y.; Tang, B. Z., Full-Range Intracellular pH Sensing by an Aggregation-Induced Emission-Active Two-Channel Ratiometric Fluorogen. *Journal of the American Chemical Society* **2013,** *135* (13), 4926-4929.
204. Hu, R.; Gómez-Durán, C. F. A.; Lam, J. W. Y.; Belmonte-Vázquez, J. L.; Deng, C.; Chen, S.; Ye, R.; Peña-Cabrera, E.; Zhong, Y.; Wong, K. S.; Tang, B. Z., Synthesis, solvatochromism, aggregation-induced emission and cell imaging of tetraphenylethene-containing BODIPY derivatives with large Stokes shifts. *Chemical Communications* **2012,** *48* (81), 10099-10101.
205. Leung, C. W. T.; Hong, Y.; Chen, S.; Zhao, E.; Lam, J. W. Y.; Tang, B. Z., A Photostable AIE Luminogen for Specific Mitochondrial Imaging and Tracking. *Journal of the American Chemical Society* **2013,** *135* (1), 62-65.
206. Liang, G.; Lam, J. W. Y.; Qin, W.; Li, J.; Xie, N.; Tang, B. Z., Molecular luminogens based on restriction of intramolecular motions through host–guest inclusion for cell imaging. *Chemical Communications* **2014,** *50* (14), 1725-1727.
207. Wang, X.; Morales, A. R.; Urakami, T.; Zhang, L.; Bondar, M. V.; Komatsu, M.; Belfield, K. D., Folate Receptor-Targeted Aggregation-Enhanced Near-IR Emitting Silica Nanoprobe for One-Photon in Vivo and Two-Photon ex Vivo Fluorescence Bioimaging. *Bioconjugate Chemistry* **2011,** *22* (7), 1438-1450.
208. Yu, Y.; Feng, C.; Hong, Y.; Liu, J.; Chen, S.; Ng, K. M.; Luo, K. Q.; Tang, B. Z., Cytophilic Fluorescent Bioprobes for Long-Term Cell Tracking. *Advanced Materials* **2011,** *23* (29), 3298-3302.

209. Wang, H.; Liu, G.; Dong, S.; Xiong, J.; Du, Z.; Cheng, X., A pH-responsive AIE nanoprobe as a drug delivery system for bioimaging and cancer therapy. *Journal of Materials Chemistry B* **2015,** *3* (37), 7401-7407.
210. Zhang, X.; Zhang, X.; Yang, B.; Liu, M.; Liu, W.; Chen, Y.; Wei, Y., Fabrication of aggregation induced emission dye-based fluorescent organic nanoparticles via emulsion polymerization and their cell imaging applications. *Polymer Chemistry* **2014,** *5* (2), 399-404.
211. Ding, D.; Mao, D.; Li, K.; Wang, X.; Qin, W.; Liu, R.; Chiam, D. S.; Tomczak, N.; Yang, Z.; Tang, B. Z.; Kong, D.; Liu, B., Precise and Long-Term Tracking of Adipose-Derived Stem Cells and Their Regenerative Capacity via Superb Bright and Stable Organic Nanodots. *ACS Nano* **2014,** *8* (12), 12620-12631.
212. Feng, G.; Tay, C. Y.; Chui, Q. X.; Liu, R.; Tomczak, N.; Liu, J.; Tang, B. Z.; Leong, D. T.; Liu, B., Ultrabright organic dots with aggregation-induced emission characteristics for cell tracking. *Biomaterials* **2014,** *35* (30), 8669-8677.
213. Li, K.; Qin, W.; Ding, D.; Tomczak, N.; Geng, J.; Liu, R.; Liu, J.; Zhang, X.; Liu, H.; Liu, B.; Tang, B. Z., Photostable fluorescent organic dots with aggregation-induced emission (AIE dots) for noninvasive long-term cell tracing. *Scientific Reports* **2013,** *3*, 1150.
214. Li, K.; Zhu, Z.; Cai, P.; Liu, R.; Tomczak, N.; Ding, D.; Liu, J.; Qin, W.; Zhao, Z.; Hu, Y.; Chen, X.; Tang, B. Z.; Liu, B., Organic Dots with Aggregation-Induced Emission (AIE Dots) Characteristics for Dual-Color Cell Tracing. *Chemistry of Materials* **2013,** *25* (21), 4181-4187.
215. Qin, W.; Li, K.; Feng, G.; Li, M.; Yang, Z.; Liu, B.; Tang, B. Z., Bright and Photostable Organic Fluorescent Dots with Aggregation-Induced Emission Characteristics for Noninvasive Long-Term Cell Imaging. *Advanced Functional Materials* **2014,** *24* (5), 635-643.
216. Feng, H.-T.; Song, S.; Chen, Y.-C.; Shen, C.-H.; Zheng, Y.-S., Self-assembled tetraphenylethylene macrocycle nanofibrous materials for the visual detection of copper(ii) in water. *Journal of Materials Chemistry C* **2014,** *2* (13), 2353-2359.
217. Hong, Y.; Chen, S.; Leung, C. W. T.; Lam, J. W. Y.; Liu, J.; Tseng, N.-W.; Kwok, R. T. K.; Yu, Y.; Wang, Z.; Tang, B. Z., Fluorogenic Zn(II) and Chromogenic Fe(II) Sensors Based on Terpyridine-Substituted Tetraphenylethenes with Aggregation-Induced Emission Characteristics. *ACS Applied Materials & Interfaces* **2011,** *3* (9), 3411-3418.
218. Liu, L.; Zhang, G.; Xiang, J.; Zhang, D.; Zhu, D., Fluorescence "Turn On" Chemosensors for Ag+ and Hg2+ Based on Tetraphenylethylene Motif Featuring Adenine and Thymine Moieties. *Organic Letters* **2008,** *10* (20), 4581-4584.
219. Wang, X.; Hu, J.; Liu, T.; Zhang, G.; Liu, S., Highly sensitive and selective fluorometric off–on K+ probe constructed via host–guest molecular recognition and aggregation-induced emission. *Journal of Materials Chemistry* **2012,** *22* (17), 8622-8628.
220. Zhao, N.; Lam, J. W. Y.; Sung, H. H. Y.; Su, H. M.; Williams, I. D.; Wong, K. S.; Tang, B. Z., Effect of the Counterion on Light Emission: A Displacement Strategy to Change the Emission Behaviour from Aggregation-Caused Quenching to Aggregation-Induced Emission and to Construct Sensitive Fluorescent Sensors for Hg2+ Detection. *Chemistry – A European Journal* **2014,** *20* (1), 133-138.
221. Cai, Y.; Li, L.; Wang, Z.; Sun, J. Z.; Qin, A.; Tang, B. Z., A sensitivity tuneable tetraphenylethene-based fluorescent probe for directly indicating the concentration of hydrogen sulfide. *Chemical Communications* **2014,** *50* (64), 8892-8895.
222. Han, T.; Lam, J. W. Y.; Zhao, N.; Gao, M.; Yang, Z.; Zhao, E.; Dong, Y.; Tang, B. Z., A fluorescence-switchable luminogen in the solid state: a sensitive and selective

sensor for the fast "turn-on" detection of primary amine gas. *Chemical Communications* **2013,** *49* (42), 4848-4850.
223. Liu, Y.; Tang, Y.; Barashkov, N. N.; Irgibaeva, I. S.; Lam, J. W. Y.; Hu, R.; Birimzhanova, D.; Yu, Y.; Tang, B. Z., Fluorescent Chemosensor for Detection and Quantitation of Carbon Dioxide Gas. *Journal of the American Chemical Society* **2010,** *132* (40), 13951-13953.
224. Feng, H.-T.; Zheng, Y.-S., Highly Sensitive and Selective Detection of Nitrophenolic Explosives by Using Nanospheres of a Tetraphenylethylene Macrocycle Displaying Aggregation-Induced Emission. *Chemistry – A European Journal* **2014,** *20* (1), 195-201.
225. Kumar, M.; Vij, V.; Bhalla, V., Vapor-Phase Detection of Trinitrotoluene by AIEE-Active Hetero-oligophenylene-Based Carbazole Derivatives. *Langmuir* **2012,** *28* (33), 12417-12421.
226. Qin, A.; Lam, J. W. Y.; Tang, L.; Jim, C. K. W.; Zhao, H.; Sun, J.; Tang, B. Z., Polytriazoles with Aggregation-Induced Emission Characteristics: Synthesis by Click Polymerization and Application as Explosive Chemosensors. *Macromolecules* **2009,** *42* (5), 1421-1424.
227. Wang, J.-H.; Feng, H.-T.; Zheng, Y.-S., Synthesis of tetraphenylethylene pillar[6]arenes and the selective fast quenching of their AIE fluorescence by TNT. *Chemical Communications* **2014,** *50* (77), 11407-11410.
228. Liu, Z.; Xue, W.; Cai, Z.; Zhang, G.; Zhang, D., A facile and convenient fluorescence detection of gamma-ray radiation based on the aggregation-induced emission. *Journal of Materials Chemistry* **2011,** *21* (38), 14487-14491.
229. Sanji, T.; Nakamura, M.; Kawamata, S.; Tanaka, M.; Itagaki, S.; Gunji, T., Fluorescence "Turn-On" Detection of Melamine with Aggregation-Induced-Emission-Active Tetraphenylethene. *Chemistry – A European Journal* **2012,** *18* (48), 15254-15257.
230. Chen, S.; Liu, J.; Liu, Y.; Su, H.; Hong, Y.; Jim, C. K. W.; Kwok, R. T. K.; Zhao, N.; Qin, W.; Lam, J. W. Y.; Wong, K. S.; Tang, B. Z., An AIE-active hemicyanine fluorogen with stimuli-responsive red/blue emission: extending the pH sensing range by "switch + knob" effect. *Chemical Science* **2012,** *3* (6), 1804-1809.
231. Jia, X.; Yang, X.; Li, J.; Li, D.; Wang, E., Stable Cu nanoclusters: from an aggregation-induced emission mechanism to biosensing and catalytic applications. *Chemical Communications* **2014,** *50* (2), 237-239.
232. Song, P.; Chen, X.; Xiang, Y.; Huang, L.; Zhou, Z.; Wei, R.; Tong, A., A ratiometric fluorescent pH probe based on aggregation-induced emission enhancement and its application in live-cell imaging. *Journal of Materials Chemistry* **2011,** *21* (35), 13470-13475.
233. Li, D.-M.; Wang, H.; Zheng, Y.-S., Light-emitting property of simple AIE compounds in gel, suspension and precipitates, and application to quantitative determination of enantiomer composition. *Chemical Communications* **2012,** *48* (26), 3176-3178.
234. Li, D.-M.; Zheng, Y.-S., Single-Hole Hollow Nanospheres from Enantioselective Self-Assembly of Chiral AIE Carboxylic Acid and Amine. *The Journal of Organic Chemistry* **2011,** *76* (4), 1100-1108.
235. Li, D.-M.; Zheng, Y.-S., Highly enantioselective recognition of a wide range of carboxylic acids based on enantioselectively aggregation-induced emission. *Chemical Communications* **2011,** *47* (36), 10139-10141.
236. Zheng, Y.-S.; Hu, Y.-J., Chiral Recognition Based on Enantioselectively Aggregation-Induced Emission. *The Journal of Organic Chemistry* **2009,** *74* (15), 5660-5663.
237. Li, S.-T.; Lin, Y.-C.; Kuo, S.-W.; Chuang, W.-T.; Hong, J.-L., Aggregation induced emission enhancement in relation to the secondary structures of poly(γ-benzyl-l-

glutamate) containing a fluorescent tetraphenylthiophene moiety. *Polymer Chemistry* **2012,** *3* (9), 2393-2402.
238. Shih, K.-Y.; Hsiao, T.-S.; Deng, S.-L.; Hong, J.-L., Water-Soluble Poly(γ-propargyl-l-glutamate) Containing Pendant Sulfonate Ions and Terminal Fluorophore: Aggregation-Enhanced Emission and Secondary Structure. *Macromolecules* **2014,** *47* (12), 4037-4047.
239. Tang, L.; Jin, J. K.; Qin, A.; Zhang Yuan, W.; Mao, Y.; Mei, J.; Zhi Sun, J.; Zhong Tang, B., A fluorescent thermometer operating in aggregation-induced emission mechanism: probing thermal transitions of PNIPAM in water. *Chemical Communications* **2009,** (33), 4974-4976.
240. Yang, C.-M.; Lai, Y.-W.; Kuo, S.-W.; Hong, J.-L., Complexation of Fluorescent Tetraphenylthiophene-Derived Ammonium Chloride to Poly(N-isopropylacrylamide) with Sulfonate Terminal: Aggregation-Induced Emission, Critical Micelle Concentration, and Lower Critical Solution Temperature. *Langmuir* **2012,** *28* (44), 15725-15735.
241. Li, J.; Zhang, Y.; Mei, J.; Lam, J. W. Y.; Hao, J.; Tang, B. Z., Aggregation-Induced Emission Rotors: Rational Design and Tunable Stimuli Response. *Chemistry – A European Journal* **2015,** *21* (2), 907-914.
242. Scalise, R. E.; Caradonna, P. A.; Tracy, H. J.; Mullin, J. L.; Keirstead, A. E., 1,1-Dimethyl-2,3,4,5-tetraphenylsilole as a Molecular Rotor Probe to Investigate the Microviscosity of Imidazolium Ionic Liquids. *Journal of Inorganic and Organometallic Polymers and Materials* **2014,** *24* (2), 431-441.
243. Guan, W.; Lu, J.; Zhou, W.; Lu, C., Aggregation-induced emission molecules in layered matrices for two-color luminescence films. *Chemical Communications* **2014,** *50* (80), 11895-11898.
244. Jin, J.-K.; Sun, J.-Z.; Dong, Y.-Q.; Xu, H.-P.; Yuan, W.-Z.; Tang, B. Z., Aggregation-induced emission of an aminated silole: A fluorescence probe for monitoring layer-by-layer self-assembling processes of polyelectrolytes. *Journal of Luminescence* **2009,** *129* (1), 19-23.
245. Li, J.; Li, Y.; Chan, C. Y. K.; Kwok, R. T. K.; Li, H.; Zrazhevskiy, P.; Gao, X.; Sun, J. Z.; Qin, A.; Tang, B. Z., An Aggregation-Induced-Emission Platform for Direct Visualization of Interfacial Dynamic Self-Assembly. *Angewandte Chemie International Edition* **2014,** *53* (49), 13518-13522.
246. Zhu, C.; Pang, S.; Xu, J.; Jia, L.; Xu, F.; Mei, J.; Qin, A.; Sun, J.; Ji, J.; Tang, B., Aggregation-induced emission of tetraphenylethene derivative as a fluorescence method for probing the assembling/disassembling of amphiphilic molecules. *Analyst* **2011,** *136* (16), 3343-3348.
247. Zhu, Q.; Huang, L.; Su, J.; Liu, S., A sensitive and visible fluorescence-turn-on probe for the CMC determination of ionic surfactants. *Chemical Communications* **2014,** *50* (9), 1107-1109.
248. Li, Y.; Xu, L.; Su, B., Aggregation induced emission for the recognition of latent fingerprints. *Chemical Communications* **2012,** *48* (34), 4109-4111.
249. Xu, L.; Li, Y.; Li, S.; Hu, R.; Qin, A.; Tang, B. Z.; Su, B., Enhancing the visualization of latent fingerprints by aggregation induced emission of siloles. *Analyst* **2014,** *139* (10), 2332-2335.
250. Iasilli, G.; Battisti, A.; Tantussi, F.; Fuso, F.; Allegrini, M.; Ruggeri, G.; Pucci, A., Aggregation-Induced Emission of Tetraphenylethylene in Styrene-Based Polymers. *Macromolecular Chemistry and Physics* **2014,** *215* (6), 499-506.
251. Kokado, K.; Nagai, A.; Chujo, Y., Poly(γ-glutamic acid) Hydrogels with Water-Sensitive Luminescence Derived from Aggregation-Induced Emission of o-Carborane. *Macromolecules* **2010,** *43* (15), 6463-6468.

252. Taniguchi, R.; Yamada, T.; Sada, K.; Kokado, K., Stimuli-Responsive Fluorescence of AIE Elastomer Based on PDMS and Tetraphenylethene. *Macromolecules* **2014,** *47* (18), 6382-6388.
253. De Acha, N.; Elosúa, C.; Corres, M. J.; Arregui, J. F., Fluorescent Sensors for the Detection of Heavy Metal Ions in Aqueous Media. *Sensors* **2019,** *19* (3), 599.
254. Steinfeld, J. I.; Wormhoudt, J., EXPLOSIVES DETECTION: A Challenge for Physical Chemistry. *Annual Review of Physical Chemistry* **1998,** *49* (1), 203-232.
255. Yang, Z.; Qin, W.; Lam, J. W. Y.; Chen, S.; Sung, H. H. Y.; Williams, I. D.; Tang, B. Z., Fluorescent pH sensor constructed from a heteroatom-containing luminogen with tunable AIE and ICT characteristics. *Chemical Science* **2013,** *4* (9), 3725-3730.
256. Tyagi, A.; Chu, K. L.; Abidi, I. H.; Cagang, A. A.; Zhang, Q.; Leung, N. L. C.; Zhao, E.; Tang, B. Z.; Luo, Z., Single-probe multistate detection of DNA via aggregation-induced emission on a graphene oxide platform. *Acta Biomaterialia* **2017,** *50*, 334-343.
257. Yu, Y.; Liu, J.; Zhao, Z.; Ng, K. M.; Luo, K. Q.; Tang, B. Z., Facile preparation of non-self-quenching fluorescent DNA strands with the degree of labeling up to the theoretic limit. *Chemical Communications* **2012,** *48* (51), 6360-6362.
258. Sun, J.; Lu, Y.; Wang, L.; Cheng, D.; Sun, Y.; Zeng, X., Fluorescence turn-on detection of DNA based on the aggregation-induced emission of conjugated poly(pyridinium salt)s. *Polymer Chemistry* **2013,** *4* (14), 4045-4051.
259. Hong, Y.; Chen, S.; Leung, C. W. T.; Lam, J. W. Y.; Tang, B. Z., Water-Soluble Tetraphenylethene Derivatives as Fluorescent "Light-Up" Probes for Nucleic Acid Detection and Their Applications in Cell Imaging. *Chemistry – An Asian Journal* **2013,** *8* (8), 1806-1812.
260. Hong, Y.; Häußler, M.; Lam, J. W. Y.; Li, Z.; Sin, K. K.; Dong, Y.; Tong, H.; Liu, J.; Qin, A.; Renneberg, R.; Tang, B. Z., Label-Free Fluorescent Probing of G-Quadruplex Formation and Real-Time Monitoring of DNA Folding by a Quaternized Tetraphenylethene Salt with Aggregation-Induced Emission Characteristics. *Chemistry – A European Journal* **2008,** *14* (21), 6428-6437.
261. Hong, Y.; Xiong, H.; Lam, J. W. Y.; Häußler, M.; Liu, J.; Yu, Y.; Zhong, Y.; Sung, H. H. Y.; Williams, I. D.; Wong, K. S.; Tang, B. Z., Fluorescent Bioprobes: Structural Matching in the Docking Processes of Aggregation-Induced Emission Fluorogens on DNA Surfaces. *Chemistry – A European Journal* **2010,** *16* (4), 1232-1245.
262. Li, Y.; Kwok, R. T. K.; Tang, B. Z.; Liu, B., Specific nucleic acid detection based on fluorescent light-up probe from fluorogens with aggregation-induced emission characteristics. *RSC Advances* **2013,** *3* (26), 10135-10138.
263. Wang, G.; Zhang, R.; Xu, C.; Zhou, R.; Dong, J.; Bai, H.; Zhan, X., Fluorescence Detection of DNA Hybridization Based on the Aggregation-Induced Emission of a Perylene-Functionalized Polymer. *ACS Applied Materials & Interfaces* **2014,** *6* (14), 11136-11141.
264. Wang, H.; Ma, K.; Xu, B.; Tian, W., Tunable Supramolecular Interactions of Aggregation-Induced Emission Probe and Graphene Oxide with Biomolecules: An Approach toward Ultrasensitive Label-Free and "Turn-On" DNA Sensing. *Small* **2016,** *12* (47), 6613-6622.
265. Hiremath, S. D.; Gawas, R. U.; Mascarenhas, S. C.; Ganguly, A.; Banerjee, M.; Chatterjee, A., A water-soluble AIE-gen for organic-solvent-free detection and wash-free imaging of Al3+ ions and subsequent sensing of F− ions and DNA tracking. *New Journal of Chemistry* **2019,** *43* (13), 5219-5227.
266. Huang, J.; Wang, M.; Zhou, Y.; Weng, X.; Shuai, L.; Zhou, X.; Zhang, D., Visual observation of G-quadruplex DNA with the label-free fluorescent probe silole with

aggregation-induced emission. *Bioorganic & Medicinal Chemistry* **2009,** *17* (22), 7743-7748.
267. Xu, L.; Zhu, Z.; Zhou, X.; Qin, J.; Yang, C., A highly sensitive nucleic acid stain based on amino-modified tetraphenylethene: the influence of configuration. *Chemical Communications* **2014,** *50* (49), 6494-6497.
268. Schärer, O. D., Chemistry and Biology of DNA Repair. *Angewandte Chemie International Edition* **2003,** *42* (26), 2946-2974.
269. Vesnaver, G.; Chang, C. N.; Eisenberg, M.; Grollman, A. P.; Breslauer, K. J., Influence of abasic and anucleosidic sites on the stability, conformation, and melting behavior of a DNA duplex: correlations of thermodynamic and structural data. *Proceedings of the National Academy of Sciences of the United States of America* **1989,** *86* (10), 3614-3618.
270. De Bont, R.; van Larebeke, N., Endogenous DNA damage in humans: a review of quantitative data. *Mutagenesis* **2004,** *19* (3), 169-185.
271. Gates, K. S., An Overview of Chemical Processes That Damage Cellular DNA: Spontaneous Hydrolysis, Alkylation, and Reactions with Radicals. *Chemical Research in Toxicology* **2009,** *22* (11), 1747-1760.
272. Lukin, M.; de los Santos, C., NMR Structures of Damaged DNA. *Chemical Reviews* **2006,** *106* (2), 607-686.
273. Nakamura, J.; Walker, V. E.; Upton, P. B.; Chiang, S.-Y.; Kow, Y. W.; Swenberg, J. A., Highly Sensitive Apurinic/Apyrimidinic Site Assay Can Detect Spontaneous and Chemically Induced Depurination under Physiological Conditions. *Cancer Research* **1998,** *58* (2), 222-225.
274. Park, J.-H.; Troxel, A. B.; Harvey, R. G.; Penning, T. M., Polycyclic Aromatic Hydrocarbon (PAH) o-Quinones Produced by the Aldo-Keto-Reductases (AKRs) Generate Abasic Sites, Oxidized Pyrimidines, and 8-Oxo-dGuo via Reactive Oxygen Species. *Chemical Research in Toxicology* **2006,** *19* (5), 719-728.
275. Lindahl, T., Instability and decay of the primary structure of DNA. *Nature* **1993,** *362* (6422), 709-715.
276. Lindahl, T.; Nyberg, B., Rate of depurination of native deoxyribonucleic acid. *Biochemistry* **1972,** *11* (19), 3610-3618.
277. de Gruijl, F. R.; van Kranen, H. J.; Mullenders, L. H. F., UV-induced DNA damage, repair, mutations and oncogenic pathways in skin cancer. *Journal of Photochemistry and Photobiology B: Biology* **2001,** *63* (1), 19-27.
278. Kawanishi, S.; Hiraku, Y.; Oikawa, S., Mechanism of guanine-specific DNA damage by oxidative stress and its role in carcinogenesis and aging. *Mutation Research-Reviews in Mutation Research* **2001,** *488* (1), 65-76.
279. Berthet, N.; Constant, J.-F.; Demeunynck, M.; Michon, P.; Lhomme, J., Search for DNA Repair Inhibitors: Selective Binding of Nucleic Bases−Acridine Conjugates to a DNA Duplex Containing an Abasic Site. *Journal of Medicinal Chemistry* **1997,** *40* (21), 3346-3352.
280. Boiteux, S.; Guillet, M., Abasic sites in DNA: repair and biological consequences in Saccharomyces cerevisiae. *DNA Repair* **2004,** *3* (1), 1-12.
281. Drohat, A. C.; Maiti, A., Mechanisms for enzymatic cleavage of the N-glycosidic bond in DNA. *Organic & Biomolecular Chemistry* **2014,** *12* (42), 8367-8378.
282. Singer, B.; Grunberger, D., Molecular Biology of Mutagens and Carcinogens. Springer Verlag: **2011**.
283. Wu, R. R.; Chen, Y.; Rodgers, M. T., Mechanisms and energetics for N-glycosidic bond cleavage of protonated 2′-deoxyguanosine and guanosine. *Physical Chemistry Chemical Physics* **2016,** *18* (4), 2968-2980.

284. Iocono, J. A.; Gildea, B.; McLaughlin, L. W., Mild acid hydrolysis of 2-pyrimidinone-containing DNA fragments generates apurinic/apyrimidinic sites. *Tetrahedron Letters* **1990,** *31* (2), 175-178.
285. Laayoun, A.; Décout, J.-L.; Defrancq, E.; Lhomme, J., Hydrolysis of oligonucleotides containing 8-substituted purine nucleosides. A new route for preparing abasic oligodeoxynucleotides. *Tetrahedron Letters* **1994,** *35* (28), 4991-4994.
286. Laayoun, A.; Décout, J.-L.; Lhomme, J., Hydrolysis of 2′-deoxypurine nucleosides. The effect of substitution at the C-8 position. *Tetrahedron Letters* **1994,** *35* (28), 4989-4990.
287. Stuart, G. R.; Chambers, R. W., Synthesis and properties of oligodeoxynucleotides with an AP site at a preselected position. *Nucleic Acids Research* **1987,** *15* (18), 7451-7462.
288. Vasseur, J. J.; Rayner, B.; Imbach, J. L., Preparation of a short synthetic apurinic oligonucleotide. *Biochemical and Biophysical Research Communications* **1986,** *134* (3), 1204-1208.
289. Pochet, S.; Huynh-Dinh, T.; Neumann, J. M.; Tran-Dinh, S.; Taboury, J. A.; Taillandier, E.; Igolen, J., Modele de jonction B-Z danz un oligonucleotide synthetique comportant un site apurinique. *Tetrahedron Letters* **1985,** *26* (17), 2085-2088.
290. Raap, J.; Dreef, C. E.; van der Marel, G. A.; van Boom, J. H.; Hilbers, C. W., Synthesis and Proton-NMR Studies of Oligonucleotides Containing an Apurinic (AP) Site. *Journal of Biomolecular Structure and Dynamics* **1987,** *5* (2), 219-247.
291. Takeshita, M.; Chang, C. N.; Johnson, F.; Will, S.; Grollman, A. P., Oligodeoxynucleotides containing synthetic abasic sites. Model substrates for DNA polymerases and apurinic/apyrimidinic endonucleases. *Journal of Biological Chemistry* **1987,** *262* (21), 10171-10179.
292. Thomas, M.; Castaing, B.; Fourrey, J.-L.; Zelwer, C., Synthesis of an Enantiomerically Pure Carbocyclic DNA Abasic Site Analogue. *Nucleosides and Nucleotides* **1999,** *18* (2), 239-243.
293. Manoharan, M.; Gerlt, J. A.; Wilde, J. A.; Withka, J. M.; Bolton, P. H., Coexistence of conformations in a DNA heteroduplex revealed by site specific labeling with carbon-13 labeled nucleotides. *Journal of the American Chemical Society* **1987,** *109* (23), 7217-7219.
294. Manoharan, M.; Ransom, S. C.; Mazumder, A.; Gerlt, J. A.; Wilde, J. A.; Withka, J. A.; Bolton, P. H., The characterization of abasic sites in DNA heteroduplexes by site specific labeling with carbon-13. *Journal of the American Chemical Society* **1988,** *110* (5), 1620-1622.
295. Wilde, J. A.; Bolton, P. H.; Mazumder, A.; Manoharan, M.; Gerlt, J. A., Characterization of the equilibrating forms of the aldehydic abasic site in duplex DNA by oxygen-17 NMR. *Journal of the American Chemical Society* **1989,** *111* (5), 1894-1896.
296. Bailly, V.; Derydt, M.; Verly, W. G., Delta-elimination in the repair of AP (apurinic/apyrimidinic) sites in DNA. *Biochemical Journal* **1989,** *261* (3), 707-713.
297. Bailly, V.; Verly, W. G., Possible roles of beta-elimination and delta-elimination reactions in the repair of DNA containing AP (apurinic/apyrimidinic) sites in mammalian cells. *Biochemical Journal* **1988,** *253* (2), 553-559.
298. Latham, K. A.; Lloyd, R. S., .delta.-Elimination by T4 Endonuclease V at a Thymine Dimer Site Requires a Secondary Binding Event and Amino Acid Glu-23. *Biochemistry* **1995,** *34* (27), 8796-8803.
299. Goljer, I.; Kumar, S.; Bolton, P. H., Refined Solution Structure of a DNA Heteroduplex Containing an Aldehydic Abasic Site. *Journal of Biological Chemistry* **1995,** *270* (39), 22980-22987.

300. Goljer, I.; Withka, J. M.; Kao, J. Y.; Bolton, P. H., Effects of the presence of an aldehydic abasic site on the thermal stability and rates of helix opening and closing of duplex DNA. *Biochemistry* **1992,** *31* (46), 11614-11619.
301. Singh, M. P.; Hill, G. C.; Peoc'h, D.; Rayner, B.; Imbach, J.-L.; Lown, J. W., High-Field NMR and Restrained Molecular Modeling Studies on a DNA Heteroduplex Containing a Modified Apurinic Abasic Site in the Form of Covalently Linked 9-Aminoellipticine. *Biochemistry* **1994,** *33* (34), 10271-10285.
302. Withka, J. M.; Wilde, J. A.; Bolton, P. H.; Mazumder, A.; Gerlt, J. A., Characterization of conformational features of DNA heteroduplexes containing aldehydic abasic sites. *Biochemistry* **1991,** *30* (41), 9931-9940.
303. Gelfand, C. A.; Plum, G. E.; Grollman, A. P.; Johnson, F.; Breslauer, K. J., Thermodynamic Consequences of an Abasic Lesion in Duplex DNA Are Strongly Dependent on Base Sequence. *Biochemistry* **1998,** *37* (20), 7321-7327.
304. Sági, J.; Guliaev, A. B.; Singer, B., 15-mer DNA Duplexes Containing an Abasic Site Are Thermodynamically More Stable with Adjacent Purines Than with Pyrimidines. *Biochemistry* **2001,** *40* (13), 3859-3868.
305. Coppel, Y.; Berthet, N.; Coulombeau, C.; Coulombeau, C.; Garcia, J.; Lhomme, J., Solution Conformation of an Abasic DNA Undecamer Duplex d(CGCACXCACGC)·d(GCGTGTGTGCG): The Unpaired Thymine Stacks Inside the Helix. *Biochemistry* **1997,** *36* (16), 4817-4830.
306. Turner, C. J.; Case, D. A.; Dupradeau, F.-Y.; Chen, J.; Stubbe, J., DNA oligonucleotides with A, T, G or C opposite an abasic site: structure and dynamics. *Nucleic Acids Research* **2007,** *36* (1), 253-262.
307. Turner, C. J.; Stubbe, J.; Hoehn, S. T., Solution structure of an oligonucleotide containing an abasic site: evidence for an unusual deoxyribose conformation. *Nucleic Acids Research* **2001,** *29* (16), 3413-3423.
308. Cline, S. D.; Jones, W. R.; Stone, M. P.; Osheroff, N., DNA Abasic Lesions in a Different Light: Solution Structure of an Endogenous Topoisomerase II Poison. *Biochemistry* **1999,** *38* (47), 15500-15507.
309. Lhomme, J.; Constant, J.-F.; Demeunynck, M., Abasic DNA structure, reactivity, and recognition. *Biopolymers* **1999,** *52* (2), 65-83.
310. Atamna, H.; Cheung, I.; Ames, B. N., A method for detecting abasic sites in living cells: Age-dependent changes in base excision repair. *Proceedings of the National Academy of Sciences* **2000,** *97* (2), 686-691.
311. Langenegger, S. M.; Häner, R., A Simple, Non-Nucleosidic Base Surrogate Increases the Duplex Stability of DNA Containing an Abasic Site. *Chemistry & Biodiversity* **2004,** *1* (2), 259-264.
312. Malinovskii, V. L.; Wenger, D.; Häner, R., Nucleic acid-guided assembly of aromatic chromophores. *Chemical Society Reviews* **2010,** *39* (2), 410-422.
313. Langenegger, S. M.; Häner, R., Remarkable Stabilization of Duplex DNA Containing an Abasic Site by Non-Nucleosidic Phenanthroline and Pyrene Building Blocks. *ChemBioChem* **2005,** *6* (5), 848-851.
314. Fukui, K.; Morimoto, M.; Segawa, H.; Tanaka, K.; Shimidzu, T., Synthesis and Properties of an Oligonucleotide Modified with an Acridine Derivative at the Artificial Abasic Site. *Bioconjugate Chemistry* **1996,** *7* (3), 349-355.
315. Tanaka, K.; Fukui, K., The Acridine Ring Selectively Intercalated into a DNA Helix at Various Types of Abasic Sites: Double Strand Formation and Photophysical Properties. *Nucleic Acids Research* **1996,** *24* (20), 3962-3967.
316. Millican, T. A.; Mock, G. A.; Chauncey, M. A.; Patel, T. P.; Eaton, M. A.; Gunning, J.; Cutbush, S. D.; Neidle, S.; Mann, J., Synthesis and biophysical studies of short

oligodeoxynucleotides with novel modifications: a possible approach to the problem of mixed base oligodeoxynucleotide synthesis. *Nucleic Acids Research* **1984,** *12* (19), 7435-7453.
317. de los Santos, C.; Kool, E. T.; Smirnov, S.; Matray, T. J., Integrity of duplex structures without hydrogen bonding: DNA with pyrene paired at abasic sites. *Nucleic Acids Research* **2002,** *30* (24), 5561-5569.
318. Kool, E. T.; Morales, J. C.; Guckian, K. M., Mimicking the Structure and Function of DNA: Insights into DNA Stability and Replication. *Angewandte Chemie International Edition* **2000,** *39* (6), 990-1009.
319. Matray, T. J.; Kool, E. T., Selective and Stable DNA Base Pairing without Hydrogen Bonds. *Journal of the American Chemical Society* **1998,** *120* (24), 6191-6192.
320. Matray, T. J.; Kool, E. T., A specific partner for abasic damage in DNA. *Nature* **1999,** *399* (6737), 704-708.
321. Wojciechowski, F.; Lietard, J.; Leumann, C. J., 2-Pyrenyl-DNA: Synthesis, Pairing, and Fluorescence Properties. *Organic Letters* **2012,** *14* (20), 5176-5179.
322. Bag, S. S.; Kundu, R.; Talukdar, S., Unnatural triazolyl nucleoside stabilizes an abasic site containing DNA duplex equally as the stabilization of a natural A–T pair. *RSC Advances* **2013,** *3* (44), 21352-21355.
323. Greco, N. J.; Tor, Y., Simple Fluorescent Pyrimidine Analogues Detect the Presence of DNA Abasic Sites. *Journal of the American Chemical Society* **2005,** *127* (31), 10784-10785.
324. Lee, S. H.; Wang, S.; Kool, E. T., Templated chemistry for monitoring damage and repair directly in duplex DNA. *Chemical Communications* **2012,** *48* (65), 8069-8071.
325. Valis, L.; Amann, N.; Wagenknecht, H.-A., Detection of single base mismatches and abasic sites using phenanthridinium as an artificial DNA base and charge donor. *Organic & Biomolecular Chemistry* **2005,** *3* (1), 36-38.
326. Yamauchi, T.; Takeda, T.; Yanagi, M.; Takahashi, N.; Suzuki, A.; Saito, Y., C2-substituted 8-aza-7-deaza-2′-deoxyadenosines as environmentally sensitive fluorescent nucleosides for discriminating apurinic/apyrimidinic sites in DNA duplex. *Tetrahedron Letters* **2017,** *58* (2), 117-120.
327. Buzzeo, M. C.; Barton, J. K., Redmond Red as a Redox Probe for the DNA-Mediated Detection of Abasic Sites. *Bioconjugate Chemistry* **2008,** *19* (11), 2110-2112.
328. Hirose, T.; Ohtani, T.; Muramatsu, H.; Tanaka, A., Direct Visualization of Abasic Sites on a Single DNA Molecule Using Fluorescence Microscopy¶. *Photochemistry and Photobiology* **2002,** *76* (2), 123-126.
329. Yoshimoto, K.; Nishizawa, S.; Minagawa, M.; Teramae, N., Use of Abasic Site-Containing DNA Strands for Nucleobase Recognition in Water. *Journal of the American Chemical Society* **2003,** *125* (30), 8982-8983.
330. Ni, Z.; Ye, T.; Yu, Y.; Gao, L.; Fei, Y.; Li, Q.; Zhou, Y.; Shao, Y.; Zeng, L., Triplex-forming oligonucleotide as a lighting-up switch for a DNA abasic site-binding fluorescent ligand. *Journal of Luminescence* **2018,** *198*, 193-197.
331. Sato, Y.; Kudo, M.; Toriyabe, Y.; Kuchitsu, S.; Wang, C.-x.; Nishizawa, S.; Teramae, N., Abasic site-binding ligands conjugated with cyanine dyes for "off–on" fluorescence sensing of orphan nucleobases in DNA duplexes and DNA–RNA hybrids. *Chemical Communications* **2014,** *50* (5), 515-517.
332. Sato, Y.; Saito, H.; Aoki, D.; Teramae, N.; Nishizawa, S., Lysine linkage in abasic site-binding ligand–thiazole orange conjugates for improved binding affinity to orphan nucleobases in DNA/RNA hybrids. *Chemical Communications* **2016,** *52* (100), 14446-14449.

333. Wu, W.; Wang, Y.; Zhou, Y.; Shao, Y.; Zhang, L.; Liu, H., Selective fluorescence lighting-up recognition of DNA abasic site environment possessing guanine context. *Sensors and Actuators B: Chemical* **2015,** *206*, 449-455.
334. Wang, Y.; Hu, Y.; Wu, T.; Zhang, L.; Liu, H.; Zhou, X.; Shao, Y., Recognition of DNA abasic site nanocavity by fluorophore-switched probe: Suitable for all sequence environments. *Spectrochimica Acta Part A: Molecular and Biomolecular Spectroscopy* **2016,** *153*, 645-650.
335. Bag, S. S.; Pradhan, M. K.; Talukdar, S., Trifunctional fluorescent unnatural nucleoside: Label free detection of T-T/C-C base mismatches, abasic site and bulge DNA. *Journal of Photochemistry and Photobiology B: Biology* **2017,** *173*, 165-169.
336. Ma, K.; Wang, H.; Li, H.; Xu, B.; Tian, W., Label-free detection for SNP using AIE probes and carbon nanotubes. *Sensors and Actuators B: Chemical* **2017,** *253*, 92-96.
337. Morris, G. M.; Goodsell, D. S.; Halliday, R. S.; Huey, R.; Hart, W. E.; Belew, R. K.; Olson, A. J., Automated docking using a Lamarckian genetic algorithm and an empirical binding free energy function. *Journal of Computational Chemistry* **1998,** *19* (14), 1639-1662.
338. Morris, G. M.; Huey, R.; Lindstrom, W.; Sanner, M. F.; Belew, R. K.; Goodsell, D. S.; Olson, A. J., AutoDock4 and AutoDockTools4: Automated docking with selective receptor flexibility. *Journal of Computational Chemistry* **2009,** *30* (16), 2785-2791.
339. Maestro, version 9.0. *Schrödinger, LLC, New York, NY* **2009**.
340. Lying, R.; Rodger, A.; Nordén, B., The CD of ligand–DNA systems. I. Poly(dG-dC) B-DNA. *Biopolymers* **1991,** *31* (14), 1709-1720.
341. M. J. Frisch, G. W. T., H. B. Schlegel, G. E. Scuseria, M. A. Robb, J. R. Cheeseman, G. Scalmani, V. Barone, B. Mennucci, G. A. Petersson, H. Nakatsuji, M. Caricato, X. Li, H. P. Hratchian, A. F. Izmaylov, J. Bloino, G. Zheng, J. L. Sonnenberg, M. Hada, M. Ehara, K. Toyota, R. Fukuda, J. Hasegawa, M. Ishida, T. Nakajima, Y. Honda, O. Kitao, H. Nakai, T. Vreven, J. A. Montgomery, Jr., J. E. Peralta, F. Ogliaro, M. Bearpark, J. J. Heyd, E. Brothers, K. N. Kudin, V. N. Staroverov, R. Kobayashi, J. Normand, K. Raghavachari, A. Rendell, J. C. Burant, S. S. Iyengar, J. Tomasi, M. Cossi, N. Rega, J. M. Millam, M. Klene, J. E. Knox, J. B. Cross, V. Bakken, C. Adamo, J. Jaramillo, R. Gomperts, R. E. Stratmann, O. Yazyev, A. J. Austin, R. Cammi, C. Pomelli, J. W. Ochterski, R. L. Martin, K. Morokuma, V. G. Zakrzewski, G. A. Voth, P. Salvador, J. J. Dannenberg, S. Dapprich, A. D. Daniels, Ö. Farkas, J. B. Foresman, J. V. Ortiz, J. Cioslowski, and D. J. Fox, *Gaussian, Inc. Wallingford CT* **2009**.
342. Bag, S. S.; Jana, S., Axially chiral amino acid scaffolds as efficient fluorescent discriminators of methanol–ethanol. *New Journal of Chemistry* **2017,** *41* (22), 13391-13398.

SUMMARY AND OUTLOOK

Summary and Outlook

Major findings and the future outlook of the present investigations described in this dissertation have been summarized below:

This dissertation has a total of five chapters out which **Chapter 1** is a review chapter on the applications of C5-substituted 2′-deoxyuridines. Two chapters (**Chapter 2** and **Chapter 4**) are devoted to the synthesis of C5-substituted 2′-deoxyuridines containing donor-acceptor triazolyl aromatics *via* Sonogashira cross-coupling and azide-alkyne cycloaddition reaction under "Click" conditions. Other chapters (**Chapter 3** and **Chapter 5**) describe the biophysical properties of one triazolyl C5-substituted nucleoside, one tetrazolyl unnatural nucleoside and one triazolyl aromatic amino acid scaffold, all of them are labeled with pyrene moiety.

Thus, in **Chapter 2**, we have described the synthesis of few new C5-substituted 2′-deoxyuridines via Sonogashira cross-coupling followed by azide-alkyne cycloaddition reaction ("Click") and studied their photophysical properties in various organic solvents. Therefore in this chapter, we have demonstrated the rational design and synthesis of triazolyl push-pull fluorophore-labeled uridines via the intermediacy of C5-{4-(2-propynyl(methyl)amino)}phenylacetylene as a universal linker. Our design involves the synthesis of a universal linker, 4-(Propynyl(methyl)amino)phenyl acetylene and its incorporation into C5-position of 2′-deoxyuridine. The universal linker containing 2′-deoxy uridine can then undergo Huisgen 1, 3-dipolar cycloaddition reaction with donor-acceptor chromophore containing fluorogenic azides to afford the target fluorescent uridines. The donor aromatic substituted triazole moiety is thought to allow an intramolecular charge transfer (ICT) process from triazole-linked moiety to the fluorophoric units leading to solvatochromic fluorescence at a longer wavelength. Moreover, the fluorophores, such as pyrene, coupled electronically with donor aryltriazoles, could show dual fluorescence property or interesting modulated solvatochromic emission response. Thus, our design would ultimately lead to predetermined photophysical properties of the fluorophores and hence of the nucleoside.

Thus, the synthesized nucleosides show interesting solvatochromic characteristic and/or intramolecular charge transfer (ICT) feature. Few of them also exhibit dual emitting characteristics evidencing our designing concept. The HOMO-LUMO distribution shows that the emissive states of these nucleosides are characterized with more significant electron redistribution between the C5-{4-(2-propynyl(methyl)amino)}phenyl triazolyl donor moiety

and the aromatic chromophores linked to it leading to modulated emission property. The solvent polarity sensitivity of these nucleosides has also been tested. The synthesized triazolyl benzonitrile-, naphthyl- and pyrenyl- nucleosides have been found to exhibit interesting intramolecular charge transfer (ICT) and dual (LE/ICT) emission property. The dual fluorescent nucleosides having ratiometric fluorescence property could be utilized for DNA analysis if incorporated in a DNA for the generation of fluorescent oligonucleotide probes.

In **Chapter 3** we have studied the interaction of biomolecular microenvironment with our previously reported triazolylpyrene nucleoside (**Chapter 2**) and tetrazolylpyrene nucleoside. In particular, we have exploited the interesting emissive property of these nucleosides to study their interactions with bovine serum albumin (BSA) spectroscopically. The photophysical study has revealed that both nucleosides exhibit enhanced fluorescence signal upon binding to the hydrophobic pocket of BSA which is also supported by a molecular docking study. These observations indicate a strong interaction between these nucleosides and BSA. The study of protein-ligand interaction is very important for the development of newer drug candidates. Therefore, our nucleoside probes might find application in studying such events in pharmaceutical sciences. The most attractive result of this chapter is that the triazolylpyrene nucleoside exhibits its dual emitting properties even after complexation with BSA and enabled a ratiometric fluorescence analysis of the binding event. As the ratiometric fluorescence sensing is highly advantageous compared to a single wavelength emission, the ratiometric fluorescent triazolylpyrene nucleoside probe would find wide future application in chemistry, biology and in material sciences.

In **Chapter 4**, we have described the synthesis of few new fluorene labeled C5-substituted 2′-deoxyuridines via the same methodologies as described in **Chapter 2** i.e. Sonogashira cross coupling and azide-alkyne cycloaddition reaction (“Click”). We have explored the photophysical properties of the synthesized nucleosides. The UV-visible and fluorescence study of these nucleosides revealed interesting dual emissive properties in various organic solvents in particular, the fluorenyl and cyanofluorenyl nucleosides. Therefore, these two nucleosides might find application in DNA microenvironment sensing. Furthermore, we have demonstrated the interaction of cyanofluorenyl nucleoside with ctDNA. Thus, it exhibits an enhanced fluorescence signal on binding to the ctDNA in the minor groove which is also supported by a molecular docking study. Therefore, these nucleosides would find applications in the investigation of DNA-drug interactions. In addition, these nucleosides might find applications in DNA analysis if incorporated into a DNA sequence in the future.

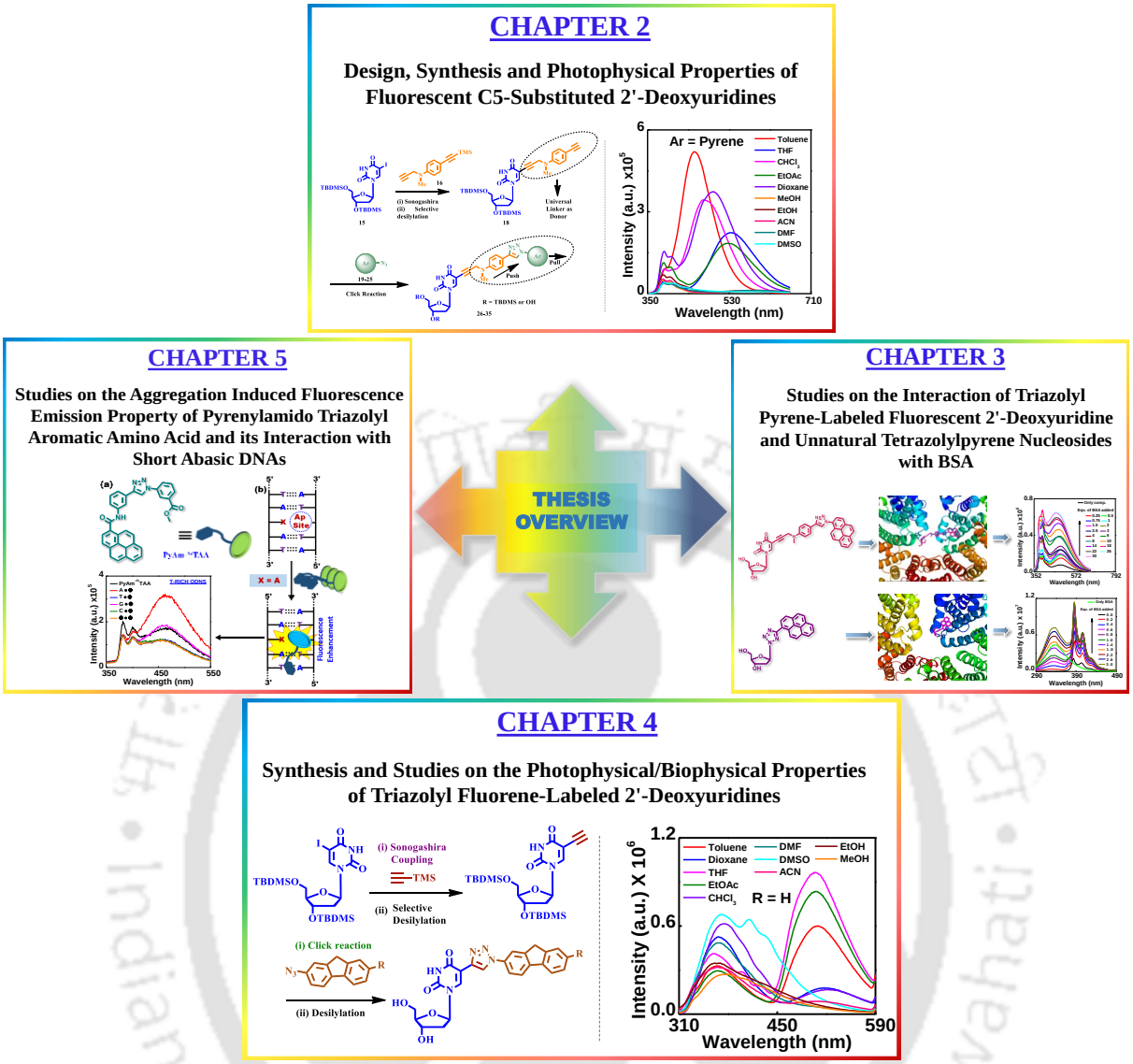

Finally, **Chapter 5**, demonstrates a label-free strategy for studying the interaction of an AIE probe, **PyAm-^{Ar}TAA**, with abasic DNA. Thus, we have successfully shown that the probe is able to sense an abasic DNA duplex via an enhancement of fluorescence when the abasic site lies opposite to base adenosine (A) of a T-rich 13-mer abasic DNA duplex. On the other hand, it also serves as a sensor for the abasic site opposite to base G and/or C of C-rich 13-mer DNAs via a drastic fluorescence quenching. A docking study reveals that the probe encompasses the minor groove extending the amidopyrenyl unit to the gap created at the abasic site and the scaffold unit remained on the groove site involving π-π-stacking and H-bonding interaction. Therefore, the aromatic amino acid scaffold probe, **PyAm-^{Ar}TAA** might find applications in the detection and targeting of other DNA lesions and G-quadruplex DNAs.

Therefore, these novel and important findings presented in this dissertation are expected to further define research to establish and to create more of such conceptually designed fluorescent nucleosides and scaffolds amino acids as probes for future applications in chemistry, biology and material sciences. Our result is sufficient enough to advance the on-going examination of such related fluorescent molecules and thus, attract the interest of the broad scientific community. The concept of designing fluorescent triazolyl- and tetrazolyl- and fluorenyl-nucleosides might find special attention in future in the field of chemical genomics. The rapidly growing research toward the expansion of genetic alphabet as well as growing demand of nucleic acid-based diagnostics and sensing materials necessitates the design and synthesis of modified/unnatural nucleosides with tuned photophysical properties such as ICT and dual emission. The incorporation of such fluorescent nucleosides/fluorophores into DNAs would extend our vision in the realm of molecular genetics/recognition. With the advancement of knowledge and strategies of chemistry and biology, fluorescently labeled nucleosides/small fluorescent probes/fluorescent scaffolds expectedly would continue to be at the forefront in aiding researchers to gain insights into fundamental questions concerning life's essential biological functions involving DNA/protein interactions, recognition, and synthesis. Many more advancements in the field of fluorescent nucleosides/fluorescent oligonucleotide probes/fluorescent biosensor are expected in the near future.

PUBLICATION

JOC The Journal of Organic Chemistry Cite This: J. Org. Chem. 2018, 83, 7606−7621 Article pubs.acs.org/joc

Design of "Click" Fluorescent Labeled 2′-deoxyuridines via C5-[4-(2-Propynyl(methyl)amino)]phenyl Acetylene as a Universal Linker: Synthesis, Photophysical Properties, and Interaction with BSA

Subhendu Sekhar Bag* and Hiranya Gogoi

Bioorganic Chemistry Laboratory, Department of Chemistry, Indian Institute of Technology Guwahati 781039, India

Supporting Information

ABSTRACT: Microenvironment-sensitive fluorescent nucleosides present attractive advantages over single-emitting dyes for sensing inter-biomolecular interactions involving DNA. Herein, we report the rational design and synthesis of triazolyl push−pull fluorophore-labeled uridines via the intermediacy of C5-[4-(2-propynyl(methyl)amino)]phenyl acetylene as a universal linker. The synthesized nucleosides showed interesting solvatochromic characteristic and/or intramolecular charge transfer (ICT) features. A few of them also exhibited dual-emitting characteristics evidencing our designing concept. The HOMO−LUMO distribution showed that the emissive states of these nucleosides were characterized with more significant electron redistribution between the C5-[4-(2-propynyl(methyl)amino)]phenyl triazolyl donor moiety and the aromatic chromophores linked to it, leading to modulated emission property. The solvent polarity sensitivity of these nucleosides was also tested. The synthesized triazolyl benzonitrile (**10C**), naphthyl (**10E**), and pyrenyl (**10G**) nucleosides were found to exhibit interesting ICT and dual (LE/ICT) emission properties. The dual-emitting pyrenyl nucleoside maintained a good ratiometric response in the BSA protein microenvironment, enabling the switch-on ratiometric sensing of BSA as the only protein biomolecule. Thus, it is expected that the new fluorescent nucleoside analogues would be useful in designing DNA probes for nucleic acid analysis or studying DNA−protein interactions via a drastic change in fluorescence response due to a change in micropolarity.

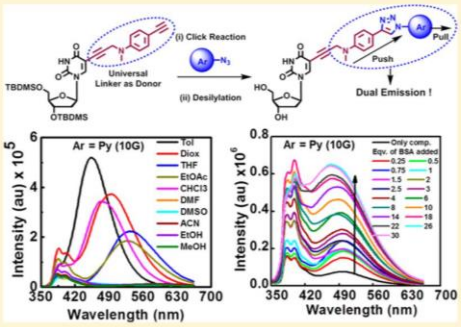

INTRODUCTION

Polarity-sensitive fluorescent molecules are ubiquitous for sensing of biomolecules and studying inter-biomolecular interactions inside a cell.[1] In particular, sensing of the local microenvironment of DNA is highly important in connection with the detection of DNA mutations causing deleterious effects on cellular survival, high-throughput screening, and many other biotechnological applications.[2] All these events in DNA rely on novel fluorescent probes—either as bare or unnatural fluorescent nucleosides or fluorescently labeled natural nucleosides.[3] Though many such probe systems in relation to DNA have been reported, the probes suffer from fluorescence quenching by neighboring nucleobases, short wavelength emission, or poor microenvironment sensitivity.[3a,4] Therefore, design of novel emissive probes, particularly, fluorescent nucleosides with unique fluorescence properties, extreme sensitivity to change in DNA microenvironment, and interactions are highly desirable. Among the three approaches, linking a fluorophore in nucleoside bases is the major approach to generate a fluorescent nucleoside useable for DNA sensing.[2−5] As a result of tremendous research efforts, a large number of fluorescently labeled nucleosides and corresponding oligonucleotide probes have been designed and utilized for a variety of applications that include probing DNA hybridization,[6] typing single nucleotide polymorphism (SNP),[7] and monitoring the inter-biomolecular interaction,[8] to name a few. However, the majority of the reported environment-sensitive fluorescent nucleosides exhibited single band emission that sense the differences in micropolarity either by change in emission intensity or wavelength.[9−12] Among these, Saito's ESF nucleosides[13] and fluorene-linked nucleoside by Hocek et al.[14] are highly attractive for monitoring the micropolarity changes within DNA. However, often the majority of such probes suffer from several shortcomings such as poor microenvironment sensitivity and low quantum yields.[2−5,13,14]

Therefore, to overcome these limitations, the concept of two-band emission would be more advantageous over commonly utilized single-band fluorescent probes/nucleosides.[15] Thus, recording a ratio of the intensities at two wavelengths would allow ratiometric sensing, which is more advantageous than sensing based on single-wavelength emission.[16] Basically, ratiometric sensing results in an intrinsically calibrated emission response.[15] Ratiometric probing of DNA, though reported, is based on labeling of DNA by two interacting dyes such as a FRET pair or excimer/exciplex pair.[6a,7b,17] However, labeling with two dyes is difficult, time-consuming, and highly uneconomical.[15−17] On the contrary, a

Received: January 23, 2018
Published: June 7, 2018

DOI: 10.1021/acs.joc.7b03097
J. Org. Chem. 2018, 83, 7606−7621

Tetrahedron 74 (2018) 2218–2229

Contents lists available at ScienceDirect

Tetrahedron

journal homepage: www.elsevier.com/locate/tet

Design of a fused triazolyl 2-quinolinone unnatural nucleoside via tandem CuAAC-Ullmann coupling reaction and study of photophysical property

Subhendu Sekhar Bag*, Suman Kalyan Das, Hiranya Gogoi

Bioorganic Chemistry Laboratory, Department of Chemistry, Indian Institute of Technology Guwahati, North Guwhati 781039, Assam, India

ARTICLE INFO

Article history:
Received 26 January 2018
Received in revised form
15 March 2018
Accepted 17 March 2018
Available online 20 March 2018

Dedicated to Professor Isao Saito (Emeritus Prof. of Nihon University and Kyoto University) on his 77th Birth day.

Keywords:
Fused triazolylquinolinone nucleoside
Fluorescent
Tandem CuAAC-Ullmann coupling
Widen nucleo base
BSA interaction
Spectroscopy

ABSTRACT

This report presents the design and synthesis of a novel fused triazolyl 2-quinolinone (**FTQuon**) nucleoside as a new generation of angularly widened unnatural nucleobase surrogate with two possible H-bonding faces-one H-bond acceptor and another donor. The synthesis via a tandem CuAAC-Ullmann coupling, the study of photophysical properties and theoretical calculation in the context of DNA are the main contents of this report. The newly designed nucleoside shows interesting photphysical property with slight blue shifted solvatochromicity. It also shows pH sensitive emission. All the theoretical DNA duplexes containing the **FTQuon** show right–handed B-form helicity as revealed from a molecular dynamics simulation using Schrodinger Macromodel. A theoretical (DFT) study indicates a good stabilizing property of **FTQuon** via pairing with natural pyrimidine bases. It also shows good interaction property with BSA protein signalled via a switch on fluorescence response.

1. Introduction

The Nature's power of delegation for encoding the complex information necessary for life is given to DNA orchestrated only by H-bonded two base pairs.[1a] However, the motivation toward enhancement of functional ability has spurred the research to expand the genetic alphabets via the design of unnatural nucleobases by mimicking the natural H-bonded base pairing.[1] The pioneering work by Professor Alex Rich and later on by Prof. Steven A. Benner have led to expand the genetic alphabet from four to six letters featuring orthogonal H-bonding complementarity.[1] Since then an increasing amount of research works has resulted in the acceleration of progress towards expanding the genetic alphabets via the design and synthesis of unnatural H-bonded base pairs.[2,3]

The creation of non-H-bonded unnatural nucleobase surrogates by Kool et al., has opened a new dimension in the design of hydrophobic DNA base analogues.[4a–c] Since then, much efforts have been put forth to develop non-natural, stable, hydrophobic nucleosides.[4d–j] Many of such hydrophobic base pairs are found to be recognized by polymerase enzymes creating an increased numbers of genetic alphabets. In recent time, the development of size expanded DNA bases as well as widened base pairs has impacted greatly in the field of design of hydrophobic as well as H-bonded nucleosides.[5] Furthermore, the lack of practical fluorescence property of the natural nucleobases and harnessing for the nucleic acid based diagnostics and sensing materials, have greatly drawn interest, in recent time, toward the design of unnatural DNA base pairs with tuned photophysical properties.[6a–c] Toward this end, several unnatural nucleosides have appeared in the literature for the development of functional nucleic acids.[6d–f]

Therefore, the attractive forces like H-bonding, aromatic stacking, hydrophobic or CH-π interactions have well been explored in the context of design of isomorphic or other unnatural DNA bases.[1–5] In general, in the design of isomorphic DNA bases, the structural modification of purine in the five-membered ring is considered mostly. Several studies have reflected that such modifications, especially for 2′-deoxyisoguanosine, are tolerated as long

* Corresponding author. Tel.: +91 361 258 2324; fax: +91 361 258 2349.
E-mail address: ssbag75@iitg.ernet.in (S.S. Bag).

https://doi.org/10.1016/j.tet.2018.03.037
0040-4020/